New Materials for Sustainable Hydrogen Generation

By

Jane Louise Inglis

B.Sc. Chemical and Pharmaceutical Science

M.Sc. Advanced Chemical and Pharmaceutical Analysis

A Thesis presented to Dublin City University for the
Degree of Doctor of Philosophy

Supervisors: Professor Johannes G. Vos/Dr. Brian J. MacLean/
Dr. Mary T. Pryce

School of Chemical Sciences

Dublin City University

2013

Authors Declaration

I hereby certify that this material, which I now submit for assessment on the programme of study leading to the award of Doctor of Philosophy by research and thesis, is entirely my own work, and that I have exercised reasonable care to ensure that the work is original, and does not to the best of my knowledge breach any law of copyright, and has not been taken from the work of others save and to the extent that such work has been cited and acknowledged within the text of my work.

Signed: _____

Jane Louise Inglis

Candidate I.D. No.: 52084287

Date: 14th August 2013

Acknowledgements

Firstly, I'd like to thank Professor Han Vos to whom I'm very grateful for giving me the opportunity to do this PhD. Thank you for your support and guidance over the last 4 years.

To Dr. Brian MacLean, I don't know where to even start! You have been a fantastic supervisor over the last couple of years. I'm so grateful for all your help and advice. And I really appreciate all the help you gave me in preparing this thesis. Thank you so much!

To Dr. Danilo Dini, the past HVRG, Jen and Mary Pryce, and to the technicians; Veronica, Damien, Ambrose, Mary, Vinny and John and to everyone else in DCU...thank you for all your help.

A big thank you to the Dr's!. Debbie, Sonia and Yvonne, all of you have listened to me give out over the last few months (and years!). Thanks for all your help and for keeping me on track! x

Thanks to my parents, Anne and Chris and to my sister Suzanne for their words of encouragement and constant support through all the years. xx

And lastly, I would like to thank my fiancé Michael. Thank you for listening to me over the years (you didn't really have a choice!). It's done now, at last. xxx

Abstract

The focus of this thesis is the investigation of modified electrodes for the electrochemical generation of hydrogen. The catalysts employed consist of a series of metal perfluorinated phthalocyanines. Modified electrode films were made my physical adsorption of the complexes onto carbon surfaces and by dispersing them in Nafion® prior to casting them onto glassy carbon electrodes. These systems were evaluated in terms of TOF (hr^{-1}), moles of hydrogen generated and current density. As non-renewable sources of energy are currently the main energy providers or global consumption, there is now, more than ever, a demand for green, cheap, reliable and stable renewable energy sources.

Chapter 1 comprises of a literature review of electrocatalytic studies on similar catalysts.

Chapter 2 introduces the theory and practical aspects of this thesis. The experimental techniques employed (mainly cyclic voltammetry, bulk electrolysis and gas chromatography) in the studies presented in the later chapters are discussed, as well as the featured materials, methods and calculations.

Chapter 3 presents the characterisation of the catalysts, using absorbance spectroscopy and solution electrochemistry. The adsorbed modified electrodes are also characterised in this chapter.

Chapter 4 is concerned with three substituted metal (II) phthalocyanines; $CoPcF_{16}$, $CuPcF_{16}$ and $ZnPcF_{16}$ for use as electrocatalysts for H_2 formation. Factors including temperature, electrolyte and electrolysis potential play a major role in the development of such systems. Optimising the parameters for increasing these catalysts' performance for the electrocatalytic proton reduction remained the focus of this work.

Chapter 5 details the activity of the three catalysts incorporated in Nafion®. The introduction of a polymer matrix is expected to alter the electrocatalytic activity. Similarly to Chapter 4, important conditions are investigated such as electrolyte,

temperature and electrolysis potential. The effect of varying the ratio of catalyst to Nafion® is also studied.

Chapter 6 explores the use of a different electrode material for electrocatalytic generation of hydrogen. Nano-porous carbon monolith fragments were used in an effort to increase the catalytic performance but also to investigate the hydrogen storage properties of this material.

Chapter 7 is concluding remarks made for each experimental chapter and suggestions for future work.

Abbreviations

Ag	Silver wire
Ag/AgCl	Silver/Silver Chloride
BCM	Blank carbon monolith
BE	Bulk electrolysis with coulometry
CM	Carbon monolith
CME	Chemically modified electrode
$CoPcF_{16}$	Cobalt (II) 1, 2, 3, 4, 8, 9, 10, 11, 15, 16, 17, 18, 22, 23, 24, 25 hexadecafluoro-29 H, 31 H phthalocyanine
$CuPcF_{16}$	Copper (II) 1, 2, 3, 4, 8, 9, 10, 11, 15, 16, 17, 18, 22, 23, 24, 25 hexadecafluoro-29 H, 31 H phthalocyanine
CV	Cyclic voltammetry
DPV	Differential pulse voltammetry
FE	Faradaic efficiency
FID	Flame ionisation detector
GC	Gas chromatography
GCE	Glassy carbon electrode
MCM	Modified carbon monolith
MPc	Metal phthalocyanine
MTPP	Metal tetraphenyl porphyrin
MV	Methyl viologen
Nf	Nafion®
PE	Potentiostatic electrolysis
PSCAS	Potential step chromoamperometry

PVP	Poly-4vinylpyridine
2-PVP	Poly-2vinylpyridine
PVP-(St)	Poly-4vinylpyridine (co-styrene)
QRE	Quasi-reversible electrode
$Ru(bpy)_3$	Ruthenium tri(bipyridine)
TCD	Thermal conductivity detector
TOF	Turnover frequency (hr^{-1})
TON	Turnover number
$ZnPcF_{16}$	Zinc (II) 1, 2, 3, 4, 8, 9, 10, 11, 15, 16, 17, 18, 22, 23, 24, 25 hexadecafluoro-29 H, 31 H phthalocyanine

Table of Contents

Chapter One

Introduction

An overview of work carried out for the investigation of electrocatalytic pathways towards sustainable fuel production from water. The electrocatalytic properties of metallophthalocyanines and metalloporphyrins on chemically modified electrodes for electrochemical H_2 formation are discussed. Important parameters are examined for such catalysts immobilised on electrode surfaces including, catalytic efficiency, the overpotential required, pH of electrolytes used, the applied potential, methods used for catalyst immobilisation, and polymer supports. Possible mechanistic pathways are investigated for both reactions. Where available, turnover numbers are reported and provided in a table format.

1.1 Introduction

In recent years the need for renewable energy sources has become a major cause for concern. Now more than ever, there is a serious demand for renewable energy supplies. The rapid expansion of human populations and its attending energy demands have seriously taxed our ability to live in a sustainable manner. It has been suggested that the world's largest energy source, oil, will be exhausted by the middle of the 21st century.[1,2] Our dependence on fossil fuels for energy sources has created a second, far-reaching problem, which is climate change. In a recent review by Roy *et al*., the environmental impact of the increasing CO_2 levels was discussed, with an expected 6 degree increase in global temperature being predicted before the end of the current century.[3] This increase in temperature will have serious environmental consequences, including greatly diminished arable lands and no polar ice cap.[4] It is alarming that trends in both population growth and fossil fuel energy consumption continue, seemingly unabated. Thus, there is an urgent need for the development of novel approaches for obtaining energy, which should be carbon-neutral and therefore not exacerbate atmospheric CO_2 levels.

The development of new energy technologies should be efficient and cheap enough to replace present fossil fuel-based energy sources. Wind and solar energy are possible solutions. The advantage with using wind energy is that it is a well-developed science; however the variable energy output remains a disadvantage (with concerns of locations of wind turbines and the irregular strength of winds).

Solar energy is widely considered to be one of the most promising avenues for energy in future times, because of the virtually unlimited amount of solar energy that is available. In the last number of years considerable improvements have been made in the construction of fuel cells which mimic artificial photosynthesis.[5] However, solar energy, like wind, is an intermittent energy source, and both of these technologies produce electricity that must be stored. Compared to liquid hydrocarbon fuels, batteries can only store a small fraction of the energy and other

means of storing electricity, such as supercapacitors are not yet developed to the point that they can be considered for large-scale use.[6]

It is these issues, along with a greatly established fossil fuel-based energy infrastructure which makes displacing fossil fuels as a primary energy source for the world a daunting task.

A study of global energy consumption for 2010 conducted by BP (British Petroleum) revealed that at present, renewable energy sources (solar, wind, tidal, hydro and geothermal energy) constitute only 1% of the world's energy consumption; oil and gas remain the leading non-renewable sources of energy, accounting for 37% and 23% of global energy usage figures, respectively.[7] Thus, a novel energy technology needs to be capable of producing energy in a stored format.[8]

The electrocatalytic formation of hydrogen and the transformation of CO_2 into useful chemical products are of great interest in this endeavour. If renewable energy sources are used to generate fuels from cheap and widely available materials, this goal can be accomplished. Because of the sheer scale that would be involved in supplying the world's billions with energy, water has often been considered as a suitable starting material for the synthesis of H_2. It is present in large quantities on the earth's surface and hydrogen produced from aqueous solutions can be combusted to produce energy, yielding no carbon footprint. Hydrogen is an ideal energy carrier, but currently, its generation is mostly carried out using fossil fuels. As hydrogen has a low volumetric energy density, its storage and transportation is inconvenient, requiring high pressures (at an extra energy cost). However, on-board generation for immediate use in vehicles could aid to partly alleviate this drawback.

For the generation of hydrogen, water electrolysis is a well-established process but it employs expensive electrode materials and the transformation to H_2 requires high temperatures, reducing energy gains.[9] Thus, a more environmentally friendly H_2 production method is of interest.[10] The electrocatalytic formation of hydrogen is of particular interest for this reason. CO_2 is another widely available material that might be considered for energy storage purposes. As it is the by-product of most industrial operations and because of the problems that are

associated with its build-up in the atmosphere, CO_2 would be the cheapest type of starting material.

Electrochemical energy storage routes have been explored as early as 1800, with the first report of water electrolysis by Nicholson and the first battery by Volta appearing in the same year.[11] Starting from the 1980's there has been an interest in developing electrocatalytic methods for hydrogen production and the transformation of CO_2 into useful chemicals. Studies of electrochemical H_2 evolution and CO_2 reduction are well-known, and are typically carried out with the use of catalysts. The reduction of acidic solutions on platinised platinum surfaces forms the basis for the standard hydrogen electrode (SHE) ($a_{H2} = a_{H+} = 1$; $T = 25^oC$), which yields the reversible potential for proton reduction to molecular hydrogen.[12,28]

The reduction of H^+ on other surfaces and using different conditions requires a greater energy investment for this transformation, observed experimentally in the form of an overpotential (section 1.2.2.1). Large-scale use of platinum for obtaining energy in this manner is not feasible, hence much time has been devoted toward the discovery of more abundant and cheaper materials for electrochemical H^+ reduction at minimal overpotentials, concerning a range of electrode materials, semiconductors, molecular catalysts dissolved in electrolyte solutions and surfaces that incorporate immobilised catalyst centres (chemically-modified electrodes, CMEs). This thesis concerns CMEs that consist of substituted metal phthalocyanines (MPc's) in surface-confined arrangements for electrochemical H_2 evolution. These MPc's are advantageous for this work in that they provide reactive catalyst centres whose electronics may be influenced by the nature of the coordination sphere. These systems are sometimes active at lower overpotentials than metallic catalysts, and may present "open" coordination sites for catalytic transformations in the form of easily-substituted ligands.[13]

Along with using molecular complexes as catalysts for these reactions, a popular method for the immobilisation of electrocatalysts on electrodes is dispersing them in polymer matrices. In certain cases, electroactive polymers may be used, which facilitates the regeneration of the active forms of the electrocatalysts.[14] Superior electron transport is possible in systems that involve conjugated organic

backbones (conjugated metallopolymers). These materials have been targeted for use in electrocatalysis since their discovery in the mid 1990's, due to their fast electron transport properties which can greatly enhance the regeneration of electrocatalyst centres during catalytic oxidation/reduction cycles.[15] For these materials, a fast superexchange mechanism operates, which provides electron transport at rates up to two orders of magnitude greater than those reported for comparable vinlypyridine-based metallopolymers.[16] The direct coordination of metal centres to the conjugated π-system of the polymer backbone in a conjugated metallopolymer also yields materials which possess interesting combinations of redox and spectral properties. However, these pre-synthesised ligands that yield conjugated metallopolymers are not yet commercially available, thus investigative work with these materials would require additional synthetic effort. Still, the attachment of groups that enable *in-situ* oxidative or reductive electropolymerisation (e.g. thiophenes, pyrroles) may be achieved through well-established carbon-carbon bond formation reactions in reasonably good yields.[17,18,19]

This chapter gives a brief overview of the work carried out for the electrocatalytic generation of hydrogen in the last 30 years using electrodes in which surfaces are modified with a range of substituted metal phthalocyanines. The experimental conditions are listed in Table 1.1 for the electrocatalytic production of hydrogen.

[M-no.]	***Polymer/Electrode***	***Potential (V) vs. Ag/AgCl***	***pH of Solvent System***	***TOF (hr^{-1})***
[Co-**1**]	P(VP-St)[a]/BPG[b]	-0.9[c]	pH 1.0[o]	2×10^5
[Co-**2**]	P(VP-St)[a]/BPG[b]	-0.9[c]	pH 1.0[o]	5×10^4
[Co-**3**]	P(VP-St)[a]/BPG[b]	-0.9[c]	pH 1.0[o]	1×10^3
[Cu-**1**]	Nf[d]/GCE[e]	-1.22[f]	pH 2.7, 7.3, 10.4[o]	[g]
[Cu-**4**]	GCE[e]	-0.84[f]	pH 9.2[o]	[g]
[Co-**4**]	GCE[e]	-1.04[f]	pH 9.2[o]	[g]
[Zn-**1**]	P(VP-St)[a]/BPG[b]	-0.9[c]	pH 1.0[o]	3×10^4
[Zn-**1**]	Nf[d]/BPG[b]	-0.9[c]	pH 1.0[o]	4×10^4
[Co-**5**]	GCE[e]/epc[c,h]	-0.98[f]	pH 2.4[o]	[g]
[Co-**5**]	GCE[e]/dc[m]	[g]	pH 2.4[o]	[g]
[Co-**5**]	GCE[e]/sc[n]	[g]	pH 2.4[o]	[g]
[Ti-**6a-c**]	Nf[d]/GCE[e]	[g]	pH 3.4, 5.6, 10[o]	[g]
[Co-**7**]	Nf[d]/ITO[i]	-0.45[f]	pH 1.4[p]	20.[j]
[Co-**7**]	Nf[d]/ITO[i]	-0.50[f]	pH 2.2[p]	40[j]
[Co-**7**]	Nf[d]/ITO[i]	-0.54[f]	pH 4.0[p]	32[j]
[Co-**7**]	Nf[d]/ITO[i]	-0.58[f]	pH 7.2[p]	6[j]
[Co-**7**]	Nf[d]/ITO[i]	-0.60[f]	pH 10.3[p]	34[j]
[Co-**8**]	Nf[d]/Pt	-0.3[c]	pH 1.0[o]	2×10^2
[Co-**8**]	Nf[d]/BPG[b]	-0.7[c]	pH 1.0[o]	70
[Mn-**8**]	Nf[d]/Pt	-0.8[c]	pH 1.0[o]	[g]
[Fe-**8**]	Nf[d]/Pt	-0.8[c]	pH 1.0[o]	[g]
[M-**8**]	Nf[d]/BPG[b]	-0.8[c]	pH 1.0[o]	5×10^2
[Zn-**8**]	PVP[k]/Pt	-0.4[l]	pH 4.4[o]	[g]
[Zn-**8**]	Nf[d]/Pt	-0.25[c]	pH 1.01[o]	[g]

Table 1.1: *Comparison of reported experimental details and hydrogen generation turnover numbers (TON's) for the electrocatalysts discussed.*

[a] P(VP-St) = poly(4-vinylpyridine-co-styrene); [b] Basal pyrolytic graphite; [c] Potentiostatic Electrolysis ; [d] Nafion® ; [e] Glassy Carbon Electrode ;[f] Calculated from published data *vs*. SCE ; [g] Not given ; [h] Electro polymerization technique; [i] Indium Titanium Oxide; [j] Calculated by subtracting the amount of hydrogen evolved on an ITO/Nf® electrode to the amount evolved on ITO/Nf®/CoPc, No indication of length of time TON have been calculated, [k] Poly(4-vinylpyridine); [l] Potential at which photocurrent is observed ; [m] Dip cast ; [n] Spin coat, [o] 0.1 M aq. NaH_2PO_4/H_3PO_4 ; [p] 0.1 M aq. $NaCl/NaH_2PO_4/H_3PO_4$.

1.2 Electrocatalytic systems based on modified electrodes

When hydrogen is used as an energy source, it generates no emissions other than water. Thus, it seems sensible to pursue this fuel as an energy source for meeting our future energy needs. The emergence of an environmental hydrogen economy has been advocated for some time. However, at present most hydrogen is produced from fossil fuels, a method that is clearly neither sustainable, nor environmentally friendly. A smaller amount (about 4%) is obtained from the electrolysis of water. Although attractive in principle, the direct electrolysis of water has several drawbacks. This process mainly uses platinum working electrode surfaces, and to enhance the efficiency of the process, high pressure and high temperatures (up to 850^{o}C) are frequently used, yielding an overall efficiency of 50-70%. Therefore, there is an urgent need for the development of cheap and low-temperature production methods for hydrogen. The challenge for today's scientists is to develop sustainable techniques to produce hydrogen economically. Because the use of Pt catalysts for meeting global energy needs is not a realistic idea (a hurdle which also confronts fuel cell technology), molecular catalysts using first row transition metals have been investigated for their potential application in hydrogen generation reactions. The main molecular catalysts which will be discussed in detail in this chapter are metal phthalocyanines and porphyrins, although a recent review has been published detailing various types of metal compounds which have been employed as electrocatalysts for the production of fuel from water.[20]

1.2.1 Modification of electrode surfaces

A variety of techniques have been published which detail the immobilisation methods of catalysts onto electrode surfaces.[21,22,23] Three techniques that are frequently encountered in the literature for producing these modified films are drop-casting of catalyst solutions, dip-coating of catalyst solutions and electrochemical coating.

The first technique simply involves casting a small volume of the catalyst solution onto the surface of an electrode, hence the term drop-casting.[24] Providing that the complex is not soluble in the electrolysis solvent, this method is a convenient route to the creation of modified electrode surfaces. Dip-coating is a related, alternative technique in which the electrode is immersed into the catalyst solution, removed and allowed to dry.[25,26] The third technique is electrochemical coating. An electrode is placed into the catalyst solution where the potential of the electrode is fixed (for a period of time) in which the coat is 'grown' directly onto the surface. The catalyst consists of a monomeric electroactive species which contains polymerisable groups (such as vinyl-substituted metal complexes) for the creation of a modified electrode surface. In this technique, the use of chemical/electrochemical reactions generate new bonds between the electrocatalyst and the electrode surface.[26,27]

Several important advantages over solution-phase experiments are achieved when electrocatalysts are introduced as insoluble films on electrode surfaces. A high concentration of the catalyst exists in the region of the electrochemical reaction (compared to the concentration of the electroactive species in at the interface in solution phase). Furthermore, because the electrode is coated with a thin layer of the catalyst, the approach uses minimal quantities of catalyst materials. Importantly, removal of the electrocatalyst following the reaction is facile.

1.2.2 Catalytic Activity

It is evident from the examples of work carried out in this field over the years that there are a number of factors which dictate a catalyst's performance for electrocatalytic reduction of H^+ to H_2. These factors are applied electrolysis

potential, pH of electrolyte, influence of the metal centre, substituent effects, and polymer support.

1.2.2.1 Overpotential (η)

For H_2 evolution, the reaction of interest is;

$$2H^+ + 2e^- \leftrightarrow H_2 \qquad E^\circ = 0.00\ V\ vs.\ SHE \qquad \textbf{Equation 1.1}$$

The reaction in Equation 1.1 occurs at a platinum electrode, at an equilibrium potential of -0.197 V vs. Ag/AgCl. Over-potential, η, is defined as the additional potential beyond the thermodynamic requirement needed to drive a reaction at a certain rate.[28] The equilibrium potential, E_{eq}, is related to the overpotential through equation 1.2:

$$\eta = E - E_{eq} \qquad \textbf{Equation 1.2}$$

An ideal system is one which has a low overpotential for the proton reduction reaction to molecular hydrogen. A large overpotential involves a significant extra energy investment for driving the electrochemical reaction at the desired rate. Thus the development of catalysts which can carry out the desired process at small overpotentials is highly desirable.

It is apparent from the literature reviewed that different research groups report the experimental potential (*E*) for the electrolyses in different manners. This, of course, influences the determination of the overpotential. Artero *et al.*[29] report using the half-wave potential at which catalytic currents are measured while Koca referred to the onset of the reduction wave for the calculation of η.[30] The onset potential is described as the minimum potential at which the catalytic process is observable. Peters *et al.*[31] interpret the potential *E* to be that of the reduction process of the species involved in the catalytic reaction (i.e. catalyst and not the potential at which the catalytic current occurs) whereas DuBois takes the potential *E* as the corresponding potential to where the current is half its maximum value.[32]

With regards to the overpotential, two remarks must be made. The first is that the standard electrode potential, E°, for the reduction to H_2 is measured at *standard* conditions (298 K, 1 atm with H^+(aq) and H_2(g) at unit activity) using platinised platinum electrodes.[28,33] However these conditions do not reflect the experimental

conditions employed for the reactions carried out in this thesis or in any of the works cited above.

In order investigate the possibility of using a complex as an electrocatalyst for this kind of work, experiments should be performed using a bare working electrode first in order to gauge the overpotential requirements (E_{bare}), for the reaction This potential can be compared to the potential for the same reaction using a modified working electrode E_{mod}. If E_{mod} is less negative (for a reduction) than the E_{bare}, then the modifying layer is an effective electrocatalyst, decreasing the overpotential with respect to the bare electrode and thus requiring less energy for the reaction to ensue.

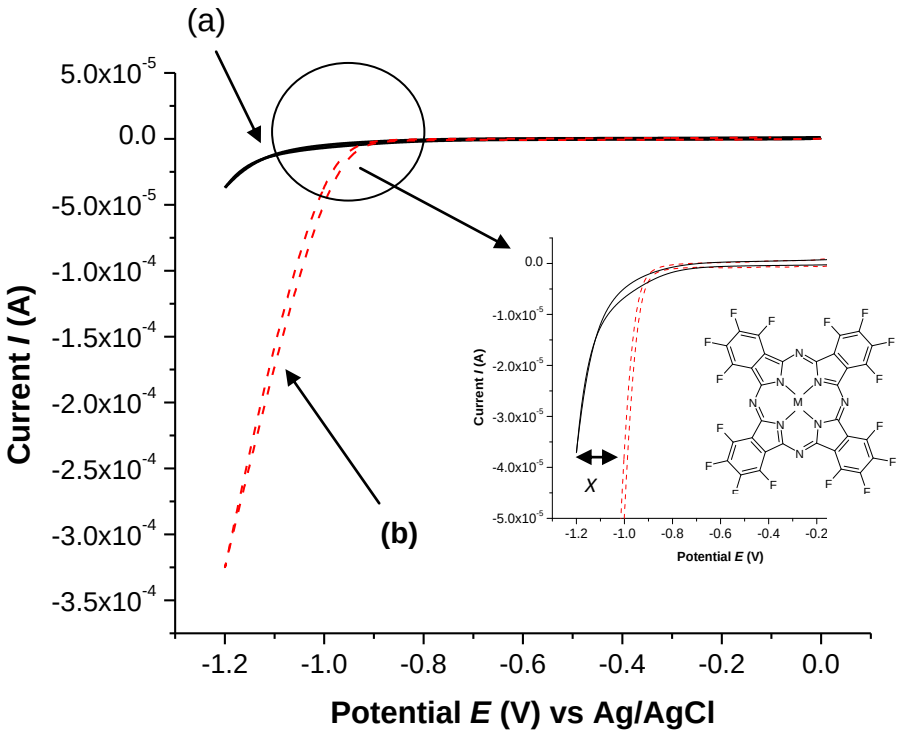

Figure 1.1: *Cyclic voltammogram of (a) bare GCE and (b) modified electrode (coated with $CoPcF_{16}$ -inset) (vs. Ag/AgCl) at 100 mV/s in 0.1 M NaH_2PO_4/H_3PO_4 (pH 2) for hydrogen production. Inset: enlarged CV, where x represents the difference in potential at which similar currents are observed by E_{bare} and E_{mod} thus decreasing the overpotential.*

For illustrating this point, the voltammogram shown in Figure 1.1 compares a bare glassy carbon electrode to a coated GCE modified with $CoPcF_{16}$. The generation

of H_2 using a bare glassy carbon electrode in pH 2 phosphate buffer conditions would require a potential (E_{bare}) more negative than -1.2 V to produce a current of the same magnitude as the current produced by $CoPcF_{16}$ (E_{mod}), Figure 1.1 inset. The same current is observed at a potential that is almost 200 mV less negative for $CoPcF_{16}$, which suggests that $CoPcF_{16}$ is effective for electrocatalytic H_2 generation.

1.2.2.2 Turnover Frequency (TOF) and Current Density (J)

Turnover frequency *TOF* and current density *J* are performance indicators used to evaluate how effective an electrocatalyst is at contributing to the reaction. The turnover number, *TON*, reports the number of moles of product generated per mole of immobilised, electrochemically active catalyst during the experiment (Equation 1.3) whereas the TOF reports the number of moles of product obtained in the context of a *certain timeframe*, (i.e. *per hour*). Current density *J* is defined as the rate at which electrons pass across the electrode-solution interface, divided by the electrode's surface area. *J* offers important information concerning the rate of electrolysis (Equation 1.4). The current density in this thesis is determined in two ways; the first is by taking the maximum current observed in a cyclic voltammetry (CV) experiment and dividing it by the geometrical area of the working electrode (0.070 cm^2 for a glassy carbon electrode). The catalytic current observed in the voltammogram is assumed to be a result of proton reduction. The current density was also calculated by taking the average current passed over the period of electrolysis and dividing it by the area of the working electrode. The problem associated with calculating the current density in this way is that oxidation of water occurs at the counter electrode. In the timeframe of an electrolysis experiment (one hour) it is expected that diffusion of dissolved O_2 (created by this oxidation) would be sufficient to permit movement of O_2 to the cathode, where it would subsequently compete with H^+ ions for reaction at the working electrode. However, because the products at both the working and counter electrodes are gases, convection caused by the movement of these bubbles (and by periodic bumping of the cell to dislodge adhered H_2 bubbles at the working electrode) is expected to greatly enhance the ability of O_2 to reach the working electrode during an electrolysis. Unfortunately, phthalocyanine complexes are known to catalyse the reduction of O_2. Thus the current that passes

during an electrolysis will have some component that is caused by O_2 reduction. Because there is not sufficient time for this to occur during a cyclic voltammetry experiment (approximately 1 minute in length), current density calculated by the former approach is expected to be more useful for probing the performance of a catalyst for H^+ reduction. (The current densities can later be related to post-electrolysis data like TOF, mol product, etc.) The current density values given in the experimental chapters are calculated by both electrochemical techniques which can be compared.

$$TON = \frac{moles\ of\ H_2}{moles\ of\ catalyst} \qquad \textbf{Equation 1.3}$$

$$J = \frac{i}{A} \qquad \textbf{Equation 1.4}$$

Turnover figures can suffer from several drawbacks. First, the amount of product is dependent on the electrolysis time, thus reporting turnover frequency (TOF) instead of TON (which is defined as TON divided by time) may be more useful. However, non-linear current densities/amounts of product can be observed over time for such studies, and thus even TOF data must be used with some care when comparing the performance of different catalysts and different conditions.

Another important factor that influences TOF/TON in modified electrode studies (which is not always considered) is the fact that not all catalyst material within a modified electrode film necessarily participates in oxidation/reduction, due to limitations imposed by electron transport, and diffusion of the catalyst during electrolyses. For bulky catalysts that diffuse slowly within a non-conducting polymer film (e.g. phthalocyanine complexes), this may limit oxidation/reduction of the catalyst to regions very close to the electrode surface and preclude such processes in more remote regions of the film. For TOF/TON calculations, this is a source of error that can amount to an order of magnitude or more in reported data. Thus the quantity of electroactive catalyst material within the film should be determined by an electrochemical technique (e.g. cyclic voltammetry). This data has been used in the determination of TOF figures for this thesis; however, there is significant variation in the data which makes trends in TOF figures sometimes difficult to interpret.

1.2.3 Metal phthalocyanine modified electrodes

Metallophthalocyanines (MPc's) have attracted much attention over the years in areas ranging from commercial use as dyes in the paper and textile industry[34], environmental and chemical sensors used in the detection of heavy metals[35,36] and in pharmacology, for use as therapeutic agents.[37]

Important properties of MPc's include a rich redox chemistry that is associated with an 18π-electron arrangement, which allows for π-stacking interactions between these planar macrocycles in even fairly dilute solutions. They offer chemical and thermal stability, varied coordination properties, absorbance in the visible spectrum and highly efficient intermolecular electron transfer processes.[38] Metal phthalocyanines can be deposited from solutions onto electrodes forming aggregated systems which exhibit low solubility in H_2O, making these ideal candidates for use as electrocatalysts in aqueous solutions. It is these properties which make them attractive for use as catalysts for hydrogen evolution.

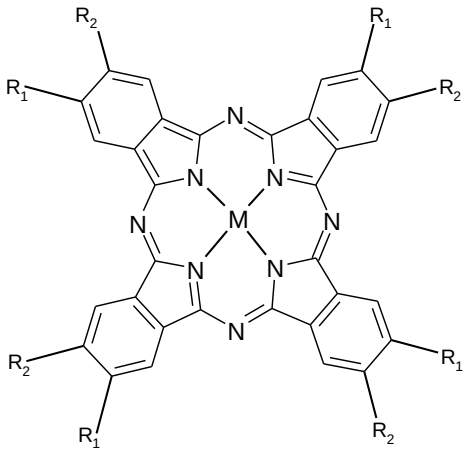

Figure 1.2: *Structures of metal phthalocyanine where M = Co, Zn, Cu, Fe, Mn, Ni, Pd; $R_1 = R_2 = H$ for [Co-**1**], [Zn-**1**], [Cu-**1**], [Fe-**1**], [Mn-**1**], [Ni-**1**] and [Pd-**1**].*

A considerable amount of research has demonstrated that MPc's can catalyse photoinduced proton reduction reactions to generate molecular hydrogen in the presence of sacrificial donors.[39,40] Although such results are very important with regards to alternative energy technology, the need for sacrificial donors will not directly lead to a sustainable hydrogen production technology. Modified electrodes for hydrogen evolution bypass the sacrificial donor step, since the

catalytically active states are generated by electron transfer at the film-solution interface at a modified electrode.

MPc's have been investigated for many years as materials for H_2 evolution, in studies that consider different metal centres as well as the effect of various substituents on the Pc ring. The electronic/steric nature of the substituents can affect the redox chemistry of the Pc ring, which can influence the electrocatalytic activities of complexes involving these structures. Electron withdrawing substituents tend to facilitate reduction of the complex (shift the reduction potential of MPc's to more positive values), while electron donating groups generally lower the ease of their reduction.[41] The catalytic activities of MPc's have been ascribed to the relative energy of the metal *d* orbital energies, which may be positioned between the HOMO and the LUMO of the Pc ring.[38, 42, 43, 44, 45, 46, 47] Although the first oxidation and first reduction processes are assigned as metal based for MPc's containing central metal ions of Mn, Fe and Co,[47] Lever *et al.* reported that for MPc's containing Ni, Zn and Cu as the central metal ion, no reduction redox processes take place on these centres but on the ring itself.[39] Therefore, there is much interest in the modification of MPc's concerning the effects of various substituents and central metal ions on their electrochemical properties. This is discussed further in Chapter 3.

1.2.3.1 Cobalt(II) phthalocyanine as an electrocatalyst

Because the electronic properties of ring substituents have been shown to play a key role in the catalytic activity of MPc's towards H_2 evolution, many researchers have explored this idea by varying both the nature of the metal and the phthalocyanine ring structure. Kaneko *et al.* reported the electrocatalytic properties of a series of Co(II) phthalocyanines. [Co-**1**], [Co-**2**] and [Co-**3**] shown in Figure 1.3 were incorporated in P(VP-St) polymer and adsorbed onto a BPG electrode. All three Pc's displayed electrocatalytic activity for hydrogen formation.[25]

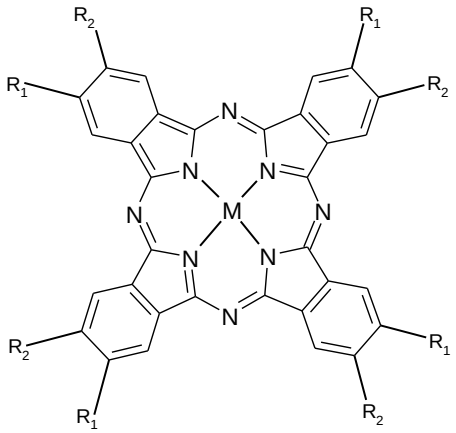

Figure 1.3: *Structure of metal phthalocyanine where M = Co for [Co-**2**] where R_1 = R_2 = CN and [Co-**3**] where R_1 = H, R_2 = (SO_3H).*

For [Co-**1**] embedded in a P(VP-St) polymer matrix, a TOF as high as 2 x 10^5 in 1 hour was determined when held at a constant potential of -0.9 V vs. Ag/AgCl in acidic phosphate buffer, Table 1.1. This TOF is one of the highest values reported when compared with other molecular based catalysts and is the standard against which our catalysts are compared throughout the thesis. Upon substitution of the [Co-**1**] with cyano- or sulphato- groups, the catalytic efficiency (and apparent diffusion coefficient D_{app} – see 1.2.4.1) decreased in the order [Co-**1**] > [Co-**2**] > [Co-**3**]. This decrease in efficiency is reflected in TOF data for [Co-**2**] and [Co-**3**] (5 x 10^4 and ~ 1.2 x 10^3 h^{-1}, respectively, Table 1.1) under the same conditions as used for [Co-**1**]. This trend suggests that catalytic efficiency is dependent upon the rate of electron transport within the matrix. Clearly the nature of the functional groups which are substituted on the Pc ring strongly affect catalytic efficiency. This is reflected in the mechanism and also in redox potentials observed for the compounds where the redox potentials (E½) for [Co-**1**], [Co-**2**] and [Co-**3**] are -0.25 V, -0.20 V and -0.55 V respectively. Some suggested mechanisms for H_2 production by proton reduction are illustrated in Scheme 1.1.[25]

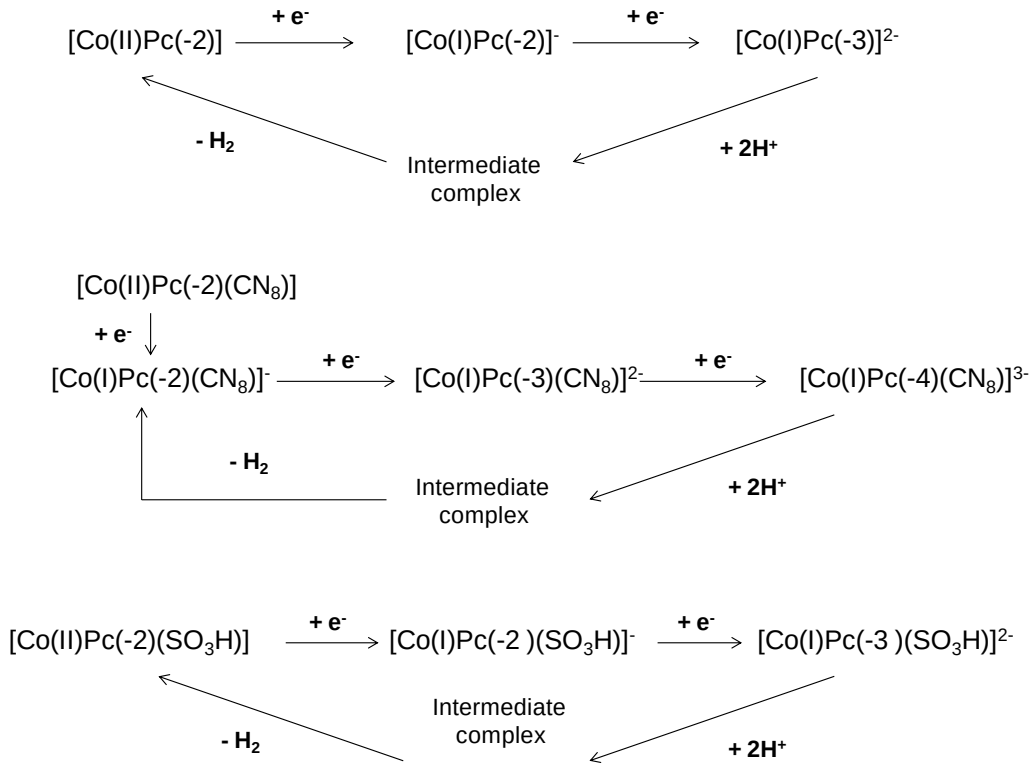

Scheme 1.1: *Proposed electrocatalytic mechanisms for the reduction of protons to hydrogen, where [Co-**1**] is the unsubstituted CoPc, [Co-**2**] is CoPc(CN_8) and [Co-**3**] is CoPc($SO_3H)_4$ (which are all embedded in the P(VP-St) matrix). Mechanism reported by Kaneko, reference 25.*

Osmanbaş *et al.* reported cobalt, copper and zinc phthalocyanines bearing thiophenes for investigation as electrocatalysts for the production of H_2 ([Co-**4**], [Cu-**4**] and [Zn-**4**]).[26] These electrodes were prepared using various modification techniques such as dip-casting, spin casting and electropolymerisation. The structure of this type of MPc is shown in Figure 1.4.

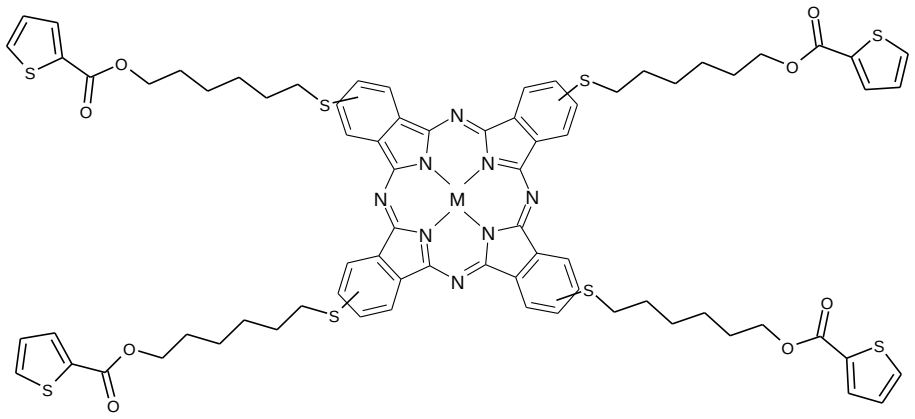

Figure 1.4*: Structure of [M-**4**] where M = Co, Cu and Zn.*

Although no TOF were given, the rate of H_2 production was determined by the rate of electrolysis where for both the zinc and copper phthalocyanines, the charge passed over 1 hour was low, compared to the charge passed for cobalt [Co-**4**], Figure 1.5. It was suggested that the enhanced catalytic activity of the thiophene based CoPc derivatives compared to the copper and zinc derivatives was due to the metal/ligand processes as metal based reduction processes were postulated to play an important role for the reduction of protons.[39,47]

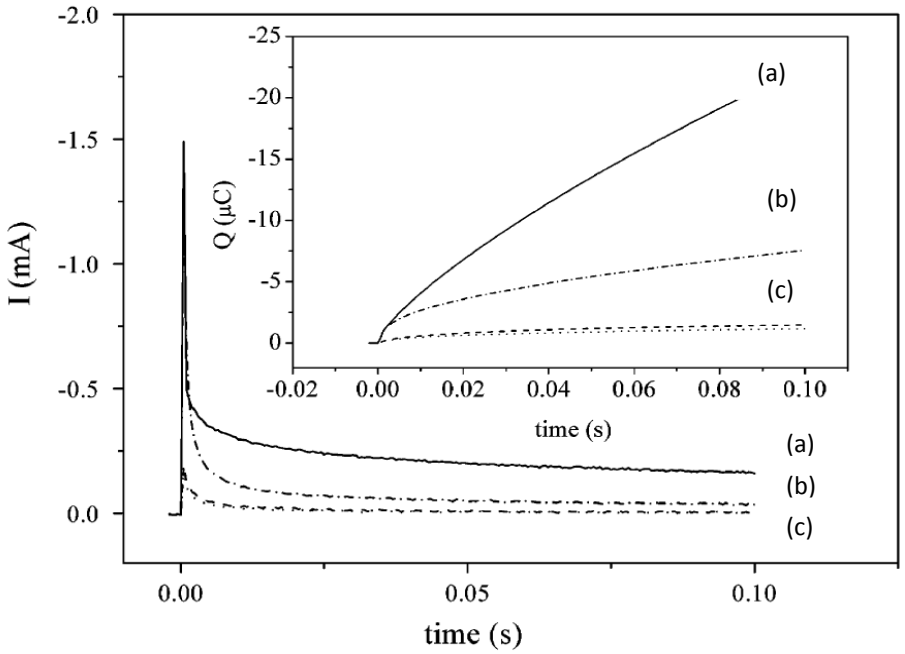

Figure 1.5: *Current-time profiles (inset: charge-time profile) for [M-**4**], (a) [Co-**4**] (black line), (b) [Zn-**4**] (dot dash line) and (c) [Cu-**4**] (dot line) (vs. SCE) at*

100 mV/s in 0.1 M NaH_2PO_4/NaCl. Electrode modified by electropolymerisation. Adapted from reference 26.

The substitution of the thiophene functional group shifts the redox potential in a negative direction, where the cathodic wave for the first reduction of metal Co(II) to Co(I) occurs at -0.43 V, compared to the unsubstituted [Co-**1**] at -0.25 V vs. Ag/AgCl.[25] The effect of pH on hydrogen generation on these MPc derivatives is discussed in Section 1.2.6.

1.2.4 Electron transport within a catalyst/polymer layer

The efficiency of the CME's will be dictated by electron transport steps between the substrate and the underlying electrode surface which are mediated by the catalytic centres. There are three mechanisms of transport by which electron transport in the polymer layer may be controlled. Depending on the experimental conditions and the nature of the polymer matrix, the rate determining step may be governed by: 1) polymer movement (in cases where the catalytic centres are strongly bound to the polymer chain) or diffusion of the catalysts within the polymer (when interactions are not strong); 2) diffusion of the substrate and/or counter ions, or; 3) electron transport.[48] Diffusion of the electrocatalysts in the polymer matrices (example: Nafion®) considered in this work is proposed to be faster than electron hopping and, therefore, is the most likely mechanism for the electron transport.[25,49,50] This is due to the weak interaction of the polymer matrix and the complex. This type of electron transport mechanism is observed for CoTPP (TPP = tetraphenylporphyrin) incorporated in P(VP-St) and Nafion® and also for MV^{2+}/ MV^{+} in Nafion® (MV^{2+} = methyl viologen)[51]. An electron-hopping mechanism is expected to be dominant for $[Ru(bpy)_3]^{3+}$/ $[Ru(bpy)_3]^{2+}$ in Nafion®.[52]

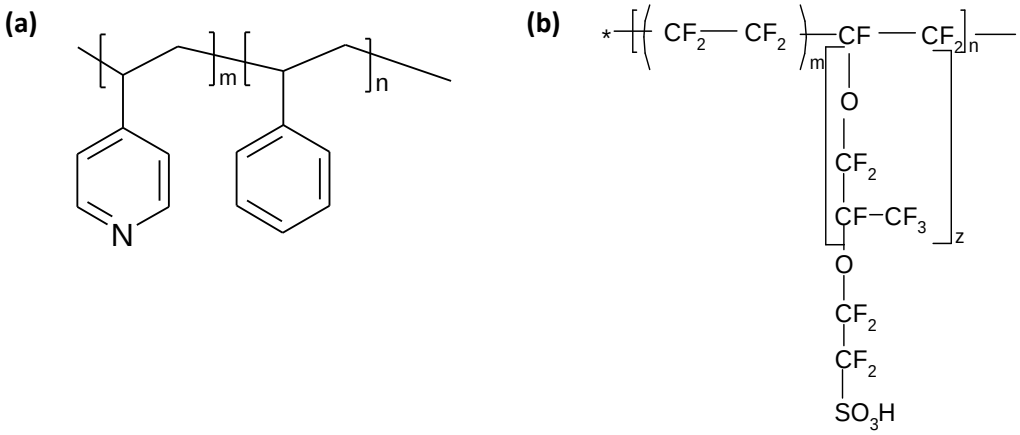

Figure 1.6: *(a) Structure of polyvinylpyridine co-styrene P(VP-St), (b) structure of Nafion®.*

When reduction of the complex occurs within the polymer film, the charge on the reduced form must be compensated. This may happen by one of two pathways: 1) cation migration from the electrolyte solution into the polymer film or 2) by anion migration from the polymer matrix to the solution. This charge compensation influences the electron transport rate. In Nafion® the sulphonate anions are immobilised in the polymer and so charge compensation takes place by movement of ions from the bulk electrolyte into the Nafion® film. Charge migration by cations is accomplished with H^+ ions, as protons have higher mobilities than any other cations in the film (e.g. Na^+). Similarly, charge compensation in P(VP-St) occurs via proton migration from the bulk solution to the layer (a process that is more likely than the migration of bulky anions such as $H_2PO_4^-$ from the polymer layer to the bulk solution). However, positively charged ions may be prevented from moving into the polymer matrix by the protonated pyridines of the P(VP-St) matrix, resulting in a lower electron transport rate.[49]

1.2.4.1 Apparent diffusion coefficient D_{app}

Charge-transport a polymer film can be described by the apparent diffusion coefficient, D_{app}, assuming semi-infinite diffusion behaviour, as defined by Cottrell's equation,[28]

$$i = \frac{nFAC_O{D_{app}}^{1/2}}{\pi^{1/2}t^{1/2}} \qquad \textbf{Equation 1.5}$$

where *i* is the current (A), *n* is the electron stoichiometry, *F* is Faraday's constant (96,485 $C \cdot mol^{-1}$), C_O is the concentration of the electroactive catalyst in the bulk solution ($mol \cdot cm^{-3}$) and *t* is time (s).

D_{app} values were obtained following a potential step from 0 V to -0.6 V vs. Ag/AgCl for electrode modified with [Zn-**1**] embedded in P(VP-St) and Nafion® matrices (denoted [Zn-**1**]/P(VP-St) and [Zn-**1**]/Nafion®, respectively) adsorbed on basal plane pyrolytic graphite (BPG) electrodes. At low catalyst concentrations (< 20 mM), the D_{app} values calculated were almost independent of the concentration of the catalyst (MPc complex) in the matrix.[49] Reported D_{app} values for [Zn-**1**]/Nafion® (~ 1.9 x 10^{-8} cm^2s^{-1}) were almost four times higher than those observed for [Zn-**1**]/P(VP-St) (~ 5.5 x 10^{-9} cm^2s^{-1}) due to the interaction of the redox complex with the polymer matrix and counterion migration. In acidic conditions the pyridine groups of P(VP-St) are protonated and so the Zn complex can be axially coordinated to the free vinyl-pyridine groups, thus the electron transport rate is slower compared to Nafion® due to these stronger interactions. This rate of charge transport through the modified layer is also reflected by the TOF, where [Zn-**1**]/Nafion® reached a TOF as high as 4 x 10^4 while TOF obtained for [Zn-**1**]/P(VP-St) was 2 x 10^4, Table 1.1.

Similar behaviour was also observed for [Co-**1**], [Co-**2**] and [Co-**3**] complexes incorporated in P(VP-St). For [Co-**1**] and [Co-**2**] (where films were prepared using low concentrations of catalysts; 2.5 mM to 10 mM), comparison of D_{app} values and catalyst concentration revealed an independent relationship. However, D_{app} values decreased for [Co-**3**] with an increase of the complex concentration in the polymer matrix, implying an inverse relationship exists between D_{app} and concentration. The most efficient catalyst, in terms of D_{app} was [Co-**1**] (~2.1 x 10^{-8} cm^2s^{-1}) while the least efficient catalyst was [Co-**3**] (~3.7 x 10^{-10} cm^2s^{-1}). As for [Zn-**1**]/Nafion® and [Zn-**1**]/P(VP-St) the rate of charge transport through the modified layer is also reflected by the TOF, where [Co-**1**]/ P(VP-St) reached a TOF as high as 2 x 10^5 while TOF obtained for [Co-**3**]/P(VP-St) was ~1.2 x 10^3. The electron transport rate is highly dependent upon interactions between complex and matrix, with physical diffusion of the complexes ascribed as the mechanism of electron transport for each of the three complexes. These D_{app}

values, which illustrate the rate of charge transport through the catalytic layer, highlight the importance of the choice of polymer matrix.

1.2.5 Catalysis

It was initially assumed that redox-active metals are required to catalyse hydrogen evolution; however, ring-based mediation has been observed.[26,30,40,49,53,54,55] This shift in the location of the catalytically active redox state is related to the metal *d*-orbital energies of the central metal ion. If the central metal has no *d* orbital levels within the HOMO-LUMO energy gap of Pc, the metal ion will not be involved when the complex is either oxidised or reduced, implying that electrocatalytic processes can be mediated by the phthalocyanine ring. MPc's based on Ni(II), Zn(II), Pb(II), Pd(II) and Cu(II) display this type of electrochemical behaviour [30, 42, 44, 45,46,49] while Mn(II), Fe(II) and Co(II) can experience metal-based and ligand-based reductions [40,42,44,45,46,54,56]. Koca *et al.* studied a range of copper (II) complexes adsorbed on a GC working electrode, where [Cu-**1**] exhibited ligand-based redox processes that efficiently catalysed proton reduction to H_2.[30]

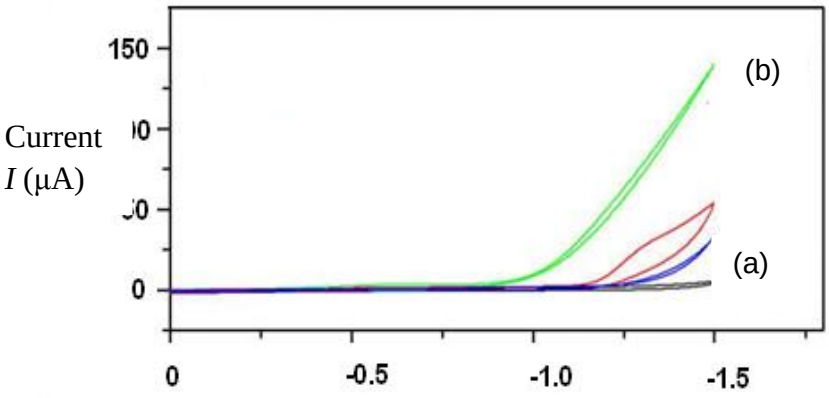

Figure 1.7: *Cyclic voltammogram of (a) bare glassy carbon electrode, (b) [Cu-**1**] in Nafion® polymer in aqueous phosphate buffer at pH 2.70 at 100 mV/s. Adapted from reference 30.*

In acidic phosphate buffer, a decrease in overpotential for H^+ reduction was observed for [Cu-**1**], compared to the potential required for H_2 formation using a bare GCE [2.5 x 10^{-9} mol cm^{-2}], Figure 1.7. Nafion® was employed as a

supporting matrix in an effort to enhance the catalytic activity. For [Cu-**1**]/Nafion® on a GCE, a decrease in overpotential for H_2 formation was observed compared to the adsorbed complex by almost 600 mV in phosphate buffer in basic conditions (pH 10.4); however, TOF were not reported for this catalyst.

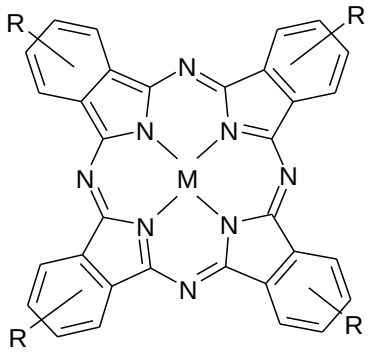

Figure 1.8: *Structure of [Co-**5**] and [Cu-**5**], R = $O(C_6H_4)_2CF_3$*

For [Cu-**5**] containing fluorophenoxy functional groups, Figure 1.8, adsorbed onto a GCE [2.5 x 10^{-9} mol cm^{-2}], higher electrocatalytic activity for proton reduction was observed than for the cobalt analogue, [Co-**5**]. While the onset potential for catalysis on bare GC electrode is observed at -1.27 V (vs. Ag/AgCl at pH 9.2) the onset of catalytic hydrogen evolution (as indicated by the appearance of a sharp cathodic process) begins at -0.84 V and -1.04 V for [Cu-**5**] and [Co-**5**], respectively; however, no TOF data were reported for these compounds.[55]

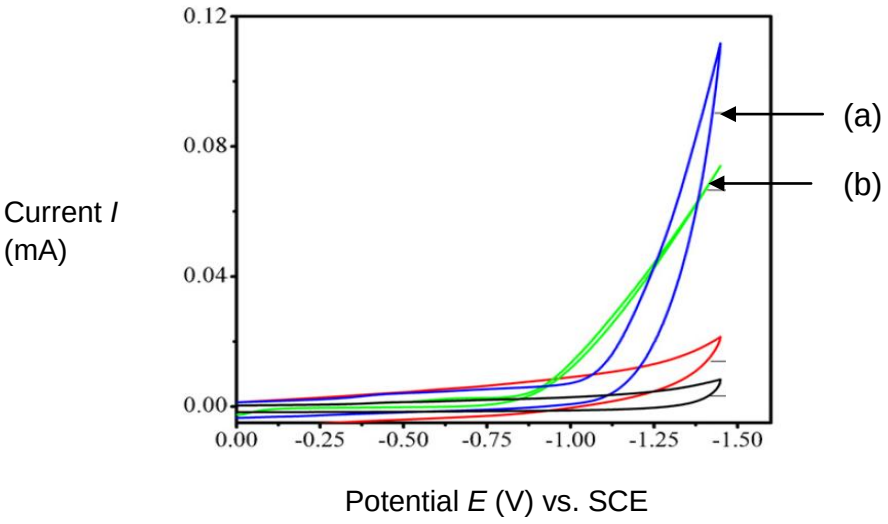

Figure 1.9: *Cyclic voltammogram of (a) [Co-**5**] and (b) [Cu-**5**] (vs. SCE) at 100 mV/s at pH 9.2 in 0.1 M NaH_2PO_4/NaCl. Adapted from reference 55.*

Kaneko *et al.* examined [Zn-**1**] embedded in Nafion® and [P(VP-St)] matrices adsorbed on BPG electrodes, which displayed ring-based redox processes that catalysed hydrogen formation.[49] TOF values reached 4.3 x 10^4 and 2.9 x 10^4 for [Zn-**1**]/Nafion® and [Zn-**1**]/P(VP-St), respectively, after 1 hour electrolysis at -0.9 V vs. Ag/AgCl [5 x 10^{-8} mol cm^{-2}], Table 1.1. This activity indicates that although Zn does not undergo a metal-based reduction, this metallophthalocyanine can still act as an electrocatalyst for H_2 evolution.

1.2.6 Effect of pH

The Nernst equation for these processes reveals that the pH of the electrolyte solution plays an important role in the potential required for the hydrogen evolution reaction at a bare electrode surface with the thermodynamic effect of pH on the half wave potential, E½ is a shift of 0.059 V. The Nernst equation is described below;[28]

$$E = E^{\circ\prime} + 2.303\frac{RT}{nF}\,log\frac{[O]}{[R]} \qquad \textbf{Equation 1.6}$$

where E is the applied potential, E^o is the standard potential, R is the gas constant (J mol^{-1} K^{-1}), T is temperature (K), n is the number of electrons transferred and F is the Faraday constant (C mol^{-1}). For [Co-**1**], electrocatalytic activity has been found to vary with pH due to the multiple mechanistic pathways. Formation of a proposed metal-hydride intermediate is proposed to occur after the first reduction of the complex, which is dependent upon electron transfer rate and electrolyte pH. Osmanbaş *et al.* reported varied catalytic behaviour over a range of pH buffer solutions. When [Co-**4**] was employed in acidic media, electrocatalytic activity was high while in neutral conditions, the lowest electrocatalytic activity was observed.[26] The mechanism proposed suggests that at low pH, the first catalytic step involves reduction of [Co(II)Pc(-2)] to [Co(I)Pc(-2)], which is subsequently protonated to form a stable hydride complex, [Co(I)Pc(-2)·H^+]. Proton reduction occurs following a second protonation step of the protonated, reduced species [Co(I)Pc(-2)·H^+] to yield molecular H_2. Thus in acidic conditions, [Co-**4**] can bind a proton firmly, thus the electrocatalytic activity increases. Suggested mechanisms for H_2 production by proton reduction for [Co-**4**] are illustrated in Scheme 1.2.

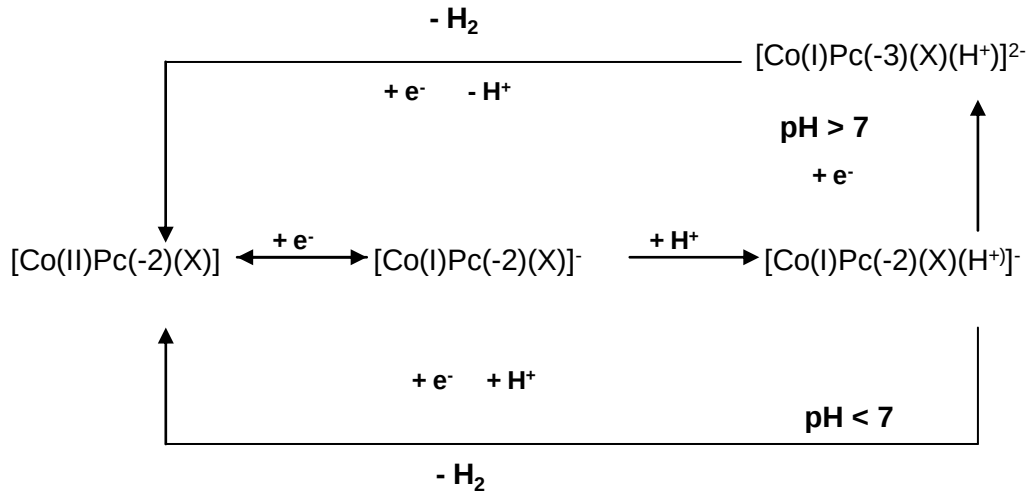

Scheme 1.2: *Proposed electrocatalytic mechanisms for the reduction of protons to hydrogen for [Co-**4**] where X denotes the thiophene functional group ($S(CH_2)_6OCO(C_4H_3S)$) on the Pc ring. Mechanism adapted from reference 26.*

The suggested mechanism for the electrocatalytic proton reduction using [Co-**4**] has two pathways; the top represents the mechanism in basic conditions while the bottom is in acidic media.

This pathway in acidic media is in agreement with work reported by Koca *et al.* using titanyl phthalocyanines adsorbed on GCE's, Figures 1.10.

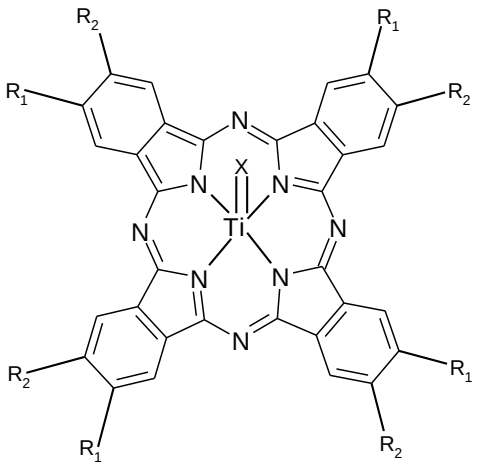

Figure 1.10: *Structure of [Ti-**6**], where **6a**; R_1= R_2 = $S(CH_2)_2N(CH_3)_2$, X = $C_6H_4O_2$, **6b**; R_1= R_2 = $S(CH_2)_2N(CH_3)_2$, X = $C_{10}H_6O_2$ and **6c**; R_1= R_2 = $S(CH_2)_2N(CH_3)_2$, X = O.*

At low pH, [Ti-**6a-c**] complexes were reduced and subsequently protonated to form stable hydrides yielding H_2 through 1 proton, 1 e^- sequences (ECCE overall), Scheme 1.3.[57]

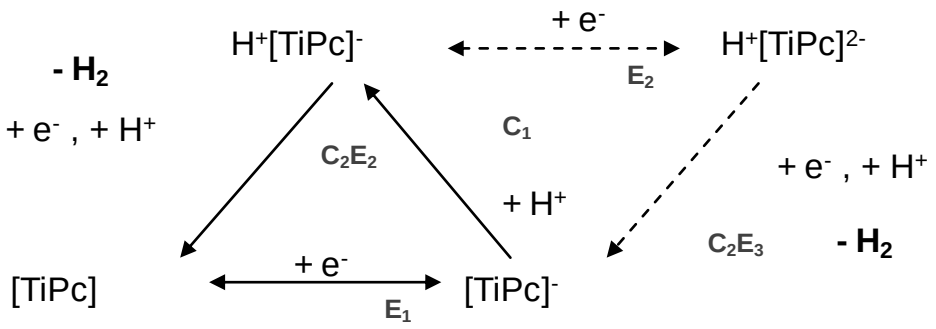

Scheme 1.3: *Proposed ECCE mechanism for the catalytic proton reduction in acidic conditions (black arrows) and basic conditions (dashed arrows). Adapted from reference 57.*

Increasing the pH to neutral conditions causes the electrocatalytic activity of the complexes to decrease. When the pH is made more basic for [Ti-**6a**] and [Ti-**6c**], the potential difference between the [M(II)Pc(-2)]/ [M(I)Pc(-2)]$^-$ process and the proton reduction process increases, and it is suggested that this difference may cause deprotonation of the hydride form before its reduction can occur to evolve hydrogen. For [Ti-**6a**] however, electrocatalytic activity increases in basic media. This increase may arise from the axially bound ligand, X. Following reduction to [Ti-**6a**]$^-$ and protonation to H^+[Ti-**6a**]$^-$, a second reduction yields H^+[Ti-**6a**]$^{2-}$, which then can undergo another protonation (to $H^+{\cdot}H^+$[Ti-**6a**]$^{2-}$) leading to the increase in catalytic activity. At different pH's, different electrocatalytic activity is observed for [Ti-**6a-c**] complexes due to 1) differing abilities bind a proton and 2) differing abilities to form a stable metal-hydride intermediate.

[Ti-**6a-c]**/Nafion® on a GCE surface sees an enhancement in electrocatalytic activity for [Ti-**6a,b**] in neutral and acidic media compared to the adsorbed complexes in the same conditions. This observation suggests that the nature of the ring substituents (along with the axial ligands) can affect the ability of the polymer/catalyst to bind a proton and that the nature of the polymer matrix plays an important role in the electrocatalytic activity over a range of pH's. Overall, the

complex which displayed the best catalytic activity over the range of pH is [Ti-**6c**].

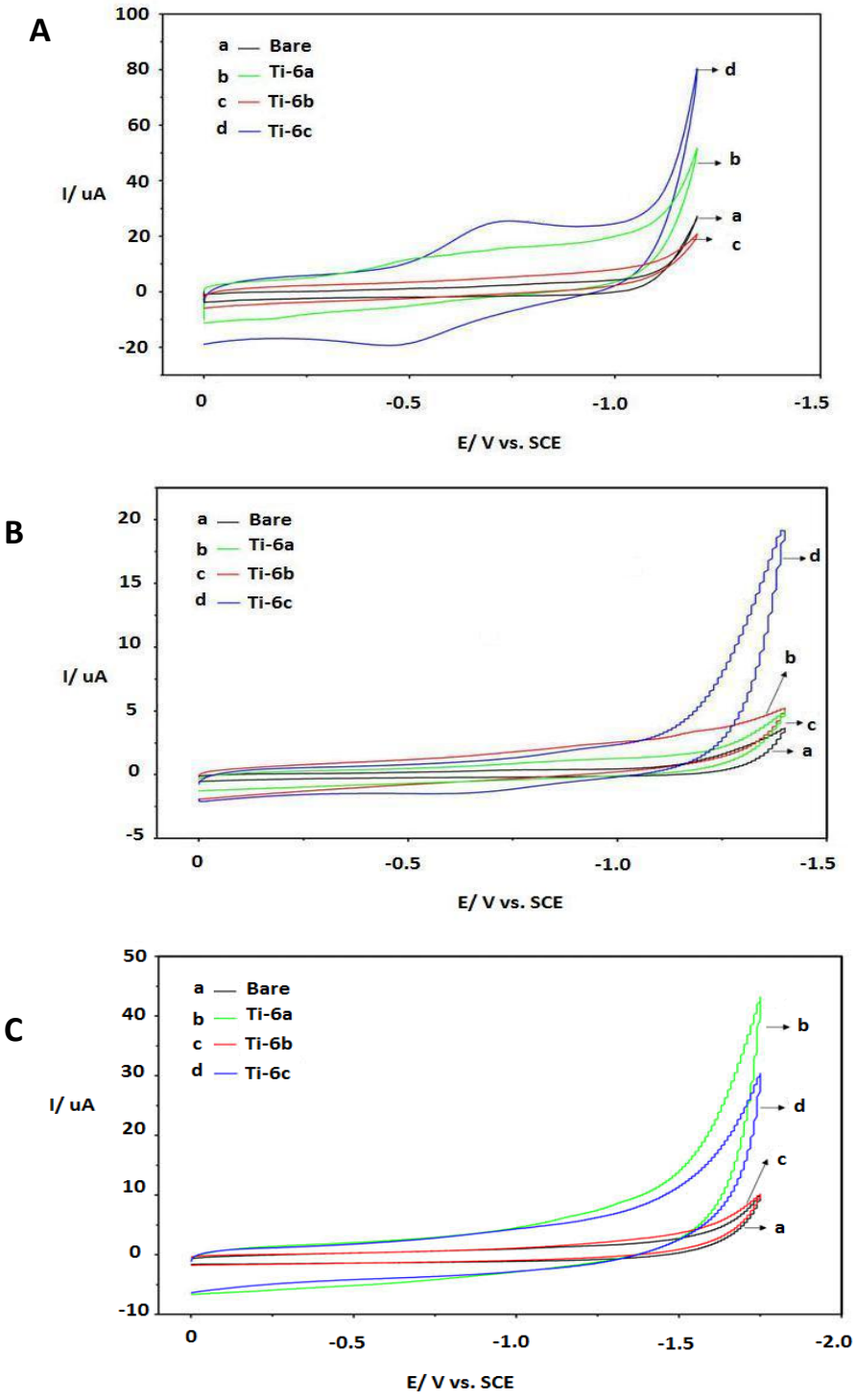

Figure 1.11: *Cyclic voltammograms of bare and modified electrodes of [Ti-**6a-c**]. Where a = bare GCE, [Ti-**6a**] = b, [Ti-**6b**] = c and [Ti-**6c**] = d. Performed in 0.1 M aqueous phosphate buffer at 100 mV/s. A = pH 3.4, B = 5.6 and C = 10.0. Adapted from reference 57.*

However, for some MPc complexes, mechanisms different to those described above have been reported. Koca *et al.* noted the effect of changing pH of the electrolyte buffer for [Co-**7**]/Nafion® adsorbed on the surface of an ITO working electrode, Figure 1.12.

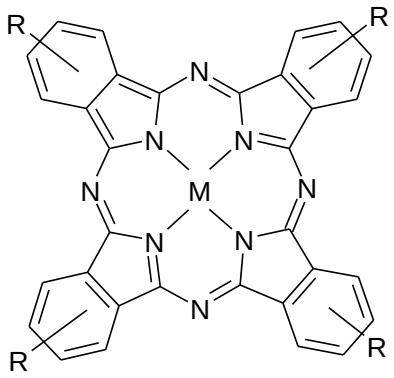

Figure 1.12: *Structure of [Co-7] where M = Co, R = $C(COOC_2H_5)_3$ incorporated into Nafion®.*

In acidic conditions, the first reduction process assigned as Co(II)/ Co(I) was found to be pH-dependent until the electrolyte solution reached neutral pH. TOFs reported for [Co-**7**]/Nafion® were 20.1, 39.9 and 31.5 at pH 1.4, 2.2, and 4.0, respectively, Table 1.1. As these electrocatalytic experiments were carried out on an ITO electrode, the concentration of catalyst immobilised on the surface was not given. At neutral pH (7.2), [Co-**7**] /Nafion® displayed poor activity for binding protons, reflected by the TOF of 6.18. The reduction potential for [Co-**7**] /Nafion® is shifted negatively in basic media, yielding an increase in the electrocatalytic activity for proton reduction. At pH 10.3, a TOF for H_2 formation was recorded as 34.2. As the central metal ion contributes to electrocatalytic activity in a range of pH's with the formation of a metal hydride intermediate; however, it appears that proton reduction is also reliant upon the nature of the substituents in both acidic and basic conditions.[40]

1.2.7 Metalloporphyrins as electrocatalysts

Metalloporphyrins are macrocyclic metal complexes which are closely related to metal phthalocyanines,[58] with the positioning of the nitrogen's at the meso (α)

position and substitution of the benzene rings fused on each of the 4 pyrolitic subunits at β position as the obvious structural difference, Figure 1.13.

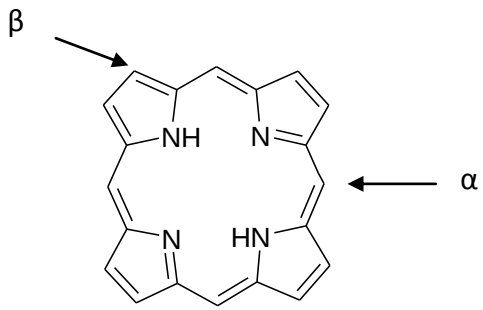

Figure 1.13: *Structure of metal free porphyrin with structural differences between porphyrin/ phthalocyanine at α and β position.*

Metalloporphyrins are used for various applications such as, phototherapeutic agents for treatment of cancer (PDT)[59] and as catalysts for the reduction of H^+ to H_2 in solution.[60,61,62] Kaneko *et al.* reported the electrocatalytic properties of various metal porphyrins on electrode surfaces.[63,64,65] Investigations concerning substitution at the porphyrin ring with a range of functional groups and different central metal ions revealed diverse electrocatalytic activities for the hydrogen evolution reaction. The nature of the substituent and central metal ion were crucial for the reaction to proceed.

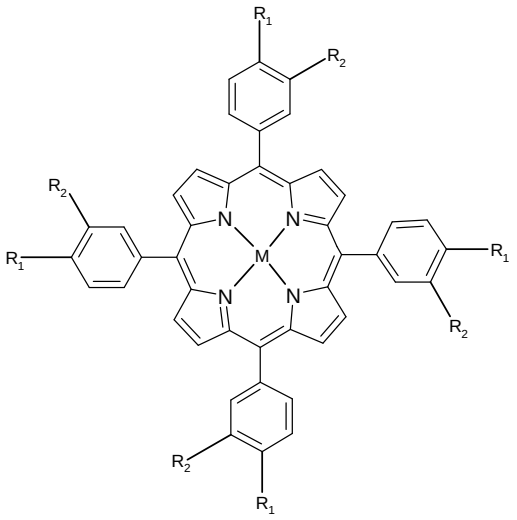

Figure 1.14: *Structure of metal tetraphenylporphyrin; where M = Co, Fe, Mn, Zn; $R_1 = R_2 = H$ for [Co-**8**], [Fe-**8**], [Mn-**8**] and [Zn-**8**] respectively.*

Cobalt tetraphenylporphyrin [Co-**8**] adsorbed on a Pt working electrode was examined for hydrogen evolution.[64] This assembly acted as a catalyst in acidic conditions at -0.25 V vs. Ag/AgCl, a potential close to the standard redox potential for H^+/H_2. Dispersing the catalyst into Nafion® appeared to result in an enhanced catalytic activity compared to [Co-**8**] immobilised directly on a bare Pt electrode. Hydrogen evolution occurred at potentials more positive than the bare Pt electrode in these studies as shown in Figure 1.15 below.

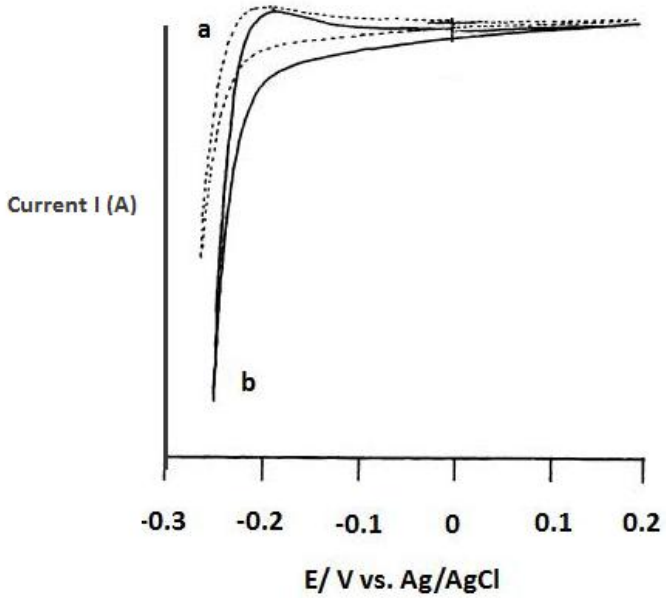

Figure 1.15: *Cyclic voltammogram of (a) bare Pt electrode and (b) [Co-**8**] embedded in a Nafion® layer coated onto a Pt electrode, using 0.1 M aqueous phosphate solution at pH 1. Scan rate = 1 mV/s. Adapted from reference 64.*

After a 1 hour potentiostatic electrolysis at -0.3 V in acidic condition (pH 1), the TOF reached 2.3 x 10^2 [2 x 10^{-9} mol cm^{-2}], Table 1.1. However, the values obtained were lower than those for [Co-**1**] where TOF reached 2 x 10^5 [1.25 x 10^{-8} mol cm^{-2}] when incorporated in P(VP-St) for 1 hr.[25] The high electrocatalytic activity of [Co-**8**]/Nafion® were assigned to the strongly acidic properties of Nafion®, where a high concentration of protons in the Nafion® membrane at pH 1 favours H_2 production.[66] As previously discussed for metal-phthalocyanines, diffusion-based electron transport occurs for this system due to a weak interaction between the redox couple and the polymer matrix and as a result, electron transfer

occurs faster by this route than by the electron-hopping mechanism.[25] For [Co-**8**]/Nafion®, it is suggested that a bimolecular catalysis mechanism is responsible for the reduction of Co(II)-TPP to catalyse H_2 formation. The formation of two intermediates was proposed; 1) metal-hydride formation and 2) a phenyl group of the TPP substituents act as an active site to form a protonated intermediate-complex due to a cation (H^+)-π interaction.

[Mn-**8**] and [Fe-**8**][63] complexes shown in Figure 1.14 are also active as catalysts, although they are less effective than [Co-**1**].[25] Similar to the findings for [Co-**8**], proton reduction appeared for these complexes at more positive potentials (approx. 50 mV) than for a bare Pt electrode. These complexes were also dispersed into Nafion® ([M-**8**]/Nafion®) to investigate the effect of a polymer matrix for the electrocatalytic proton reduction. A comparison of the amounts of H_2 produced after the potentiostatic electrolysis step for [Mn-**8**]/Nafion®, [Fe-**8**]/Nafion®, and [Mn-**8**] and [Fe-**8**] films adsorbed directly on Pt surfaces showed that the [M-**8**]/Nafion® system exhibited the highest electrocatalytic activity (in terms of volumes (μL) for H_2 evolution, however a time frame was not given). Thus these modified electrodes can electrocatalytically generate hydrogen. The TOF reported for [M-**8**] was 5×10^2 hr^{-1} at -0.8 V in pH 1 buffer solution (1×10^{-8} mol cm^{-2}/surface). Similarly for [Co-**8**], a bimolecular catalysis mechanism for electron transport was considered. Importantly, Buttry and Anson reported the presence of Co-TPP in the hydrophobic region of the Nafion®[67] which may suggest the formation of the second intermediate. Ryan *et al.* reported similar behaviour for [Fe-**8**] and [Mn-**8**] complexes.[68]

Abe *et al.* investigated the effect of using light (λ = 420 nm) to enhance the electrocatalytic activity of [Zn-**8**] immobilised in a matrix and adsorbed on a Pt electrode. This modified electrode produced a photocurrent upon an applied electrolysis potential of -0.55 V vs. Ag/AgCl when a PVP support was employed at pH 4.4 (1×10^{-7} mol cm^{-2}), Figure 1.16.[65a]

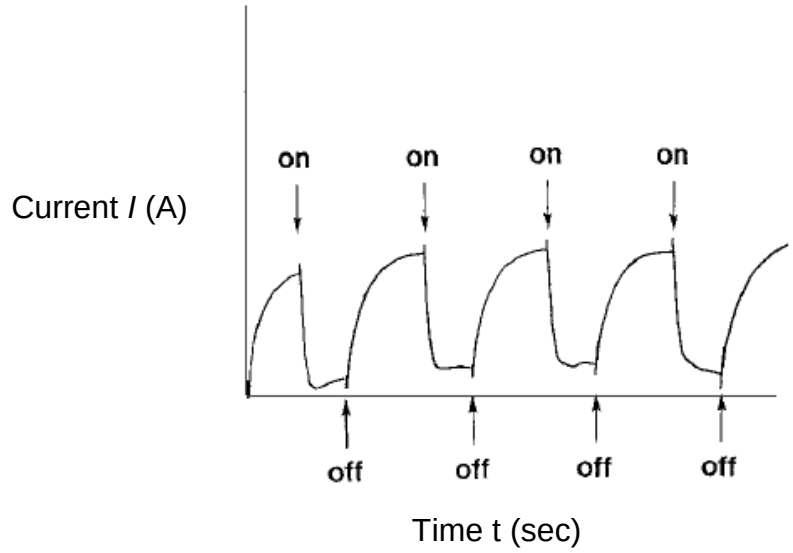

Figure 1.16: *Current response induced by on/off irradiation of light at 420 nm (vs. Ag/AgCl) for [Zn-**8**]/PVP in pH 4.4 phosphate buffer solution. Adapted from reference 65a.*

[Zn-**8**] worked as a photosensitiser in the visible region for photoinduced electron transfer.[69,70,71,72] These findings suggested that quenching of the singlet [Zn-**8**]* species to [Zn-**8**]$^{\cdot-}$ occurred by reduction of the Pt electrode. This reduced [Zn-**8**]$^{\cdot-}$ species was expected to mediate proton reduction to H_2. Nafion® was also used as a polymer for these photoelectrochemical experiments ([1 x 10^{-8} mol cm^{-2}).[65b] Potentiostatic electrolyses were carried out at -0.25 V vs. Ag/AgCl for 1 hour in pH 1 aqueous solution. It was observed that photoinduced H_2 formation takes place efficiently for this system, however no TOF were given. Thus, the system [Zn-**8**] when either PVP or Nafion® were employed as polymers, displayed photoelectrochemical H_2 production without employing an electron relay, while [Zn-**8**] acted as the sensitizer in the polymer membrane.

1.3 Why perfluorinated metal phthalocyanines?

Developing feasible alternatives for H_2 production is scientifically challenging an endeavour. However using bare metal cathodes such as Hg, Cu, Pd or Au is not practical, as large overpotentials are required or, in the case of Au, low abundance makes large-scale use impractical. The literature review for this thesis is based on

macrocyclic metal complexes for the electrocatalytic production of hydrogen, mainly metal phthalocyanines. These metal phthalocyanines described are substituted with various substituents and by doing so the electrochemical properties of the complex are altered. Hence, choosing a catalyst which possess attractive electrochemical properties, such as reversible reduction processes which have only moderately low potentials (close to 0 V, the standard potential for H^+ reduction) in order to enhance the electrocatalytic activity for proton reduction is highly desirable.

1,2,3,4,8,9,10,11,15,16,17,18,22,23,24,25-Hexadecafluoro-29*H*,31*H* phthalocyanine (PcF_{16}) contains electro-withdrawing groups at all available sites on the four fused phenyl rings. The tetraaza nitrogen's on the phthalocyanines offer greater thermal stability and are less susceptible to oxidation. By substituting all 16 hydrogen's on the fused phenyl rings with fluorines, a positive shift in the reduction potential occurs (-0.43 V vs. Ag/AgCl). The electrochemical properties can be further tuned by substitution of both protons at positions 29 and 31 in the central cavity with metal cations. Kaneko *et al.* reported TOF as high as 2 x 10^5 for the unsubstituted CoPc ([Co-**1**]) in aqueous phosphate solution (pH 1).[25] Substitution with an electron withdrawing group, fluorine, yielded an increase in catalytic activity (compared to CoPc) leading to higher TOF (2 x 10^6) and current densities and a decrease in overpotential (discussed later in chapter 4).

Several research groups have reported $MPcF_{16}$ as catalysts which displays good catalytic activity for the reduction of O_2 where M denotes Co, Fe, Mn and Zn. Considering these $MPcF_{16}$ catalysts show good catalytic activity for the reduction of O_2 from water,[73,74,75,76,77] which is a four-electron transfer reaction, these catalysts should be applicable for the investigations of the more kinetically feasible electron transfer reaction, $2H^+ + 2e^- \rightarrow H_2$. The electrocatalytic proton reduction reaction to hydrogen using these perfluorinated metal (II) phthalocyanines ($CoPcF_{16,}$ $CuPcF_{16}$ and $ZnPcF_{16}$) as electrocatalysts has not been reported to the best of our knowledge.

1.4 Scope of Thesis

The aim of this project was to identify a range of electrocatalysts for H_2 evolution. Platinum is widely used for electrochemical H_2 evolution; however, it is not an ideal electrode material as it is not abundant and is an expensive material. Hence employing transition metal complexes such as metal phthalocyanines would be an excellent alternative, considering these materials are abundant and thus cost effective. As non-renewable sources are currently the main energy supplies for global consumption, there is an ever-increasing demand for green, cheap, and reliable, renewable energy sources.

Chapter 2 deals with the electrochemical and gas chromatography theory. Important performance indicators and calculations, such as TOF are described here.

Chapter 3 in this thesis will introduce and discuss the three substituted perfluorinated metal (II) phthalocyanines, Figure 1.17. The main electrochemical technique used for the characterisation in both solution phase and as a thin films was cyclic voltammetry (CV). Characterisation of the electrocatalytic activity is also introduced in this chapter.

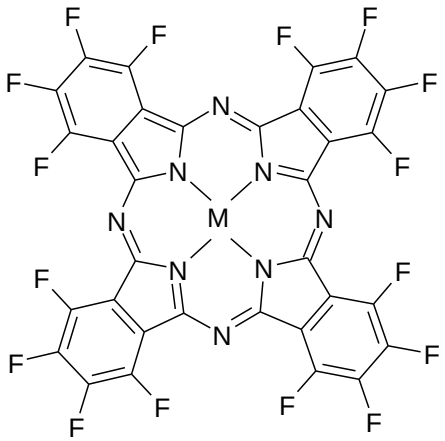

Figure 1.17: *Structure of molecular catalysts for the electrocatalytic reduction of H^+ to H_2 where M = Co, Cu and Zn.*

Chapters 4, 5 and 6 in this thesis will discuss these perfluorinated metal (II) phthalocyanines as adsorbed catalysts, as catalysts embedded in a polymer and in

graphitised porous carbon monolith material for the electrocatalytic generation of hydrogen.

Chapter 4 will discuss the results of electrocatalytic studies for the selected catalysts shown in Figure 1.17 as adsorbed films. Various factors are explored to determine which parameters influence the catalysis for H_2 production. These factors include electrolysis potential, overpotential, electrolytes, temperature, influence of light and a range of other parameters. Their potential in the application as electrocatalysts are ascertained by performance indicators, mainly TOF, moles of hydrogen and current density.

Chapter 5 will discuss the results of immobilising these catalysts within a polymer matrix. The development of a 3-D catalytic layer such as this, has been known to lead to greater performance due to the increase in concentration of electroactive species at the electrode surface.[20] The polymer matrix employed in these studies is Nafion®, an anionic polymer which allows for the passage of H^+ through the layer. The influential parameters investigated in chapter four will be discussed in this chapter.

Chapter 6 details the activity of these three catalysts when dispersed on a nano-porous carbon monolith material. The construction of these new catalytic systems on a conducting GCE will be discussed. Nano-porous polymers have been reported as materials which are capable for H_2 storage,[78,79] thus in combination with an electrocatalyst, the construction of a new electrocatalytic system, which can both produce and store hydrogen is the main focus of this chapter. The optimum catalyst and conditions identified from Chapter 4 and 5 are applied to this nano-porous material and the results following the investigation will be discussed.

Chapter 7 outlines the main concluding remarks from each chapter. The proposed future work for each of the studies carried out in previous sections is also outlined in this chapter. A series of refereed papers have been published on the work can be found in Appendix A. Supplementary Figures and Tables of work carried out and described in Chapters 3 to 6 are located in Appendix B to E respectively.

1.5 References

[1] M. Momirlan, T. N Veziroglu, *Int. J. Hydrogen Ener*., *30*, **2005**, 795.

[2] T. Abe, M. Kaneko, *Prog. Polym. Sci., 28,* **2003**, 1441.

[3] S. C. Roy, O. K. Varghese, M. Paulose, C. A. Grimes, *ACS Nano, 4*, **2010**, 1259.

[4] J. Hansen, P. Kharecha, D. Beerling, R. Berner, V. Masson Delmotte, M. Pagani, M. Raymo, D. L. Royer, J. C. Zachos, *J. Open Atmos. Sci.*, 2, **2008**, 217.

[5] D. Gust, T. A. Moore, A. L. Moore, *Acc. Chem. Res., 42,* **2009**, 1890.

[6] G. Centi, S. Perathoner, *Greenhouse Gas Sci. Technol., 1,* **2011**, 21.

[7] BP Statistical Review of World Energy 2010, Christof Rühl, June, **2010** http://www.bp.com/genericarticle.do?categoryId=98&contentId=7062807. Last accessed 10/01/2012.

[8] S. Dahl, I. Chorkendorff, *Nature Materials, 11*, **2012**, 100.

[9] NREL Technical report NREL/TP-581-40605.

[10] European Fuel Cells and Hydrogen Joint Undertaking, EU Call FCH-JU-2011-1.

[11] http://www.rsc.org/chemistryworld/Issues/2003/August/electrolysis.asp Last accessed 01/04/2012

[12] D. T. Sawyer, A. Sobkowiak, J. L. Roberts Jr, *Electrochemistry for Chemists, 2nd Ed*., John Wiley & Sons Ltd., **1995**, New York.

[13] A. Deronzier, J.C. Moutet, *Electrochemical Reactions Catalysed by Transition Metal Complexes,* in: M.D. Ward (Ed.) Comprehensive Coordination Chemistry, Vol. II, Elsevier, **2003**, Amsterdam.

[14] A. Deronzier, J. C. Moutet, *Accounts Chem. Res., 22,* **1989**, 249.

[15] B. J. MacLean, P. G. Pickup, *J. Phys. Chem. B, 106*, 18, **2002**, 4658.

[16] C. G. Cameron, B. J. MacLean, P. G. Pickup, *Macromol. Symp., 196*, **2003**, 165.

[17] B. J. MacLean, P. G. Pickup, *Chem. Commun.*, **1999**, 2471.

[18] D. T. Walker, C. G. Douglas, B. J. MacLean, *Can. J. Chem., 87*, 6, **2009**, 729.

[19] A. H. Murray, Z. Yue, A. L. Wallbank, T. S. Cameron, R. Vadavi, B. J. MacLean, M.A.S. Aquino, *Polyhedron, 27*, **2008**, 1270.

[20] J. L. Inglis, B. J. MacLean, M. T. Pryce, J. G. Vos, *Coord. Chem. Rev*., 256, **2012**, 2571.

[21] R. W. Murray, *Accounts Chem. Res., 13*, **1980**, 135.

[22] W. J. Albery, A. R. Hillman, *RSC Annual Report*, 78, **1981**, 377.

[23] J. G Vos, M. R. Smyth, *Analytical Voltammetry*, Chapter 7, Elsevier, **1992**, New York.

[24] T. Yoshida, K. Kamato, M. Tsukamoto, T. Iida, D. Schlettwein, D. Wohrle, M. Kaneko, *J. Electroanal. Chem., 385*, **1995**, 209.

[25] F. Zhao, J. Zhang, T. Abe, D. Wöhrle, M. Kaneko, *J. Mol. Catal. A: Chem*., *145*, **1999**, 245.

[26] Ö. A. Osmanbaş, A. Koca, M. Kandaz, F. Karaca, *Int. J. Hydrogen Ener., 33*, **2008**, 3281.

[27] P. Denisevich, H. D. Abruña, C. R. Leidner, T. J. Meyer, R.W. Murray, *Inorg. Chem.*, 21 **1982**, 2153.

[28] A. J. Bard, L.R. Faulkner, *Electrochemical Methods: Fundamentals and Applications*, *2nd Ed*., John Wiley & Sons, Inc., **2001,** USA.

[29] V. Fourmond, P.A. Jacques, M. Fontecave, V. Artero, *Inorg Chem.*, *49*, **2010**, 10338.

[30] A. Koca, *Electrochem. Commun.*, *11*, **2009**, 838.

[31] X. Hu, B. S. Brunschwig, J. C. Peters, *J. Am. Chem. Soc.*, *129*, **2007**, 8988.

[32] A. D. Wilson, R. H. Newell, M. J. McNevin, J. T. Muckerman, M. R. DuBois, D. L. DuBois, *J. Am. Chem. Soc.*, *128*, **2006**, 358.

[33] J. Wang, *Analytical Electrochemistry*, *2nd Ed*., Wiley-VCH, **2001**, New York.

[34] P. Gregory, *J. Porphyr. Phthalocya.*, *4*, **2000**, 432.

[35] S. O'Malley, B. Schazmann, D. Diamond, K. Nolan, *Tetrahedron Lett.*, *48*, **2007,** 9003.

[36] G. Guillaud, J. Simon, J.P. Germain, *Coord. Chem. Rev.*, *180*, **1998**, 1433.

[37] (a) N. B. McKeown, *Phthalocyanine Materials: Synthesis, Structure and Function*, Cambridge University Press, **1998**, Cambridge. (b) I. Rosanthal, *Photochem. Photobio. 53*, **1991**, 859.

[38] C.C Leznoff, A. B. P. Lever, *Phthalocyanines: Properties and Applications, Vol. I*, VCH, **1989**, New York.

[39] J. R. Darwent, P. Douglas, A. Harriman, G. Porter, M-C. Richoux, *Coord. Chem. Rev.*, *44*, **1982**, 83.

[40] A. Koca, M. K. Şener, M. B Koçak, A. Gül, *Int. J. Hydrogen Ener*., *31*, **2006**, 2211.

[41] K. Hesse, D. Schlettwein *J. Electroanal. Chem., 476*, **1999**, 148.

[42] M. K. Şener, A. Koca, A. Gül, M. B. Koçak, *Polyhedron, 26*, **2007**, 1070.

[43] M. N. Yarasir, M. Kandaz, A. Koca, B. Salih, *Polyhedron, 26*, **2007**, 1139.

[44] A. Koca, M. K. Şener, M. B. Koçak, A. Gül, *Transit. Metal Chem., 30*, **2005,** 399.

[45] A. Koca, Ş. Bayar, H.A. Dinçer, E. Gonca, *Electrochim. Acta, 54*, **2009,** 2684.

[46] M. Ozer, A. Altindal, A. R. Özkaya, M. Bulut, Ö. Bekaroglu *Polyhedron, 25,* **2006**, 3593.

[47] N. Chebotareva, T. Nyokong, *Electrochim. Acta, 42*, **1997**, 23-24 3519.

[48] (a)W. J. Albery A. R. Hillman, *Annu. Rep. Prog. Chem., C78*, **1981**, 317. (b) C. P. Andrieux, J. M. Dumas-Bouchiat, J. M. Saveant, *J. Electroanal. Chem., 131*, **1982**, 131.

[49] F. Zhao, J. Zhang, D. Wöhrle, M. Kaneko, *J. Porphyr. Phthalocya., 4*, **2000**, 31.

[50] F. Zhao, J. Zhang, T. Abe, M. Kaneko, *J. Porphyr. Phthalocya., 3*, **1999**, 238.

[51] J. Zhang, T. Abe, M. Kaneko, *J. Electroanal. Chem., 438*, **1997**, 133.

[52] J. Zhang, M. Yagi, X. Hou, M. Kaneko, *J. Electroanal. Chem., 412*, **1996**, 159.

[53] A. Koca, A. Kalkan, Z. Altuntaş Bayir, *Electroanal., 22*, **2010**, 310.

[54] A. Alemdar, A. R. Özkaya, M. Bulut, *Polyhedron, 28*, **2009**, 3788.

[55] A. Koca, A. Kalkan, Z. Altuntaş Bayir, *Electrochim. Acta, 56,* **2011**, 5513.

[56] A. Koca, M. Özçeşmeci, E. Hamuryudan, *Electroanal., 14*, **2010**, 1623.

[57] A. Koca, *Int. J. Hydrogen Ener*., *34*, **2009**, 2107.

[58] N. B. McKeown, *J. Mater. Chem.*, *10,* **2000**, 1979.

[59] D. Wohrle, A. Wendt, A. Weitemeyer, J. Stark, W. Spiller, G. Schneider, S. Muller, U. Michelsen, H. Kliesch, A. Heuermann, A. Ardeschirpur, *Russ. Chem. B+*, *43*, **1994**, 1953.

[60] (a) I. Bhugan, D. Lexa, J. M. Savéant, *J. Am. Chem. Soc.*, *118*, **1996**, 3982. (b) V. Grass, D. Lexa, J. M. Savéant, *J. Am. Chem. Soc*., *119*, **1997**, 7526.

[61] R. M. Kellett, T. G. Spiro, *Inorg. Chem*., *24*, **1985**, 2373.

[62] R. M. Kellett, T. G. Spiro, *Inorg. Chem.*, *24*, **1985**, 2378.

[63] F. Taguchi, T. Abe, M. Kaneko, *J. Mol. Catal. A: Chem*., *140*, **1999**, 41.

[64] T. Abe, F. Taguchi, H. Imaya, F. Zhao, J. Zhang, M. Kaneko, *Polym. Adv. Technol., 9*, **1998**, 559.

[65] (a) T. Abe, H. Imaya, S. Tokita, D. Wöhrle, M. Kaneko, *J. Porphyr. Phthalocya*., *1*, **1997**, 215.
(b) T. Abe, H. Imaya, M. Endo, M. Kaneko, *Polym. Adv. Technol*., *11*, **2000**, 167.

[66] M. Yagi, K. Kinoshita, M. Kaneko, *J. Phys. Chem. B, 101*, **1997**, 3957-3960.

[67] D. A. Buttry, F.C. Anson, *J. Am. Chem. Soc.*, *106*, **1984**, 59.

[68] I.K. Choi, Y. Liu, Z. Wei, M. D. Ryan, *Inorg. Chem., 36*, **1997**, 3113-3118.

[69] K. Kalyanasundaram, N. Vlachopoulos, V. Krishnan, A. Monnier, M. Grätzel, *J. Phys. Chem*., *91*, **1987**, 2342

[70] E. Tsuchida, M. Kaneko, H. Nishide, M. Hoshino, *J. Phys. Chem., 90*, **1986**, 2283.

[71] M. Kaneko, E. Tsuchida, Y. Imai, *J. Chem. Soc. Faraday Trans. 87*, **1991**, 1 83.

[72] M. Kaneko, I. Okura Ed. *Photocatalysis- Science and Technology*, Kodansha-Springer, **2002**, Japan.

[73] R. Baker, D. P. Wilkinson, J. Zhang, *Electrochim. Acta, 53*, **2008**, 6906.

[74] L. Mao, K. Arihara, T. Sotomura, T. Ohsaka, *Electrochim. Acta, 49,* **2004**, 2515.

[75] C. Song, L. Zhang, J. Zhang, D. P. Wilkinson, *Fuel Cells, 1*, **2007**, 9.

[76] J. Ouyang, K. Shigehara, A. Yamada, F. C. Anson, *J. Electroanal. Chem., 297*, **1991**, 2, 489.

[77] C. Song, L. Zhang, J. Zhang, *J. Electroanal. Chem., 587*, **2006**, 293.

[78] J. Germain, J. M. Frechet, F. Svec, *Polymeric Materials: Science & Engineering*, *97,* **2007**, 272.

[79] (a) B. Assfour, S. Leoni, G. Seifert, I.A. Baburin, *Adv. Mat., 23*, **2011**, 1237. (b) J. M. Blackman, J. W. Patrick, A. Arenillas, W. Shi, C. E. Snape, *Carbon*, *44*, **2006**, 8, 1376. (c) M. Hirscher, M. Becher, M. Haluska, A. Quintel, V. Skakalova, Y. M. Choi, *J. Alloys Comp., 330*, **2002,** 654. (d) A. Züttel, P. Sudan, P. Mauron, T. Kiyobayashi, C. Emmenegger, L. Schlapbach, *Int. J. Hydrogen Ener., 27, 2,* **2002,** 203. (e) M. Volpe, F. Cleri. *Surf. Sci., 544,* **2003,** 24.

Chapter Two

Experimental Procedures and an Introduction to Techniques

This chapter discusses the theory and background of electrochemistry. This includes a discussion of the factors affecting the reactions at the electrode/solution interface. The thermodynamic and kinetic parameters which influence the rate of reaction are discussed. An introduction into the importance of modified electrodes and the different parameters which affect the rate of electrolysis are presented.

The electrochemical techniques used throughout the thesis, cyclic voltammetry and bulk electrolysis with coulometry are discussed.

This chapter also presents an introduction to the analytical instrumentation employed for the detection of a gas product, hydrogen, including the calculations used for the determination of product formed and the efficiency of the electrocatalytic systems.

2.1 Electrochemistry

2.1.1 Introduction

Electrochemistry is the science of electron transfer across an electrode-solution interface. The origin of electrochemistry began over 200 years ago when Volta invented the Voltaic Pile and Nicholson and Carlisle discovered electrolysis.[1] It was these findings which lead to a scientific revolution at the beginning of the 19th century. A new science was born. Michael Faraday established quantitative electrochemistry, with the publication of Faraday's two laws, relating the extent of an electrochemical reaction to the charge passed at the electrode. Advances in methods and technology have made electrochemistry an increasingly popular technique for qualitative and quantitative analysis of a chemical reaction.

2.1.2 Faradaic Processes

An electrochemical reaction involves the application of a potential to an electrode in order to remove or supply an electron(s) to some electroactive species in solution, represented as O and R in Equation 2.1 below.

$$O + ne^- \leftrightarrow R \qquad \textbf{Equation 2.1}$$

where O and R denote the oxidised and reduced forms, respectively, of a redox couple. When a species becomes oxidised/reduced, a Faradaic current (i_F) is produced. This current arises from the movement of the electrons from/to the electrode to effect a change in the oxidation state of the electroactive species at the electrode/solution interface. A Faradaic current is one which obeys Faraday's law which states that the quantity of a chemical species produced or consumed by electrolysis is proportional to the amount of charge passed across the electrode/solution interface (the passage of 96,485 C causes a 1 mole equivalent of a 1-electron reaction).[2] Faradaic processes will occur at potentials where they are thermodynamically and kinetically feasible and the resulting current due to these processes provides a measure of the rate of the reaction. Non-Faradaic processes can also occur. These processes are commonly due to adsorption of ions on the electrode surface in response to an applied potential, resulting in the formation of an electrical double layer at the interface (discussed below) and the current produced (i_C, the charging current) is thus not a result of electron transfer

across the interface. Although such processes are not generally of interest, experimental conditions may cause i_C to become large relative to i_F and make data interpretation difficult. Conditions which minimise i_C (high electrolyte concentrations, slower scan rates, or perhaps microelectrodes) may need to be considered.

2.1.3 Electrical double layer

As mentioned above, non-Faradaic processes can occur as a result of the re-organisation of charge at the electrode/solution interface. When the potential of an electrode is moved from the equilibrium potential, charge will generated at the surface. This charge can create strong interactions between the electrode and ions and molecules in the solution adjacent to the electrode, resulting in the formation of the double layer. Species close to the electrode and species in the bulk solution behave differently due to the effect of the electric field which exists at the electrode surface. The species in the bulk solution are said to experience an isotropic environment (due to the absence of an electric field) while species at the electrode/solution interface are influenced by an anisotropic electric field. Thus as the distance from the electrode interface increases, the influence of the electric field on the species in solution decreases.[3]

The first model to be presented by Helmholtz in 1879 proposed that the interactions between the ions in solution and electrode surface were electrostatic interactions. It was suggested that a charge density was held on the electrode, arising from an excess or deficiency of electrons at the electrode surface and this charge at the electrode could be balanced by redistributing ions close to the electrode. However Helmholtz's proposed structure of the double layer did not consider additional factors, such as diffusion of such charges due to thermal agitation (into the bulk solution) and interactions between solvent dipoles and the electrode.[4]

The next model to address these factors was by Gouy and Chapman in the early 1900's, which proposed that the solution side of the electrode/solution interface possesses a diffuse layer of charges, with the greatest concentration of charge closest to the electrode. Like the Helmholtz model described above, this model was not realistic. Stern suggested a model in 1924 which combined both the

Helmholtz and Gouy-Chapman models. The Stern model takes into consideration that ions have defined radii and when in solution, become solvated.[5] The distance of these ions to the electrode surface thus will always be greater than zero. In 1947 Grahame suggested a model for the double layer, very similar to that of the Stern model described above. The difference between this model and the former is the existence of specific adsorption of ions which lose the solvation shell upon approaching closer to the electrode surface as shown in Figure 2.1.[6] These ions can bind strongly to the metal electrode surface and are thus said to exist in the IHP (inner Helmholtz plane), Figure 2.1 (a).

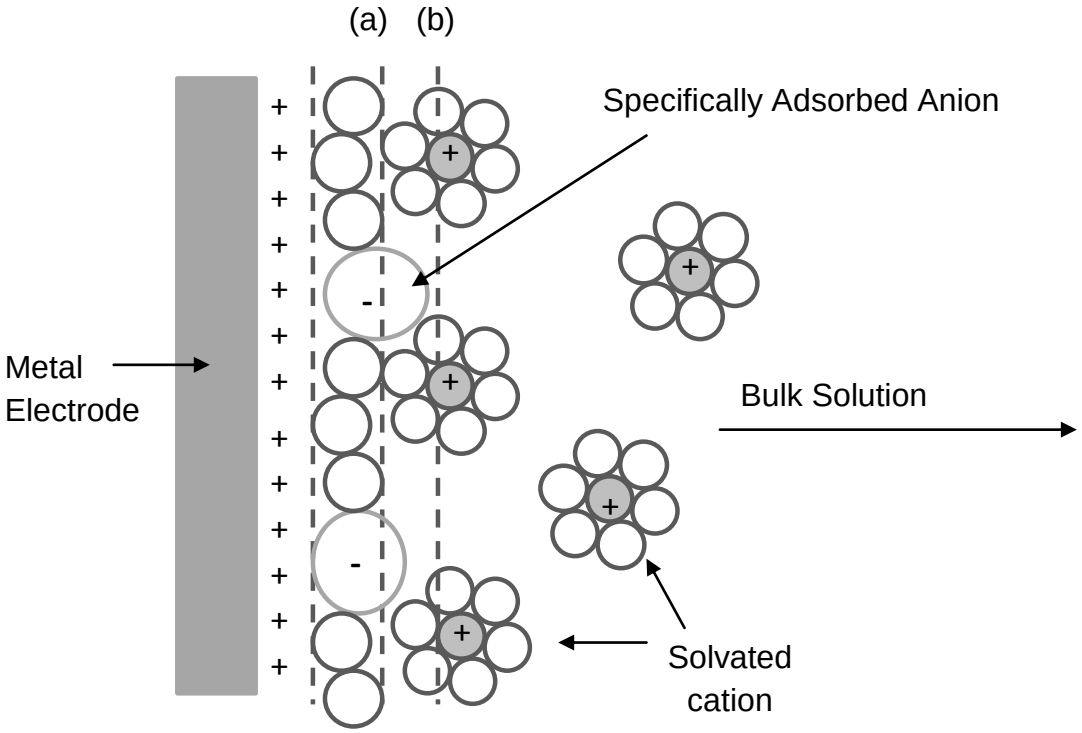

Figure 2.1: *Model of a double layer as proposed by Stern and Grahame, where (a) and (b) indicate the inner and outer Helmholtz planes respectively. Adapted from references 4, 5 and 6.*

Two regions exist in this model adjacent to the electrode interface, the first (closest to the electrode) is the inner Helmholtz plane (IHP) while the second region is known as the outer Helmholtz plane (OHP), labelled (a) and (b) in the diagram. The IHP contains specifically adsorbed ions and solvent molecules. The OHP extends from the inner layer out to the bulk solution. This outer diffuse layer

is comprised of solvated ions and other adsorbed species. A region of no net charge can exist, termed a potential of zero charge (PZC). This exists when there is no specific adsorption; hence the net charge is zero. The number of cations is equal to that of the anions.[7]

2.1.4 Nernst behaviour and Interfacial Reactions

Electrode reactions can be described by the Nernst equation which relates the electrode potential and the concentration of the electroactive species at the interfacial region.[3]

$$E = E^{\circ\prime} + 2.303\frac{RT}{nF}\log\frac{[O]}{[R]} \qquad \textbf{Equation 2.2}$$

Where E° is the standard potential for the redox reaction, R is the gas constant, T is the temperature, n is the number of electrons transferred and F is Faraday's constant. The reaction at the electrode/solution interface can involve a series of steps. Factors which may affect the rate of the electrode reaction include, mass transport (movement of reactants to and products from the electrode surface), chemical processes (e.g. accompanying chemical reactions), surface processes (e.g. adsorption/desorption) which precede or follow electron transfer. Where a reaction is controlled by the rate at which the electroactive species reaches the electrode surface, the current produced is described as mass transport limited. A simplified model shown in Figure 2.2 represents the electrochemical reaction of a redox species at the electrode/solution interface.

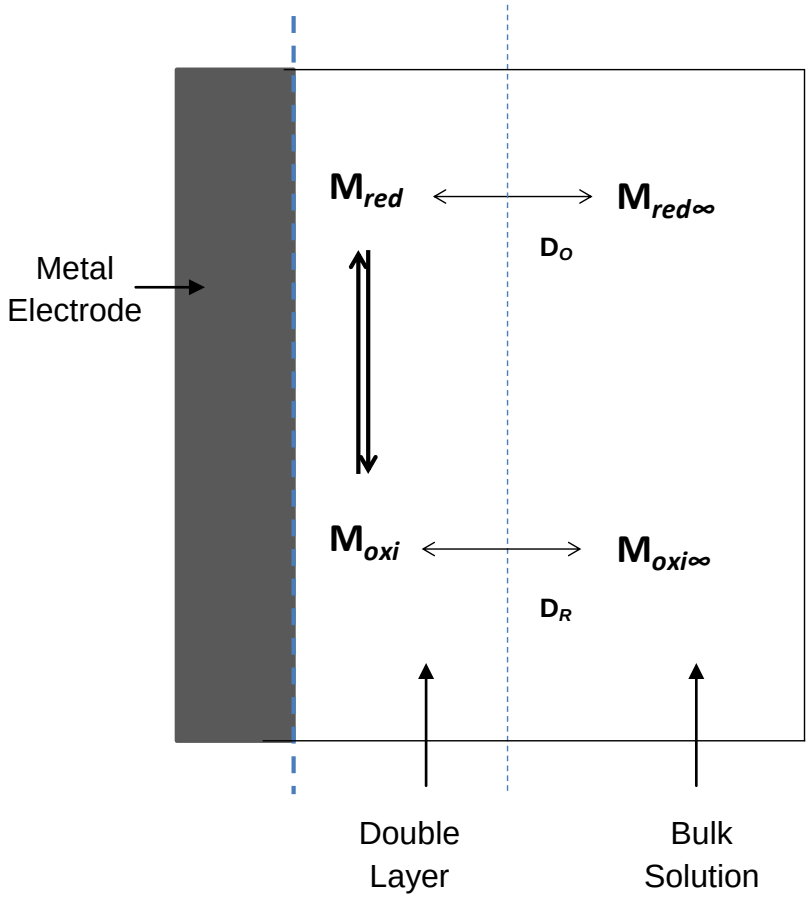

Figure 2.2: *Illustration of electron transfer at the electrode/solution interface. D_O and D_R represent the diffusion coefficients for the mass transport of electroactive species (oxidised and reduced) in and out of the bulk solution from/to the double layer. Adapted from reference 6.*

2.1.5 Mass Transport

There are 3 modes of mass transport; diffusion, convection and migration. The first type diffusion concerns mass transport driven by a concentration gradient, such that diffusion of the species occurs from regions of high concentration to lower concentrations. Transport of species to the electrode by convection occurs by physical movement such as stirring. The third mode of mass transport is the migration of charged particles through an electric field. Typically, migration effects are minimised by the use of an electrolyte (salt) and because mass transport in regions very close to the electrode surface occurs through a compact layer adjacent to the electrode (2.1.5.1), convection here is assumed to be zero.[8]

2.1.5.1 Diffusion

Diffusion is the movement of species in a solution under the influence of a concentration gradient. The rate of diffusion can be quantified by use of Fick's 1st law of diffusion, Equation 2.3, where the rate of diffusion (flux) is proportional to the slope of the concentration gradient.[3]

$$j = -D\frac{\partial C(x,t)}{\partial x} \qquad \textbf{Equation 2.3}$$

where D is the diffusion coefficient, $\frac{\partial C(x,t)}{\partial x}$ is the concentration gradient and *j* is the flux. The flux is the number of moles passing through a unit area per unit time, (moles·cm^{-2}·s^{-1}) and is also given by Equation 2.4 where the flux of species to the electrode surface is directly proportional to the current produced.

$$j = -\frac{i}{nFA} \qquad \textbf{Equation 2.4}$$

Where i is the current (A), n is the number of electrons transferred in the reaction, F is Faraday's constant (C/mol e$^-$) and A is the area of the electrode (cm^2). These two equations can be combined to yield an expression for the current response due to the flux.

$$i = \text{nFAD}\frac{\partial C(x,t)}{\partial x} \qquad \textbf{Equation 2.5}$$

Therefore the current is first order with respect to the concentration gradient of the electroactive species. The mathematical expressions given above indicate that the diffusional flux is time dependent, which is taken into account by Fick's second law, Equation 2.6 illustrating the rate of change of the concentration between two planes *x* and (*x*+d*x*) which are parallel.

$$\frac{\partial C(x,t)}{\partial t} = D\frac{\partial^2 C(x,t)}{\partial x^2} \qquad \textbf{Equation 2.6}$$

This law is only valid for conditions where the diffusional planes are parallel to one another and the direction of diffusion is perpendicular to the planes, shown in Figure 2.3. These conditions described above are valid for linear diffusion.[3,4]

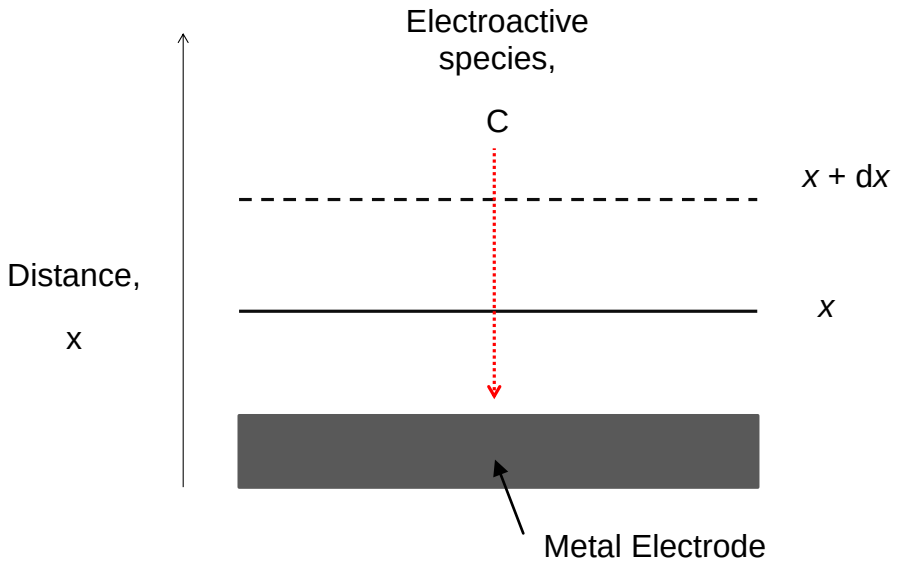

Figure 2.3: *Illustration to represent the direction of flux and diffusion planes which are at 90° indicative of linear diffusion at a planar electrode. Adapted from reference 5.*

As discussed above the diffusional flux is time dependent, thus a concentration-time profile can be generated for a potential step experiment where a potential is chosen for which reactant O is completely reduced to product R. Upon application of this potential, the surface concentration of O falls to zero and a concentration gradient is immediately created adjacent to the electrode surface. This region is known as the diffusion layer where the thickness, δ is time dependent (becoming thicker with time).

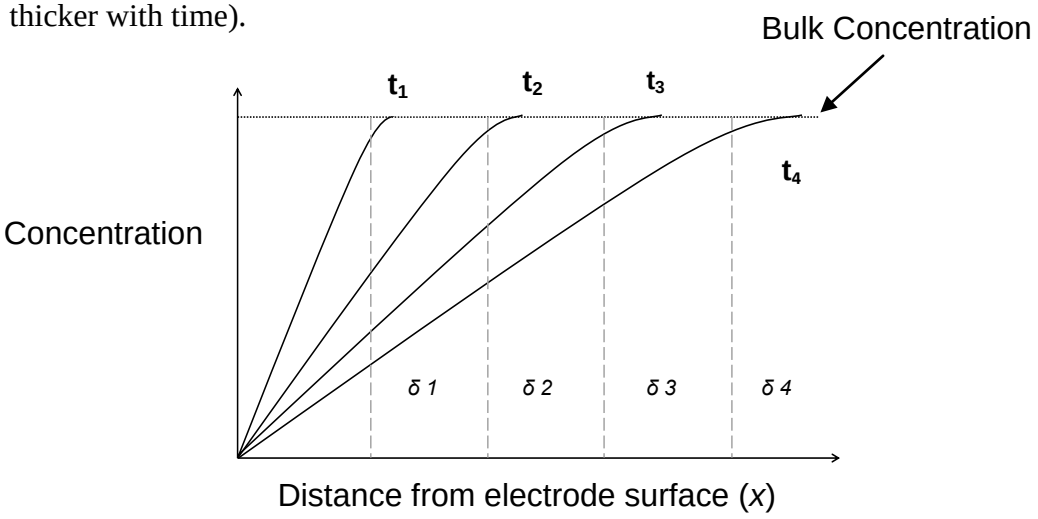

Figure 2.4: *The growth of the diffusion layer thickness (δ) with increasing distance from the electrode surface as a function of time. T_x indicates the period of time after electrolysis. Adapted from reference 3.*

A new mathematical expression is shown in Equation 2.8 which considers the concentration gradient at the surface and the current response due to the diffusional flux (Equation 2.6). The validity of this equation assumes a set of boundary conditions and are described as the following equations:

$$C_{O(x,0)} = C_O^* \qquad \textbf{Equation 2.7a}$$

Initial condition: the concentration of the electroactive species C_o at the electrode/solution interface at time zero (i.e. prior to an electrolysis reaction) is the same concentration of that in the bulk solution $C^*_{o.}$

$$C_{O(0,t)} = 0 \qquad \textbf{Equation 2.7b}$$

The concentration of species at the electrode/solution interface is zero when the experiment begins (time t) as the species is converted to either its oxidised or reduced species (depending on the direction of the reaction).

$$\lim_{x\to\infty} C_{o(x,t)} = C_O^* \qquad \textbf{Equation 2.7c}$$

while the concentration of the electroactive species at some distance beyond the diffusion layer from the electrode remains C^*_o at time t (semi-infinite condition)

This equation is known as the Cottrell equation, where the current (for semi infinite linear diffusion) decreases proportionally to the square root of time.

$$i = \frac{nFAC_O D^{1/2}}{\pi^{1/2} t^{1/2}} \qquad \textbf{Equation 2.8}$$

For this equation, n is the number of electrons, F is Faraday's constant, A is the electrode area (cm^2), C_O is the concentration of the electroactive species in the bulk solution ($mol \cdot cm^{-3}$), D is the diffusion coefficient ($cm^2 \cdot s^{-1}$) and t is the time (s). The application of this equation relies on the semi infinite linear diffusion being the controlling condition for mass transport.[4,20]

2.1.6 Electron transfer

Reactions for which the current is controlled by the rate at which electrons are transferred at the interface occur when the mass transport is sufficiently fast compared to electron transfer. Heterogeneous electron transfer involves the

transfer of electrons across an interface, in these studies, across an electrode/solution (or electrode-coating) interface. For both of these cases, transfer of electrons from the electrode to a catalyst occurs, and this catalyst may be present in solution form or fixed at the electrode surface in the form of a film/coating.

A metal electrode consists of closely packed atoms which overlap and so continuum of electron energy levels exists where the available electrons fill the states according to the Aufbau principle.[5] The Fermi level is an energy level of which the highest energy electrons are located. Upon the application of a voltage, the Fermi level can be moved to higher or lower energy. Depending on the position of the Fermi level, it may be thermodynamically feasible for electron transfer to occur; that is for the oxidation or reduction of a species in solution to take place. If the potential is increased to more negative potentials then the Fermi level will rise to a higher energy level while the energy will decrease when the voltage is made more positive. The processes of reduction and of oxidation are shown in Figure 2.5 where (a) depicts the addition of an electron to the LUMO level of species *A* while (b) illustrates the removal of an electron from the HOMO level of species *A*.[9]

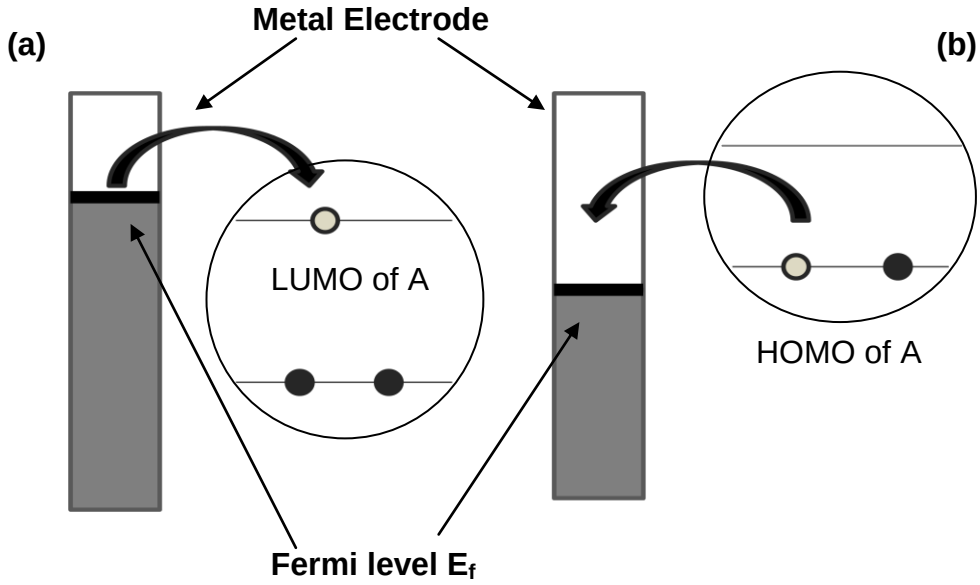

Figure 2.5: *Electron transfer process between a metal electrode and species A in solution. (a) represents reduction of the species A, while (b) demonstrates the oxidation of A. Adapted from reference 5 and 9.*

When the highest energy electrons on the electrode are above the LUMO of A, A will be reduced by the electrode, ($A + e^- \rightarrow A^-$). When the highest energy electrons of the electrode are below the HOMO of A, A will be oxidized, ($A – e^- \rightarrow A^+$).[10] The factors which govern the rate of electron transfer for the oxidation and reduction processes are discussed here. For a one electron reaction, a heterogeneous rate constant k is used to quantify the rate of the forward and reverse reaction.[3]

$$O + ne^- \underset{k_r}{\overset{k_f}{\leftrightarrow}} R \qquad \textbf{Equation 2.9}$$

$$V_x = k_x C_{y(0,t)} \qquad \textbf{Equation 2.10}$$

where V_x is the rate of the reaction ($mol \cdot cm^{-2} \cdot s^{-1}$); where x = f is the forward direction and x = r in the reverse direction, k_x is the heterogeneous rate constant ($cm^2 \cdot s^{-1}$) and C_y is the concentration of species y at the electrode surface after time t. For the forward reaction ($O + ne^- \rightarrow R$), y = O; and reverse reaction, ($R \rightarrow O + ne^-$) y = R.

As the current is a measure of the rate of a redox reaction, then the rate V_x (of the forward and backward reactions) is first order with respect to C_y thus V_x is proportional to the predicted current produced i_x, Equation 2.11.

$$i_x = nFAV_x \qquad \textbf{Equation 2.11}$$

where i_x is the current (where x = f is the forward direction and x = r in the reverse direction) V_x is the rate (where y = f for the forward reaction and y = r for the reverse reaction) and n, F, A are as described in 2.1.5.1. The overall current can be calculated by combining both reactions, to obtain Equation 2.12.

$$i = i_f - i_b = nFA\left[(V_f - V_r)\right] \qquad \textbf{Equation 2.12}$$

As electron transfer reactions behave in a similar manner to chemical processes, the transition state model (thermodynamics) can be employed, shown (Figure 2.6) to establish the parameters affecting electron transfer. This model represents a reaction in which the reactant *O* must overcome an energy barrier, the summit (transition state) $G^‡$ in order to produce products *R*.

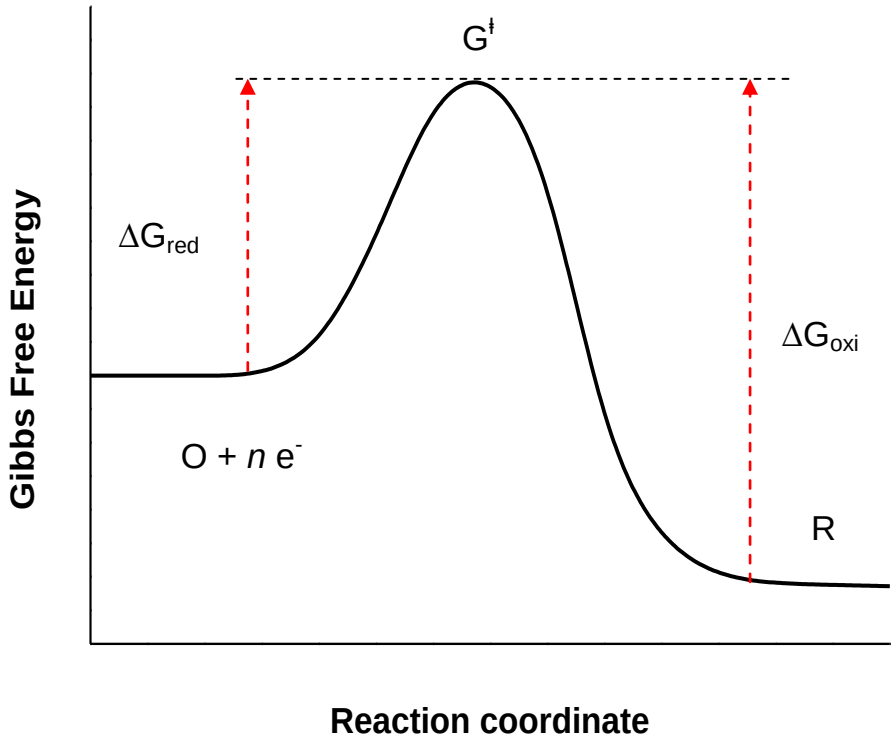

Figure 2.6: *Free energy ΔG plot for the one electron reduction of O to R at a fixed potential. Adapted from reference 5.*

The free energy ΔG_x for the electrode reactions can be calculated using Equations 2.13 and 2.14 for the oxidation and reduction reactions respectively.

$$\Delta G_{red} = G^{\ddagger} - G^{o} \qquad \textbf{Equation 2.13}$$

$$\Delta G_{oxi} = G^{\ddagger} - G^{R} \qquad \textbf{Equation 2.14}$$

Where ΔG_{red} and ΔG_{oxi} represent the activation free energy for the product of the forward (reduction) and back (oxidation) reactions respectively, $G^{\ddagger}$ is the transition state (energy barrier) and G^{O} and G^{R} are the energies associated with the reactants of each the reactions. This free energy model predicts the corresponding rate of an electrode transfer process k_x (where $_x$ can represent oxidation or reduction), Equation 2.15.

$$k_x = A\, e^{\frac{-\Delta G_x^{\ddagger}}{RT}} \qquad \textbf{Equation 2.15}$$

Where A is the frequency factor, ΔG_x is the free energy of activation, (*x* is oxidation/reduction), R is the ideal gas constant and T is absolute temperature. (ΔG_x is also referred to as E_A, the activation energy barrier which is used in the Arrhenius equation.) The influence of applied potential on the heterogeneous rate constants can be understood by examining the thermodynamics of the process. Using the transition state model, it demonstrates how the rate constants are dependent upon applied potential.[5,6] Figure 2.7 illustrates how the free energy plots change as a function of applied potential. Similar to Figure 2.6 at a single potential, this shows the dependence of the reactant on voltage as the potential is now changed to a value beyond the equilibrium potential (*Eq*). The free energy associated with product remains fixed, independent of applied potential.

Figure 2.7 illustrates how the free energy plots change as a function of applied potential (transition state model). Similar to Figure 2.6, at a single potential, this shows the dependence of the reactant on voltage as the potential is now changed to a value beyond the equilibrium potential (E_{eq}). The free energy associated with product remains fixed, independent of applied potential.

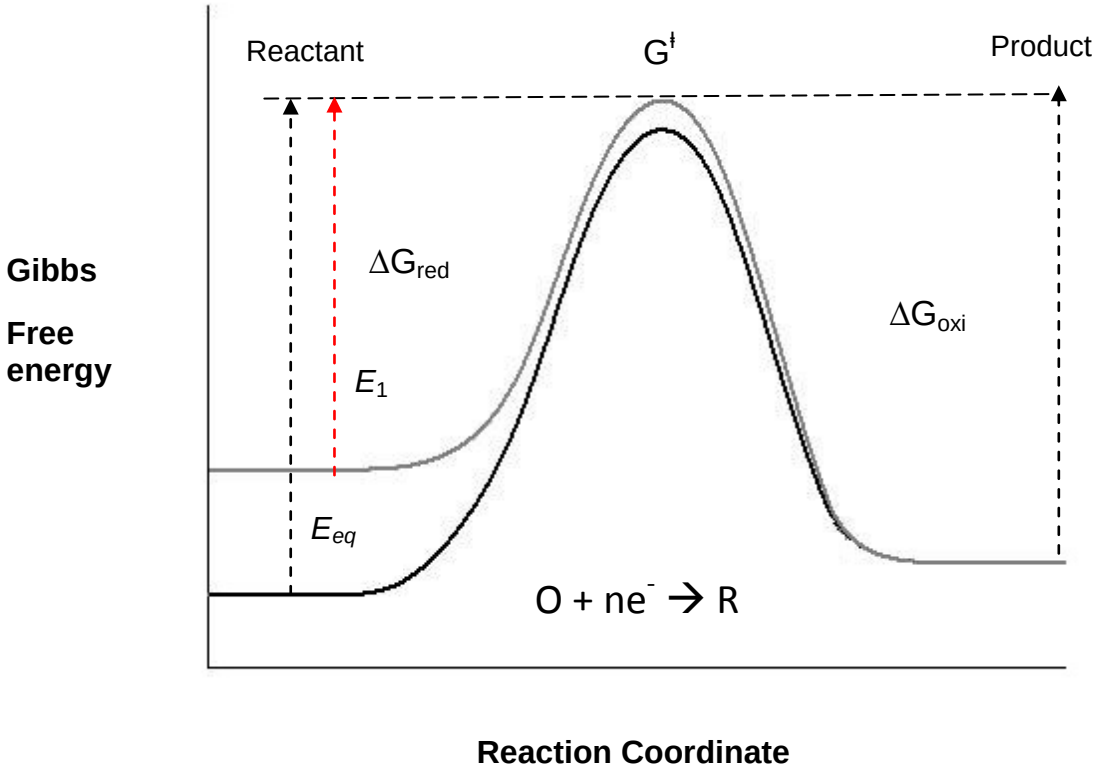

Figure 2.7: *Free energy ΔG profiles at varying potentials E_{eq} and E_1.*

As the potential is changed from the initial equilibrium potential E_{eq} to a final potential E_1, it is evident that the activation energy is shifted with varying potential, hence the reaction of O to R becomes more thermodynamically favoured. The free energy terms for the oxidation/reduction can be expressed in terms of the heterogeneous rate constants k_{oxi} and k_{red} in Equations 2.16 and 2.17 respectively. The expressions below indicate that the rate constants for the electron transfer steps are proportional to the exponential of the applied potential, thus the rate of an electrode reaction can be altered by changing the potential of the working electrode.[11]

$$k_{oxi=}A\ e\left(\frac{\Delta G_{red}}{RT}\right)e\left(\frac{(1-\alpha)FE}{RT}\right) \qquad \textbf{Equation 2.16}$$

$$k_{red=}A\ e\left(\frac{\Delta G_{oxi}}{RT}\right)e\left(\frac{-\alpha FE}{RT}\right) \qquad \textbf{Equation 2.17}$$

where E is the applied potential and α is the symmetry factor (which affects the shape of the free energy potential plots).

2.1.7 Modified electrode surfaces

The structure of the electrode/solution interface is of great importance for an electrode reaction, as discussed. The application of a thin layer of material onto an electrode surface can provide a greater control of the electrode's properties, including its ability to transfer electrons to some species of interest. The development of modified electrodes for the current work was done in order to facilitate this sort of process and enhance catalytic reactions. The reactivity of the modified surface electrode is determined by the electrode potential (which is controlled by a potentiostat) and by the nature and structure of the electrode surface (in particular, the modifying layer).[12,13]

Although the modifying layer prevents direct contact between the underlying electrode surface and the solution, it must allow for transfer of electrons between the electrode and the species in solution undergoing oxidation/reduction. As electron transfer occurs between the Fermi level of the electrode and HOMO/LUMO of electroactive species in a solution (in the work of Chapter 3),

electron transfer is mediated by redox groups present in the layer. These redox groups are specifically chosen to mediate charge transfer i.e. participate in an electrochemical reaction, whether it be to catalyse or block a reaction.[12] A model for mediated electron transfer is shown in Figure 2.8

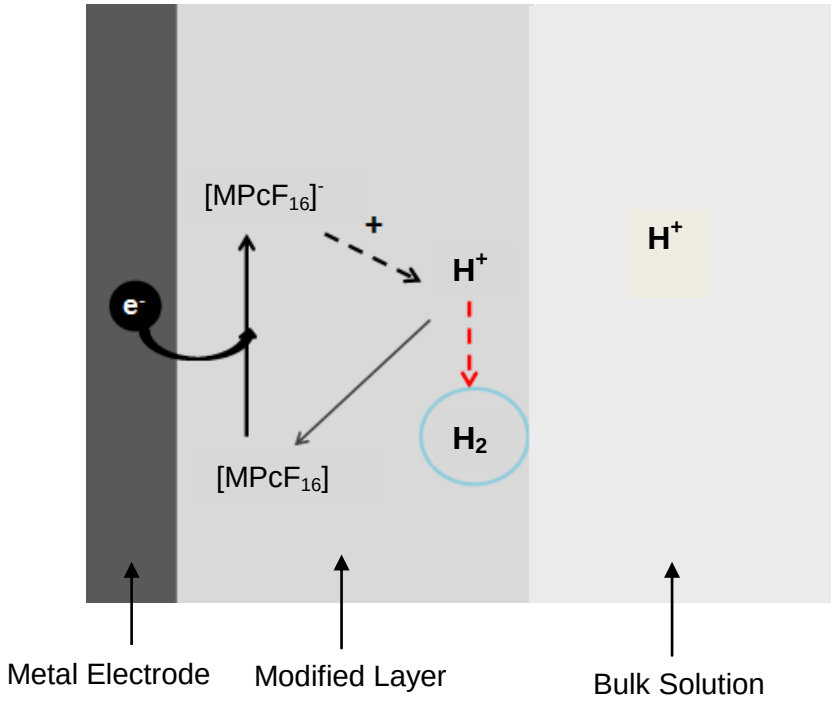

Figure 2.8: *Electron transfer model of a modified electrode surface consisting of $MPcF_{16}$ as an example. Adapted from references 12 and 13.*

This scheme is similar to the model shown in Figure 2.2; however, electron transfer occurs between the electrode and the mediator *M* and not directly with the substrate H^+. Equations 2.18 and 2.19 demonstrate the mediated reaction sequence. The original active form of the mediator is electrochemically regenerated and reduced substrate can diffuse away into the bulk solution. For the hydrogen evolution reaction occurring in work presented in this thesis, the mediator M_{ox} is [$MPcF_{16}$], the substrate *A* is H^+ in the electrolyte which are electrocatalytically reduced to H_2. As the reduced substrate is a gas, it diffuses away from the electrode surface to fill the headspace volume at the top of the electrochemical cell.[3]

$$M_{ox} + ne^- \rightarrow M_{red} + A_{ox} \rightarrow M_{ox} + A_{red} \qquad \textbf{Equation 2.18}$$

$$[MPcF_{16}] + e^- \rightarrow [MPcF_{16}]^- + 2H^+ \rightarrow [MPcF_{16}] + H_2 \qquad \textbf{Equation 2.19}$$

Thus the catalytic reaction in the simplistic form is given in Equation 2.19, where the catalyst is regenerated with the evolution of hydrogen.

2.1.7.1 Construction of modified electrodes

Polymers which are capable of moving charge (electrons/ions) between the electrode surface and the catalyst are an important feature of the work reported in this thesis, as the reduction of the catalyst requires both electrons and counterion movement within the modifying layer. Production of these layers can be achieved in various ways, such as direct electropolymerisation, dip coating of the electrode into a solution of the mediator/polymer, electrostatic binding of a mediator directly via drop-casting from a solution, or incorporating the mediator in a polymer matrix.[3,4,12,13]

In this last technique, the polymeric material and the mediator, an electrocatalyst in this case, are dissolved in a volatile solution. A known volume (μL) of the mediator/polymer solution is transferred to the electrode surface. The solvent can be removed in a number of ways, including air drying, *in vacuo* drying, and evaporation in a solvent-saturated chamber followed by air curing. Vos *et al*. report the importance of the rate of solvent removal, where slow removal is the optimum method for the production of organised films.[13] Exposure of a large surface area is important as it allows for greater contact with the substrate in the electrolyte solution, leading to large and rapid responses. If the catalyst within whole layer is electroactive (rather than just a thin layer at the polymer/solution or electrode/polymer interface) then a thick, 3-D film structure should lead to enhanced product yields.

2.1.7.2 Stability

An important factor for such thin modifying films is the stability of the coating. Employing modified electrodes in a variety of pH environments (acidic, neutral and basic solutions) may affect the long-term response (stability) of the coating. Another important factor to consider is the stability associated with the mediator and the ability of the redox centre to be repeatedly cycled through reduction/oxidation steps. Repeated movement of the charge-compensating

counterions in and out of the film can lead to breaks in the film. This can hinder the mechanical stability of the film after repeated redox cycling.[13]

2.1.7.3 Characterisation

The nature of the modified layer can be determined using cyclic voltammetry. This technique allows for important parameters to be obtained, such as redox potential and stability. Using slow scan rates, the area under the cyclic voltammogram can provide a measure of the amount of electroactive mediator species which is present on the electrode surface.

The appearance of a cyclic voltammogram for a redox species in a very thin modifying layer is different to that of a redox couple in solution phase that follows Nernst behaviour.

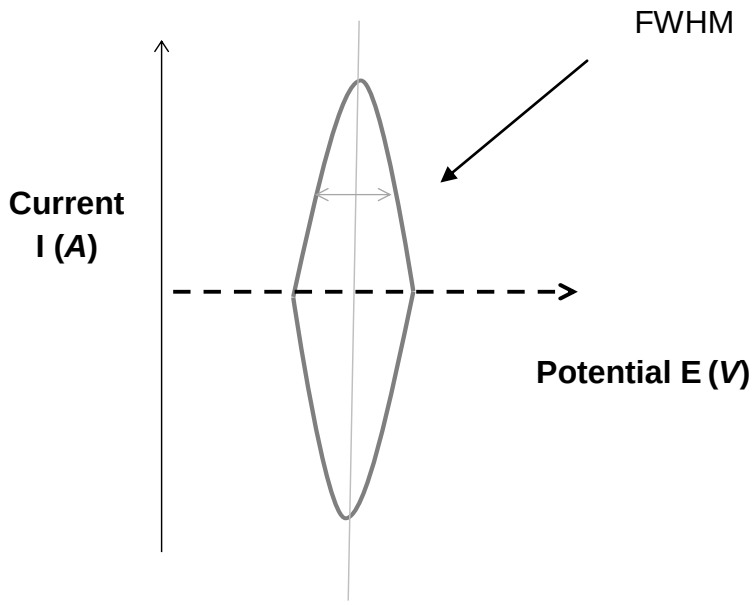

Figure 2.9: *Cyclic voltammetry of an ideal reversible redox species in a modified layer. FWHM ($\Delta E_{p½}$) is the full width a half maximum for the redox species. Adapted from reference 4.*

The anodic wave of a reversible surface confined redox couple is generally the mirror image of its corresponding cathodic wave. Considering that the redox species within the modified layer is not present in the bulk solution then electron transfer will not be limited by mass transport to the electrode. Thus, for an ideal Nernstian reaction where $E_{pa} = E_{pc}$, the full width at half height (FWHM or $E_{p,½}$) of either the cathodic or anodic wave is given by the following expression,[4]

$$E_{p,1/2} = 3.53\frac{RT}{nF} = \frac{90.6}{n}\ mV\ (25°C) \qquad \textbf{Equation 2.20}$$

Monitoring the peak current and position as a function of time allows for the stability of the coating to be studied. For surface-confined redox species, the current is directly proportional to the scan rate (Equation 2.21) whereas the current produced by the reversible oxidation/reduction of a redox couple which is freely diffusing in solution is proportional to the square root of the scan rate (Equation 2.22). Thus investigating the sweep rate dependence of the modified layer can provide information about the charge transfer process within the modifying layer.[12]

$$i_p \propto \nu \qquad \textbf{Equation 2.21}$$

$$i_p \propto \sqrt{\nu} \qquad \textbf{Equation 2.22}$$

As stated above, the amount of the electroactive species in the modified layer can be calculated from the area under the redox wave, allowing for the number of moles of electroactive species to be determined. Assuming that the Faradaic response is due to the redox species in the modified layer and not from the bulk solution (which is electrolyte only, therefore the concentration of redox species in solution is zero), then the surface coverage, in terms of molecules can also be calculated for the film by Equation 2.23.

$$\Gamma = \frac{Q}{nFA} \qquad \textbf{Equation 2.23}$$

Where Γ is the surface coverage (mol cm^{-2}), Q is Faradaic charge (C), n is the number of electrons transferred, F is the Faraday constant (C/mol e) and A is the area of the electrode surface (cm^2).[4]

This can be further extended to determine the area occupied by a molecule A_{molec} ($Å^2$) using Equation 2.24.[14]

$$A_{molec} = \frac{10^{16}}{N_A\Gamma} \qquad \textbf{Equation 2.24}$$

where N_A is Avogadro's number. The surface coverage term can be used in combination with Equation 2.20 to give an expression which relates surface

coverage, peak current and the potential scan rate (ν, $V \cdot s^{-1}$) for a reversible surface controlled process by Equation 2.25 where n_M is the number of electrons transferred.[3,4,15]

$$i_p = \frac{n_M^2}{4} \frac{F^2}{RT} A\nu\Gamma_M \qquad \textbf{Equation 2.25}$$

The surface coverage term is important as it allows for an understanding of the behaviour of the redox species within the modified layer. By comparing the experimental surface coverage values Γ_{exp} with theoretical surface coverage values Γ_{theo}, a description of the film in terms of flat monolayers of redox species can be determined.[15,16]

2.2 Electrochemical Materials

2.2.1 Electrochemical Cell

The experimental work in Chapters 3 to 6 presented in this thesis employed the use of a three electrode cell set up in order to perform the necessary electrochemical techniques, such as cyclic voltammetry, differential pulse voltammetry and bulk electrolysis. The three electrodes used consist of a working electrode, a reference electrode and a counter electrode which are housed in a V-shaped glass cell as shown in Figure 2.10.

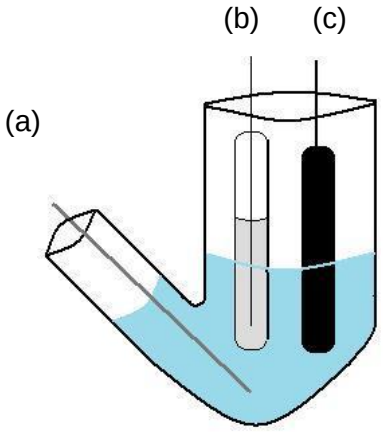

Figure 2.10: *Diagram of a basic 3 electrode electrochemical set up, consisting of (a) counter electrode, (b) reference electrode and (c) working electrode.*

The working electrode is the surface at which the electrochemical reaction of interest occurs while the counter electrode provides the surface for which the accompanying electron-transfer reaction occurs during the overall redox reaction. Current is measured between the working electrode and the counter electrode. The reference electrode is an electrode which has a defined electrochemical potential that is stable upon the passage of a small current (non-polarisable electrode). The applied potential (working electrode) is measured between the working electrode and reference electrode. When setting up the three-electrode cell, it is important to place the working and reference electrodes close to each other to minimise the solution resistance. From Ohm's Law, it can be seen that resistance is a function of potential and current; $iR = E$. Thus, the working electrode potential which is reported includes Ohmic potential drop, where $E_{real} = E_{applied} + iR$.[4] It is important to note that there will always be a residual resistance, which will remain uncompensated and thus is termed R_u. This uncompensated resistance R_u can be calculated using Equation 2.26 when planar working electrodes are employed. As this electrode surface is uniform, this means the current density is also uniform and not shielded from the adjacent reference electrode.

$$R_u = \frac{x}{\kappa A} \qquad \textbf{Equation 2.26}$$

In this equation, x denotes the distance between the working and reference electrodes, κ is the conductivity of the solution and A is the area of the working electrode.[4] Another means of reducing the resistance of the solution is the use of an electrolyte of high ionic strength, i.e. 1 M concentration. The high ionic strength of an electrolyte allows for a high conductivity therefore reducing the resistance of the solution.

2.2.2 Electrodes

2.2.2.1 Working Electrode

Glassy carbon (GCE) working electrodes were employed for the electrocatalytic studies; however, Chapter 6 discusses these studies whilst using a carbon monolith as an electrode material. GCEs possess the advantages of low cost, little pretreatment and a large overpotential for the evolution of H_2, compared to Pt surfaces.[17]

2.2.2.2 Counter Electrode

The counter electrode, also known as the auxiliary electrode, provides a route for the 'other' half reaction to occur. Most counter electrodes possess a high surface area. Metal wires are commonly used as they are excellent conductors. Similar to using Pt as working electrodes, it is often a good choice for use as a counter electrode as it is chemically inert.[17]

2.2.2.3 Reference electrodes

A reference electrode is one whose chemical composition is known and fixed. Its potential should be stable with respect to time. The primary reference electrode used is the standard hydrogen electrode, SHE (also known as the normal hydrogen electrode NHE). It is composed of platinised platinum which is immersed in an acidic medium in which H_2 gas is bubbled through.[4,17]

$$2H^+ + 2e^- \rightarrow H_2 \qquad \textbf{Equation 2.27}$$

For use as a reference electrode, the potential of the SHE is defined as 0 V, where a = 1 (unit activity) for both H_2 and H^+, and are maintained at unity during operation. This electrode is not practical for everyday use in the sense that it requires a constant stream of H_2 gas bubbled through the acidic solution. Nonetheless, potentials are often quoted *vs*. SHE. It is far more common to see the use of an Ag/AgCl or SCE reference electrode during routine electrochemical studies involving aqueous solutions.

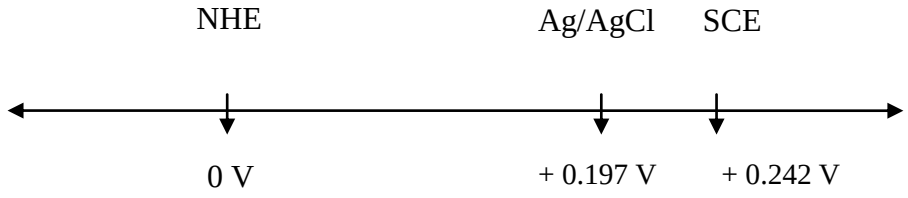

Figure 2.11: *Schematic of potential scale (V) of reference electrodes.*

Simple conversion of potentials collected using one reference electrode to those versus another can be calculated as shown below in Equations 2.28. The NHE and Ag/AgCl reference electrodes are used as examples.

$$E_{NHE}(V) = E_{Ag/AgCl}(V) + (0.197\ V) \qquad \textbf{Equation 2.28}$$

The reference electrode used for the electrocatalytic experiments discussed in Chapters 4-6 is an aqueous (aq.) Ag/AgCl electrode. This is a popular choice of reference electrode when aqueous conditions are employed. The half reaction for this reference electrode is shown below in Equation 2.29.

$$AgCl_{(s)} + e^{-} \leftrightarrow Ag_{(s)} + Cl^{-}_{(aq)} \qquad \textbf{Equation 2.29}$$

The constant activity of the chloride ion is achieved by coating a silver wire with silver chloride and immersing this into an internal solution of saturated potassium chloride, thus the concentration of the chloride ion remains fixed at the saturation limit. A salt bridge is used to make electrical contact between the silver wire and solution to be analysed as it allows for slow leakage of the internal potassium chloride solution.[4] At 25°C the formal potential for the AgCl half reaction is + 0.197 V vs. SHE in saturated chloride solution.

Non aqueous reference electrodes have been used for the characterisation of MPc's by solution electrochemistry in Chapter 3 (the use of aqueous reference electrodes is unwanted due to problems posed by the possible leakage of water into the non-aqueous solvent and liquid junction potentials). Therefore, using a silver wire within a non-aqueous solvent is preferred. Although the potential of the Ag wire is not defined, it doesn't change significantly during the measurements. These electrodes are often referred to as quasi-reference electrodes (QRE) and using an internal standard such as ferrocene is required in order to obtain a true reference potential.[3,4]

2.2.2.4 Using Ferrocene as an Internal Standard

Because the potential of the Ag wire is not defined, it is essential to use an internal standard. Ferrocene (Fc/Fc^{+}) is suitable for this purpose. Ferrocene exhibits a reversible redox process at +0.40 V vs NHE[18] in water (~0.69 V vs. NHE in MeCN).[20] Its oxidised species ferrocenium Fc^{+}, is also soluble and stable in a range of solvents and the redox couple displays Nernstian behaviour. Thus, a value for $E^{o}_{Fc/Fc+}$ *vs.* Ag wire can be obtained and the potentials of other reactions may be reported against Fc/Fc^{+}. Although the potential of the Fc/Fc^{+} wave will

vary with the type of reference electrode material used (e.g. Ag wire, Cu wire, SCE), the potentials of other redox processes vs. the ferrocene wave will not. It also allows for reproducible formal potentials because variables (including electrode degradation) are eliminated. Therefore using ferrocene as an internal standard is convenient and it allows for the quantitative comparison of potentials measured in a range of solvents.[19,20]

2.2.3 Electrochemical Methods and Techniques

Cyclic voltammetry is a widely used technique for the analysis of electrochemical reactions. Voltammetric methods based on linear potential sweep techniques are used throughout this thesis allowing for the identification of diffusion-controlled and surface-confined properties of metal phthalocyanines.

2.2.3.1 Cyclic Voltammetry

For the linear sweep voltammetry technique, the potential is scanned at a constant rate between an initial and final potential (E_1 and E_2, respectively) following the waveform shown in Figure 2.12. The current produced by this experiment is measured as a function of the applied potential, as well as the potentials observed for oxidation/reduction processes, which relate to orbital energies of the analyte. Cyclic voltammetry operates on the same basis with the difference being that a reverse scan is employed whereby the potential is scanned back from E_2 toward to the initial potential E_1, Figure 2.12. Analysis of the resulting voltammogram (CV) offers added information about the properties of the electrochemical reaction as well as any additional follow up chemical processes that may occur following electron transfer, to or from the species involved.[3,20]

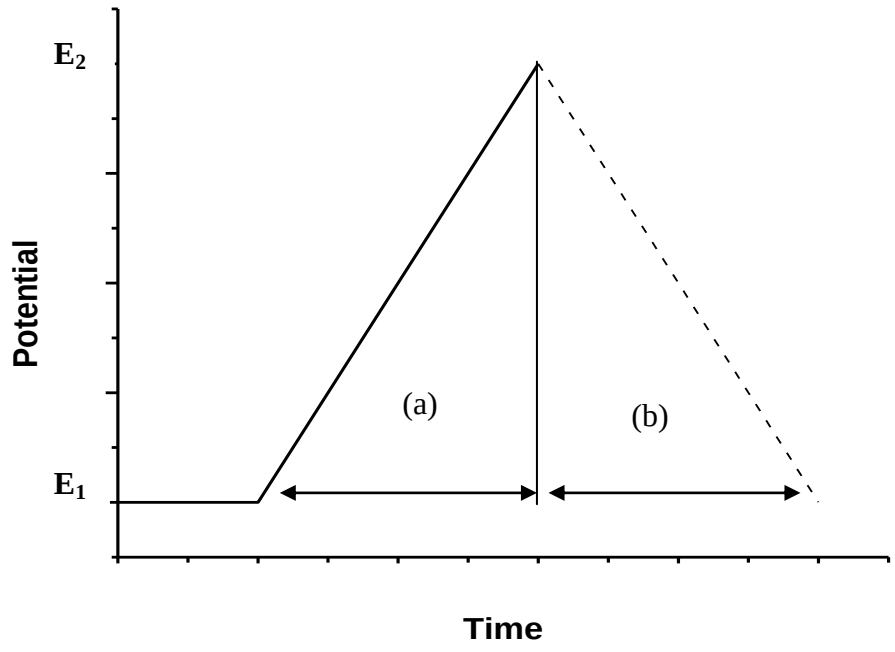

Figure 2.12: *Potential-time profile; Linear-sweep voltammetry, forward sweep (a) and cyclic voltammetry (1 cycle), reverse sweep (b).*

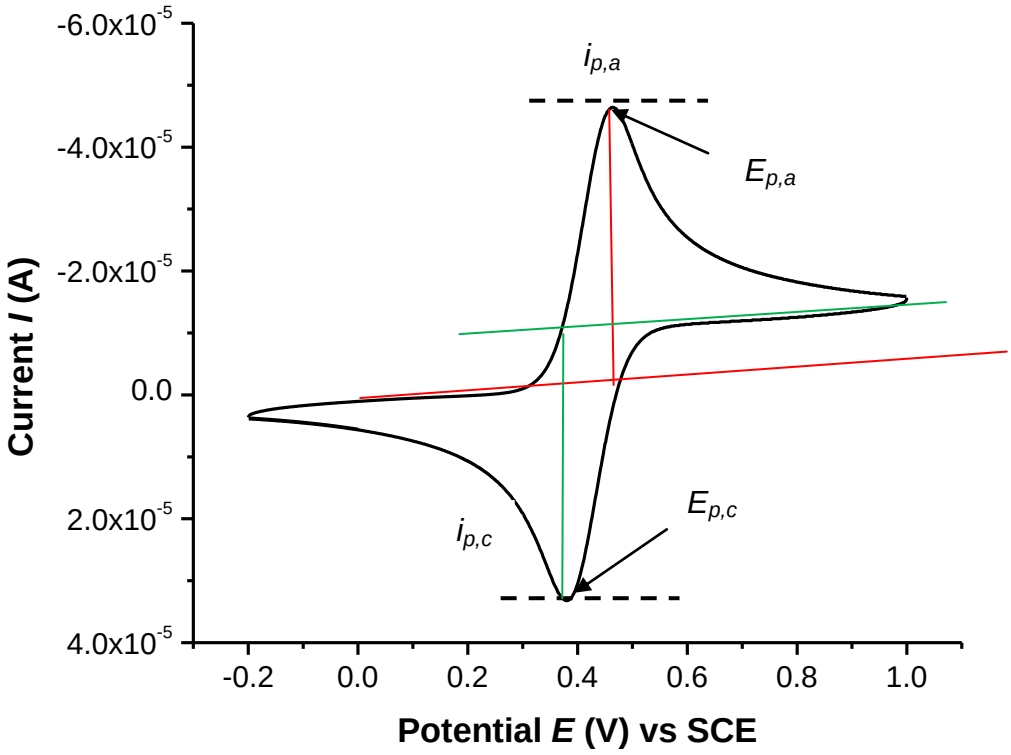

Figure 2.13: *Cyclic voltammogram of ferrocene (Fc^{2+}/Fc^{3+}) in 0.1 M TBA PF_6 in MeCN vs. SCE.*

The cyclic voltammogram of the oxidation of ferrocene to ferrocenium is shown in Figure 2.13. As the potential is scanned in a positive direction, it approaches the standard potential E° for the redox process, an anodic current begins to increase until a maximum current is reached. During this period of the scan, Fc is oxidized at the electrode surface (to Fc^+). At the potential that corresponds to the peak current, the movement of Fc through the bulk solution to the edge of the diffusion layer occurs at a maximum rate. Beyond this potential, Fc becomes depleted in the region adjacent to the diffusion layer and the current consequently drops until it reaches the final potential E_2. The direction of the potential sweep is then reversed and scans back toward E_1, where the ferrocenium molecules at the electrode surface (generated by the forward sweep) are reduced back to ferrocene (generating a corresponding cathodic peak). This CV is characteristic of a redox couple in solution undergoing a one electron electrochemical process at which the scan rate is faster than the rate of diffusion.[4,6]

The Fc/Fc^+ couple is a reversible redox couple, and several important characteristics of this couple can be deduced from the cyclic voltammogram, including peak potential, E_p and peak current maximum, i_p.

The half wave potential, $E_{½}$ is positioned between the anodic ($E_{p,a}$) and cathodic ($E_{p,c}$)[4] peak potentials shown by Equation 2.30.

$$E_{1/2} = \frac{E_{p,a} + E_{p,c}}{2} \qquad \textbf{Equation 2.30}$$

The separation of peaks $E_{p,a}$ and $E_{p,c}$ for a reversible couple is shown by Equation 2.31.

$$\Delta E_p = E_{p,a} - E_{p,c} = \frac{0.059}{n} V \qquad \textbf{Equation 2.31}$$

Therefore for a process exhibiting Nernstian behaviour, the separation for a one electron transfer ΔE_p is 59 mV.[4] The half peak potential can also be calculated where the peak potential at half the maximum is related to $E_{p/2}$ as shown by Equation 2.32.

$$E_p - E_{p/2} = \frac{2.20RT}{nF} = 0.0565\, V\ (25°C) \qquad \textbf{Equation 2.32}$$

The peak current for a reversible redox reaction, where diffusion of the electroactive species is considered to be planar, is expressed according to the Randles-Sevcik equation.[3,4]

$$i_p = (2.69\ x\ 10^5)n^{3/2}AD_O^{1/2}C_O^*v^{1/2}(25°C) \quad \textbf{Equation 2.33}$$

The peak current (i_p) is directly proportional to the concentration of electroactive species (for a reversible electrochemical process), and the current increases with the square root of the scan rate, as described previously in Equation 2.22. For a reversible couple, the ratio of the cathodic and anodic peak currents will equal 1.

$$\frac{i_{p,a}}{i_{p,c}} = 1 \qquad \textbf{Equation 2.34}$$

2.2.3.2 Differential Pulse Voltammetry

This technique differs from that of potential sweep voltammetry in that the potential is applied in a staircase manner, rather than being ramped at a constant rate. The current is measured before and after an application of a pulse potential[6], as shown in Figure 2.14 where i_1 and i_2 represent the points in which the currents are measured.

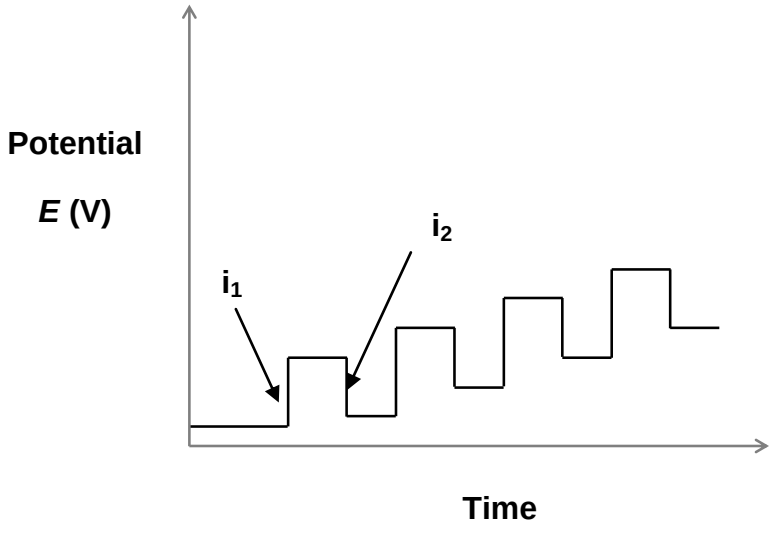

Figure 2.14: *Differential Pulse Voltammetry (DPV).*

The advantage of this technique over potential ramp techniques is that it offers a greater sensitivity by optimising the ratio of the Faradaic current (i_F) to the capacitive current (i_C).

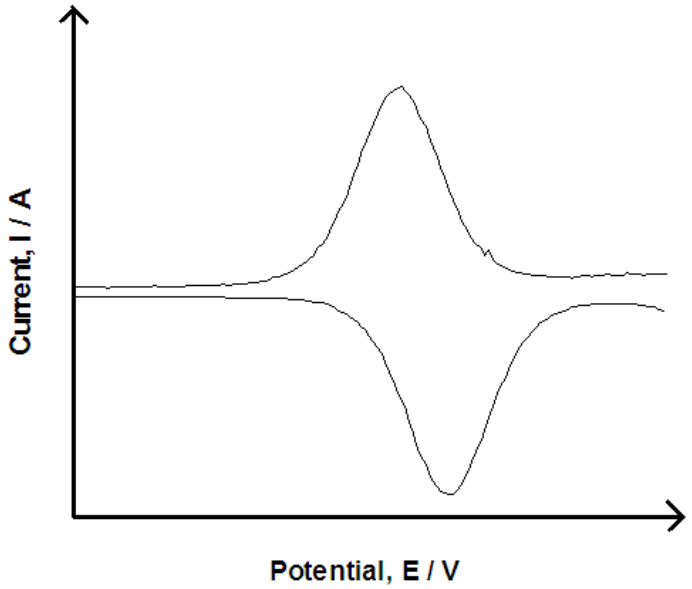

Figure 2.15: *An example of a Differential Pulse Voltammogram of a redox couple* $O + ne \leftrightarrow R$.

The current is sampled over a series of increasing potential pulses. The difference in the current is measured before and at the end of each pulse. The resulting i-E curve is shown in Figure 2.15, similar to that of a cyclic voltammogram, but the contribution of the capacitive charging current now is diminished.

2.2.3.3 Bulk Electrolysis with Coulometry

Bulk electrolysis (also known as potentiostatic electrolysis PE) with coulometry is another electrochemical technique in which a constant potential is applied (for a period of time) and the resulting current is recorded as a function of time.[21] The potential waveform, E-t (a), current-time profile, i-t (b) and charge- time profile, Q-t (c) for a bulk electrolysis experiment are shown in Figure 2.16. During the time before the potential step (the rest period), the cell should be at open-circuit (i.e. zero current); this makes the solution homogeneous near the electrode surface, like in the rest of the solution. Then, when the step is applied, mass transport changes the surface (and nearby) concentrations, and a Faradaic current flows.[4]

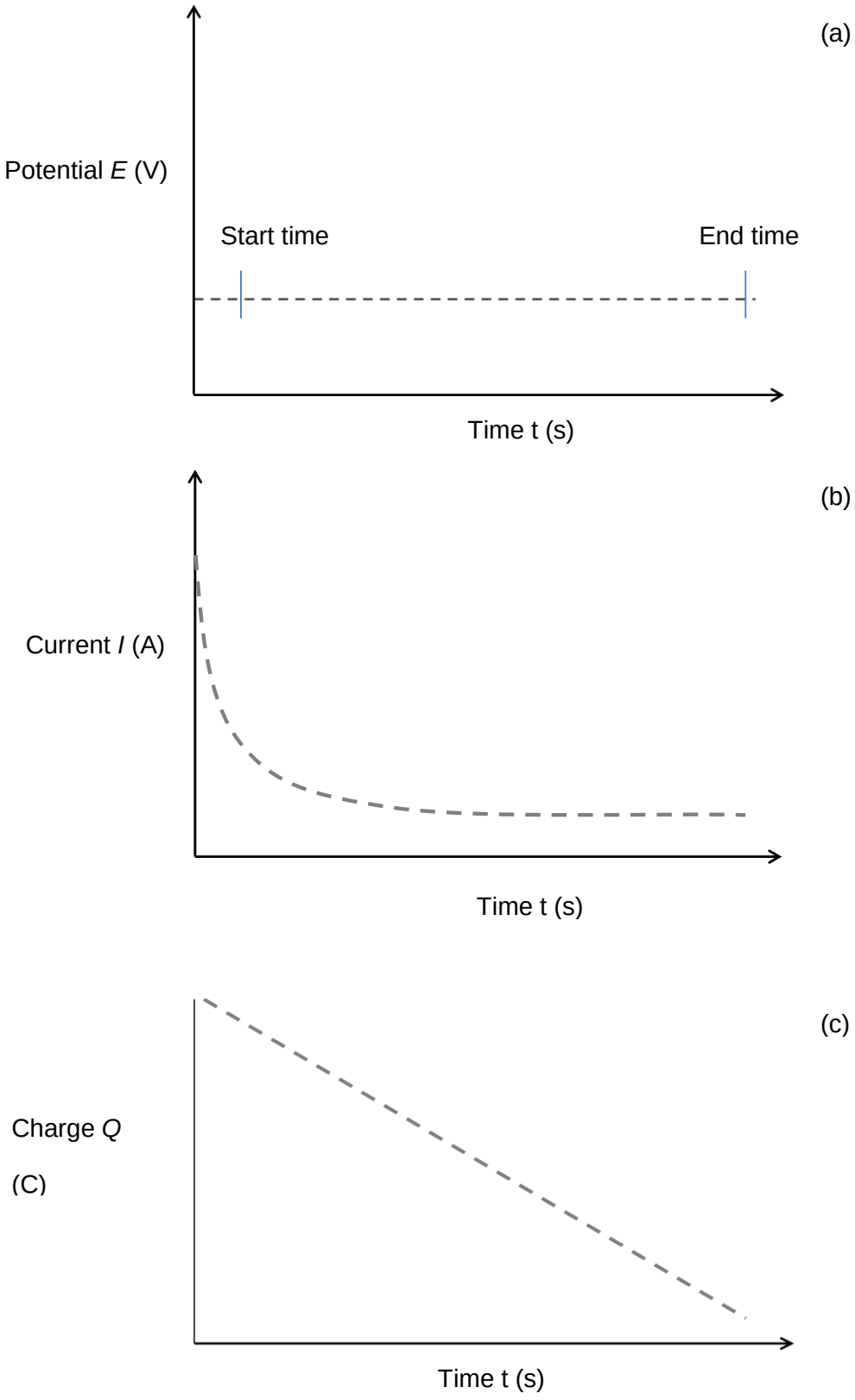

Figure 2.16: *(a) potential waveform E-t, (b) current-time i-t and (c) charge-time Q-t for a bulk electrolysis.*

This technique is different from a potential ramp technique in that the potential is stepped into the mass transport-limited region so that the electrochemical reaction is diffusion controlled. As the current is related to the rate of electrolysis, it can be used to calculate the charge passed at any period of time during the reaction. The area under the i-t curve can be calculated to give the charge passed for that period of time as 1 A = 1C/s.

2.3 Hydrogen Quantification using Electrochemistry

In this section, the manner in which the electrochemical data is obtained and analysed is described. In Chapters 4 to 6 the amount of product formed by electrolyses and the turn-over frequency per hour (TOF hr^{-1}) for each system is discussed. The electrochemical determination of the moles of product (H_2) formed during an electrolysis assumes only H_2 formation (i.e. not other processes, such as O_2 reduction that may also produce current, and other side-reactions that involve the catalyst) and so this figure represents the upper limit for H_2 formation – the maximum amount of product that may be obtained if 100% of the charge passed during the experiment is utilised for forming H_2. The potential imposed on the working electrode during electrolysis will also generate a non-Faradaic current that will contribute towards the overall charge reported. The TOF values which are obtained by the total current, given as TOF (electrochemistry) are listed in relevant Appendix section, in order to simplify the experimental data used to calculate the Faradaic efficiency mentioned throughout this thesis.

Furthermore, it is possible that gaseous products like H_2 may leak during the electrolysis or during transfer to the GC instrument. The first factor (electrochemical) will make the mol of H_2 (and TON) determined through electrochemical data artificially high, while the last factor will lower the value of the mol of H_2 determined by GC. Importantly, the ratio of the mol H_2 determined for electrolysis and by GC (or other instrumental method) gives an indication of the proportion of the total current that yields H_2 (Faradaic efficiency) but does not account for any hydrogen which may have leaked from the cell.

2.3.1 Calculation of moles of reactant/ product

The number of electrons that cross the electrode interface during the time of an electrolysis step is related stoichiometrically to the extent of the electron-transfer processes occurring at the electrode. This number of electrons is expressed as the total charge *Q* and is accumulative for the duration of an electrolysis step. The relationship between charge and the amount of product formed is given by Faradays law which states that a 1 mole equivalent for a 1 electron reaction causes 96,485 Coulombs to pass.[4] Thus, the number of moles electrolysed can be determined by Equation 2.35.

$$N = Q/nF \qquad \textbf{Equation 2.35}$$

Where N is the number of moles electrolysed (mol), Q is the charge (Coulombs), n is the stoichiometric number of electrons consumed in the electrochemical reaction and F is Faraday's Constant (C/mol).

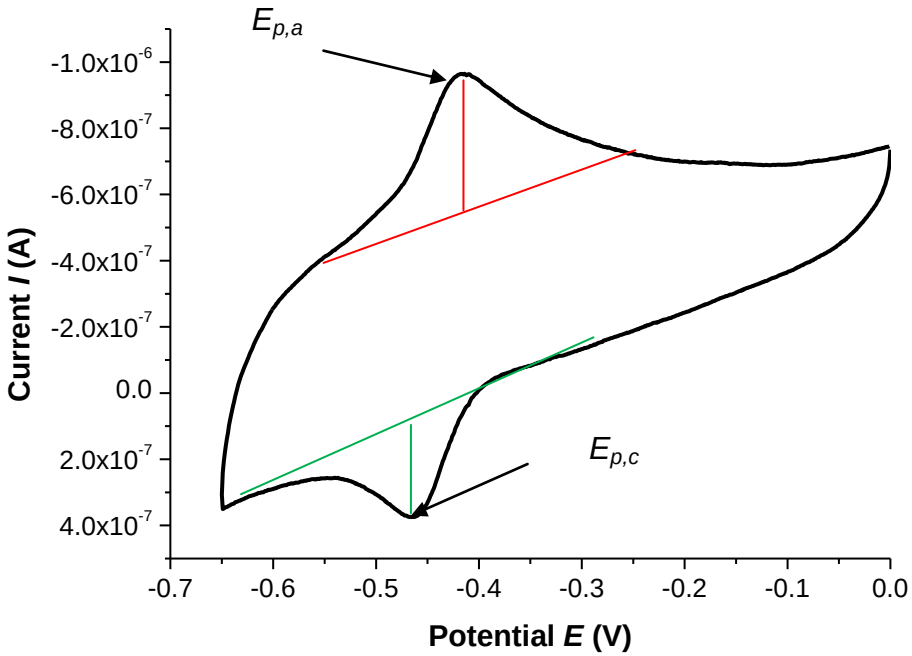

Figure 2.17: *Cyclic voltammogram of $CoPcF_{16}$ in 0.1 M NaH_2PO_4/H_3PO_4 (pH 2) vs. Ag/AgCl. Scan rate = 100 mV/s.*

The cyclic voltammogram shown in Figure 2.17 shows the reduction of Co(II) to Co(I). The area under the peak can be integrated to determine the charge passed

for this process (for the data shown, a charge of 5.1 x 10^{-7} C was passed). Using equation 2.35, the number of moles of catalyst deposited on the electrode surface (or, at least, the number of moles of catalyst that is able to undergo reduction/oxidation for this modified electrode) is calculated as 5.3 x 10^{-12} mol.

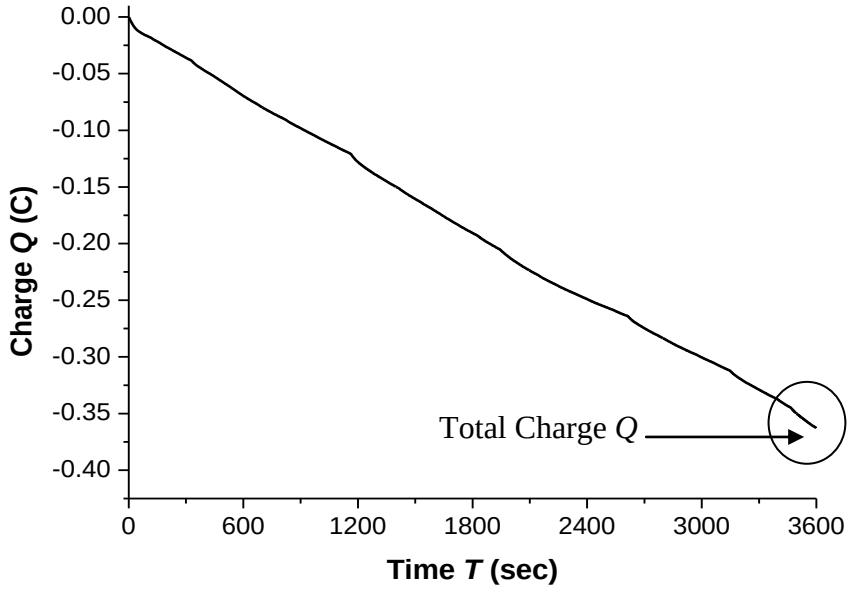

Figure 2.18: *Charge-time profile (Q-t) for electrolysis step for 1 hour.*

2.3.2 Calculation of percentage of electroactive catalyst

The determination of the number of electroactive moles is described above in 2.3.1. As the volume of catalyst (1.5 μL) drop cast onto the electrode and the concentration of the catalyst solution (2.8 x 10^{-5} M for $CoPcF_{16}$) are known, calculating the percentage (%) electroactive catalyst in the modifying layer can be determined.

$$\frac{mol\ of\ electroactive\ catalyst\ (mol)}{mol\ of\ catalyst\ drop\ cast\ onto\ electrode\ surface}\ x\ 100\ \% \qquad \textbf{Equation 2.36}$$

2.3.3 Calculation of turnover frequency (electrochemically)

The potentiostatic electrolysis experiment involves the imposition of a potential step to the modified working electrode for 1 hour, during which time, H_2 is

produced. A charge-time profile is generated from which the total charge, *Q*, is obtained as - 0.36 C (from Figure 2.18). For the electrochemical production of H_2, 2 electrons are required, thus through Equation 2.35, the number of moles of product formed can be determined. For the reaction of interest, the stoichiometric value n is 2 (number of electrons). Using the number of moles of H_2 produced, the average TON (or TOF (hr^{-1})) can be obtained by using Equation 2.37.

$$Av.\ TOF\ (electrochemical, hr^{-1}) = \frac{moles\ of\ H_2}{moles\ of\ catalyst}\ x\ \frac{1}{hr} \quad \textbf{Equation 2.37}$$

TOF values obtained in this way in Chapters 3 to 6 by Equation 2.37 are available in Appendix B to E respectively.

2.4 Chromatography

2.4.1 Introduction and Gas Chromatography

Chromatography is a procedure for separating an analyte of interest from other compounds in a sample mixture. All chromatographic techniques depend on the differing distributions of individual compounds between two immiscible phases, the mobile (liquid or gas) and the stationary phases (fixed in a column or on a solid surface). The mobile phase passes through or over the stationary phase. As the mixture of compounds is eluted, the compound appearing first at the end of the stationary phase has the smallest distribution into the stationary phase, thus has the smallest retention time. As the separated compounds appear at the end of the stationary phase, they are detected by means of a detector which may be a general purpose detector or one that is specific for the analyte of interest. The quantification of the separated compounds is determined by the detector.

Gas chromatography (GC) involves a sample which can be vapourised easily (or is already in a gaseous state) and injected onto the head of the chromatographic column. The sample is transported through the column by the flow of an inert or unreactive gaseous mobile phase. There are two packed columns which are used to separate a mixture of gases such as H_2, O_2, CO_2, CO and CH_4 which will be discussed now in more detail.

The rate at which the gas molecules progress along the column depends on the strength of adsorption or distribution, which in turn depends on the type of molecule and on the column chosen for separation. Gas species are identified by

the order in which they emerge from the column and by the residence time of the species in the column. There are many parameters which influence the effect of molecular adsorption and the rate of progression along the column, temperature and the flow rate of carrier gas are just two of these parameters and thus are carefully controlled.[22]

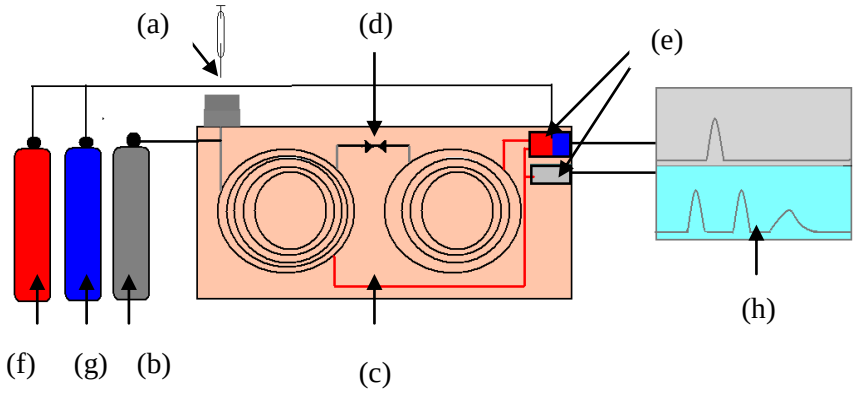

Figure 2.19: *Basic diagram of a typical GC, consisting of (a) gas tight syringe and injector port, (b) carrier gas N_2, (c) temperature controlled oven, (d) two packed columns, (e) Detectors, TCD and FID, (f) & (g) compressed air and H_2 for FID and (h) software for conversion of signal output to chromatographs. Adapted from reference 22.*

A gaseous mixture containing H_2, O_2, CO_2, CO and CH_4 is injected into the sample loop *L1*, through the injector port using a gas tight syringe. This mixture is swept along by the mobile phase i.e. N_2 carrier gas, to the first column, Hayesep C.[23] This packed column consists of a macro-porous polymer in which CO_2 has a high affinity for while the other gas molecules are not retained and quickly elute to the second column through sample loop *L2*. At this point the columns, which were arranged in series (see Figure 2.20- (d)) are now switched to bypass mode (Figure 2.20-(e)) to prevent CO_2 moving onto the second column from the Hayesep column. As CO_2 bypasses the second column, it moves directly towards the TCD and FID detectors and can be identified easily on the chromatogram. The second column consists of a molecular sieve column which is commonly used for the separation of gases such as H_2, O_2, CH_4 and CO, argon, neon, and other rare gases.[24] The lighter gases tend to elute first while the larger gas molecules will be retained for a longer time. The column is moved back into series mode and the

column effluent passes through both the detectors and methanizer, with H_2 being eluted first.[25]

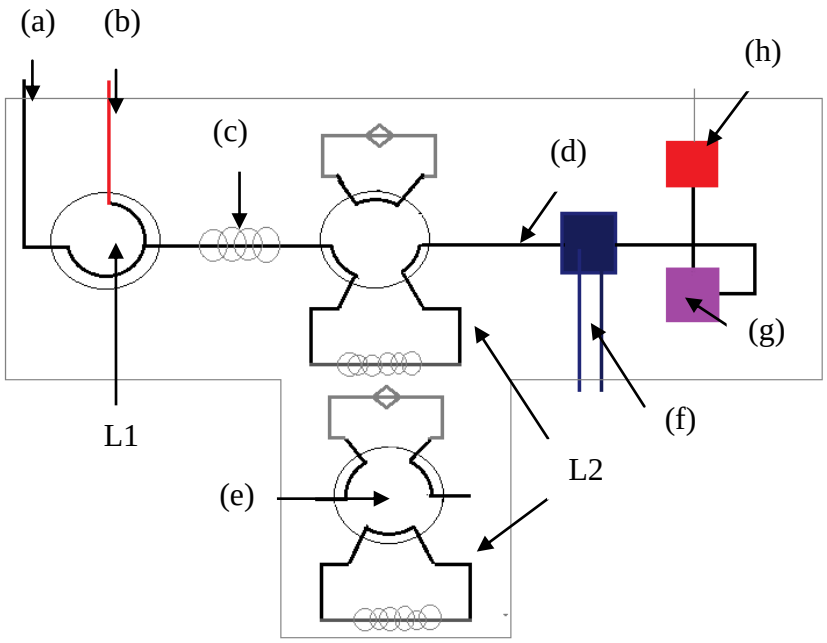

Figure 2.20: *Schematic of the flow of gas mixture through GC; (a) Sample in loop L1, (b) Carrier gas in loop L1, (c) Hayesep C column, (d) Molecular sieve column in series mode on loop L2 (e) Molecular sieve column in bypass mode on loop L2, (f) TCD reference sample in/out, (g) Methanizer and (h) FID. Adapted from Reference 25.*

2.4.2 Detectors

2.4.2.1 Thermal Conductivity Detector (TCD)

The thermal conductivity detector (TCD) was one of the first detectors to be used for gas analysis and is still a popular choice for use today as it possesses desirable properties. This detector works on the basis that it measures a constant thermal conductivity of the carrier gas (reference gas) so any change in this due to a species with a different thermal conductivity relative to that of the carrier gas can be detected.

A TCD is basically a metal block consisting of two pathways in which electrically heated filaments are fitted. The block which houses these filaments is temperature controlled at all times. The filaments are usually made of an alloy so it has a high temperature coefficient of resistance. These filaments are inserted into a

Wheatstone bridge circuit as illustrated in Figure 2.21. Nitrogen carrier gas passes through one pathway while the column effluent is allowed to pass through the second. A basic TCD normally consists of two filaments (Varian© CP 3800 GC consists of four filaments which enhances the response). The carrier gas is passed over two filaments, labelled R_{R1} and R_{R2} at a constant flow rate and temperature. The column effluent consists of the carrier gas, N_2 and the analytes separated by the columns before reaching the detectors. Therefore the conductivity of the column effluent is different to that of the reference and this passes by the sample filaments labelled S_1 and S_2. The change in conductivity causes the filament temperature to change (heat up or cool down), subsequently altering the resistance of the sample resistors of the Wheatstone bridge.[26,27]

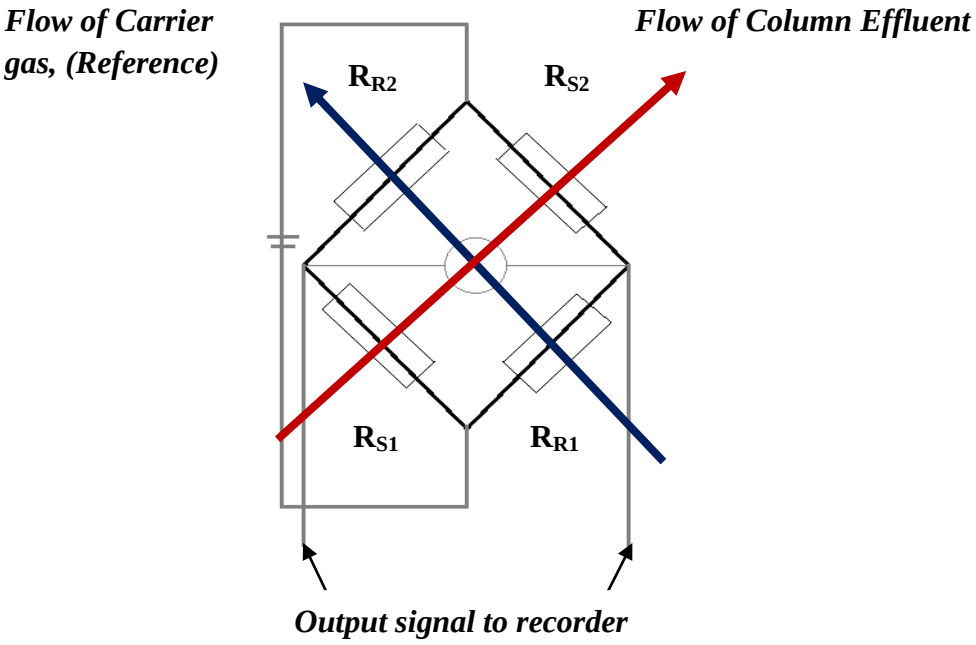

Figure 2.21: *A TCD consists of a Wheatstone bridge circuit. The blue arrow indicates the direction of carrier gas which passes by the filaments labelled R_{R1} and R_{R2}, while the red arrow indicates the direction of column effluent which passes by the filaments labelled R_{S1} and R_{S2}. Four filaments are used, typical for a Varian GC detector. Adapted from Reference 26.*

When a current is applied to the filaments, this causes the filaments heat up to a required temperature. A change in resistance is monitored as the filaments 'sense' a change in temperature. When an analyte passes both filaments, the resistance of R_{S1} and R_{S2} changes and the bridge becomes unbalanced. This generates a

potential which is proportional to the skew and proportional to the concentration of analyte in the effluent stream.

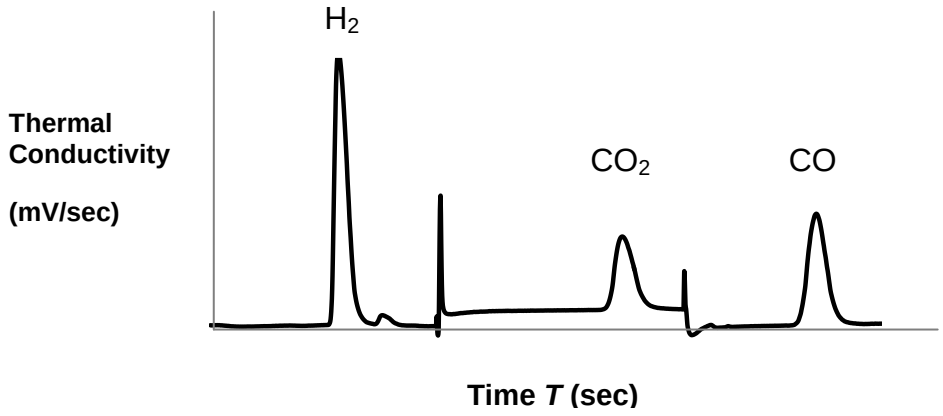

Figure 2.22: *Gas chromatogram of a separated mixture of gases detected by the TCD.*

A typical chromatogram of a 1 ml injection of a 1000 ppm mixed gas is shown in Figure 2.22, produced by the TCD detector. The gases are separated and identified (output signal is mV/sec).

2.4.3 Method Validation

Quantification of the gas product formed by electrolysis is vital, as it allows for the efficiency of the system to be calculated by comparing GC results with electrochemical results. Quality control (precision) and method validation can be used as a measure to verify that an experiment/procedure is working properly, and to ensure that the results generated by this are correct. Precision is how well an instrument can reproduce the same result over time and under varying operating conditions. Method validation is a process of testing a measurement procedure to assess its performance and to validate that performance is acceptable for its intended purpose.[28,29,30] This approach was taken for the research carried out throughout the experimental chapters of this thesis. Not only does this provide assurance in the instrumentation, it also gives confidence in the results obtained.

A calibration curve shows the response of an analytical method to known quantities of an analyte.[28] As a calibration curve is used to determine a sample of an unknown concentration by comparing it to a standard set of samples of known

concentration, a plot of concentration versus instrument response yields a linear relationship (Figure 2.23). The unknown's response is measured and using the equation of the line from the calibration curve, the concentration can be attained. A measure of linearity is denoted by the square of the correlation coefficient R^2.

A volume of a mixture of standard gases was injected onto the GC on a daily basis to account for the reproducibility and reliability of the instrument. The response of this gas sample was inserted into a calibration curve to ensure there was no deviation from the linear fit.

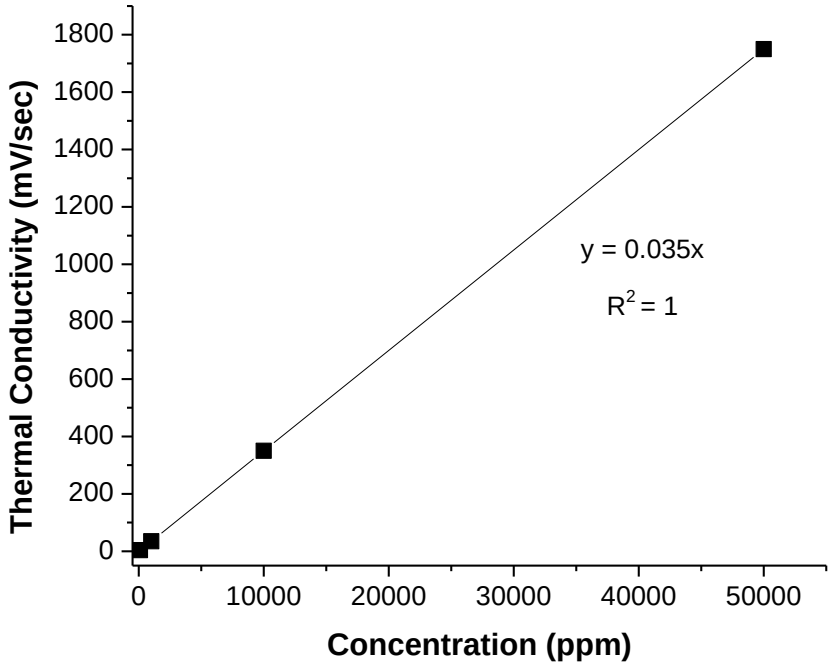

Figure 2.23: *Example of a calibration curve for the determination of concentration of a H_2 sample of unknown concentration.*

2.4.4 Hydrogen Quantification using Gas chromatography

As described in section 2.3, the electrochemical determination of the moles of product (H_2) formed during electrolysis is an indication of the upper performance limit (H_2 evolution), thus the GC value is always expected to be less than this value. By taking a certain volume of gas from the headspace of an electrochemical cell as shown in Figure 2.10, this can be injected into the GC and

the concentration of the headspace can be calculated. Using the Ideal gas law, the moles of product *n* can be determined for each system. Assume that the injection of a 10000 ppm calibration standard of H_2 yielded a signal of 350 mV/sec, as obtained by TCD. If an injection of a sample containing *x* ppm of H_2 from the headspace is recorded as *245* mV/sec, then this corresponds to a concentration of 7000 ppm of H_2. The concentration of the gas can be converted to partial pressure by assuming standard pressure is present in the electrochemical cell (1 atm). The concentration is divided by 1 x 10^6 and then multiplied by 101,325 Pa. Thus the partial pressure due to hydrogen is determined as 709.3 Pa (1 atm = 101,325 Pa). Assuming ideal gas behaviour, this value can be substituted into the Ideal gas law as P, V, R and T are known, therefore *n*, number of moles of product can be solved.

$$PV = nRT \qquad \textbf{Equation 2.38}$$

The turnover frequency TOF (hr^{-1}) can be obtained by using Equation 2.37 as the number of moles of catalyst is determined by electrochemistry, discussed above in section 2.3.1.

The Faradaic efficiency of the system can also be determined by taking the chromatographic data; the moles of H_2 calculated and dividing it by the total amount of moles of H_2 formed (obtained by electrochemistry) and multiplying it by 100, Equation 2.39. If no other process or reaction is taking place in the cell (and no leakage of product occurs), then the Faradaic efficiency should be 100 %. (Note: all TOF (hr^{-1}) values given in the experimental Chapters 4 to 6 are obtained by gas chromatography, unless otherwise stated).

$$\%\ Efficiency = \frac{moles\ of\ H_2\ (GC)}{moles\ of\ H_2\ (Electrochemical)}\ x\ 100\% \qquad \textbf{Equation 2.39}$$

2.4.5 Sources of Error

As with any measurement taken, a level of uncertainty will be present, known as experimental error. Although experimental errors are unavoidable, it is important however to firstly identify where the source of error may lie and to recognise the degree of error (or the degree of confidence). There are two types of errors which

can occur; systematic and random. A systematic error is described as a consistent error which can be detected and corrected. An example of a systematic error is one which may occur due to a fault within an instrument, such as an uncalibrated pipette or use of a wrongly labelled solution. A systematic error affects the accuracy however, a feature of systematic error is that it is reproducible and can be taken into account by careful examination of results produced. Random error is one which is unpredictable and can't be eliminated. An example of this error is reading the scale of a syringe; reading of the same scale several times might report several different readings. As random errors affect the precision of a result, repetition can reduce the degree of experimental error.[28]

In an effort to reduce the amount of errors, the experimental errors have been identified and extra care taken to minimise these, thus leading a greater degree of confidence in the accuracy and precision in the results presented in the thesis. The errors identified are discussed in the experimental chapters.

2.5 Experimental Materials and Conditions

2.5.1 Solution electrochemistry

Cyclic voltammograms described in Chapter 3 were recorded against a silver wire (Ag/Ag^+) reference electrode. GCEs macro (area = 0.07 cm^2) were used as the working electrode and a platinum wire was employed as the counter electrode. Ferrocene was used as an internal standard for which the potentials obtained using the Ag^+ wire were converted to the Ag/AgCl reference electrode.

A 0.1 M solution of tetrabutylammonium hexafluorophosphate, *TBA* PF_6 (Fluka, electrochemical grade) in DMSO (Aldrich, anhydrous, 99.8%) was used as the supporting electrolyte unless otherwise stated.

Electrochemical experiments were carried out using CH Instruments Version 8.15 software controlled electrochemical bipotentiostat CHI750C. Prior to each experiment, the electrochemical cell was degassed for at least 20 minutes using argon and a blanket of argon was maintained throughout each experiment to allow for the removal of oxygen from the cell.

2.5.2 Modified electrodes for electrocatalytic studies

Cyclic voltammograms, differential pulse voltammograms and bulk electrolyses were recorded against a silver/ silver chloride (Ag/AgCl, 3 M KCl) reference electrode using a platinum wire as the counter electrode. GCEs were mainly used for these experiments. All cyclic voltammograms were recorded at a scan rate of 100 mV/s unless otherwise stated.

Sodium dihydrogen phosphate (Merck 98-100 %) was used as the electrolyte/buffer for the electrocatalytic experiments. Altering the ratio of sodium dihydrogen phosphate and phosphoric acid allowed for the formulation of buffer solutions covering a range of pH. Basic solutions were attained by using NaOH and as described for the lower pH buffers, the ratios of each were altered to achieve a range of basic aqueous solutions. The ionic strength of these solutions was kept constant at 0.1 M unless otherwise stated.

2.5.2.1 Coating of electrodes

Modified GC electrodes were prepared by drop-casting a known volume (1.5 µL) of each catalyst/polymers onto the surface of a clean electrode. The electrode was allowed to dry overnight in an oven set at 21°C (in an effort to form a homogeneous reproducible film).

2.5.2.2 Cleaning of working electrodes

The working electrodes required cleaning before each use. This was carried out by polishing with 0.3 µm alumina paste (alumina powder and water), followed by sonication in deionised water for 5 minutes and further polishing with 0.05 µm alumina paste and sonicated again in deionised water for 5 minutes. For solution electrochemical analysis, the electrodes were sonicated for 5 minutes in DMSO before being placed in the electrochemical cell. All cyclic voltammograms were recorded at a scan rate of 100 mV/s unless otherwise stated.

2.5.3 Catalysts and polymers

Metal phthalocyanines employed for the investigation of suitable catalysts for the electrocatalytic proton reduction to H_2 were Cobalt (II) 1,2,3,4,8,9,10,11,15,16,17,18,22,23,24,25-hexadecafluoro-29*H*,31*H*-

phthalocyanine (Aldrich, 95% dye content), Copper (II) 1,2,3,4,8,9,10,11,15,16,17,18,22,23,24,25-hexadecafluoro-29*H*,31*H*-phthalocyanine (Aldrich, 80% dye content) and Zinc (II) 1,2,3,4,8,9,10,11,15,16,17,18,22,23,24,25-hexadecafluoro-29*H*,31*H*-phthalocyanine (90-95 % purity), which was synthesised by Dr. Brian Murphy of Dr. Kieran Nolan's research group, Dublin City University. Nafion® resin (5 wt % in mix of lower aliphatic alcohols and water) was used to investigate the suitability of a polymer matrix for electrocatalytic production to H_2.

2.5.4 Preparation of Catalyst solutions

2.5.4.1 Adsorbed Catalysts

0.0012 g of $CoPcF_{16}$ was dissolved in 20 mL of DMF or ethyl acetate and sonicated. The solution was allowed to stand overnight and was decanted the following day. The undissolved catalyst was dried and weighed on pre-weighed filter paper. The amount catalyst which remained undissolved was calculated as 60 %, thus the concentration of the catalyst solution in DMF is 2.8×10^{-5} M. The concentration of $CoPcF_{16}$ prepared in ethyl acetate was calculated as 8.2×10^{-5} M with 53 % of undissolved catalyst remaining in solution.

$CuPcF_{16}$ and $ZnPcF_{16}$ solutions were prepared as described for $CoPcF_{16}$ with solution concentrations calculated as 5.6×10^{-5} M and 3.7×10^{-4} M (69 % and 48 % undissolved catalyst remaining in solution for $CuPcF_{16}$ and $ZnPcF_{16}$ respectively).

2.5.4.2 Catalysts dispersed in Nafion®

1 mL of Nafion® was added to 4 mL of $CoPcF_{16}$ solution (above) and sonicated for 5 minutes. $CuPcF_{16}$/Nafion® and $ZnPcF_{16}$/Nafion® solutions were prepared as described for $CoPcF_{16}$.

Solution concentrations when dispersed in a 4:1 $CoPcF_{16}$:Nf volume ratio are as follows: 2.2×10^{-5} M ($CoPcF_{16}$:Nf); in a 1:1 ratio 1.4×10^{-5} M (*2*-$CoPcF_{16}$:Nf) and in a volume ratio of 1: 4, 5.6×10^{-6} M (*3*-$CoPcF_{16}$:Nf). Solution concentrations when dispersed in a 4:1 $CuPcF_{16}$/Nf volume ratio are as follows: 4.4×10^{-5} M ($CuPcF_{16}$:Nf); in a 1:1 ratio 2.2×10^{-5} M (*2*-$CuPcF_{16}$:Nf) and in a

volume ratio of 1: 4, 1.1 x 10^{-5} M (*3*-$CuPcF_{16}$:Nf). Solution concentrations when dispersed in a 4:1 $ZnPcF_{16}$/Nf volume ratio are as follows: 3.0 x 10^{-4} M ($ZnPcF_{16}$:Nf); in a 1:1 ratio 1.9 x 10^{-4} M (*2*-$ZnPcF_{16}$:Nf) and in a volume ratio of 1: 4, 7.4 x 10^{-5} M (*3*-$ZnPcF_{16}$:Nf).

2.5.5 Preparation of catalysts using graphitized carbon monolith material as electrodes

The modified electrodes prepared using porous graphitized carbon monolith material described in Chapter 6 were synthesised by Xiaoyun He[31] of Professor Brett Paul's research group, Dublin City University.

Two methods were used to prepare the modified electrodes. The first involved placing the carbon rod into a solution of $CoPcF_{16}$ (2.8 x 10^{-5} M $CoPcF_{16}$) which was stirred for 72 hours and allowed to dried after this time. This modified carbon monolith rod adsorbed with the cobalt catalyst was denoted MCM (modified carbon monolith). The next stage involved crushing the carbon monolith fragment into a fine powder by a mortar and pestle. A 10 mg/mL of CCM/ 10 mM DDAB (dodecyldimethylammonium bromide) solution was prepared to allow for drop casting of the material onto a glassy carbon electrode.

The second method of electrode preparation followed the method outlined above (see Chapter 6). Modified electrodes consisted (blank carbon monolith material, denoted CM) of varying ratios of CM: $MPcF_{16}$(DMF) where each component which was mixed and then drop cast (1.5 μL, unless otherwise stated) onto the electrode surface. Prior to drop casting of the carbon monolith materials, each solution was sonicated for 1 hour. Modified electrodes were allowed to dry in an oven (at 21°C) overnight.

2.5.6 Gas Chromatography

Varian© CP3800 GC equipped with a TCD and FID detector was used for the quantification of gas in the headspace of the experiments described in chapters 4 to 6. Gas mixtures were separated using two packed columns; Hayesep C porous polymer column of dimensions 2 m x 1/8" x 2.0 mm and a Molecular Sieve 13x 60-80 mesh with dimensions 1.5 m x 1/8" x 2.0 mm. Nitrogen (BIP grade- Air

Products) was used as a carrier gas and compressed air and hydrogen (Air Products) were used for the FID to maintain a lighting flame. Varian software version was used to interpret the chromatograms. A range of standard calibration gases were used containing H_2, O_2, CO_2, CO and CH_4 in the range of 10^2 ppm to 5 x 10^4 ppm (0.01% to 5%). These were used to plot a calibration curve on a weekly basis to account for accuracy and reliability in the measurements.

Flow rates were controlled by electronic flow controllers (EFC). Column pressure was set to 40 psi with total flow of 50 ml/min N_2 carrier gas. The TCD reference was set at 20ml/min and it was important that the actual column flow matches that of the TCD flow rate to allow the TCD to function correctly. The methaniser flow was set at 10 ml/min of H_2 at 40 psi. The gases which pass through the FID consisted of compressed air at 300 ml/min, H_2 at 20 ml/min and makeup flow at 10 ml/min. The following are the temperatures for which each component were set: Injector 150°C, Middle Valve Oven 170°C, Column Oven 70°C, TCD block temperature 200°C, filament temp 250°C, FID oven 200°C and methaniser 400°C. A 1 ml gas tight syringe (Hamilton) and 23 gauge needle was used to inject the gas sample into the injector port.

2.5.6.1 Elution times of gases

The run time was 7 minutes, with the order of elution and retention times as follows; TCD: H_2 0.85 min, O_2 1.20 min, CO_2 2.30 min, CO 5.00 min; FID: O_2 1.20 min, CO_2 2.30 min, CO 5.00 min and CH_4 5.50 min.

2.6 Concluding Remarks

In this chapter, the theory of important electrochemistry terms is discussed, such as double layer formation, mass transport and electron transport. The use of modified electrodes consisting of an electroactive species is discussed, where the structure of the electrode/solution interfaces is of great importance for an electrode reaction to occur. The development of modified electrodes has been widely reported to facilitate and enhance catalytic reactions, such as the catalytic reaction reported in this thesis. The main electrochemical techniques employed in this thesis are cyclic voltammetry and bulk electrolysis with coulometry. The current responses produced as a result of the application of a potential allow for valuable information to be obtained by each technique employed.

Gas chromatography is a separation technique which can detect gases and thus was chosen to detect hydrogen produced by electrolysis experiments outlined in Chapter 4 to 6. The basic theory of gas chromatography is discussed, along with a detailed description of the workings of the detectors. As with any analytical instrumentation, the importance of the accuracy and reproducibility is highlighted with the discussion of method validation, use of calibration curves and identification of errors associated with the experimental work carried out. The chapters detailing the electrocatalytic studies consist of both electrochemical and chromatographic calculations. These calculations, which allow for hydrogen quantification, are described in detail. The electrochemical and chromatographic determination of moles of hydrogen evolved by electrolysis allow for the determination of the Faradaic efficiency of each catalytic system.

2.7 References

[1] http://www.rsc.org/chemistryworld/Issues/2003/August/electrolysis.asp (Last accessed 01/04/2012).

[2] D. B. Hibbert, *Introduction to Electrochemistry*, Macmillan Press Ltd, **1993**, London, UK.

[3] J. Wang, *Analytical Electrochemistry, 2nd Ed.*, Wiley-VCH, **2001**, New York.

[4] A. J. Bard, L. R. Faulkner, *Electrochemical Methods: Fundamentals and Applications*, 2nd Ed., John Wiley & Sons, Inc., **2001,** USA.

[5] A. C. Fischer, *Electrode Dynamics,* Oxford Chemistry Primers, **1996**, Oxford, UK.

[6] C. M. A. Brett, A. M. O. Brett, *Electrochemistry: principles, methods and applications, 1st Ed.*, Oxford science publications, **1993,** USA.

[7] R. J. Forster, T. E. Keyes, J. G. Vos, *Interfacial Supramolecular Assemblies*, John Wiley & Sons, **2003**, Chichester, UK.

[8] R. G. Compton, G. H. W. Sanders, *Electrode Potentials*, Oxford Chemistry Primers, **1996**, Oxford, UK.

[9] D. R. Crow, *Principles and Applications of Electrochemistry, 4th Ed*., Blackie Academic & Professional, **1994**, Glasgow, UK.

[10] J. Koryta, J. Dvořák, L. Kavan, *Principles of Electrochemistry*, *2nd Ed*., Wiley, **1993**, Chichester, England.

[11] http://www.cheng.cam.ac.uk/research/groups/electrochem/JAVA/electrochemistry/ELEC/l2html/l2kin.html Last accessed 23/08/2012

[12] W. J. Albery, A. R. Hillman, *RSC Annual Report, 78*, **1981**, 377.

[13] J. G Vos, M. R. Smyth, *Analytical Voltammetry, Chapter 7*, Amsterdam, Elsevier, **1992**, New York, USA.

[14] M. P. Soriaga, A. T. Hubbard, *J. Am. Chem. Soc.*, *104*, **1982**, 10.

[15] R. Baker, D. P. Wilkinson, J. Zhang, *Electrochim. Acta*, *53*, **2008**, 6906.

[16] C. Song, L. Zhang, J. Zhang, H. Wang, D. P. Wilkinson, R. Baker, *Fuel Cells*, 7, **2007**, 9.

[17] *Educator's Reference Guide for Electrochemistry*, Pine Instrument Company, **2000**, Pennsylvania, USA.

[18] H. M. Koepp, H. Wendt, H. Z. Strehlow, *Elektrochem.*, *64*, **1960**, 483.

[19] R. R. Gagne, C. A. Koval, G. C. Lisensky, *Inorg. Chem*., *19*, **1980**, 2854.

[20] D. T. Sawyer, A. Sobkowiak, J. L. Roberts Jr, *Electrochemistry for Chemists*, *2nd Ed*., John Wiley & Sons Ltd., **1995**, New York, USA.

[21] CHI Instruments, *Model 750C, Electrochemical Analyzer/Workstation Manual*, **2012**, Texas, USA.

[22] G. McMahon, *Analytical Instrumentation, A Guide to Laboratory, Portable and Miniaturised Instruments*, John Wiley & Sons Ltd., **2007**, Chichester, UK.

[23] Hayesep C column http://www.vici.com/hayesep/hayesep.php Last accessed 16/06/2012.

[24] Molecular sieve www.supelco.com.tw/A-3%20%20%20236-241.pdf Last accessed 16/06/2012.

[25] Varian© CP 3800 GC, *Getting Started Manual*, Varian© Inc., **1999**, USA.

[26] J. E. Willett, *Gas Chromatography*- Analytical Chemistry by Open Learning, John Wiley & Sons Ltd., **1987**, Chichester, UK.

[27] R. Bramston-Cook, H. Neumann, *Operating Parameters for the Thermal Conductivity Detector in Varian 3800 and 3900 Gas Chromatographs*, Lotus Flower Inc., **2007**, USA.

[28] D. C. Harris, *Quantitative chemical analysis, 6th Ed.*, W.H. Freeman and Company, ***2006***, New York, USA.

[29] D. A. Skoog, S. R. Crouch, F. J. Holler, *Principles of Instrumental Analysis*, *6th Ed.*, Thomson Brooks/Cole, **2007**, Belmont, California, USA.

[30] K. Grob, *Direct Verification within Methods*, http://www.restek.com/Technical-Resources/Technical-Library/Editorial/editorial_A025 Last accessed 30/06/2012**.**

[31] X. He, L. Zhou, E. P. Nesterenko, P. N. Nesterenko, B. Paull, J. O. Omamogho, J. D. Glennon, J.H.T Luong, *Anal. Chem*., **2012**, *84*, 2351.

Chapter Three

Characterisation of Perfluorinated Metal (II) Phthalocyanines

Three perfluorinated metal (II) phthalocyanine complexes where M is Co, Cu and Zn, have been studied as potential catalysts for electrocatalytic generation of molecular hydrogen. Characterisation of the metallophthalocyanines is carried out using UV-Vis spectroscopy and cyclic voltammetry in solution, while characterisation of the electrocatalytic activity of the adsorbed metallophthalocyanines is done by cyclic voltammetry.

3.1 Introduction

Some of the features characteristic of metal phthalocyanines are the following; they can be synthesised from a metallic element, facile design of special characteristics through symmetric and asymmetric substitution of the main Pc ring and through axial ligation to the central metal, its efficient energy absorption and redox nature which make these metallophthalocyanine complexes valuable.[1] The electrochemistry of both unsubstituted and substituted cobalt phthalocyanine derivatives has been previously reported[2]. The electrochemistry of metallophthalocyanine species in solution typically shows multiple redox processes localised on the metal centre and/or on the phthalocyanine ring. Diverse electrochemical properties may be achieved by incorporating different metals into the central cavity of the Pc ring and by varying the ring substituents. The redox processes are influenced by the nature and oxidation state of the central metal, the nature of the substituents on the Pc ring and the nature of any axial ligands and solvents.

The charge on the deprotonated phthalocyanine ring is -2 (Pc^{2-}). Application of negative potential (i.e. cathodic direction) can reduce the Pc ring with up to 4 electrons; from $Pc^{(2-)}$, $Pc^{(3-)}$, $Pc^{(4-)}$, $Pc^{(5-)}$ to $Pc^{(6-)}$. The central metal ion can be both oxidised and reduced which can yield a variety of possible net oxidation states. Ni(II), Zn(II), Pb(II), Pd(II), and Cu(II) display ring based oxidations while Mn(II), Fe(II) and Co(II) can experience metal-based reductions as well as ligand-based reductions.[3,4,5,6,7,8,9,10,11] The reason for which these metals experience metal based reductions is due to the energies of the molecular orbitals. If these lie at values within the highest occupied molecular orbital HOMO (a_{1u}) and lowest unoccupied molecular orbital LUMO (2_{eg}) gap of the ring, oxidation or reduction (or both) may occur on the central metal.

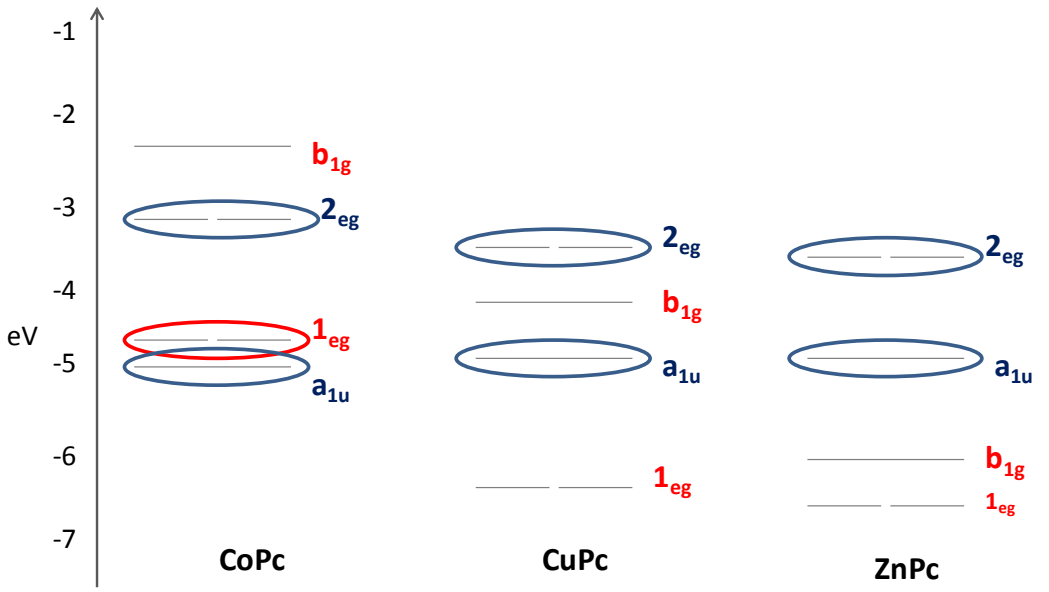

Figure 3.1: *Molecular energy orbitals for the outer orbitals of Co, Cu and Zn phthalocyanines. Metal based orbitals are labelled in red while ring based orbitals are in navy. Adapted from reference 12.*

The energies of the highest occupied molecular orbital (HOMO) and lowest unoccupied molecular orbital (LUMO) are displayed in Figure 3.1 for neutral metal phthalocyanines bearing Co, Cu and Zn central metal ions. Under the D_{4h} point group, the 5 metal d-orbitals are termed b_{1g}, b_{2g}, a_{1g} and $1e_g$ for $d_{x^2-y^2}$, d_{xy}, d_{z^2} and d_{xz}, d_{yz} respectively. The molecular orbitals of the phthalocyanine ring are labelled a_{1u} and 2_{eg} for the bonding π and antibonding π* orbitals respectively. These orbitals are the HOMO and LUMO of the phthalocyanine ring.

The square planar symmetry offers good stabilisation as the $d_{x^2-y^2}$ is high in energy and remains unfilled. The molecule lies in the xy plane and thus the d_{xy} and d_{yz} orbitals have π character.

Comparison of the orbitals for each of the metals in Figure 3.1 reveals similar energies for the HOMO (a_{1u}) and LUMO (2_{eg}) orbitals of the phthalocyanine ring. The a_{1u} level remains at the same energy for all three metal ions, suggesting that substitution of the central cavity of the phthalocyanine ring with different metal *d* ions has little effect on this orbital. In the case for cobalt (II) which is a d^7 ion, the 1_{eg} orbital of the metal lies in between these orbitals, thus allowing for reduction to occur on this partially filled orbital. However for copper (d^9) and

zinc (d^{10}), the 1_{eg} orbitals lie beneath the a_{1u} level hence these complexes don't experience a metal based reduction. The addition of an electron to the copper phthalocyanine occurs on the ring (2_{eg}), even though a level of lower energy b_{1g} (in comparison to 2_{eg}) is available. It is postulated however that the reason the electron 'bypasses' this metal based orbital is due to repulsion of the electron with a localised metal orbital and so reduction is favoured on the delocalised Pc ring.[12] The 1_{eg} orbital of ZnPc lies at lower energy compared to that of both Co and Cu hence reductions for this complex occur only from the a_{1u} and 2_{eg} orbitals of the phthalocyanine ring. All three metals can experience a removal of an electron from the a_{1u} of orbital of the phthalocyanine ring.

It should be noted that the order of molecular orbitals for the perfluorinated [M(II)PcF_{16}] does not change from [M(II)PcH_{16}] shown above in Figure 3.1; however there is a slight shift to higher energy (eV) for the high energy orbitals (b_{1u} and 2_{eg}) of both the metal and ring orbitals.[12] This shift is attributed to the electronic properties of the substituted fluorine atoms on the Pc ring.

3.2 Results and Discussion

3.2.1 Characterisation- Absorption Spectroscopy

The absorption spectrum of the perfluorinated Co(II) phthalocyanine is displayed in Figure 3.2. The solubility of this catalyst is quite poor in most organic solvents, however the spectrum was obtained at a low concentration of $CoPcF_{16}$ in DMF (concentration ~ 5 x 10^{-6} M). (Absorbance spectra of $CuPcF_{16}$ and $ZnPcF_{16}$ are displayed in Appendix B, Figures B.1 and B.2).

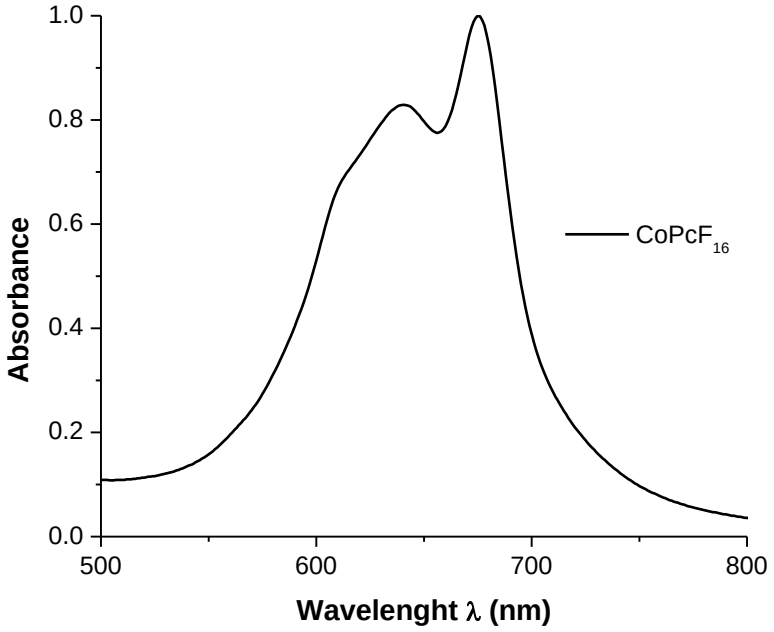

Figure 3.2: *Absorbance spectrum of $CoPcF_{16}$ in DMF solution.*

The absorbance spectrum of $CoPcF_{16}$ is shown in Figure 3.2. This catalyst exhibits a Q band at a maximum absorbance 675 nm, with a shoulder at 640 nm which are features which are characteristic of metallophthalocyanines.[13,14] The Q band is attributed to the π-π* electronic transitions from the HOMO (a_{1u}) to the LUMO (2_{eg}) of the Pc ring.[15] The Q band is influenced by the central metal ion, the solvent and valence state.[16] Aggregation of metallophthalocyanines is often indicated by the emergence of a second absorbance band at higher energy relative to the Q band, thus the appearance of the shoulder at 640 nm indicates aggregation in the catalyst solution.[17] The absorbance spectra of $CuPcF_{16}$ and $ZnPcF_{16}$ also display these features.

Comparing the wavelengths at which these catalysts exhibit the maximum absorbance (Q band), it appears that substituting the central metal ion with copper or zinc results in a slight blue shift to 673 nm for $CuPcF_{16}$, while for $ZnPcF_{16,}$ the shoulder which appears at 638 nm is larger than the Q band which is observed at 670 nm. This also indicates the presence of two Pc species (aggregates) in solution.[14,18] Thus, it can be deduced that for these metallophthalocyanines, the spectral features exhibited by all 3 catalysts are similar, with $ZnPcF_{16}$ experiencing the largest blue shift of the Q band.

3.2.2 Electrochemical Characterisation- Redox Properties

Two electrochemical techniques were employed in the characterisation of these complexes; cyclic voltammetry (CV) and differential pulse voltammetry (DPV). The redox potentials for each of the three metallophthalocyanines were obtained using these 2 techniques and are listed in Table 3.1.

The first phthalocyanine discussed [$CoPcF_{16}$] is the only complex which experiences a metal based reduction; the addition of an electron according to the following process: $M(II) + e^- \rightarrow M(I)$. No metal based reductions are observed for the phthalocyanines bearing copper and zinc as central metal cations. The theoretical peak to peak separation between the anodic and cathodic waves of a redox process (ΔE_p) for a one electron process is 59 mV at room temperature (an experimental range between 60 – 100 mV for a one electron process is not uncommon).[19,20,21] Values in the range of 55 – 90 mV were observed for ΔE_p of each the metallophthalocyanines investigated in this thesis. All three phthalocyanines experience several ring based reductions, revealing an addition of an electron to the LUMO (2_{eg}) of the molecular Pc ring orbital.[22] ($Pc^{(2-)} + e^- \rightarrow Pc^{(3-)}$, $Pc^{(3-)} + e- \rightarrow Pc^{(4-)}$).

Redox processes observed at more positive potentials for these metallophthalocyanines are assigned as the oxidation of the metal with the removal of an electron; $M(II) \rightarrow M(III) + e^-$ for cobalt.

Variations in the redox potentials of each of these perfluorinated phthalocyanines are due to the influence of the metal cation located in the central cavity of the Pc

ring as shown in Figure 3.1. To aid the assignment of the processes, the redox potentials of the unsubstituted M(II)$Pc^{(2-)}$ complexes are reported. The presence of 16 fluorine atoms on the four fused benzo-rings shifts the redox potentials towards positive values, as the fluorine substituents are electron withdrawing in nature, Figure 3.3.

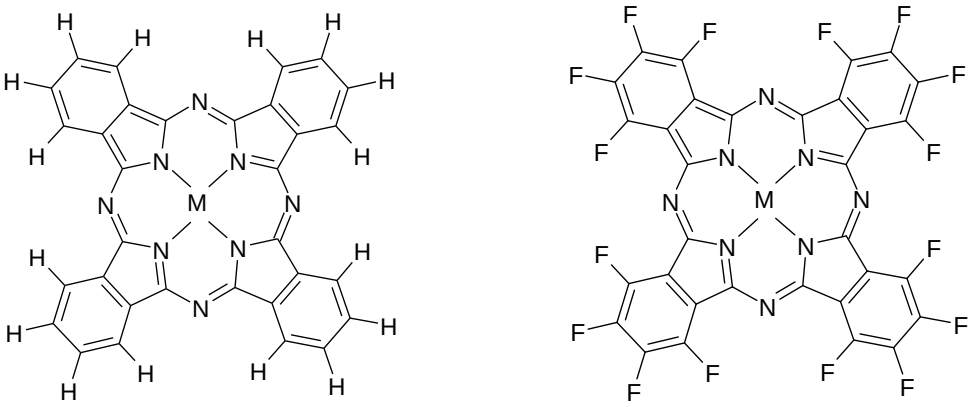

Figure 3.3: *Structures of (a) unsubstituted M(II)$Pc^{(2-)}$ and (b) perfluorinated M(II)$Pc^{(2-)}F_{16}$ metallophthalocyanines where M = Co, Cu and Zn.*

[M(II)Pc($^{2-}$)]	Oxidation[a] E ½ (V) vs. Ag^+	Oxidation[a] E ½ (V) vs. vs. Fc/Fc^+	E_{pa}-E_{pc} (mV)	Reduction[a] E ½ (V) vs. Ag^+	Reduction[a] E ½ (V) vs. Fc/Fc^+	E_{pc}-E_{pa} (mV)
$[CoPcF_{16}]$[b]	0.21	-0.20	80	-0.54	-0.95	[f]
	0.67	+0.26	75	-1.11	-1.52	65
				-1.54	-1.95	80
$[CuPcF_{16}]$[b]	0.37	-0.05	160	-0.80	-1.21	70
				-1.05	-1.46	70
$[ZnPcF_{16}]$[b]	0.77	+0.38	[f]	-0.65	-1.07	50
				-0.86	-1.29	70
				-0.96	-1.39	30
				-1.43	-1.86	55
[CoPc][c,e,22,23]		-0.23[f]	n/a		-1.07	n/a
		+0.32[f]				
[CuPc][c,d,22,24]		+0.53[f]	n/a		-1.29[f]	n/a
[ZnPc][c,22,23]		+0.23[f]	n/a		-1.33[f]	n/a
$[H_2Pc]$[d,24]		+0.41[f]	n/a		-1.03[f]	n/a

Table 3.1: *Electrochemical potentials of the metallophthalocyanines (vs Fc/Fc^+) at 100 mV/s. The unsubstituted metallophthalocyanines $Co(II)Pc^{(2-)}$, $Cu(II)Pc^{(2-)}$ and $Zn(II)Pc^{(2-)}$ are included for comparison purposes. Experiments performed using a Ag/Ag^+ wire in 0.1 M TBA PF_6 in acetonitrile.*

[a]Potentials converted from Ag^+ to Fc/Fc^+, [b]Dimethylsulphoxide, [c]1-chloronaphthalene[20], [d]Dimethylforamide[22], [e]Pyridine[21], [f]Irreversible process, [g]Potentials converted from vs. SCE to vs. Fc/Fc^+ using E° = 0.69 V vs. NHE in MeCN.[25]

Due to time constraints, assignment of redox processes with the aid of spectroelectrochemistry was not carried out. However, as the redox potentials of these perfluorinated phthalocyanines shifted only slightly compared to the unsubstituted phthalocyanines, and with comparison of redox potentials of similar MPc's reported in the literature, assignments could be carried out. All three metallophthalocyanines have similar voltammetric responses in solution, displaying multi electron reduction processes. The reason for the difference in redox potentials for the three MPc's lies in the nature of the metal occupying the central cavity of the Pc ring. (Note: the complexes denoted CoPc, CuPc and ZnPc in this chapter are the same complexes labelled [Co-**1**], [Cu-**1**] and [Zn-**1**] respectively in Chapter 1).

As Table 3.1 above lists the redox potentials of the unsubstituted metallophthalocyanines previously reported by Wolberg[22], Lever[23] and Turek[24], it was expected that effect of substituting the hydrogen atoms in the fused benzene rings with fluorines would yield a shift to positive potentials. Due to the extremely poor solubility of these metallophthalocyanines (concentration < 1 mM) the currents observed were quite weak.

3.2.2.1 Cobalt hexadecafluorophthalocyanine $CoPcF_{16}$

Cobalt phthalocyanines can undergo both metal based oxidations and metal based reductions.[1] For the perfluorinated complex under investigation here and examination of the redox potentials observed for the unsubstituted CoPc displayed in Table 3.1, it was expected that two oxidation processes would be observed,

each for the metal centre and the Pc ring. Similarly for the reduction processes, the appearance of three cathodic waves was expected.

The electrochemistry of the $CoPcF_{16}$ reveals two anodic processes, both of which are reversible. These findings are in agreement with the expected electrochemical behaviour. These processes occurring at 0.21 V and 0.67 V vs. Ag/Ag^+ are in agreement with the potentials reported for the oxidation of the unsubstituted CoPc.[23,24,26] The first process, observed at the least positive potential is attributed to the removal of an electron from the metal centre as the metal dπ (1_{eg}) can experience a metal based oxidation due to the position of this level within the MO of the Pc ring. Hence it can be assumed that the first oxidation and also the first reduction processes occur on the metal 1_{eg} in polar solvents, such as DMSO.[27] Hence the oxidation process at 0.21 V vs. Ag/Ag^+ can be easily assigned as M(II) $\rightarrow$ M(III) + e^-. The second process at 0.67 V vs. Ag/Ag^+ is characteristic of a ring based oxidation, $Pc^{(2-)} \rightarrow Pc^{(1-)} + e^-$. The cyclic voltammogram showing the oxidation of $CoPcF_{16}$ is shown in Figure 3.4.

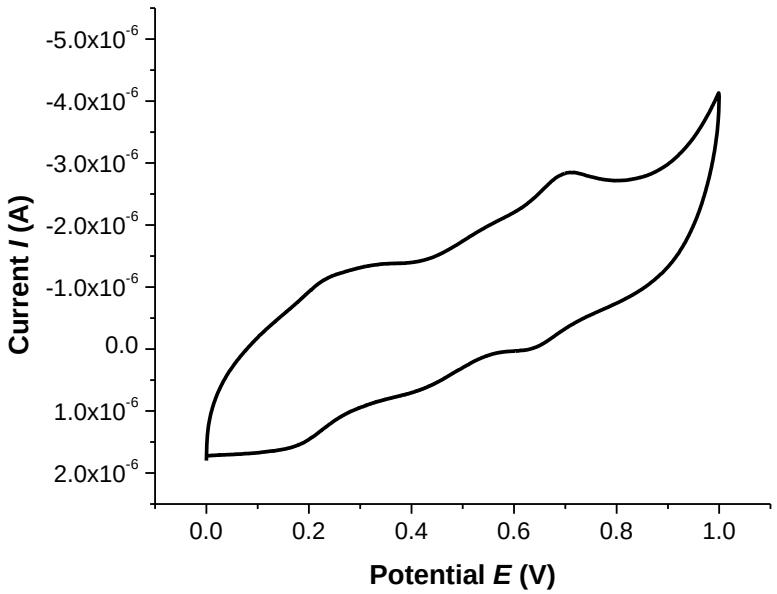

Figure 3.4 *Cyclic voltammogram of $CoPcF_{16}$ at a GC electrode (0.07 cm^2 area), vs. Ag/Ag^+, using 0.1 M $TBAPF_6$ as the supporting electrolyte in DMSO. Scan rate: 100 mV/s.*

The appearance of these processes at more positive potentials than those displayed by CoPc is attributed to the electron withdrawing ability of the hexadecafluoro groups on the 4 fused benzo subunits of the phthalocyanine ring. The electron withdrawing substituents on the Pc ring leads to greater π-acceptor capabilities and the π-delocalization results in a stabilisation of the metal d_π orbitals (1_{eg}). Compared to the unsubstituted Pc ring, the presence of the electron withdrawing groups pull even more electron density away from the metal accounting for the additional process observed at higher redox potentials. The potentials at which these processes are observed are comparable with similar CoPc derivatives; Ünlü *et al*. report comparable redox potentials for a Co(II) phthalocyanine with fluorophenoxy substituents.[28] The metal based oxidation for the Co(II)/Co(III) redox couple is observed at 0.77 V vs. Fc/Fc^+ (1.13 V vs. SCE). Koca *et al.* also report oxidation potentials slightly more positive at 0.87 V vs. Fc/Fc^+ (1.23 V vs. SCE) for a Co(II) phthalocyanine with long chain chlorobenzyl substituents on each of the 4 fused benzene rings.[30] Similarly Golovin *et al.* describe the oxidation potentials of $Co(II)PcCl_{16}$ to be more positive than those of the unsubstituted Co(II) phthalocyanine, observed at 0.68 V vs. Fc/Fc^+ (1.09 V vs. Ag/AgCl, DPV).[29] It is clear that substituting metal (II) phthalocyanines which can undergo metal based oxidations with electro withdrawing substituents causes a shift to more positive potentials.

The assignments of such processes reported by Koca[11,30,31] and Ünlü[28] are based on spectroelectrochemistry in which a typical oxidative spectrum of a Co(II)Pc can reveal an increase in both the Q band and the B bands in the 400–500 nm region and an accompanying red shift to lower energy, indicative of the removal of an electron from the metal centre. Ring based oxidative processes are shown by a decrease of the Q band and appearance of other absorbance bands.

In DMSO, several cathodic processes were observed within the available potential window. The redox potentials and peak-to-peak separations are listed in Table 3.1

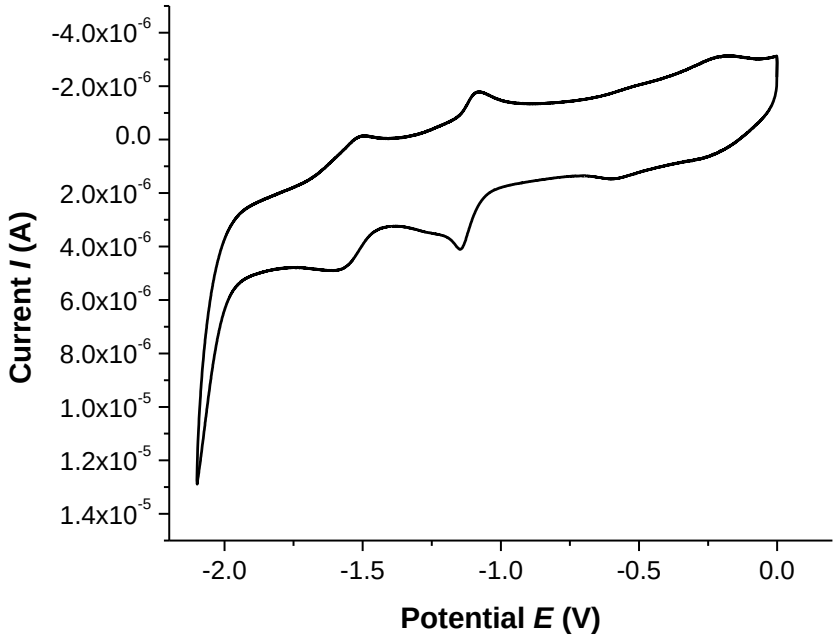

Figure 3.5: *Cyclic voltammogram of the reductions of $CoPcF_{16}$ at a GC electrode vs. Ag/Ag^+, using 0.1 M $TBAPF_6$ in DMSO. Scan rate: 100 mV/s.*

There are three processes evident in the voltammogram shown in Figure 3.5. The process observed at the least negative potential, E_{pc} = -0.54 V vs. Ag/Ag^+ does not appear to be electrochemically reversible at this scan rate as the peak to peak separation for this process with the corresponding anodic wave is larger than 59 mV/n. The reduction potentials of the Co(II) phthalocyanine substituted with fluorophenoxy substituents described by Ünlü *et al.*[28] and for Co(II) phthalocyanines with fluorinated aryloxy groups reported by Koca *et al.*[11] are comparable to some of the processes observed here. Thus this process is attributed to the addition of an electron to the metal 1_{eg} orbital, Figure 3.1. The metal dπ (1_{eg}) can experience a metal based reduction due to the position of this level, hence the first reduction process at -0.54 V vs. Ag^+ is assigned as Co(II) + e^- → Co(I).

Thus the remaining 2 cathodic processes are attributed to the phthalocyanine ring, which is in good agreement with previous reports.6,[11,22,23,30,31] These reduction waves are indicative of a reversible redox processes where a one electron reversible process exhibits a peak to peak separation of 59 mV (however it is not uncommon to observe separation values of 60-100 mV/n).

The electron-withdrawing properties of the fluorine substituents cause a shift to less negative potentials, -0.95 V compared to -1.07 V vs. Fc/Fc^{+} in the absence of the fluorine atoms. In the potential window shown in Figure 3.5, the reductive processes can be observed at -1.11 V and -1.54 V vs. Ag/Ag^{+}. Such potentials reported for the MPc's appear to be characteristic of phthalocyanines bearing fluoro-moieties.[10,31,32] As described for the assignments of the oxidative processes, these assignments are based on spectroelectrochemistry in which reduction of Co(II)Pc to form Co(I)Pc, results in a shift of the Q band to longer wavelengths with a simultaneous decrease in intensity and development of a new absorption band between the Q and B bands in the 400–500 nm region. This new absorption band is associated with the metal-to-ligand charge transfer (MLCT) from Co(I) to the Pc ring.[33]

3.2.2.2 Copper (II) Hexadecafluorophthalocyanine $CuPcF_{16}$

Copper phthalocyanines can only undergo ring based reductions due to the positioning of the HOMO/LUMO energies. For this complex it was expected that one oxidation process would be observed for the Pc ring and the appearance of two cathodic waves was also expected attributed to the reduction of the Pc ring. The electrochemistry of $CuPcF_{16}$ reveals one oxidation and two reductions which is in agreement with the predicted behaviour.

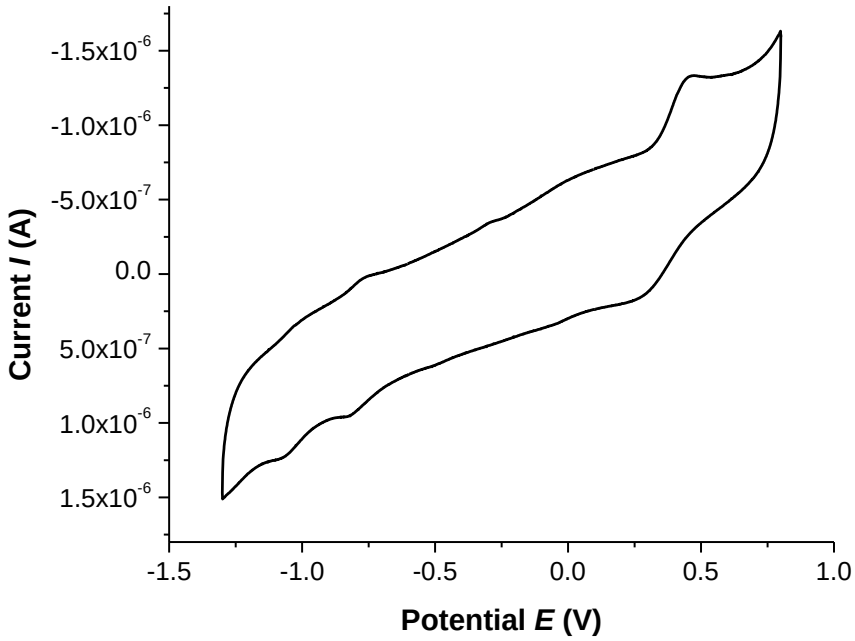

Figure 3.6: *Cyclic voltammogram of both the oxidation and reductions of $CuPcF_{16}$ at a GC electrode vs. Ag/Ag^+, using 0.1 M $TBAPF_6$ in DMSO. Scan rate: 100 mV/s.*

The anodic process is observed at 0.37 V vs. Ag^+ with a peak to peak separation of 160 mV. Lever *et al.* report that metallophthalocyanines in solution can experience the removal of two electrons on the phthalocyanine ring, where the oxidation state of the ring becomes Pc(0).[1] Referring back to Figure 3.1 which presents the molecular orbital energies of the three hexadecafluoro substituted metallophthalocyanines, it is apparent that the oxidation and reductions reactions can only occur on the a_{1u} and 2_{eg} orbitals of the Pc ring.

Thus the removal of the electron takes place on the a_{1u} (HOMO) orbital and is assigned as a 2 electron oxidation ($Pc^{(2-)} \rightarrow Pc^{(0)}$). Comparing the Cu and Co phthalocyanines, the Co exhibits a reversible Pc ring process at a more positive oxidation potential (0.67 V vs. Ag^+) than for Cu (0.37 V vs. Ag^+).

Two reduction processes are observed in Figure 3.6, which was expected. These two cathodic processes at –0.80 V and -1.05 V vs. Ag/Ag^+ exhibit Nernstian behaviour. The reduction reactions occur as follows: $Pc^{(2-)} \rightarrow Pc^{(3-)} \rightarrow Pc^{(4-)}$. Comparing the cathodic potential of the unsubstituted CuPc which occurs at -1.29

V vs Fc/Fc^+ with the first reduction process for $CuPcF_{16}$ at -1.21 V vs. Fc/Fc^+ (-0.80 V vs. Ag^+), these potentials are in good agreement. The slight shift towards less negative potentials for $CuPcF_{16}$ is attributed to the electron withdrawing nature of the fluorines. The electrochemical behaviour of this complex can be compared to the existing literature of similar MPc's. Günsel *et al*. reported comparable redox potentials for a Cu(II) phthalocyanine with tetra-fluorophenoxy substituents.[34] The cathodic processes occurring at -0.75 V, -1.05 V and -1.85 V vs. SCE were attributed to ring based reductions. Similar to the experimental results presented here, these potentials are shifted in a positive direction due to the enhanced π-acceptor properties of the substituents. Spectroelectrochemical studies carried out by Koca *et al.* report ring based reduction for a Cu(II) phthalocyanine bearing trifluorophenoxy substituents. These three Pc ring based reductions, $Pc^{(2-)} \rightarrow Pc^{(3-)}$, $Pc^{(3-)} \rightarrow Pc^{(4-)}$ and $Pc^{(4-)} \rightarrow Pc^{(5-)}$ are observed by a decrease in the Q band in the 650-690 nm regions with a corresponding increase in absorbance bands in the 500 and 700 nm regions; indicative of the addition of an electron on the Pc ring.[3]

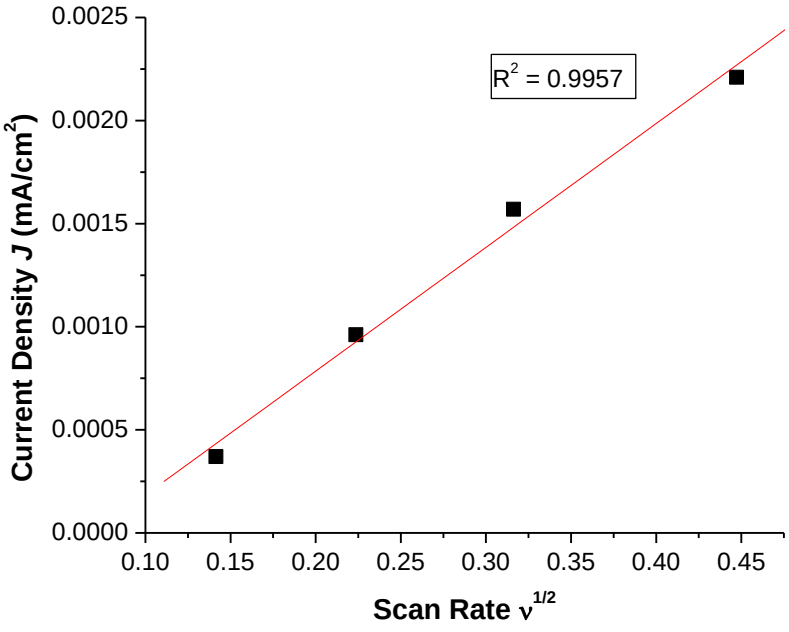

Figure 3.7: *Plot illustrating the relationship between the current density, J, of the first cathodic process, with the square root of the scan rate, $v^{1/2}$ for $CuPcF_{16}$.*

For $CuPcF_{16}$, the anodic process at 0.37 V and the two reductions at -0.80 V and -1.05 V vs. Ag/Ag^+ were observed to exhibit linear peak current versus square root of scan rate dependence (see Figure 3.7). For simplicity, the plot of scan rate vs. current density is only shown for the first cathodic process, however the plot for the oxidation and second reduction show the same behaviour as the one shown above.

3.2.2.3 Zinc hexadecafluorophthalocyanine $ZnPcF_{16}$

Zinc phthalocyanines can undergo both ring based oxidations and reductions. For this perfluorinated ZnPc under investigation here and examination of the redox potentials observed for the unsubstituted ZnPc displayed in Table 3.1, it was expected that one oxidation process would be observed (occurring on the Pc ring). While for the reduction processes, the appearance of two cathodic waves was expected. The behaviour of this complex was expected to display processes similar to those exhibited by $CuPcF_{16}$ (discussed above). The electrochemistry of $ZnPcF_{16}$ reveals one irreversible oxidation, Figure 3.8 and reductions, Figure 3.9.

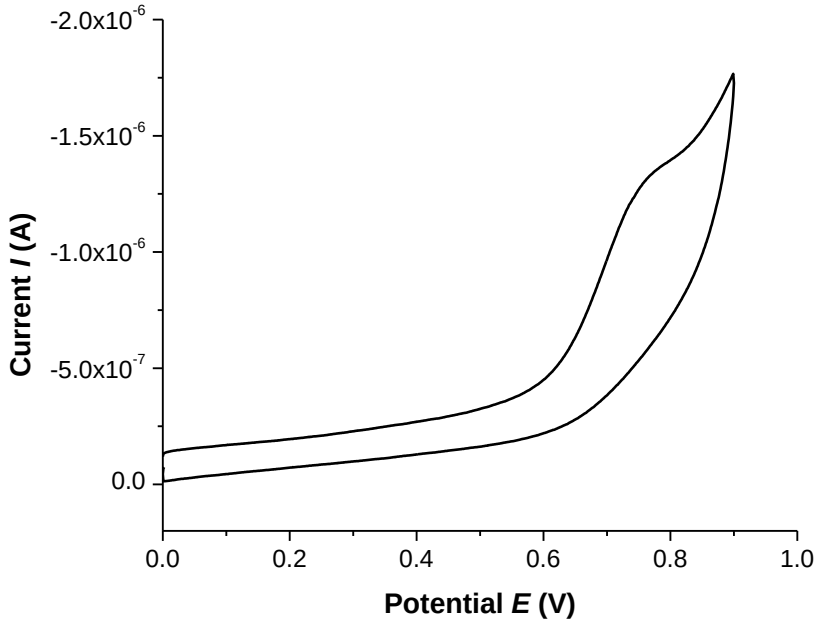

Figure 3.8: *Cyclic voltammogram of the oxidation of $ZnPcF_{16}$ at a GC electrode vs. Ag/Ag^+, using 0.1 M $TBAPF_6$ in DMSO. Scan rate: 100 mV/s.*

The anodic process observed at 0.77 V vs. Ag/Ag^+ is assigned as a ring based oxidation, $Pc^{(2-)} \rightarrow Pc^{(1-)}$. Koca *et al*. report comparable redox potentials for a Zn(II) phthalocyanine with tri-fluorophenoxy substituents; the anodic process at 0.66 V vs. SCE is attributed to a ring based oxidation.[31] Replacement of the tri-fluorophenoxy substituents with tetra- and penta-fluorophenoxy moieties causes the oxidation potential to increase to 0.79 V and 0.99 V vs. SCE respectively.[11] This is a result of the electron-withdrawing nature of the fluorinated groups, requiring more energy to remove an electron from the ring, as the number of fluorine atoms on the ring increases.

Comparing this $ZnPcF_{16}$ complex to $CoPcF_{16}$, the Zn exhibits an irreversible Pc ring process at +0.77 V vs. Ag/Ag^+ which is similar to the potential of the ring based oxidation of $CoPcF_{16}$ at +0.67 V vs. Ag/Ag^+.

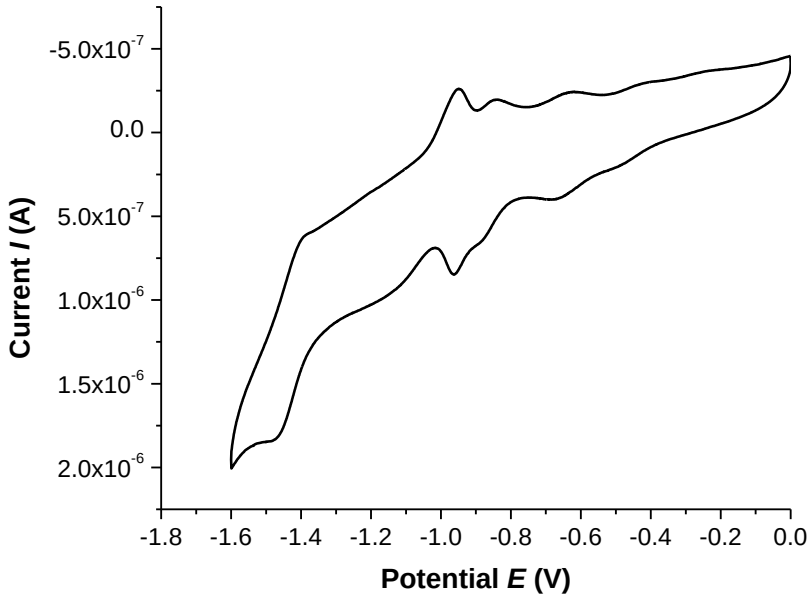

Figure 3.9: *Cyclic voltammogram of the reductions of $ZnPcF_{16}$ at a GC electrode vs. Ag/Ag^+, using 0.1 M $TBAPF_6$ in DMSO. Scan rate: 20 mV/s.*

Four prominent reduction processes can be observed from cyclic voltammogram, at $E_{½}$ = -0.65 V, -0.86, -0.96 V and -1.43 V as shown above in Figure 3.9. The appearance of 4 reduction processes was not expected and without the use of spectroelectrochemistry, assigning each of these processes is difficult. However, comparing the cathodic potentials of CuPc and CoPc, it appears that the reduction

potentials of the Cu are mostly similar to this Zn phthalocyanine, as both exhibit ring based reduction processes. These potentials are also similar to those reported for the unsubstituted analogues. Koca *et al*. report similar cathodic potentials for a Zn(II) phthalocyanine with penta-fluorophenoxy moieties.[3] The reductions occurring at -0.63 V and -1.03 V vs. SCE are attributed to a ring based reduction. Hesse *et al*. also describe the reduction potentials observed for a similar fluoro-substituted phthalocyanine at -0.60 V, -0.90 and -1.9 V vs. SCE.[35] These processes are in good agreement with the experimental potentials for this $ZnPcF_{16}$ phthalocyanine.

3.2.3 Electrochemical Characterisation- Redox Properties of Immobilised MPc's

Cyclic voltammetry was employed in the characterisation of these complexes immobilised on a glassy carbon electrode. The redox potentials for each of the three metallophthalocyanines are listed in Table 3.2. Preparation of these modified electrodes is described in the experimental section of Chapter 2. A further discussion will be given in Chapter 4, describing the cyclic voltammograms and onset potentials for the electrocatalytic currents.

Complex	Reduction E ½ (V) vs. Ag/AgCl	E_{pc}- E_{pa} (mV)
$CoPcF_{16}$	-0.43	70
$CuPcF_{16}$	-0.30	30
$ZnPcF_{16}$	-0.27	120

Table 3.2: *Electrochemical potentials of the metallophthalocyanines (vs Ag/AgCl) at 100 mV/s. Experiments performed in 0.1 M NaH_2PO_4/H_3PO_4 (pH 2).*

3.2.3.1 Electrochemical Characterisation- Cobalt hexadecafluorophthalocyanine $CoPcF_{16}$

The cyclic voltammogram of Co (II) phthalocyanine adsorbed on a glassy carbon working electrode is shown in Figure 3.11. A well resolved reversible redox couple at -0.43 V vs. Ag/AgCl, with a peak to peak separation of 70 mV is observed. Comparing this cathodic wave with the assignment in solution phase, this reduction is attributed as the one electron reduction of the Co(II)/Co(I) process. The reduction potential of the adsorbed metallophthalocyanine lies at approximately 110 mV less negative than in solution.

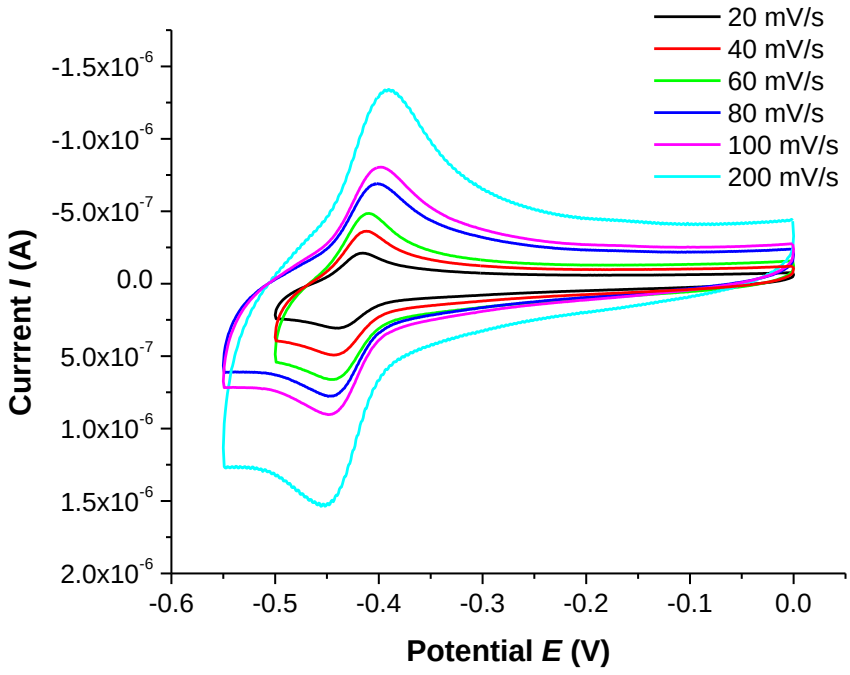

Figure 3.11: *Cyclic voltammogram of $CoPcF_{16}$ modified electrode vs. Ag/AgCl in 0.1 M NaH_2PO_4/H_3PO_4 (pH 2). Scan rates: 20mV/s- 200 mV/s.*

3.2.3.2 Copper and Zinc hexadecafluorophthalocyanine ($CuPcF_{16}$ and $ZnPcF_{16}$)

The cyclic voltammograms of both Cu and Zn (II) phthalocyanines adsorbed on GCEs are shown in Figure 3.12. Cu and Zn both exhibit ring based reductions

only as the 1_{eg} orbital of these metals do not lie in the energy gap of the a_{1u} and 2_{eg} orbitals. Cu displays a well resolved redox couple at -0.30 V vs. Ag/AgCl, with a peak to peak separation of 30 mV. A broader cathodic wave is observed for Zn at a slightly less negative potential of -0.27 V vs. Ag/AgCl. The peak to peak separation for the addition of an electron to the Pc ring of the Zn complex is 120 mV. Comparing these cathodic waves to the corresponding reduction process in solution phase, there appears to be an anodic shift for both processes. The reduction potential of the adsorbed metallophthalocyanine lies at approximately 400 mV less negative than in solution while the largest shift is revealed by the reduction of Cu(II) to Cu(I) which occurs in solution almost 500 mV more negative than the adsorbed phthalocyanine.

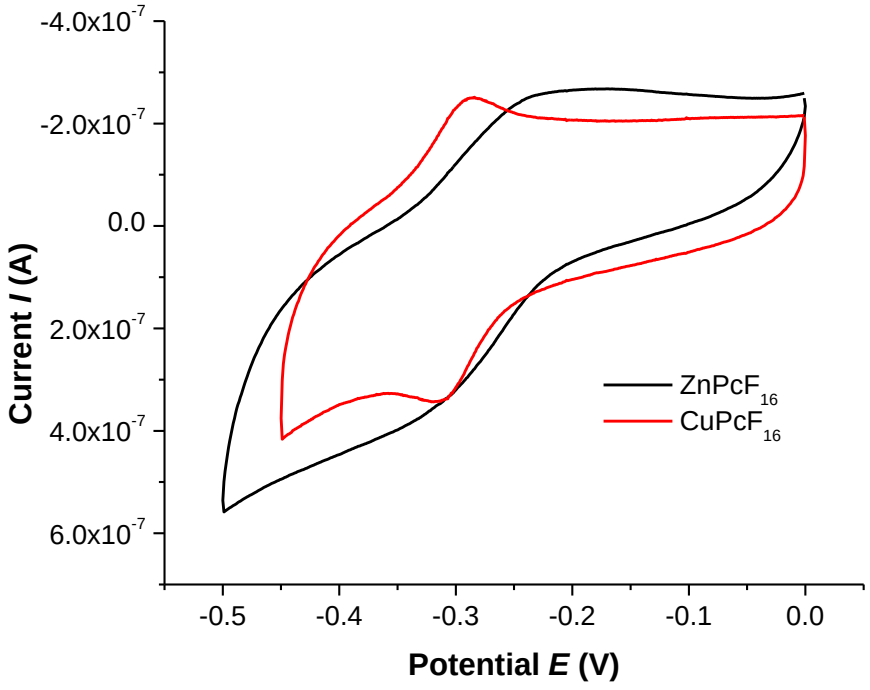

Figure 3.12: *Cyclic voltammograms of $CuPcF_{16}$ and $ZnPcF_{16}$ modified electrodes in 0.1 M NaH_2PO_4/H_3PO_4 (pH 2), vs. Ag/AgCl. Scan rate: 100mV/s*

Scan rate dependence studies are displayed in Appendix B, Figures B.3-B.4 for each of these catalysts.

3.2.4 Characterisation of the Electrocatalytic activity

Scanning to further negative potentials (0 to -0.8 V vs. Ag/AgCl) reveals an additional return wave with an E_{pa} = -0.6 V and the appearance of the well resolved Co(II)/Co(I) process observed in the smaller potential window (0 V to -0.6 V vs. Ag/AgCl) changes to a broader process, Figure 3.13 inset. The additional return wave is most likely attributed to the reduction of the Pc ring, however the E_{pc} is not clearly observed. It is suggested that this occurs at a potential close to the onset of the catalytic process at -0.90 V. A sharp catalytic current displayed at -1.2 V vs. Ag/AgCl is indicative of the consumption of protons with the simultaneous evolution of H_2.

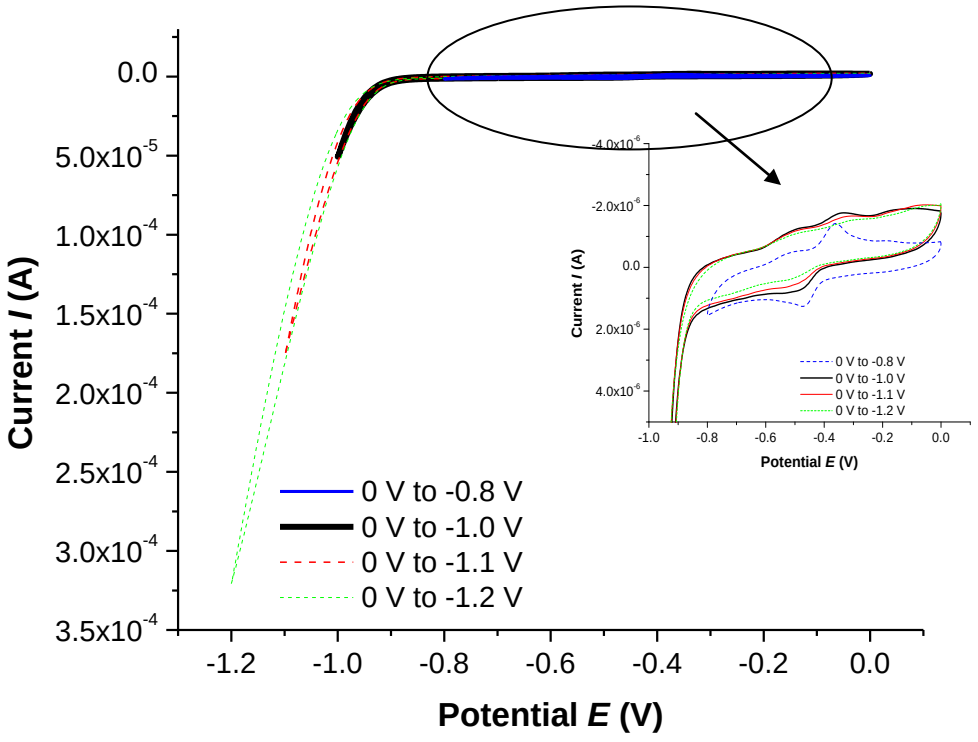

Figure 3.13: *Electrocatalytic activity of the adsorbed $CoPcF_{16}$ modified GCE over a range of potential windows in 0.1 M NaH_2PO_4/H_3PO_4 (pH 2) vs. Ag/AgCl. Scan rate: 100 mV/s.*

The same catalytic response can be seen for both $CuPcF_{16}$ and $ZnPcF_{16}$ upon scanning in a negative direction, Figures 3.14 and 3.15. However, no additional ring based processes are observed, unlike Co. The catalytic current for Cu appears

to commence at a slightly less negative potential of -0.83 V compared to that for Co, whilst this onset potential for the Zn phthalocyanine appears marginally more negative, -0.85 V. The currents observed are enhanced greatly at potentials beyond the onset potential, indicative of the catalytic current for the generation of H_2.

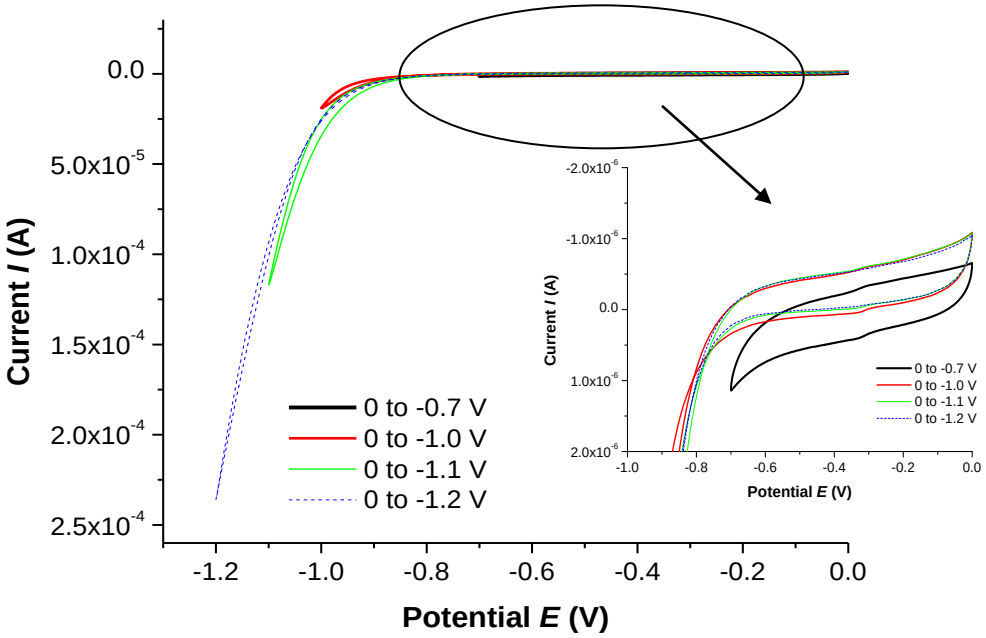

Figure 3.14: *Electrocatalytic activity of the adsorbed $CuPcF_{16}$ modified GCE over a range of potential windows in 0.1 M NaH_2PO_4/H_3PO_4 (pH 2) vs. Ag/AgCl. Scan rate: 100 mV/s.*

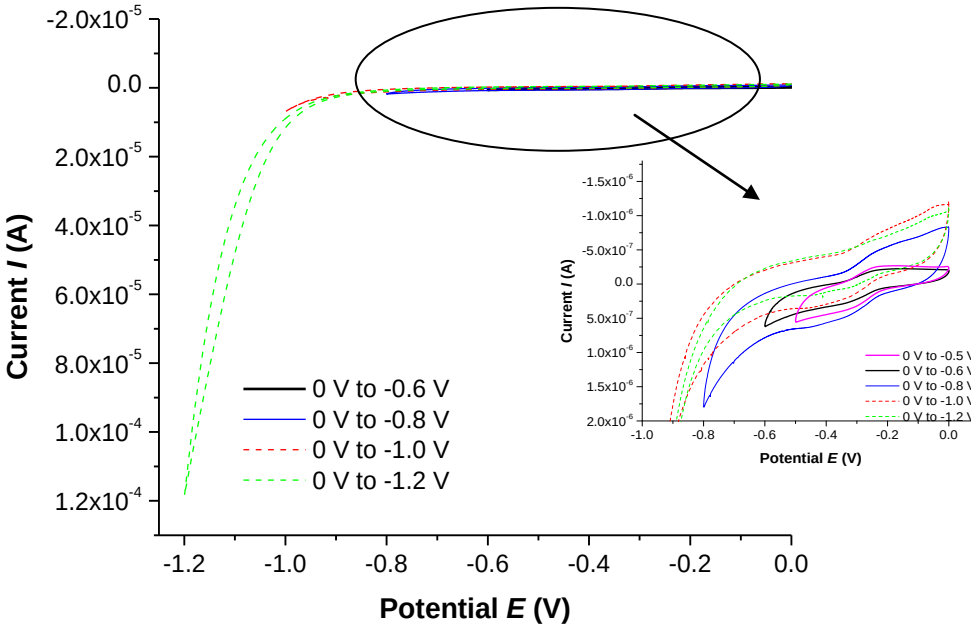

Figure 3.15: *Electrocatalytic activity of the adsorbed $ZnPcF_{16}$ modified GCE over a range of potential windows in 0.1 M NaH_2PO_4/H_3PO_4 (pH 2) vs. Ag/AgCl. Scan rate: 100 mV/s.*

3.3 Concluding Remarks

Cobalt, copper and zinc perfluorinated phthalocyanines were characterised by absorbance spectroscopy and cyclic voltammetry. The expected electrochemical behaviour was observed. Comparing these potentials to those displayed by the unsubstituted MPc's reveals a shift in potentials. For $CoPcF_{16}$, two oxidation processes are assigned as the removal of an electron from the metal followed by the Pc ring. Three cathodic processes are displayed, attributed to the addition of an electron to the metal and Pc ring. Copper and zinc display ring based oxidations and reductions. This is a result of the position of the HOMO and LUMO energies with respect to the Fermi level of the electrode.

When these catalysts are immobilised on a glassy carbon electrode, the redox potentials are observed. For $CoPcF_{16,}$ the metal based reduction is 100 mV more negative compared to $CuPcF_{16}$ and $ZnPcF_{16.}$ The electrocatalytic activity is introduced; the cyclic voltammograms reveal a sharp increase in the cathodic current at ~ -1.2 V, with an onset potential at approximately -0.90 V, indicative of the catalytic proton reduction reaction to H_2.

3.4 References

[1] A. B. P. Lever, *J. Porphyr. Phthalocya., 3*, **1999**, 488.

[2] A. B. P. Lever, P. C. Minor, *Inorg. Chem. 20*, **1981**, 4015.

[3] A. Koca, *Electrochem. Commun., 11*, **2009**, 838.

[4] M. K. Şener, A. Koca, A. Gül, M.B. Koçak, *Polyhedron, 26*, **2007**, 1070.

[5] A. Koca, M.K. Şener, M.B. Koçak, A. Gül, *Transit. Metal Chem., 30,* **2005,** 399.

[6] A. Koca, Ş. Bayar, H.A. Dinçer, E. Gonca, *Electrochim. Acta, 54,* **2009,** 2684.

[7] M. Ozer, A. Altindal, A.R. Özkaya, M. Bulut, Ö. Bekaroglu *Polyhedron, 25,* **2006**, 3593.

[8] F. Zhao, J. Zhang, D. Wöhrle, M. Kaneko, *J. Porphyr. Phthalocya.,4*, **2000**, 31.

[9] A. Koca, M.K. Şener, M.B Koçak, A. Gül, *Int. J. Hydrogen Ener., 31*, **2006**, 2211.

[10] A. Alemdar, A. R. Özkaya, M. Bulut, *Polyhedron, 28*, **2009**, 3788.

[11] A. Koca, M. Özçeşmeci, E. Hamuryudan, *Electroanal., 22*, **2010**, 1623.

[12] M. S Liao, T. Kar, S. M. Gorun, S. Schneiner, *Inorg. Chem., 43*, **2004**, 22, 7151.

[13] E. Kol'tsov, T. Bosova, P. Semyannikov, I. Igumenov, *Mats. Chem. Phys., 86*, **2004**, 222.

[14] H. Ogata, R. Higashi, N. Kobayashi, *J. Porphyr. Phthalocya., 7*, **2003**, 551.

[15] (a) L. Edwards, M. Gouterman, *J. Mol. Spectr., 33,* **1970,** 293. (b) M. J. Stillman, A. J. Thomson, *RSC.* **1974,** 790. (c) F. Ma, S. Wang, X. Li, *J. Phys. Chem. Solids, 73*, **2012**, 589.

[16] S. Mho, B. Ortiz, S. M. Park, D. Ingersoll, N. Doddapaneni, *J. Electrochem. Soc., 142, 5,* **1995,** 1436.

[17] M. Handa, A. Suzuki, S. Shoji, K. Kasuga, K. Sogabe, *Inorg. Chim. Acta, 230*, **1995**, 41.

[18] I. Yilmaz, M. B. Koçak, *Polyhedr., 23*, **2004**, 1279.

[19] A. J. Bard, L.R. Faulkner, *Electrochemical Methods: Fundamentals and Applications*, 2nd Ed., John Wiley & Sons, Inc., **2001,** USA.

[20] J. Wang, *Analytical Electrochemistry*, 2nd Ed., Wiley-VCH, **2001**, New York, USA.

[21] C. M. A. Brett, A. M. O. Brett, *Electrochemistry: principles, methods and applications, 1st Ed.*, Oxford science publications, **1993,** USA.

[22] A. Wolberg, J. Manassen, *J. Am. Chem. Soc.*, *92*, **1970**, 10, 2982.

[23] A. B. P. Lever, J. P. Wilshire, *Can. J. Chem.*, *54*, **1976**, 2514.

[24] P. Turek, P. Petit, J-J. André, J. Simon, R. Even, B. Boudjema, G. Guillaud, M. Maitrota, *J. Am. Chem. Soc.*, *109*, **1987**, 5119.

[25] D. T. Sawyer, A. Sobkowiak, J.L. Roberts Jr, *Electrochemistry for chemists*, 2nd Ed., John Wiley & Sons Ltd., **1995**, New York, USA.

[26] S. H. Kim, *Functional Dyes*, Elsevier, **2006**, Amsterdam.

[27] A. B. P. Lever, E. R. Milaeva, G. Speier; *Phthalocyanines: Properties and Applications*, VCH, 3, **1993**, New York, USA.

[28] S. Ünlü, M. Yaraşir, M. Kandaz, A. Koca, B. Salih, *Polyhedron*, *27*, **2008,** 2805.

[29] M. N. Golovin, P. Seymour, K. Jayaraj, Y. Fu, A. B. P. Lever, *Inorg. Chem.*,*29*, **1990**, 1719.

[30] A. Koca, A. Kalkan, Z. A. Bayir, *Electroanal.*, *22*, **2010**, 3, 310.

[31] A. Koca, A. Kalkan, Z. A. Bayir, *Electrochimica Acta, 56*, **2011**, 5513.

[32] A. T. Bilgiçli, M. Kandas, A. R. Özkaya, B. Salih, *Heteroatom Chem.*, *20*, **2009**, 5, 262.

[33] N. Kobayashi, S-I. Nakajima, H. Ogata, T. Fukuda, *Chem. Eur. J., 10*, **2004**, 6294.

[34] A. Günsel, M. Kandaz, A. Koca, B. Salih, *J. Fluor. Chem., 129*, **2008,** 662.

[35] K. Hesse, D. Schlettwein, *J. Electroanal. Chem.*, *475*, **1999**, 148.

Chapter Four

Factors Influencing the Electrocatalytic Generation of Hydrogen using modified Metal (II) Perfluorinated Phthalocyanine Electrodes

The electrocatalytic generation of H_2 from water using modified electrodes of metal (II) perfluorinated phthalocyanine complexes where M is Co, Cu and Zn are discussed. Various parameters influencing the electrocatalytic activity were investigated including pH, temperature, choice of solvent, volume of coatings, number of coatings and applied electrolysis potential.

The performance of each of the three catalysts was evaluated by TOF (hr^{-1}) and current density. The results generated were significantly higher compared to the data for unsubstituted CoPc reported by Kaneko et al., reaching a TOF (hr^{-1}) as high as 2×10^5. The catalyst which exhibited the highest TOF (hr^{-1}) reaching 3.5×10^6 was $CuPcF_{16}$ at $20^{\circ}C$ in pH 2 aqueous solution. $CoPcF_{16}$ displayed the largest current density for the electrocatalytic reaction while $ZnPcF_{16}$ required the least overpotential to electrocatalytically produce H_2.

4.1 Introduction

Metal phthalocyanine derivatives have been studied as potential candidates for solar energy devices. The potential for application of these MPc's owes to their electronic properties; their ability to efficiently transfer electrons to facilitate electrocatalytic reactions, such as the hydrogen evolution reaction and the more challenging, reduction of carbon dioxide to useful fuels. [1,2,3,4,5]

For the work conducted in this thesis, three metals were chosen to investigate the role of the central metal ion for the catalytic reduction of H^+ in aqueous solutions. The three metal ions, Co^{2+}, Cu^{2+} and Zn^{2+} have electronic configurations of d^7, d^9 and d^{10} respectively, thus the positions of the molecular orbitals lie at different energies. It has been documented that if the central metal has no available *d* orbital levels which fall within the HOMO-LUMO energy gap of phthalocyanine ring, the metal cation will not be involved when the complex is either oxidised or reduced, therefore the electrocatalytic process can be mediated by the phthalocyanine ring itself.[6] Originally however it was assumed that redox-active metals are required to catalyse hydrogen evolution such as Mn(II), Fe(II) and Co(II) which undergo metal-based reductions as well as ligand-based reductions.[7,8,9,10,11] Metals which experience no metal based reductions include Ni(II), Zn(II), Pb(II), Pd(II), and Cu(II).[7,11,12,13]

This chapter will discuss the results of the investigations performed using $CoPcF_{16}$, $CuPcF_{16}$ and $ZnPcF_{16}$. The effects of various parameters which influence the electrocatalytic hydrogen evolution reaction are presented. Additional experimental considerations are also discussed. All TOF (hr^{-1}) figures presented in this chapter are calculated by values obtained by gas chromatography. Faradaic efficiencies discussed here are calculated using TOF (hr^{-1}) values obtained by gas chromatography and TOF (hr^{-1}) values determined by electrochemistry. These electrochemical TOF (hr^{-1}) values are located in Appendix C.

4.2 Results and Discussion

4.2.1 Characterisation-Cyclic voltammetry and onset potential

The characterisation and peak assignments for each of the three metallophthalocyanines considered in this chapter have been previously discussed in Chapter 3. The potentials for which the redox processes of metallophthalocyanines are commonly reported for adsorbed films on various electrode materials. [14] The cyclic voltammogram displayed in Figure 4.1 represents GCEs modified with $CoPcF_{16}$, $CuPcF_{16}$, $ZnPcF_{16}$ and a bare, uncoated GCE in acidic phosphate (0.1 M NaH_2PO_4/H_3PO_4) electrolyte at pH 2 measured under argon.

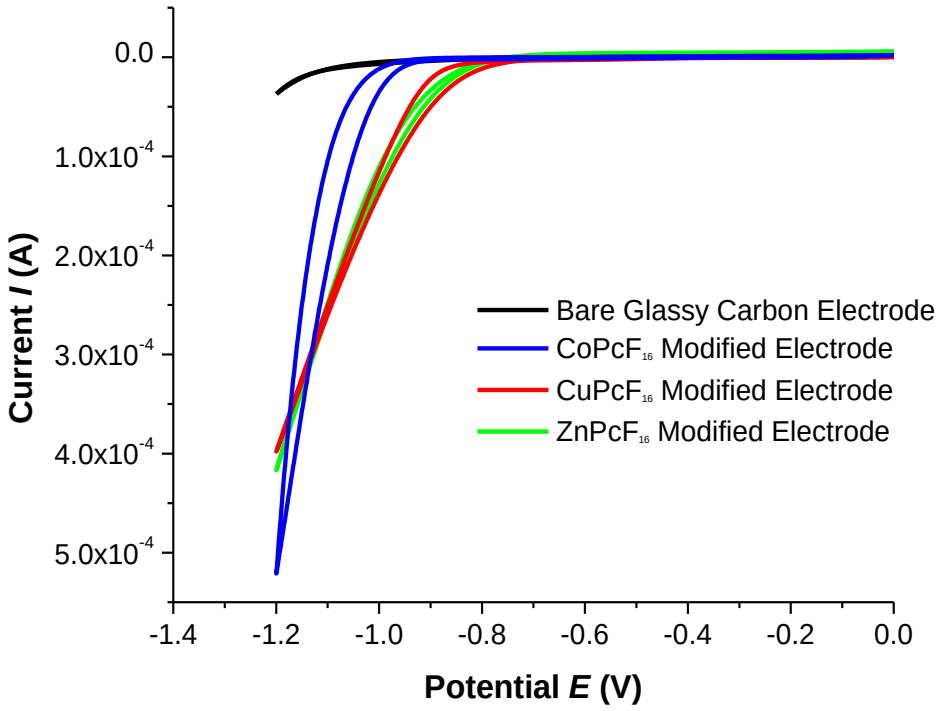

Figure 4.1: *Comparison of typical currents observed in the potential window of 0 to -1.2 V vs. Ag/AgCl for electrodes modified with $CoPcF_{16}$, $CuPcF_{16}$, $ZnPcF_{16}$ and a bare GCE. Scan rate = 100 mV/s in 0.1 M NaH_2PO_4/H_3PO_4 (pH 2) at 20°C.*

The onset for hydrogen evolution occurs at -0.45 V vs. Ag/AgCl when a bare Pt macro electrode is used in this buffer solution (see Appendix C, Figure C.10). At -0.7 V a maximum current of 6 x 10^{-4} A is observed with a corresponding current

density obtained by CV of 20.30 mA/cm^2 (based on the geometrical area of 0.03 cm^2). With this is mind, Figure 4.1 demonstrates the onset potentials for $MPcF_{16}$-modified electrodes. The cathodic current can be seen to increase at approximately – 0.83 V and -0.85 for $CuPcF_{16}$ and $ZnPcF_{16}$ respectively, while for $CoPcF_{16}$, the current increases substantially near -0.9 V. This behaviour suggests an electrocatalytic reaction, which in these experiments is due to the reduction of H^+ to H_2. As a measure of comparison, the same experiment was conducted on an uncoated (bare) GCE. The onset potential in these voltammograms was determined by examining the point at which the current significantly increases, hence for these experiments as shown in Figure 4.1 above, the onset potentials are said to be at the point of the first curvature of the E-i plot. In the absence of a catalyst, it can be seen that the current at this surface is much less than for the modified electrodes near -0.8 to -0.9 V. Even at a potential of -1.2 V, the current at the GC electrode is less than 10% of the current observed for the $CoPcF_{16}$ film. The overpotential may be quoted with respect to this bare electrode (see Chapter 2).[15,16] The potential which is required in order to produce a cathodic current of a similar magnitude in the phosphate electrolyte is approximately -1.4 V vs. Ag/AgCl. Thus these catalysts significantly lower the overpotential required for the electrocatalytic generation of hydrogen thus requiring less energy for promotion of the reaction.[13]

Electrode	Onset Potential (V)
Co	-0.90
Cu	-0.83
Zn	-0.85
Bare GCE	-1.10

Table 4.1: *Onset potentials (V) at which the catalytic current are observed vs. Ag/AgCl in 0.1 M NaH_2PO_4/H_3PO_4 (pH 2) at 20°C for $CoPcF_{16}$, $CuPcF_{16}$, $ZnPcF_{16}$ modified electrodes and an uncoated GCE.*

The maximum current observed at 100 mV/s for catalytic hydrogen evolution reaches a value of 5 x 10^{-4} A for $CoPcF_{16}$ and approximately 4 x 10^{-4} A for both $CuPcF_{16}$, and $ZnPcF_{16.}$ Although the largest catalytic current is observed for films of the Co catalyst, films of the Cu and Zn complexes (which exhibit only ring based reductions) display less negative onset potentials. From the onset potential for the bare GCE (about -1.10 V vs. Ag/AgCl) it can be deduced that the overpotential for electrocatalytic H_2 evolution in these experiments is reduced by at least 200 mV using electrodes modified with $MPcF_{16}$ films. Comparing these values to those obtained when a bare Pt electrode (see Appendix, Figure C.10) was used in an identical experiment, it appears that an overpotential of approximately 500 mV is required when the catalysts are employed (with respect to Pt).

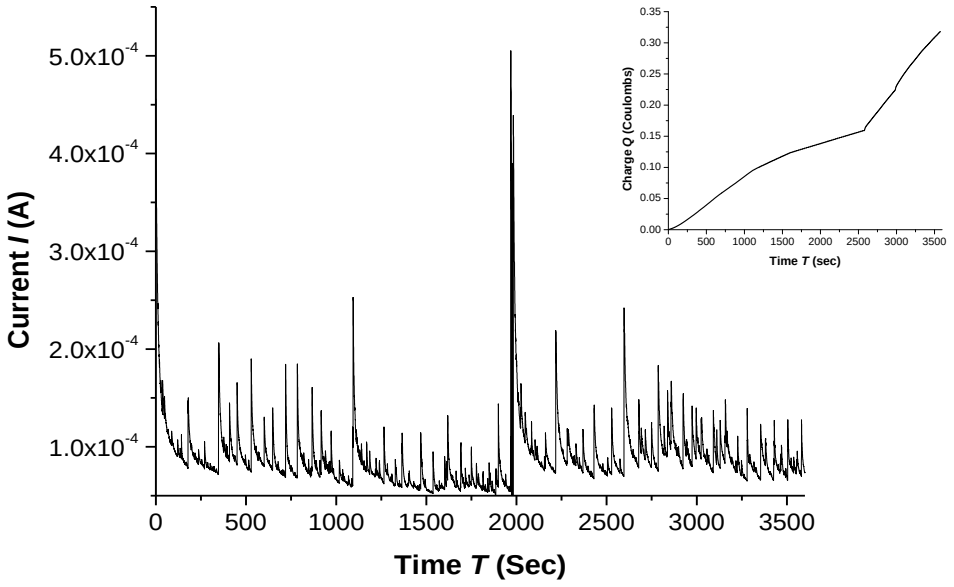

Figure 4.2*: Current- time profile (inset: charge-time profile) as a result of potentiostatic electrolysis of $CoPcF_{16}$ at -1.2 V vs. Ag/AgCl.*

Potentiostatic electrolyses were carried out under argon in the acidic phosphate buffer solution for the adsorbed metallophthalocyanines. A typical electrolysis experiment is shown in Figure 4.2, where the potential was fixed at -1.2 V for $CoPcF_{16}$ corresponding to the potential at which a large steep catalytic current was

observed. Investigating the optimum applied electrolysis potential was carried out in an effort to further reduce the overpotential for the generation of H_2, discussed in 4.2.2.1. The current-time profile for this type of experiment is shown in Figure 4.2. In this figure, the current appears to be very noisy due to the constant build up of small hydrogen bubbles occurring at the electrode surface. The bubbles block the working electrode surface and impede the electrocatalytic reaction, as shown in Figure 4.3.

Figure 4.3: *Images of experimental set up for the potentiostatic electrolysis of $CoPcF_{16}$ at -1.2 V vs. Ag/AgCl in 0.1 M NaH_2PO_4/H_3PO_4 (pH 2). The build up of hydrogen gas bubbles can be clearly seen on the working electrode.*

However when the hydrogen gas bubbles diffuse away, the working electrode (modified) surface is exposed, yielding a greater surface area for electron transfer and thus an immediate increase in the observed current. It was often necessary to manually tap the side of the electrochemical cell to "encourage" the hydrogen gas bubbles away from the surface of the electrode. As the current is related to the rate of electrolysis, it can be used to calculate the charge passed after any period of time during the reaction (charge is the integral of current with respect to time).

4.2.1.1 Surface Coverage of M(II)PcF_{16}

For each of the electrocatalysts discussed in this section, the volume of $MPcF_{16}$ solution applied to the working electrode was 1.5 uL. Thus for a solution of a

concentration of 2.8 x 10^{-5} M (for $CoPcF_{16}$) the number of moles of catalyst deposited on the surface of the electrode was calculated as 4.2 x 10^{-11} mol. The amount of electrochemically active catalyst in the coated layer was determined using the peak area of the M(II)/M(I) couple for $CoPcF_{16}$ (or $Pc^{(2-)}$/ $Pc^{(3-)}$ for $CuPcF_{16}$ and $ZnPcF_{16}$). The average percentage of this $CoPcF_{16}$ species which is electroactive on the electrode surface was calculated to be about 6% of the total amount deposited. Although this represents only a small fraction of material, Abe *et al*. reported similar findings in which 4% of CoPc coated on a basal plane pyrolitic graphite (BPG) working electrode was found to be electroactive.[17] For $CuPcF_{16}$ and $ZnPcF_{16}$, the average number of moles of catalyst coated on the surface of the electrode was calculated as 8.3 x 10^{-11} mol and 5.6 x 10^{-10} mol respectively. The average percentage of electroactive catalyst was found to be 0.1 % and 1 % for $ZnPcF_{16}$ and $CuPcF_{16}$ respectively. Although the percentage of active species for the Cu and Zn catalyst was lower compared to Co, the concentration of the catalyst solutions prepared are higher. The average surface coverage of each catalyst is shown below in Figure 4.4.4

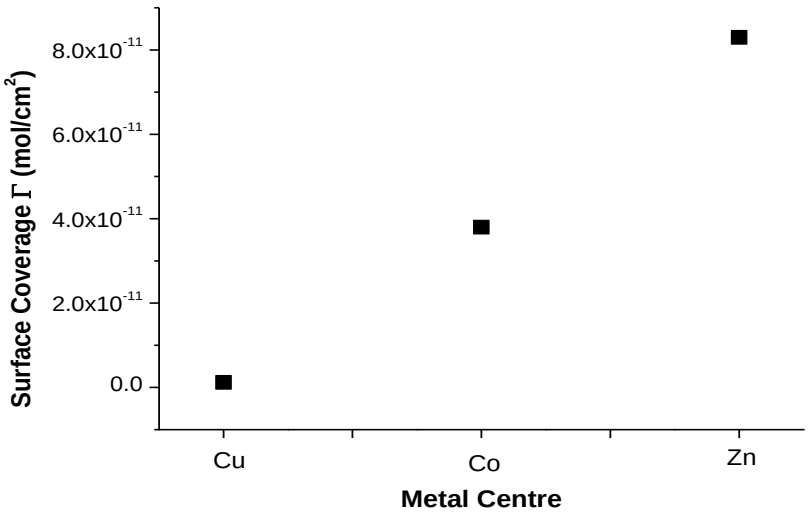

Figure 4.4: *Typical surface coverage Γ calculated for Co, Cu and Zn metallophthalocyanine complexes using the electrochemically active amount of catalyst, where the geometrical area of a glassy carbon electrode is 0.07 cm^2.*

It appears that for these types of metallophthalocyanines, only a small fraction of the catalyst participates in the electrocatalytic reaction. Investigations were carried out in an effort to increase the amount of electroactive species present in the modified layer, including coating the electrode surfaces with more than one "layer", increasing the volume of catalyst solution deposited and using a more volatile solvent to increase rate at which the solvent can evaporate, allowing for additional layers to be cast in a short amount of time. These investigations are discussed later in this chapter. Ouyang *et al.* reported the use of $CoPcF_{16}$ as an electrocatalyst for the reduction of O_2. However, in this work, it was found that approximately 33 % of the coated layer of the catalyst was electroactive, as determined by cyclic voltammetry when deposited on a BPG electrode.[18] Suguwara *et al*. reported similar findings to the catalysts employed in this thesis, where a lower percentage of catalyst is electroactive of ~3 %.[19] It has been proposed that the small percentage of catalyst which is electroactive in these layers is due to limited conductivity of metallophthalocyanines.[20,21] The various factors which appear to affect the electrocatalytic behaviour of the $MPcF_{16}$ modified electrodes in this thesis will be discussed for each of the three metallophthalocyanines. The results of these potentiostatic electrolysis experiments are discussed in terms of moles of hydrogen produced and TOF data.

4.2.1.2 Proposed Reaction Pathways

In this thesis, the centre of attention has been the optimisation of the electrocatalytic behaviour of the modified electrodes. No specific experiments were carried out to investigate the reaction pathway of this process. However in the literature,[22] such mechanisms have been proposed and are suitable for the compounds studied in this thesis. For $CoPcF_{16}$ modified electrodes, the reaction pathway for hydrogen evolution is assumed to occur in a manner described by Kaneko *et al*. for the unsubstituted CoPc modified electrodes.[14] Following the reduction of the metal centre, the charge on this reduced complex $[Co(I)Pc^{(-2)}F_{16}]^-$ needs to be compensated by cation migration from the electrolyte solution into the modifying layer, $[Co(I)Pc^{(-2)}F_{16}]^-H^+$. In aqueous media at pH 2, this charge

migration occurs in the form of protons from the bulk solution, as protons have a higher mobility than any other cations in the film. There are conflicting reports as to how the next step evolves. The formation of the proposed metal-hydride intermediate can occur after the first reduction. In acidic conditions, this pathway is plausible; however in neutral and basic conditions, the lower concentration of protons in the solution can hinder the formation of the metal hydride. The third step involves the reduction of the protonated anionic species $[Co(I)Pc^{(-2)}F_{16}]^{-}\cdot H^{+}$, where the addition of an electron takes place on the phthalocyanine ring $[Co(I)Pc^{(-3)}F_{16}]^{-}\cdot H^{+}$ with a subsequent protonation step $H^{+}\cdot H^{+}[Co(I)Pc^{(-3)}F_{16}]^{2-}$ to electrocatalytically evolve hydrogen.[2,14,23] This step is denoted EC, Scheme 4.1.

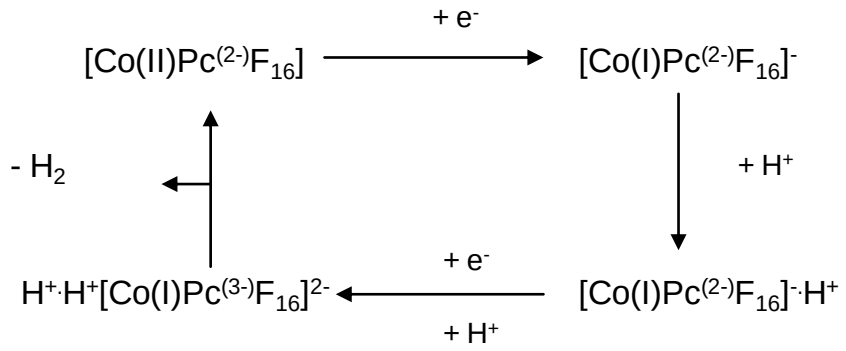

Scheme 4.1: *Proposed ECEC pathway for the electrocatalytic generation of hydrogen using $CoPcF_{16}$ as the catalyst in acidic conditions. (Pathway adapted from Kaneko, reference 14).*

When different pH's of an electrolyte solution are employed, the difference in electrocatalytic activity is due to the ability of the catalyst to bind a proton and to form a stable metal-hydride intermediate. In basic conditions, a third reduction of a di-anionic protonated species can occur with a second protonation step to subsequently eliminate hydrogen gas. This pathway has been proposed by Osmanbaş *et al.* who reported a Co based phthalocyanine bearing thiophenes which exhibited varied behaviour when aqueous electrolytes of varying pH are employed in these studies.[24]

For catalysts where no metal based reductions take place (i.e. $CuPcF_{16}$ and $ZnPcF_{16}$), the reductions can only occur on the phthalocyanine ring.[13,25] The proposed reaction pathway for these catalysts is described by Scheme 4.2, where

an *ECEC* route is suggested. The reaction pathway for hydrogen evolution proposed here is suggested to occur in a manner described by Koca *et al*. when modified electrodes consisting of CuPc and ZnPc derivatives were employed in these studies.[13,24,25]

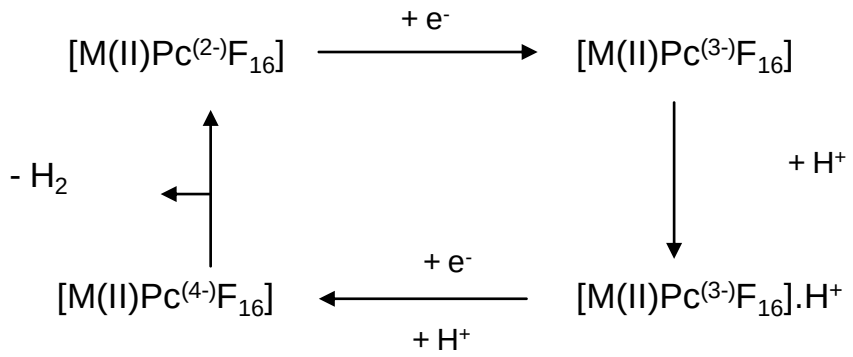

Scheme 4.2: *Proposed ECEC pathway for the electrocatalytic generation of hydrogen where M is Cu and Zn as the catalyst in acidic conditions. Pathway adapted from reference 23.*

4.2.2 Conditions affecting electrocatalytic generation of hydrogen

It is important to note that all the performance data given in these experimental chapters are based on several modified electrodes for each set of experiments, hence the performance data values are an average of a given number of modified electrodes.

4.2.2.1 Electrolysis potential

The potential at which the electrocatalytic reaction proceeds efficiently is an important factor, as it determines the energy cost for hydrogen evolution. In an ideal electrocatalytic system, a potential close to -0.2 V vs. Ag/AgCl would be all that is needed for the driving force for this reaction. Examination of the cyclic voltammograms of each of the catalysts reveals large cathodic currents which are attributed to H_2 evolution are observed at -1.2 V vs. Ag/AgCl (however, as noted, the onset potentials occurs at less negative potentials). These potentials have been utilised for the generation of hydrogen. Kaneko *et al.* reported a TOF of 2 x 10^5

hr^{-1} using an electrolysis potential of -0.9 V vs. Ag/AgCl for CoPc in a phosphoric acid at pH 1.[17] Similar potentials have been employed for other Cu and Zn phthalocyanines.[12,13,25]

Lower (more negative) applied potentials result in increased reaction kinetics, which is observed by the increasing TOF figures obtained for H_2 evolution (determined by GC measurements, Figure 4.5, charge passed in the electrolyses (Table 4.2 and Table 4.3) and current densities in Figure 4.6. (Additional TOF values in Appendix C, Tables C.1-C.3). It is important to reiterate that the charge passed in these experiments is likely to be complicated by the reduction of O_2 produced at the anode, by solvent oxidation. Without this complication, it would be possible to assess the Faradaic efficiency of the catalytic reactions (amount of H_2 determined by GC divided by amount of H_2 calculated from the charge passed during the electrolysis, multiplied by 100%). However, the design of the cells used in this work (no salt bridge, small physical separation (< 2.5 cm) between working and counter electrode) did not include measures aimed at impeding the movement of O_2 throughout the solution. This factor also limits the performance of the modified electrodes as H_2 evolution catalysts, since the O_2 reduction reaction will compete with H^+ reduction.[18,26,27] Interestingly, when potentials more negative than -1.1 V are applied for a $ZnPcF_{16}$-modified electrode, a decrease in catalytic activity (in terms of TOF values) is observed. It appears that the optimum electrolysis potential required for the electrocatalytic generation of hydrogen using $ZnPcF_{16}$ as the catalyst is -1.1 V vs. Ag/AgCl. Examination of the moles of hydrogen produced can further help to identify the optimum catalyst used for these studies.

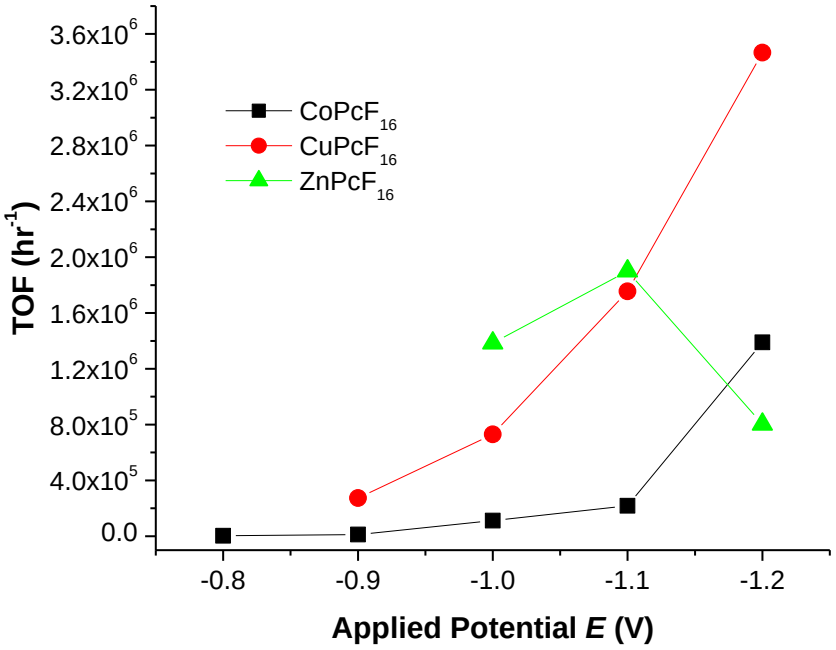

Figure 4.5: *Effect of applied potential on turnover frequencies TOF (hr^{-1}) obtained by gas chromatography for $CoPcF_{16}$, $CuPcF_{16}$ and $ZnPcF_{16}$ represented by the black, red and green lines respectively in 0.1 M NaH_2PO_4/H_3PO_4 (pH 2).*

The TOF values are shown in Figure 4.5 for all modified electrodes. The TOF values obtained increase with increasingly negative applied electrolysis potentials when $CoPcF_{16}$ is employed. For this catalyst, the highest TOF data are obtained at -1.2 V (1.9×10^6 (electrochemical) and 1.4×10^6 (gas chromatography)) while at -0.8 V, the lowest TOF was determined as 2.5×10^3. Analysis of the gas phase was carried out by injecting a volume of gas from the headspace of the electrochemical cell using a gas-tight syringe. Detection of hydrogen gas was achieved via gas chromatography using a thermal conductivity detector (see Chapter 2). There are a number of possible reasons for such low TOF values at less negative potentials, such as leakage of hydrogen gas from the electrochemical cell (which would matter more for experiments that produce less H_2). It is likely that the weaker performances are the result of a low driving force (i.e. applied potential) for the reaction to proceed because rate constants for electron transfer are potential-dependent. Greater overpotentials will yield higher currents and more product within a given timeframe.

Applied Potential (V)	***-0.8***	***-0.9***	***-1.0***	***-1.1***	***-1.2***
Charge (C)	*0.02*	*0.03*	*0.10*	*0.15*	*0.28*
Moles of H_2 (mol)	*3.1×10^{-9}*	*6.4×10^{-9}*	*7.6×10^{-8}*	*1.2×10^{-7}*	*1.2×10^{-6}*
Faradaic Efficiency (%)	*27*	*39*	*15*	*16*	*74*
[1]Current Density J (mA/cm^2)	*8×10^{-2}*	*0.1*	*0.4*	*0.6*	*1.1*
[2]Current Density J (mA/cm^2)	*2×10^{-2}*	*0.2*	*0.6*	*3.1*	*7.5*
(%) Electroactive Co	*4.0*	*3.7*	*4.2*	*4.6*	*6.3*

Table 4.2: *Average performance data obtained by CV and BE vs. Ag/AgCl for 1 hour for $CoPcF_{16}$ with varying electrolysis potentials in 0.1 M NaH_2PO_4/H_3PO_4 (pH 2). [1]Current density obtained using BE data and [2]current density obtained using the last scan of the CV.*

The TOF data for $CuPcF_{16}$ and $ZnPcF_{16}$ are shown in Figure 4.5. Analysis of the gas phase was performed and the measured amount of hydrogen and the resulting TOF data was determined as 1.7×10^6 when $ZnPcF_{16}$ is used (-1.1 V). When the electrolysis potential of -0.8 V was applied, the amount of H_2 gas present in the headspace was lower than the limit of detection for the TCD (100 ppm H_2). The performance indicators displayed in Table 4.3 reflect the poor activity at this electrolysis potential. The reduced activity of this catalyst at this potential was expected and is suggested to be the result of a low driving force for the reaction.

As mentioned above, $ZnPcF_{16}$ was found to exhibit some interesting applied potential-TOF behaviour. This is illustrated by the data obtained from cyclic voltammetry and electrolysis experiments (Table 4.3). The maximum TOF value was found for this modified electrode at -1.1 V (Figure 4.5). Since the TOF value

is calculated using the moles of electroactive catalyst, it is worth noting here that at a potential of -1.2 V, the amount of catalyst that underwent reduction at the working electrode was found to be noticeably higher than at all other potentials. However, because the amount of product detected in the cell headspace was not found to increase proportionally, the TOF value for this experiment was lower than expected. The moles of hydrogen produced also reflects this trend (Table 4.5). When an electrolysis potential of -1.2 V was applied for the $CuPcF_{16}$-modified electrode, the highest TOF of all three experiments was noted (3.5×10^6).

Applied Potential (V)	***-0.8***	***-0.9***	***-1.0***	***-1.1***	***-1.2***
$CuPcF_{16}$					
Average Charge (C)	*9.2×10^{-3}*	*0.07*	*0.08*	*0.1*	*0.2*
[1]Current Density *J* (mA/cm^2)	*4×10^{-2}*	*0.3*	*0.3*	*0.4*	*0.9*
[2]Current Density *J* (mA/cm^2)	*0.4*	*0.8*	*2.2*	*3.9*	*5.7*
Moles of H_2 (mol)	-	*9.1×10^{-8}*	*1.3×10^{-7}*	*3.2×10^{-7}*	*8.8×10^{-7}*
Faradaic Efficiency (%)	-	*25*	*32*	*56*	*74*
(%)Electroactive	*0.4*	*0.5*	*0.4*	*0.4*	*1.0*
$ZnPcF_{16}$					
Average Charge (C)	*5.4×10^{-4}*	*2.0×10^{-3}*	*0.3*	*0.4*	*0.2*
[1]Current Density *J* (mA/cm^2)	*2×10^{-3}*	*8×10^{-3}*	*1.2*	*1.7*	*0.8*
[2]Current Density *J* (mA/cm^2)	*0.3*	*0.7*	*2.1*	*3.9*	*5.9*
Moles of H_2 (mol)	-	-	*1.1×10^{-6}*	*1.2×10^{-6}*	*4.4×10^{-7}*
Faradaic Efficiency (%)	-	-	*68*	*54*	*40*
(%) Electroactive	*0.1*	*0.1*	*0.2*	*0.1*	*0.4*

Table 4.3: *Performance data obtained by CV and BE for 1 hour for $CuPcF_{16}$ and $ZnPcF_{16}$ at varying electrolysis potentials vs. Ag/AgCl in 0.1 M NaH_2PO_4/H_3PO_4 (pH 2).Current densities obtained by [1]BE and [2]current density obtained using the last scan of the CV.*

.

Examination of the electrochemical results obtained using $ZnPcF_{16}$ shows that the lowest current density at -0.8 V is obtained while at -0.9 V a significant jump in current density is noted, indicating that the rate of electron-transfer at the modified electrode has increased with this small additional driving force. Because O_2 has a less negative reduction potential than H^+ for these kinds of modified electrodes in aqueous solutions,[18,28,29,30,34,35] it is possible that the current which is produced at these potentials is directed towards O_2 reduction, but at more negative potentials, H_2 evolution from H^+ becomes more competitive. When a potential of -1.1 V was applied the Faradaic efficiency (described in Chapter 2) calculated for H_2 evolution for this modified electrode was 54 %. Bearing in mind the complications mentioned earlier in this chapter with regards to Faradaic efficiency data, it appears that at this potential, H^+ reduction is faster than reduction of O_2. However, a significant portion of the electrolysis charge still involves some process other than H_2 evolution.

The amount of catalyst which is electrochemically active in these experiments reveal no obvious trends other than that at the lowest potentials, the amount of catalyst available for catalysis appears to be highest. For the Cu and Zn films, this factor is several times lower compared to the Co films. It is obvious that most of the catalyst in the modifying films does not participate in the catalytic reaction.

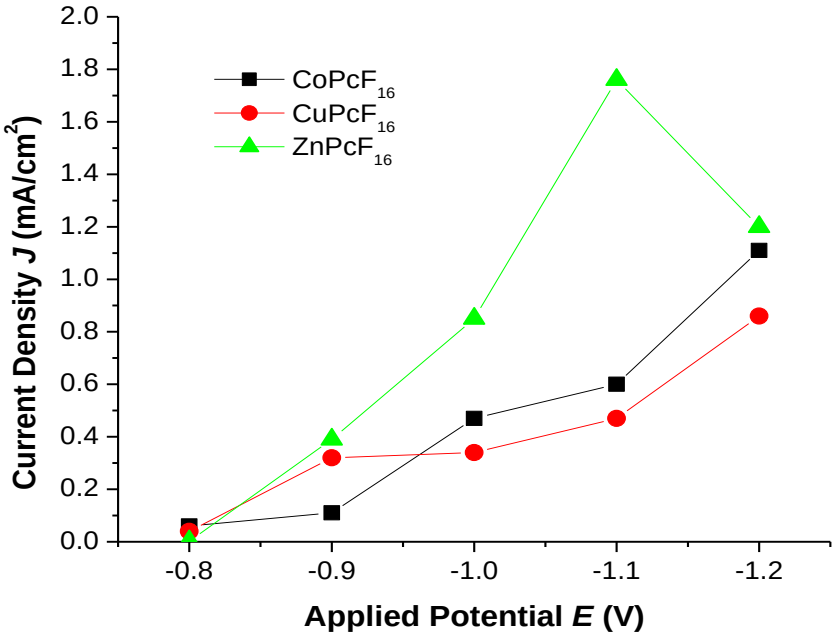

Figure 4.6: *Average current density (obtained by BE) as a function of applied potential. The black, red and green lines represent the data obtained for $CoPcF_{16}$, $CuPcF_{16}$ and $ZnPcF_{16}$ respectively.*

$ZnPcF_{16}$ demonstrates better performance at less negative potentials (-1.1 V electrolysis potential) than the other two modified electrodes in these studies, in terms of moles of hydrogen, TOF and current density (which can be considered important as it is a measure of the rate of the electrolysis reaction), however as mentioned previously, the current density value obtained is not solely due to the hydrogen evolution reaction occurring at the modified electrode as O_2 reduction is likely to contributes to a significant amount of the current density in these experiments.[31,32,33] Thus, the catalyst displaying the largest current density due to proton reduction alone is $CoPcF_{16}$ (7.5 mA/cm^2).

Examination of the moles of hydrogen determined by GC reveals the $CoPcF_{16}$ as the catalyst which produces the largest number of moles (1.2 x 10^{-6} mol) compared to $CuPcF_{16}$ and $ZnPcF_{16}$ when an electrolysis potential of -1.2 V is applied.

4.2.2.2 Effect of Temperature

The experimental results discussed so far are concerned with the employment of the catalyst systems for electrocatalytic hydrogen generation at room temperature (i.e. 20°C). Therefore it is worthwhile investigating how these systems function at temperatures both above and below room temperature, thus the temperatures chosen for investigation are 0°C, 20°C and 40°C. For all of these studies, the electrochemical cell was placed in a stirring water bath at a constant temperature. An ice bath was employed for the experiments performed at 0°C where ice was continuously added to maintain the cold temperature (actual temperature of the ice bath was ~ 3°C).

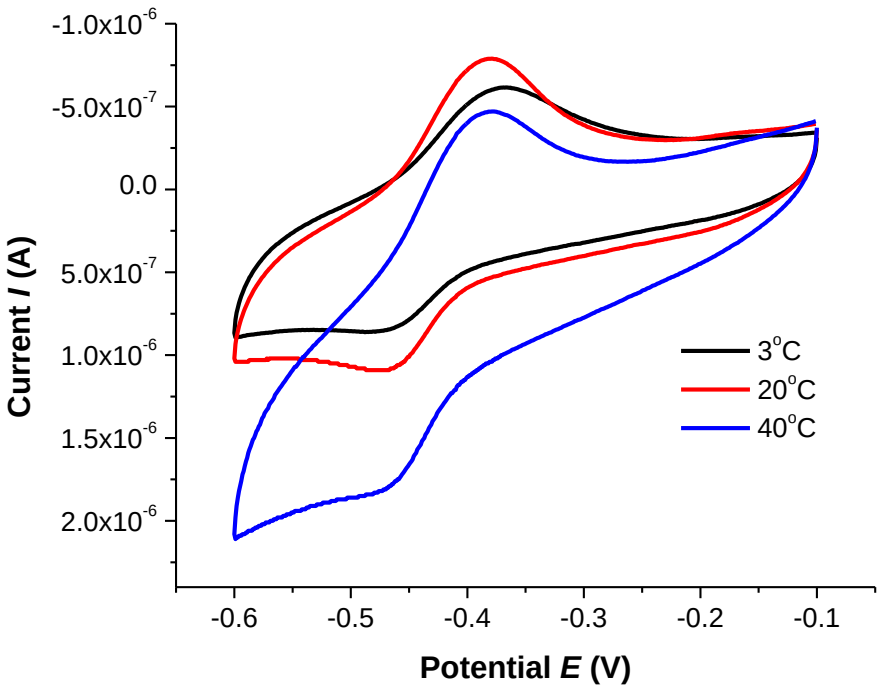

Figure 4.7: *Cyclic voltammetry of $CoPcF_{16}$ vs. Ag/AgCl in 0.1 M NaH_2PO_4/H_3PO_4 (pH 2) at 3°C (black line), 20°C (red line) and 40°C (blue line).*

It is evident that temperature affects both the electrochemical behaviour of the redox couple and also the subsequent proton reduction reaction. Although the appearance of the Co(II)/Co(I) redox couple at each temperature are slightly different, the height of the waves are quite similar against the background. The

difference is most likely attributed to the increase in kinetics with the hydrogen evolution reaction itself at the electrode surface with increasing temperature rather than a change in electrochemical behaviour with the Co(II)/Co(I) process.[34,35] The effect of temperature on electrocatalytic hydrogen evolution for each catalyst is shown in Figures 4.8, 4.10 and 4.11. The accompanying experimental data are displayed in Tables 4.4 and Table 4.5 for catalysts employed. (Additional TOF data in Appendix C, Tables C.4-C6).

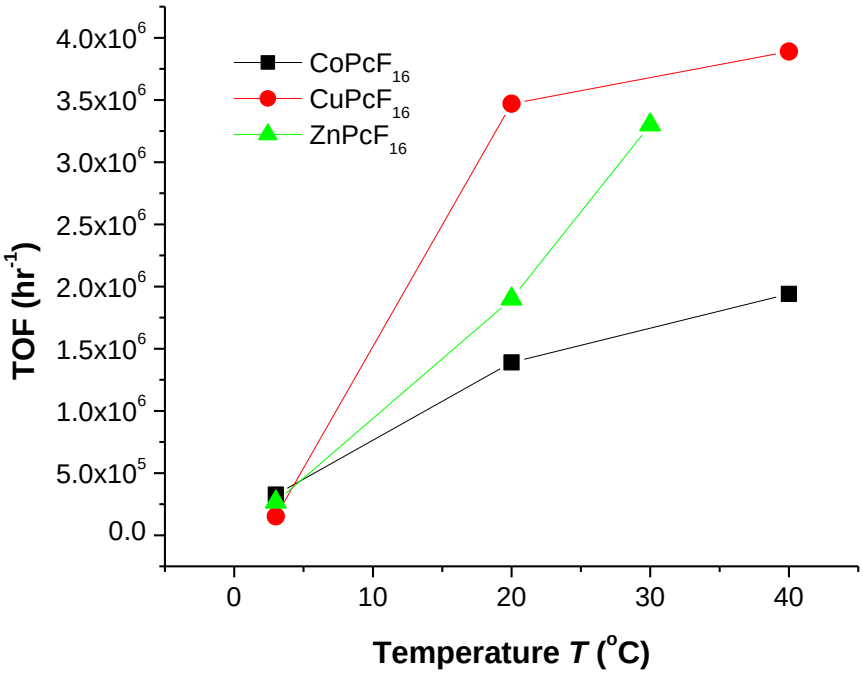

Figure 4.8: *Effect of temperature on turnover frequencies TOF (hr^{-1}) for $CoPcF_{16}$, $CuPcF_{16}$ and $ZnPcF_{16}$ represented by the black, red and green lines respectively.*

A trend is observed for all catalysts where the TOF increases with increasing temperature. Analysis of the gas in the headspace of the cell for the $CoPcF_{16}$ system reveals the following data; at 40°C, TOF was determined of 1.9 x 10^6, at 20°C, TOF = 1.4 x 10^6 and at 3°C, TOF = 3.3 x 10^5, Figure 4.8. It is important to note that temperature influences the solubility of H_2 (as well as O_2), with higher temperatures lowering gas solubility. This will affect the quantity of H_2 in the headspace (above the solution) as well as the amount of H_2 that remains in

solution (which is inaccessible as far as GC determination of TOF is concerned).[36,37]

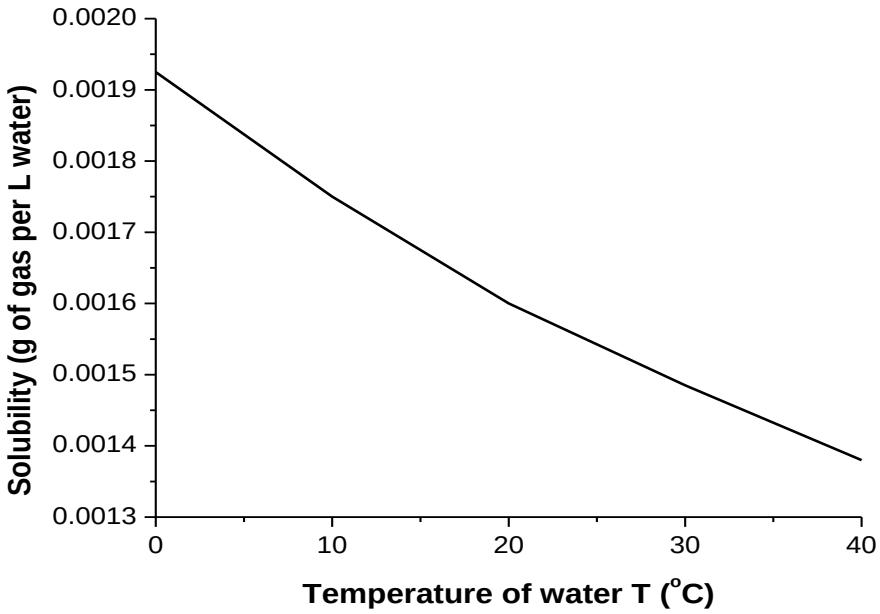

Figure 4.9: *Solubility of hydrogen in water at various temperatures. Adapted from reference 36.*

The effect of solubility of hydrogen in water is observed in Figure 4.9. It shows the expected inverse relationship between the solubility of H_2 in water at various temperatures; the solubility decreases with increasing temperature.[36,37] The temperature at which H_2 has the highest solubility in water (3°C) correlates with the lowest TOF for $CoPcF_{16}$. Thus the most efficient system (40°C) is the one in which H_2 has the lowest solubility as well as increased reaction kinetics at higher operating temperatures. It is worth noting that O_2 generated at the counter electrode will also be less soluble at higher temperatures. Thus the optimum operating conditions of the cell used in this work for H_2 production would best be carried out at elevated temperatures. The cyclic voltammograms for $CoPcF_{16}$ at the various temperatures are shown in Figure 4.10.

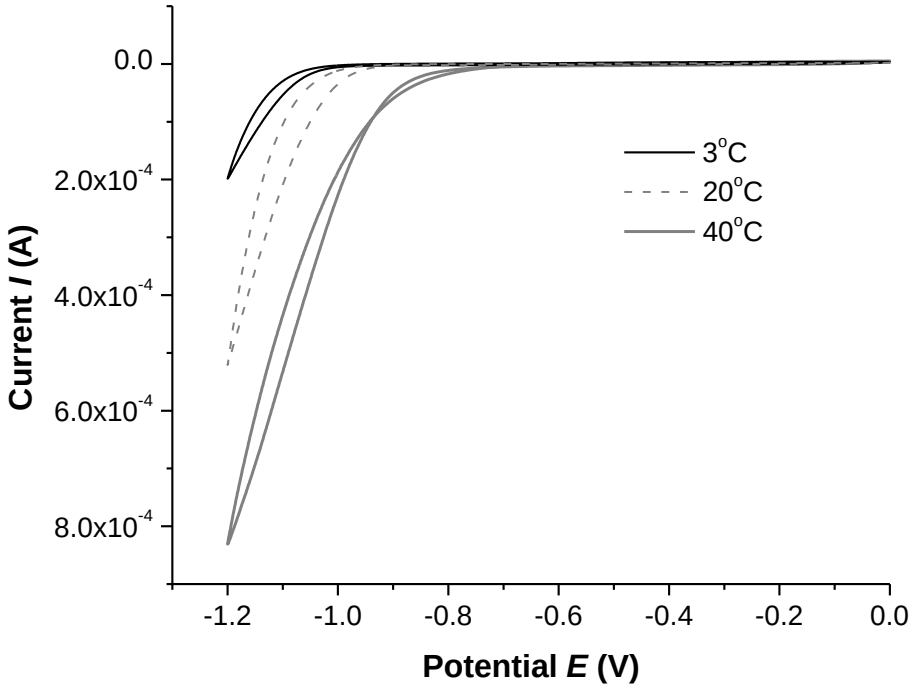

Figure 4.10: *Cyclic voltammogram of $CoPcF_{16}$ vs. Ag/AgCl in 0.1 M NaH_2PO_4/H_3PO_4 (pH 2) at 100 mV/s where the black, dashed and grey lines represent the catalytic currents at 3°C, 20°C and 40°C respectively.*

This figure shows that the onset potential for reduction shifted to less negative values with increasing temperature. The onset potential for work conducted at 0°C was -1.08 V vs. Ag/AgCl. When the temperature was increased to 20°C, the onset potential was observed at -0.90 V vs. Ag/AgCl. Increasing the temperature by a further 20°C shifts the onset potential for the electrocatalytic reduction of H^+ to -0.85 V vs. Ag/AgCl. This shift is a result of an increase in the rate constant for the electrocatalytic reaction and a lowering of the overpotential is thus observed..[34,38] Data describing charge passed at the electrode surface after 1 hour potentiostatic electrolysis, current density, Faradaic efficiency and % of electroactive catalyst in the films are shown in Table 4.4.

Temperature (°C)	***3***	***20***	***40***
Charge (C)	*0.13*	*0.28*	*0.80*
Moles of H_2 (mol)	*3×10^{-7}*	*1.2×10^{-6}*	*2.1×10^{-6}*
Faradaic Efficiency (%)	*46*	*74*	*50*
[1]Current Density *J* (mA/cm^2)	*0.5*	*1.1*	*3.1*
[2]Current Density *J* (mA/cm^2)	*2.9*	*7.5*	*11.8*
(%) Electroactive $CoPcF_{16}$	*2.7*	*6.3*	*6.8*

Table 4.4: *Average performance data obtained by CV and BE (-1.2 V vs. Ag/AgCl for 1 hour) for $CoPcF_{16}$ at varying temperatures in 0.1 M NaH_2PO_4/H_3PO_4 (pH 2). Current density obtained by [1]BE and [2]current density obtained using the last scan of the CV.*

.

It can be seen from the data that the fraction of the catalyst that is electroactive is enhanced at higher temperatures. This observation suggests that the conductivity of the films is improved at higher temperatures. Saravanan *et al*. showed this to be true for films of CoPc studied over a wide range of temperatures.[39] The improved conductivity is a likely result of improved charge hopping at higher temperatures. In these experiments, the ability of H^+ ions to diffuse through the films during catalytic reactions may also be enhanced by structural changes brought about by temperature changes.[40] The effect of temperature on the electrocatalytic activity for $CuPcF_{16}$ and $ZnPcF_{16}$ has also been studied. Analysis of the gas in the headspace yielded TOF values of 1.5×10^5, 3.5×10^6 and 3.9×10^6 at 3°C, 20°C and 40°C respectively when $CuPcF_{16}$ was employed as the catalyst. This trend was also observed for $ZnPcF_{16}$ was employed where TOF values of 2.7×10^5, 1.7×10^6 and 3.4×10^6 at 3°C, 20°C and 30°C, were obtained respectively. The current densities determined for both of these catalysts with

increasing temperature are shown in Figure 4.11. The current densities for $CoPcF_{16}$ experiments are included for comparison.

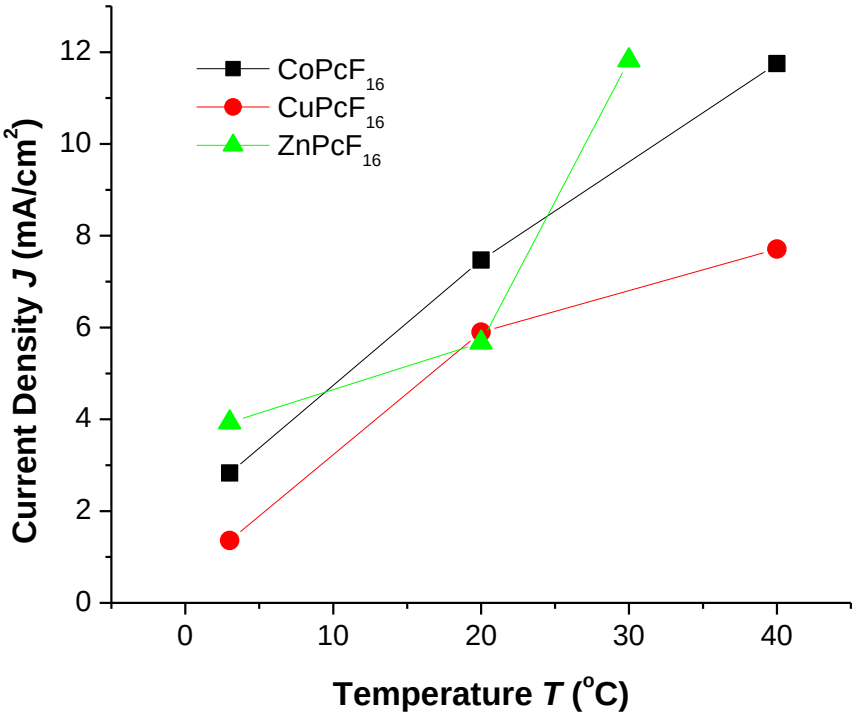

Figure 4.11: *Average current densities (mA/cm^2) at -1.2 V as a function of temperature for $CoPcF_{16}$ (black line), $CuPcF_{16}$ (red line) and $ZnPcF_{16}$ (green line). (Current densities obtained using CV).*

The current density data can be obtained by using either CV and/or BE data (Chapter 2). Figure 4.11 above displays the current densities determined by cyclic voltammetry as these values correspond to the catalytic production of hydrogen and are not complicated by the reduction of O_2 evolved at the anode.

It can be clearly seen that $CuPcF_{16}$ displays very similar behaviour to $CoPcF_{16}$, where higher temperatures yield an increase in reaction rates as a result of improved kinetics.[34,35] However the current densities values are lower for $CuPcF_{16}$ compared to $CoPcF_{16}$ over the temperature range investigated. The trend is also observed for $ZnPcF_{16}$ where an increase in temperature results in a rise in current density values.

Although there is no experimental data for the catalytic activity for $ZnPcF_{16}$ at 40°C, the increase in current densities displayed by this catalyst when the

temperature is increased from 20°C to 30°C suggests that this trend would be also be observed at 40°C as a result of improved kinetics.

Catalyst	**$ZnPcF_{16}$**			**$CuPcF_{16}$**		
Temperature (°C)	***3***	***20***	***30***	***3***	***20***	***40***
Charge (C)	*0.04*	*0.44*	*0.81*	*0.11*	*0.23*	*0.59*
Mols of H_2 (mol)	*1.1×10^{-7}*	*1.2×10^{-6}*	*3.7×10^{-6}*	*8.6×10^{-8}*	*8.9×10^{-7}*	*1.4×10^{-6}*
Faradaic Efficiency (%)	*36*	*54*	*89*	*15*	*74*	*46*
[1]Current Density *J* (mA/cm^2)	*0.2*	*1.7*	*3.2*	*0.4*	*0.9*	*2.3*
[2]Current Density *J* (mA/cm^2)	*2.4*	*5.9*	*11.8*	*1.4*	*5.7*	*7.7*
% Electroactive	*0.02*	*0.1*	*0.2*	*1.1*	*1.0*	*3.6*

Table 4.5: *Average performance data obtained by CV and BE at -1.1 V and -1.2 V vs. Ag/AgCl for 1 hour for $ZnPcF_{16}$ and $CuPcF_{16}$ respectively at varying temperatures in 0.1 M NaH_2PO_4/H_3PO_4 (pH 2). Current density obtained by [1]BE and [2]current density obtained using the last scan of the CV.*

The current densities (J) obtained by cyclic voltammetry and bulk electrolysis can be compared. As mentioned, the current density obtained by cyclic voltammetry is a result of proton reduction at the modified electrode, hence it can be viewed as an indicator of the catalyst's performance for the catalytic reaction. However, the current density determined by bulk electrolysis is averaged over the timeframe of the electrolysis experiment that involved times longer than ~ 1 minute, and is assumed to be a contribution of proton reduction and O_2 reduction, which drifts from the anode to the modified electrode. To evaluate the performance for proton reduction alone, it is best to consider the current densities obtained by cyclic

voltammetry. For these catalysts, the largest J at 20°C was observed when $CoPcF_{16}$ was employed, (7.5 mA/cm^2), compared to $CuPcF_{16}$ (5.7 mA/cm^2) and $ZnPcF_{16}$ (5.9 mA/cm^2) in Table 4.5 respectively. Increasing the temperature to 40°C results in increased electrode kinetics (as discussed) which was observed by higher current densities, 11.8 mA/cm^2 for both $CoPcF_{16}$ and $CuPcF_{16}$. The cyclic voltammograms displaying the catalytic currents for $CuPcF_{16}$ and $ZnPcF_{16}$ at the various temperatures are shown in the Appendix C, Figures C.1 and C.2.

Comparison of the moles of hydrogen generated by these catalysts over the range of temperature reveals $ZnPcF_{16}$ as the optimum catalyst for the employment for hydrogen production at 30°C (3.7 x 10^{-6} mols at an applied potential of -1.1 V).

4.2.2.3 Effect of using ethyl acetate for preparation of catalyst solutions

The catalyst layers under investigation in this thesis were prepared using DMF as the most appropriate solvent. The solubility of metallophthalocyanines in most organic solvents is quite poor and in DMF, it was found that a maximum concentration of 2.8 x 10^{-5} M of $CoPcF_{16}$ could be achieved in this solvent.

In an effort to increase the amount of catalyst material on the electrode surface, ethyl acetate was chosen, a solvent which is more volatile than in DMF and also one which the catalyst exhibited better solubility. A 8.2 x 10^{-5} M $CoPcF_{16}$ solution was prepared, (almost 3 times more concentrated than when prepared in DMF). As ethyl acetate has a boiling point of 77° C, much lower than that of DMF (153° C), this allowed for solvent evaporation to occur faster than for DMF. Hence modified electrodes could be constructed with multiple layers cast onto the surface (the ethyl acetate catalyst solution evaporated almost immediately upon casting on the electrode). The results of these studies are shown below. A trend can be observed upon increasing the number of layers (Table 4.6), in terms of charge passed during electrolyses, current density (mA/cm^2), and the percentage of the catalyst that is electroactive.

No. of layers drop cast	***1***	***2***	***5***
Charge (C)	*0.12*	*0.09*	*0.08*
Moles of H_2 (mol)	*3.7×10^{-7}*	*2.6×10^{-7}*	*2.3×10^{-7}*
Faradaic Efficiency %	*60*	*56*	*56*
[1]Current Density *J* (mA/cm^2)	*0.5*	*0.4*	*0.3*
[2]Current Density *J* (mA/cm^2)	*3.4*	*3.6*	*3.1*
(%) Electroactive $CoPcF_{16}$	*0.9*	*0.6*	*0.1*

Table 4.6: *Average charge (C), current density (mA/cm^2) moles of electroactive catalyst (mol) and % electroactive catalyst for $CoPcF_{16}$ prepared in ethyl acetate. Current density obtained by [1]BE and [2]current density obtained using the last scan of the CV.*

From the experimental results, it appears that increasing the number of layers on the electrode leads to a slight decrease in catalytic performance. This is indicated by the charge passed after 1 hour electrolysis; 0.12 C using 1 layer, 0.09 C using 2 layers and 0.08 C for 5 layers. This is also shown by the current density values obtained after the 1 hour electrolysis period. It might be assumed that thicker films would be less able to pass charge due to problems associated with counterion diffusion through thicker films. However, it is expected that the evaporation of the solvent on the electrode is not an entirely predictable process. Evaporation rates at different regions on the electrode (i.e. exterior of the drop cast on the surface vs. the interior of the drop) are not uniform, and thus films produced by this method can be expected to be somewhat irregular. It is expected that the film's appearance would look similar to a film left by a drop of coffee, for example, on a tabletop, thickest at the outside and thin in the centre. When multiple drops are cast, they dry on the surface created by the previous drops. Furthermore, the solid that remains following solvent evaporation will be, to at least some extent, crystalline, and the crystallinity of the film will be highly

dependent on evaporation rate.[41] In short, although the data might suggest simple "thick film-poor performance" behaviour, the topography of the films is likely complex and comparisons in these data are not necessarily straightforward.

Comparison of the cyclic voltammograms of the modified electrode coated with 1 layer and 5 layers are shown in Figure 4.12. A reversible redox couple $E_{½}$ at -0.43 V vs. Ag/AgCl is observed for the electrode modified with one coat of catalyst, while the electrode coated with 5 layers of catalyst reveals a less pronounced redox process. This reversible process has been previously assigned (Chapter 3) as the addition of an electron to the catalyst with the subsequent re-oxidation reaction.

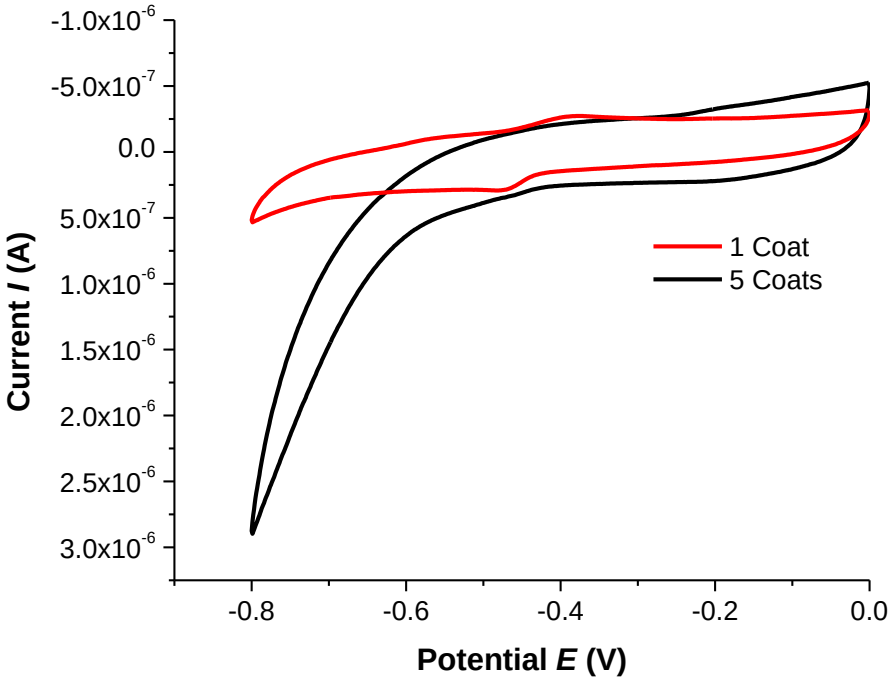

Figure 4.12: *Cyclic voltammogram of modified electrodes coated with $CoPcF_{16}$ vs. Ag/AgCl in 0.1 M NaH_2PO_4/H_3PO_4 (pH 2). The catalyst was prepared using ethyl acetate. The red line represents the CV of the single layered modified electrode while the black line depicts the CV of the electrode modified with 5 layers of catalyst. Scan rate = 100 mV/s.*

Using cyclic voltammetry, the area (C) under the wave can be converted to number of moles of catalyst which are electroactive by using Faraday's constant.

Table 4.6 displays the number of moles of catalyst which are electroactive and the percentage of electroactive species. From the data, it can be seen that as the number of layers coated increase, this factor becomes progressively worse. These results correlate with the charge and current density parameters previously discussed. In terms of turnover frequencies TOF (hr^{-1}), the graph below compares the TOF to the modified electrodes coated with various layers of catalyst.

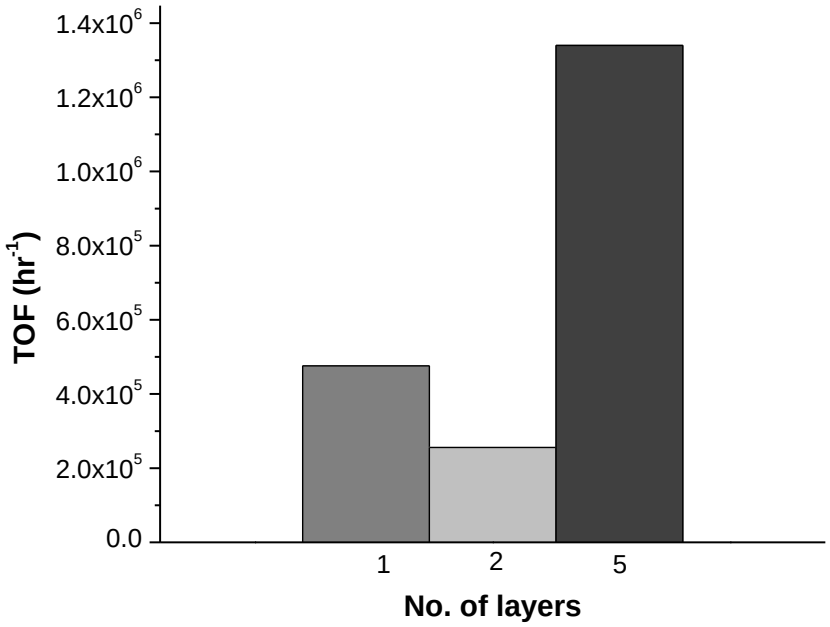

Figure 4.13: *Number of layers coated on a modified electrode vs. TOF (hr^{-1}) for the electrocatalytic generation of hydrogen.*

The modified electrode with 5 layers of catalyst deposited on the surface revealed the most promising current density and also displayed the largest TOF (1.3 x 10^6). The electrode modified with just one layer of catalyst revealed a TOF of 4.8 x 10^5. A greater amount of catalyst should yield more product; however, TOF numbers should be independent of catalyst amount, as the greater amount of H_2 produced would be divided by a greater quantity of catalyst. Comparing the moles of hydrogen produced is a better way of comparing the catalytic activity for these modified electrodes. Increasing the catalyst layers from 1 film to 5 films resulted in a decrease in hydrogen formation; 3.7 x 10^{-7} mols (1 layer) compared to 2.3 x 10^{-7} mols (5 layers). As small variations in the amount of catalyst will result in

significant fluctuations in TOF data, the trend shown in Figure 4.13 should be viewed with caution.

Vos *et al.* reported the rate of solvent removal is important if the aim is to produce smooth films, with slow removal being preferable.[42] Since DMF is much less volatile than ethyl acetate, slower evaporation of the solvent is achieved using DMF. The fraction of active catalyst for a DMF film (1 drop/layer) was significantly higher than for ethyl acetate (6% compared to 0.9%). It is possible that the larger fraction of active catalyst is a result of better film quality due to the slow evaporation of DMF, producing good crystallinity and leading to an increase in conductivity in the film.[43]

The drop casting method for electrode modification presents a number of factors that may lead to variations in film quality. These factors include solution preparation, accuracy in the delivery by the auto pipette, rate of solvent evaporation, and human error. Solvent evaporation rate will affect the surface characteristics of the film, while the other factors listed will only contribute to uncertainty in the total amount of catalyst deposited.[42]

Assuming that coating the electrode in layers has some effect on the performance of the modified electrodes, one way that this could be assessed is using cyclic voltammetry to investigate the amount of catalyst that is able to undergo reduction/oxidation. This is important because the amount of catalyst that is electroactive within the film will influence the amount of H_2 that can be generated. The mean and standard deviation results for one and five layer films are presented in Table 4.7.

Number of layers	**1**	**5**
Mean no. of moles of electroactive catalyst (mol)	1.1×10^{-12}	1.7×10^{-13}
Standard Deviation (mol)	4.6×10^{-13}	1.0×10^{-13}
% Distribution of data about the mean	*45*	*56*
No. of modified electrodes	*6*	*6*

Table 4.7: *Catalyst solution prepared in ethyl acetate; Data obtained for twelve modified electrodes in total, six of which are coated with 1 layer of catalyst and the remaining six coated with 5 layers of catalyst. These electrodes were placed in an oven where the temperature was maintained at 21°C for solvent evaporation.*

From the data in the table, it can be seen that the standard deviation for data acquired from the electrodes formed with 1 film versus 5 is not really that different. There is a slightly greater variability for the electrodes coated with 5 layers of catalyst, relative to the electrodes modified with one layer. However, it does still appear that a thicker film presents less catalyst that is available for reduction/oxidation. (Additional TOF data in Appendix C, Table C.7).

4.2.2.4 Casting additional layers using DMF catalyst solution

In an effort to increase the amount of electroactive catalyst present in the modifying layer which is available to participate in the electrocatalytic reaction, the casting of additional layers was investigated. While the effect of increasing the number of layers cast using a catalyst solution prepared in ethyl acetate has been discussed above (4.2.2.3), investigating the effect of altering the number of layers cast onto the electrode using a catalyst solution prepared in DMF was carried out. For comparison purposes, the performance indicators for each catalyst when just one coat was drop cast onto a glassy carbon electrode in the construction of a modified electrode is given. The effect of the additional layer is shown in Table 4.8.

Catalyst	***$CoPcF_{16}$***	
No. of layers cast	***1***	***2***
Charge (C)	*0.28*	*0.17*
TOF (hr^{-1})	*1.4×10^{6}*	*4.1×10^{5}*
Moles of H_2 (mol)	*1.2×10^{-6}*	*8.2×10^{-7}*
Faradaic Efficiency %	*74*	*43*
[1]Current Density J (mA/cm^2)	*1.1*	*0.7*
[2]Current Density J (mA/cm^2)	*7.5*	*6.9*
(%) Electroactive $CoPcF_{16}$	*6.3*	*4.8*

Table 4.8: *Average performance data obtained for $CoPcF_{16}$ by CV and BE vs. Ag/AgCl in 0.1 M NaH_2PO_4/H_3PO_4 (pH 2) with varying the number of layers of catalyst deposited (from a catalyst solution prepared in DMF) on the electrode. Current density calculated using [1]BE and [2]current density obtained using the last scan of the CV.*

When a modified electrode was coated with 2 layers of $CoPcF_{16}$, the average current density, obtained during the electrolysis step (0.7 mA/cm^2) was just over half of that obtained when 1 coat was applied (1.1 mA/cm^2). These results indicate that the rate of the electrocatalytic reaction decreased significantly when an additional layer was coated. Consider Equation 4.1 where A_{ox} represent the protons in the electrolyte solution, M_{ox} is Co (II), M_{red} is Co (I) and A_{red} is H_2. The electrocatalytic reaction occurs by the following equation;

$$M_{ox} + ne^{-} \rightarrow M_{red} + A_{ox} \rightarrow M_{ox} + A_{red} \qquad \textbf{Equation 4.1}$$

The protons must diffuse through the second layer (adjacent to the bulk solution) before it reaches the catalyst at the first modifying layer close to the electrode in order to participate in the electrocatalytic reaction. Thus the decrease in activity may be a result of slow mass transport of the protons into the modifying layer, as the layer thickness has increased and the electrode kinetics may be sluggish due to the additional layer, hindering the catalytic activity.[41, 44, 45] This trend is also observed when 2 layers of $CuPcF_{16}$ and $ZnPcF_{16}$ are cast (from DMF) onto a working electrode. As the catalytic activity was not enhanced with the additional casting of layers (evident for all 3 catalyst), the resulting TOF values obtained were lower than those compared to using one layer of catalyst. (see Appendix C, Tables C.8 and C.9).

4.2.2.5 Effect of varying the pH and ionic strength of electrolyte

The experimental results for each of the catalyst systems for electrocatalytic hydrogen generation at room temperature using a solution which works as an electrolyte and a buffer will be discussed. The pH was changed by altering the ratio of NaH_2PO_4/H_3PO_4 and by using NaOH for basic conditions, while maintaining an ionic strength of 0.1 M NaH_2PO_4.

Examination of the cyclic voltammograms of each of the catalysts in phosphate solution at pH 2, 4, 7 and 9 reveals a shift towards more negative potentials for the redox couples, Co(II)/Co(I) for $CoPcF_{16}$ (and $Pc^{(2-)}/Pc^{(3-)}$ $CuPcF_{16}$ and $ZnPcF_{16}$) with decreasing acidity, see Table 4.9. For $CoPcF_{16}$ at pH 4, the Co(II)/Co(I) process is observed at -0.54 V vs. Ag/AgCl, but as the pH of the electrolyte solution increases to more basic conditions, the redox process becomes broader and the anodic peak is difficult to see (making E_{pa} more difficult to determine).

pH	E ½ (V) vs. Ag/AgCl	E_{pa}- E_{pc} (mV)
2	*-0.43*	*60*
4	*-0.54*	*60*
7	*-0.67*	*110*
9	*-0.91*	*130*

Table 4.9: *Reduction potentials of immobilised Co(II)/ Co(I) for $CoPcF_{16}$ in 0.1 M NaH_2PO_4 electrolyte over a range of pH at room temperature.*

It is evident that a concurrent shift in the onset potential for H^+ reduction is also observed as a result of a increase in pH of the electrolyte solution, Figure 4.14-4.15. The Nernst equation predicts that the $2H^+ + 2e^- \rightarrow H_2$ reaction will be more thermodynamically favourable at lower solution pH (Equation 4.2).[46]

$$E = E^\circ + \frac{RT}{nF} \ln \frac{[H^+]^2}{[H_2]} \qquad \textbf{Equation 4.2}$$

As expected by the equation, a cathodic shift in potential was observed when the pH of the electrolyte solution increased, Equation 4.3.

$$E = E^\circ - 2.303 \frac{RT}{F}(pH) \qquad \textbf{Equation 4.3}$$

In neutral and basic conditions, the H_2 evolution reaction is expected to be $2H_2O + 2e^- \rightarrow H_2 + 2OH^-$, because $[H^+]$ in these cases is very low.[47,48] For this equation, in more basic media, $[OH^-]$ is high, and increasing $[OH^-]$ shifts the H_2 evolution reaction to more negative potentials. Application of a reduction potential of -1.2 V to a modified electrode of $CoPcF_{16}$ immersed in a phosphate solution at pH 4, revealed a weak cathodic current, producing a TOF of 1.3×10^4.

pH	***2***	***4***	***7***	***9***
Charge (C)	*0.28*	*0.02*	*8.4×10^{-4}*	*6.5×10^{-4}*
TOF (hr^{-1})	*1.4×10^{6}*	*1.3×10^{4}*	-	-
Moles of H_2 (mol)	*1.2×10^{-6}*	*2×10^{-8}*	-	-
Faradaic Efficiency %	*74*	*19*	-	-
[1]Current Density *J* (mA/cm^2)	*1.1*	*0.1*	*3×10^{-3}*	*2×10^{-3}*

Table 4.10: *Effect of varying the pH of electrolyte on the (average) performance indicators for $CoPcF_{16}$ obtained by CV and B at -1.2 V vs. Ag/AgCl. [1]Current densities determined using data obtained by BE.*

The activity at -1.2 V became progressively lower upon increasing the pH of the solution. At neutral conditions, no visible sharp increase in a cathodic current at -1.2 V was observed indicating that at this potential, the hydrogen evolution reaction was hindered. The current density obtained of 3×10^{-3} mA/cm^3 reflects this weak activity. No gaseous product was detected by gas chromatography, indicating that the concentration of hydrogen (if any) lies below the LOD of the TCD. Similar to the activity of the catalyst at pH 7, when more basic conditions were employed (pH 9), no hydrogen was detected by gas chromatography. These results indicate that the electrocatalytic reaction proceeds at a much lower rate in neutral and basic conditions, as expected, Figure 4.14.

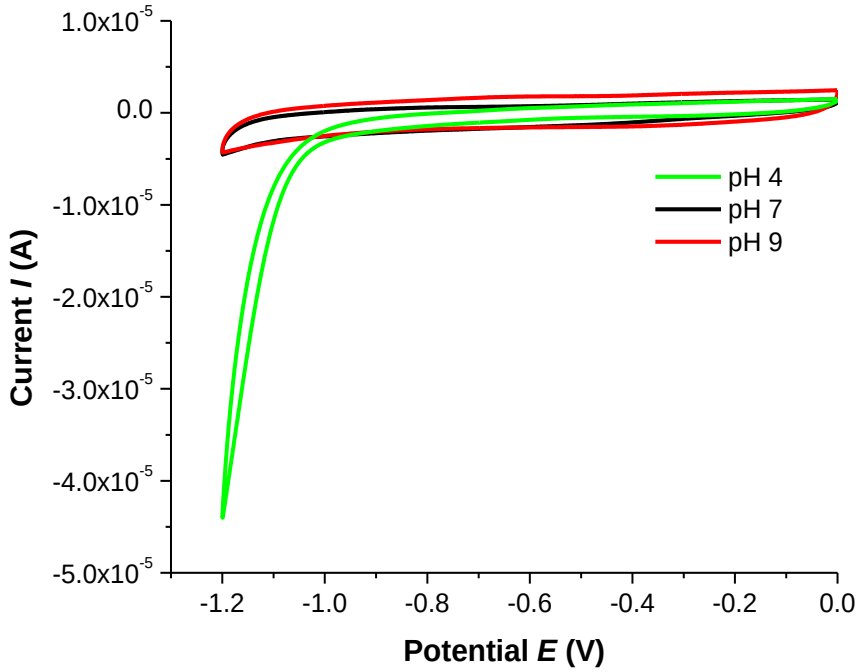

Figure 4.14: *Cyclic voltammetry of $CoPcF_{16}$ in 0.1 M NaH_2PO_4 at pH 4, 7 and 9 represented by green, black and red lines respectively.*

As mentioned above, the reason for such poor catalytic activity for the electrocatalytic generation of hydrogen is due to the decrease in the concentration of protons in solution with increasing pH. Also, it is evident that the electrolysis potential of -1.2 V is clearly not a sufficient driving force for H_2 evolution when such a low concentration of protons in solution are available. In order for $CoPcF_{16}$ to work as an efficient catalyst at higher pH, a more negative overpotential will be required to improve the performance.

Thus, work was carried out on these catalysts to investigate the potential required to initiate the hydrogen evolution reaction over a range of pH values. The results for $CoPcF_{16}$ are described in Figure 4.15.

In pH 4 conditions, a catalytic current was observed having a peak value at -1.4 V, indicating that at this potential, hydrogen evolution can take place. The onset potential is shifted negatively relative to what was found when pH 2 buffer was used, observed at -1.03 V.

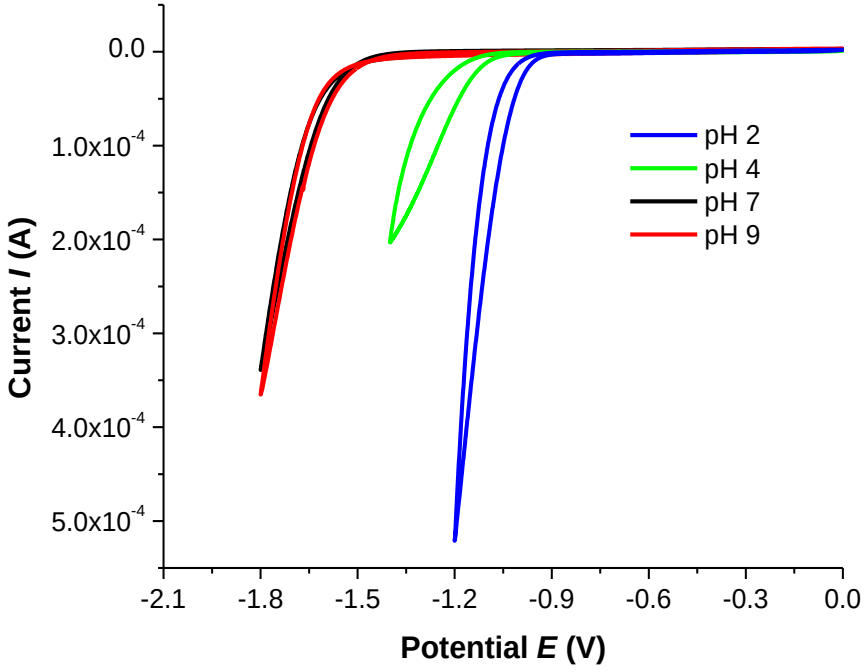

Figure 4.15: *Cyclic voltammetry of the catalytic currents for $CoPcF_{16}$ in 0.1 M NaH_2PO_4 over a range of pH.*

The electrochemical behaviour of $CoPcF_{16}$ at neutral pH and in basic conditions was similar (see Figure 4.15). Significantly enhanced currents at pH 7 and pH 9 conditions were noted to begin near -1.5 V for this catalyst at both pH.

Comparing the catalytic currents shown in the cyclic voltammograms by $CoPcF_{16}$ to those of the bare GCE in Figure 4.16, a similar response in the absence of the catalyst is observed. The appearance of these catalytic currents over a range of pH with decreasing (more negative) electrolysis potential implies that the hydrogen evolution reaction can occur in the absence of the catalyst providing enough of a driving force is applied, i.e. an overpotential.

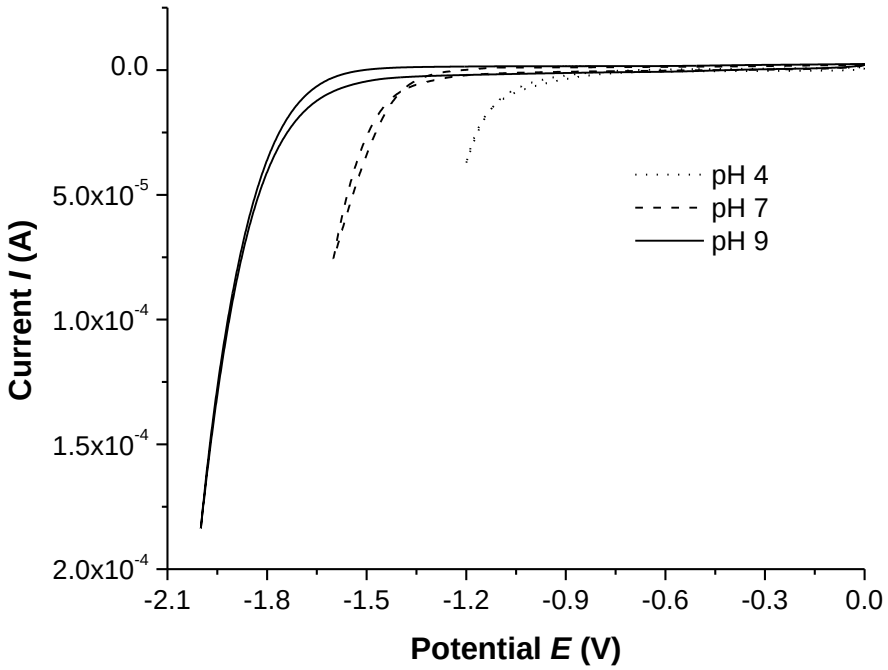

Figure 4.16: *Cyclic voltammetry of the catalytic currents for bare GCE in 0.1 M NaH_2PO_4 over a range of pH.*

The performance data for $CoPcF_{16}$ at each pH is displayed in Table 4.8. At pH 7, the H_2 evolution process was noted to begin near -1.45 V. At -1.8 V, the characteristic, sharp rise in reduction current (indicative of the catalytic reaction) was observed, reaching a maximum of 3.5 x 10^{-4} A. As the pH of the electrolyte increased, a lower (more negative) electrolysis potential was required. The charge passed after 1 hour electrolysis at each of the applied potentials discussed above increased as the pH increased. The catalytic activity of $CoPcF_{16}$ was quite similar in both basic and neutral conditions. The TOF values are shown in Table 4.10 (Appendix C, Table C.10). The performance in these experiments, as evaluated by TOF, was largest at pH 7 followed closely by the pH 9 study (2.2 x 10^6 and 2.0 x 10^6, respectively). High Faradaic efficiencies for these systems were determined (82 % and 77 %, respectively). The lowest TOF were obtained when the pH 4 electrolyte was employed; 5.5 x 10^5. The current density observed in a cyclic voltammetry experiment is a reasonable predictor of the quantity of charged that will be passed during an electrolysis, assuming the reaction at the electrode is uncomplicated. The peak current for the pH 4 study was the smallest of the

currents observed of all the pH studies. Thus it should not be surprising that the TOF data found for pH 4 is significantly less than those found at other pH values.

Applied Potential (V)	***-1.2*** *(pH 2)*	***-1.4*** *(pH 4)*	***-1.8*** *(pH 7)*	***-1.8*** *(pH 9)*
Charge (C)	*0.28*	*0.33*	*1.04*	*1.02*
Moles of H_2 (mols)	*1.1×10^{-6}*	*9×10^{-7}*	*4.4×10^{-6}*	*2.3×10^{-6}*
TOF (hr^{-1})	*1.4×10^{6}*	*5.5×10^{5}*	*2.2×10^{6}*	*2.0×10^{6}*
Faradaic Efficiency %	*74*	*60*	*82*	*77*
(%) Electroactive $CoPcF_{16}$	*6.3*	*4.5*	*5.0*	*5.9*

Table 4.11: *Effect of pH of electrolyte on the average performance indicators for $CoPcF_{16}$ obtained by CV and BE (using varying applied potentials).*

The catalytic reaction of proton reduction in acidic conditions should result in the largest amount of hydrogen formation, however in Table 4.10, this is not the case. In neutral and basic conditions, an increase in the number of moles of hydrogen was observed as a result of the negative applied potential. Thus, it is difficult to gauge the pH-catalyst performance as hydrogen evolution due to an overpotential influences the experimental results. Thus for each of the catalytic systems presented here, the experimental results for $CuPcF_{16}$ and $ZnPcF_{16}$ over a range of pH are not discussed but the cyclic voltammograms and TOF data are presented in Appendix C, Tables C.11-C12 and Figures C.3-C.4.

The experiments which have been discussed so far have all been performed in a phosphate (NaH_2PO_4/H_3PO_4) solution at pH 2 (varied for pH study) of 0.1 M ionic strength. Kaneko and Koca reported electrocatalytic results concerning metallophthalocyanines when their modified electrodes were placed in an electrochemical cell containing 0.1 M NaH_2PO_4/H_3PO_4.[1,2,12,14,17] To the best of our knowledge, varying the concentration of the electrolyte has not been reported,

therefore it was of interest to investigate the effect of lowering the concentration on the electrocatalytic generation of hydrogen.

As the potential was held constant and the pH was increased, the cathodic current decreased, which is evident in Figure 4.14 which compares the currents at different pH cycled in the same potential window (0 V to -1.20 V). This was expected as the equilibrium potential E_{eq} becomes more and more negative with increasing pH, indicated by the magnitude of the currents (0.059 V per pH unit change). In order for the same current to be produced by each of these systems operated over a range of pH, the applied potential E_{app} was pushed to more negative potentials. At pH 4, the equilibrium potential becomes more negative by 0.118 V, compared to the equilibrium potential at pH 2. Thus the overpotentials can be calculated for at each pH unit change; 1.0 V at pH 4, 1.1 V at pH 7 and 1.2 V at pH 9 when all compared at a current of 1 x 10^{-4} A.

In Figure 4.17 the effect of the ionic strength of the buffer solution on the activity for hydrogen evolution is observed.

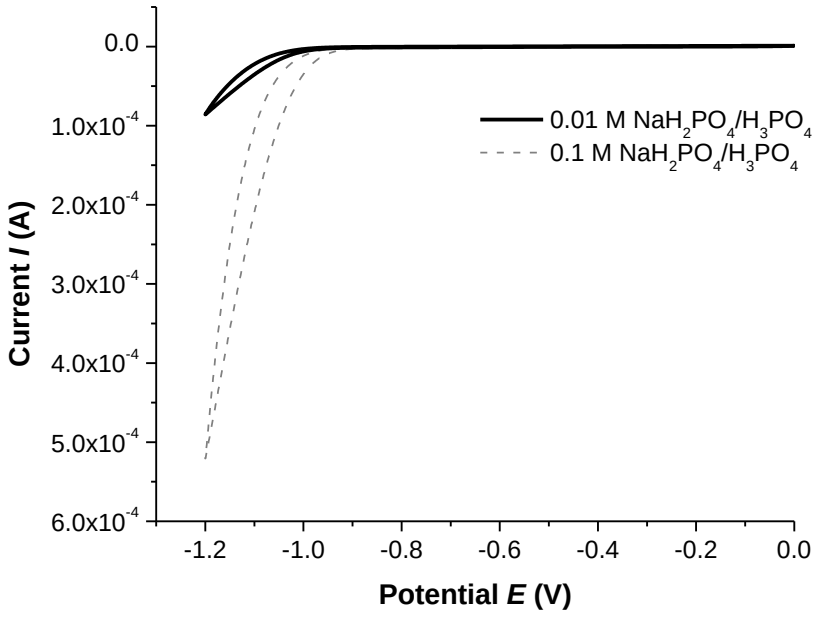

Figure 4.17: *Cyclic voltammogram of $CoPcF_{16}$ vs. Ag/AgCl at 100 mV/s where the black line is the modified electrode immersed in 0.1 M NaH_2PO_4/H_3PO_4 (pH 2) and the grey dashed line is using 0.01 M NaH_2PO_4/H_3PO_4 (pH 2).*

When an electrolyte containing 0.1 M NaH_2PO_4/H_3PO_4 at pH 2 was employed, a large cathodic catalytic current was observed with a corresponding onset potential of -0.90 V vs. Ag/AgCl. By altering the concentration of the electrolyte to 0.01 M, an cathodic current at -1.2 V was observed, although it is of less magnitude, compared to the current produced at -1.2 V in 0.1 M electrolyte. The onset potential shifted negatively by 100 mV as the ionic strength decreases, observed now at -1.0 V vs. Ag/AgCl. The ionic strength of the electrolyte plays a significant role in the electrocatalytic reaction.[49]

A plausible explanation for the reduced catalytic activity for $CoPcF_{16}$ using the lower ionic strength buffer (0.01 M NaH_2PO_4/H_3PO_4) is an increase in resistance between the working and reference electrodes in the cell. It was observed that the charge can be passed more easily using a higher concentration of buffer, which can be attributed to a lower resistance when the solution of higher ionic strength is employed. This, coupled with the importance of proton concentration leads to an improved performance for the hydrogen evolution reaction when the solution of higher ionic strength is used i.e. 0.1 M NaH_2PO_4/H_3PO_4

4.2.2.6 Varying the catalyst concentration in coating solution

The experimental results discussed so far are concerned with the employment of these catalyst systems where a volume of catalyst of known concentration is deposited onto the surface of the GCE. The effect of varying the concentration of the $CoPcF_{16}$ catalyst was investigated and the experimental results are displayed in Figures 4.18 and 4.19 and Table 4.12. Three solutions were prepared from a stock solution (2.8×10^{-5} M) of the following concentrations; 7×10^{-6} M, 1.4×10^{-5} M and 2.1×10^{-5} M. Kaneko *et al.* reported that the number of moles of cobalt phthalocyanine increased with increasing solution concentration; the hydrogen evolved (measured in uL) was proportional with the concentration of catalyst solution (3 mM to 10 mM).[14] For $CoPcF_{16}$, the number of moles of hydrogen electrocatalytically produced increased as the concentration of catalyst increased also, shown in Figure 4.18.

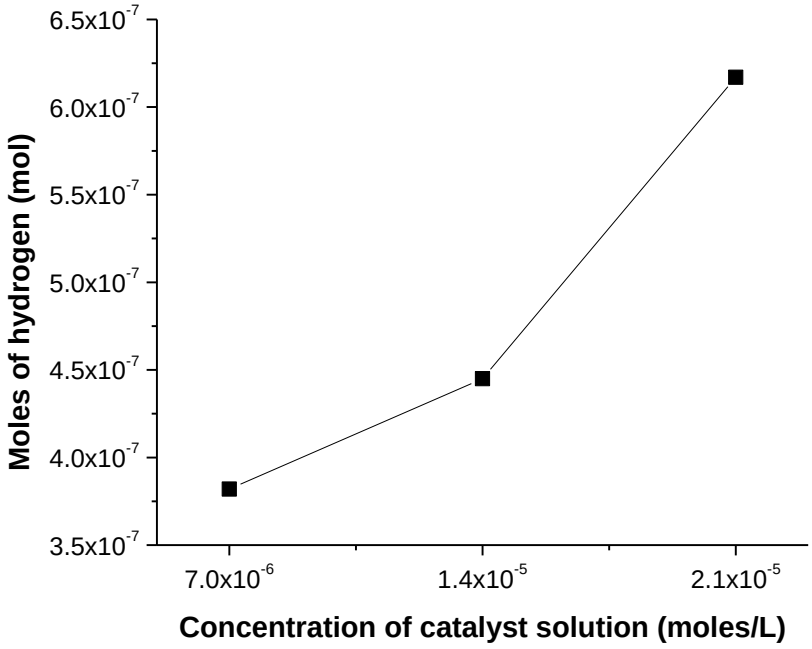

Figure 4.18: *Moles of hydrogen as a function of concentration of catalyst solution (used for depositing films) in 0.1 M NaH_2PO_4/H_3PO_4 (pH 2) at -1.2 V vs. Ag/AgCl.*

A linear relationship was described for the evolved hydrogen using CoPc by Kaneko with increasing catalyst solution concentration.[14] This unsubstituted catalyst was assumed as being 100 % electroactive in the layer for each of the concentrations of catalyst solutions, thus the resulting TOF was invariant. This behaviour was not observed for the $CoPcF_{16}$ catalyst discussed here, as the highest percentage of electroactive species varied with each concentration of catalyst investigated. Table 4.12 presents electrochemical data that were obtained in these experiments. It is evident that the charge obtained during 1 hour potentiostatic electrolysis increased as a function of increasing concentration of catalyst solution; the lowest electrolysis charge of 0.16 C was observed when a catalyst concentration of 7 x 10^{-6} M was used while this increased to 0.26 C when 2.1 x 10^{-5} M catalyst solution was employed. The current density appeared to increase slightly when the concentration of catalyst in solution increased, this is a feature which was observed for a ZnPc macrocycle, where it was assumed that the

increase in current density with increasing concentration of catalyst was a result of improved intermolecular contact (higher electrical conductivity).[50]

Catalyst Concentration (x 10^{-5} M)	***0.7***	***1.4***	***2.1***
Charge (C hr^{-1})	*0.16*	*0.22*	*0.26*
Moles of H_2 (mol)	*3.8 x 10^{-7}*	*4.4 x 10^{-7}*	*6.1 x 10^{-7}*
Faradaic Efficiency (%)	*46*	*39*	*45*
[1]Current Density *J* (mA/cm^2)	*0.6*	*0.9*	*1.0*
[2]Current Density *J* (mA/cm^2)	*0.8*	*1.4*	*4.3*
Electroactive $CoPcF_{16}$ (%)	*1.6*	*3.2*	*3.4*

Table 4.12: *Average performance data obtained for $CoPcF_{16}$ by CV and BE (at -1.2 V for 1 hour) vs. Ag/AgCl in 0.1 M NaH_2PO_4/H_3PO_4 (pH 2) with varying catalyst concentration. Current densities obtained by [1]BE and [2]CV data.*

The TOF figures obtained by headspace analysis using gas chromatography are displayed in Figure 4.19.

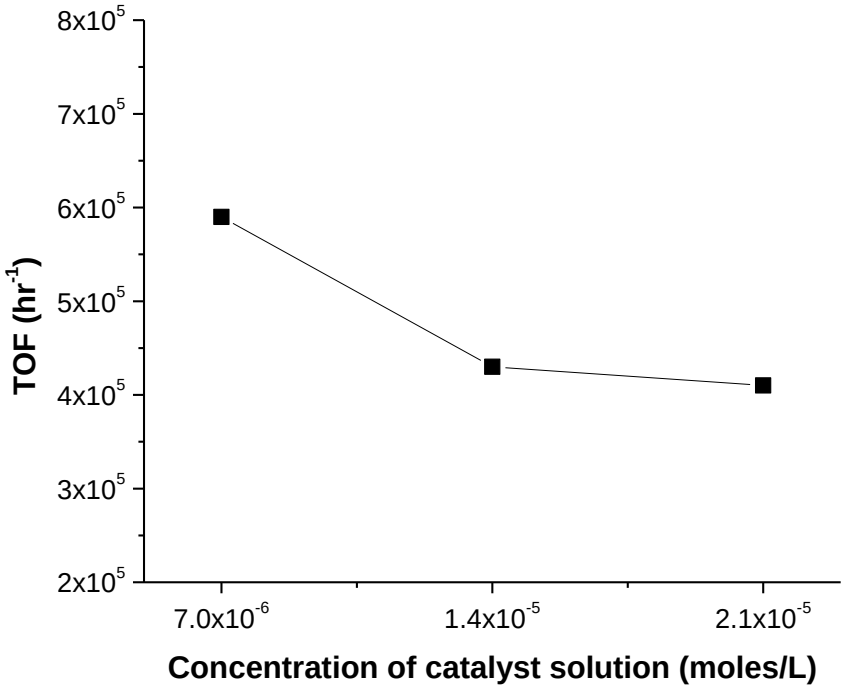

Figure 4.19: *Turnover frequencies TOF (hr^{-1}) as a function of concentration of catalyst solution for $CoPcF_{16}$ in 0.1 M NaH_2PO_4/H_3PO_4 (pH 2).*

The TOF values calculated do not appear to change significantly with catalyst solution concentration; However, the Faradaic efficiencies were poor in these studies, calculated as 46 %, 39 % and 45 % with increasing concentrations of catalyst solutions using a potential of -1.2 V (Appendix C, Table C.13).

4.2.2.7 Varying the volume of catalyst deposited

As the concentration of the catalyst was varied (4.2.2.6) and the results have been discussed above, the effect of casting a lower volume of catalyst was hence investigated. The experimental data discussed in this chapter are a result of casting 1.5 μL of each of the catalysts onto a GCE to construct a modified layer. As varying the catalyst concentration revealed an increase in the catalytic activity, determined by product yield (mols) and current density. The expected results when the volume of catalyst deposited was lowered (0.5 μL and 1.0 μL) was a subsequent decrease in electrocatalytic activity for the hydrogen evolution reaction. The experimental results did not indicate the expected trend with varying the volume of catalyst deposited onto the electrode. Hence the catalytic activity is

independent when volumes of 0.5 μL, 1.0 μL and 1.5 μL of catalyst solution are cast onto the electrode. By casting a volume of 0.5 μL, the maximum number of electroactive moles in the film is 1.4 x 10^{-11}, while increasing the volume to 1.5 μL would allow 4.2 x 10^{-11} mols of $CoPcF_{16}$ (assuming 100 % electroactive). However metallophthalocyanines are reported to have limited conductivity, as illustrated by the modified layers shown in this chapter and by Ouyang and Sugawara.[18,19]

4.2.2.8 Using Chloride as an electrolyte

The cyclic voltammetry of $CoPcF_{16}$ immersed in 0.1 M HCl/KCl (~pH 1) is displayed in Figure 4.20. Comparing the cyclic voltammogram using this electrolyte to one obtained in a phosphate solution reveals similar characteristics, however it is evident a shift in potential occurred (in HCl/KCl) for the most prominent process, assigned as the reduction of the metal centre of $CoPcF_{16}$.

The cyclic voltammogram of $CoPcF_{16}$ shows a reversible redox process at -0.39 V vs. Ag/AgCl and is assigned as the reduction of Co(II)/ Co(I) process (E ½ = -0.43 V vs. Ag/AgCl in pH 2 phosphate buffer), experiencing a 40 mV positive shift. A broad cathodic wave is observed in the potential region of -0.7 V and a re-oxidation process E_{pa} is observed at -0.52 V. This process is assigned as the reduction of the phthalocyanine ring. The potentials at which these processes occur shift in an anodic direction, as the pH of this solution is more acidic compared to the phosphate buffer.

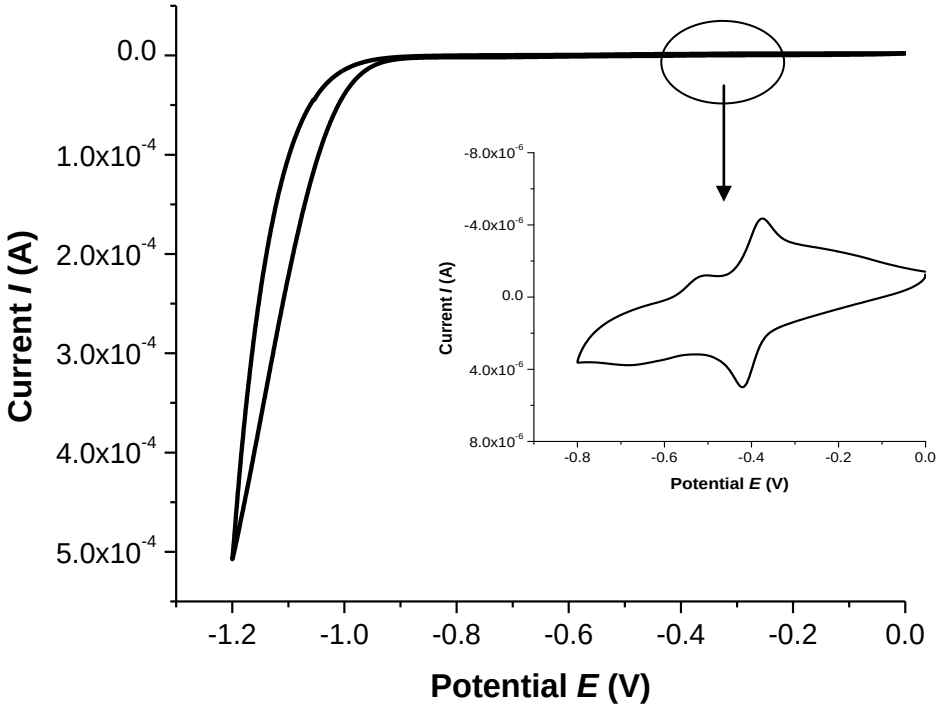

Figure 4.20: *Cyclic voltammogram of $CoPcF_{16}$ vs. Ag/AgCl in 0.1 M HCl/KCl (~pH 1) at 100 mV/s. Inset: Redox couple Co(II)/Co(I) in the potential window 0 to -0.9 V.*

A large sharp cathodic current is observed when the potential is scanned negatively to -1.2 V, Figure 4.20. As described previously for this catalyst using the phosphate electrolyte, this is indicative of a catalytic current. An onset potential occurs at -0.93 V using this electrolyte similar to when the phosphate electrolyte is employed.

The effect of varying the temperature using the HCl electrolyte was investigated and the results are shown in Table 4.13 below. Similar to the trend observed using the phosphate buffer, an increase in catalyst performance was observed with increasing temperature.

Temperature (°C)	***0***	***20***	***40***
Charge (C)	*0.15*	*0.37*	*0.54*
Moles of H_2 (mol)	*5×10^{-7}*	*1.7×10^{-6}*	*2.5×10^{-6}*
Faradaic Efficiency %	*64*	*89*	*89*
[1]Current Density (mA/cm^2)	*0.6*	*1.5*	*2.1*
[2]Current Density (mA/cm^2)	*1.7*	*7.2*	*9.6*
% Electroactive catalyst	*3.4*	*6.7*	*8.1*

Table 4.13: *Average performance data obtained for $CoPcF_{16}$ by CV and BE (at -1.2 V for 1 hour) vs. Ag/AgCl in 0.1 M HCl/KCl (~pH 1) with varying temperature. Current densities obtained by [1]BE and [2]current density obtained using the last scan of the CV.*

The TOF (hr^{-1}) values as a function of temperature are shown in Figure 4.21 (Appendix C, Table C.14). As the temperature increased, the TOF values for $CoPcF_{16}$ also increased. At 40°C, TOF figures reached 7.3×10^5, whereas at 20°C and 0°C, TOF values were 6.1×10^5 and 3.4×10^5, respectively. The Faradaic efficiencies at 20°C and 40°C were determined to be 89 % at both temperatures. The high Faradaic efficiencies for these experiments (relative to what was found in the phosphate buffer) may be a result of less water oxidation at the anode, since Cl^- should undergo oxidation at a similar potential, resulting in less O_2 generated at the counter electrode and potentially less interference by O_2 reduction at the working electrode. Furthermore, higher temperatures should decrease H_2 and O_2 solubility.[36] Lower H_2 solubility will enhance H_2 in the cell headspace and lower O_2 solubility would lower competition for electrons at the working electrode. Thus both should result in higher Faradaic efficiencies. It is also noted that the amount of product obtained in these experiments is about the same as what was found in the phosphate buffer at each temperature.

Similarly to the previous discussion in section 4.2.2.2, these Faradaic efficiencies given are a lower limit and do not take into consideration the solubility of H_2 in water at various temperatures (Figure 4.9).

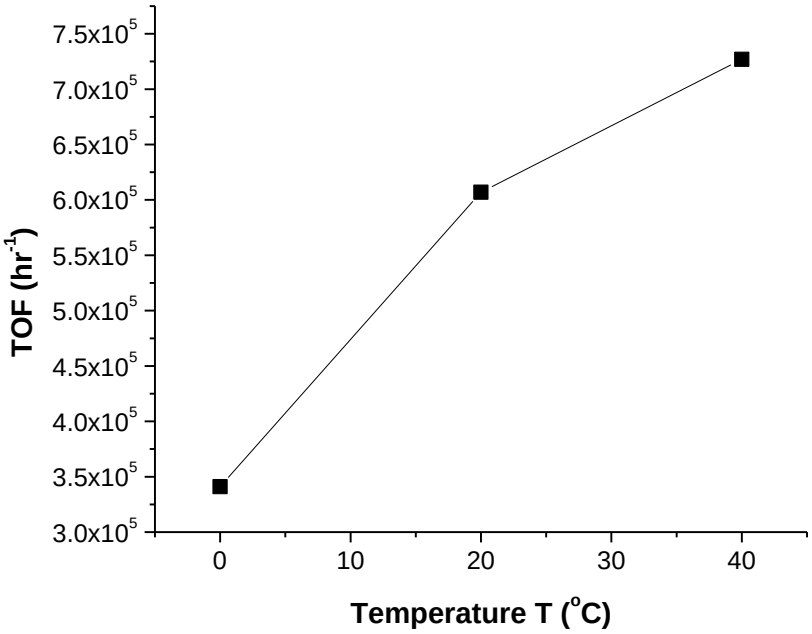

Figure 4.21: *Turnover frequencies TOF (hr^{-1}) as a function of temperature for $CoPcF_{16}$ in 0.1 M HCl/KCl.*

Comparing the TOF calculated using both these electrolyte systems, lower TOF values were obtained using 0.1 M HCl/KCl. Although these TOF data are lower, a larger number of moles of catalyst were determined to be active in these studies (the percentage of electroactive catalyst increased when higher temperatures are employed: 6.7 % and 8.1 % at 20°C and 40°C, respectively).

4.2.2.9 Stability

The stability of these catalysts is observed upon examining the cyclic voltammograms recorded prior to and after the potentiostatic electrolysis. Before an electrolysis step is performed using the modified electrode, the voltage is scanned to low potentials until the potential at which the maximum catalytic current is reached. The stability of these catalysts in the modifying layer is indicated by a cathodic catalytic current of similar magnitude after the potentiostatic electrolysis. The appearance of this current suggests a stable

electrochemical response. A decrease in the current produced after the electrolysis step would indicate instability of the catalyst in the modifying layer to serve as a catalyst for the electrocatalytic generation of hydrogen.[42] As the number of moles of electroactive catalyst is relatively low (less than 6 % electroactive for $CoPcF_{16}$, 1.0 % for $CuPcF_{16}$ and 0.1 % for $ZnPcF_{16}$) it is difficult to observe the redox couple in the CV after electrolysis (See Appendix C, Figures C.5-C.7).

4.2.2.10 Duration of Electrolysis

For the generation of H_2, the potential of the working electrode is fixed at a negative value. For $CoPcF_{16}$ and $CuPcF_{16}$, the optimum reduction potential for the electrolysis step was determined to be -1.2 V while this potential increases slightly to -1.1 V when $ZnPcF_{16}$ is used for the electrocatalytic reaction.

The aim of this study was to investigate the length of time the catalyst could be used to electrochemically generate hydrogen before the performance of the modified layer was observed to be adversely affected. The modified electrodes were prepared in the same manner as described earlier for one hour electrolyses, however the duration of the electrolysis reaction was increased from 1 hour to 5, 11 and 24 hours. These experiments were conducted using just the Co catalyst. The performance indicators are reported in Table 4.14 and the corresponding TON values are displayed in Figure 4.22.

Time (hr)	***1***	***5***	***11***	***24***
Charge (C)	*0.28*	*2.3*	*6.5*	*71.4*
[1]Current Density *J* (mA/cm^2)	*1.1*	*9.1*	*25.8*	*16.9*
(%) Electroactive $CoPcF_{16}$	*6.3*	*3.2*	*3.6*	*4.9*

Table 4.14: *Average performance data obtained for $CoPcF_{16}$ by CV and BE (at -1.2 V for 1 hour) vs. Ag/AgCl in 0.1 M NaH_2PO_4/H_3PO_4 (pH 2) as a function of time. [1]Current density obtained by BE data.*

The results presented in Table 4.14 indicate that as the length of time of the potentiostatic electrolysis increased the performance did not appear to diminish suggesting that metallophthalocyanine modified electrodes are quite stable as catalysts for the electrocatalytic hydrogen evolution reaction. When the electrolysis was carried out over 5 hours, an increase in charge passed was observed which was more than 8 times larger than the charge passed after 1 hour. After a 24 hour period, a large charge passed of 71.4 C. These results indicate that $CoPcF_{16}$ can act as a catalyst for the electrocatalytic hydrogen evolution reaction over long periods of time. The current densities obtained increased as the period of electrolysis increased, however the contribution of increasing O_2 concentration produced at the anode over time complicates these results.

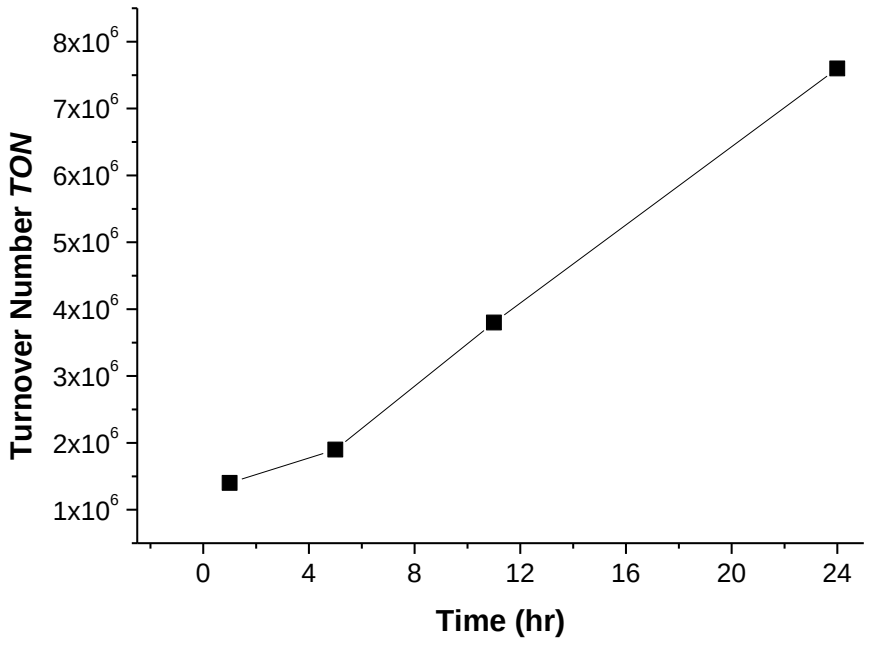

Figure 4.22: *Turnover numbers (TON) as a function of time for $CoPcF_{16}$ in 0.1 M NaH_2PO_4/H_3PO_4 (pH 2).*

The turnover numbers are displayed in Figure 4.22 for $CoPcF_{16}$ (Appendix C, Table C.15). The turnover figures presented so far in this chapter are turnover frequencies, where TOF reports the number of moles produced over a given time frame, i.e. per hour. The turnover number TON reports the number of moles of product generated per mole of immobilised, electrochemically active catalyst over

the duration of the experiment. The TON obtained by gas chromatography revealed an increase with time however, the increase in TON from 11 hours to 24 hours was more rapid. At 11 hours, the TON calculated by gas chromatography is 3.8 x 10^6, while after 24 hours, the TON reached 7.9 x 10^6. The Faradaic efficiency after 24 hours was quite poor, only 20 % efficient compared to 74 % Faradaic efficiency after 1 hour period.

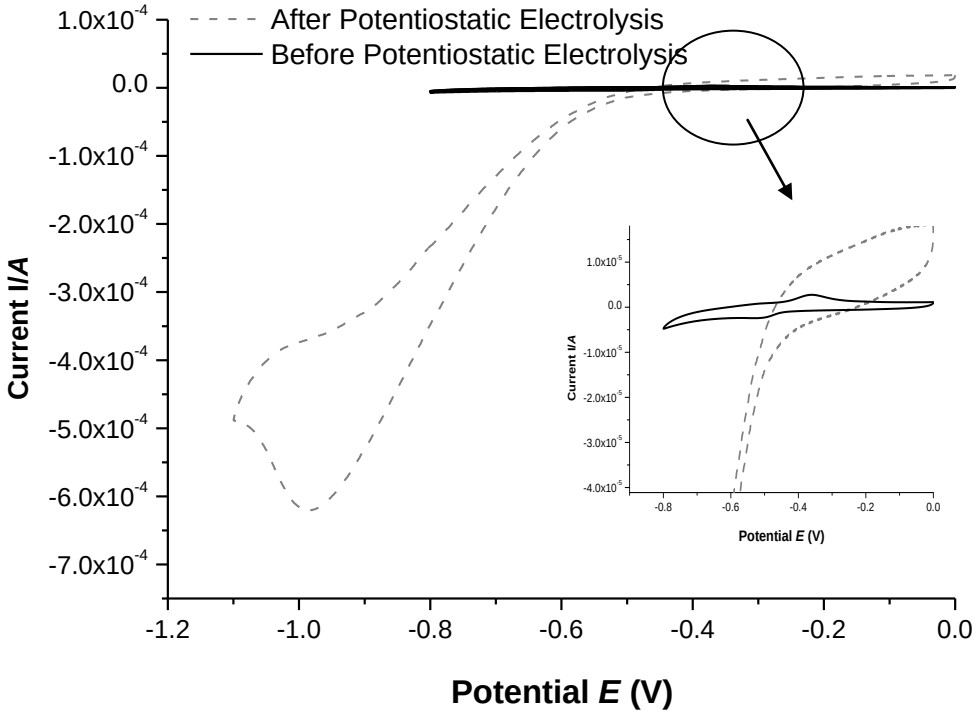

Figure 4.23: *Cyclic voltammetry of $CoPcF_{16}$ in 0.1 M NaH_2PO_4/H_3PO_4 (pH 2) vs. Ag/AgCl. The black line indicates the CV before electrolysis (Co(II)/Co(I) process) and the grey dashed line is the CV after the electrolysis step after 5 hours. Inset: enlarged potential window of 0 to -0.9 V.*

Figure 4.23 shows the voltammograms prior to electrolysis and 5 hours after electrolysis. It is evident that the onset potential shifted significantly in a positive direction and appeared at the potential at which the Co(II)/Co(I) process was observed. A subsequent increase in current is also observed, further indicating the stability of the modified electrode.

4.2.2.11 Repeated use of a modified electrode

The stability of the catalyst in the modified layer has been discussed, where the stability after the potentiostatic electrolysis is indicated by a catalytic current of similar magnitude to the initial catalytic current prior to electrolysis. Work was carried out to investigate if the modified electrode could be used for a second time; in a separate experiment with fresh electrolyte and de-aerated for 20 minutes, as per previous experiment set-ups. An overlay of the currents observed in a potential window of 0 to -1.2 V vs. Ag/AgCl when the modified electrode was used for the first and second time is shown in Figure 4.24. The magnitude of the catalytic current is slightly less in the second experiment than observed the first time the electrode was used. The redox couple of Co(II)/ Co(I) is less prominent that compared to the voltammogram obtained the first time the modified electrode was used. The number of moles which were electroactive in the modifying layer was calculated as 4.8 x 10^{-13} moles, less than half of the electroactive catalyst that was determined after the first experiment.

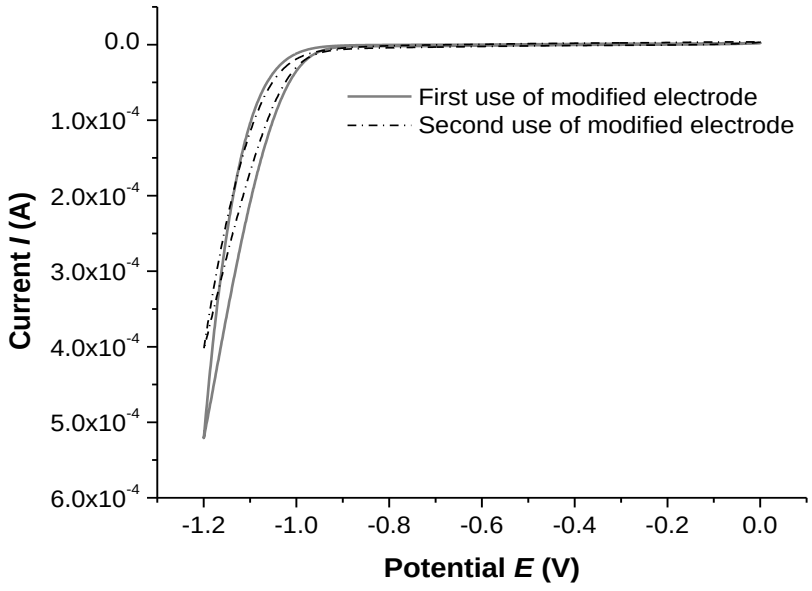

Figure 4.24: *Cyclic voltammogram of $CoPcF_{16}$ vs. Ag/AgCl in 0.1 M NaH_2PO_4/H_3PO_4 (pH 2) at 100 mV/s. The grey line indicates the catalytic current obtained prior to the first electrolysis step while the dashed line shows the catalytic current obtained prior to the second electrolysis step.*

From Table 4.15, it can also be seen that the charge which passed during the second electrolysis was only 50 % of the charge passed when the modified electrode was used the first time.

Re-use of Electrodes	***First Use***	***Second Use***
Charge (C)	*0.24*	*0.12*
Moles of H_2 (mol)	*6.1×10^{-7}*	*1.2×10^{-7}*
Faradaic Efficiency %	*49*	*19*
[1]Current Density *J* (mA/cm^2)	*0.9*	*0.4*
[2]Current Density *J* (mA/cm^2)	*7.8*	*2.4*
Moles of electroactive catalyst (mol)	*1.1×10^{-12}*	*4.8×10^{-13}*
(%) Electroactive $CoPcF_{16}$	*2.5*	*1.1*

Table 4.15: *Average performance data obtained for $CoPcF_{16}$ by CV and BE (at -1.2 V for 1 hour) vs. Ag/AgCl in 0.1 M NaH_2PO_4/H_3PO_4 (pH 2) after the first and second use. Current density obtained using data from [1]BE and [2]current density obtained using the last scan of the CV.*

The TOF (hr^{-1}) values obtained when the electrode is used for a second time for the hydrogen evolution reaction are 2.4×10^5 (and 5.7×10^5 for the first use). (See Appendix for additional TOF data, Table C.16).

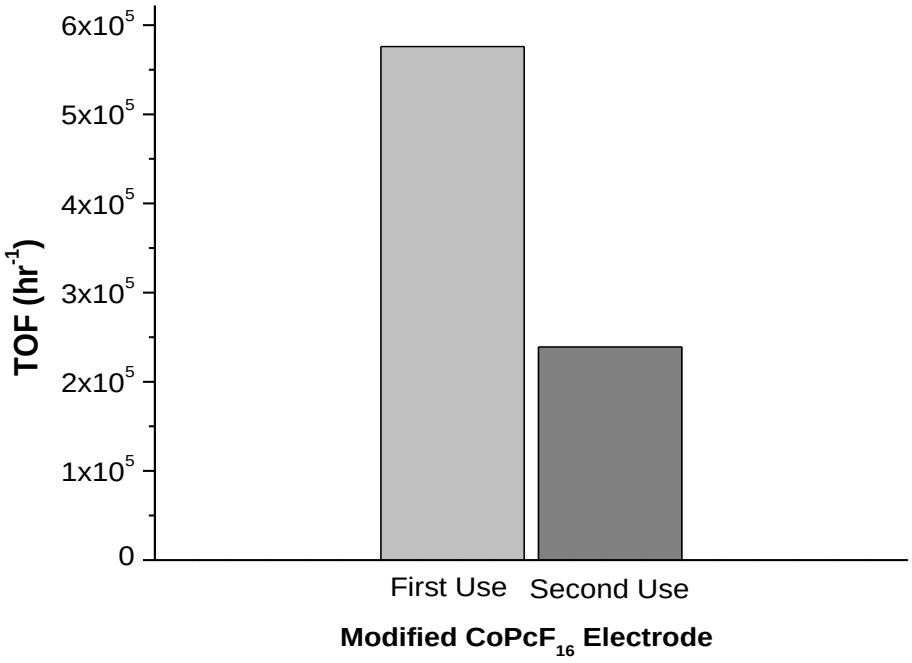

Figure 4.25: *Turnover frequencies obtained for $CoPcF_{16}$ where the light grey and dark grey columns correspond to the first and second use of the modified electrode respectively.*

From the data, it appears that this systems performance deteriorates with use. This is further shown by comparing the moles of hydrogen produced; 6.1 x 10^{-7} mols of H_2 is produced for the first used and when used for a second time, only 1.2 x 10^{-7} mols are generated.

4.2.2.12 Photo- electrocatalytic generation of hydrogen

Phthalocyanines can play a role as active components for processes driven by light. This is been reported by many groups, including Klofta[51] and Kaneko *et al.* who reported an increase in electrocatalytic activity when modified electrodes containing zinc macrocycles were irradiated with light.[52,53,54] The experiments discussed so far in this chapter were all carried out in natural daylight. As metal phthalocyanines can absorb light at both the blue and red regions, it was necessary to investigate the effect of the absence of light on these modified electrodes containing $CoPcF_{16}$, $CuPcF_{16}$ and $ZnPcF_{16}$.

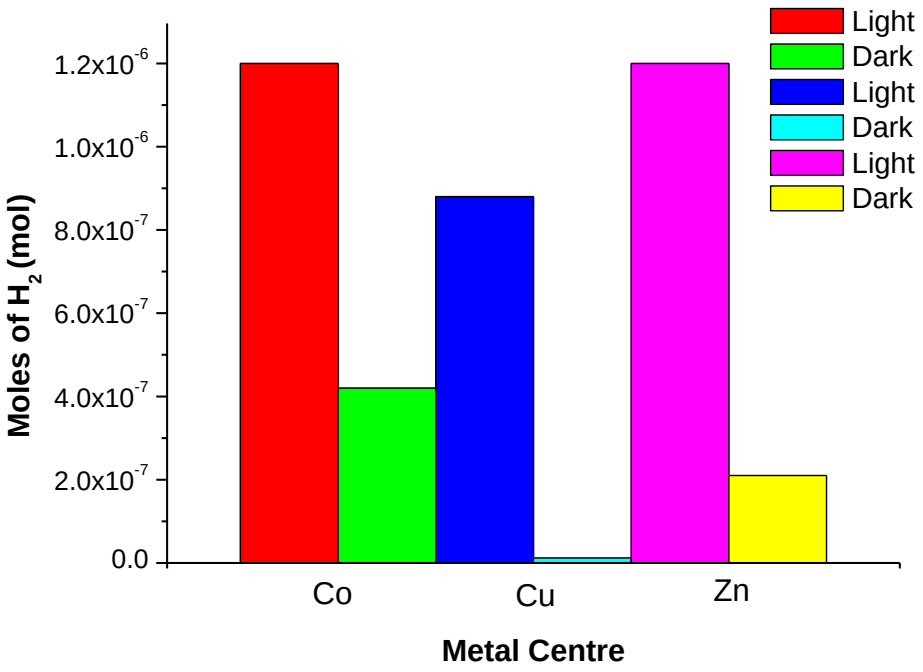

Figure 4.26: *Moles of hydrogen obtained by gas chromatography after 1 hour potentiostatic electrolysis at -1.2 V vs. Ag/AgCl for $CoPcF_{16}$, $CuPcF_{16}$ and $ZnPcF_{16}$ in 0.1 M NaH_2PO_4/H_3PO_4 (pH 2).*

The cell was placed in a dark cupboard and the potentiostatic electrolysis experiments in the absence of light were performed. The resulting experimental data are displayed in Tables 4.16-4.17 for $CoPcF_{16}$ and $CuPcF_{16}$/ $ZnPcF_{16}$ respectively. The moles of hydrogen obtained in the light and the dark are shown in Figure 4.26 above.

Variable	Dark	Light
Charge (C)	*0.13*	*0.28*
Moles of H_2 (mol)	*4.2×10^{-7}*	*1.2×10^{-6}*
Faradaic Efficiency %	*63*	*74*
[1]Current Density (mA/cm^2)	*0.6*	*1.1*
[2]Current Density (mA/cm^2)	*1.8*	*7.5*
% Electroactive	*1.5*	*6.3*

Table 4.16: *Average performance data obtained for $CoPcF_{16}$ by CV and BE (at -1.2 V for 1 hour) vs. Ag/AgCl in 0.1 M NaH_2PO_4/H_3PO_4 (pH 2) in daylight and in darkness. Current density obtained using [1]BE and [2]current density obtained using the last scan of the CV.*

Examination of the data shown in the table revealed a decrease in activity when the electrolyses were conducted in the absence of light. This suggests that the electrocatalytic generation of hydrogen is aided when performed in daylight. For $CoPcF_{16}$, the charge passed after an hour electrolysis was doubled when carried out in daylight (0.28 C) compared to the charge obtained in darkness; 0.13 C. Hence it appears that the light contributes to the catalytic activity for hydrogen evolution using this catalyst.

	$CuPcF_{16}$		$ZnPcF_{16}$	
Variable	**Dark**	**Light**	**Dark**	**Light**
Charge (C)	*0.03*	*0.23*	*0.13*	*0.44*
Moles of H_2 (mol)	*1.2×10^{-8}*	*8.8×10^{-7}*	*2.1×10^{-7}*	*1.2×10^{-6}*
Faradaic Efficiency %	*8*	*74*	*31*	*54*
[1]Current Density (mA/cm^2)	*0.1*	*0.9*	*0.5*	*1.8*
[2]Current Density (mA/cm^2)	*1.5*	*5.7*	*2.6*	*5.9*
% Electroactive	*0.3*	*1.0*	*0.9*	*0.1*

Table 4.17: *Average performance data obtained for $CuPcF_{16}$ and $ZnPcF_{16}$ by CV and BE vs. Ag/AgCl in 0.1 M NaH_2PO_4/ H_3PO_4 (pH 2) in daylight and in darkness. Current density obtained using data from [1]BE and [2]CV.*

Comparing the resulting data obtained when $CuPcF_{16}$ and $ZnPcF_{16}$ were employed as catalysts, the same trend determined for $CoPcF_{16}$ was observed. For $ZnPcF_{16}$, the charge passed after an hour electrolysis was less than one third of that when carried out in daylight (0.44 C) compared to the charge obtained in darkness; 0.13 C. The current density also confirmed that the absence of light appeared to cause a decrease in the catalytic activity. When the reaction takes place in daylight, a current density of 1.8 mA/cm^2 was obtained by bulk electrolysis, however when the electrochemical cell was placed in darkness, the resulting current density falls to 0.5 mA/cm^2, again, only one third of the value obtained when the cell was placed in light (however these current densities are complicated by the presence of O_2 after an hour electrolysis). Similarly, the current density obtained by cyclic voltammetry was reduced by more than half when the cell was placed in the dark, a direct indication of the effect of light on proton reduction at -1.2 V vs. Ag/AgCl.

Thus for phthalocyanines with Cu and Zn as central metal cations, the light contributes to the rate at which the hydrogen is evolved.[55] This behaviour was observed by Tachikawa *et al*. where in the darkness, no significant cathodic current for the electrocatalytic reduction of O_2 using ZnPc was observed.[56]

The largest affect the absence of light has on the generation of hydrogen electrocatalytically was when $CuPcF_{16}$ was employed. The lowest charge passed after 1 hour electrolysis, 0.03 C in darkness was observed. This is 7 times lower than the charge obtained in daylight of 0.23 C. The current density also confirmed that when the electrochemical cell was placed in darkness, a decrease in the catalytic activity was observed. In daylight, a current density of 0.9 mA/cm^2 was obtained, however when the electrochemical cell was placed in darkness, the resulting current density decreased to 0.1 mA/cm^2, again, almost 7 times smaller compared to the current density value obtained when the cell was placed in light, (4 times less when comparing current densities obtained by CV). The catalyst which displayed the weakest electrocatalytic activity when placed in darkness, relative to the activity observed in daylight was $CuPcF_{16}$, while the most efficient catalyst which can perform in the absence of light was $CoPcF_{16}$, as determined by the current density. These findings are in agreement with the literature for CoPc derivatives, where these complexes can act as efficient electrocatalysts for the reduction of O_2 in the dark.[57,58,59] Thus, the performance indicators displayed in Tables 4.16 and 4.17 indicate that these catalysts can work in both light and dark conditions, with the optimum conditions being in daylight. (See Appendix C, Table C.17 and Figure C.8 and C.9).

4.3 Experimental considerations

4.3.1 Pressure

The equations required to calculate TOF values by gas chromatography are described in Chapter 2. An important assumption which has been made for all the TOF data calculated throughout this thesis is that the pressure remains as 1 atm (101325 Pa) during the potentiostatic electrolysis. Accumulation of the product of the electrolysis reaction ($H_{2(g)}$) subsequently changes (increases) the pressure in the headspace of the cell at fixed volume (5.5 mL). The increase in H_2 pressure could affect the kinetics by slowing down the rate of the reaction at the working electrode.

For the experiments carried out in this thesis, there are no visible signs of an increase in pressure which would be expected if there was a significantly large increase in pressure building up in the cell; a bulge in the rubber septa was not observed. Also, if the pressure in the cell was much larger than 1 atm, it is assumed the plunger of the needle would rise instantly to fill the syringe. This is also not observed upon taking a gas sample from the headspace of the electrochemical cell. Finally, as the average partial pressure due to hydrogen evolution in the electrochemical cell was 700 Pa, this is the equivalent of a 0.69 % rise in pressure in the cell and thus may be considered as negligible.

4.3.1.1 Effect of using a larger cell volume

The effect of pressure can be further illustrated by using a larger cell with a headspace volume of 21 mL. This headspace is 4 times larger than the standard cell, denoted cell 1. By carrying out an identical potentiostatic electrolysis using the larger cell, denoted cell 2, this increased volume was thought to alleviate some of the pressure due to the change in the partial pressure component as a result of the evolution of hydrogen gas at the working electrode. Also it was expected if the increase in pressure is a dominant factor in the standard cells and subsequently hinders the rate of the reaction in an hour potentiostatic electrolysis experiment, then this larger cell should allow for the rate of the reaction to be unaffected as the

headspace volume is almost 4 times larger. Thus, an increase in the performance indicators is expected when cell 2 is employed.

In order to analyse the results of an increase in volume of headspace, it is sensible to replicate an experiment which generates a large current density and also one where a large TOF is determined by gas chromatography. The system which displayed the greatest catalytic activity when the operating temperature was set to 40°C was $CoPcF_{16}$. The solubility of hydrogen also plays a vital role as discussed in section 4.2.2.2; the solubility of hydrogen in water decreases with increasing temperature. The experimental results of using both the standard cell 1 and the larger cell 2 are displayed in Table 4.18.

	Cell 1	***Cell 2***
Charge (C)	*0.80*	*0.68*
Moles of H_2 (mol)	*2.1×10^{-6}*	*1.2×10^{-6}*
Faradaic Efficiency %	*50*	*35*
[1]Current Density *J* (mA/cm^2)	*2.3*	*2.4*
[2]Current Density *J* (mA/cm^2)	*7.5*	*10.7*
Moles of electroactive catalyst (mol)	*2.9×10^{-12}*	*2.5×10^{-12}*
Electroactive $CoPcF_{16}$ (%)	*6.8*	*6.0*

Table 4.18: *Average results obtained for $CoPcF_{16}$ by CV and BE (at -1.2 V for 1 hour) vs. Ag/AgCl in 0.1 M NaH_2PO_4/H_3PO_4 (pH 2) using cell 1 (total volume of headspace = 5.5 ml) and using cell 2 (total volume of headspace = 21 ml) at 40°C. Current density obtained using data from [1]BE and [2]current density obtained using the last scan of the CV.*

Examination of the performance indicators showed that employing a cell with a larger headspace did not significantly change these parameters for the electrocatalytic generation of hydrogen. These results were not expected if the catalytic activity was hindered by the increase in pressure with a fixed volume. As cell 2 contains a larger headspace, it was expected that higher performance indicators would be observed if the pressure is a dominant factor in the electrolysis reaction. These results above suggest that the pressure in the cell did not rise significantly enough to affect the rate of the hydrogen evolution reaction. In fact, it appeared that the kinetics is slightly improved while housed in the standard cell, where a charge of 0.80 C is obtained during the 1 hour potentiostatic electrolysis, compared to 0.68 C in cell 2 at 40°C. However the average current density, obtained during one hour electrolysis was marginally larger in cell 2 of 2.4 mA/cm^2.

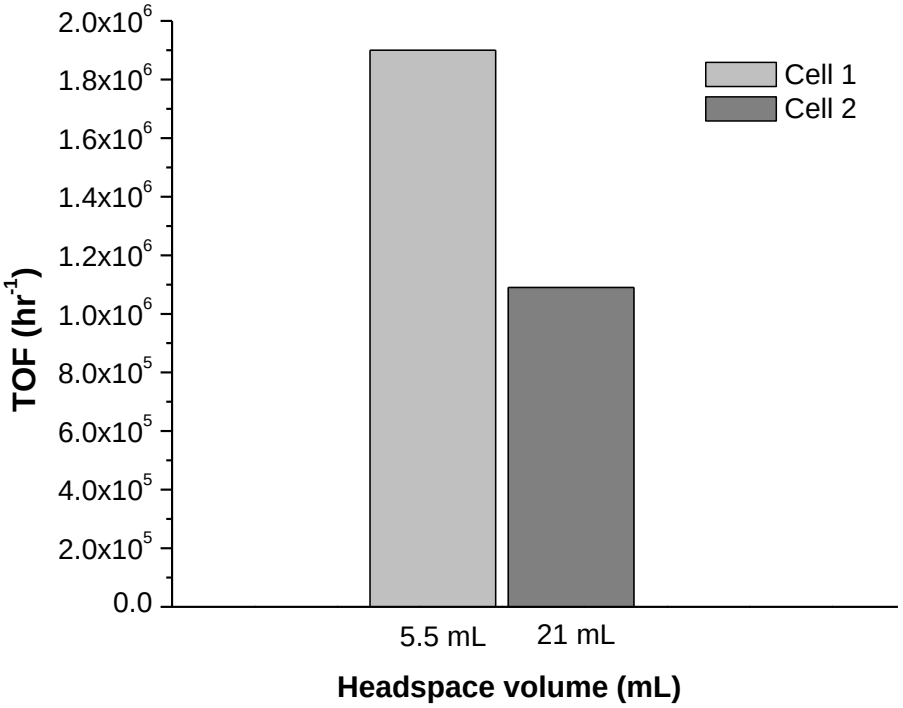

Figure 4.27: *Turnover frequencies TOF (hr^{-1}) obtained for $CoPcF_{16}$ where the dark grey and light grey columns correspond to the TOFs by gas chromatography for the modified electrodes placed in cell 1 and cell 2 respectively.*

Comparing the TOF determined in the standard cell 1 with the TOF obtained in the larger cell 2, it is evident that the highest TOF values are attained using the smaller cell 1. Using the larger cell 2, the TOF values calculated are one third less, 1 x 10^6 than those determined using the standard cell 1, 1.9 x 10^6. Hence it is concluded that the catalytic activity is not affected by the volume of cell headspace when 1 hour potentiostatic electrolysis is carried out. It is also concluded that the pressure does not deviate significantly from 1 atm when hydrogen gas is produced electrocatalytically, therefore the equations for calculating TOF determined by gas chromatography are valid (albeit a level of error exists).

4.3.2 Effect of temperature on solvent evaporation and film quality

Two sets of results are shown in Table 4.21 below; the first are the number of electroactive moles present on the electrode surface when dried overnight in a cupboard and the second represent the number of electroactive moles present on the electrode surface when dried overnight in an oven set at 21°C.

Air-Temperature of electrodes for solvent evaporation	**21°C**	**Varied**
Mean no. of moles of electroactive catalyst (mol)	*4.6x* 10^{-12}	*1.4 x* 10^{-12}
Standard Deviation (mol)	*2.8 x* 10^{-12}	*1.2 x* 10^{-12}
% Distribution of data about the mean	*60*	*90*

Table 4.19: *Catalyst solution prepared in DMF; Data obtained for modified electrodes when the temperature is maintained at 21°C and when the temperature can fluctuate.*

The data suggests that the drying rate does exhibit some influence over film features. It appears that the fraction of catalyst that is electroactive is lower for

films that are not dried under constant temperature conditions. If there is a real effect here, it is expected that regulated drying conditions would improve the regularity of the film. It is evident from the statistical data presented above that construction of these modified electrodes is influenced by the temperature as it affects the rate of removal of the solvent evaporation. By placing the modified electrodes in an oven set at a constant temperature (21°C), it allows for the formation of a homogenous layer, thus the measure of uncertainty is reduced. The electrodes which are placed in a cupboard overnight are affected deeply by the temperature. Considering that the solvent is allowed to evaporate over the course of approximately 18 hours, the temperature of the laboratory overnight may decrease, possibly leading to an irregular rate of solvent removal and hence an inhomogeneous layer formation as the temperature is inconsistent.[42]

4.3.3 Seal Integrity

The construction of the electrochemical cells used for the electrocatalytic generation of hydrogen consists of a v-shaped glass cell filled with 15 mL of electrolyte solution with the working modified electrode, reference electrode and counter electrode. These are placed in the cell, where in one side, the reference and counter electrode are fitted. A rubber septum is used to hold both electrodes in place and also to seal the cell as the product of the electrolysis reaction is a gas. A second rubber septum is used and is placed in the second neck of the cell in which the modified electrode is placed. When the cell is sealed, a stream of argon is allowed to flow through the cell by piercing these seals with the inlet needle (Ar) and an outlet needle which allows the gas to escape from the cell. When the cell has been de-aerated after 20 minutes (see Appendix C, Figure C.11), the needles are removed and the septa are covered with a layer of parafilm. As the rubber seals have been pierced, it is important to investigate the integrity of the seal. It is possible that H_2 may escape at a faster rate, before the headspace analysis takes place. Therefore it was necessary to investigate the rate of loss of gas when a seal has been previously pierced.

A schlenk flask was filled with hydrogen gas and sealed with a rubber septum. Using a gas tight syringe, the seal was pierced with the needle and a volume of

hydrogen gas was injected into the GC. The amount of hydrogen was obtained by the chromatogram generated by the TCD. A second injection was taken and importantly, the needle pierced a different part of the rubber septum. This sample was injected into the GC for analysis. This procedure of piercing the seal in different locations of the rubber septum was continued until a large area of the seal had been pierced (carried out over one week). The chromatograms revealed that continuous piercing of the rubber septa did not significantly allow the hydrogen gas to escape, as the concentration of hydrogen present after one week decreased by 40 %.

4.4 Concluding Remarks

The parameters and operating conditions which affect the activity of $MPcF_{16}$ where M is Co, Cu or Zn to electrocatalytically generate hydrogen from water were investigated. Important conditions such as pH, temperature and electrolysis potential have been discussed. The onset potentials for $CuPcF_{16}$, $ZnPcF_{16}$ and $CoPcF_{16}$ were determined to be -0.85, -0.87 and -0.90 V vs. Ag/AgCl in pH 2 phosphate solution (0.1 M NaH_2PO_4/H_3PO_4). At least a 200 mV decrease in overpotential for H_2 evolution was achieved using these modified electrodes, with respect to the bare electrodes in identical conditions. It was found that the best overall performance at pH 2 and at 20°C was provided by $ZnPcF_{16}$ (largest moles of hydrogen of 1.2×10^{-6} mol at -1.1 V).

When the temperature was varied, the three catalysts each revealed lower electrocatalytic activity at 0°C due to slower electron transfer kinetics. Increasing the temperature to 20°C and 40°C provided better kinetics and improved performance. The solubility of hydrogen in water with increasing temperature is taken into consideration in the discussion of these electrocatalytic results.

Employing ethyl acetate as a solvent permitted the investigation of the affect of the rate of solvent evaporation during film casting (the results obtained using thicker films created by deposition of several layers of catalyst material). Coating an electrode with 5 layers through fast evaporation of a catalyst solution prepared using ethyl acetate revealed a low charge and a decrease in current densities relative to a single coated electrode. This decrease in electrocatalytic performance is ascribed to the slow electron transfer through the increased number of layers of catalysts.

When the pH of the electrolyte solution was increased (neutral, basic conditions) the potential at which the redox couple and the onset potential for the electrocatalytic reaction was observed shifted to lower potentials. However the catalyst which acts the most efficiently at all pH, reflected by the overpotentials, charge and current densities was $CoPcF_{16}$. Altering the ionic strength of the electrolyte solution to 0.01 M displayed a decrease in catalytic activity when $CoPcF_{16}$, which was reflected in the performance indicators which revealed a

decrease by approximately 50 % compared to using 0.1 M phosphate solution. It is plausible that solution resistance gives rise to this performance. Increasing the number of layers (from a DMF solution) applied to the electrode of the modifying layer exhibited a decrease in electrocatalytic activity, observed in the current density, charge and TOF obtained for each of the catalysts. Varying the concentration of the catalysts cast into the electrode reveals the highest current density for $CoPcF_{16}$ when the most concentrated catalyst was applied, 2.1 x 10^{-5} M, however the largest TOF values obtained when the least concentrated solution of catalyst cast, 7.x 10^{-6} M, which was due to the low number of electroactive moles in the modifying layer at this concentration.

The stability of the layers was investigated through running experiments over different durations. After 24 hours, a plateau or a decrease in charge would be expected if the modifying layer deactivated or decomposed on the electrode. However this was not observed, indicated by the large charge and TON obtained after 24 hours of electrolysis, reaching 71.4 C and 9.7 x 10^{6} respectively. To further investigate the stability of these layers, the modified electrodes containing $CoPcF_{16}$ were subjected to repeated use for the electrocatalytic generation of hydrogen. Lastly, the effect of light was investigated for all catalysts. When these electrocatalytic experiments were performed in the dark the activity fell for all three metallophthalocyanines indicated by a decrease in the current density, charge, TOF and percentage electroactive in the layer. The largest difference was observed using $CuPcF_{16}$ as the catalyst, where the number of moles of H_2 produced in the dark (1.1 x 10^{-7} moles) was more than 7 times less than the moles of hydrogen produced in the light (8.8 x 10^{-7} moles). Thus light plays a role in the electrocatalytic generation of hydrogen.

The practical experimental considerations are discussed, such as the effect of pressure in a standard cell compared to a cell of larger headspace volume. It is concluded that the volume of headspace available does not affect these electrocatalytic reactions over the 1 hour potentiostatic electrolysis, thus the effect of increasing pressure is not evident in this experimental set up. The rate of which hydrogen gas escapes from the electrochemical cell sealed using rubber septa and the errors which are associated with these experiments have also been discussed.

4.4 References

[1] D. Wöhrle, D. Schlettwein, G. Schnurfeil, G. Schneider, E. Karmann, T. Yoshida, M. Kaneko, *Polymers Adv. Tech., 6,* **1995**, 3, 118.

[2] T. Yoshida, K. Kamato, M. Tsukamoto, T. Iida, D. Schlettwein, D. Wohrle, M. Kaneko, *J. Electroanal. Chem. 385*, **1995**, 209.

[3] T. Abe, F. Taguchi, T. Yoshida, S. Tokita, G. Schnurpfeil, D. Wohrle, M. Kaneko, *J. Mol. Catal. A-Chem. 112*, **1996**, 55.

[4] T. Abe, H. Imaya, T. Yoshida, S. Tokita, D. Schlettwein, D. Wohrle, M. Kaneko, *J. Porphyr. Phthalocya. 1*, **1997**, 315.

[5] E. E. Benson, C.P. Kubiak, A.J. Sathrum, J.M. Smieja, *Chem. Soc. Rev. 38*, **2009**, 89.

[6] N. Chebotareva, T. Nyokong, *Electrochim. Acta, 42,* **1997**, 23-24 3519.

[7] M. K. Şener, A. Koca, A. Gül, M.B. Koçak, *Polyhedron, 26*, **2007**, 1070.

[8] A. Koca, M.K. Şener, M.B. Koçak, A. Gül, *Transit. Metal Chem., 30,* **2005,** 399.

[9] A. Koca, Ş. Bayar, H.A. Dinçer, E. Gonca, *Electrochim. Acta, 54*, **2009,** 2684.

[10] M. Ozer, A. Altindal, A.R. Özkaya, M. Bulut, Ö. Bekaroglu *Polyhedron, 25,* **2006**, 3593.

[11] A. Alemdar, A. R. Özkaya, M. Bulut, *Polyhedron, 28*, **2009**, 3788.

[12] F. Zhao, J. Zhang, D. Wöhrle, M. Kaneko, *J. Porphyr. Phthalocya.,4*, **2000**, 31.

[13] A. Koca, *Electrochem. Commun., 11*, **2009**, 838.

[14] F. Zhao, J. Zhang, T. Abe, D. Wöhrle, M. Kaneko, *J. Mol. Catal. A: Chem., 145*, **1999**, 245.

[15] V. Fourmond, P.A. Jacques, M. Fontecave, V. Artero, *Inorg Chem, 49*, **2010**, 10338.

[16] C. Costentin, S. Drouet, M. Robert, J.M. Savéant, *J. Am. Chem. Soc, 134*, **2012**, 11235.

[17] T. Abe, T. Yoshida, S. Tokita, F. Taguchi, H. Imaya, M. Kaneko, *J. Electroanal. Chem., 412*, **1996**, 125.

[18] J. Ouyang, K. Shigehara, A. Yamada, F. C. Anson, *J. Electroanal. Chem., 297*, **1991**, 2, 489.

[19] K. Sugawara, S. Hoshi, K. Akatsuka, K. Shimazu, *J. Electroanal. Chem., 414*, **1996,** 253.

[20] A. Elzing, A. van der Putten, W. Visscher, E. Barendrecht, *J. Electroanal. Chem. 233,* **1987**, 99.

[21] P. Janda, N. Kobayashi, P.R. Auburn, H. Lam, C.C. Leznoff , A.B.P. Lever, *Can. J. Chem. 67*, **1989**, 1109.

[22] (a) J. Masassen, B. Ilan, *J. Catal., 17,* **1970**, 86. (b) J. P. Randan, *Electrochim. Acta, 19,* **1974**, 83.

[23] A. Koca, *Int. J. Hydrogen Ener. 34*, **2009**, 2107.

[24] Ö.A. Osmanbaş, A. Koca, M. Kandaz, F. Karaca, *Int. J. Hydrogen Ener. 33*, **2008**, 3281.

[25] A. Koca, A. Kalkan, Z. Altuntaş Bayir, *Electrochim. Acta, 56,* **2011**, 5513.

[26] J. H. Zagal, R. K. Sen, E. yaeger, *J. Electroanal. Chem., 83*, **1977**, 207.

[27] J. P. Collman, P. Denisevich, Y. Konai, M. Marrocco, C. Koval, F. C. Anson, *J. Am. Chem. Soc., 102*, **1980**, 6027.

[28] S. Sun, X. Jiang, D. Xia, *J. Phys. Chem. C, 115*, **2011**, 9511.

[29] P. Mashazi, T. Mugadza, N. Sosibo, P. Mdluli, S. Vilakazi, T. Nyokong, *Talanta, 85*, **2011**, 2202.

[30] L. Mao, K. Arihara, T. Sotomura, T. Ohsaka, *Electrochim. Acta, 49*, **2004**, 2515.

[31] J. H. Zagal, Coord. *Chem. Rev. 119*, **1992,** 89.

[32] J. H. Zagal, M. Paez, A.A. Tanaka, J. R. Dossantos, C. A. Linkous, *J. Electroanal. Chem. 359, 1*, **1992**, 13.

[33] M. Dieng, O. Contamin, M. Savy, *Electrochim. Acta*, *33*. **1988**, 121.

[34] R. Baker, D. P. Wilkinson, J. Zhang, *Electrochim. Acta., 53*, **2008**, 6906.

[35] C. Song, L. Zhang, J. Zhang, D. P. Wilkinson R. Baker, *Fuel Cells, 1*, **2007**, 9.

[36] http://www.engineeringtoolbox.com/gases-solubility-water-1148.html. Last referenced 20/10/2012

[37] P. Ruetschi, R. F. Amlie, *J. Phys. Chem., 70*, 8, **1966**, 718.

[38] S. Baranton, C. Coutanceau, C. Roux, F. Hahn, J. M. Leger, *J. Electroanal. Chem., 577*, **2005**, 223.

[39] Saravanan, C. J. Mathai, M. R. Anaantharaman, S. Venkatachalam, P. V. Prabhakaran, *J. Appl. Polym. Sci., 91*, **2004**, 2529.

[40] A. H. Schroeder, F. B. Kaufman, *J. Electroanal. Chem., 113*, **1980**, 209.

[41] J. M. Savéant, *Chem. Rev., 108*, **2008**, 2378.

[42] J. G Vos, M. R. Smyth, Analytical Voltammetry, Chapter 7, Amsterdam, New York, Elsevier, **1992**.

[43] O. Haas, J. G. Vos, *J. Electroanal. Chem. 113*, **1980**, 139.

[44] W. J. Albery, A. R. Hillman, *RSC Annual Report*, 78, **1981**, 377.

[45] N. Oyama, T. Ohsaka, T. Ushirogouchi, *J. Phys. Chem., 88*, **1984**, 5274.

[46] A. J. Bard, L.R. Faulkner, *Electrochemical Methods: Fundamentals and Applications*, 2nd Ed., John Wiley & Sons, Inc., **2001,** USA.

[47] B. E. Conway, M. Salomon, *Electrochim. Acta, 9*, **1964,** 1599.

[48] M. G. Walter, E. L. Warren, J. R. McKone, S. W. Boettcher, Q. Mi, E. A. Santori, N. S. Lewis, *Chem. Rev., 110,* **2010**, 6446.

[49] G. Inzelt, *Electrochim. Acta, 34*, **1989**, 83.

[50] D. Wöhrle, H. Kaune, B. Schumann, N. Jaeger, *Makromol. Chem. 187*, **1986**, 2947.

[51] (a) T. J. Klofta, J. Danziger, P. Lee, J. Pankow, Y. W. Nebesny, N. R. Armstrong, *J. Phys., Chem., 91*, **1987**, 5646. (b) T. J. Klofta, T. D. Sims, , J. W. Pankow, J. Danziger, K. Nebesny, N. R. Armstrong, *J. Phys., Chem., 91*, **1987**, 5651. (c) T. J. Klofta, P. C. Rieke, C. A. Linkous, W. J. Buttner, A. Nanthankumar, T. D. Newborn, N. R. Armstrong, *J. Electrochem. Soc., 132*, **1985**, 2134.

[52] T. Abe, H. Imaya, S. Tokita, D. Wöhrle, M. Kaneko, *J. Porphyr. Phthalocya., 1*, **1997**, 215.

[53] M. Kaneko, E. Tsuchida, Y. Imai, *J. Chem. Soc. Faraday Trans. 87*, **1991**, 1 83.

[54] D. Schlettwein, M. Kaneko, A. Yamada, D. Wöhrle, N.I. Jaeger, *J. Phys. Chem., 95*, **1991**, 1748.

[55] M. Kaneko, D. Wöhrle, D. Schlettwein, V. Schmidt, *Makromol. Chem., 189*, **1988**, 2419.

[56] H. Tachikawa, L. R. Faulkner, *J. Am. Chem. Soc., 100*, **1978**, 4379.

[57] D. Wöhrle, *Adv. Polym. Sci., 50*, **1983,** 48.

[58] E. Yaeger, *Electrochim. Acta, 29*, **1984**, 152.

[59] T. Hirai, J. Yamaki, *J. Electrochem. Soc., 132*, **1985**, 2125.

Chapter Five

Electrocatalytic Hydrogen Generation using modified Metal (II) Perfluorinated Phthalocyanine Electrodes dispersed in Nafion® polymer

The electrocatalytic generation of H_2 from water using modified electrodes of three metal (II) perfluorinated phthalocyanine complexes (where M is Co, Cu and Zn) incorporated in Nafion® are discussed. Various parameters influencing the catalytic activity discussed in the previous chapter were investigated in these studies also. The effect of varying the ratio of metallophthalocyanine to polymer matrix was conducted, which revealed the optimum catalyst system as 3-$MPcF_{16}$:Nf of (volume ratio of 1:4 MPc: Nafion®) for each of the catalysts employed.

The performance of each of the catalysts embedded in the polymer weere evaluated by TOF (hr^{-1}) and current density. The performance data were found to be significantly lower than for the adsorbed catalyst films discussed in the previous chapter, although a larger percentage of catalyst in the polymer is electroactive. The catalyst which displayed the highest catalytic activity for the electrocatalytic generation of hydrogen at 20°C in 0.1 M phosphate solution at pH 2 was $CoPcF_{16}$/Nf, achieving 4.4 x 10^5 TOF with a corresponding Faradaic efficiency of 71%.

Comparisons between adsorbed catalysts and polymer-supported forms are made throughout the discussion.

5.1 Introduction

Modified electrodes incorporating polymer matrices have been a subject of interest for many years now, with widespread applications in areas such as electroanalysis [1], electrocatalysis, [2] information storage [3] and solar energy conversion [4]. The role of the modifying layer is to allow electrochemical communication between the underlying electrode material and the solution containing the analyte of interest.[5] This is achieved by employing an electroactive species, such as metallophthalocyanines within the layer. This electroactive species can also be dispersed within an electroactive polymer. As the name suggests, electroactive polymers are polymers which allow for charge transfer to occur. There are many classes of polymers, such as electronically conducting π-conjugated polymers (polypyrole), redox species covalently linked to polymer chains (poly(vinylferrocence)) and ion exchange polymers (Nafion®, poly4-vinylpyridine-co-styrene). The appeal of employing polymers in conjunction with a redox active molecule is their properties. Electroactive polymers which are used as films in contact with an electrode can permit an electrical current and they possess a semi-rigid mechanical property.[6] It is this mechanical stability which is attractive, as it can allow for repeated ingress/ egress of reactants and products through the polymer matrix (for the duration of an electrolysis step), thus the redox species immobilised within the matrix should remain intact.

For the investigations carried out in this chapter, an ion exchange polymer Nafion® was employed. The attractive properties of this anionic polymer include thermal stability and it is chemically inert. Nafion® consists of hydrophilic sulphonate groups immobilised on hydrophobic fluorocarbon chains.[7] The redox active metallophthalocyanines are held due to hydrophobic forces within the polymer matrix, however these redox active molecules are not anchored and are considered as mobile. As the structure of this polymer contains hydrophilic and hydrophobic groups, Figure 5.1, these regions can be identified and are expected to play a vital role in oxidation/reduction processes within the polymer-catalyst layer. [8, 13, 14, 21]

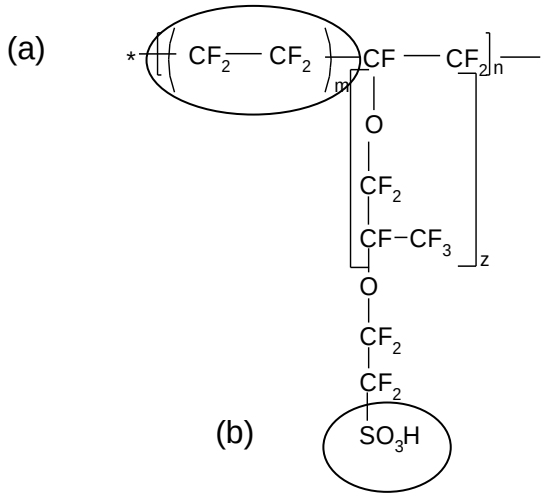

Figure 5.1: *Structure of Nafion® where the (a) hydrophobic and (b) hydrophilic regions are circled. Adapted from reference 14.*

Modified electrodes incorporating a polymer can be described by Figure 5.2.9

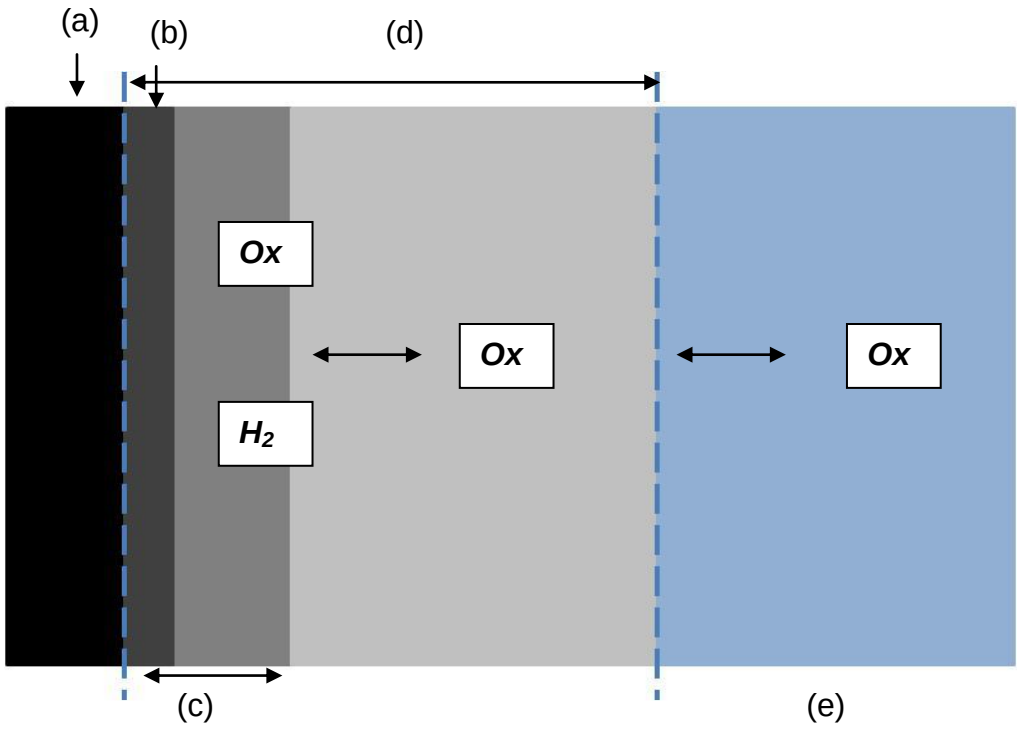

Figure 5.2: *Illustration of a modified electrode incorporating an electroactive polymer matrix where (a) Electrode, (b) Transfer layer, (c) Diffusion double layer, (d) diffusion layer and (e) bulk solution.*

In the absence of a modified layer, the electrode/solution interface consists of the electrode, electrical double layer and the bulk solution (desribed in Chapter 2). However, for a modified electrode, the electrical double layer is now identified as the "transfer layer" and the "diffuse double layer" (b) and (c), while the ionically conductive phase incorporates the transfer layer, diffusion double layer, and diffusion layer, and expands to the bulk solution, (b) – (e). The definition of the electrode/solution interface is broadened to incorporate a modified electrode.[9] Modifying layers designed to catalyse a specific target reaction, such as the hydrogen evolution reaction can be constructed.

An important factor to consider is the transport of electrons and ions through the matrix when electroactive polymers are employed. Electron transport through polymer films such as these have been thoroughly investigated over the years providing an insight into the mechanisms for reactions.[10,11,12] The electron transfer and charge transport mechanisms involving ion exchange polymer and metallophthalocyanines have been reported,[20,21] and thus pathways that describe the transport of electrons and ions in these M(II)PcF_{16} modified electrodes may be deduced.

Kaneko *et al.* described the two forms of charge transfer which can occur in redox reactions through a polymer matrix.[13,14,21] For redox-active molecules bound to a polymer matrix by strong chemical interactions (chemical binding or coordination), the ability of the redox species to move within the polymer framework is hindered and as a result, charge propagation takes place by an electron-hopping mechanism. Redox molecules which are physically bonded by electrostatic or hydrophobic interactions achieve charge propagation through charge-hopping and/or diffusion mechanisms.[15] Physical interactions between the redox molecules and the polymer matrix are considered as less restricting, thus the mobility of the redox molecules is increased. Blauch and Savéant investigated charge transport through polymer films and reported that charge propagation in a matrix is fundamentally a percolation process.[12]

This chapter will discuss the results of the investigations performed using $CoPcF_{16}$, $CuPcF_{16}$ and $ZnPcF_{16}$, each incorporated in Nafion® films, denoted

$CoPcF_{16}$/Nf, $CuPcF_{16}$/Nf and $ZnPcF_{16}$/Nf (4:1 volume ratio of M(II)PcF_{16}: Nafion®), described in Chapter 2. The effect of the varying the parameters which influence electrocatalytic hydrogen evolution are presented. The effect of varying the ratio of metallophthalocyanine to Nafion® polymer has been investigated and will be discussed in section 5.2.3. (All TOF (hr^{-1}) values presented in this chapter are based on values obtained by gas chromatography. TOF values obtained electrochemically are in Appendix D).

5.2 Results and Discussion

5.2.1 Characterisation of $MPcF_{16}$:Nafion®

Characterisation of the three metallophthalocyanines employed here are described in Chapter 3 previously. The effect of incorporating these catalysts into the Nafion® polymer is observed using cyclic voltammetry, Figure 5.3. A slight shift in the redox potential of the prominent process is observed relative to the adsorbed metallophthalocyanines. As this shift in potential is relatively small, the assignments for redox processes here are assumed to be unchanged.

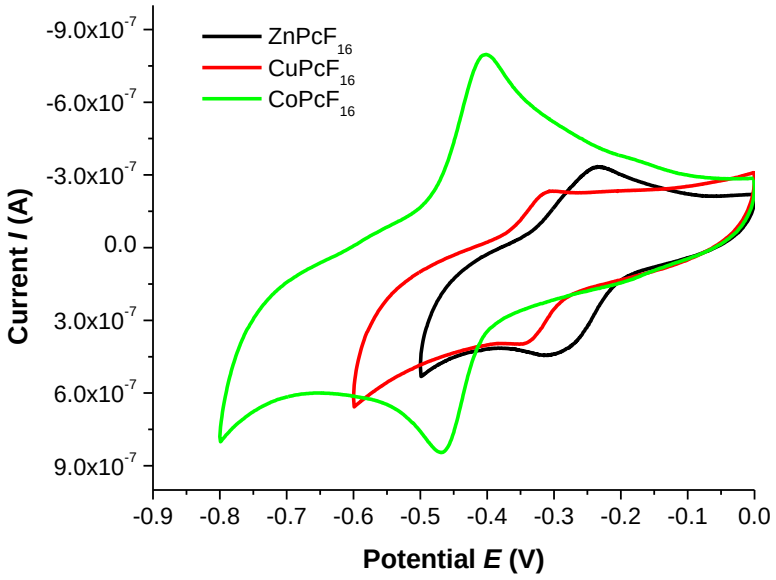

Figure 5.3: *Redox processes observed for electrodes modified with $CoPcF_{16}$/Nf, $CuPcF_{16}$/Nf, and $ZnPcF_{16}$/Nf vs. Ag/AgCl Scan rate = 100 mV/s in 0.1 M NaH_2PO_4/H_3PO_4 (pH 2).*

The potentials observed for these MPc's are similar to phthalocyanine derivatives which are commonly reported for adsorbed films, presumably due to their low solubility in common solvent-electrolyte systems.[16] For comparison purposes, the redox potentials reported by Zhao of various cobalt phthalocyanine derivates dispersed in polyvinylpyridine co-styrene (P-VPSt) are listed. Similar to the perfluorinated catalysts discussed in this work, incorporation of these catalysts in a polymer matrix causes a slight shift in potentials relative to adsorbed catalyst films.

Catalyst	**$E_{½}$ Potential (V)**	**$E_{pc} - E_{pa}$ (V)**
$CoPcF_{16}$/Nf	-0.43	0.06
$CuPcF_{16}$/Nf	-0.32	0.03
$ZnPcF_{16}$/Nf	-0.25	0.10
CoPc[(a)]	-0.57	-
CoPc/PVP[(b)]	-0.25	-
$CoPc(CN)_8$/P(VP-St)[(b)]	-0.20	-
$CoPc(SO_3H)_4$/ P(VP-St) [(b)]	-0.50	-

Table 5.1: *Potentials at which the redox couple is observed vs. Ag/AgCl in 0.1 M NaH_2PO_4 (pH 2) at 20°C for $CoPcF_{16}$/Nf, $CuPcF_{16}$/Nf, and $ZnPcF_{16}$/Nf, modified electrodes. (a) denotes the redox potentials of various cobalt phthalocyanine derivates reported by Ouyang et al.[17] (b) denotes the redox potentials of various cobalt phthalocyanine derivates reported by Zhao et al.[16]*

The redox potentials displayed in Table 5.1 reveal relatively small shifts when compared to the potentials in the absence of a polymer matrix; no shift in potential for $CoPcF_{16}$, a 20 mV cathodic shift when $CuPcF_{16}$/Nf is used and a 20 mV anodic shift for $ZnPcF_{16}$ when compared to the adsorbed catalysts.

5.2.1.1 Onset Potential

The cyclic voltammogram displayed in Figure 5.4 illustrates the results of experiments involving GCE modified with $CoPcF_{16}$/Nf, $CuPcF_{16}$/Nf and $ZnPcF_{16}$/Nf where H_2 is electrochemically generated. Data for a bare GCE and Nafion®-coated GCE are shown also in 0.1 M NaH_2PO_4/H_3PO_4 electrolyte at pH 2.

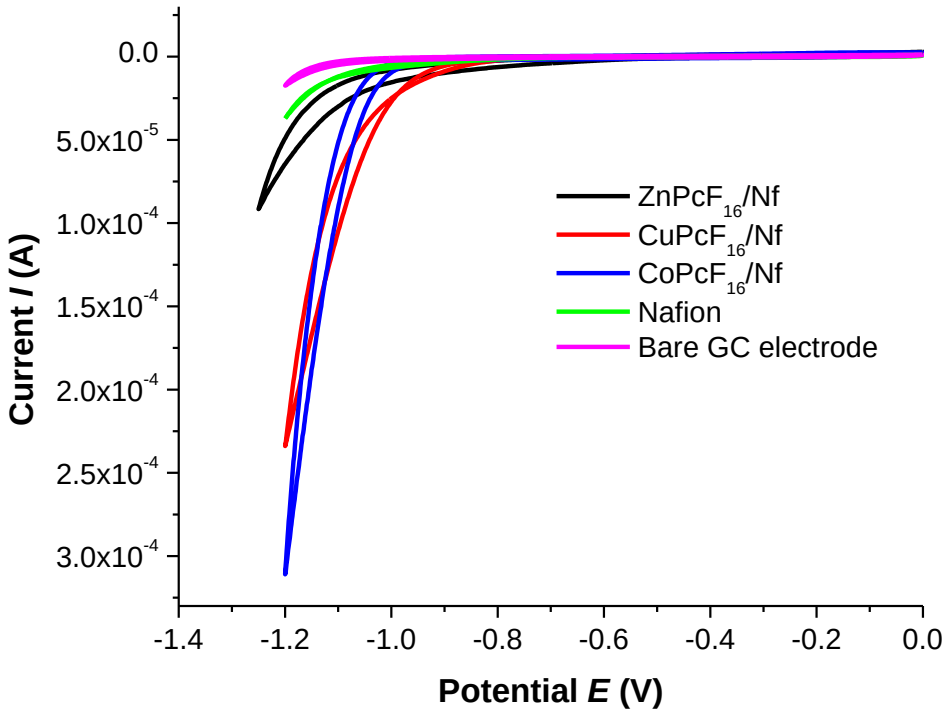

Figure 5.4: *Comparison of typical currents observed for electrodes modified with $CoPcF_{16}$/Nf, $CuPcF_{16}$/Nf, $ZnPcF_{16}$/Nf, Nafion® and a GCE, vs. Ag/AgCl. Scan rate = 100 mV/s in 0.1 M NaH_2PO_4/H_3PO_4 (pH 2)buffer.*

When $CuPcF_{16}$/Nf is employed in these studies, the cathodic current begins to increase at approximately – 0.90 V vs. Ag/AgCl. This potential is the most positive onset potential displayed of all three catalysts. In the absence of the catalyst/polymer layer (i.e. bare GCE surface) the onset potetnial was not observed until near -1.10 V. The potential which is necessary to produce currents of the same magnitude (to the bare) in the phosphate electrolyte is approximately -1.40 V vs. Ag/AgCl. Somewhat similar behaviour is observed when an electrode cast with Nafion® is employed. The overpotential for H^+ reduction using the

modified electrodes is less than for the bare electrode and Nafion®-coated surfaces. Incorporation of the catalysts into Nafion® causes a negative shift in the onset potentials for H^+ reduction; where $CuPcF_{16}$/Nf and $CoPcF_{16}$/Nf both experience small shifts (0.05 mV and 0.07 mV respectively), $ZnPcF_{16}$/Nf lowers the onset potential by 0.13 mV relative to the adsorbed catalyst.

	Onset Potential (V)
Co	-0.98
Cu	-0.90
Zn	-1.00
Nafion®	-1.05
Bare GCE	-1.10

Table 5.2: *Onset potentials (V) at which the catalytic current is produced vs. Ag/AgCl in 0.1 M NaH_2PO_4/H_3PO_4 (pH 2) at 20°C for $CoPcF_{16}$/Nf, $CuPcF_{16}$/Nf, $ZnPcF_{16}$/Nf, Nafion® modified electrode and an uncoated GCE.*

The cyclic voltammograms for the modified electrodes shown in Figure 5.4 are indicative of the catalytic H^+ reduction reaction. The resulting current from the catalytic reduction of H^+ reached a value of 3.0×10^{-4} A for $CoPcF_{16}$/Nf and 2.3×10^{-4} A for $CuPcF_{16}$/Nf. The weakest catalytic current was observed for $ZnPcF_{16}$/Nf, 1×10^{-4} A. From Figure 4.1, it can be seen that the currents for the catalysts adsorbed directly onto the electrodes (i.e. without Nafion®) are greater than those shown in Figure 5.4. Also, the onset potential for H^+ reduction is observed at less negative potentials for adsorbed films as mentioned. The current-time profile for an electrolysis experiment is shown in Figure 5.5

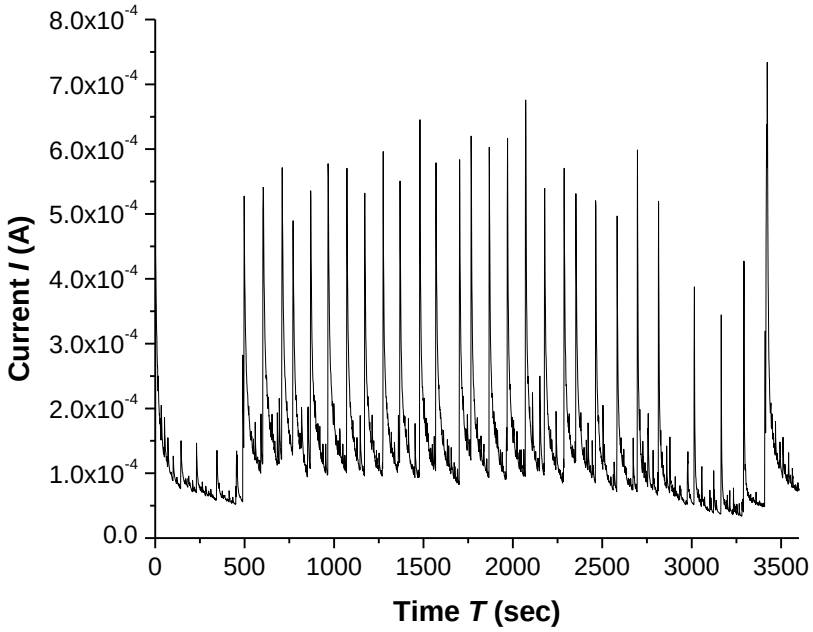

Figure 5.5*: Current- time profile as a result of potentiostatic electrolysis of $CoPcF_{16}$/Nf at -1.2 V vs. Ag/AgCl in 0.1 M NaH_2PO_4/H_3PO_4 (pH 2).*

A typical electrolysis experiment is shown in Figure 5.5, where the potential was fixed at -1.2 V for $CoPcF_{16}$/Nf corresponding to the potential at which a large steep catalytic current was observed. As the current is related to the rate of electrolysis, it can be used to calculate the charge passed after any period of time during the reaction (charge is the integral of current with respect to time).

5.2.1.2 Electrochemical reactivity of M(II)PcF_{16} embedded in Nafion®

For each of the electrocatalysts discussed here, modified electrodes were created by casting ~ 22 μM solutions (1.5 μL) of the catalyst (in Nafion®/DMF). The surface coverage of the catalyst in the Nafion® film was thus ~5 x 10^{-10} mol/cm^2 of geometric electrode area (see Appendix D, Figure D.0). The amount of reactive catalyst in the coated layer was determined using the peak area of the M(II)/ M(I) couple for $CoPcF_{16}$/Nf and $Pc^{(2-)}/Pc^{(3-)}$ for $CuPcF_{16}$/Nf and $ZnPcF_{16}$/Nf respectively, as described in Chapter 2. The average percentage of this $CoPcF_{16}$ species which was found to be electroactive was calculated as ~10.5 % of the total amount deposited. This percentage is significantly larger than for

adsorbed $CoPcF_{16}$ (~6.3 %). For $CuPcF_{16}$/Nf and $ZnPcF_{16}$/Nf, the fraction of electroactive catalyst was ~3.4 % and 1.2 % for Cu and Zn catalysts, respectively. It is perhaps worth noting that the concentrations of the catalyst solutions used for preparing $CuPcF_{16}$/Nf and $ZnPcF_{16}$/Nf modified electrodes was higher than for the Co catalyst films. Similar to what was observed for $CoPcF_{16}$/Nf, a greater fraction of the total catalyst deposited in these experiments (in $CuPcF_{16}$/Nf and $ZnPcF_{16}$/Nf films) was found to be electractive compared to corresponding adsorbed catalysts (1 % and 0.1 % $CuPcF_{16}$ and $ZnPcF_{16}$ respectively). This behaviour might be ascribed to improved charge transport properties of the catalysts in the Nafion® matrix compared to what exists with the adsorbed layers of the metallophthalocyanines. Similar to Chapter 4, investigations were carried out in an effort to increase the amount of electroactive species present in the modified layer, including coating more than one layer, increasing the volume of catalyst deposited and increasing the ratio of Nafion® matrix in the modifying layer. These investigations are discussed later in the chapter.

5.2.1.3 Surface electrochemical response

The surface behaviour of the adsorbed metallophthalocyanines on a GCE has been described in Chapter 3. For modified electrodes constructed by dispersing these metallophthalocyanines in Nafion®, a linear relationship between current and square root of scan rate in cyclic voltammetry experiments was found, illustrated in Figure 5.6 for $CoPcF_{16}$/Nf. The electrochemical response of this catalyst is also representative of the behaviour exhibited by $CuPcF_{16}$/Nf and $ZnPcF_{16}$/Nf. This behaviour suggests that these redox molecules which are physically trapped in the Nafion® matrix by hydrophobic forces move by diffusion within the matrix.[21] The effect of altering the ratio of Nafion® and metallophthalocyanine in the modifying film is investigated in section 5.2.3 of this chapter.

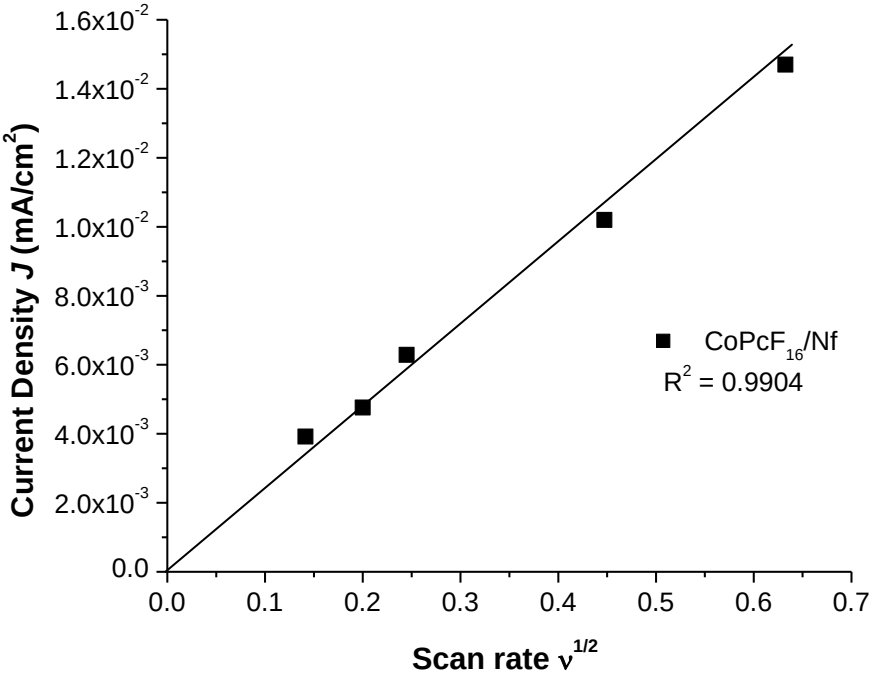

Figure 5.6: *Current density J, of $CoPcF_{16}$/Nf (4:1 vol ratio) as a function of the square root of the scan rate, v½ at 20°C.*

5.2.1.4 Proposed Reaction Pathways

The reaction pathways proposed in Chapter 4 are applicable for these metallophthalocyanines embedded in Nafion®. Following the reduction of the metal centre (Co(II)/Co(I)), the charge on the reduced complex $[Co(I)Pc^{(-2)}F_{16}/Nf]$ is compensated by cation migration from the electrolyte solution into the modifying layer, $[Co(I)Pc^{(-2)}F_{16}/Nf]^{\cdot}H^{+}$. In aqueous media at pH 2, this charge migration occurs in the form of protons from the bulk solution to balance the negative charge associated with the reduced catalytic species at the electrode surface, as protons have a higher mobility than any other cations in the film. As Nafion® is an anionic polymer, protons are easily accepted. Also, as this metallophthalocyanine is immobilised (some movement is permitted, known as bounded motion[12]) within the anionic polymer matrix, proton migration from the bulk solution into the polymer framework is favoured.

The addition of an electron on the phthalocyanine ring $[Co(I)Pc^{(-3)}F_{16}/Nf]\cdot H^+$, with the subsuqent protonation of the complex, $H^+\cdot H^+[Co(I)Pc^{(-3)}F_{16}/Nf]$ yields molecular hydrogen. These reaction steps are illustrated in Scheme 5.1.

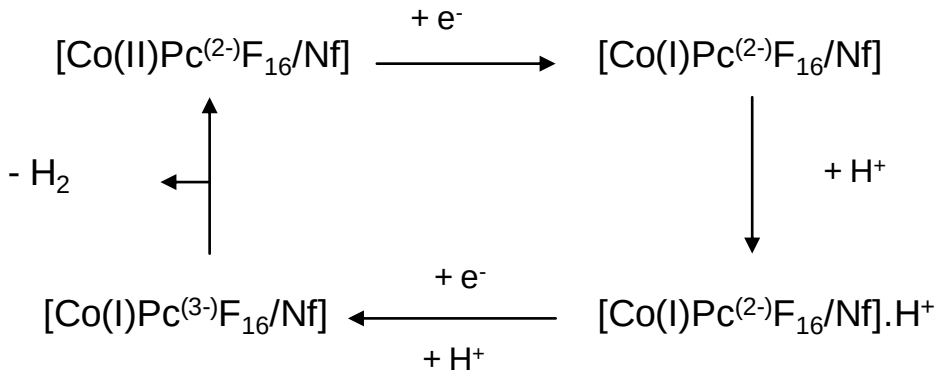

Scheme 5.1: *Proposed ECEC pathway for the electrocatalytic generation of hydrogen using $CoPcF_{16}$ embedded in Nafion® as the catalyst.*

However employing catalysts such as copper and zinc in a polymer matrix which exhibit no metal based reductions, the addition of an electron can only take place on the phthalocyanine ring.[18] As the formation of a metal hydride cannot occur, protonation can only take place on the phthalocyanine ring.[19,20] A suggested pathway is displayed in Scheme 5.2, where an *ECEC* route is postulated.

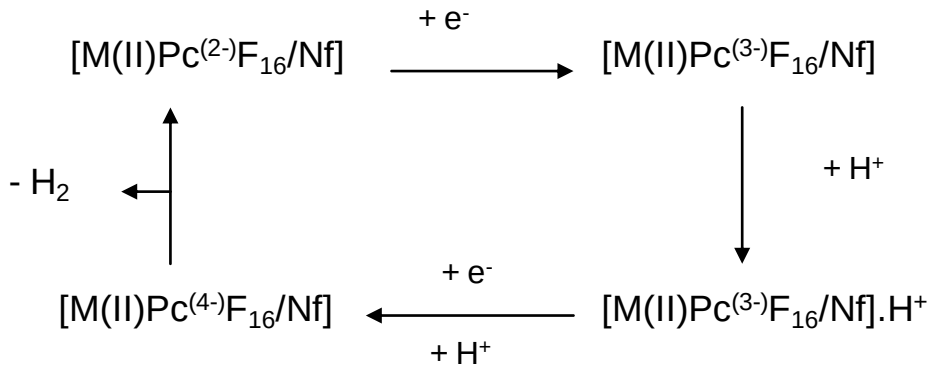

Scheme 5.2: *Proposed ECEC pathway for the electrocatalytic generation of hydrogen where M is Cu or Zn as the catalyst.*

Zhao *et al.* report an unsubstituted ZnPc embedded in Nafion® as a catalyst for the electrocatalytic generation of hydrogen.[21] Two fundamental steps are required for the catalytic reaction to proceed; the first is the electron propagation (diffusion) by the reduction of $Zn(II)Pc^{(2-)}$ to $Zn(II)Pc^{(3-)}$ and the second is the

hydrogen evolution reaction facilitated by the catalytic proton reduction by the reduced Zn(II)$Pc^{(3-)}$ catalyst. The pathway proposed by Zhao is similar to the pathway described in Scheme 5.2, however the formation of an intermediate molecule occurs upon the coordination of a proton by the reduced Zn(II)$Pc^{(3-)}$ species. The evolution of dihydrogen occurs when two of these molecules are close in proximity where Zn(II)$Pc^{(3-)}$ is oxidized back to the original Zn(II)$Pc^{(2-)}$ form and eliminating hydrogen in the process.[21]

5.2.2 Conditions affecting electrocatalytic generation of hydrogen

5.2.2.1 Applied electrolysis potential

The results for adsorbed catalyst films discussed in Chapter 4 describe the importance of the applied potential used for driving the hydrogen evolution reaction. In order to investigate the importance of the polymer matrix (Nafion®) a GCE was coated with Nafion® and used as a modified electrode for H^+ reduction experiments. Following an hour potentiostatic electrolysis at -1.2 V, the following data were collected (Table 5.3):

Charge (C)	*0.04*
[1]Current Density J (mA/cm^2)	*0.3*
[2]Current Density J (mA/cm^2)	*0.2*
Moles of hydrogen (mol)	*1 x 10^{-7}*
Faradaic Efficiency* %	*52*

Table 5.3: *Average performance data obtained by CV and BE vs. Ag/AgCl for 1 hour at -1.2 V for Nafion® with in 0.1 M NaH_2PO_4/H_3PO_4 (pH 2). [1]Current density obtained using BE data and [2]current density obtained using the last scan of the CV.*

It is evident that H^+ reduction is accelerated in the presence of a Nafion® coating compared to a bare GCE, indicated by the number of moles of hydrogen produced. The Faradaic efficiency was calculated using the charge passed and the number of moles of H_2 gas chromatography. This catalytic behaviour was noted by Zhao *et al*. when Nafion® was coated onto a BPG electrode, the Faradaic efficiency was 52 % in pH 2 conditions also.[21] A comparison of the amount of charge passed in this electrolysis experiment with one conducted for a $CoPcF_{16}$/Nf modified electrode at -1.2 V (Table 5.4) shows that much less H_2 is produced using the Nafion® modified electrode alone.

When the applied potential is decreased (to more negative potentials), an increase in the reaction kinetics can occur, displayed in Tables 5.4- 5.5 and in Figures 5.7 to 5.9 respectively (see Appendix D, Tables D.1-D.3 for additional TOF data).

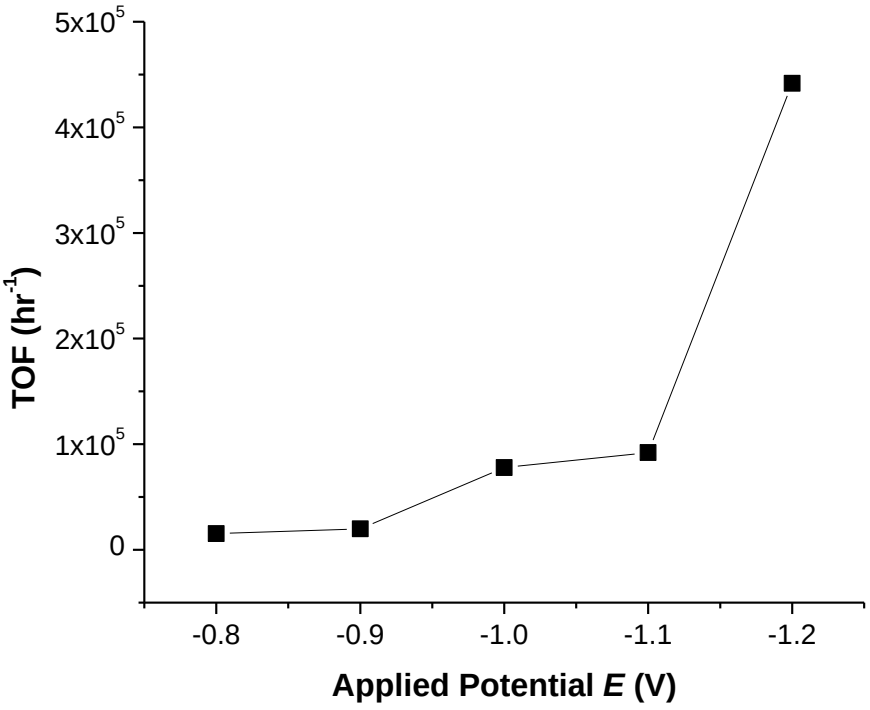

Figure 5.7: *Effect of applied potential on turnover frequencies TOF (hr^{-1}) for $CoPcF_{16}$/Nf.*

The TOF (hr^{-1}) values are shown in Figure 5.7 where $CoPcF_{16}$/Nf is the catalyst employed for the modified electrode. The TOF values obtained are in agreement with the expected response; these values increase with decreasing applied

electrolysis potentials. The highest TOF obtained at -1.2 V is 4.4 x 10^5 with a corresponding Faradaic efficiency of 71 %.

Applied Potential (V)	**-0.8**	**-0.9**	**-1.0**	**-1.1**	**-1.2**
Charge (C)	*2 x 10^{-3}*	*0.03*	*0.05*	*0.12*	*0.19*
Moles of H_2 (mol)	*7.4 x 10^{-9}*	*3.7 x 10^{-8}*	*1 x 10^{-7}*	*2.6 x 10^{-7}*	*7 x 10^{-7}*
Faradaic Efficiency %	*68*	*25*	*41*	*42*	*71*
[1]Current Density J (mA/cm^2)	*8 x 10^{-3}*	*0.1*	*0.2*	*0.5*	*0.8*
[2]Current Density J (mA/cm^2)	*2 x 10^{-2}*	*3 x 10^{-2}*	*0.1*	*1.5*	*4.4*
(%) Electroactive $CoPcF_{16}$	*3.0*	*6.2*	*9.2*	*8.7*	*10.5*

Table 5.4: *Average performance data obtained by CV and BE vs. Ag/AgCl for 1 hour for $CoPcF_{16}$/Nf with varying electrolysis potentials in 0.1 M NaH_2PO_4/H_3PO_4 (pH 2). [1]Current density obtained using BE data and [2]current density obtained using the last scan of the CV.*

The current density profile observed in Figure 5.8 below follows the trend cited above: increased reaction kinetics at lower applied potentials. At -1.2 V, the highest charge and current density were obtained of 0.19 C and 1.1 mA/cm^2 (4.4 mA/cm^2 by CV) respectively. The current density obtained here using an electrolysis potential of -1.2 V compares with the current density obtained using the $CoPcF_{16}$ adsorbed species revealing no further increase in current density. This suggests that when the catalyst is embedded in a Nafion® polymer, the polymer offers no real performance enhancement. This is further realised by comparing the moles of hydrogen produced when the catalyst is immobilised in

the absence of Nafion® (1.2 x 10^{-6} mols). This is, perhaps, because only the catalyst near the electrode is able to participate in the catalytic reaction. Diffusion of the phthalocyanine complex is expected to be slow within the polymer. The metallophthalocyanine which is situated in the film closest to the electrode may decompose in the matrix faster than if adsorbed on the surface itself. As percolation of charge transport is assumed a gradual process through the film, the remaining catalyst in the rest of the film is transported by either a hopping or diffusion mechanism.[13] Blauch and Savéant report both of these percolation processes within polymer matrices as sluggish.[12]

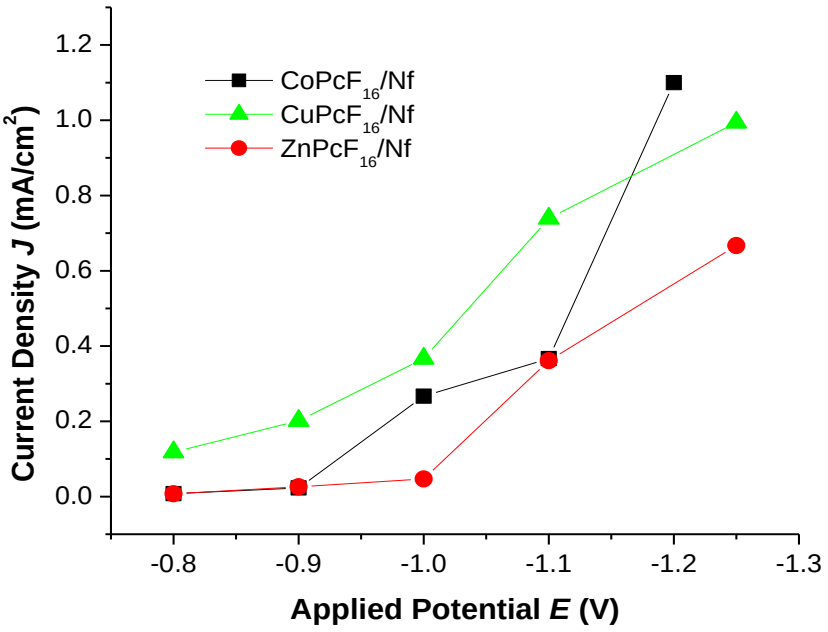

Figure 5.8: *Average current density (mA/cm^2) obtained by BE function of varying applied electrolysis potentials. The black, green and red lines represent CoPcF$_{16}$/Nf, CuPcF$_{16}$/Nf and ZnPcF$_{16}$/Nf respectively.*

The TOF (hr^{-1}) values shown in Figure 5.9 represent the data for CuPcF$_{16}$/Nf modified electrodes. When a potential of -1.2 V was applied for this electrode system, the TOF was found to be 2.3 x 10^5. Comparison of these TOF values displayed in Figure 5.9 with those obtained in the absence of Nafion® (Chapter 4) reveals that they are considerably less (3.5 x 10^6). However as TOF values are calculated based on the number of moles of electroactive species in the modifying layer, it is difficult to directly compare the catalytic performance of these systems based on TOF data alone. Comparing the number of moles of hydrogen obtained

(by gas chromatography) can further aid the determination of which metallophthalocyanine displays the optimum performance.

Applied Potential (V)	**-0.8**	**-0.9**	**-1.0**	**-1.1**	**-1.2**
$CuPcF_{16}$/Nf					
Charge (C)	*2.9×10^{-2}*	*4.6×10^{-2}*	*0.11*	*0.16*	*0.17*
Moles of H_2 (mol)	*5.7×10^{-8}*	*6×10^{-8}*	*7.2×10^{-8}*	*1.6×10^{-7}*	*1.8×10^{-7}*
Faradiac Efficiency %	*19*	*18*	*25*	*29*	*39*
[1]Current Density *J* (mA/cm^2)	*0.1*	*0.2*	*0.4*	*0.6*	*0.7*
[2]Current Density *J* (mA/cm^2)	*4×10^{-2}*	*0.2*	*0.4*	*1.6*	*3.5*
Electroactive $CuPcF_{16}$/Nf (%)	*2.1*	*2.0*	*1.6*	*2.3*	*3.4*
$ZnPcF_{16}$/Nf					
Charge (C)	*1.9×10^{-3}*	*6.5×10^{-3}*	*1.2×10^{-2}*	*0.14*	*0.24*
Moles of H_2 (mol)	-	-	-	*1.6×10^{-7}*	*2.7×10^{-7}*
Faradiac Efficiency %	-	-	-	*25*	*22*
[1]Current Density *J* (mA/cm^2)	*8×10^{-3}*	*3×10^{-2}*	*5×10^{-2}*	*0.6*	*1.0*
[2]Current Density *J* (mA/cm^2)	*0.1*	*0.1*	*0.3*	*0.4*	*1.4*
Electroactive $ZnPcF_{16}$/Nf (%)	*1.6*	*1.2*	*1.8*	*2.1*	*1.2*

Table 5.5: *Average performance data obtained by CV and BE for 1 hour for $CuPcF_{16}$/Nf and $ZnPcF_{16}$/Nf at varying electrolysis potentials vs. Ag/AgCl in 0.1*

M NaH_2PO_4/H_3PO_4 (pH 2). [1]Current density obtained using BE data and [2]current density obtained using the last scan of the CV.

At potentials of -0.8 V to -1.0 V for $ZnPcF_{16}$/Nf, electrochemical data suggested the formation of H_2 (Appendix D, Table D.3); however, the amounts produced fell below the LOD and thus the performance of this catalyst at these potentials is not able to be fully studied with the techniques available. At -1.1 V and -1.2 V, enough H_2 was generated during the 1 hour electrolysis period to permit the calculation of TOF (hr^{-1}) values. The largest TOF for $ZnPcF_{16}$/Nf was calculated as 5.6×10^4.

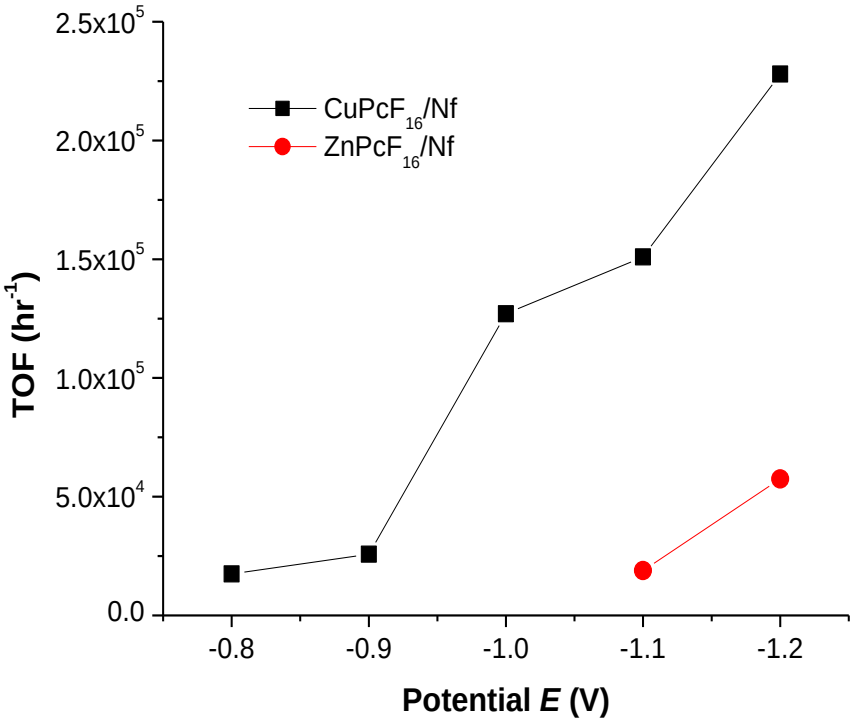

Figure 5.9: *Effect of applied potential on turnover frequencies TOF (hr^{-1}) for $CuPcF_{16}$/Nf and $ZnPcF_{16}$/Nf represented by the black line and red lines respectively.*

For catalyst/Nafion® modified electrodes overall, the largest TOF values were obtained for $CoPcF_{16}$/Nf, followed by $CuPcF_{16}$/Nf and the lowest TOF was determined for $ZnPcF_{16}$/Nf. The TOF values obtained for catalysts supported in Nafion® are considerably less than those displayed for adsorbed catalysts.

Nafion® is an excellent H^+ conductor, and the concentration of H^+ ions within the polymer film should be quite high, so it is postulated that the lower performance of metallophthalocyanine catalysts in Nafion® is a result of slow mass transport through the polymer film, indicated by the moles of H_2 produced by these catalysts.

5.2.2.2 Effect of Temperature

The experimental results discussed throughout this chapter are concerned with the employment of these catalyst systems for electrocatalytic hydrogen generation at room temperature, i.e. 20°C. Therefore the effect of varying the operating temperature of these electrochemical cells was investigated. The temperatures chosen for investigation were 3°C, 20°C and 40°C, the same as in Chapter 4.

The cyclic voltammogram in Figure 5.12 shows the effect of temperature on the appearance of the Co(II)/Co(I) redox couple for $CoPcF_{16}$/Nf. The potential at which the redox couple was observed shifts very slightly as the temperature is increased. The half wave potentials measured for Co(II)/Co(I) for $CoPcF_{16}$/Nf at both 3°C and 20°C were -0.44 V and -0.43 V respectively, and -0.43 V when the temperature of the cell was increased to 40°C. At 40°C, the current was observed to increase in the region of -0.60 V. This behaviour was observed by Baker *et al*. for the electrocatalytic reduction of O_2 using $CoPcF_{16}$. This behaviour is not observed when the temperature is maintained at 3°C and 20°C. [22,23]

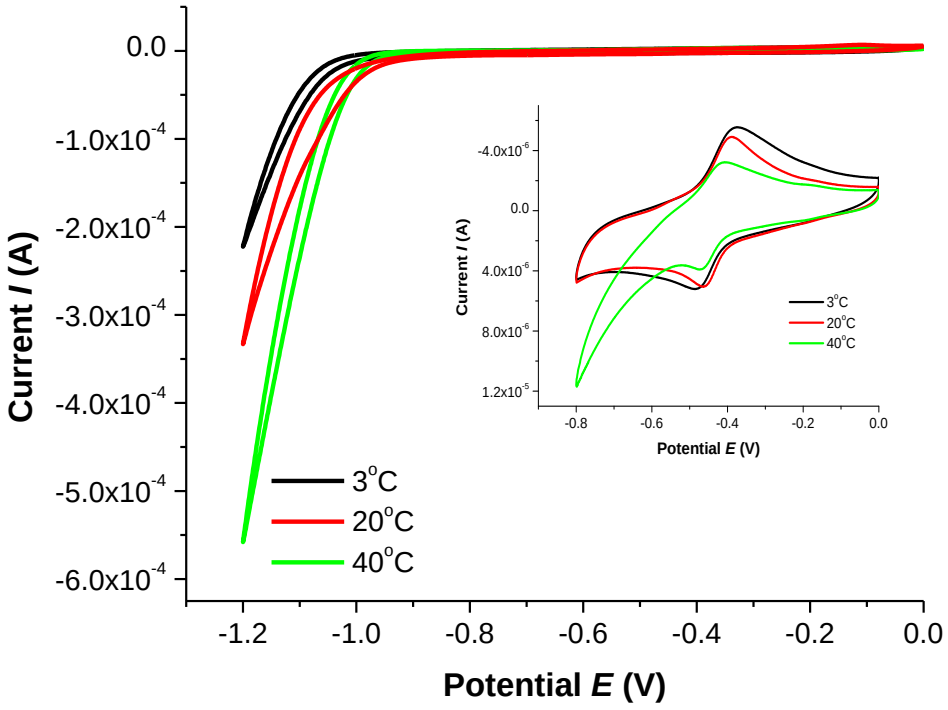

Figure 5.10: *Cyclic voltammetry of $CoPcF_{16}$/Nf vs. Ag/AgCl in 0.1 M NaH_2PO_4/H_3PO_4 (pH 2) at 3°C (black line), 20°C (red line) and 40°C (green line). Scan rate = 100 mV/s.*

Figure 5.10 illustrates the effect of temperature on the H^+ reduction reaction. The onset potentials for H^+ reduction for the Nafion®-modified electrodes appeared to be slightly shifted to more negative potentials compared to adsorbed films, but the onset potential was again observed to shift to less negative potentials with increasing temperature. At higher temperatures, the charge passed during the electrolysis experiment was observed to rise (Table 5.6 below). The voltammograms at each temperature revealed a sharp rise in current at -1.2 V vs. Ag/AgCl, indicative of the catalytic reaction for $CoPcF_{16}$/Nf. The increase in the catalytic currents with increasing temperatures are due to the increased reaction kinetics as discussed previously.[23,24]

Comparing the magnitudes of these currents produced by $CoPcF_{16}$/Nf to the currents obtained using the adsorbed $CoPcF_{16}$ catalyst alone, the currents observed at 3°C are approximately the same magnitude, however the rise in temperature caused a larger performance enhancement for adsorbed $CoPcF_{16}$ films than for

Nafion®-supported catalysts. The effect of temperature on electrocatalytic hydrogen evolution for $CoPcF_{16}$/Nf species is shown in Figure 5.10. The accompanying experimental data for $CoPcF_{16}$/Nf is displayed in Table 5.6.

Temperature (°C)	**3**	**20**	**40**
Charge (C)	*0.09*	*0.19*	*0.42*
Moles of H_2 (mol)	*3×10^{-7}*	*7×10^{-7}*	*1.7×10^{-6}*
Faradaic Efficiency %	*66*	*71*	*77*
[1]Current Density *J* (mA/cm^2)	*0.4*	*0.8*	*1.7*
[2]Current Density *J* (mA/cm^2)	*3.2*	*4.5*	*8.0*
(%) Electroactive $CoPcF_{16}$/Nf	*5.5*	*10.5*	*14.1*

Table 5.6: *Average performance data obtained by CV and BE (-1.2 V vs. Ag/AgCl for 1 hour) for $CoPcF_{16}$/Nf at varying temperatures in 0.1 M NaH_2PO_4/H_3PO_4 (pH 2). [1]Current density obtained using BE data and [2]current density obtained using the last scan of the CV.*

A linear relationship was observed for the $CoPcF_{16}$/Nf system for TOF (hr^{-1}) and temperature. The highest Faradaic efficiency (77 %) for these experiments was found at 40°C. The Faradaic efficiency of the systems at 3°C and 20°C are 66 % and 71 % respectively. It is expected that these efficiencies are a reflection of both improved reaction kinetics at higher temperatures and also poorer H_2 and O_2-solubility with increasing temperature (Figure 4.9).[25]

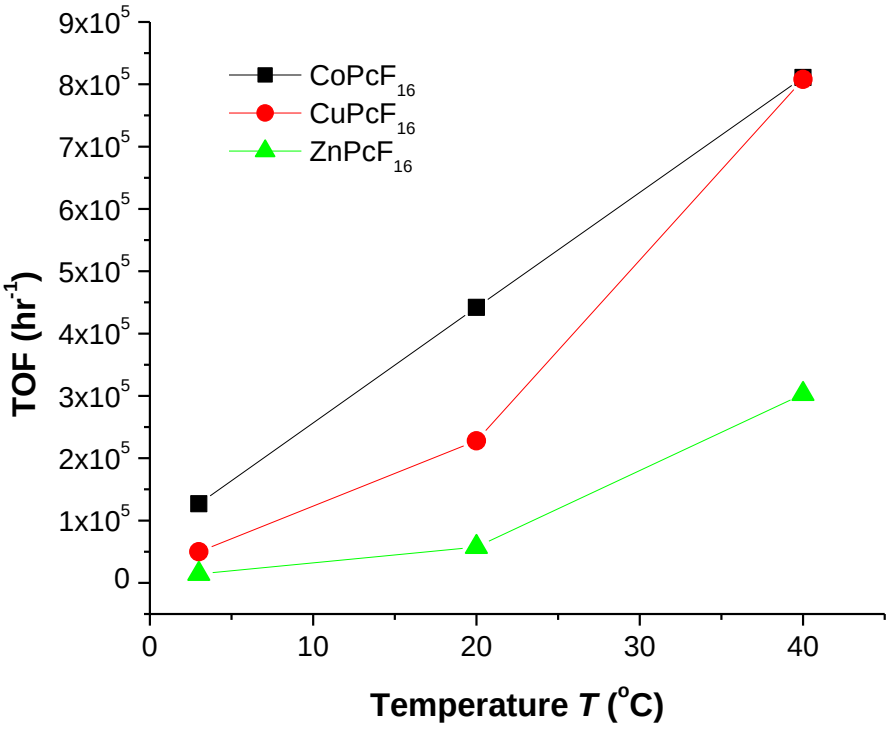

Figure 5.11: *Effect of temperature on turnover frequencies TOF (hr^{-1}) for $CoPcF_{16}$/Nf (black line), $CuPcF_{16}$/Nf (red line), $ZnPcF_{16}$/Nf (green line) respectively.*

Examination of the data obtained for $CoPcF_{16}$/Nf at the various temperatures in Table 5.6 also reveals an increase in the performance indicators with increasing temperature. The current density determined at 3°C reached 0.4mA/cm^2, almost two thirds as less than the current density observed at room temperature of 1.1 mA/$cm^{2.}$ Likewise the current density at 20°C is more than half of that obtained at 40°C (1.9 mA/cm^2). Similarly, this trend was observed in the charge obtained after an electrolysis step where at 3°C then charge obtained was 0.09 C while at 20°C the charge doubled to 0.19 C. This was also observed at 40°C, where the charge measured of 0.42 C was about twice the charge obtained at 20°C. Thus it can be concluded that the charge was first order with respect to increasing temperature of the electrochemical cell while the current density also increases with increasing temperatures.

The performance indicators obtained for modified electrodes involving the adsorbed Co catalyst indicated superior catalytic performance for these films over Nafion®-supported films.

The cyclic voltammograms in Figure 5.12 exhibits the redox couple of the Pc ring of $CuPcF_{16}$/Nf. The half wave potentials measured for $Pc^{(2-)}$/ $Pc^{(3-)}$ for $CuPcF_{16}$/Nf at 3°C and 20°C were -0.33 V and -0.32 V respectively, while this potential shifted anodically to -0.26 V when the temperature of the electrochemical cell was increased to 40°C. At 40°C, it appeared that an increase in catalytic activity occured as the current started to increase in the region of the potential onset at -0.85 V; due to improved reactions kinetics at the electrode/catalyst interface. The onset potentials for H^+ reduction for the Nafion®-modified electrodes were signicantly shifted to less negative potentials with increasing temperature.

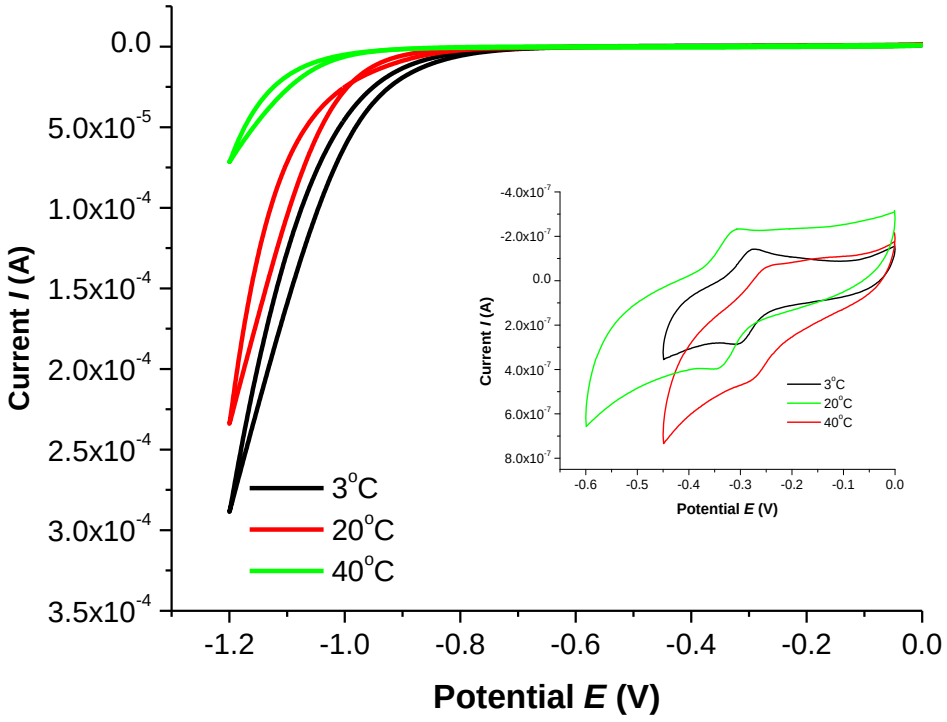

Figure 5.12: *Cyclic voltammograms of $CuPcF_{16}$/Nf vs. Ag/AgCl in 0.1 M NaH_2PO_4/H_3PO_4 (pH 2) at 100 mV/s where the black line is at 3°C, the red line is at 20°C and the green line is at 40°C. Scan rate = 100 mV/s.*

The cyclic voltammograms for $CuPcF_{16}$/Nf at the various temperatures are shown in Figure 5.12. The catalytic current at 40°C is more than 3 times greater than that of the current produced at 3°C. The stability of this catalyst dispersed in Nafion® is also evident at the various temperatures. The effect of temperature on electrocatalytic hydrogen evolution for $CuPcF_{16}$/Nf species is shown in Table 5.7. (see Appendix D, Tables D.4 to D.6 for additional data).

	$ZnPcF_{16}$/Nf			**$CuPcF_{16}$/Nf**		
Temperature (°C)	**3**	**20**	**40**	**3**	**20**	**40**
Charge (C)	*0.04*	*0.24*	*0.60*	*0.04*	*0.17*	*0.33*
Moles H_2 (mol)	*5.6×10^{-8}*	*2.7×10^{-7}*	*2.2×10^{-6}*	*7.9×10^{-8}*	*1.8×10^{-7}*	*1.2×10^{-6}*
Faradaic Efficiency %	*25*	*24*	*70*	*39*	*39*	*74*
[1]Current Density J (mA/cm^2)	*0.2*	*1.0*	*2.4*	*0.2*	*0.7*	*1.3*
[2]Current Density J (mA/cm^2)	*0.4*	*1.4*	*3.1*	*1.0*	*3.4*	*4.1*
% Electroactive	*0.4*	*1.2*	*0.9*	*2.0*	*3.4*	*2.3*

Table 5.7: *Average performance data obtained by CV and BE at -1.2 V vs. Ag/AgCl for 1 hour for $ZnPcF_{16}$/Nf and $CuPcF_{16}$/Nf respectively at varying temperatures in 0.1 M NaH_2PO_4/H_3PO_4 (pH 2). [1]Current density obtained using BE data and [2]current density obtained using the last scan of the CV.*

Analysis of the gas in the headspace of the cell by gas chromatography revealed a TOF of 2.3×10^5 at 20°C, while at 40°C a TOF value of $8. \times 10^5$ was obtained. When the temperature of the electrochemical cell was maintained at 40°C, the highest Faradaic efficiency was calculated as 74 %.

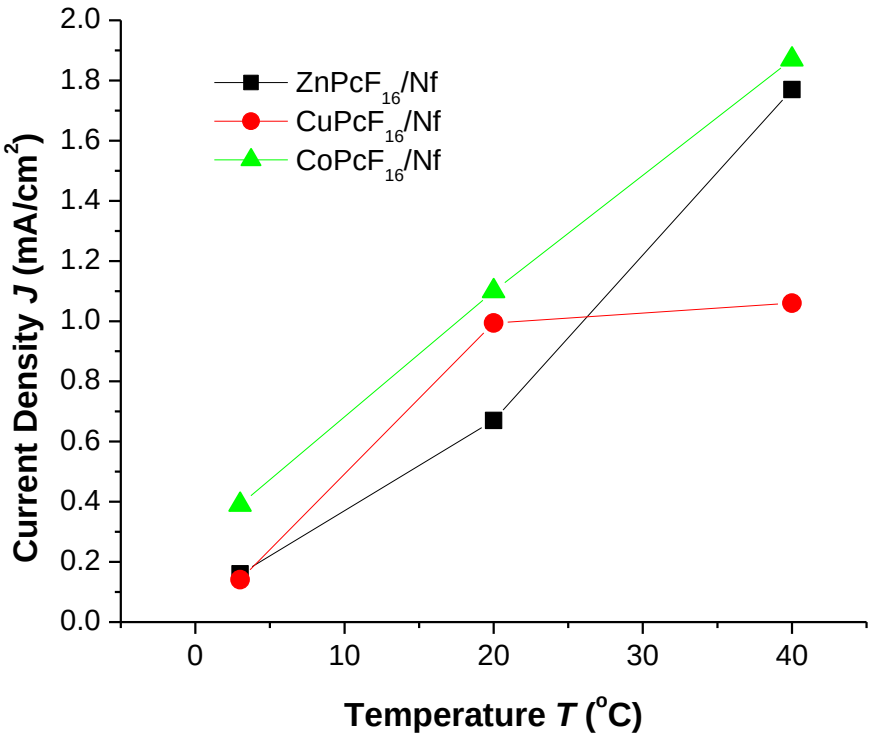

Figure 5.13: *Current densities (mA/cm^2, obtained by bulk electrolysis) as a function of temperature for $CoPcF_{16}$/Nf (green line), $CuPcF_{16}$/Nf (red line) and $ZnPcF_{16}$/Nf (black line).*

It is clear to see that $ZnPcF_{16}$/Nf displays a similar profile to $CoPcF_{16}$/Nf, Figure 5.14 however the current densities obtained for $ZnPcF_{16}$/Nf were almost half those obtained for $CoPcF_{16}$/Nf at 3°C and 20°C. The current density for $CuPcF_{16}$ at 40°C was also lowered than expected (1.1 mA/cm^2). As discussed in the previous chapter, the effect of O_2 reduction (produced at the anode) and the continuous build up of gas bubbles on the working electrode results in a lower passage of current, thus the current densites obtained over an hour electrolysis step are lower than expected.

The redox couple of $ZnPcF_{16}$/Nf is displayed in Figure 5.14 over the range of temperatures. The potential at which the redox couple was observed did not change with varying the temperature, however it was evident that altering the temperature effected both the electrochemical behaviour of the redox couple and also the subsequent proton reduction reaction. The appearance of the $Pc^{(2-)}$/ $Pc^{(3-)}$ redox couple at -0.25 V vs. Ag/AgCl changed as the temperature increased.

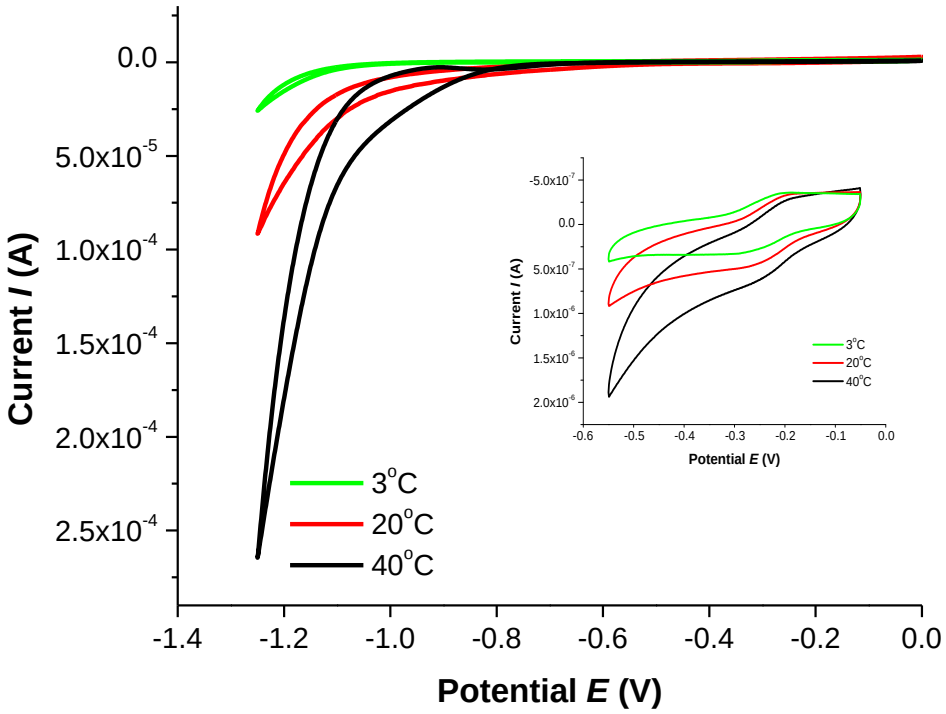

Figure 5.14: *Cyclic voltammetry of $ZnPcF_{16}$/Nf vs. Ag/AgCl in 0.1 M NaH_2PO_4/H_3PO_4 (pH 2) at 3°C (black line), 20°C (green line) and 40°C (red line). Scan rate = 100 mV/s.*

The onset potential of H^+ reduction at $ZnPcF_{16}$/Nf at 3°C occured at -1.10 V, and, shifted to -0.9 V when the temperature was increased to 40°C. The shift to a more negative potential at 3°C is a result of slower rate of reaction due to the temperature, while the opposite is true at 40°C. The magnitudes of the currents shown in Figure 5.14 are comparable to the currents observed for the adsorbed species (see Appendix C, Figure C.2). The TOF/temperature profile for results obtained by gas chromatography are shown in Figure 5.11. At 3°C, 20°C and 40°C, the TOF obtained were 1.4 x 10^4, 5.8 x 10^4 and 3.0 x 10^5 respectively. The Faradaic efficiency of each of these systems was calculated and when the temperature of the electrochemical cell was maintained at 40°C, the highest Faradaic efficiency was calculated as 70 %.

5.2.2.3 Effect of varying the pH and ionic strength of electrolyte

The experimental results for each of the catalyst systems for electrocatalytic hydrogen generation at room temperature discussed so far with varying potential and temperature were carried out using 0.1 M NaH_2PO_4/H_3PO_4 buffer at pH 2. The effect of the catalytic performance whilst varying the pH of the phosphate buffer solution was investigated using these catalysts incorporated in Nafion®. Preparation of the phosphate solutions over a range of pH is described in Chapter 2. Examination of the cyclic voltammograms of each of the catalysts in the phosphate buffer over the range of pH revealed a shift in redox potential towards more negative potentials of the first redox couple (Co(II)/Co(I) and $Pc^{(2-)}/Pc^{(3-)}$ for $CoPcF_{16/}Nf$ and $CuPcF_{16}/Nf$/ $ZnPcF_{16}/Nf$, respectively). For $CoPcF_{16}/Nf$ at pH 4, the Co(II)/Co(I) process is observed at -0.47 V vs. Ag/AgCl while it shifts to more negative potentials at neutral pH. As the pH of the electrolyte solution was increased to more basic conditions, the Co(II)/Co(I) wave became broader and the anodic peak was difficult to see, Table 5.8.

pH	E ½ Potential (V)	$E_{pc} - E_{pa}$ (V)	Onset Potential (V)
2	-0.43	0.06	-0.98
4	-0.47	0.07	-0.98
7	-0.67	0.10	-1.10
9	-	-	-1.47

Table 5.8: *Reduction potentials of $CoPcF_{16}/Nf$ in 0.1 M NaH_2PO_4 over a range of pH.*

The influence of pH on the potential of the Co(II)/Co(I) process should be due to the influence of ring protonation, which would be promoted at lower pH. Cyclic voltammograms for $CoPcF_{16}/Nf$ in phosphate buffers of various pH are shown in Figure 5.15. Application of a reduction potential of -1.25 V to a modified electrode of $CoPcF_{16}/Nf$ immersed in a phosphate solution at pH 4, revealed only a weak cathodic current; with no detectable amount of gaseous product

determined. Comparing this to an experiment conducted at pH 2, the current density obtained was significantly less (0.1 mA/cm^2) suggesting weak activity at pH 4 when an electrolysis potential of -1.2 V was applied, Table 5.9.

pH	***2***	***4***	***7***	***9***
Charge (C)	*0.19*	*3 x10^{-2}*	*2.2 x10^{-3}*	*3.7x10^{-4}*
[1]Current Density J (mA/cm^2)	*0.8*	*0.1*	*9 x 10^{-3}*	*1.5 x 10^{-3}*

Table 5.9: *Effect of varying the pH of electrolyte on the average performance indicators for $CoPcF_{16}$/Nf obtained by CV and BE at -1.2 V vs. Ag/AgCl.*

The activity at -1.2 V was found to be progressively weaker with increasing pH for $CoPcF_{16}$/Nf. At neutral pH, a gradual increase in cathodic current was observed at -1.2 V with no H_2 detected by gas chromatography. As before, the poor activity for the electrocatalytic generation of hydrogen in these experiments ascribed to the decrease in the concentration of protons in solution with increasing pH. (see Appendix D, Table D.7 and Figure D.1).

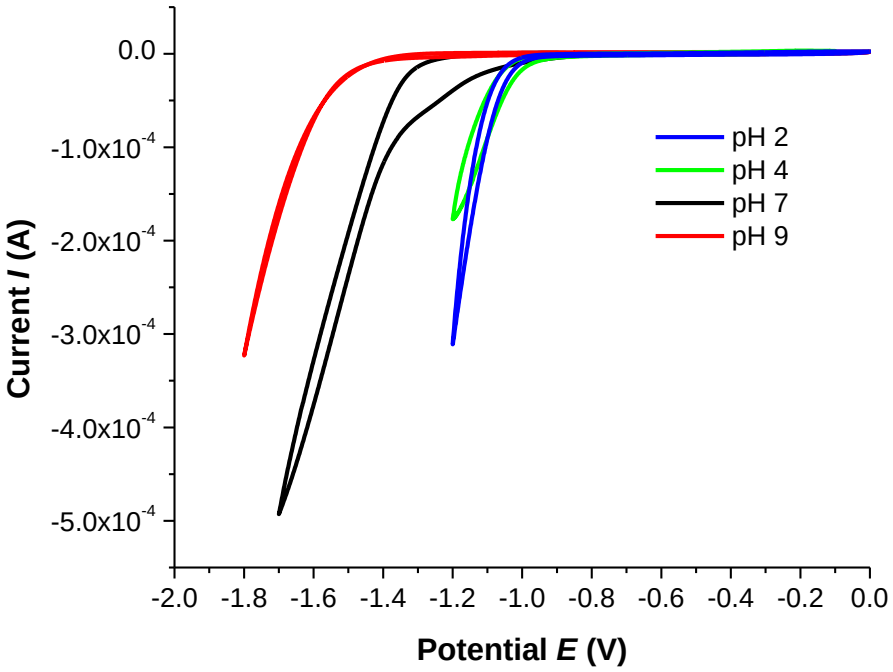

Figure 5.15: *Typical currents observed for $CoPcF_{16}$/Nf in phosphate buffer at various pH, vs. Ag/AgCl. Scan rate = 100 mV/s.*

Upon scanning in a further cathodic direction to -1.7 V, the current begins to increase grealty, 5.8 x 10^{-3} mA/cm^2 at -1.2 V to 7.1 mA/cm^2 at -1.7 V.

Applied Potential (V)	***-1.2*** *(pH 2)*	***-1.25*** *(pH 4)*	***-1.7*** *(pH 7)*	***-1.8*** *(pH 9)*
Charge (C)	*0.19*	*0.05*	*0.67*	*1.24*
Moles of H_2 (mol)	*7 x 10^{-7}*	*2.5 x 10^{-7}*	*3.5 x 10^{-6}*	*6.4 x 10^{-6}*
Faradaic Efficiency %	*71*	*55*	*35*	-
[1]Current density *J* (mA/cm^2)	*4.4*	*2.6*	*7.1*	*4.6*
Electroactive $CoPcF_{16}$/Nf (%)	*10.5*	*3.8*	*2.4*	*0.5*

Table 5.10: *Effect of pH of electrolyte on the average performance indicators for $CoPcF_{16}$/Nf obtained by CV and [1]BE (using varying applied potentials).*

In order to get some idea of the performance of the $CoPcF_{16}$/Nf modified electrode in different pH conditions, the applied electrolysis potentials were varied according to the maximum currents that were obtained in CV experiments. These potentials are shown in Table 5.10 and can be seen in Figure 5.15. Although the H_2 generation data will thus involve a combination of influences (pH and applied potential) it is expected that the latter factor is a greater influence here. Thus the high pH data does not necessarily reflect superior performance. The amount of H_2 actually determined in these measurements is shown in Figure 5.16.

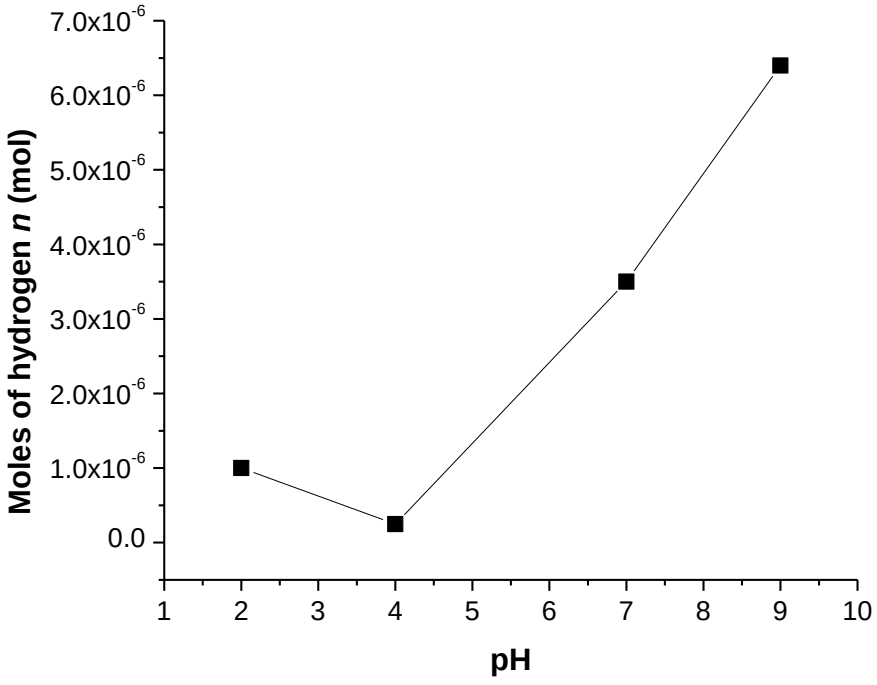

Figure 5.16: *Moles of hydrogen gas produced as a function of pH of electrolyte as determined by gas chromatography respectively for $CoPcF_{16}$/Nf in phosphate buffer.*

It is difficult to compare the activity illustrated above as the performance at each pH is a result of a different driving force. The catalytic reaction of proton reduction in acidic conditions should result in the largest amount of hydrogen formation, however in Figure 5.16 above, this is not the case. In neutral and basic conditions, an increase in the number of moles of hydrogen is observed as a result of the applied potential. It is difficult to gauge the pH-catalyst performance as hydrogen evolution in these cases because the data would involve two influences: pH and applied potential. However, the Nernst equation predicts the equilibrium potential E_{eq} to change by 0.059 V per pH unit change, thus, in order for the same current to be produced by each of these systems operated over a range of pH, the applied potential E_{app} was driven to negative potentials. At pH 4, the equilibrium potential becomes more negative by 0.118 V, compared to the equilibrium potential at pH 2. Thus the overpotentials can be calculated for at each pH unit change; 0.9 V at pH 4, 1.0 V at pH 7 and 1.1 V at pH 9 when all compared at a current of 1 x 10^{-4} A.

The experimental data obtained using $CuPcF_{16}$ and $ZnPcF_{16}$ dispersed in Nafion® are shown in Appendix D, Figures D.2- D.5 and Tables D.8- D.11. These catalyst systems exhibit the same behaviour as discussed here for $CoPcF_{16}$:Nf. As the overpotential for the catalytic reaction varies for each of the catalysts, direct comparisons cannot be drawn.

The electrocatalytic activity of these metallophthalocyanines incorporated in a Nafion® polymer discussed so far in this chapter has been measured in 0.1 M NaH_2PO_4/H_3PO_4 at pH 2 (with the exception of the pH study). As observed with the adsorbed catalysts described in Chapter 4, it appears that the catalytic activity for the production of hydrogen is highly dependent upon the concentration of protons in the electrolyte solution. In Figure 5.17 the effect of the ionic strength of the buffer solution is evident as a catalytic current a smaller magnitude is observed when a 0.01 M NaH_2PO_4/H_3PO_4 buffer was employed.

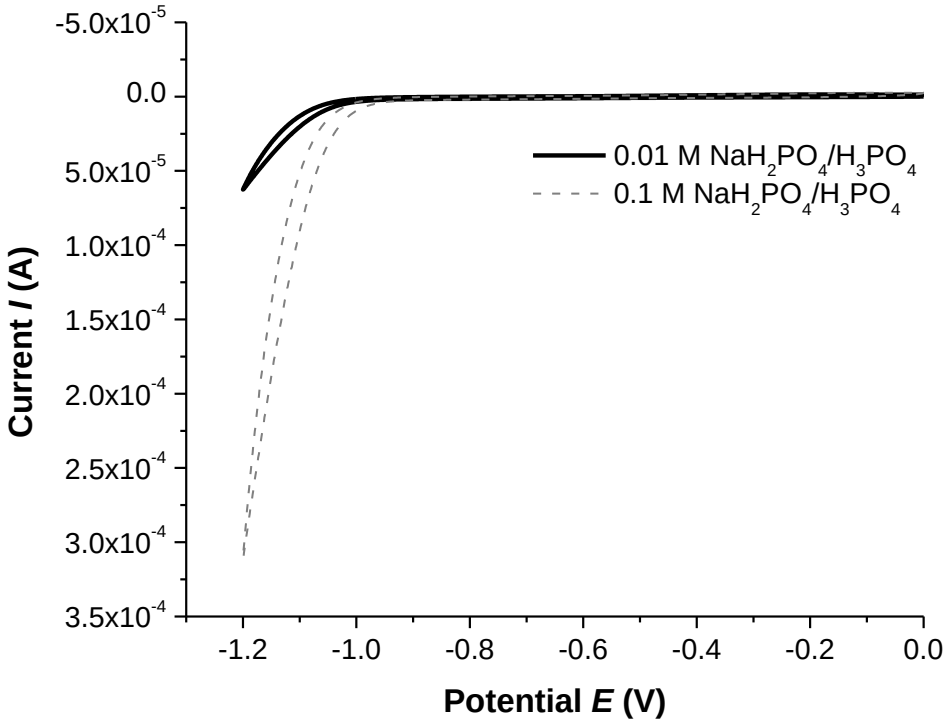

Figure 5.17: *Cyclic voltammogram of $CoPcF_{16}$ vs. Ag/AgCl at 100 mV/s where the grey dashed line is the modified electrode immersed in 0.1 M*

NaH_2PO_4/H_3PO_4 (pH 2) and the black line is using 0.01 M NaH_2PO_4/H_3PO_4 (pH 2).

Similar to the results observed in Chapter 4, the ionic strength and resistance of a result of a lower ionic strength of the electrolyte plays a significant role in the electrocatalytic reduction of protons to hydrogen.[26]

As these metallophthalocyanines catalysts are insoluble in water due to the hydrophobicity of the Pc ring,[13] it is assumed that the catalysts are located either at the hydrophobic region i.e. at the fluorocarbons chains, or possibly located in the interfacial regions as the M(II)PcF_{16} molecule is neutral. This is assumed by Zhao *et al.* for an unsubstituted ZnPc embedded in Nafion® where electron propagation as the rate determining step was reported to occur at a faster rate (indicated by the D_{app}) in Nafion® than in P(VP-St) due to the mobility of ZnPc in the Nafion® polymer framework.[21]

The reason for this lies in the interaction of the catalyst with the polymer framework. Charge transport through the Nafion® is assumed faster due to diffusive interaction compared to a restricted interaction with P(VP-St). Charge compensation is another factor which influences the rate of electron transfer. When an electrochemical reduction occurs, an additional negative charge is localised on the catalyst, thus to maintain electroneutrality a cation is required to balance the charge within the modifying layer. Nafion® works on the basis of charge exclusion, such that anionic interference is excluded from the surface through electrostatic repulsion with the negatively charged sulphonated groups. As the sulphonate anions cannot move into from the polymer matrix, charge compensation occurs through proton migration from the bulk solution into the Nafion® film. As protons are highly mobile in solution and due to the high concentration in pH 2 electrolyte solution, proton migration is favoured. Also Nafion® is an anionic polymer, protons are easily attracted to this matrix thus facilitating electron transfer. Hence the presence of the catalysts dispersed in a Nafion® polymer plays a vital role in the rate of the electrocatalytic reaction for hydrogen evolution.8,[13,27,29]

No gaseous product was detected by gas chromatography, therefore the amount of gas present in the headspace was lower than the LOD using 0.01 M

NaH_2PO_4/H_3PO_4 solution. A plausible explanation for the reduced catalytic activity for $CoPcF_{16}$ dispersed in Nafion® using the lower ionic strength buffer (0.01 M NaH_2PO_4/H_3PO_4) is an increase in resistance between the working and reference electrodes in the cell. It appears that the charge is passed more easily using the 0.1 M buffer, which can be attributed to a lower resistance when the solution of higher ionic strength is employed.

5.2.2.4 Using chloride as an electrolyte

The cyclic voltammogram for $CoPcF_{16}$/Nf immersed in 0.1 M HCl/KCl (~pH 1) is displayed in Figure 5.31. Comparing the cyclic voltammogram for the modified electrode in this electrolyte to one obtained in a phosphate solution reveals similar characteristics, however there is a clear shift in the potential for the Co(II)/Co(I) process, Figure 5.18.

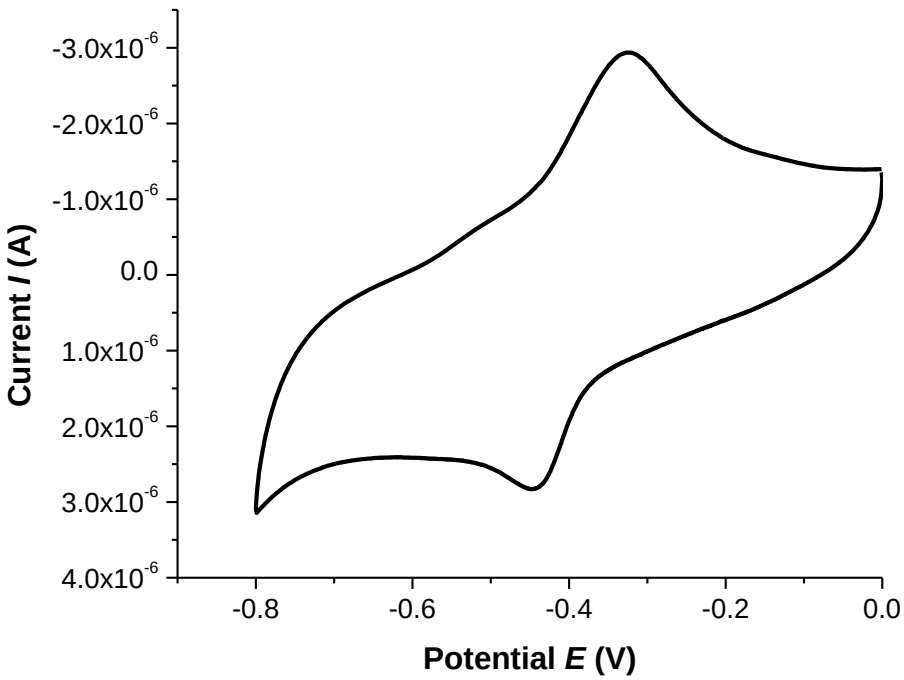

Figure 5.18: *Cyclic voltammogram of $CoPcF_{16}$ vs. Ag/AgCl in 0.1 M HCl/KCl (~pH 1) at 100 mV/s.*

The cyclic voltammogram for $CoPcF_{16}$/Nf shows a reversible redox process at -0.39 V vs. Ag/AgCl and is assigned as the reduction of Co(II)/Co(I) process. The potential at which this processes occured shifted in an anodic direction as the pH

of the electrolyte solution decreased to approximately pH 1. The cyclic voltammogram displayed here occured at the same potential for the adsorbed species in this electrolyte, however no ring based reduction was observed $CoPcF_{16}$/Nf.

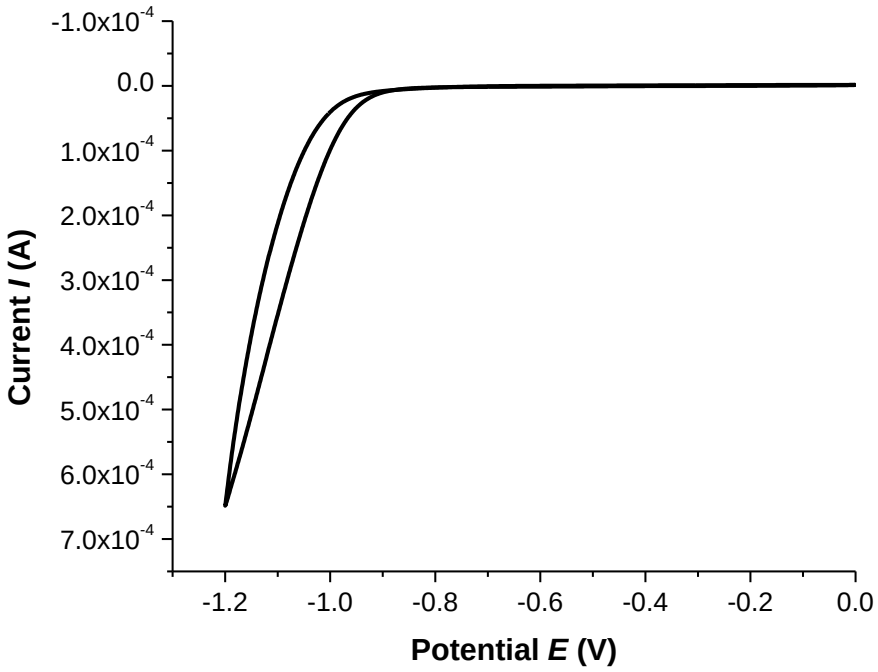

Figure 5.19: *Cyclic voltammogram of $CoPcF_{16}$ vs. Ag/AgCl in 0.1 M HCl/KCl at 100 mV/s.*

A large sharp cathodic current, corresponding to H^+ reduction, was observed beginning near -0.94 V, which is 40 mV less negative than for the corresponding phosphate electrolyte experiment. Similar to experiments performed in the phosphate buffer, the current measured after an electrolysis experiment was virtually unchanged compared to the voltammogram measured before the experiment, further suggesting that the $CoPcF_{16}$/Nf modified electrode is stable to the conditions employed in this experiment. A larger catalytic current (and hence current density) is observed using this solution; 6.5 x 10^{-4} A and 9.3 mA/cm^2 respectively). As discussed in Chapter 4, the larger current density indicates the reduction of O_2 is slower when this KCl electrolyte is employed.

Temperature effects are shown in Table 5.11, below. Similar to the trend observed using the phosphate buffer, increased performance is observed with increasing temperature.

Temperature (°C)	**3**	**20**	**40**
Charge (C)	*0.08*	*0.28*	*0.58*
Moles of H_2 (mol)	*2.6×10^{-7}*	*1.0×10^{-6}*	*2.3×10^{-6}*
Faradaic Efficieny %	*63*	*69*	*77*
[1]Current Density (mA/cm^2)	*5.2*	*11.3*	*13.6*
[2]Current Density (mA/cm^2)	*0.3*	*1.1*	*2.3*
% Electroactive catalyst	*7.0*	*6.2*	*8.6*

Table 5.11: *Average performance data obtained for $CoPcF_{16}$/Nf by CV and BE (at -1.2 V for 1 hour) vs. Ag/AgCl in 0.1 M HCl/KCl with varying temperature. [1]Current density obtained using the last scan of the CV and using [2]bulk electrolysis data.*

The TOF values as a function of temperature are shown in Figure 5.20. TOF values at 0°C and 20°C reached 9.2 x 10^4 and 3.5 x 10^5, respectively. The TOF obtained at 40°C was 8.1 x 10^5. Large Faradaic efficiencies were determined for the catalyst with increasing temperatures. (see Appendix D, Table D.13)

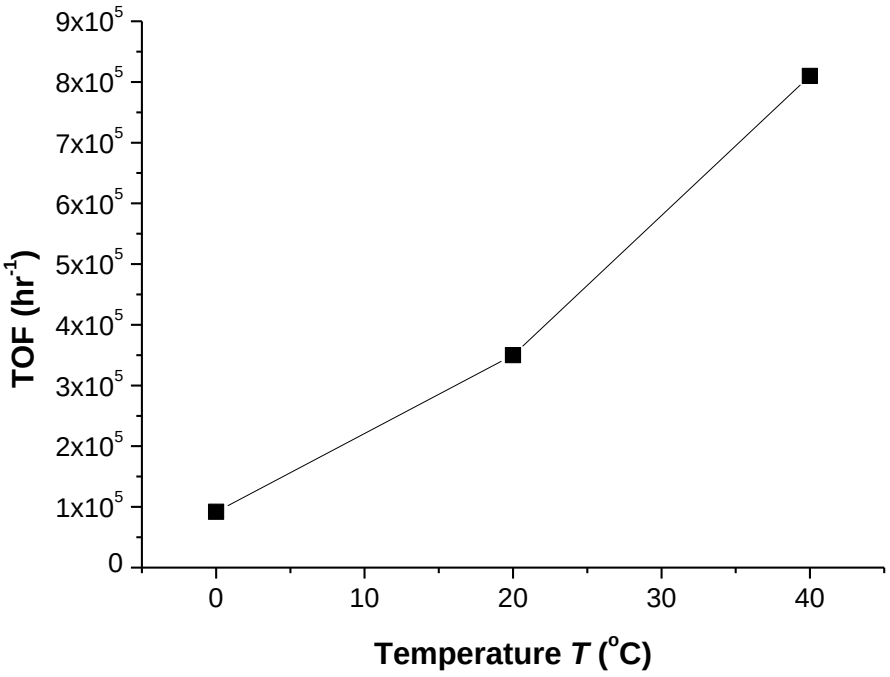

Figure 5.20: *Turnover frequencies TOF (hr^{-1}) as a function of temperature for $CoPcF_{16}$/Nf in 0.1 M HCl/KCl.*

Comparing the performance parameters in Table 5.12, it appears the better performance data were achieved when 0.1 M HCl/KCl electrolyte was employed. For instance, at 40°C, the charge and current density obtained using this electrolyte were 0.58 C and 13.6 mA/cm^2 respectively, while lower values were determined using 0.1 M NaH_2PO_4/H_3PO_4 of 0.42 C and 8.0 mA/cm^2 respectively.

5.2.2.5 Varying the catalyst concentration in coating solution

The effect of varying the concentration of the $CoPcF_{16}$/Nf catalyst was investigated and the experimental results are displayed in Figure 5.21 and Table 5.12. Three solutions were prepared from a 2.2 x 10^{-5} M stock CoPc/Nf solution of the following concentrations; 5.6 x 10^{-6} M, 1.1 x 10^{-5} M and 1.7 x 10^{-5} M. Kaneko *et al.* reported that the number of moles of H_2 produced for CoPc/Nf modified electrodes increased with increasing catalyst concentration.[16] For $CoPcF_{16}$/Nf, a similar result was found. However, Kaneko *et al.* found that TOF was independent of catalyst concentration (3 mM to 10 mM). For $CoPcF_{16}$ decreasing TOF values were obtained with increasing catalyst concentration. For

Kaneko's work, it was assumed that 100% of the catalyst deposited onto the electrode was involved in the catalytic reaction. However, decreasing TOF values with increasing $CoPcF_{16}$ concentration was found here (regardless of whether all of the catalyst or only the amount determined to be electroactive in the films is used). The expected trend is one where the amount of catalyst in the film produces a proportional quantity of H_2; however, TOF should be fairly constant, giving consideration to influences such as experimental error. (see Appendix D, Table D.14).

Catalyst Concentration (x 10^{-5} M)	**0.6**	**1.1**	**1.7**
Charge (C)	*0.12*	*0.14*	*0.17*
Moles of H_2 (mol)	*5.0 x 10^{-7}*	*5.5 x 10^{-7}*	*6.4 x 10^{-7}*
Faradaic Efficiency %	*90*	*89*	*74*
[1]Current Density *J* (mA/cm^2)	*0.5*	*0.6*	*0.7*
[2]Current Density *J* (mA/cm^2)	*1.4*	*0.9*	*1.1*
(%) Electroactive $CoPcF_{16}$	*2.8*	*2.7*	*2.5*

Table 5.12: *Average performance data obtained for $CoPcF_{16}$/Nf by CV and BE (at -1.2 V for 1 hour) vs. Ag/AgCl in 0.1 M NaH_2PO_4/H_3PO_4 (pH 2) with varying catalyst concentration. [1]Current density obtained using BE data and [2]current density obtained using the last scan of the CV.*

The current density appeared to increase slightly when the concentration of catalyst in solution increased, a feature which was observed for a ZnPc macrocycle, assumed as a result of improved intermolecular contact (higher electrical conductivity).[28] For this work, solutions were prepared from a stock 2.2 x 10^{-5} M $CoPcF_{16}$ solution containing ~ 5 % w/w Nafion® by dilution in DMF. Thus, the solutions have differing amounts of Nafion® (from the most dilute to most concentrated solution, the relative quantity of Nafion® increases by a factor

of 3). This may suggest that the thicknesses of the films that are produced after drying will depend largely on the amount of Nafion® in the casting solution (thicker films with increasing amounts of Nafion® in the casting solution).[29,33] The best catalytic behaviour should be obtained for the thinnest film, assuming that diffusion within the film is a limiting factor in this work. Thus the TOF data shown in Figure 5.21 appear to be influenced by film thickness.

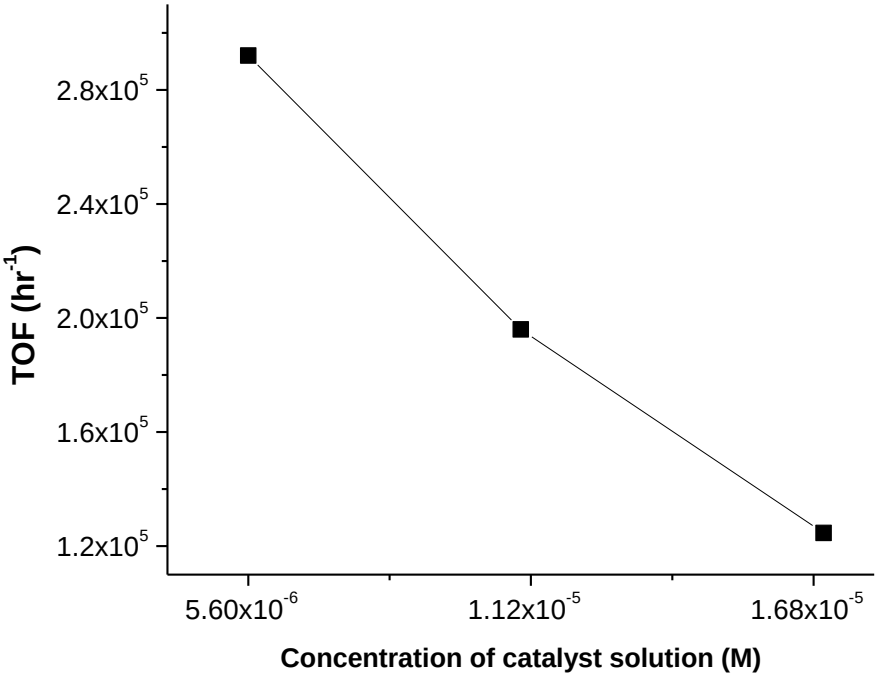

Figure 5.21: *Turnover frequencies as a function of catalyst solution concentration for $CoPcF_{16}$/Nf.*

5.2.2.6 Varying the volume of catalyst deposited

The effect of varying the concentration of the catalyst embedded in a Nafion® matrix discussed above prompted a study to investigate the effect of casting a lower volume of catalyst. The experimental results did not indicate the expected trend; an increase in active with increasing the volume of catalyst deposited onto the electrode since the catalytic activity was independent when volumes of 0.5 μL, 1.0 μL and 1.5 μL of catalyst solution dispersed in Nafion® were cast onto the electrode.

5.2.2.7 Casting additional layers from DMF catalyst solution

While the effect of increasing the volume of catalyst is discussed above, investigating the effect of altering the number of layers cast onto the electrode was carried out in an effort to increase the amount of electroactive catalyst present in the modifying layer which is available to participate in the electrocatalytic reaction. The performance indicators for each catalyst when just one coat was drop cast onto a GCE are displayed for comparison purposes. The effect of the additional layer is observed in Table 5.13 which displays the electrocatalytic activity of $CoPcF_{16}$/Nf. (see Appendix D, Table D.15).

Catalyst	**$CoPcF_{16}$/Nf**	
No. of layers cast	***1***	***2***
Charge (C)	*0.19*	*0.18*
Moles of H_2 (mol)	*7×10^{-7}*	*6×10^{-7}*
Faradaic Efficiency %	*71*	*65*
[1]Current Density J (mA/cm^2)	*0.8*	*0.7*
[2]Current Density (J) (mA/cm^2)	*4.4*	*7.2*
% Electroactive	*10.5*	*6.5*

Table 5.13: *Average performance data obtained for $CoPcF_{16}$/Nf by CV and BE at -1.2 V vs. Ag/AgCl in 0.1 M NaH_2PO_4/H_3PO_4 (pH 2) with varying the number of layers of catalyst deposited on the electrode. [1]Current density obtained using BE data and [2]current density obtained using the last scan of the CV.*

Examination of the data displayed in Table 5.13 reveals that applying a second layer of catalyst onto the modifed electrode did not alter the electrocatalytic activity for the hydrogen evolution reaction. It is proposed that facile diffusion can occur when a second layer is cast. As Nafion® allows for the uptake of protons, it

is postulated that as the ratio of Nafion® increases, the uptake of protons occurs readily in pH 2 acidic conditions, thus contributing to the steady catalytic activity.[7,21] Although no experimental data is available for an electrode with 10 layers of $CoPcF_{16}$/Nf cast, it would be expected that an increase in thickness of the modifying layer would result in a decrease in the rate of the catalytic activity as mass transport of the reactant (protons) and catalyst to the electrode surface and product leaving the electrode surface would become sluggish.[29,30,31,32]

Catalyst	**$CuPcF_{16}$/Nf**		**$ZnPcF_{16}$/Nf**	
No. of layers cast	***1***	***2***	***1***	***2***
Charge (C)	*0.17*	*0.17*	*0.24*	*0.05*
Moles of H_2 (mol)	*1.8×10^{-7}*	*1.4×10^{-7}*	*2.7×10^{-7}*	*2.7×10^{-7}*
Faradaic Efficiency %	*39*	*16*	*22*	*45*
[1]Current Density *J* (mA/cm^2)	*0.7*	*0.7*	*1.0*	*0.2*
% Electroactive $MPcF_{16}$/Nf	*3.4*	*1.5*	*1.2*	*1.3*

Table 5.14: *Average performance data obtained for $CuPcF_{16}$/Nf and $ZnPcF_{16}$/Nf by CV and BE at -1.2 V, vs. Ag/AgCl in 0.1 M NaH_2PO_4/H_3PO_4 (pH 2) with varying the number of layers of catalyst deposited on the electrode. [1]Current density obtained by BE.*

When 2 layers of $CuPcF_{16}$/Nf and $ZnPcF_{16}$/Nf were cast onto a working electrode, the catalytic activity decreased. The charge recorded after the hour electrolysis was slightly less that the charge obtained when only one coat is applied to the working electrode for $CuPcF_{16}$/Nf. However, when a second layer of $ZnPcF_{16}$/Nf was cast, the charge accumulated after an hour is 20 % of the charge passed when

1 layer was coated. These results indicate that the rate of the electrocatalytic reaction decreases when an additional layer is coated.

The TOF values obtained for each of the catalysts employed revealed a decrease in the values determined (See Appendix D, Table D.15). The largest TOF obtained is when $CuPcF_{16}$/Nf was employed of 1.7 x 10^5, however this is 3.5 times smaller than the TOF obtained using 1 modifying layer. The lowest TOF is observed when $ZnPcF_{16}$/Nf was used, 4.7 x 10^4.

As TOF values are determined by the number of electroactive moles on the modifying layer and this can vary with each modified electrode, it is more appropriate to use the current density, charge and number of moles of hydrogen produced to determine the electrocatalytic activity of a catalyst. As the number of moles of hydrogen produced when the second coat of catalyst is cast are marginally smaller than those compared to only one coat, it is therefore assumed that when a second layer of $CoPcF_{16}$/Nf is cast onto a modified electrode, the electrocatalytic behaviour is independent of this additional layer. As the aim of casting an additional layer was to increase the moles of electroactive catalyst and hence improve the electrocatalytic activity for the generation of hydrogen, this was not achieved. Casting a second layer of $CoPcF_{16}$/Nf resulted in the same catalytic activity, while a decrease in activity occurs when additional layers of $CuPcF_{16}$/Nf and $ZnPcF_{16}$/Nf are cast.

5.2.2.8 Stability

The stability of these catalysts is observed upon examining the cyclic voltammograms recorded prior to and after the potentiostatic electrolysis. Before an electrolysis step is performed using the modified electrode, the voltage is scanned in a cathodic direction to the corresponding potential at which the maximum catalytic current is observed. The stability of these catalysts in the modifying layer is indicated by a cathodic catalytic current of similar magnitude after the potentiostatic electrolysis. A decrease in the current produced after the electrolysis step would indicate instability of the catalyst in the modifying layer to serve as a catalyst for the electrocatalytic generation of hydrogen.5 Similar to the

adsorbed catalysts, as the number of moles of electroactive catalyst is relatively low (10.5 % electroactive for $CoPcF_{16}$/Nf, 3.4 % for $CuPcF_{16}$/Nf and 1.2 % for $ZnPcF_{16}$/Nf), it is difficult to observe the redox couple in the voltammogram after electrolysis (See Appendix D, Figures D.6-D.9). This is also observed for the adsorbed catalysts in Chapter 4.

5.2.2.9 Duration of Electrolysis

The aim of this study was to investigate the length of time the catalyst can electrocatalytically generate hydrogen before the activity of the modified layer decreased. The modified electrodes were prepared in the same manner as for a one hour electrolysis experiment; however the duration of the electrolysis reaction was increased from 1 hour to 6 hours and to 24 hours. These experiments were conducted using just the $CoPcF_{16}$/Nf catalyst. The performance indicators are reported in Table 5.15 and the corresponding TON displayed in Figure 5.22. (see Appendix D, Table D.16).

Time (hr)	**1**	**6**	**24**
Charge (C)	*0.2*	*2.2*	*30.5*
Current Density *J* (mA/cm^2)	*0.8*	*8.7*	*121*
(%) Electroactive $CoPcF_{16}$	*10.5*	*9.2*	*10.6*

Table 5.15: *Average performance data obtained for $CoPcF_{16}$/Nf by CV and BE (at -1.2 V) vs. Ag/AgCl in 0.1 M NaH_2PO_4/H_3PO_4 (pH 2) as a function of time.*

The results presented in Table 5.15 indicate that as the length of time of the potentiostatic electrolysis increased, performance did not appear to diminish suggesting these modified electrodes dispersed in Nafion® were stable as catalysts for the electrocatalytic hydrogen evolution reaction. When the electrolysis was carried out over 6 hours, an increase in charge passed was

observed which is more than 11 times larger than the charge passed after 1 hour. After a 24 hour period, the charge continued to rise indicating the catalytic reaction can continue over long periods of time. As discussed in chapter 4, the current densities obtained by bulk electrolysis increase as the period of electrolysis increases, however the contribution of increasing O_2 concentration over time complicates these results.

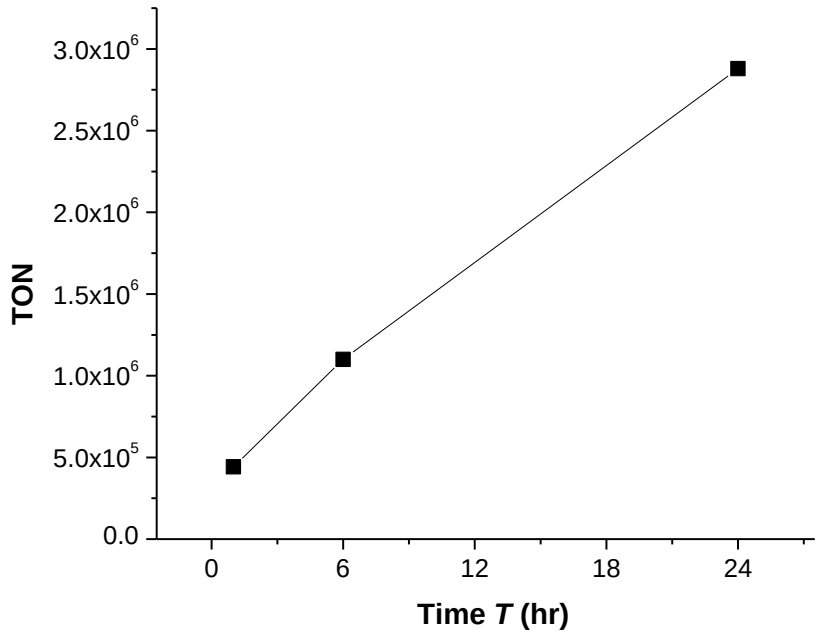

Figure 5.22: *Turnover Numbers (TON) as a function of time for $CoPcF_{16}$ in 0.1 M NaH_2PO_4/H_3PO_4 (pH 2).*

The turnover figures are displayed in Figure 5.22 for $CoPcF_{16}$/Nf over time. The turnover figures presented so far in this chapter are turnover frequencies, where TOF reports the number of moles produced over a given time frame, i.e. per hour. The turnover number TON reports the number of moles of product generated per mole of immobilised, electrochemically active catalyst over the duration of the experiment. The TON's increased steadily over the 24 hour period, reaching 2.9 x 10^6. Although the Faradaic efficiency decreases with increasing periods of potentiostatic electrolyses (17 %), O_2 reduction contribues to the large current densities. The stability of this catalyst is demonstrated and can work as a catalyst for longer electrolysis periods. These findings are very similar to those observed

for the adsorbed catalysts, therefore Nafion® doesn't offer any further stability for longer electrolysis periods.

5.2.2.10 Photo- electrocatalytic generation of hydrogen

The experiments discussed so far in this chapter were all carried out in natural daylight. Therefore the importance of light on the electrocatalytic activity was investigated using modified electrodes containing $CoPcF_{16}$, $CuPcF_{16}$ and $ZnPcF_{16}$ embedded in Nafion®. Performing these experiments in the presence of light has been reported where an increase in the electrocatalytic activity was obtained when a modified electrode containing a zinc macrocycle was irradiated with light.[33,34,35] The effect of light on the catalytic actiivty can also be observed in Chapter 4 (4.2.2.12). For these electrocatalytic experiments, the cell was placed in a dark cupboard and the potentiostatic electrolysis experiments in the absence of light were performed. The resulting experimental data are displayed in Tables 5.16 and 5.18 for $CoPcF_{16}$/Nf, and $CuPcF_{16}$/Nf and $ZnPcF_{16}$/Nf respectively. (see Appendix D, Table D.17).

Variable	Dark	Light
Charge (C)	*0.11*	*0.19*
Moles of H_2 (mol)	*4×10^{-7}*	*7×10^{-7}*
Faradaic Efficiency %	*64*	*71*
[1]Current Density (mA/cm^2)	*0.4*	*0.8*
[2]Current Density (mA/cm^2)	*1.1*	*4.5*
% Electroactive	*2.8*	*10.5*

Table 5.16: *Average performance data obtained for $CoPcF_{16}$/Nf by CV and BE (at -1.2 V for 1 hour) vs. Ag/AgCl in 0.1 M NaH_2PO_4/H_3PO_4 (pH 2) in daylight and in darkness. [1]Current density obtained using BE data and [2]current density obtained using the last scan of the CV.*

Examination of all the performance indicators when this metallophthalocyanine dispersed in Nafion® was employed as a catalyst revealed a decrease in activity when the potentiostatic electrolyses were conducted in the absence of light. This suggests that the electrocatalytic generation of hydrogen is aided when performed in daylight. When the reaction takes place in daylight, a current density of 4.5 mA/cm^2 is observed by CV, however when the electrochemical cell is placed in darkness, the resulting current density falls to 1.1 mA/cm^2. Hence it appears that the light contributes to the rate at which the hydrogen is evolved using this catalyst. The current densities calculated by CV when the reactions were performed in the dark were lower than those determined for the adsorbed catalysts (described in Chapter 4). This trend was been noted by Schlettwein for the light induced oxygen reduction using ZnPc (in a variety of polymers, including Nafion®) were investigated.[33]

	$CuPcF_{16}$/Nf		**$ZnPcF_{16}$/Nf**	
Variable	**Dark**	**Light**	**Dark**	**Light**
Charge (C)	*0.12*	*0.17*	*0.05*	*0.24*
Moles of H_2 (mol)	*1.4×10^{-7}*	*1.8×10^{-7}*	*4.2×10^{-8}*	*2.7×10^{-7}*
Faradaic Efficiency %	*24*	*39*	*16*	*24*
[1]Current Density (mA/cm^2)	*0.5*	*0.7*	*0.2*	*1.0*
[2]Current Density (mA/cm^2)	*0.7*	*3.5*	*0.7*	*1.4*
% Electroactive	*2.4*	*3.4*	*1.3*	*1.2*

Table 5.17: *Average performance data obtained for $CuPcF_{16}$/Nf and $ZnPcF_{16}$/Nf by CV and BE vs. Ag/AgCl in 0.1 M NaH_2PO_4/H_3PO_4 (pH 2) in daylight and in darkness. [1]Current density obtained using BE data and [2]current density obtained using the last scan of the CV.*

Examination of the experimental data when $CuPcF_{16}$/Nf and $ZnPcF_{16}$/Nf were employed as catalysts, the same trend determined for $CoPcF_{16}$/Nf was observed here. For $ZnPcF_{16}$/Nf, the charge passed after an hour electrolysis in darkness was almost 5 times less than the charge obtained when carried out in daylight. Comparing this to the activity when $CuPcF_{16}$/Nf was used, the absense of light did not appear to have a significant effect on the catalytic performance. The current density confirmed that the absence of light appeared to cause a decrease in the electrocatalytic activity for both catalysts embedded in Nafion® (however these current densities are complicated by the presence of O_2 after 1 hour electrolysis).[36,37] This activity correlates to the findings reported by Kaneko and Hirai when ZnPc was incorporated into Nafion® and PVP.[21,38]

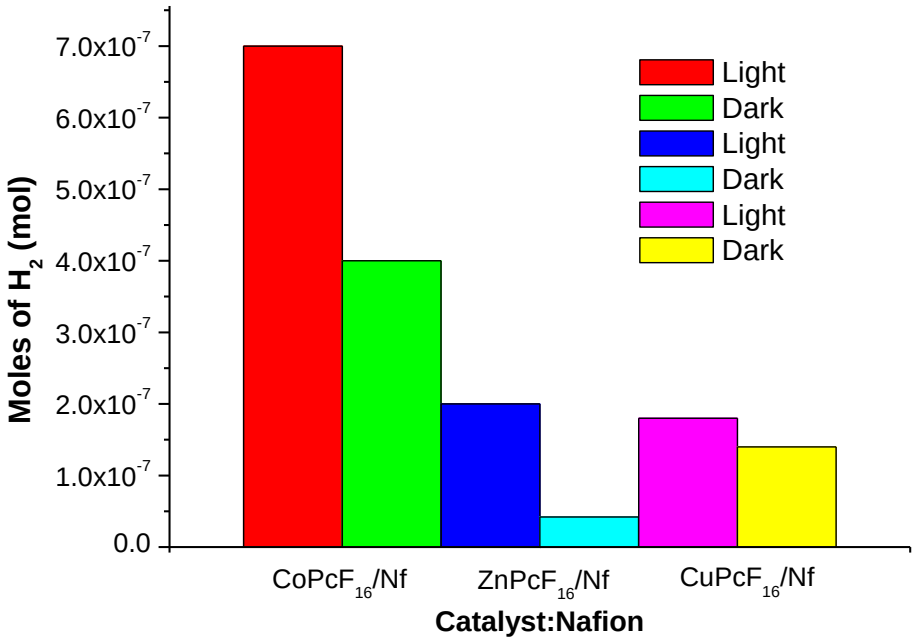

Figure 5.23: *TOF values obtained by gas analysis after 1 hour potentiostatic electrolysis at -1.2 V vs. Ag/AgCl for $CoPcF_{16}$/Nf, $CuPcF_{16}$/Nf and $ZnPcF_{16}$/Nf.*

The TOF (hr^{-1}) values determined are displayed in Figure 5.23. The largest activity exhibited by $CoPcF_{16}$/Nf in the darkness was indicated by a TOF value of 3.8 x 10^5, followed by $CuPcF_{16}$/Nf of 2.1 x 10^5 while the lowest was obtained by $ZnPcF_{16}$/Nf of 4.3 x 10^4. The Faradaic efficiencies of these systems were

calculated as 64 %, 54 % and 16 % for $CoPcF_{16}$/Nf, $CuPcF_{16}$/Nf and $ZnPcF_{16}$/Nf respectively (see Appendix D, Table D.17). The data displayed for these catalysts indicated that these catalysts incorporated in Nafion® can work in both darkness and in daylight, with the optimum conditions being in daylight.[39,40,41]

5.2.3 Effect of varying the ratio of MPc to Nafion® for the electrocatalytic generation of hydrogen

The purpose of employing Nafion® was to investigate the influence of a polyionic support on the electrocatalytic activity of the metallophthalocyanines for the generation of hydrogen. Nafion® alone displayed weak catalytic activity for this reaction. When each of the catalysts were dispersed into this polymer matrix, the resulting activity was found to decrease when compared to the corresponding adsorbed catalysts. The experimental results discussed so far are concerned with the employment of the catalyst in Nafion® in a volume ratio of 4: 1; a small ratio of polymer is employed (see Chapter 2 for description). The experimental results discussed in this section will examine the effect on the electrocatalytic activity when the ratio of polymer is increased to 1:1 and 1:4 MPc:Nf, denoted *2*-MPc:Nf and *3*-MPc/Nf respectively. The experimental data for varying ratios of $CoPcF_{16}$/Nf and $ZnPcF_{16}$/Nf are displayed in Appendix D, Tables D.18-D.20 and Figures D.10-D.11.

5.2.3.1 Varying the ratio of $CuPcF_{16}$:Nafion®

Phthalocyanine complexes are expected to undergo electron transfer via a diffusion mechanism, rather than by a charge-hopping scheme.[42] Analysis of the diffusion properties of the catalysts in Nafion® is possible through use of the Randles-Sevcik equation, as a plot of peak current versus square root of scan rate for cyclic voltammetry experiments (Figures 5.24 and 5.26) provides a means of investigating an apparent diffusion coefficient, D_{app}, of the catalysts in the modified electrode films.[43]

Because the dominant mechanism of charge transport is via diffusion, it is expected that the diffusion coefficient will be independent of catalyst

concentration. The catalyst concentration in the film would be required in order to calculate D_{app}. Since values for C are not able to be determined here, the diffusion data may be expressed as $D_{app}^{1/2}C$. In this way, direct comparisons may be made between films cast from *2*-$CuPcF_{16}$:Nf and *3*-$CuPcF_{16}$:Nf solutions. The results for these experiments are shown in Figures 5.25 to 5.27. The slopes of the lines for these plots show that for *2*-$CuPcF_{16}$:Nf, $D_{app}^{1/2}C$ is approximately 4 times larger. However, the concentration of the catalyst in the *2*-$CuPcF_{16}$:Nf film is 4 times greater. Thus, the diffusion coefficients are equivalent. Assuming a nominal catalyst concentration of 1 mM in the Nafion film, D_{app} would be calculated from the Randles Sevcik equation as approximately 5 x 10^{-9} cm^2/s. This value is in good agreement with D_{app} figures reported by Kaneko *et al.* for CoPc in poly(4-vinylpyridine)-co-styrene using chronoamperometry experiments.[16] Additional calculations are shown in Appendix D.

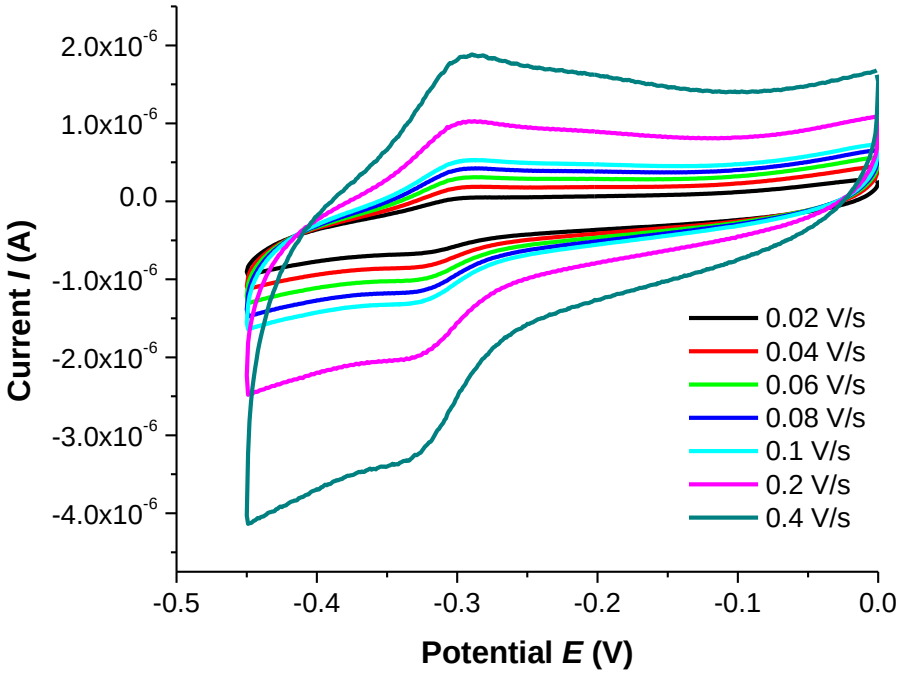

Figure 5.24*: Scan rate dependence of 2-$CuPcF_{16}$/Nf; (1: 1 Cu: Nf ratio), vs. Ag/AgCl in 0.1 M NaH_2PO_4/H_3PO_4 (pH 2).*

.

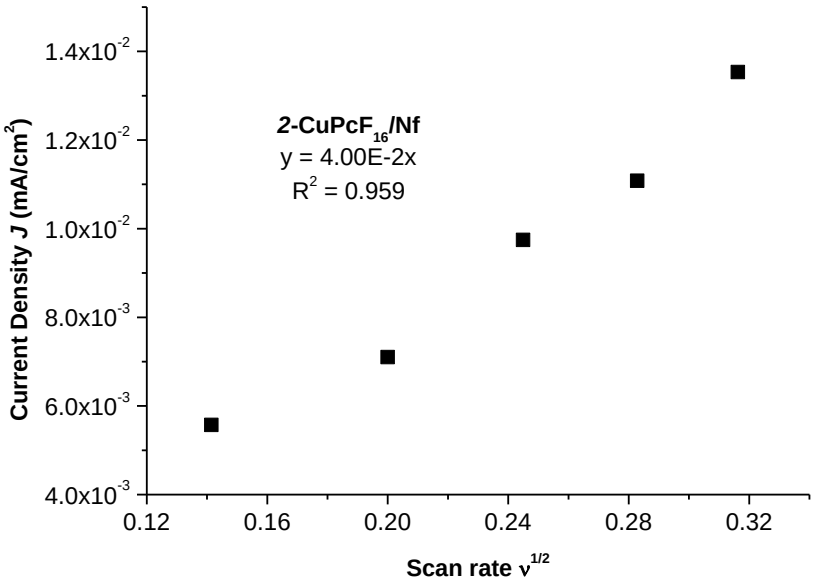

Figure 5.25: *Current density J, as a function of scan rate v, for 2-CuPcF$_{16}$/Nf (1: 1 Cu: Nf ratio) in 0.1 M NaH$_2$PO$_4$/H$_3$PO$_4$ (pH 2), vs. Ag/AgCl.*

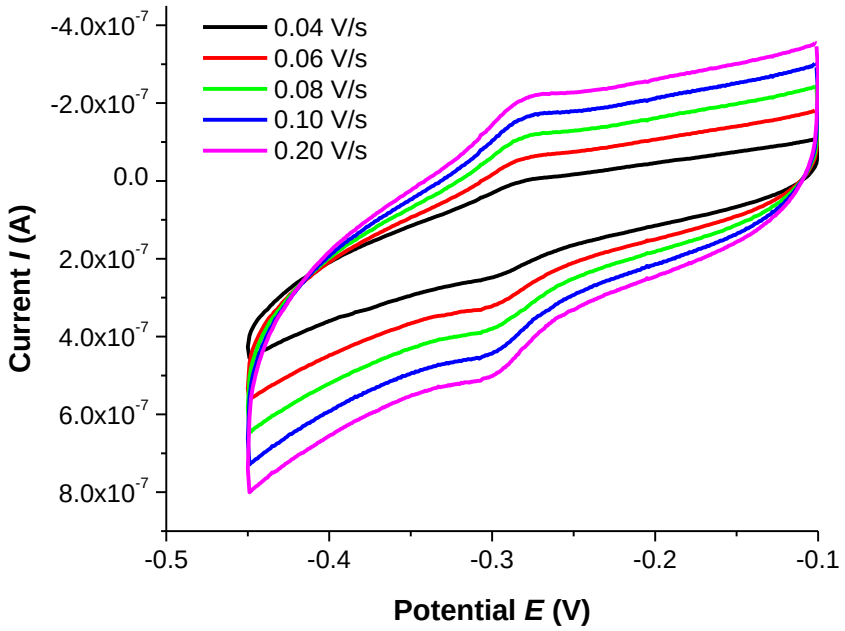

Figure 5.26*: Scan rate dependence of 3-CuPcF$_{16}$/Nf (1: 4 Cu: Nf ratio) in 0.1 M NaH$_2$PO$_4$/H$_3$PO$_4$ (pH 2), vs. Ag/AgCl.*

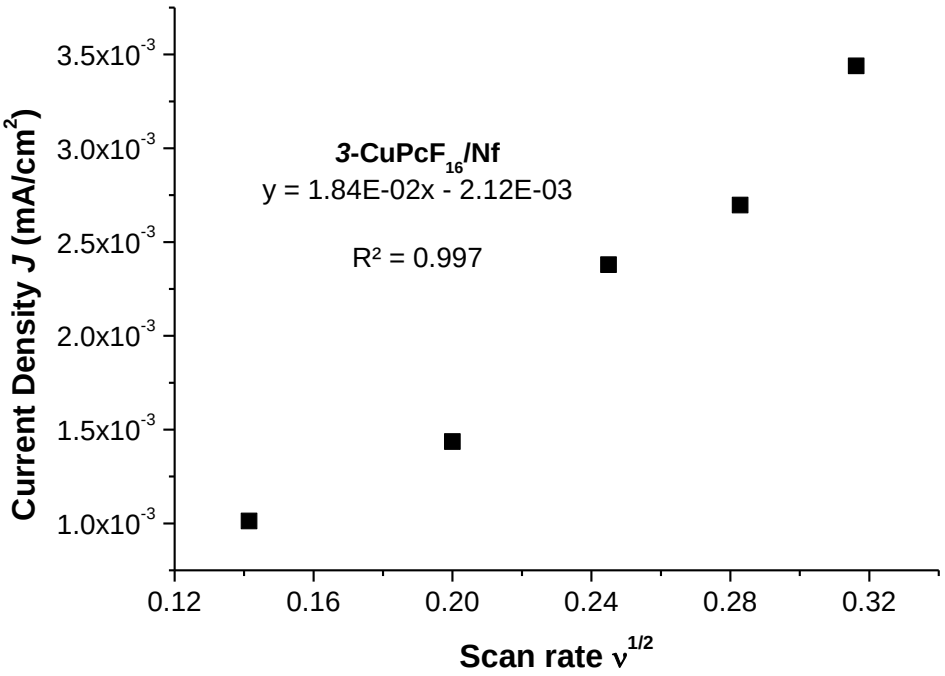

Figure 5.27: *Current density J, as a function of scan rate ν, for 3-CuPcF$_{16}$/Nf (1: 4 Cu: Nf ratio) in 0.1 M NaH$_2$PO$_4$/H$_3$PO$_4$ (pH 2), vs. Ag/AgCl.*

The performance indicators for CuPcF$_{16}$/Nf of varying ratios are displayed in Table 5.18. As the ratio of Nafion® to CuPcF$_{16}$ increased, the charge accumulated after a one hour electrolysis increased also. The catalyst *3*-CuPcF$_{16}$/Nf resulted in the largest charge of 0.28 C while the lowest charge was observed of 0.19 C when a ratio of 4:1 Cu: Nf was used. Examination of the current densities revealed the highest (3.9 mA/cm^2) was obtained when *3*-CuPcF$_{16}$/Nf was employed.

$CuPcF_{16}$:Nafion®	***1*-$CuPcF_{16}$/Nf**	***2*-$CuPcF_{16}$/Nf**	***3*-$CuPcF_{16}$/Nf**
Charge (C)	*0.17*	*0.27*	*0.28*
Mol of H_2 (mol)	*3.3×10^{-7}*	*6.7×10^{-7}*	*1.7×10^{-7}*
Faradaic Efficiency %	*39*	*48*	*13*
[1]Current Density *J* (mA/cm^2)	*0.7*	*1.1*	*1.1*
[2]Current Density *J* (mA/cm^2)	*3.5*	*3.8*	*3.9*
Electroactive $CuPcF_{16}$/Nf (%)	*3.4*	*2.4*	*3.7*

Table 5.18: *Average performance data obtained for $CuPcF_{16}$/Nf by CV and BE at -1.2 V vs. Ag/AgCl in 0.1 M NaH_2PO_4/H_3PO_4 (pH 2) with varying ratios of catalyst: Nafion® deposited on the electrodes. [1]Current density obtained using BE data and [2]current density obtained using the last scan of the CV.*

It appeared that *2*-$CuPcF_{16}$/Nf resulted in the largest catalytic activity for proton redcution. This is further indicated by the moles of H_2 generated of 6.7×10^{-7} mols and TOF (1.1×10^6) in Figure 5.28. Comparing the performance indicators at this ratio with those obtained using the adsorbed catalyst $CuPcF_{16}$, revealed that the optimum system was when this perfluorinated copper phthalocyanine (*2*-$CuPcF_{16}$/Nf) was dispersed in Nafion® polymer in a 1:1 ratio respectively.

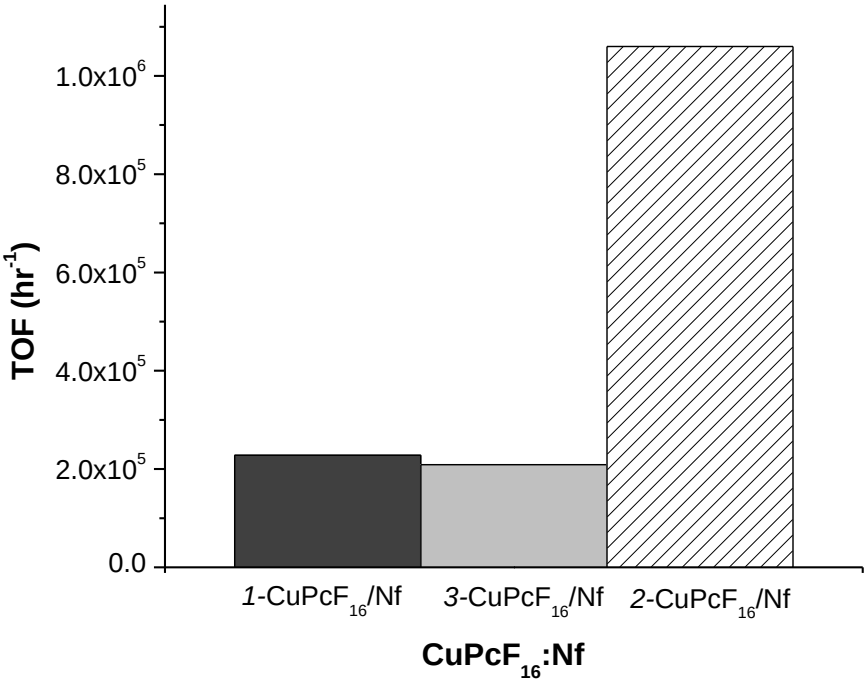

Figure 5.28: *Effect of varying the ratios of $CuPcF_{16}$ and Nafion® on turnover frequencies TOF (hr^{-1}) for catalysts 1-$CuPcF_{16}$/Nf, 2-$CuPcF_{16}$/Nf and 3-$CuPcF_{16}$/Nf respectively.*

Although the number of moles of H_2 produced by this catalytic system was the largest, it is difficult to directly compare all three systems. Comparing the systems *1*-$CuPcF_{16}$/Nf and *2*-$CuPcF_{16}$/Nf is straighforward, as the difference in these systems lies in the amount of catalyst in the film. However, for 3-*$CuPcF_{16}$/Nf,* the film morphology is expected to change considering there is more Nafion® per unit volume of the solution. Therefore this modified electrode is unlike the ones modified with *1*-$CuPcF_{16}$/Nf and *2*-$CuPcF_{16}$/Nf.

5.2.3.2 Varying the ratio of Catalyst:Nafion® using KCl as the electrolyte

The effect of varying the catalyst/polymer ratio while using 0.1 M HCl/KCl as the electrolyte for the electrocatalytic generation of hydrogen is shown in Table 5.19.

MPc: Nafion®	***1*-$CoPcF_{16}$/Nf**	***2*-$CoPcF_{16}$/Nf**	***3*-$CoPcF_{16}$/Nf**
Charge (C)	*0.28*	*0.23*	*0.24*
Moles of H_2 (mol)	*1.4×10^{-6}*	*1.1×10^{-6}*	*1.1×10^{-6}*
Faradaic Efficiency %	*97*	*93*	*88*
^{1}Current Density (mA/cm^2)	*1.1*	*0.9*	*1.0*
^{2}Current Density (mA/cm^2)	*11.3*	*10.5*	*11.9*
% Electroactive catalyst	*6.2*	*0.8*	*1.1*

Table 5.19: *Average performance data obtained for $CoPcF_{16}$/Nf by CV and BE (at -1.2 V for 1 hour) vs. Ag/AgCl in 0.1 M HCl/KCl (pH 1.8) at 20°C with varying ratios of catalyst: Nafion®. ^{1}Current density obtained using BE data and ^{2}current density obtained using the last scan of the CV.*

The performance values in Table 5.19 above indicates that varying the ratio of catalyst to Nafion® polymer did not significantly alter the electrocatalytic activity for the generation of hydrogen. The lowest current density (obtained by BE) and charge was obtained when *1*-$CoPcF_{16}$/Nf was employed; 0.9 mA/cm^2 and 0.23 C respectively. When 2-$CoPcF_{16}$/Nf was used, the largest current density was obtained of 1.1 mA/cm^2, yet the largest charge of 0.28 C was obtained when *1*-$CoPcF_{16}$/Nf was used. However, the differences in these performance indicators are small, thus it appears that the Co catalyst can exhibit catalytic activity when a different electrolyte is used and with varying ratios of Nafion® polymer. As discussed previously in chapter 4 (4.2.2.8), the affect of O_2 reduction decreases when KCl/HCl is employed as a buffer. This is observed by the larger amounts of H_2 produced; 1.4 x 10^{-6} mols compared to when the acidic phosphate buffer is used 7 x 10^{-7} mols respectively.

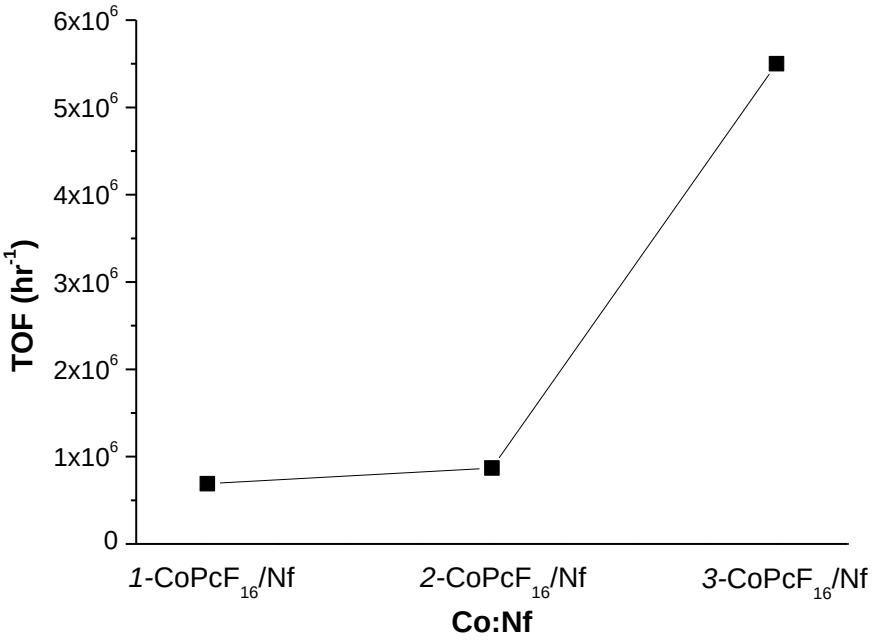

Figure 5.29: *Turnover frequencies TOF (hr^{-1}) as a function of varying ratios of Nafion® polymer for $CoPcF_{16}$/Nf in 0.1 M HCl/KCl.*

Similar to the behaviour exhibited by the performance parameters in Table 5.20 above, the TOF values obtained by gas chromatography are comparable. The TOF values determined using *1*-$CoPcF_{16}$/Nf and 2-$CoPcF_{16}$/Nf were 6.9 x 10^5 and 8.7 x 10^5 respectively. The corresponding Faradaic efficiencies for these systems were calculated as 94 % and 93 % respectively. The largest TOF values determined for *3*-$CoPcF_{16}$/Nf were significantly larger compared to the TOF values for the other ratios. The Faradaic efficiency calculated for this system was 88 %, however these large TOF values are attributed to the lowest percentage of electroactive catalyst in the polymer of the modifying layer. (see Appendix D, Table D.21).

5.3 Concluding Remarks

The parameters and operating conditions which affect the activity of $MPcF_{16}$ (where M is Co, Cu or Zn dispersed in Nafion®) to electrocatalytically generate hydrogen from water have been investigated including temperature, applied potentiostatic electrolysis, pH and varying the ratio of polymer matrix to catalyst. The potentials at which the redox processes of the metallophthalocyanines are observed are shifted slightly in comparison with the adsorbed catalysts to -0.43 V, -0.32 V and -0.25 V vs. Ag/AgCl for $CoPcF_{16}$/Nf, $CuPcF_{16}$/Nf and $ZnPcF_{16}$/Nf respectively. Similarly the onset potentials for which the catalytic currents are observed also experience a small shift to more negative potentials occurring at -0.98 V, -0.90 V and -1.0 V vs. Ag/AgCl for $CoPcF_{16}$/Nf, $CuPcF_{16}$/Nf and $ZnPcF_{16}$/Nf respectively.

At least a 200 mV decrease in overpotential with respect to a bare glassy carbon electrode and a Nafion-coated GCE in identical conditions exists, indicating their promise as electrocatalysts for the hydrogen evolution reaction in aqueous solutions. It was found that the best overall performance at pH 2 (phosphate buffer) and at 20^{o}C was provided by $CoPcF_{16}$/Nf (largest TOF of 4.4 x 10^5 and current density (4.5 mA/cm^2 at 20°C). Larger values were obtained when a solution of 0.1 M KCl/HCl was employed using *3*-$CoPcF_{16}$/Nf; (5.5 x 10^6 TOF hr^{-1} and 11.9 mA/cm^2).

Importantly, the TOF (hr^{-1}) values obtained by gas chromatography are significantly less than the TOF values determined when the adsorbed catalysts are employed, where the highest TOF is 2.1 x 10^5 (for $CoPcF_{16}$/Nf) compared to 3.5 x 10^6 (for adsorbed $CuPcF_{16}$ described in Chapter 4). Although the TOF values calculated are low, their corresponding Faradaic efficiencies are large, typically 70 %.

Although turnover frequency (TOF) values are an indication of hydrogen produced per catalyst, evaluating the catalytic activities of these metallophthalocyanines in Nafion® is not only based on TOF values but also other performance indicators, such as charge (accumulated after 1 hour potentiostatic electrolysis) and current density.

When the temperature is varied, the three catalysts each reveal a decrease in electrocatalytic activity at 0°C, a possible indication of a sluggish electron transfer which is reflected in the current densities obtained at this temperature. Increasing the temperature to 40°C reveals a increase in the kinetics of the reaction as suggested by the rise in current densities for all three catalysts. The solubility of hydrogen in water with increasing temperature is taken into consideration in the discussion of these electrocatalytic results

When the pH of the electrolyte solution is increased to basic conditions, the potential at which the redox couple and the onset potential for the electrocatalytic reaction is observed shifts to lower potentials. Comparing the number of moles of hydrogen produced is difficult as the change on pH of the electrolyte and the overpotential required should be taken into consideration. However the catalyst which acts the most efficiently at all pH, reflected by the overpotentials, charge and current densities is $CoPcF_{16}$/Nf. Altering the ionic strength of the electrolyte solution to 0.01 M results in a decrease in catalytic activity for $CoPcF_{16}$/Nf, , however it is plausible that an increase in solution resistance gives rise to this performance.

Varying the concentration of the catalysts cast into the electrode reveals the highest current density and moles of evolved hydrogen for $CoPcF_{16}$/Nf when the most concentrated catalyst is applied, 1.7×10^{-5} M, however the largest TOF values are obtained when the least concentrated solution of catalyst is cast, 5.6×10^{-6} M, which is due to the low number of electroactive moles in the modifying layer at this concentration.

Similar to the results observed by the adsorbed catalyst, the stability of the layers was investigated. After 24 hours, a plateau or a decrease in charge would be expected if the modifying layer deactivated or decomposed on the electrode. However this was not observed, indicated by the large charge and TON obtained after 24 hours of electrolysis, reaching 30.5 C and 2.9×10^{6} respectively. It is suggested that the presence of O_2 complicates the current as the duration of electrolysis increases, as O_2 can drift towards the cathode and contribute to the performance measured.

Lastly, the effect of the absence of light was investigated using all three catalysts which displayed similar behaviour. When these electrocatalytic experiments were performed in the dark, remarkably the activity fell for all three metallophthalocyanines as indicated by a decrease in the current density, charge, TOF and percentage electroactive in the layer. The largest difference was observed using $ZnPcF_{16}$/Nf; the TOF obtained in the dark 25 % less than the TOF obtained in the daylight. Thus, it appears that light plays a role in the electrocatalytic generation of hydrogen.

5.4 References

[1] (a) A.P. Doherty, M.A. Stanley, J.G. Vos, *Analyst, 120*, **1995**, 2371; (b) A.P. Doherty, M.A. Stanley, D. Leech, J.G. Vos, *Anal. Chim. Acta, 319*, **1996**, 111; (c) A. Heller, Acc. *Chem. Res. 23,* **1990**, 128.

[2] J. L. Inglis, B.J. MacLean, M.T. Pryce, J.G. Vos, *Coord. Chem. Rev*., 256, **2012,** 2571.

[3] C. E. D. Chidsey, R. W. Murray, *J. Phys. Chem., 90*, **1986**, 4733, 1479.

[4] T. J. Meyer, *Acc. Chem. Res. 22*, **1989**, 163.

[5] J. G Vos, M. R. Smyth, *Analytical Voltammetry*, Chapter 7, Amsterdam, Elsevier, **1992**, New York.

[6] C. E. D. Chidsey, R. W. Murray, *Science, 231*, **1986**, 4733, 25.

[7] D.A. Buttry, F.C. Anson, *J. Am. Chem. Soc. 106*, **1984**, 59.

[8] M. Yagi, K. Nagai, A. Kira, M. Kaneko, *J. Electroanal. Chem., 394*, **1995**, 169.

[9] M. Fujihira, I. Rubenstein, J. F. Rusling, *Modified Electrodes*, *Encyclopedia of Electrochemistry, Vol. 10*, **2007**, Wiley-VCH, Weinheim.

[10] P. G. Pickup, R. W. Murray, *J. Am. Chem. Soc, 105*, **1983**, 14, 4510.

[11] P. G. Pickup, W. Kutner, C. R. Leidner, R. W. Murray, *J. Am. Chem. Soc, 106,* **1984**, 7, 1991.

[12] D. N. Blauch, J. M. Savéant, *J. Am. Chem. Soc,114*, **1992**, 9, 3323.

[13] J. Zhang, F. Zhao, M. Kaneko, *J. Porphyrins Phthalocyanines, 4*, **2000**, 65.

[14] F. Zhao, J. Zhang, M. Kaneko, *J. Porphyrins Phthalocyanines, 4*, **2000**, 158.

[15] J. Zhang, F. Zhao, T. Abe, M. Kaneko, *Electrochimica Acta, 45*, **1999**, 399.

[16] F. Zhao, J. Zhang, T. Abe, D. Wöhrle, M. Kaneko, *J. Mol. Catal. A: Chem., 145*, **1999**, 245.

[17] J. Ouyang, K. Shigehara, A. Yamada, F. C. Anson, *J. Electroanal. Chem., 297*, **1991**, 2, 489.

[18] Ö.A. Osmanbaş, A. Koca, M. Kandaz, F. Karaca, *Int. J. Hydrogen Ener. 33*, **2008**, 3281.

[19] A. Koca, A. Kalkan, Z. Altuntaş Bayir, *Electrochim. Acta, 56,* **2011**, 5513.

[20] A. Koca, *Electrochem. Commun., 11*, **2009**, 838.

[21] F. Zhao, J. Zhang, D. Wöhrle, M. Kaneko, *J. Porphyr. Phthalocya., 4*, **2000**, 31
.

[22] C. Song, L. Zhang, J. Zhang, D. P. Wilkinson R. Baker, *Fuel Cells, 1*, **2007**, 9.

[23] R. Baker, D. P. Wilkinson, J. Zhang, *Electrochim. Acta., 53*, **2008**, 6906.

[24] S. Baranton, C. Coutanceau, C. Roux, F. Hahn, J. M. Leger, *J. Electroanal. Chem., 577*, **2005**, 223.

[25] http://www.engineeringtoolbox.com/gases-solubility-water-1148.html. Last referenced 20/10/2012

[26] G. Inzelt, *Electrochim. Acta, 34*, **1989**, 83.

[27] H. Zhang, R. W. Murray, *J. Am. Chem. Soc., 115*, **1993**, 2335.

[28] D. Wöhrle, H. Kaune, B. Schumann, N. Jaeger, *Makromol. Chem. 187*, **1986**, 2947.

[29] N. Oyama, T. Ohsaka, T. Ushirogouchi, *J. Phys. Chem., 88*, **1984**, 5274.

[30] J. M. Savéant, *Chem. Rev., 108,* **2008**, 2378.

[31] J. G Vos, M. R. Smyth, Analytical Voltammetry, Chapter 7, Amsterdam, New York, Elsevier, **1992**.

[32] W. J. Albery, A. R. Hillman, *RSC Annual Report*, 78, **1981**, 377.

[33] D. Schlettwein, M. Kaneko, A. Yamada, D. Wöhrle, N.I. Jaeger, *J. Phys. Chem., 95*, **1991**, 1748.

---

[34] T. Abe, H. Imaya, S. Tokita, D. Wöhrle, M. Kaneko, *J. Porphyr. Phthalocya*., *1*, **1997**, 215.

[35] M. Kaneko, E. Tsuchida, Y. Imai, *J. Chem. Soc. Faraday Trans. 87*, **1991**, 1 83.

[36] M. Kaneko, D. Wöhrle, D. Schlettwein, V. Schmidt, *Makromol. Chem., 189*, **1988**, 2419.

[37] H. Tachikawa, L. R. Faulkner, *J. Am. Chem. Soc., 100*, **1978**, 4379.

[38] (a) T. Hirai, J. Yamaki, *J. Electrochem. Soc., 132*, **1985**, 2125. (b) T. Hirai, J. Yamaki,Y. Yamaji, J. Appl. Electrochem., 15, 1985, 441.

[39] D. Wöhrle, *Adv. Polym. Sci., 50*, **1983,** 48.

[40] E. Yaeger, *Electrochim. Acta, 29*, **1984**, 152.

[41] H. Tachikawa, L. R. Faulkner, *J. Am. Chem. Soc., 100*, **1978**, 4379.

[42] M. Kaneko, *Prog. Polym. Sci*., **2001**.

[43] A. J. Bard, L.R. Faulkner, *Electrochemical Methods: Fundamentals and Applications*, 2nd Ed., John Wiley & Sons, Inc., **2001,** USA.

Chapter Six

Electrocatalytic Hydrogen Generation using modified Metal (II) Perfluorinated Phthalocyanine Electrodes on Nano-porous Graphite Material

In addition to the electrocatalytic studies conducted using GCEs modified with metallophthalocyanines, the use of graphitized carbon monolith material as a modified electrode and as a storage material has been investigated.

An increase in electroactive catalyst performance is evident when dispersed onto the porous carbon material; the formation of a modified layer, close to the magnitude of a monolayer, is observed. Varying the ratio of catalyst dispersed in the carbon material reveals a current density of 2.5 mA/cm^2 for the electrocatalytic reaction of hydrogen evolution when a catalytic system consisting of 1:4 CM:CoPcF$_{16}$ is employed. Increasing the temperature of the electrochemical cell results in a further rise in current density to 3.7 mA/cm^2 using a chloride-based electrolyte by BE.

Investigation of a carbon monolith rod modified with CoPcF$_{16}$ reveals a large increase in current density relative to the values obtained for the same catalyst mixed with the carbon material and then drop-cast onto a glassy carbon electrode. The storage capabilities of this material are also examined.

6.1 Introduction

The quest for finding alternatives to non-renewable energy sources we have come to depend on remains a crucial issue. Hydrogen is an attractive solution and is considered a green technology because its combustion produces no CO_2, unlike other fuels.[1] The production of hydrogen by renewable means has been investigated for many years now, however the task of storing hydrogen remains a challenge, therefore exploring new means of storing hydrogen is also quite important. Currently, hydrogen is stored by either compression or liquefaction of the gas into pressurised tanks allowing for large volumes of hydrogen to be stored. However the low volumetric density of hydrogen relies on the use of low temperatures and high pressures for storing hydrogen in such ways, resulting in the hydrogen storage and transportation techniques being costly and inconvenient.[2,3] Thus a hydrogen economy is on the horizon, only if suitable and safe means of storage is developed.[4]

Storing hydrogen by sorption methods using porous material is an alternative strategy to the costly methods mentioned above. Solid state storage of hydrogen can be desirable due to high energy efficiencies and fast adsorption/desorption kinetics.[5] Nano-porous polymers have been reported as materials which are capable for H_2 storage[6]. Porous materials have now become the materials of choice due to their enhanced adsorption properties towards gaseous molecules.[7] Such nano-structured carbon materials can be created with high specific areas that make them good candidates for hydrogen storage.[8,9,10,11,12] Activated carbons which have a nano/microporous carbon structure have also been realised as good gas adsorbents. The nano-pores enhance adsorption of gaseous molecules while the micro-pores increase the transportation of hydrogen to the bulk of the materials.[13]

Such porous carbon materials have thus gained a great deal of attention in electrode modification. Their properties of high surface area, electronic conductivity and chemical inertness, make them attractive for the construction of modified electrodes.[14] Electrodes modified with such carbon material have been previously reported in the application of electrocatalytic reactions,[15] fuel cells,[16] sensors[17] and other energy storage devices such as batteries.[18]

For the electrocatalytic reactions discussed in this chapter, hydrogen generated by the modified electrode consisting of a $MPcF_{16}$ catalyst (where M denotes Co, Cu or Zn) can adsorb to the graphite nano-structure surface as previously reported.[19,20] However it is important to note that the forces which govern the adsorption to the carbon depends the surface chemistry, adsorbate structure and poresizes.[14]

6.2 Results and Discussion

6.2.1 Carbon monoliths as electrode material for the enhanced electrocatalytic activity of $CoPcF_{16}$

6.2.1.1 Preparation of monolith material as modified electrodes

Two methods are employed to investigate the activity of the perfluorinated cobalt phthalocyanine incorporated in these carbon monoliths as modified electrodes. The first method is described in the experimental section in Chapter 2 and is termed the adsorbed method, denoted MCM (modified carbon monolith).[21] The carbon monolith (in the form of a rod), consisting of a smooth homogenous surface (Figure 6.1a), was placed in a stirring solution containing $CoPcF_{16}$ (2.8×10^{-5} M) for 72 hours. After this time, the rod was dried and was analysed using scanning electron microscopy (SEM) and UV-Vis spectroscopy. SEM images for this chemically treated rod were collected to study the adsorption of the catalyst onto the carbon monolith material. The SEM images obtained of the cross section of the rod using a low magnification (x 5 k) revealed a defined 3-D structure, Figure 6.1b, containing the catalyst. The carbon monolith skeleton exhibited mesopores using a higher magnification, the pore sizes were estimated as approximately 5-6 nm, Figure 6.1c.

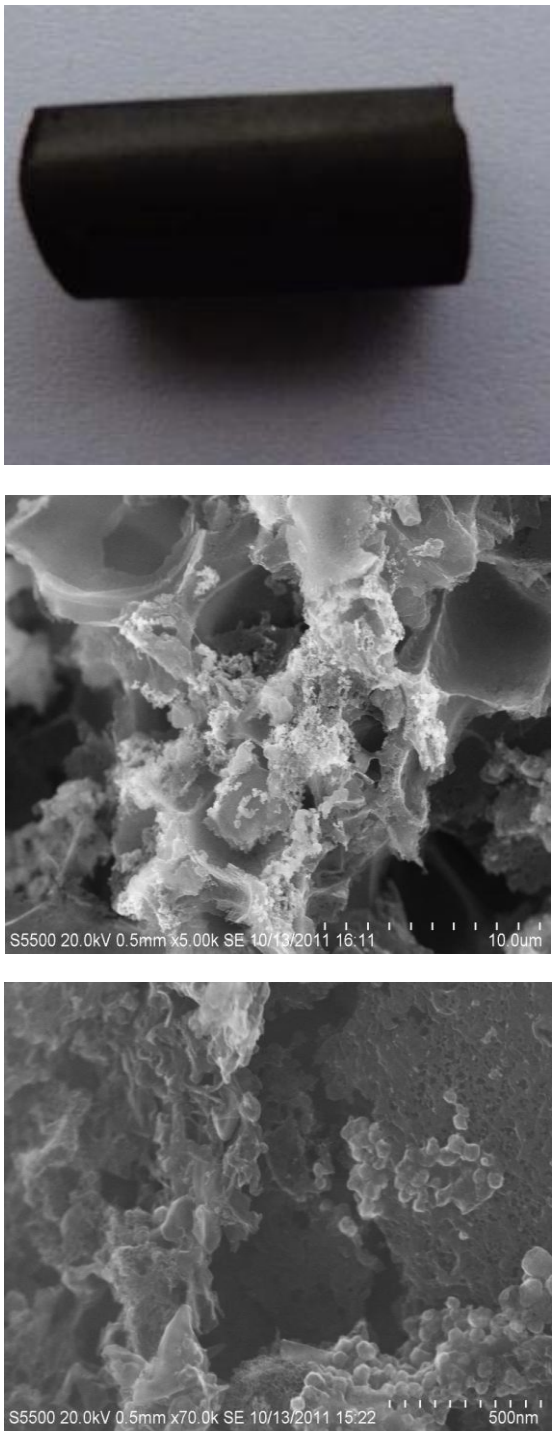

Figure 6.1: *(a) Carbon monolith rod,(b) SEM images of carbon monolith fragments with $CoPc_{16}$ (MCM) using low (×5 k) magnification, (c) SEM images of carbon monolith fragments with $CoPc_{16}$ (MCM) with high (×70 k) magnification.*

The adsorption of catalyst into the nano-porous material was confirmed by comparing the absorbance spectra of the solution of $CoPcF_{16}$ in DMF prior to placing the rod in the catalyst solution and after the 72 hour period of adsorption,

Figure 6.2. UV-visible spectroscopy shows the presence of a Q band for $CoPcF_{16}$ in DMF in the region of 675 nm which is characteristic of metallophthalocyanines. Following adsorption by the rod, the absence of this Q band confirmed that the $CoPcF_{16}$ had been adsorbed on the nano-porous material. Visual inspection of the DMF solution confirmed this as the deep blue-green colour of this solution had faded to a weak, less intense colour when the rod was removed from the $CoPcF_{16}$ solution. From the absorbance spectra, it was estimated that 89 % of the catalyst had been taken up by the porous rod.

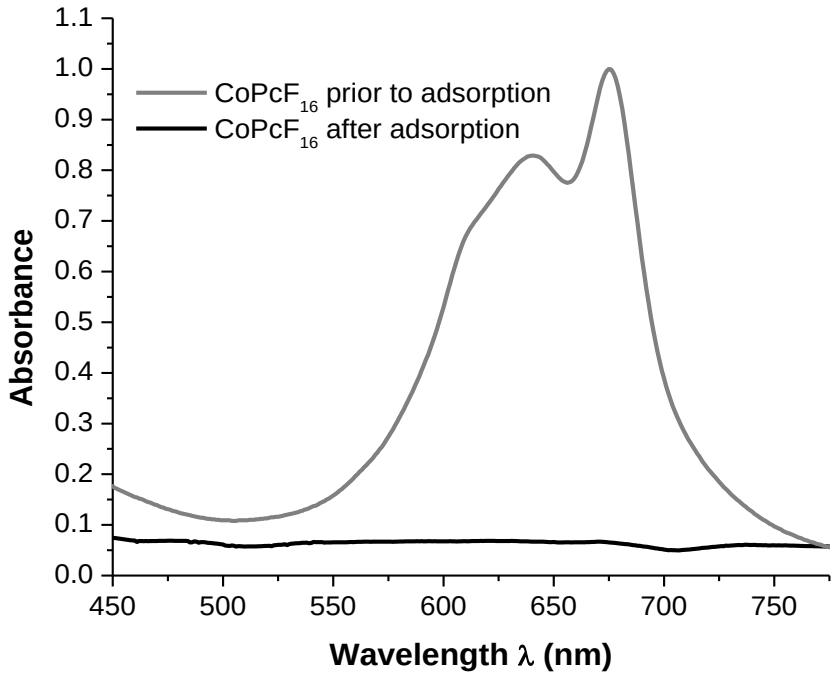

Figure 6.2: *Absorbance spectra of $CoPcF_{16}$ in DMF prior to placing the nano-porous rod in this solution (grey line) and solution after the 72 hour period (black line).*

The MCM rod was cut into half, where one part of the rod was retained for construction of a working electrode, described in section 6.2.7. The second part of the rod was crushed into a fine powder and a suspension of this modified carbon monolith was prepared using a surfactant, DDAB, allowing for facile drop casting of this carbon monolith-$CoPcF_{16}$ material onto a GCE. DDAB has been shown to be a good surfactant for immobilising analytes on the GCE.[22,23,24] The second

method of electrode fabrication involved $CoPcF_{16}$ being dispersed onto a carbon monolith-DDAB mixture in a variety of volume compositions (called $CM/CoPcF_{16}$; 1:1 $CM:CoPcF_{16}$, 1:2 $CM:CoPcF_{16}$, 1:3 $CM:CoPcF_{16}$ and 1:4 $CM:CoPcF_{16}$). A suspension of the bare carbon monolith material (i.e. no incorporation of a catalyst) denoted CM was also prepared for comparisons.

6.2.2 Characterisation of $CoPcF_{16}$/CM by cyclic voltammetry

The characterisation of $CoPcF_{16}$ employed for the work described in Chapters 4 and 5 has been previously discussed. The results for experiments where the catalysts were incorporated into the carbon monolith material (using the adsorption method described above) is shown in Figure 6.3. A shift in the redox potential of the metal centre reduction to lower potentials is observed relative to both the adsorbed $CoPcF_{16}$ (Chapter 4) and when incorporated into Nafion®, $CoPcF_{16}$/Nf (Chapter 5).

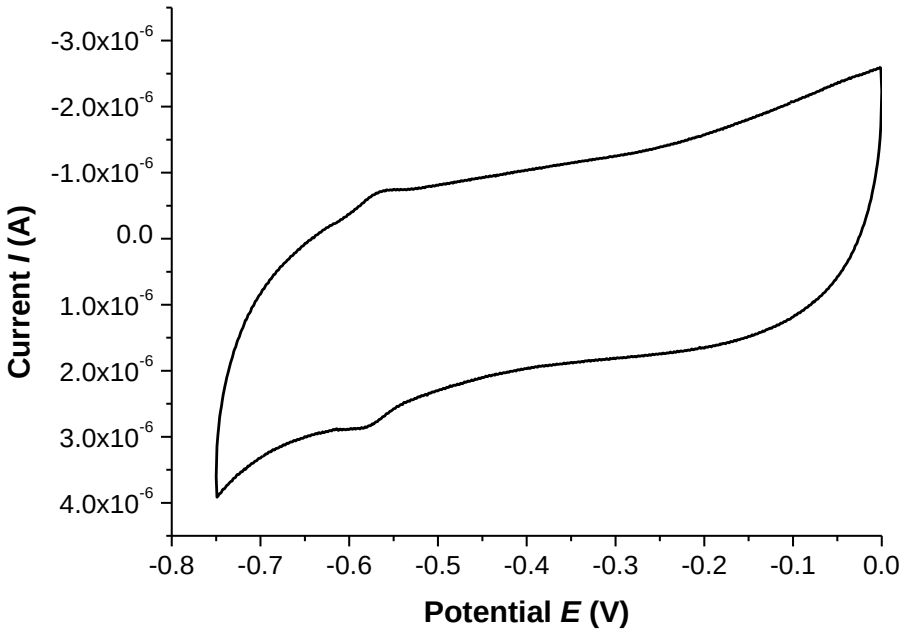

Figure 6.3: *Cyclic voltammogram of the carbon monolith powder consisting of adsorbed $CoPcF_{16}$ (MCM) in vs. Ag/AgCl in 0.1 M NaH_2PO_4/H_3PO_4 (pH 2). Scan rate = 100 mV/s.*

The half-wave potential for the Co(II)/Co(I) process was observed at -0.59 V vs. Ag/AgCl. The subsequent Pc ring reduction was not observed in this potential window. A cathodic shift of 160 mV and 150 mV was experienced by the catalyst relative to $CoPcF_{16}$ and $CoPcF_{16}$/Nf, respectively. When the catalyst was incorporated in this material by a mixture of a volume ratio 1:1 and 1:2 of CM: $CoPcF_{16}$ respectively, a negative shift is also observed in the cyclic voltammogram in Figure 6.4. For 1:1 and 1:2 CM:$CoPcF_{16}$ powder materials, the appearance of this wave was observed to depend on the catalyst loading

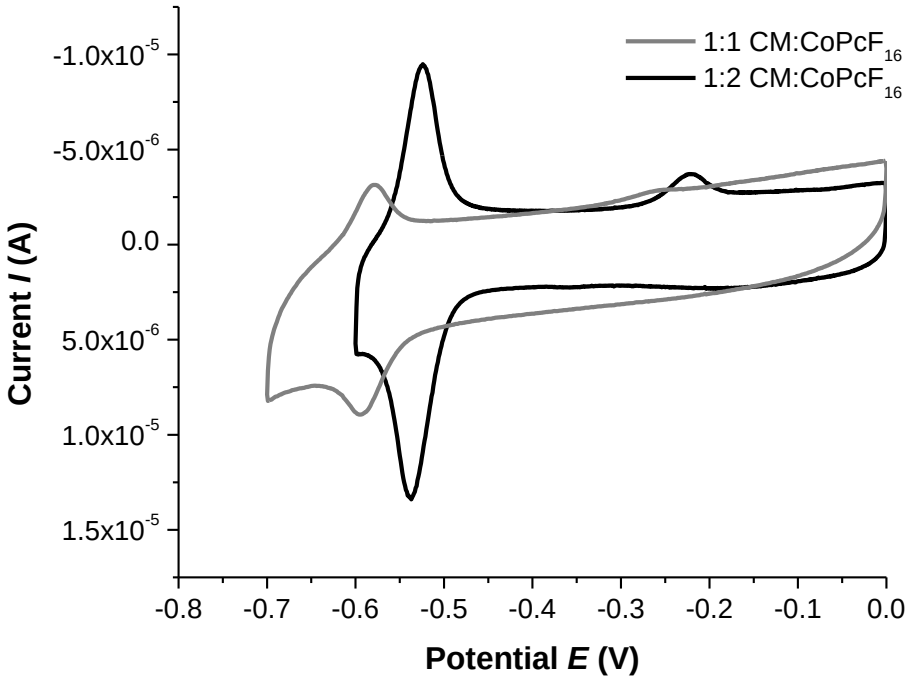

Figure 6.4: *Cyclic voltammograms of $CoPcF_{16}$ dispersed in a bare carbon monolith powder in a 1:1 and 1:2 CM:$CoPcF_{16}$ ratio (grey and black lines) respectively vs. Ag/AgCl in 0.1 M NaH_2PO_4/H_3PO_4 (pH 2). Scan rate = 100 mV/s.*

When the ratio of the CM:$CoPcF_{16}$ catalyst increased from 1:1 to 1:2, a shift to more positive potentials was observed. $E_{½}$ for 1:1 and 1:2 CM:$CoPcF_{16}$ are -0.58 V and -0.53 V vs. Ag/AgCl, respectively. An oxidation peak was also observed near -0.22V. The absence of this process in the cyclic voltammogram obtained for the bare carbon monolith material (Appendix E, Figure E1) and for MCM in Figure 6.3 suggests that this process may be the result of a following chemical

reaction involving the nano-porous material following the electrochemical reaction of the metal centre. As the ratio of $CoPcF_{16}$ increased further, this process grew in magnitude.

As the quantity of $CoPcF_{16}$ in the CM:$CoPcF_{16}$ materials increases, the magnitude of the current also increases. The area under the Co(II)/Co(I) process can be used to calculate the number of electroactive moles, as described earlier. The number of moles of $CoPcF_{16}$ increases from 5.7 x 10^{-12} mols to 4.0 x 10^{-11} moles for 1:1 and 1:2 CM:$CoPcF_{16}$ respectively.

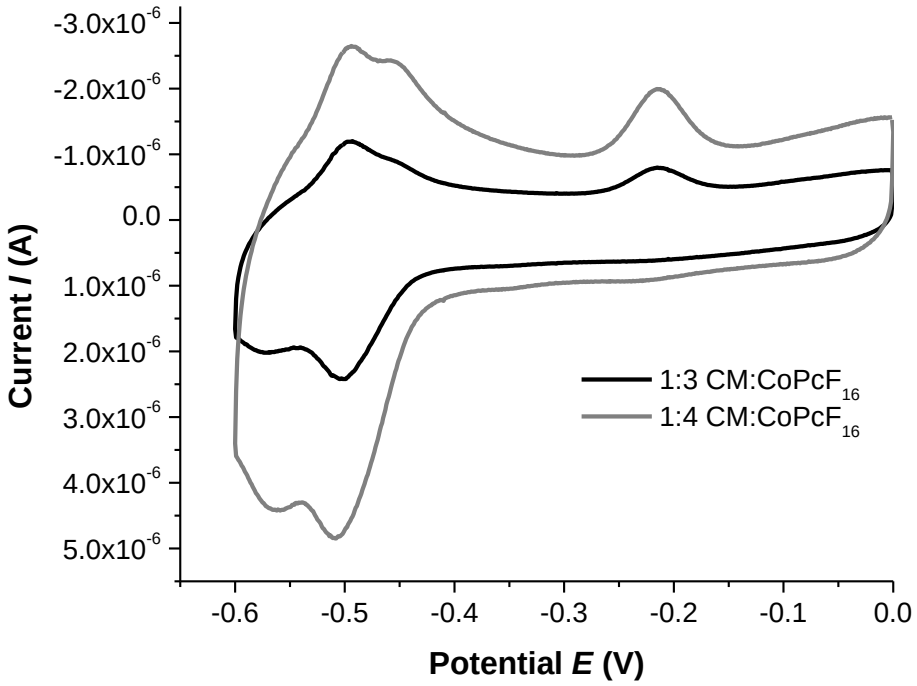

Figure 6.5: *Cyclic voltammograms of $CoPcF_{16}$ dispersed in a bare carbon monolith powder in a 1:3 and 1:4 CM:$CoPcF_{16}$ ratio (black and grey lines) respectively vs. Ag/AgCl in 0.1 M NaH_2PO_4/H_3PO_4 (pH 2). Scan rate = 100 mV/s.*

For 1:3 and 1:4 CM:$CoPcF_{16}$, two reduction processes are evident; however, the appearance of a second reduction process changed; difficulty in assigning these processes is compounded by the fact that the use of spectroelectrochemistry was not possible using these electrode materials. As the ratio of $CoPcF_{16}$ increased, a shift was observed in the redox potential assigned to Co(II)/ Co(I) to more positive potentials. Thus considering this trend and the literature, the first

reversible process is assigned as the 1 electron reduction of Co(II) to Co(I) at -0.47 V while the second process at -0.53 V is postulated as the reduction of the phthalocyanine ring.

6.2.2.1 Characterisation of immobilised $CuPcF_{16}$/CM and $ZnPcF_{16}$/CM by cyclic voltammetry

The effect of incorporating these catalysts into the carbon monolith material using the adsorbed method described above is observed in the cyclic voltammogram in Figure 6.6. The half wave potentials determined for each of these catalysts dispersed in the carbon material are similar to the potentials observed when they were embedded in the Nafion® polymer film (Chapter 5).

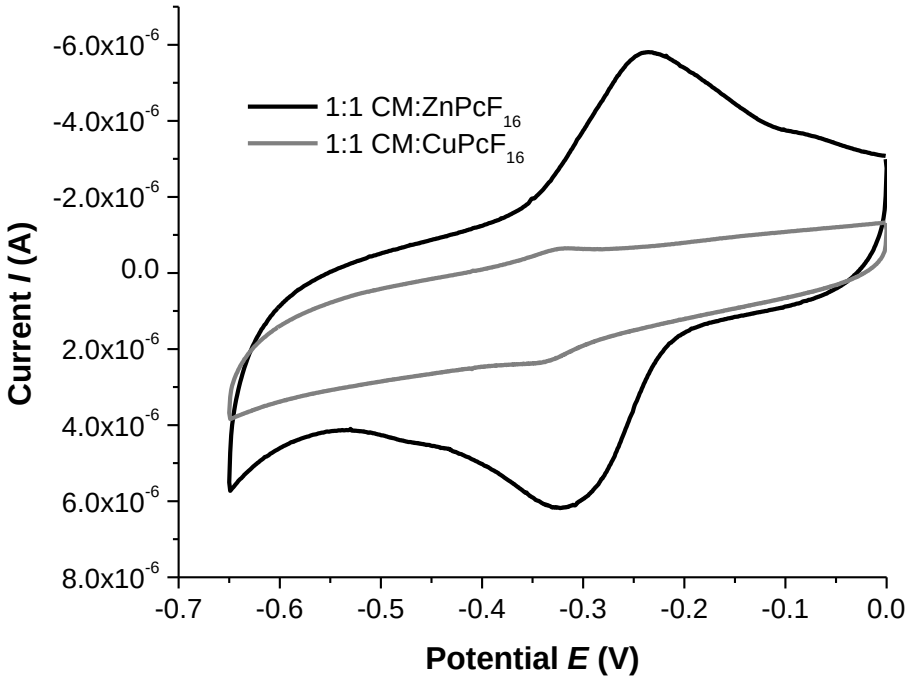

Figure 6.6: *Cyclic voltammograms of $CuPcF_{16}$ and $ZnPcF_{16}$ dispersed in a bare carbon monolith powder in a 1:1 volume ratio (grey and black lines) respectively vs. Ag/AgCl in 0.1 M NaH_2PO_4/H_3PO_4 (pH 2). Scan rate = 100 mV/s.*

As discussed previously in Chapter 3, Zn and Cu phthalocyanines are complexes which do not display a metal centred reduction due to the positioning of the HOMO and LUMO of the metal and ring, therefore these one electron reduction

processes were assigned to the Pc ring. In Figure 6.6 the half wave potentials, $E_{½}$ are observed at -0.33 V and -0.28 V vs. Ag/AgCl for 1:1 CM:$CuPcF_{16}$ and 1:1 CM:$ZnPcF_{16}$ respectively. The appearance of the irreversible process observed for CM:$CoPcF_{16}$ (E_{pa} = -0.22 V) was not observed for these materials.

6.2.3 Onset Potential

The cyclic voltammograms displayed in Figure 6.7 represent GCEs modified with DDAB/CM:$CoPcF_{16}$ (1:1, 1:2, 1:3 and 1:4 mixtures) as well as an adsorbed MCM electrode (SEM images obtained for this electrode). For comparison purposes, a bare DDAB/CM coated electrode (containing no catalyst) and a GCE coated only with 1.5 µL of 10 mM DDAB solution were employed in acidic phosphate (0.1 M NaH_2PO_4/H_3PO_4) electrolyte at pH 2 measured under argon.

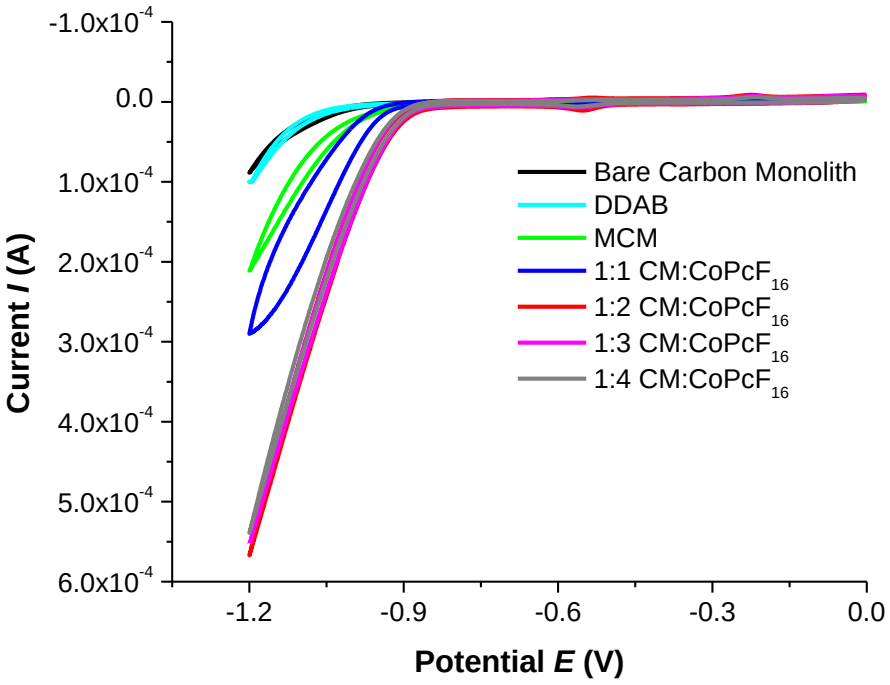

Figure 6.7: *Comparison of cyclic voltammograms of a bare DDAB/CM/GCE, one coated with surfactant DDAB/GCE, a DDAB/MCM carbon monolith and $CoPcF_{16}$ dispersed in carbon monolith powder in a 1:1, 1:2, 1:3 and 1:4 CM:$CoPcF_{16}$ ratio respectively vs. Ag/AgCl in 0.1 M NaH_2PO_4/H_3PO_4 (pH 2). Scan rate = 100 mV/s.*

A typical system for H_2 production is shown in Figure 6.7 where the least negative onset potential was noted at approximately – 0.86 V for the electrodes modified with CM:$CoPcF_{16}$ in 1:2, 1:3 and 1:4 ratios. In the absence of a catalyst ("DDAB" and "bare carbon monolith" in Figure 6.7), the onset potential was observed near -1.05 V. The cathodic current at -1.2 V was found for both these electrodes to be less than 20% of the current for the 1:2, 1:3 and 1:4 CM:$CoPcF_{16}$ mixtures. Clearly, the overpotential for H_2 evolution is lowered by the catalyst in these experiments.

Modified Electrode	Onset Potential (V)
MCM	*-0.92*
1:1 CM:$CoPcF_{16}$	*-0.92*
1:2 CM:$CoPcF_{16}$	*-0.86*
1:3 CM:$CoPcF_{16}$	*-0.86*
1:4 CM:$CoPcF_{16}$	*-0.87*
DDAB	*-1.03*
Bare CM	*-1.05*

Table 6.1: *Onset potentials (V) at which the catalytic currents are produced vs. Ag/AgCl in 0.1 M NaH_2PO_4/H_3PO_4 (pH 2) at 20°C for a range of modified electrodes of carbon monolith material.*

The largest current in these experiments was 5.5 x 10^{-4} A for $CoPcF_{16}$ dispersed in the carbon monolith powder in ratios of 1:3 and 1:4 CM:$CoPcF_{16.}$ Similarly, catalytic currents of approximately 3 x 10^{-4} A are observed with corresponding onset potentials of -0.92 V and -0.95 V when CM:$CuPcF_{16}$ and CM:$ZnPcF_{16}$ in a 1:1 ratio are used respectively in these experiments (See appendix- Figure E2).

The onset potential for the bare carbon material occurs at potentials more negative than -1.05 V vs. Ag/AgCl. Therefore the overpotential for the production of

hydrogen from aqueous solutions is reduced by at least 100 mV with respect to the bare carbon monolith electrode in the same operating conditions.

6.2.4 Electrochemical surface behaviour

For the catalysts described in this section, the expected linear relationship between the peak current i_p, (or current density j) and scan rate, v was observed (Figures 6.8 and 6.9).

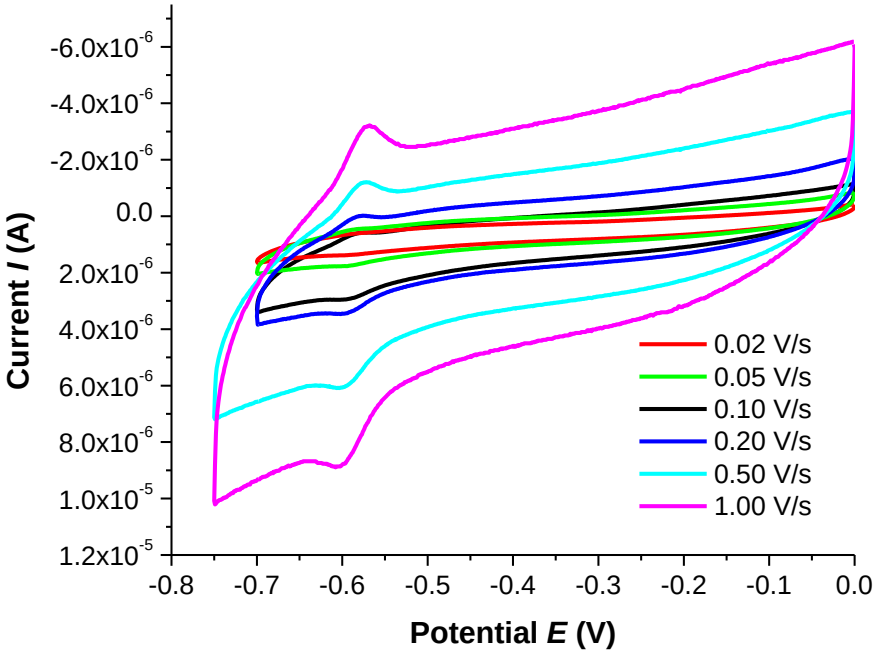

Figure 6.8: *Scan rate dependence (vs. Ag/AgCl) of the adsorbed $CoPcF_{16}$ catalyst in adsorbed in MCM in 0.1 M NaH_2PO_4/H_3PO_4 (pH 2).*

The cyclic voltammograms of the $CoPcF_{16}$ adsorbed into the carbon monolith are shown in Figure 6.8. As the sweep rate was increased, a reversible redox process at -0.59 V vs. Ag/AgCl was observed. The peak potentials for this process did not shift, indicating reversible behaviour. The resulting current density as a function of scan rate was investigated in Figure 6.9.

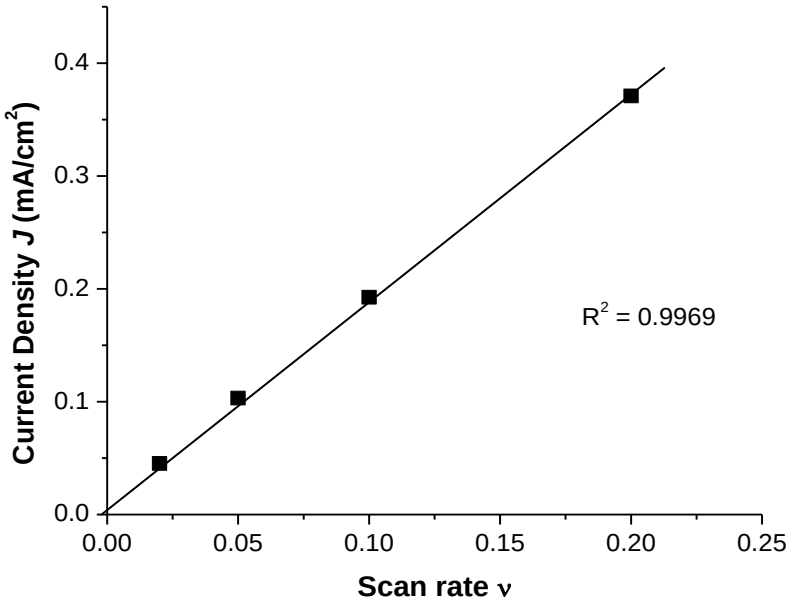

Figure 6.9: *Current density as a function of scan rate when $CoPcF_{16}$ is adsorbed in a carbon monolith powder at 20°C (taken from Figure 6.8).*

The cyclic voltammograms for 1:2 CM:$CoPcF_{16}$ with increasing scan rates are displayed in Figure 6.9.

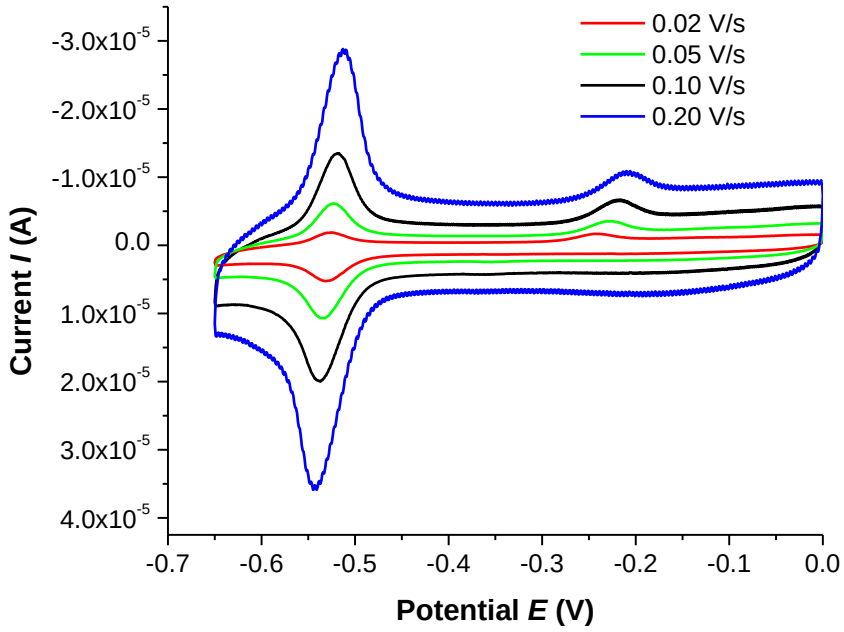

Figure 6.10: *Scan rate dependence of CM:$CoPcF_{16}$ in a 1:2 ratio vs. Ag/AgCl in 0.1 M NaH_2PO_4/H_3PO_4 (pH 2).*

The reversible redox process at -0.53 V vs. Ag/AgCl was assigned as the reduction of the metal centre, Co(II) to Co(I). The peak potentials do not appear to vary significantly with increasing scan rates, indicating reversibility. As the volume ratio of CM:$CoPcF_{16}$ was altered, the electrochemical surface behaviour remains unchanged, Figure 6.11.

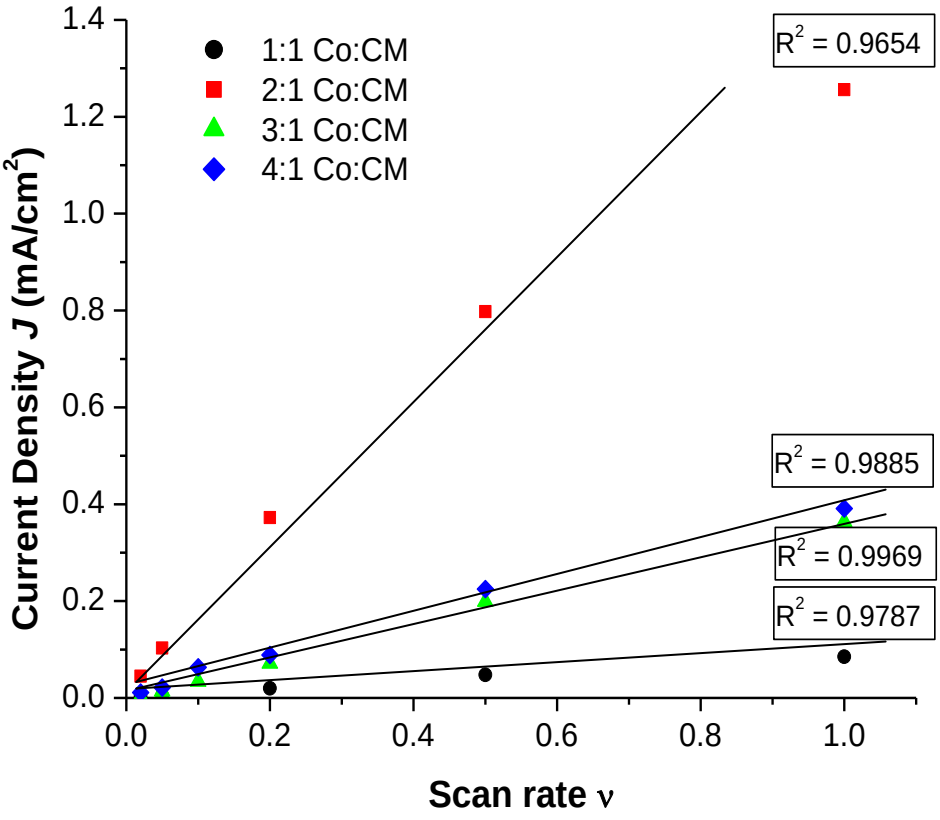

Figure 6.11*: Current density J, as a function of scan rate ν, for CM:$CoPcF_{16}$ in a ratio of 1:1, 1:2, 1:3 and 1:4 respectively.*

The percentage of electroactive catalyst in the modified layer is shown to increase significantly with respect to the catalyst in the absence of the carbon material. As the surface of the modified layer is now rougher than compared to a glassy carbon electrode due to the nanoporous carbon material, a higher percentage of catalyst can become electroactive.

6.2.5 Parameters affecting electrocatalytic hydrogen production

The factors and conditions which affect the catalytic activity of these metallophthalocyanines have been investigated and are discussed in Chapters 4 and 5. In this chapter using the carbon monolith material the effect of varying the ratio of CM:$CoPcF_{16}$; the effect of increasing the temperature on the optimum ratio of CM:$CoPcF_{16}$ and the stability of the modifying layer are examined.

6.2.5.1 Electrocatalytic activity of MCM and effect of varying the ratio of CM:$CoPcF_{16}$

The electrocatalytic experiments were conducted in the same manner as described in Chapters 4 and 5. A larger volume (5 μL) was deposited onto the working electrode compared to previous chapters. The electrolysis potential was -1.2 V vs. Ag/AgCl in 0.1 M NaH_2PO_4/H_3PO4 (pH 2) electrolyte at 20°C and the duration of the reaction was 1 hour. The moles of hydrogen and other performance indicators obtained for $CoPcF_{16}$ when adsorbed within the carbon monolith (MCM-method 1) and when the catalyst is dispersed in the carbon monolith powder (method 2) are shown in Figure 6.12 and Table 6.2, respectively. (see Appendix E, Table E1).

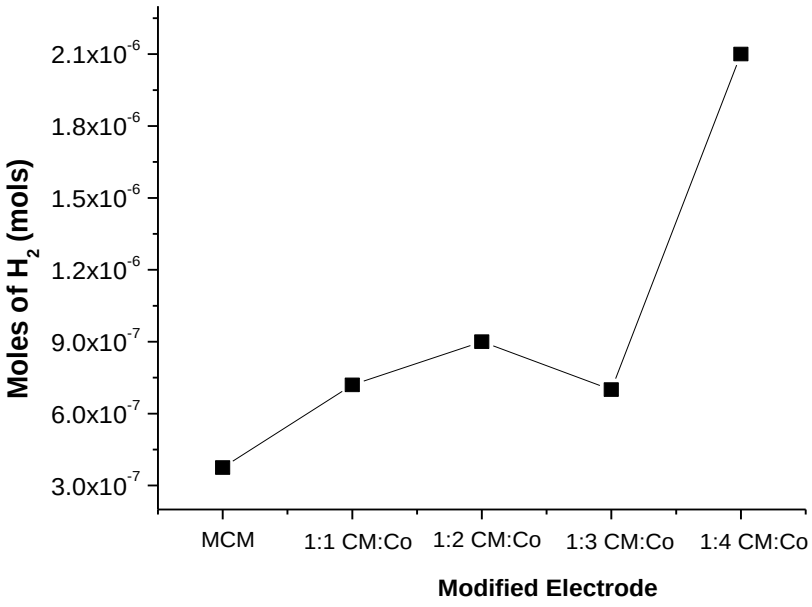

Figure 6.12: *Moles of hydrogen produced by the various modified electrodes consisting of $CoPcF_{16}$ in 0.1 M NaH_2PO_4/H_3PO_4 (pH 2).*

It is difficult to directly compare the catalytic performance of these systems based on TOF, however comparing the number of moles of hydrogen along with charge and current density can further aid the determination of which metallophthalocyanine displays the optimum performance for the electrocatalytic generation of hydrogen. The moles of hydrogen shown in Figure 6.12 indicate that the catalyst system which produced the largest moles of hydrogen from water is when the catalyst was dispersed in a ratio of 1:4 CM:$CoPcF_{16}$. This catalyst system (1:4 CM:$CoPcF_{16}$) also corresponds to the highest Faradaic efficiency of 63 %.

Modified Electrode	***MCM***	***1:1***	***1:2***	***1:3***	***1:4***
Charge (C)	*0.29*	*0.42*	*0.54*	*0.45*	*0.63*
Moles H_2 (mol)	*3.8×10^{-7}*	*7.2×10^{-7}*	*9.0×10^{-7}*	*7.0×10^{-7}*	*2.1×10^{-6}*
Faradaic Efficiency %	*25*	*32*	*33*	*33*	*63*
[1]Current Density *J* (mA/cm^2)	*1.2*	*1.6*	*2.1*	*1.7*	*2.5*
[2]Current Density *J* (mA/cm^2)	*3.0*	*4.1*	*8.1*	*7.9*	*7.8*
(%) Electroactive $CoPcF_{16}$	*2.5*	*9.0*	*12.5*	*14.6*	*29.2*

Table 6.2: *Average performance data obtained by CV and BE vs. Ag/AgCl for 1 hour for $CoPcF_{16}$ adsorbed in carbon monolith fragments MCM, and from DDAB supported catalysts on carbon using ratios of CM:$CoPcF_{16}$ in 0.1 M NaH_2PO_4/H_3PO_4 (pH 2). [1]Current density obtained using BE data and [2]current density obtained using the last scan of the CV.*

The performance indicators shown in Table 6.2 reflect the catalytic activity of the catalyst MCM and immobilised DDAB/CM:$CoPcF_{16}$ mixtures with increasing ratios of Co. Comparing all the performance indicators, the adsorbed modified carbon monolith MCM reveals the lowest catalytic activity as indicated by the charge (0.29 C) and current density (3.0 mA/cm^2) and moles of hydrogen (3.8 x 10^{-7} mols, see Figure 6.12) respectively.

It is evident that the presence of the nano-porous material significantly enhanced the percentage of electroactive catalyst, demonstrated in Table 6.2. When $CoPcF_{16}$ was employed as a catalyst and adsorbed onto a GCE (see Chapter 4), the largest percentage of electroactive species was determined at 6.3 %. This is almost 5 times less than compared to when the catalyst was embedded in the material in a ratio of 1:4 CM:$CoPcF_{16}$.

The catalytic activity of $CuPcF_{16}$ and $ZnPcF_{16}$ dispersed in the graphitized carbon monolith powder was also investigated where a 1:1 ratio of each component was mixed and drop cast onto a GCE in DDAB solution. The operating conditions were identical to those employed for $CoPcF_{16}$, in Chapter 4. The performance indicators for these catalysts are displayed in Table 6.3.

Modified Electrode	***$CuPcF_{16}$***	***$ZnPcF_{16}$***
Charge (C)	*0.44*	*0.46*
Moles H_2 (mol)	*8.2×10^{-7}*	*7.2×10^{-7}*
Faradaic Efficiency %	*36*	*32*
[1]Current Density *J* (mA/cm^2)	*1.7*	*1.8*
[2]Current Density *J* (mA/cm^2)	*4.9*	*3.9*
Electroactive M(II)PcF_{16} (%)	*4.2*	*7.6*

Table 6.3: *Average performance data obtained by CV and BE vs. Ag/AgCl for 1 hour for $CuPcF_{16}$ and $ZnPcF_{16}$ dispersed in carbon monolith fragments in a ratio of 1:1 in 0.1 M NaH_2PO_4/H_3PO_4 (pH 2). [1]Current density obtained using BE data and [2]current density obtained using the last scan of the CV.*

Comparing these values to those obtained using a 1:1 CM:$CoPcF_{16}$, the charge which passed after an hour potentiostatic electrolysis was similar, 0.44 C and 0.46 C for 1:1 CM:$CuPcF_{16}$ and 1:1 CM:$ZnPcF_{16}$ respectively. The current densities however were lower than $CoPcF_{16}$, reaching 0.6 and 1.0 mA/cm^2 for 1:1 CM:$CuPcF_{16}$ and 1:1 CM:$ZnPcF_{16}$ respectively compared to 1.3 mA/cm^2.

Examination of the hydrogen evolved revealed the lowest mols of hydrogen were obtained when 1:1 CM:$CuPcF_{16}$ was employed. The highest Faradaic efficiency calculated for was 36 %, exhibited by 1:1 CM:$CuPcF_{16}$ (See Appendix E- Table E2).

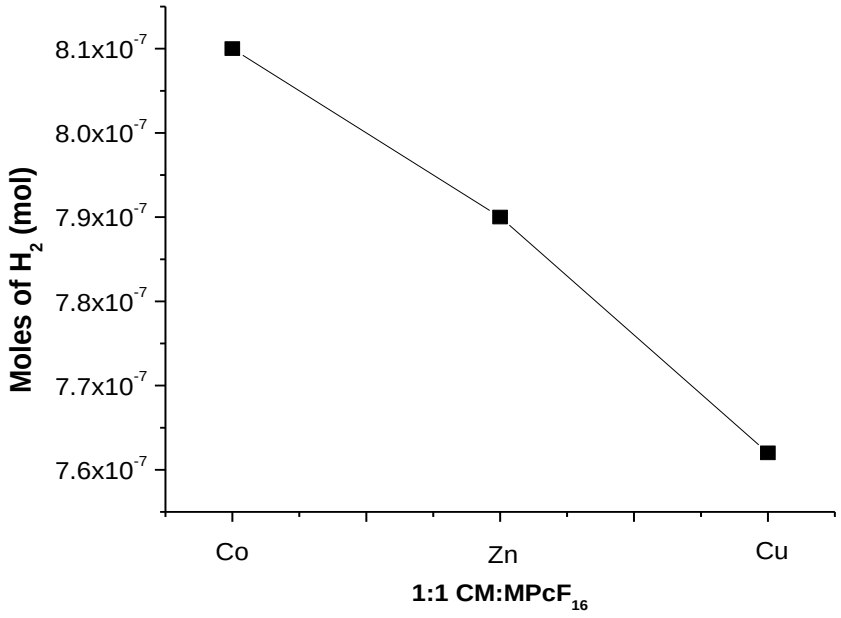

Figure 6.13: *Moles of hydrogen for 1:1 of CM:CoPcF$_{16}$, CM:CuPcF$_{16}$, CM:ZnPcF$_{16}$ in 0.1 M NaH$_2$PO$_4$/H$_3$PO$_4$ (pH 2).*

The catalytic activity of these systems can be compared to catalysts ZnPcF$_{16}$ and CoPcF$_{16}$/Nf identified previously in chapter 4 and 5 which display the best catalytic activity in terms of current density (obtained by BE data); 1.8 mA/cm^2 and 1.1 mA/cm^2 respectively. However, O_2 reduction contributes to this value, as discussed in Chapter 4. It is suggested that the nano-pores in the material offer an increase in surface area and as a result more catalyst is present at the modified electrode surface and can participate in the catalytic reaction thus leading to a the higher current density.

6.2.5.2 Effect of Temperature

The effect of increasing the temperature of the electrocatalytic cell from 20°C to 40°C was investigated. When CoPcF$_{16}$ was employed as a catalyst for the electrocatalytic generation of hydrogen at 40°C, an increase in charge, current density and TOF values were observed (previously discussed in chapter 4). Investigating the effect on increasing the operating temperature to 40°C was expected to yield a similar trend for both the adsorbed MCM and the CM:CoPcF$_{16}$ modified electrodes. Investigating the effect of increasing the temperature was

carried out; the sweep rate was increased and the resulting current was measured. The electrochemical responses of this catalyst at both 20°C and 40°C are shown in Figure 6.14.

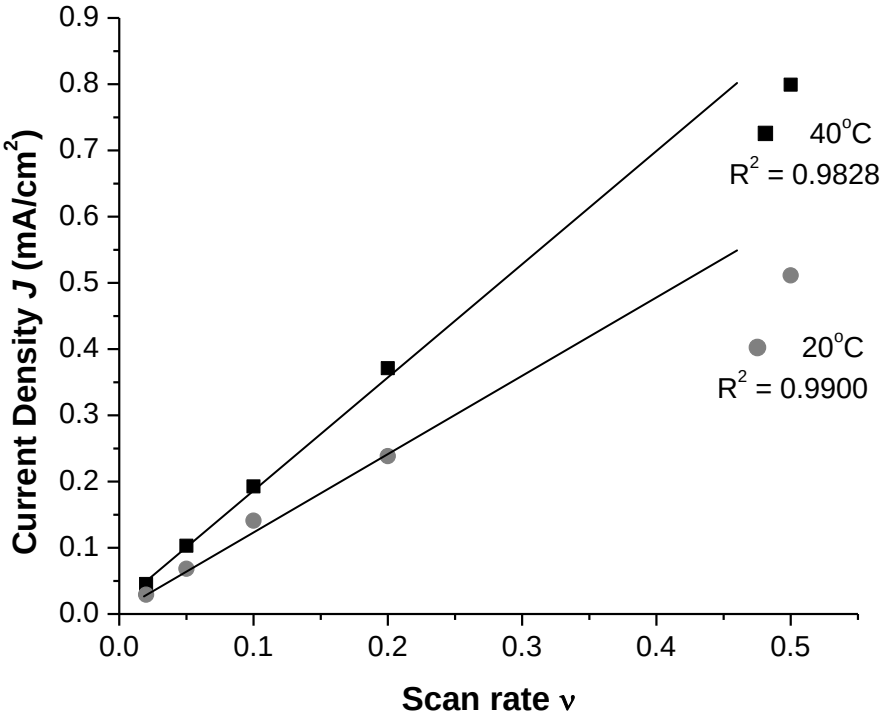

Figure 6.14: *Current density J (mA/cm^2) as a function of scan rate when $CoPcF_{16}$ is adsorbed in a carbon monolith powder (MCM) at 20°C represented by the black line and 40°C depicted by the grey line.*

ME Ratio	***1:1***	***1:2***	***1:3***	***1:4***
Charge (C)	*0.44*	*0.95*	*0.52*	*0.66*
[1]Current Density *J* (mA/cm^2)	*1.7*	*3.8*	*2.1*	*2.6*
Moles H_2 (mols)	*8.9×10^{-7}*	*2.3×10^{-6}*	*1.5×10^{-6}*	*1.7×10^{-6}*
Faradaic Efficiency %	*39*	*47*	*55*	*61*
Electroactive $CoPcF_{16}$ (%)	*7.4*	*26.0*	*14.7*	*24.0*

Table 6.4: *Average performance data obtained by CV and BE vs. Ag/AgCl for 1 hour for $CoPcF_{16}$ adsorbed in carbon monolith fragments MCM, and varying ratios of CM:$CoPcF_{16}$ in 0.1 M NaH_2PO_4/H_3PO_4 (pH 2) at 40°C. Current density obtained by [1]BE.*

Examination of the data obtained for CM:$CoPcF_{16}$ at varying ratios when the temperature was increased from 20°C to 40°C in Table 6.4 revealed an increase in performance indicators with this increase in temperature. The largest current density and moles of hydrogen were determined when 1:2 CM:$CoPcF_{16}$ was employed, reaching 6.1 mA/cm^2 and 2.3×10^{-6} mols respectively.

The charge which passes in these experiments almost doubles from 0.54 C to 0.95 C when a 20°C increase in temperature occurs for 1:2 CM:$CoPcF_{16}$, however this large increase in charge was not exhibited by the other ratios of electrodes modified with CM:$CoPcF_{16}$ (see Appendix E-Table E3).

Two important aspects are considered to account for the enhanced activity of catalysts for electrocatalytic reactions when the temperature is increased. Firstly, the solubility of hydrogen in water at 40°C is reduced,[25] hence there is an increase in concentration of hydrogen gas in the headspace of the cell.

$$k = Ae^{-E_A/RT} \qquad \textbf{Equation 6.1}$$

The next point involves the rate of the reaction. The Arrhenius equation is often used to investigate effect of the rate constant k when a change in temperature occurs. In Equation 6.1, the activation barrier, E_A, can also be understood as a change in the internal energy to the transition state. Thus, when the temperature of the cell rises to 40°C, the rate constant k for the electrolysis reaction also increases, as indicated in the equation above.

Modified Electrode	**$CuPcF_{16}$**	**$ZnPcF_{16}$**
Charge (C)	*0.51*	*0.56*
Moles of H_2 (mol)	*1.1×10^{-6}*	*1.2×10^{-6}*
Faradaic Efficiency %	*43*	*45*
[1]Current Density *J* (mA/cm^2)	*2.0*	*2.2*
[2]Current Density *J* (mA/cm^2)	*2.7*	*3.1*
Electroactive M(II)PcF_{16} (%)	*3.4*	*20.5*

Table 6.5: *Average performance data obtained for $CuPcF_{16}$ and $ZnPcF_{16}$ respectively in a 1:1 mix of carbon monolith (method 2) at 40°C in 0.1 M NaH_2PO_4/H_3PO_4 (pH 2). [1]Current density obtained using BE data and [2]current density obtained using the last scan of the CV.*

The performance indicators are displayed in Table 6.5, revealing an increase in charge and current density as a result of increasing temperature. The large TOF value obtained for $CuPcF_{16}$ was attributed to the smaller percentage of electroactive species in the modifying layer (3.4 %) in comparison to the $ZnPcF_{16}$ catalyst which exhibits over 20 % activity. The Faradaic efficiencies calculated for both of these catalyst systems are similarly 43 % and 45 % respectively. (See Appendix E, Table E4).

6.2.6 Electrocatalytic activity using a chloride electrolyte at 40°C

As discussed in chapter 4, it is postulated that formation of oxygen at the anode can drift towards the modified cathode and subsequently contribute to the charge and current density measured. Thus, in an effort to minimise this effect, a chloride based electrolyte was employed. The experimental results discussed in chapter 4 revealed an increase in the electrocatalytic activity efficiency which is expected to be a result of the decrease in oxygen in the cell. In order to achieve the highest catalytic performance, the operating conditions which yielded high catalytic activity (as shown in the previous chapters) were applied an increase in temperature to 40°C and using 0.1 M HCl/KCl as the electrolyte. The effect of both these conditions were carried out using the catalysts in a 1:1 ratio CM:$MPcF_{16}$. The performance indicators obtained under these conditions are shown in Table 6.6 for each of the catalyst systems investigated.

	$CoPcF_{16}$	***$CuPcF_{16}$***	***$ZnPcF_{16}$***
Charge (C)	*0.95*	*0.55*	*0.52*
Moles of H_2 (mol)	*4×10^{-6}*	*1.8×10^{-6}*	*2.1×10^{-6}*
Faradaic Efficiency (%)	*82*	*62*	*79*
[1]Current Density *J* (mA/cm^2)	*11.3*	*9.0*	*6.0*
Electroactive catalyst (%)	*27.5*	*5.5*	*16.6*

Table 6.6: *Average performance indicators for $CoPcF_{16}$, $CuPcF_{16}$ and $ZnPcF_{16}$ in carbon monolith in a ratio of 1:1 mix MPc:CM at 40°C using 0.1 M HCl/KCl (~pH 1). [1]Current density obtained by CV.*

An increase in catalytic activity, as expected was observed for each of the catalysts employed in the carbon monolith material. In the absence of the nano-porous material, the charge and current density of 0.55 C and 9.0 mA/cm^2 respectively was obtained at 40°C using the chloride based electrolyte for $CuPcF_{16}$. These performance indicators were less than those determined using $CoPcF_{16}$ dispersed in the graphitized carbon material which reached a charge and current density of 0.95 C and 11.3 mA/cm^2 respectively, (see Appendix E, Table E5).

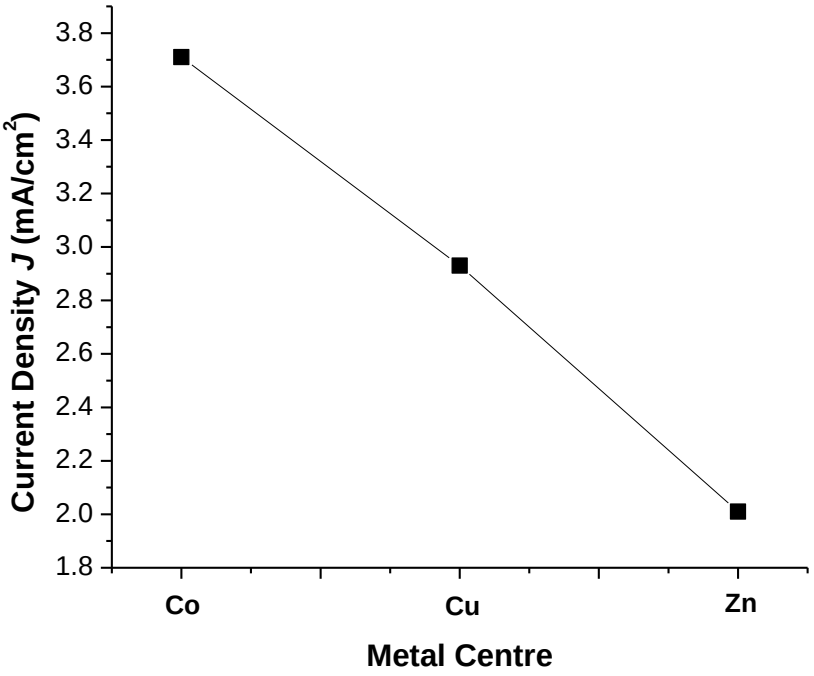

Figure 6.15: *Current density (obtained by BE) as a function of each catalyst system dispersed in the carbon monolith material in a ratio of 1:1 MPc:CM at 40°C using 0.1 M HCl/KCl.*

An increase in the moles of H_2 produced when this porous material was used, compared to the adsorbed catalysts in Chapter 4 was suggested to be a result of the decrease in oxygen produced at the anode as chloride can also undergo oxidation to form Cl_2 when HCl/KCl was employed as an electrolyte. Water oxidation at the counter electrode which produces O_2 appears to limit the rate of hydrogen production at the modified electrode.

6.2.7 Carbon monolith rod as a working electrode for the electrocatalytic generation of hydrogen using $CoPcF_{16}$

In the preparation of the modified carbon monolith material where $CoPcF_{16}$ was adsorbed into the graphitized nano-porous material (method 1), a section of this modified carbon monolith rod (*MCMR)*, was kept intact as a rod in an effort to construct a modified working electrode. The rod itself was used as a direct electrode material without the need for a GC electrode.

The construction of the working electrode involved the attachment of the modified carbon monolith rod *MCMR* to a small piece of glass by using a non-conductive glue (Superglue liquid, Loctite). This was done to provide extra support to the fragile carbon rod. The rod was covered in this glue and both ends of the rod were carefully cut. This was done in order to provide one side in which an active area was exposed and could act as a working electrode while the other end of the rod allowed for a connection to be made with a copper wire using a conducting glue (Conduct epoxy CW2400, ITW Chemtronics). The area at which the connection to the wire was made was re-coated with the non-conducting glue so the entire material could be placed in an air-tight cell for further analysis. Figure 6.16 shows a schematic of this carbon rod.

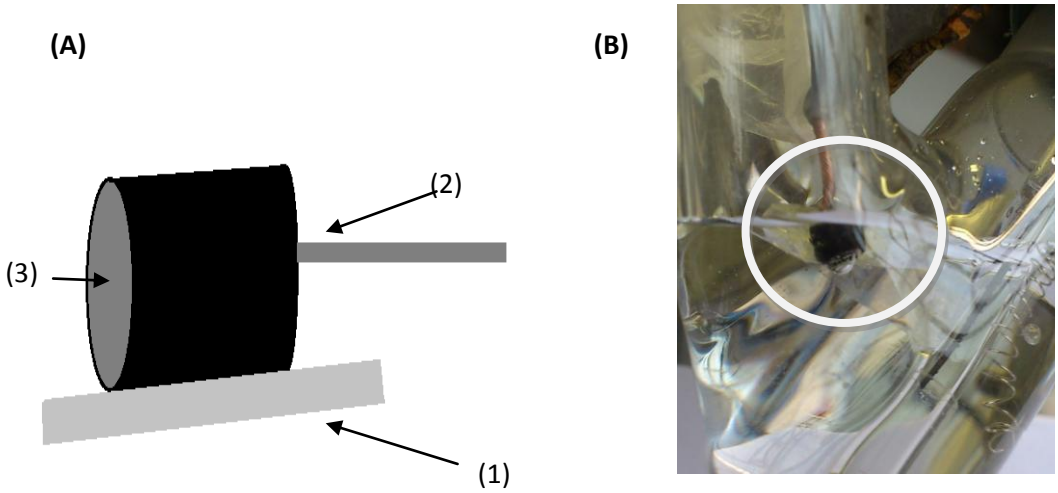

Figure 6.16: (*A) Carbon rod modified with $CoPcF_{16}$ (MCM) attached to a piece of glass (1), where two cross-sections are exposed, one for a connection (2), and the other side (3) as the exposed area for the site of the electrocatalytic production of H_2. (B) Image of experimental set up for the potentiostatic*

electrolysis of the MCMR. The build up of hydrogen gas bubbles can be clearly seen on the rod.

The experiment was conducted in the same manner as described for the electrocatalytic experiments performed throughout these experimental chapters. The rod was placed in one arm of the electrochemical cell and the electrolyte solution was filled to just enough to cover the rod. Although the geometrical surface area was a factor of ten less than compared to a glassy carbon electrode, the graphitized carbon material which consists of mesopores was expected to facilitate the electrocatalytic reaction. The performance indicators are displayed in Table 6.7.

	Carbon Rod (MCMR)
Charge (C)	*0.66*
Moles of H_2 (mol)	*1.9×10^{-6}*
Faradaic Efficiency %	*56*
[1]Current Density *J* (mA/cm^2)	*8.3*
[2]Current Density *J* (mA/cm^2)	*22.5*
Moles of Electroactive catalyst (mol)	*2.8×10^{-12}*

Figure 6.7: *Average performance indicators of MCMR in 0.1 M NaH_2PO_4/H_3PO_4 (pH 2) at 20°C. [1]Current density obtained using the last scan of the CV and by [2]bulk electrolysis.*

The average current density obtained over 1 hour potentiostatic electrolysis was 8.3 mA/cm^2. (This is based on an approximate size of the diameter 1 mm, thus the geometrical area of the circular carbon rod was estimated as 7.9×10^{-3} cm^2). This current density was significantly larger than the current densities obtained when

the monolith was crushed and used as a powder (method 2). The number of moles of $CoPcF_{16}$ which were electroactive was 2.8 x 10^{-12} mols; no increase in the number of electroactive moles was observed when the modified rod was employed.

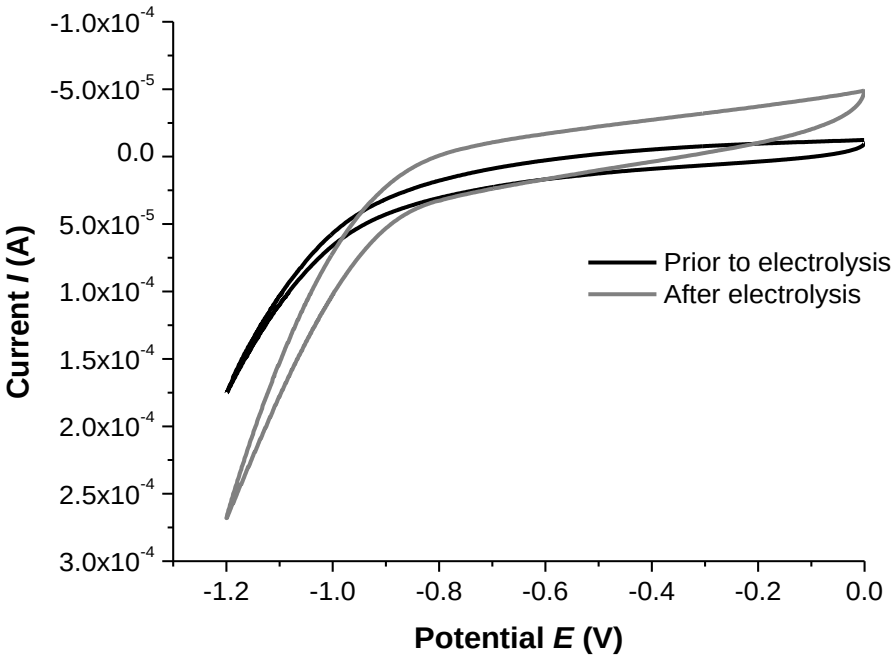

Figure 6.17: *Cyclic voltammogram of MCMR vs. Ag/AgCl in 0.1 M NaH_2PO_4/H_3PO_4 (pH 2). The black line represents the CV before electrolysis at -1.2 V while the grey line shows the CV after one hour potentiostatic electrolysis.*

Examination of the catalytic currents produced prior to and after the bulk electrolysis step indicate the stability of this new catalytic system for hydrogen generation, Figure 6.17. It is believed that the lower than expected activity of the MCMR is due to only a small cross-section of the rod exposed. An enhanced catalytic activity could be attained for this rod by improving the design/construction of the working electrode. However part of the hydrogen may also remain in the rod as outlined below.

6.2.8 Storage properties of carbon monolith material

Nano-porous carbon based materials have recently become the focus as storage material for hydrogen.6,[26,27,28,29,30] The storage of gaseous hydrogen is regarded as a challenging task, as high pressures and low temperatures are normally required to store hydrogen.2 However, it appears that in order to avoid such extreme conditions, storing hydrogen in the solid form and in the adsorbed state could be a less energy consuming solution to this problem. The graphitized carbon material (in the form of the rod) which was employed in these studies was allowed to stand in the electrocatalytic cell after a 1 hour electrolysis period (at -1.2 V) where injections of the gaseous product in the headspace of the cell were performed over time.

In order to see if this material could act as a storage material for H_2, an identical experiment was carried out simultaneously, however the graphitized carbon monolith rod was replaced with a modified ($CoPcF_{16}$) glassy carbon electrode for a comparison purposes. The corresponding amounts of hydrogen obtained in the headspace when the rod was used as a function of the amount of time passed after the electrolysis are displayed in Table 6.8.

	MCMR	***Modified GCE***
Time (mins)	***Moles of H_2 (mol)***	***Moles of H_2 (mol)***
60	1.9×10^{-6}	1.2×10^{-6}
68	1.6×10^{-6}	1.1×10^{-6}
86	1.45×10^{-6}	9.0×10^{-7}
108	1.3×10^{-6}	7.4×10^{-7}
186	7.8×10^{-7}	4.1×10^{-7}
225	7.7×10^{-7}	2.7×10^{-7}
242	6.4×10^{-7}	1.3×10^{-7}
335	5.0×10^{-7}	8.9×10^{-8}
490	4.6×10^{-7}	4.2×10^{-8}
1440	2.6×10^{-7}	n/d

Table 6.8: *Moles of hydrogen (mol) over a 24 hour time-frame for the modified rod, MCMR and modified GCE. n/d = not detected*

Although the moles of hydrogen evolved decreased as the period of time increased, it demonstrates that after a 24 hour period, some of this diffusive gas remains adsorbed when the MCMR is used. This is not observed when the GCE coated with a catalyst, in the absence of this nano-porous material is used. The

moles of hydrogen present in the cell cannot be determined by gas chromatography (below LOD) following a 24 hour period left to stand, thus the nano-porous graphite carbon monolith material can act as a storage material.1[a] It has been shown that hydrogen adsorption onto porous sorbents at atmospheric pressure is a function of surface area.6 Thus it is postulated that developing a porous carbon material with a higher surface area may lead to an increase in hydrogen adsorption.

6.3 Concluding Remarks

Graphitized carbon monolith material was used as an alternative way for the modification of carbon electrodes. In this chapter the conditions identified from the previous experimental chapters were applied.

Dispersing the metallophthalocyanines into a graphitized carbon monolith material by adsorption, and by crushing the rod into a fine powder which was cast onto an electrode in a solution containing a volume ratio of catalyst was shown to increase the number of moles which are electroactive, which was assumed to be a result of an increase in surface area due to the nano-pores. As a result of the increase in electroactive material, the TOF (hr^{-1}) values were lower than the values obtained in the absence of the meso-porous material.

Increasing the ratio of catalyst to carbon monolith ($CoPcF_{16}$:CM), the highest productivity was identified at 1:4 CM:$CoPcF_{16}$. An increase in temperature to 40°C resulted in only a slightly enhanced activity for this catalyst system, however when the phosphate electrolyte was replaced with a chloride electrolyte, a considerable increase in current density and Faradaic efficiency was observed (11.3 mA/cm^2 and 82 % respectively) at 40°C. Although the reason for this enhanced activity is not fully understood at this time, it is assumed to be due to sacrificial oxidation of the chloride electrolyte in lieu of water oxidation at the counter electrode, lowering the amount of O_2 reduction that would otherwise occur at the cathode.

Rather than evaluating the catalytic activity by the TOF values, comparing the moles of hydrogen was a better way of assessing the activity. Comparing the moles generated by the adsorbed catalysts (Chapter 4) to those obtained when the catalysts were embedded in this nano-porous material (1.2 x 10^{-6} mol), a larger number of moles of H_2 was produced (2.1 x 10^{-6} mol) when in the catalyst was dispersed in this material in a 1:4 CM:$CoPcF_{16}$ volume ratio. No significant enhancement was observed when 1:1 CM:$CuPcF_{16}$ and CM:$ZnPcF_{16}$ catalysts were used. Employment of the chloride based electrolyte at 40°C revealed a larger activity; 2.5 x 10^{-6} moles of H_2 for adsorbed $CoPcF_{16}$ catalyst (Chapter 4) compared to the catalyst dispersed in the nano-porous carbon material of 4 x 10^{-6}

moles. These results indicate that at higher temperatures, the carbon monolith material can enhance the activity of the $CoPcF_{16}$ catalyst for the electrocatalytic generation of hydrogen.

Construction of a working electrode using the carbon rod fragment yielded no significant enhanced activity. It is plausible that this smaller than expected activity was due to the physical construction of the electrode; only a cross section was exposed at which the catalytic reaction could take place.

The H_2 storage capabilities of this material were also investigated. Analysis of the gas in the headspace over a 24 hour period revealed that after this time, a percentage of hydrogen gas had remained in the nano-porous rod, which is not observed by catalysts systems in the absence of this nano-porous material. Therefore carbon monolith material can act as a storage material through adsorption interactions for this gas.

6.4 References

[1] (a) X. Xiao, S. M. Brozik, G. A. Montaño, C. M. Washburn, D. R. Wheeler, D. B. Burckel, R. Polsky, *Electronal. 24, 1*, **2012**, 153. (b) www.hydrogentechnologiesinc.com (last referenced 04/12/2012).

[2] V. Meregalli, M. Parrinello, *Appl. Phys. A, 72*, **2001**, 143.

[3] J. L. Inglis, B. J. MacLean, M. T. Pryce, J. G. Vos, *Chem. Coord. Rev.*, *256*, **2012**, 2571.

[4] J. Graetz, *Chem. Soc. Rev., 38*, **2009**, 73.

[5] C. Weidenthaler, M. Felderhoff, *Energy Environ. Sci., 4*, **2011**, 2495.

[6] J. Germain, J. M. Frechet, F. Svec, *Polymeric Materials: Science & Engineering*, *97*, **2007**, 272.

[7] J. Germain, J.M. Frechet, F. Svec, *Small, 5*, **2009**, 1098.

[8] B. Assfour, S. Leoni, G. Seifert, I.A. Baburin, *Adv. Mat., 23*, **2011**, 1237.

[9] J. M. Blackman, J. W. Patrick, A. Arenillas, W. Shi, C. E. Snape, *Carbon, 44, 8*, **2006**, 1376.

[10] M. Hirscher, M. Becher, M. Haluska, A. Quintel, V. Skakalova, Y. M. Choi, *J. Alloys Comp., 330*, **2002,** 654.

[11] A. Züttel, P. Sudan, P. Mauron, T. Kiyobayashi, C. Emmenegger, L. Schlapbach, *Int. J. Hydrogen Ener.*, *27, 2*, **2002,** 203.

[12] M. Volpe, F. Cleri. *Surf. Sci., 544*, **2003,** 24.

[13] B. Fang, M. Kim, J. H. Kim, J. S. Yu, *Langmuir, 24*, **2008**, 12068.

[14] R. L. McCreery, *Chem. Rev., 108*, **2008**, 2646.

[15] V. Raghuveer, A. Manthiram, *J. Electrochem. Soc., 152*, **2005**, A1504.

[16] K. Lee, J. Zhang, H. Wang, D. P. Wilkinson, *J. Appl. Electrochem., 36, 5,* **2006,** 507.

[17] M. S. Mauter, M. Elimelech, *Environ. Sci., Technol., 42, 16,* **2008**, 5843.

[18] M. Endo, Y. A. Kim, T. Hayashi, K. Nishimura, T. Matusita, K. Miyashita, *Carbon, 9*, **2001**, 1287.

[19] (a) W. J. Thomas, *J. Chem. Phys., 58,* **1961**, 61. (b) S. L. Kanashenko, A. E. Gorodetsky, V. N. Chernikov, A. V. Markin, A. P. Zakharov, B. L. Doyle, W. R. Wampler, *J. Nucl. Mater*., *233*, **1996**, 1207.

[20] (a) M. Saeki, *Int. J. Appl. Radiat. Isot. 43*, **1983**, 739. (b) M. Frenklach, H. Wang, *Phys. Rev. B, 43,* **1991**, 1520.

[21] X. He, L. Zhou, E. P. Nesterenko, P. N. Nesterenko, B. Paull, J. O. Omamogho, J. D. Glennon, J.H.T Luong, *Anal. Chem*., **2012**, *84*, 2351.

[22] (a) Z. Guo, J. Chen, H. Liu, C. Cha,. *Anal. Chim. Acta*, *607*, **2008**, 30. (b)Y. Hu, H. Sun, N. Hu, *J. Colloid Interface Sci*., *314*, **2007**, 131.

[23] L. Liu, L-P. Guo, X-P. Bo, J. Bai, X.-J. Cui, *Anal. Chim. Acta, 673,* **2010**, 88.

[24] Y. Xu, C. Hu, S. Hu, *Anal. Chim. Acta, 663*, **2010**, 19.

[25] (a) http://www.engineeringtoolbox.com/gases-solubility-water-1148.html. Last referenced 20/10/2012, (b) P. Ruetschi, R. F. Amlie, *J. Phys. Chem., 70,* 8, **1966**, 718.

[26] J. Y. Lee, C. D. Wood, D. Bradshaw, M. J. Rosseinsky, A. I. Cooper, *Chem. Comm.,* **2006,** 2670.

[27] J. Germain, J. Hradil, J. M. J. Fréchet, F. Svec, *Chem. Mater., 18,* **2006,** 4430.

[28] V. Fierro, A. Szczurek, C. Zlotea, J. F. Marêché, M. T. Izquierdo, A. Albiniak, M. Latroche, G. Furdin, A. Celzard, *Carbon, 48*, **2010**, 1902.

[29] M. Kunowsky, J. P. Marco-Lozar, A. Oya, A. Linares-Solano, *Carbon, 50*, **2012**, 1407.

[30] (a) A. C. Dillon,K. M. Jones, T. A. Bekkedahl, D. S. Bethune, M. J. Heben, *Nature, 386*, **1997**, 377. (b) P. Chen, X. Wu, J. Lin, K.L. Tan. *Science, 285*, **1999,** 91. (c) A. Chambers, C. Park, R. T. K. Baker , N.M. Rodriguez, *J. Phys. Chem. B, 102 (22),***1998**, 4253. (d) Y. Ye, C. C. Ahn, B. Witham, B. Fultz, J. Liu, A. G. Rinzler, *Appl Phys Lett., 74 (16),* **1999**, 2307. (e) A. Ansón, M. A. Callejas, A. M. Benito, W. K. Maser, M. T. Izquierdo, B. Rubio, *Carbon 42 (7),* **2004**, 1243. (f) B. Panella, M. Hirscher, S. Roth, *Carbon 43 (10),* **2005**, 2209. (g) K.M. Thomas, *Catal. Today, 120 (3-4)*, **2007**, 389.

Chapter Seven

Concluding Remarks and Future Work

7.1 Concluding remarks and future work

Characterisation of the metallophthalocyanines employed as catalysts has been carried out using UV-Vis spectroscopy and cyclic voltammetry (Chapter 3). Under both solution-phase and surface confined conditions, a single reversible metal centred reduction is observed for $CoPcF_{16}$ at potentials more negative than those for catalysts $CuPcF_{16}$ and $ZnPcF_{16}$. The addition of an electron takes place on the Pc ring for these two catalysts. Future work with these metallophthalocyanines includes spectroelectrochemistry (to further identify the locations of the reductions).

Chapters 3 to 6 describe the catalytic activity of the metallophthalocyanines for electrocatalytic generation of hydrogen as adsorbed species, embedded in a polymer framework (Nafion®) and dispersed in a nano-porous material respectively. The electrochemical behaviour of $CoPcF_{16}$ adsorbed on a glassy carbon electrode in aqueous acidic conditions reveals a sharp cathodic current at negative potentials (-1.2 V) indicative of proton reduction. It is suggested that proton reduction can occur following the reduction of the protonated reduced species $[Co(I)Pc(-3)^{\cdot}H^{+}]H^{+}$ to yield molecular hydrogen. Electrodes modified with $CuPcF_{16}$ and $ZnPcF_{16}$ are expected to follow in the same pathway with the first reduction occurring on the Pc ring.

The catalytic activity exhibited by these metallophthalocyanines was evaluated by a number of performance indicators; TOF (hr^{-1}), moles of hydrogen produced and current density and applied electrolysis potential. While all 3 displayed catalytic activity for proton reduction in acidic (pH 2) conditions, the catalyst which performed the best when adsorbed on a glassy carbon electrode was $ZnPcF_{16}$ as it required 100 mV less of an overpotential to generate the same amount of hydrogen (1.2×10^{-6} mol at -1.1 V mol) compared to $CoPcF_{16}$ (1.2×10^{-6} mol at -1.2 V). The stability of the catalysts in a variety of conditions such as electrolysis time (1 hour to 24 hours), electrolyte and temperature were indicated in Chapters 4 and 5. The appearance of a catalytic current of similar or larger magnitude was observed.

When these catalysts were incorporated in Nafion® in a volume ratio of 4:1 MPc:Nafion®, the catalytic activity, in terms of TOF and current density was shown to decrease. This behaviour was unexpected as Nafion® contains a region of high proton concentration, thus facile proton reduction was anticipated. TOF values obtained for these catalysts were an order of magnitude lower than those observed for the adsorbed catalyst, in the absence of a 3-D framework. The use of nano-porous carbon monolith material in Chapter 6 was investigated in addition to the electrocatalytic studies presented in Chapters 4 and 5. The increased surface area allowed for a larger percentage of electroactive species at the electrode surface. When this material was crushed into a powder and (prepared in a cationic surfactant) dispersed with $MPcF_{16}$ in a volume ratio of 1:4 CM:$CoPcF_{16}$, the catalytic activity was evaluated by the number of moles of hydrogen produced and current density. Although the percentage of electroactive species increased, the TOF, moles and current density did not significantly rise in comparison with the adsorbed catalysts/ catalysts in Nafion®. The hydrogen storage properties of these nano-porous materials were shown as the gas remained in the electrocatalytic cell containing the modified electrode when allowed to stand over a 24 hour period (as analysed by gas chromatography).

The percentage of catalyst which was electroactive in the layer for these catalysts is low, which is considered a result of possible aggregation of the metallophthalocyanines in the modified layer. This would impede the ability of the catalyst to form conductive films. As a low percentage of active catalyst (1 %) was observed for $CuPcF_{16}$ compared to a larger percentage (6 % for $CoPcF_{16}$), this led to difficulty in directly comparing the modified electrodes; hence a comparison of moles of hydrogen formed was more useful. Due to this small percentage of active catalyst adsorbed on GCE's as modified electrodes, the use of nano-porous carbon material yielded an increase in electroactive catalyst. Improvements in measuring the active catalyst could be considered for future work, such as a different approach to film formation.

It is evident from the studies carried out in this thesis that there are many variables which influence the catalytic activity of these metallophthalocyanines for the electrocatalytic generation of hydrogen, thus it was difficult to control so many of these parameters. The biggest parameter which affects the generation of hydrogen

evolution is O_2 production at the anode. When this is produced at the counter electrode, the gas can drift towards the cathode and contributes to the charge and current measured at this electrode, thus TOF values obtained by electrochemistry are not solely due to proton reduction. Hence, analysis of the headspace gas (determination of TOF) is crucial to evaluate the catalyst's performance. Future work would include the development of the cell design. The use of a separator or a two compartment cell would be useful; one which would physically stop the O_2 gas from drifting towards the cathode but allowing for the passage of current in the circuit. The use of a chloride based electrolyte in Chapters 4 and 5 resulted in an increase in catalytic activity, current density and moles of hydrogen produced. It is suggested that the reduction of chloride to chlorine at the electrode is more favourable than water oxidation. Future work may involve investigating alternative electrolyte solutions for these systems.

The formation of H_2 gas bubbles on the surface of the electrode can hinder the rate of which charge is passed through the system. Thus, developing a technique which offsets the bubbles at the electrode surface is important. This may be done by stirring or tapping the cell in order to encourage the bubbles to escape from the surface. However, stirring over a period of time would also lead to an increase in O_2 gas, which would also experience the force from stirring with a magnet; therefore the two cell compartment would be essential here. Another possible solution to this would be to employ a rotating disk working electrode in an effort to mitigate the problem of bubble formation at the surface for long periods of time.

It is important to note that the TOF (hr^{-1}) for H_2 produced by these systems is a lower limit as hydrogen is also soluble in the aqueous solution (1.6×10^{-3} g/L at 20°C) in which the catalytic reaction is carried out in. Future work would include an investigation of the determination of soluble H_2 in the cell, which would indicate a more accurate Faradaic efficiency for these systems. Also, the calculation TOF of H_2 assumes the cell pressure is at 1 atm. Although the moles of hydrogen produced (and subsequent pressure) are small ($\sim \times 10^{-6}$ mols, ~700 Pa) it would be useful to quantify the pressure correctly by using a pressure metre.

The purpose of employing Nafion® as a polymer was to investigate whether the polymeric framework would lead to an enhanced catalytic activity. The results obtained in chapter 5 revealed a decrease in activity, relative to the neat adsorbed catalysts. Investigating other polymers, such as PVP (reported by Kaneko) or co-polymers such as PVP: PMMA to create a 3-D modified electrode would be advantageous as $CoPcF_{16}$ has shown to work as an efficient catalyst for hydrogen production, therefore using the polymers in with these catalysts would be expected to yield an enhanced activity. Using nano-porous material, as shown in Chapter 6 led to an increase in electroactive species at the electrode surface. However, this does not result in an increase in catalytic activity, indicated by TOF and current density. Future work may include investigating other material for these studies, such as the use of a carbon cloth.

Finally, the significance of light on the electrocatalytic activity has been shown in Chapters 4 and 5. Although the significance was not realised until the late stages of this project, the effect of light plays a crucial role, thus future work would see further investigations being carried out, including the angle of electrode with respect to the light source, the time of day in which the electrocatalytic experiments are conducted, and the photochemical properties of the catalysts.

Appendix A

Publications

Coordination Chemistry Reviews 256 (2012) 2571–2600

Contents lists available at SciVerse ScienceDirect

Coordination Chemistry Reviews

journal homepage: www.elsevier.com/locate/ccr

Review

Electrocatalytic pathways towards sustainable fuel production from water and CO_2

Jane L. Inglis [a], Brian J. MacLean [b,**], Mary T. Pryce [a], Johannes G. Vos [a,*]

[a] SRC for Solar Energy Conversion, School of Chemical Sciences, Dublin City University, Dublin 9, Ireland
[b] Department of Chemistry, St. Francis Xavier University, P.O. Box 5000, Antigonish, Nova Scotia, B2G-2W5, Canada

Contents

ARTICLE INFO

Article history:
Received 20 January 2012
Received in revised form 1 May 2012
Accepted 5 May 2012
Available online 14 May 2012

Keywords:
Hydrogen
CO_2
Electrocatalysis
Modified electrodes
Transition metal complexes

ABSTRACT

The electrocatalytic properties of transition metal complexes with respect to the formation of H_2 and the reduction of CO_2 are discussed. The compounds are immobilized on electrode surfaces and the efficiency of the modified electrodes is considered as a function of the nature of the metal complex, the electrolytes used, the potential applied and the method used to immobilize the compounds on the electrode surfaces. Where available, turnover numbers are reported. For CO_2 reduction systems the nature of the products obtained is also considered.

1. Introduction

The rapid expansion of human populations and its energy demands seriously tax our ability to live in a sustainable manner. It has been suggested that the world's largest energy source, oil, may be exhausted by the middle of the 21st century [1,2]. Our dependence on fossil fuels for energy sources has created a second, far-reaching problem, which is climate change. In a recent review by Roy et al. the environmental impact of expected turn-of-the-century CO_2 levels was discussed, with a 6 °C increase in global temperature being predicted by that time with serious, accompanying environmental consequences, including greatly diminished arable lands and the disappearance of the polar ice cap [3]. It is alarming that trends in both population growth and fossil fuel energy consumption continue, seemingly unabated. There is, therefore, an urgent need for the development of novel approaches for obtaining energy, which should be carbon-neutral and will

* Corresponding author. Tel.: +353 1 7005307; fax: +353 1 7005503.
** Corresponding author. Tel.: +1 902 8672826; fax: +1 902 8672414.
E-mail addresses: bjmaclea@stfx.ca (B.J. MacLean), han.vos@dcu.ie (J.G. Vos).

0010-8545/$ – see front matter © 2012 Elsevier B.V. All rights reserved.
http://dx.doi.org/10.1016/j.ccr.2012.05.002

therefore not exacerbate atmospheric CO_2 levels. At the same time, new energy technologies should be efficient and cheap enough to replace present fossil fuel-based energy sources. Wind and solar energy are possible solutions. Wind energy is, at present, a well-developed science, but problems exist concerning locations of wind turbines and the irregular strength of winds, which leads to a variable energy output. Solar energy is widely considered to be one of the most promising avenues for energy in future times, because of the virtually unlimited amount of solar energy that is available. In the last number of years considerable improvements have been made in the efficiency and price for both classical silicon-based photovoltaic cells and the more recently developed Grätzel cell [4] while the artificial photosynthesis approach has also been discussed [5]. However, solar energy, like wind, is an intermittent energy source, and both of these technologies may produce excess electricity that must be stored. Batteries can only store a small fraction of the energy by weight or volume that liquid hydrocarbon fuels can, and other means of storing electricity (e.g. supercapacitors) are not yet developed to the point that they can be considered for large-scale use [6]. This fact, coupled with an already well-established fossil fuel-based energy infrastructure makes displacing fossil fuels as a primary energy source for the world a daunting task. A study of global energy consumption for 2010 conducted by BP revealed that at present, renewable energy sources (solar, wind, tidal, hydro and geothermal energy) constitute only 1% of the world's energy consumption; oil and gas remain the leading non-renewable sources of energy, accounting for 37% and 23% of global energy usage figures, respectively [7].

Against this background to fully develop the potential of renewable energy sources, novel technologies where energy is stored as fuels or chemical feed stocks need to be developed [8]. One of the most studied options in this area is the development of photocatalytic methods for the generation of solar fuels. These methods are based on photoinduced inter- or intramolecular electron transfer processes [9]. Areas studied include light-driven hydrogen generation [10] and the transformation of CO_2 into fuels or chemical feed stocks [11]. So far these studies have been carried out in solution and require sacrificial agents. The presence of sacrificial agents creates side reactions such as decomposition of the photocatalysts or spurious results by their interaction with solvents [12]. The presence of these sacrificial agents does not allow for the development of environmentally friendly and sustainable energy sources. The immobilization of such photocatalysts on active surfaces promises to be the way forward, since sacrificial agents are not needed in this case. For the same reasons the immobilization of electrocatalysts is an attractive way of storing energy as fuels and research in this area has been carried out for many years.

The electrocatalytic formation of hydrogen and the transformation of CO_2 into useful chemical products are of great interest in this endeavor. If renewable energy sources are used to generate fuels from cheap and widely available materials, this goal might be accomplished. Because of the sheer scale that would be involved in supplying the world's billions with energy, water has often been considered as a possible starting material for the synthesis of H_2. It is present in large quantities on the earth's surface and hydrogen produced from aqueous solutions can be combusted to produce energy, yielding no carbon footprint. Even though the processes by which hydrogen is obtained from water are endergonic, when coupled with renewable energies, they would yield net energy gains. Hydrogen is an ideal fuel in this regard, but currently, its generation is mostly carried out using fossil fuels. Hydrogen has a low density, and thus its storage and transportation is not only inconvenient but also requires high pressures (at an extra energy cost); however, on-board generation for immediate use in vehicles could help to partly alleviate this drawback. For the generation of hydrogen, water electrolysis is a well-established process but it requires expensive electrode materials and this transformation is carried out at high temperatures, reducing energy gains [13]. Therefore a more environmentally friendly H_2 production method based on abundant metals and at ambient temperatures is of interest [14].

CO_2 is another widely available material that might be considered for energy storage purposes. Because it is the by-product of most industrial operations and because of the problems that are associated with its build-up in the atmosphere CO_2 would have a zero-to-negative cost figure, and thus would be a very cheap starting material. Importantly, CO_2 may be hydrogenated to form a range of products – including liquid hydrocarbons – that might be used in tandem with existing energy-delivery infrastructure [15].

Electrochemical energy storage routes have been explored as early as 1800, with the first report of water electrolysis by Nicholson and the first battery by Volta appearing in the same year [16]. Starting from the 1980s there has been an interest in developing electrocatalytic methods for hydrogen production and the transformation of CO_2 into useful chemicals. Studies of electrochemical H_2 evolution and CO_2 reduction are well-known, and are typically carried out with the use of catalysts. The reduction of acidic solutions on platinized platinum surfaces, which is the basis for the standard hydrogen electrode (SHE) ($a_{H_2} = a_{H^+} = 1$; $T = 25\,^{\circ}C$), and is considered as the standard redox potential for proton reduction to molecular hydrogen. The reduction of H^+ on other surfaces and using different conditions requires a greater energy investment, observed experimentally in the form of an overpotential. Because of the costs associated with platinum, obtaining hydrogen in this manner on a large scale is not feasible. Therefore much time has been devoted toward the discovery of more abundant and cheaper materials for electrochemical H^+ reduction at minimal overpotentials, concerning electrode materials that span metal surfaces, alloys, semiconductors (photoelectrocatalysis), molecular catalysts dissolved in electrolyte solutions, and surfaces that incorporate immobilized catalyst centers (chemically modified electrodes, CMEs), to name a few. This review concerns CMEs that consist of coordination complexes in surface-confined arrangements for electrochemical H_2 evolution and CO_2 reduction. Coordination complexes are advantageous for this work in that they provide reactive catalyst centers whose electronics may be influenced by the nature of the coordination sphere. These systems are sometimes active at lower overpotentials than metallic catalysts, and may present "open" coordination sites for catalytic transformations in the form of easily substituted ligands [17].

When electrocatalysts are introduced as insoluble films on electrode surfaces, several important advantages over solution-phase experiments may be realized. First, a high effective concentration of the catalyst exists in the zone of the electrochemical reaction. This factor may create the possibility for cooperative effects (e.g. delivery of multiple redox equivalents to substrates due to the close proximity of catalyst centers to each other). Furthermore, because the electrode is coated with a thin layer of the catalyst, the approach uses minimal quantities of catalyst materials. Importantly, removal of the electrocatalyst following the reaction is facile, bypassing product-catalyst separation steps.

A variety of techniques have been published which concern the immobilization of catalysts onto electrode surfaces [18]. Two techniques that are frequently encountered in the literature are drop-casting of catalyst solutions and the use of chemical/electrochemical reactions that generate new covalent bonds between the electrocatalyst and the electrode surface. For example, glassy carbon electrode surfaces may be derivatized with chelating ligands such as phenanthrolines through the reduction of aryl diazonium salts, followed by coordination of catalyst centers to these units to produce catalytically active monolayers [19]. Simple drop-casting of catalyst solutions may be used for the creation of modified electrode surfaces via a less labor-intensive route (spin-casting

and dip-casting techniques are related alternatives) [20]. Provided the complex is not appreciably soluble in the electrolysis solvent (in the catalytically active oxidation states), this method is a convenient route to the creation of modified electrode surfaces.

A popular method for the immobilization of electrocatalysts on electrodes is dispersing them in polymer matrices. In certain cases, electroactive polymers may be used, which facilitate the regeneration of the active forms of the electrocatalysts [21]. Other supports like carbon nanotubes may serve similar purposes, while exposing a high reaction surface area [22]. Commercially available polymers like Nafion® and poly(4-vinyl)pyridine (PVP) enable drop-casting of catalyst–polymer mixtures onto electrodes. These polymers may readily permit passage of both H^+ ions and solvent. At the same time, trapped catalyst molecules can undergo electron transfer with the electrode either through slow diffusion or charge-hopping mechanisms, depending on the interactions of the electrocatalyst with the polymer support [23,24]. Such layers have been used for the design of electrochemical and glucose sensors [25].

Another strategy for the incorporation of catalyst centers in polymeric matrices is to utilize ligands which may undergo in situ electrochemical polymerization [26]. A disadvantage of this approach is the extra time and effort that must be invested in the chemical reactions that accompany the attachment of polymerizable groups to catalysts, but this need not be a major concern, since polymerizable ligands like 4-vinylpyridine are commercially available. One of the main advantages of this approach is that processibility issues which often accompany high molar mass materials are not a major concern, since the insoluble polymer is produced at the electrode surface. Examples may be found in the literature where metal complexes have been co-polymerized with molecules like bithiophene; however, use of polymerizable catalyst complexes ensures the incorporation of a high quantity of catalyst centers into the polymer coating [27–29].

The use of vinyl-substituted ligands to obtain polymer-supported complexes yields metallopolymers that have saturated organic backbones, and in these materials, catalyst regeneration

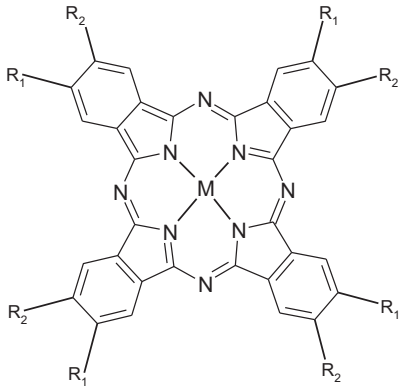

1: **M** = Zn, Co, Cu, Ni, Mn, Pd, Fe, Dy, Sn, Pb, In, Ga, Ti, Mg, V, Pt; $\mathbf{R_1} = \mathbf{R_2} = H$
2: **M** = Co; $R_1 = R_2 = CN$
3: **M** = Co; $\mathbf{R_1} = SO_3H$; $\mathbf{R_2} = H$
39: **M**= Co; $\mathbf{R_1} = \mathbf{R_2} = OC_4H_9$
40: **M** = Co, Cu; $\mathbf{R_1} = C(CH_3)_3$; $\mathbf{R_2} = H$
41: **M** = Cu; $\mathbf{R_1} = NH_2$; $\mathbf{R_2} = H$
42: **M** = Lu; $\mathbf{R_1} = \mathbf{R_2} = OC_5H_{11}$

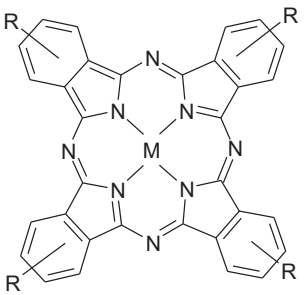

4:**M** = Co, Cu; **R** = 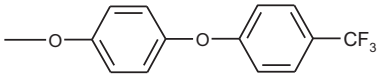

5: **M** = Co; **R** = 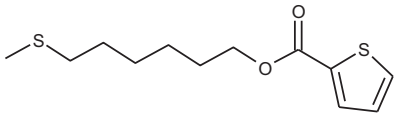

7: **M** = Co; $\mathbf{R} = C(COOC_2H_5)_3$

45: **M** = Co, Ni, Fe; $\mathbf{R} = NH_2$

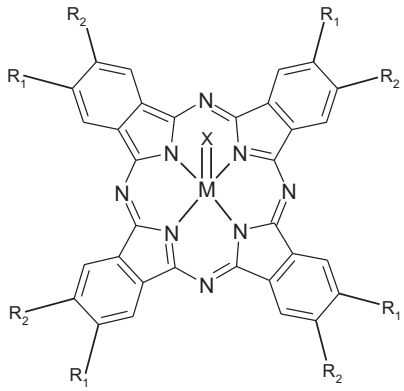

6a: **M** = Ti; $\mathbf{R_1} = \mathbf{R_2} = S(CH_2)_2N(CH_3)_2$; X = 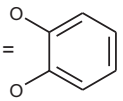

6b: **M** = Ti; $\mathbf{R_1} = \mathbf{R_2} = S(CH_2)_2N(CH_3)_2$; X = 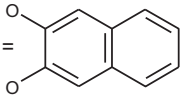

6c: **M** = Ti; $\mathbf{R_1} = \mathbf{R_2} = S(CH_2)_2N(CH_3)_2$; X = O

Fig. 1. Molecular structures of electrocatalysts discussed.

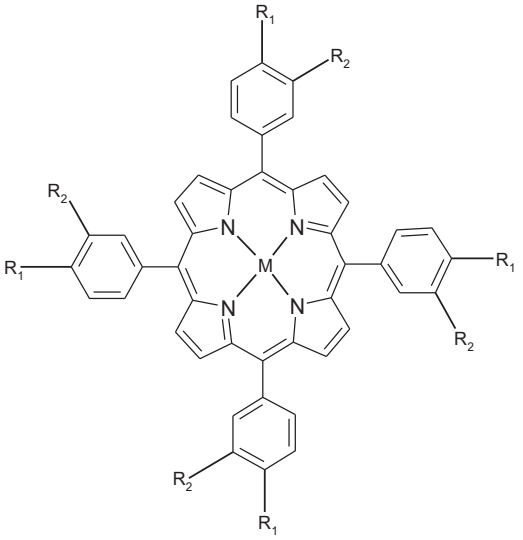

8: **M** = Co, Mn, Fe, Zn, Cu, Ni, Mg; $\mathbf{R_1}$= H; $\mathbf{R_2}$ = H

43: **M** = Co; $\mathbf{R_1}$ = OCH3; $\mathbf{R_2}$ = H

51: **M** = Co; $\mathbf{R_1}$ = H; $\mathbf{R_2}$ = NH_2

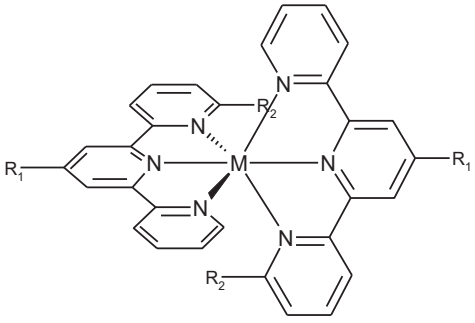

9: **M** = Cr, Fe, Co, Ni, Ru, Os; $\mathbf{R_1}$ = $\mathbf{R_2}$ = H

52: **M**= Cr, Fe, Co, Ni, Ru, Os; $\mathbf{R_1}$ = $CHCH_2$; $\mathbf{R_2}$ = H

53: **M**= Cr, Fe, Co, Ni, Ru, Os; $\mathbf{R_1}$ = H; $\mathbf{R_2}$ = $CHCH_2$

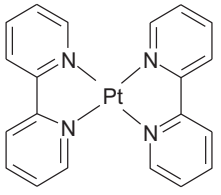

10: **M** = **Pt**

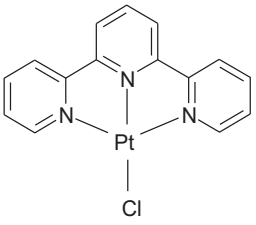

11: **M** = **Pt**

Fig. 1. (*Continued*)

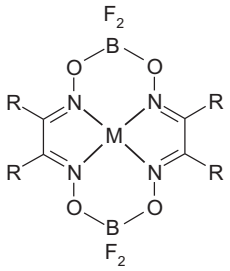

12: **M** = Co, Ni; **R** = CH_3
13: **M** = Co, Ni; **R** = C_6H_5

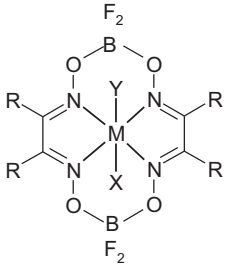

14: **M** = Co; **R** = CH_3; **X** = **Y** = $CNCH_3$
15: **M** = Co; **R** = C_6H_5; **X** = **Y** = $CNCH_3$
16: **M** = Co; **R** = C_6H_5; **X** = $CNCH_3$

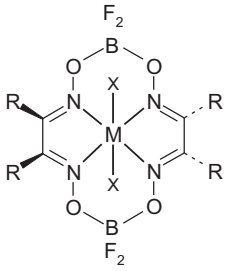

17: **M** = Co; **R** = CH_3; **X** = $CNCH_3$
18: **M**= Co; **R** = C_6H_5; **X** = $CNCH_3$

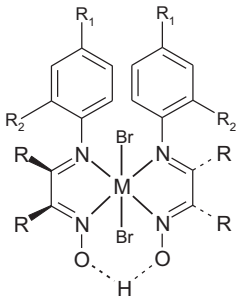

19: **M** = Co; $\mathbf{R_1}$ = H; $\mathbf{R_2}$ = H
20: **M** = Co; $\mathbf{R_1}$ = OCH_3; $\mathbf{R_2}$ = H
21: **M** = Co; $\mathbf{R_1}$ = CH_2COOH; $\mathbf{R_2}$ = H
22: **M** = Co; $\mathbf{R_1}$ = H; $\mathbf{R_2}$ = C_6H_5

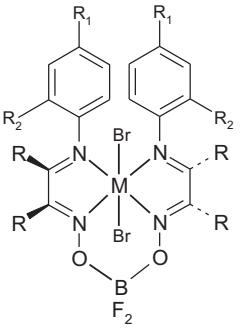

23: **M** = Co; $\mathbf{R_1}$ = $\mathbf{R_2}$ = H
24: **M** = Co; $\mathbf{R_1}$ = OCH_3; $\mathbf{R_2}$ = H
25: **M** = Co; $\mathbf{R_1}$ = CH_2COOH; $\mathbf{R_2}$ = H
26: **M** = Co; $\mathbf{R_1}$ = H; $\mathbf{R_2}$ = C_6H_5

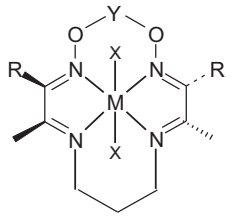

27: **M** = Co; **R** = CH_3; **X** = Br; **Y** = H
28: **M** = Co; **R** = H; **X** = Cl; **Y** = H
29: **M** = Co; **X** = Br; **Y** = BF_2

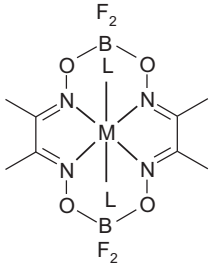

30: **M** = Co; **L** = H_2O, CH_3CN, DMF

Fig. 1. (*Continued*)

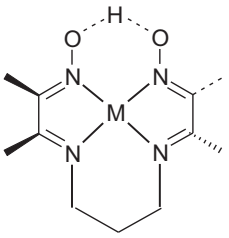

31: **M** = Ni

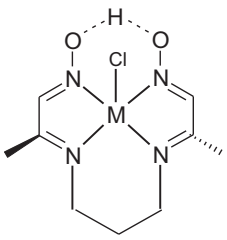

32: **M** = Ni

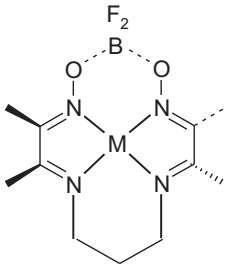

33: **M** = Ni

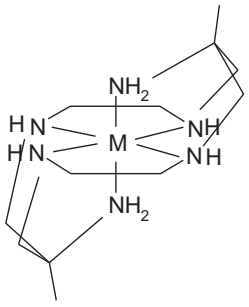

34: **M** = Co

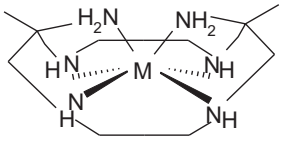

35: **M** = Co

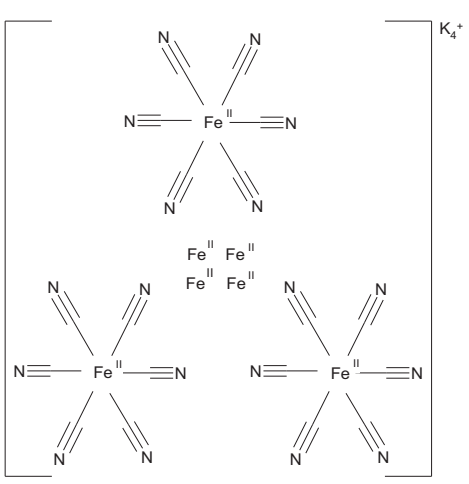

36: **M** = Fe

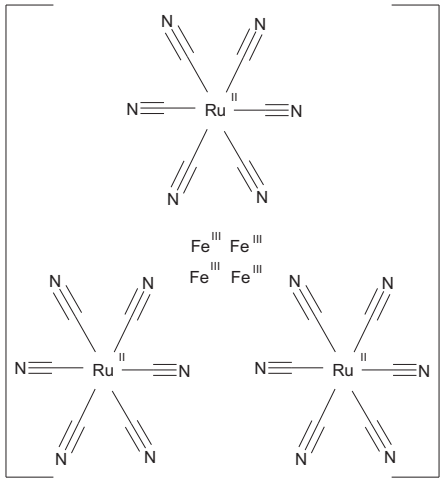

37: **M** = Ru

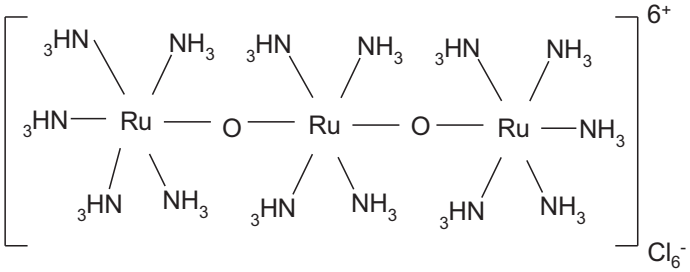

38: **M** = Ru

Fig. 1. (*Continued*)

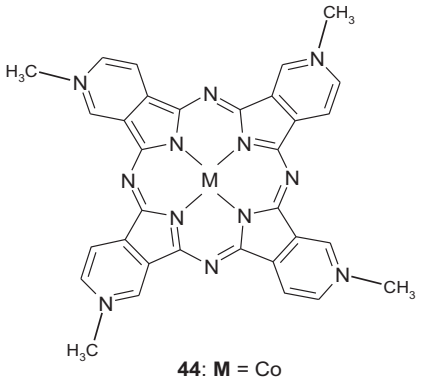

44: **M** = Co

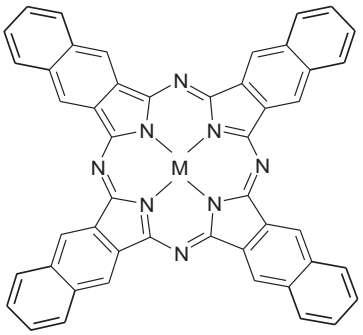

46: **M** = Co

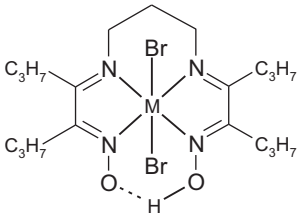

47: **M** = Co

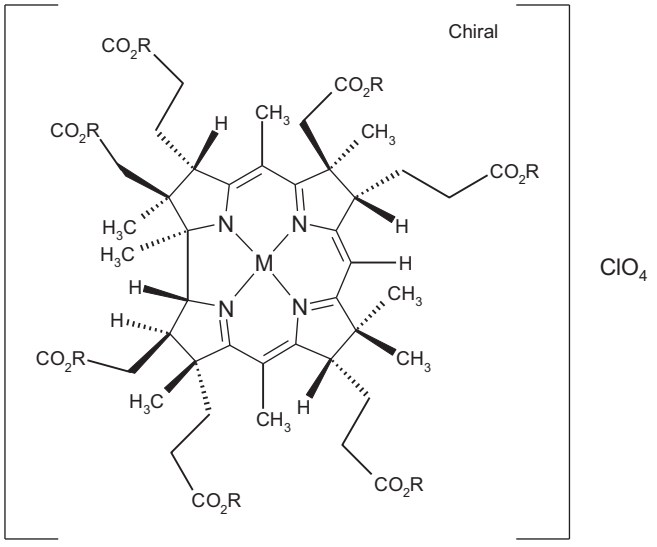

48: **M** = Co; **R** = CH_3
49: **M** = Co; **R** = $CH_2CH_2CH_3$

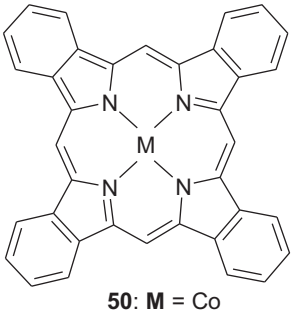

50: **M** = Co

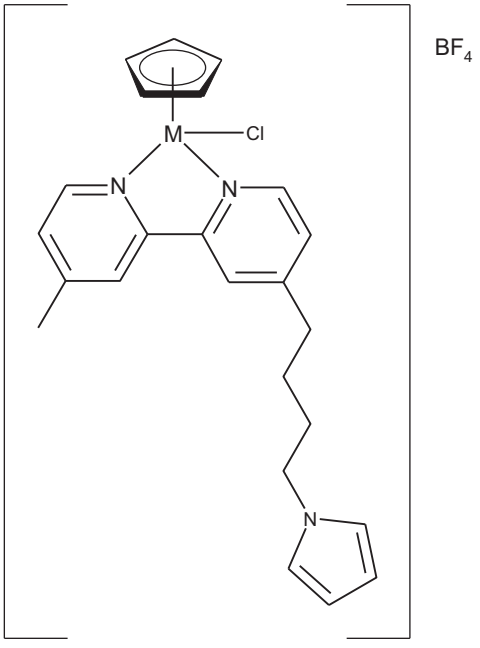

54: **M** = Rh

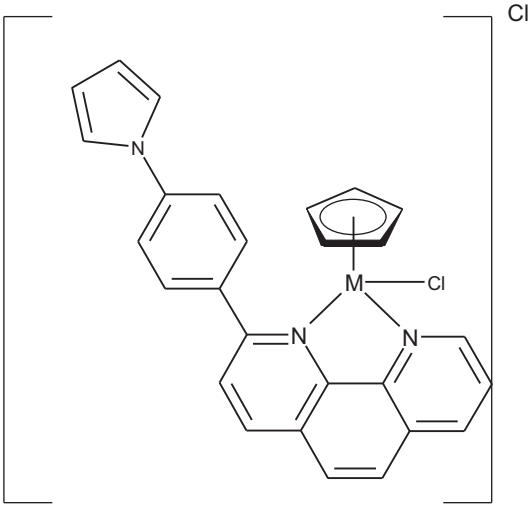

55: **M** = Ir

Fig. 1. (*Continued*)

56: **M =** Re; $\mathbf{R_1}$ = H; $\mathbf{R_2}$ = H; **X** = Br
58: **M** = Re; $\mathbf{R_1}$ = CH_3; $\mathbf{R_2}$ = $CHCH_2$; **X** = Cl

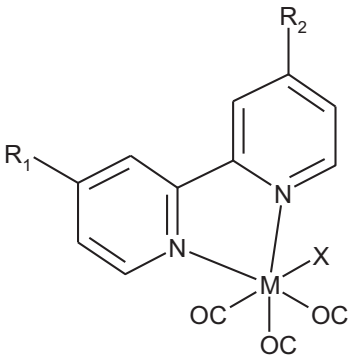

60: **M** = Re; $\mathbf{R_1}$ = CH_3; $\mathbf{R_2}$ = 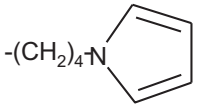

X = Cl

61: **M** = Re; $\mathbf{R_1}$ = $\mathbf{R_2}$ = 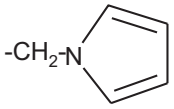

X = Cl

62: **M** = Re, $\mathbf{R_1}$ = CH_3; $\mathbf{R_2}$ = 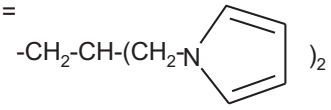

X = Cl

63: **M** = Re; $\mathbf{R_1}$ = $\mathbf{R_2}$ = 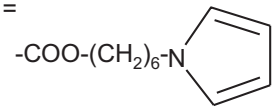

X = Cl

64: **M** = Re; $\mathbf{R_1}$ = $\mathbf{R_2}$ = 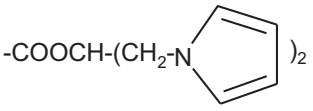

X = Cl

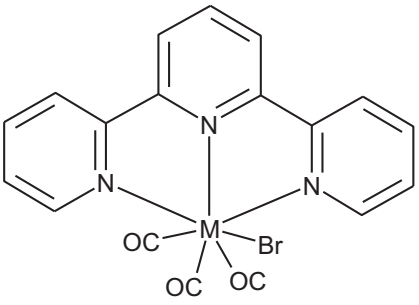

57: **M** = Re

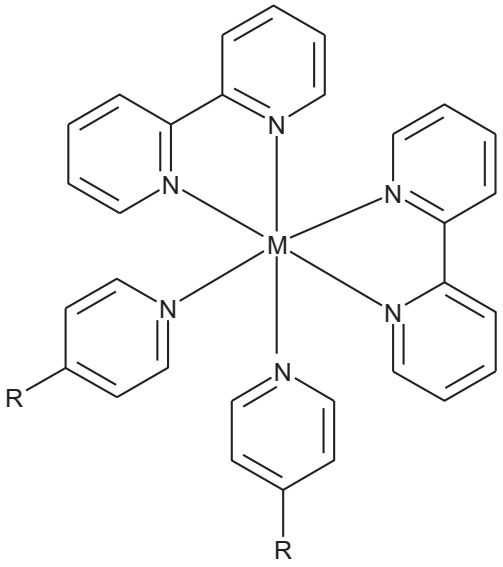

59: **M** = Ru; **R** = $CHCH_2$

Fig. 1. (*Continued*)

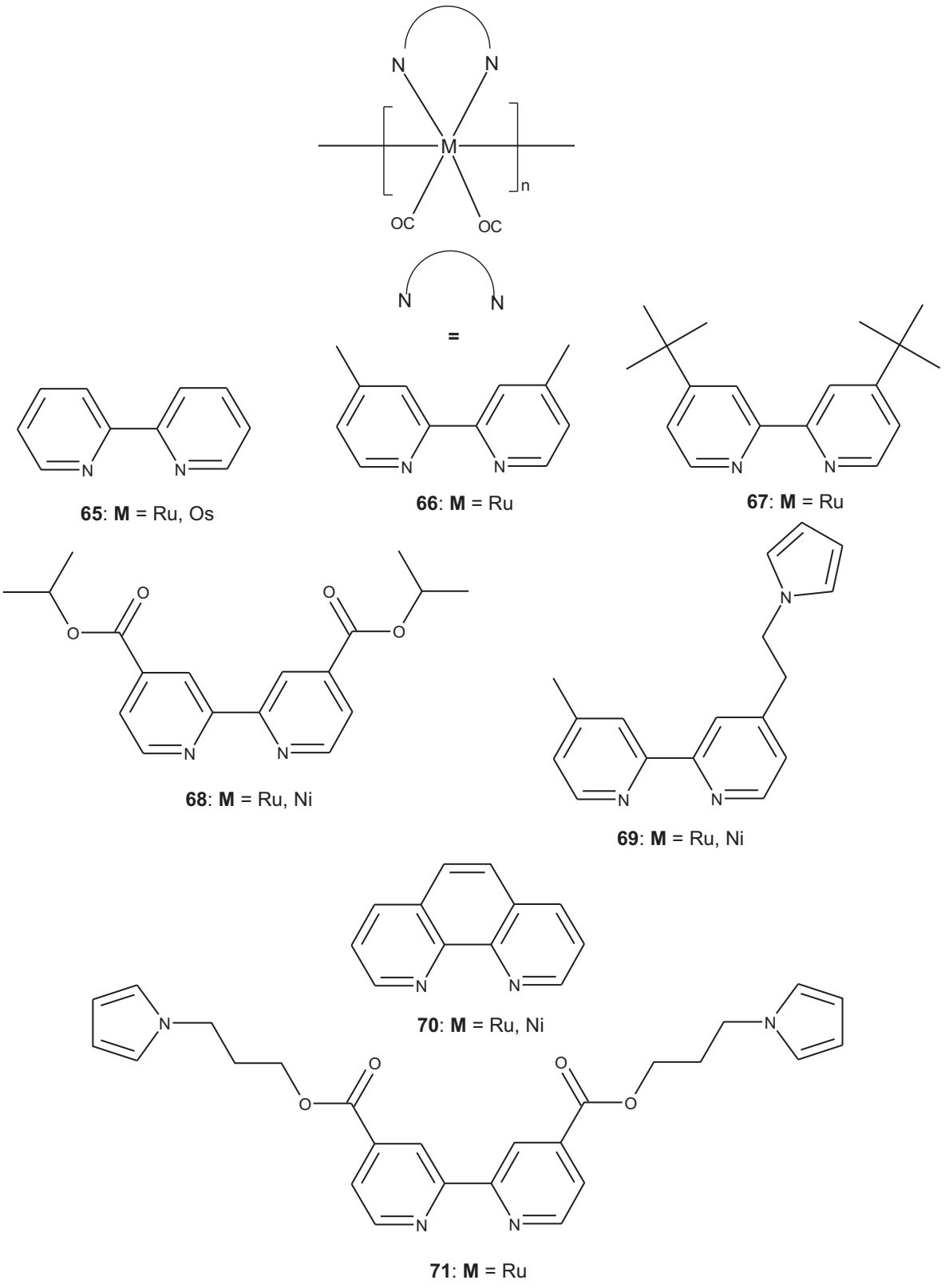

Fig. 1. (*Continued*)

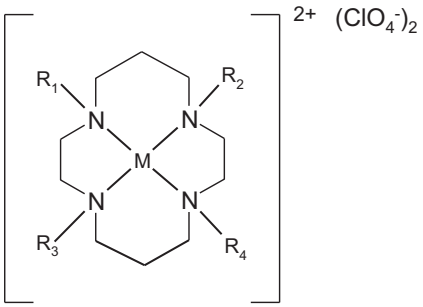

72: **M** = Ni; $\mathbf{R_1} = \mathbf{R_2} = \mathbf{R_3} = \mathbf{R_4} = C_{16}H_{33}$
73: **M** = Ni; $\mathbf{R_1} = \mathbf{R_2} = \mathbf{R_3} = H$; $\mathbf{R_4} = C_{16}H_{33}$
74:**M** = Ni; $\mathbf{R_1} = \mathbf{R_2} = \mathbf{R_3} = \mathbf{R_4} = H$
75:**M** = Ni; $\mathbf{R_1} = \mathbf{R_2} = \mathbf{R_3} = H$; $\mathbf{R_4} = CH_3$
76:**M** = Ni; $\mathbf{R_1} = \mathbf{R_2} = H$; $\mathbf{R_3} = \mathbf{R_4} = CH_3$
77:**M** = Ni; $\mathbf{R_1} = H$; $\mathbf{R_2} = \mathbf{R_3} = \mathbf{R_4} = CH_3$
78:**M** = Ni; $\mathbf{R_1} = \mathbf{R_2} = \mathbf{R_3} = \mathbf{R_4} = CH_3$
79:**M** = Ni; $\mathbf{R_1} = \mathbf{R_2} = H$; $\mathbf{R_3} = \mathbf{R_4} = C_{16}H_{33}$
80:**M** = Ni; $\mathbf{R_1} = \mathbf{R_2} = \mathbf{R_3} = H$; $\mathbf{R_4} = CH_2$-pyridine
81:**M** = Ni; $\mathbf{R_1} = \mathbf{R_2} = \mathbf{R_3} = H$; $\mathbf{R_4} = CH_2$-anthracene

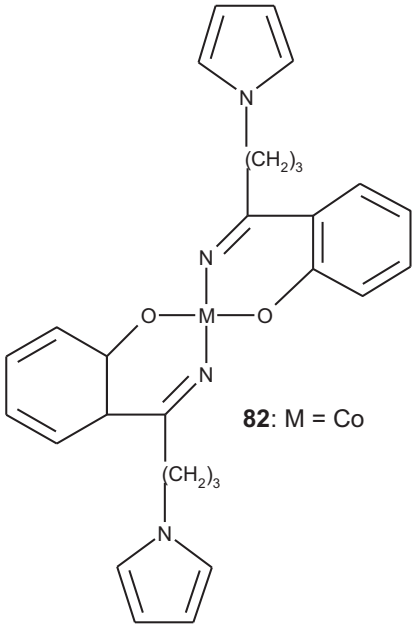

82: M = Co

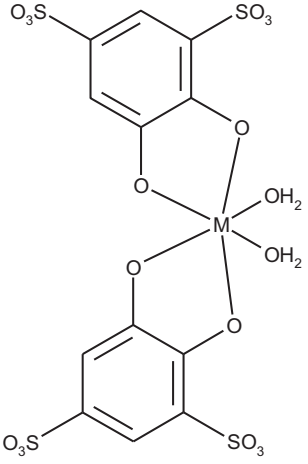

83: **M** = Fe

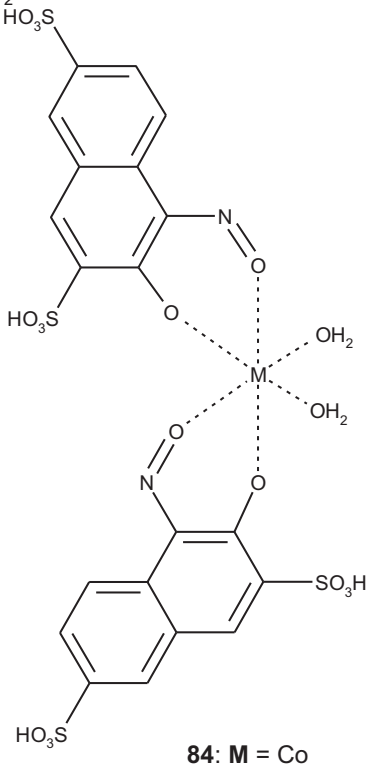

84: **M** = Co

Fig. 1. (*Continued*)

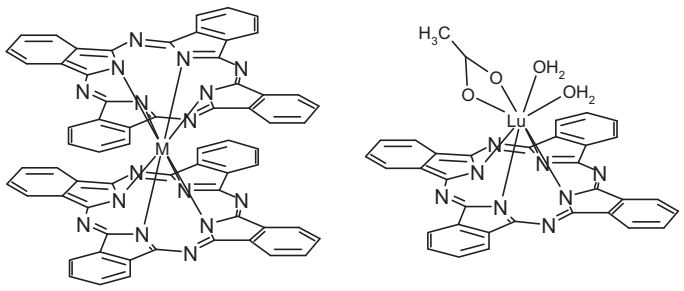

Fig. 1. (*Continued*).

is accomplished by an outer-sphere electron-hopping mechanism. Superior electron transport is possible in systems that involve conjugated organic backbones (conjugated metallopolymers). These materials have been targeted for use in electrocatalysis since their discovery in the mid 1990s, because their fast electron transport properties will greatly enhance the regeneration of electrocatalyst centers during catalytic oxidation/reduction cycles [30]. For these materials, a fast superexchange mechanism operates, which provides electron transfer at rates up to two orders of magnitude greater than those reported for comparable vinylpyridine-based metallopolymers [31]. The direct coordination of metal centers to the conjugated π-system of the polymer backbone in a conjugated metallopolymer also yields materials which possess interesting combinations of redox and spectral properties. Unfortunately, presynthesized ligands that yield conjugated metallopolymers are not yet generally available from commercial vendors, and thus investigative work with these materials requires additional synthetic effort. Still, the attachment of groups that enable in situ oxidative or reductive electropolymerization (e.g. thiophenes, pyrroles) may be achieved through well-established carbon–carbon bond formation reactions in reasonably good yields [32].

A major drawback of CO_2 electrocatalytic approaches is that CO_2 is only sparingly soluble in aqueous solutions, necessitating the use of low temperatures to enhance gas solubility and long CO_2 bubbling times. For experiments involving gaseous substances, improved performance can be achieved through the use of gas-diffusion electrodes. In a gas-diffusion electrode, CO_2 is introduced directly into the catalyst layer for conversion. The electrodes provide a high surface area for the electrochemical reaction in the form of a highly gas-permeable, porous environment upon which catalysts may be supported. A three-component electrode/gas/electrolyte interface is produced, which permits generation of much higher currents in electrochemical reactions than on planar electrodes and generally better overall performance.

This review gives an overview of the work carried out over the last 30 years using electrode surfaces modified with a range of coordination complexes mostly based on first row transition metals. The first section deals with a discussion of methods developed for the electrocatalytic generation of hydrogen, while in the second part the electrocatalytic transformation of CO_2 is discussed. The structures of the electrocatalysts employed in these studies are shown in Fig. 1. Note that compounds M-**1**–M-**38** are hydrogen producing catalysts while the compounds M-**39**–M-**84** are used for CO_2 reduction. Where compounds are used in both processes they are introduced first in the hydrogen section and listed in the first set of compounds as outlined above. The experimental conditions as well as the current efficiency of the methods utilized for hydrogen generation are listed in Table 1. The data reported for CO_2 transformation are shown in Table 2.

2. Electrocatalytic systems for hydrogen generation

When hydrogen is used as an energy source, it generates no emissions other than water. The emergence of an environmentally friendly hydrogen economy has been advocated for some time. However, at present most hydrogen is produced from fossil fuels, a method that is clearly neither sustainable, nor environmentally sound. A smaller amount (about 4%) is obtained from the electrolysis of water. Although attractive in principle, the direct electrolysis of water has several drawbacks. This process mainly uses platinum working electrode surfaces, and to enhance the efficiency of the process, high pressures and high temperatures (up to 850 °C) are frequently used. Since heat losses are considerable, overall efficiency is normally in the 50–70% range. Therefore, there is an urgent need for the development of cheap and low-temperature production methods for hydrogen. The challenge for today's scientists is to develop sustainable techniques to produce hydrogen economically. Because the use of Pt catalysts for meeting global energy (hydrogen) needs is not a realistic idea, molecular catalysts using first row transition metals have been investigated for their potential in electrocatalytic hydrogen generation reactions. Against this backdrop, the first part of this review discusses electrocatalytic hydrogen production methods at ambient temperatures, using electrodes modified with mostly first row transition metal complexes. In Section 2.1 below a brief discussion of some important issues, such as charge transport, immobilization techniques and the importance of the matrix associated with modified electrodes will be discussed first, using phthalocyanine based materials as electrocatalysts.

2.1. Metal phthalocyanine-modified electrodes

Metallophthalocyanines (MPc's) have attracted much attention over the years, as they have found applications in many different areas, ranging from commercial uses as dyes in the paper and textile industry [33], environmental and chemical sensors used for the detection of heavy metals [34,35] and in pharmacology, for use as therapeutic agents [36]. The properties of MPc's include a rich redox chemistry that is associated with an 18π-electron ring arrangement. They offer chemical and thermal stabilities, varied coordination properties, absorbance in the visible spectrum and highly efficient intermolecular electron transfer processes [37]. These properties are attractive for their use as catalysts for hydrogen evolution. A considerable amount of research has shown that in solution, MPc's can catalyze photoinduced proton reduction reactions to generate molecular hydrogen in the presence of sacrificial donors [38,39]. Although such studies are worthwhile, the need for sacrificial donors (which, as the name suggests, are consumed during the reaction process) will not directly lead to a

Table 1
Comparison of reported experimental details and hydrogen generation TON's for the electrocatalysts discussed.

	Electrode	Potential (V) vs. Ag/AgCl	Solvent system	TON	Ref.
[Co-**1**]	P(VP-St)[a]/BPG[b]	−0.9[c]	pH 1.0, 0.1 M aq. NaH_2PO_4/H_3PO_4	2×10^5 h^{-1}	[50]
[Co-**2**]	P(VP-St)[a]/BPG[b]	−0.9[c]	pH 1.0, 0.1 M aq. NaH_2PO_4/H_3PO_4	5×10^4 h^{-1}	[50]
[Co-**3**]	P(VP-St)[a]/BPG[b]	−0.9[c]	pH 1.0, 0.1 M aq. NaH_2PO_4/H_3PO_4	$\sim 1.2 \times 10^3$ h^{-1}	[50]
[Cu-**1**]	Nf[d]/GCE[e]	−1.22[f]	pH 2.7, 7.3, 10.4, 0.1 M aq. NaH_2PO_4	[g]	[55]
[Cu-**4**]	GCE[e]	−0.84[f]	pH 9.2, 0.1 M aq. NaH_2PO_4	[g]	[59]
[Co-**4**]	GCE[e]	−1.04[f]	pH 9.2, 0.1 M aq. NaH_2PO_4	[g]	[59]
[Zn-**1**]	P(VP-St)[a]/BPG[b]	−0.9[c]	pH 1.0, 0.1 M aq. NaH_2PO_4/H_3PO_4	2.92×10^4 h^{-1}	[47]
[Zn-**1**]	Nf[d]/BPG[b]	−0.9[c]	pH 1.0, 0.1 M aq. NaH_2PO_4/H_3PO_4	4.33×10^4 h^{-1}	[47]
[Co-**5**]	GCE[e]/epc[c,h]	−0.98[f]	pH 2.4, 0.1 M aq. NaH_2PO_4/H_3PO_4	[g]	[57]
[Co-**5**]	GCE[e]/dc[o]	[g]	pH 2.4, 0.1 M aq. NaH_2PO_4/H_3PO_4	[g]	[57]
[Co-**5**]	GCE[e]/sc[p]	[g]	pH 2.4, 0.1 M aq. NaH_2PO_4/H_3PO_4	[g]	[57]
[Ti-**6a**]	Nf[d]/GCE[e]	[g]	pH 3.4, 5.6, 10, 0.1 M aq. NaH_2PO_4	[g]	[61]
[Co-**7**]	Nf[d]/ITO[i]	−0.45[f]	pH 1.4, 0.1 M aq. $NaCl/NaH_2PO_4/H_3PO_4$	20.1[j]	[39]
[Co-**7**]	Nf[d]/ITO[i]	−0.50[f]	pH 2.2, 0.1 M aq. $NaCl/NaH_2PO_4/H_3PO_4$	39.9[j]	[39]
[Co-**7**]	Nf[d]/ITO[i]	−0.54[f]	pH 4.0, 0.1 M aq. $NaCl/NaH_2PO_4/H_3PO_4$	31.5[j]	[39]
[Co-**7**]	Nf[d]/ITO[i]	−0.58[f]	pH 7.2, 0.1 M aq. $NaCl/NaH_2PO_4$	6.18[j]	[39]
[Co-**7**]	Nf[d]/ITO[i]	−0.60[f]	pH 10.3, 0.1 M aq. $NaCl/NaH_2PO_4$	34.2[j]	[39]
[Co-**8**]	Nf[d]/Pt	−0.3[c]	pH 1.0, 0.1 M aq. NaH_2PO_4/H_3PO_4	2.3×10^2 h^{-1}	[67]
[Co-**8**]	Nf[d]/BPG[b]	−0.7[c]	pH 1.0, 0.1 M aq. NaH_2PO_4/H_3PO_4	70 h^{-1}	[67]
[Mn-**8**]	Nf[d]/Pt	−0.8[c]	pH 1.0, 0.1 M aq. NaH_2PO_4/H_3PO_4	[g]	[66]
[Fe-**8**]	Nf[d]/Pt	−0.8[c]	pH 1.0, 0.1 M aq. NaH_2PO_4/H_3PO_4	[g]	[66]
[M-**8**]	Nf[d]/BPG[b]	−0.8[c]	pH 1.0, 0.1 M aq. NaH_2PO_4/H_3PO_4	5×10^2 h^{-1}	[66]
[Zn-**8**]	PVP[k]/Pt	−0.4[l]	pH 4.4, 0.1 M aq. NaH_2PO_4/H_3PO_4	[g]	[68a]
[Zn-**8**]	Nf[d]/Pt	−0.25[c]	pH 1.01, 0.1 M aq. NaH_2PO_4/H_3PO_4	[g]	[68b]
[Fe-**8**]	Gold disk	−1.56[f]	DMF, 0.1 M Et_4NClO_4	[g]	[63a]
[Rh-**8**]	Gold disk	−1.56[c,f]	DMSO, 0.1 M Et_4NClO_4, 20 mM CF_3CO_2H	[g]	[68b]
[Fe-**36**]	Pt	−0.8[c]	pH 1.35, 0.05 M aq. KCl	67 h^{-1}	[87]
[Co-**9**]	Nf[d]/BPG[b]	−1.1[c]	pH 2.9, DMA:H_2O, 1 mM $NaClO_4$	13.9 h^{-1}	[76]
[Co-**9**]	Nf[d]/BPG[b]	−1.45[c]	pH 7.0, DMA:H_2O, 1 mM $NaClO_4$	20.7 h^{-1}	[76]
[Co-**12**]	Nf[d]/GCE[e]	−0.61[f]	0–20 mM $HClO_4$, 0.1 M TBAP/ACN	[g]	[82]
[Co-**13**]	Nf[d]/GCE[e]	[g]	[g]	[g]	[82]
[Ni-**12**]	Nf[d]/GCE[e]	−0.76[f]	0–20 mM $HClO_4$, 0.1 M TBAP/DMF	[g]	[82]
[Ni-**13**]	Nf[d]/GCE[e]	−0.46[f]	0–20 mM $HClO_4$, 0.1 M TBAP/DMF	[g]	[82]
[Co-**14,15**]	GCE[e]	−0.51[f]	0.1 M $[^nBu_4N][ClO_4]$, CH_3CN, $TsOH{\cdot}H_2O$	[g]	[83]
[Co-**14,15**]	GCE[e]	−0.16[f]	0.1 M $[^nBu_4N][ClO_4]$, CH_3CN, $TsOH{\cdot}H_2O$		[83]
[Co-**16**]	[g]	[g]	[g]	[g]	[83]
[Co-**34,35**]	GCE[e]	−1.0[c]	pH 2–7, 0.1 M aq. NaH_2PO_4/Na_2HPO_4	[g]	[86]
[Co-**17**]	GCE[e]	−0.55[c]	0.1 M Bu_4NClO_4 ACN, $TsOH{\cdot}H_2O$	[g]	[84]
[Co-**17–26**]	ITO[i]	[g]	0.1 M Bu_4NClO_4, $TsOH{\cdot}H_2O$, ACN	[g]	[84]
[Co-**27**]	Graphite rod[n]	−0.78[n]	50 mM p-$CN(C_6H_4)NH_3(BF)_4$, 0.1 M Bu_4NClO_4 ACN	40/(3 h)	[85]
[Co-**28**]	Graphite rod[n]	[g]	[g]	[g]	[85]
[Co-**29**]	Graphite rod[n]	−0.82[m]	50 mM p-$CN(C_6H_4)NH_3(BF)_4$, 0.1 M Bu_4NClO_4 ACN	20/(3 h)	[85]
[Co-**30**]	Graphite rod[n]	−0.92[m]	50 mM p-$CN(C_6H_4)NH_3(BF)_4$, 0.1 M Bu_4NClO_4 ACN	50/(3 h)	[85]
[Ni-**31**]	Graphite rod[n]	−1.54[m]	50 mM Et_3NHCl, 0.1 M Bu_4NClO_4 ACN	7/(3 h)	[85]
[Ni-**32**]	Graphite rod[n]	−1.1[m]	50 mM p-$CN(C_6H_4)NH_3(BF)_4$, 0.1 M Bu_4NClO_4 ACN	20/(3 h)	[85]
[Ni-**33**]	Graphite rod[n]	−0.95[m]	50 mM p-$CN(C_6H_4)NH_3(BF)_4$, 0.1 M Bu_4NClO_4 ACN	4/(3 h)	[85]
[**37**]	BPG[b]	−0.8[c]	pH 1.5, 0.1 M aq. NaH_2PO_4/H_3PO_4	5.1×10^{-2} h^{-1}	[88]
[**37**]	BPG[b]	−0.8[c]	pH 1.5, 0.1 M aq. NaCl/HCl	2.1×10^{-3} h^{-1}	[88]
[**38**]	BPG[b]	−0.6[c]	pH 1.0, 0.1 M aq. NaH_2PO_4/H_3PO_4	1.8×10^2 h^{-1}	[89]
[Pt-**10**]	Nf[d]/ITO[i]	−0.6[c]	pH 1.0, 0.1 M aq. NaH_2PO_4/H_3PO_4	6.0×10^3 h^{-1}	[80]
[Pt-**10**]	ITO[i]/Nf[d]	−0.95[c]	pH 5.9, 0.1 M aq. NaH_2PO_4/H_3PO_4	238.3 h^{-1}	[81]
[Pt-**11**]	ITO[i]/Nf[d]	−0.95[c]	pH 5.9, 0.1 M aq. NaH_2PO_4/H_3PO_4	55.2 h^{-1}	[81]

[a] P(VP-St) = poly(4-vinylpyridine-co-styrene).
[b] Basal pyrolytic graphite.
[c] Potentiostatic electrolysis
[d] Nafion®.
[e] Glassy carbon electrode.
[f] Calculated from published data vs. SCE.
[g] Not given.
[h] Electropolymerization technique.
[i] Indium titanium oxide.
[j] Calculated by subtracting the amount of hydrogen evolved on an ITO/Nf® electrode to the amount evolved on ITO/Nf®/CoPc, no indication of length of time TON has been calculated for.
[k] Poly(4-vinylpyridine).
[l] Potential at which photocurrent is observed.
[m] Calculated from published data vs. Ferrocene Fc^+/Fc^0.
[n] Graphite rod electrode.
[o] Dip cast.
[p] Spin coat.

Table 2
Comparison of reported experimental details and hydrogen generation TON's for the electrocatalysts discussed.

Comp. no.	Electrode/E[a]	Potential (V) vs. Ag/AgCl[b]	Solvent system	Major CO_2 reduction products (% efficiency)	Selectivity vs. H_2[c]	TON[d] (time, where indicated)	Ref.
[Co-**1**]	BPG	−1.06	0.1 M aqueous phosphate buffer (pH 2.3)	CO (29.6%)	0.42	6.01×10^4 (2 h)	[20]
[Co-**1**]	PVP/BPG	−1.06	0.1 M aqueous phosphate buffer (pH 2.3)	CO (49.5%)	0.98	1.31×10^6 (2 h)	[20]
[Co-**1**]	BPG	−1.16	0.1 M aqueous phosphate buffer (pH 4.4)	CO (50.7%)	2.29	1.27×10^4 (2 h)	[20]
[Co-**1**]	PVP/BPG	−1.16	0.1 M aqueous phosphate buffer (pH 4.4)	CO (71.6%)	3.41	2.94×10^5 (2 h)	[20]
[Co-**1**]	BPG	−1.26	0.1 M aqueous phosphate buffer (pH 6.8)	CO (55.3%)	2.28	3.07×10^4 (2 h)	[20]
[Co-**1**]	PVP/BPG	−1.26	0.1 M aqueous phosphate buffer (pH 6.8)	CO (77.2%)	4.65	3.66×10^5 (2 h)	[20]
[Co-**1**]	Carbon cloth	−1.11	0.05 M aqueous citrate buffer pH 5	CO 52%[f]	1.5	3.7×10^5	[103]
[Co-**2**]	BPG	−1.20	0.1 M aqueous phosphate buffer (pH 9.3)		9.5	6.0×10^4 (1 h)	[102]
[Co-**2**]	BPG	−1.15	0.1 M aqueous phosphate buffer (pH 4.4)		5.5		[102]
[Co-**2**]	PVP/BPG	−1.15	0.1 M aqueous phosphate buffer (pH 4.4)		0.75		[102]
[Co-**39**]	BPG	−1.30	Aqueous buffer pH 4.4		4.20	1.1×10^6 (1 h)	[101]
[Co-**39**]	PVP/BPG	−1.30	Aqueous buffer pH 4.4		0.49	1×10^5 (1 h)	[101]
[Co-**1**]	Graphite	−1.16 to −1.36	0.1 M $KHCO_3$	$HCOO^-$ (60%); CH_3OH (5% at pH 3)			[104]
[Cu-**40**]	Graphite	−1.80	0.1% $KHCO_3$, 0.1 M Bu_4NBF_4/MeOH	CO (1%); CH_4 (17.5%); $HCOOCH_3$ (37.5%)[g]			[106]
[Cu-**40**]	Graphite	−2.50	0.1% $KHCO_3$, 0.1 M Bu_4NBF_4/MeOH	CO (1%); CH_4 (27%); $HCOOCH_3$ (35%)[g]			[106]
[Lu-(**1**)$_2$]	Graphite	−1.20	0.1% $KHCO_3$, 0.1 M Bu_4NBF_4/MeOH	CO (12.5%); $HCOOCH_3$ (36%)[g]			[106]
[Lu-(**1**)$_2$]	Graphite	−2.50	0.1% $KHCO_3$, 0.1 M Bu_4NBF_4/MeOH	CO (9%); CH_4 (1%); $HCOOCH_3$ (47.5%)[g]			[106]
[Dy-(**1**)$_2$]	Graphite	−2.50	0.1% $KHCO_3$, 0.1 M Bu_4NBF_4/MeOH	CO (9%); CH_4 (1.4%); $HCOOCH_3$ (47.5%)[g]			[106]
[Lu-(**1**)]	Graphite	−2.50	0.1% $KHCO_3$, 0.1 M Bu_4NBF_4/MeOH	CO (9%); CH_4 (4%); $HCOOCH_3$ (42.5%)[g]			[106]
[Lu-(**42**)$_2$]	Graphite	−2.50	0.1% $KHCO_3$, 0.1 M Bu_4NBF_4/MeOH	CO (5%); CH_4 (2%); $HCOOCH_3$ (27.5%)[g]			[106]
[Cu-**41**]	Graphite	−1.60	0.1% $KHCO_3$, 0.1 M Bu_4NBF_4/MeOH	CO (2.5%); CH_4 (0.3%); $HCOOCH_3$ (40%)[g]			[106]
[Cu-**41**]	Graphite	−2.10	0.1% $KHCO_3$, 0.1 M Bu_4NBF_4/MeOH	CO (7%); CH_4 (0.3%); $HCOOCH_3$ (35%)[g]			[106]
Poly[Cu-**41**]	Graphite	−1.10	0.1% $KHCO_3$, 0.1 M Bu_4NBF_4/MeOH	CO (4%); $HCOOCH_3$ (55%)[g]			[106]
Poly[Cu-**41**]	Graphite	−1.50	0.1% $KHCO_3$, 0.1 M Bu_4NBF_4/MeOH	CO (59%); CH_4 (1.5%); $HCOOCH_3$ (27.5%)[g]			[106]
Poly[Cu-**41**]	Graphite	−2.00	0.1% $KHCO_3$, 0.1 M Bu_4NBF_4/MeOH	CO (31%); CH_4 (3%); $HCOOCH_3$ (22.5%)[g]			[106]
[Co-**1**]	PTFE GDE	−1.46	Na_2SO_4 in aqueous H_2SO_4 (pH 2)	CO 100%[h]	7.1		[107]
[Mn-**1**]	PTFE GDE	−1.96	Na_2SO_4 in aqueous H_2SO_4 (pH 2)	HCOOH 26%;			[107]
[Cu-**1**]	PTFE GDE	Not indicated	Na_2SO_4 in aqueous H_2SO_4 (pH 2)	HCOOH 13–38%			[107]
[Zn-**1**]	PTFE GDE	Not indicated	Na_2SO_4 in aqueous H_2SO_4 (pH 2)	HCOOH 5%			[107]
[Co-**1**]	GDE/ACF	−1.41	0.5 M aqueous $KHCO_3$	CO (72%)			[108]
[Cu-**1**]	GDE/ACF	−1.36	0.5 M aqueous $KHCO_3$	CO (66%)			[108]
[Co-**40**]	GDE/ACF	−1.36	0.5 M aqueous $KHCO_3$	CO (39%)			[108]
[Cu-**40**]	GDE/ACF	−1.36	0.5 M aqueous $KHCO_3$	CO (35%)			[108]
[Co-**43**]	GDE/ACF	−1.35	0.5 M aqueous $KHCO_3$	CO (70%)			[108]
[Cu-**40**]	GDE/AC	Not indicated	0.5 M aqueous $KHCO_3$	CO (82%)			[108]
[Co-**43**]	GDE/AC	Not indicated	0.5 M aqueous $KHCO_3$	CO (79%)			[108]
[Co-**1**]	GDE	−2.14	0.5 M aqueous $KHCO_3$ (pH 7.6)	CO (95%)			[110]
[Ni-**1**]	GDE	−2.14	0.5 M aqueous $KHCO_3$ (pH 7.6)	CO (93%)			[110]
[Sn-**1**]	GDE	−2.24	0.5 M aqueous $KHCO_3$ (pH 7.6)	CO (5%); HCOOH (70%)			[110]
[In-**1**]	GDE	−2.64	0.5 M aqueous $KHCO_3$ (pH 7.6)	CO (10%); HCOOH (25%)			[110]
[Pb-**1**]	GDE	−2.28	0.5 M aqueous $KHCO_3$ (pH 7.6)	CO (5%); HCOOH (65%)			[110]
[Cu-**1**]	GDE	−2.24	0.5 M aqueous $KHCO_3$ (pH 7.6)	CO (15%); CH_4 (30%)			[110]
[Ga-**1**]	GDE	−3.24	0.5 M aqueous $KHCO_3$ (pH 7.6)	CO (5%); CH_4 (40%)			[110]
[Ti-**1**]	GDE	−2.64	0.5 M aqueous $KHCO_3$ (pH 7.6)	CO (20%); CH_4 (30%)			[110]
[Pd-**1**]	GDE	−2.14	0.5 M aqueous $KHCO_3$ (pH 7.6)	CO (80%)			[110]
[Fe-**1**]	GDE	−1.84	0.5 M aqueous $KHCO_3$ (pH 7.6)	CO (50%)			[110]
[Zn-**1**]	GDE	−2.54	0.5 M aqueous $KHCO_3$ (pH 7.6)	CO (15%)			[110]
[Al-**1**]	GDE	−2.44	0.5 M aqueous $KHCO_3$ (pH 7.6)	CO (5%); HCOOH (15%)			[110]
Poly-[Co-**45**]	GC	−1.00	Aqueous	HCOOH		7.9×10^4 (4 h)	[112]
[Co-**1**]	GC	−1.26	0.1 M aqueous phosphate buffer (pH 6.3)	CO (31%)			[113]

Table 2 (*Continued*)

Comp. no.	Electrode/E[a]	Potential (V) vs. Ag/AgCl[b]	Solvent system	Major CO_2 reduction products (% efficiency)	Selectivity vs. H_2[c]	TON[d] (time, where indicated)	Ref.
[Co-**46**]	GC	−1.26	0.1 M aqueous phosphate buffer (pH 6.3)	CO (25%)			[113]
[Co-**8**]	GC	−1.26	0.1 M aqueous phosphate buffer (pH 6.3)	CO (47%)			[113]
[Co-**43**]	GC	−1.26	0.1 M aqueous phosphate buffer (pH 6.3)	CO (39%)			[113]
[Co-**48**]	GC	−1.26	0.1 M aqueous phosphate buffer (pH 6.3)	CO (38%)			[113]
[Co-**49**]	GC	−1.26	0.1 M aqueous phosphate buffer (pH 6.3)	CO (33%)			[113]
[Co-**8**]	GC/4-NHCO-py-	−1.06	Aqueous phosphate buffer (pH 6)	CO 92%		1.1×10^7	[115]
[Co-**8**]	GC/4-NH_2-py	−1.16	Aqueous phosphate buffer (pH 6.86)	CO > 50%		1×10^5 (4 h)[j]	[118]
[Co-**8**]	GC/4-NH_2-py	−1.06	Aqueous phosphate buffer (pH 6.3)	CO 59%			[119]
[Co-**8**]	GC/4-NH_2-C_2H_4-py	−1.26	Aqueous phosphate buffer (pH 6.3)	CO 63%			[119]
[Co-**8**]	GC/im	−1.06	Aqueous phosphate buffer (pH 6.3)	CO 53%			[119]
[Co-**8**]	GDE	−0.96[e]	0.5 M aqueous $KHCO_3$	CO (97.3/75%); HCOOH (0.1/1.0%)[i]			[120]
[Ni-**8**]	GDE	Not indicated	0.5 M aqueous $KHCO_3$	CO (12.0/0.9%); HCOOH (6.1/0%)[i]			[120]
[Fe-**8**]	GDE	−1.01[e]	0.5 M aqueous $KHCO_3$	CO (80.9/42%); HCOOH (3.7/0%)[i]			[120]
[Zn-**8**]	GDE	−1.24[e]	0.5 M aqueous $KHCO_3$	CO (62.4/27.5%); HCOOH (3.4/0.7%)[i]			[120]
[Cu-**8**]	GDE	−1.34[e]	0.5 M aqueous $KHCO_3$	CO (27.1/8.9%); HCOOH (22.0/10.4%)[i]			[120]
[Mg-**8**]	GDE	Not indicated	0.5 M aqueous $KHCO_3$	CO (0/0%); HCOOH (1.6/0%)[i]			[120]
[Mn-**8**]	GDE	Not indicated	0.5 M aqueous $KHCO_3$	CO (0/0%); HCOOH (0.8/0%)[i]			[120]
[**8**]	GDE	Not indicated	0.5 M aqueous $KHCO_3$	CO (0/0%); HCOOH (3.2/0%)[i]			[120]
[Co-**9**]	BPG/Nf	−1.06	Phosphate bufffer (pH ~ 7)	HCOOH (51.4%)	4	11	[122]
Poly-[Co-**52**]	GC	−1.10	0.1 M $NaClO_4$	HCHO (39%)		1.1×10^4	[124]
Poly-[Fe-**52**]	GC	−1.08	0.1 M $NaClO_4$	HCHO (27%)		1.5×10^4	[124]
Poly-[Cr-**52**]	GC	−1.10	0.1 M $NaClO_4$	HCHO (87%)		6.1×10^3	[124]
Poly-[Rh-**54**]	Carbon felt	−1.26	5% H_2O/CH_3CN/0.1 M Bu_4NClO_4	CO (5%); $HCOO^-$ (22%)			[127]
[Re-**56**]	BPG/Nf	−1.26	Phosphate bufffer (pH ~ 7)	CO (16.5%); HCOOH (48.0%)	1.65	CO: 34; HCOOH: 98 (4.3 h)	[128]
[Re-**57**]	BPG/Nf	−1.56	Phosphate bufffer (pH ~ 7)	CO (trace); HCOOH (14.5%)	0.22	401 (3.2 h)	[128]
Poly-[Re-**58**]	Pt or GC	−1.51	CH_3CN/Bu_4NPF_6	CO (92.3%)		516 (1.3 h)	[129]
RuO_2	Pt/Nf, TiO_2 NT	−0.76	0.5 M $NaHCO_3$	CH_3OH (60.5%)			[132]
RuO_2	Pt/Nf, TiO_2 NP	−0.76	0.5 M $NaHCO_3$	CH_3OH (40.2%)			[132]
Poly-[Re-**60**]	Pt	−1.51	CH_3CN/0.1 M Bu_4NClO_4	CO (50%); CO_3^{2-} (50%)			[134]
Poly[Re-**61**]	Pt	−1.51	CH_3CN/0.1 M Bu_4NClO_4	CO (46%); CO_3^{2-} (54%)			[134]
Poly[Re-**62**]	Pt	−1.51	CH_3CN/0.1 M Bu_4NClO_4	CO (50%); CO_3^{2-} (50%)			[134]
[Ru-**65**]	Carbon felt	−1.21	5% H_2O/CH_3CN/0.1 M Bu_4NClO_4	CO (100%)			[136]
[Ru-**65**]	Carbon felt	−1.21	0.1 M $LiClO_4$	CO (97%)			[136]
[Ru-**69**]	Carbon felt	−1.25	5% H_2O/CH_3CN/0.1 M Bu_4NClO_4	CO (90%)			[136]
[Ru-**69**]	Carbon felt	−1.31	0.1 M $LiClO_4$	CO (80%)			[136]
[Ru-**65**]	Pt or VC	−1.17	Phosphate buffer + 0.1 M Na_2SO_4 (pH 9)	CO (94%); $HCOO^-$ (5%)			[137]
[Ru-**68**]	Pt or VC	−1.17	Phosphate buffer + 0.1 M Na_2SO_4 (pH 12)	CO (8%); $HCOO^-$ (90%)			[137]
ppy-[Ru-**69**]	Pt or VC	−1.17	Phosphate buffer + 0.1 M Na_2SO_4 (pH 12)	CO (90%); $HCOO^-$ (10%)			[137]
ppy-[Ru-**71**]	Pt or VC	−0.75	0.1 M $NaHCO_3$ + 0.5 M K_2SO_4	$HCOO^-$ (99%)			[137]
[Os-**65**]	Carbon felt	−1.18	0.1 M $LiClO_4$	CO (60%); $HCOO^-$ (10%)			[138]
[Fe-**83**]	Pt|PAn|PB dual film	−0.76	0.5 M KCl (pH 3)	Lactic acid (87.5%)			[147]
[Co-**84**]	Pt|PAn|PB dual film	−0.56	0.5 M KCl (pH 2)	Lactic acid (1.8%); C_2H_5OH (1.2%)			[148]

[a] BPG: basal plane pyrolitic graphite; PVP: polyvinylpyridine; GC: glassy carbon; PTFE: polytetrafluoroethylene; GDE: gas-diffusion electrode; ACF: activated carbon fiber; AC: activated carbon; Nf: Nafion®; PAn: polyaniline; PB: Prussian Blue; NT: nanotubes; NP: nanoparticles; VC: vitreous carbon.

[b] Electrolysis potentials. All potentials quoted relative to Ag/AgCl (sat'd KCl).

[c] Moles of reduced CO_2 products divided by moles of H_2.

[d] Time of electrolysis indicated in brackets, where provided by reference.

[e] Galvanostatic experiment.

[f] Calculated from the % efficiency figure for all gaseous products and selectivity figure, assuming only CO and H_2 are produced.

[g] Efficiencies were reported as ranges of values. Efficiencies indicated in table are average values.

[h] Total current efficiency reported was greater than 100%.

[i] Data for 20 atm CO_2/1 atm CO_2.

[j] Overall turnover number.

sustainable hydrogen production technology. As outlined above these modified electrodes do not need sacrificial donors, since the catalytically active states are regenerated by electron transfer at the electrode–film interface. In this area of research, MPc's have been investigated for many years employing different metal centers and various substituents on the Pc ring. The electronic/steric nature of the substituents can affect the redox chemistry of the Pc ring, which can influence the electrocatalytic activities of complexes involving these structures. Electron-withdrawing substituents tend to facilitate reduction of the complex (shift the reduction potential of MPc's to more positive values) while electron-donating groups generally lower the ease of their reduction [40]. The catalytic activity of these MPc's has been ascribed to the relative energy of the metal as metal *d* orbital energies may be positioned between the HOMO and the LUMO of the Pc ring [37,41–46]. This suggests the presence of possibly two different types of redox behavior. It is indeed observed in that while the first oxidation and first reduction processes occur at the central metal ion for MPc's where M denotes Mn, Fe and Co [46], Chebotareva reported that for MPc's containing Ni, Zn and Cu as the central metal ion, no redox processes take place at the inactive metal center [46]. Therefore, there is much interest in the modification of MPc's which considers the effects of various substituents and central metal ions on their electrochemical properties, as will be discussed in the present section and electrodes based on the materials will be used to introduce some important aspects of modified electrodes in general. The performance characteristics for all compounds discussed in this section are given in Table 1, including details on the electrolysis potentials applied and reaction conditions utilized for electrochemical hydrogen evolution, as well as TON (turnover number), when available.

Many different approaches have been used to prepare modified electrodes and many different immobilization techniques have been utilized in these studies. Importantly the catalytic performance figures will depend on the mode of immobilization, since electron transfer between the electrocatalysts and the substrate, and between the electrode and the electrocatalyst, will be dependent on the matrix used.

A number of studies have appeared concerning catalytically active systems that are incorporated in polymer matrices such as Nafion® (an anionic polymer) or cationic polymers like polyvinylpyridine co-styrene P(VP-St) [47]. Nafion® is a super-acid, a thermally stable and chemically inert polymer consisting of hydrophilic sulphonate groups and strongly hydrophobic fluorocarbons. Nafion® thus consists of distinct hydrophobic and hydrophilic regions [48]. P(VP-St) is a cationic polymer at low pH (pH < 2.5), is stable, and has hydrophobic properties. The presence of pyridine groups affords the possibility of axial coordination of the catalysts so transition metal complexes incorporated in this polymer are bound by stronger interactions than those found in a Nafion® matrix. Consequently, electron transfer is a slower process in this polymer [20]. It is thus expected that the electrochemical and electrocatalytic properties of MPc's may be affected by this binding.

The current efficiency of the electrocatalytic materials when immobilized in polymer layers on electrode surfaces will be dictated by electron transfer between the substrate and the underlying electrode surface and is mediated by the catalytic centers. There are three mechanisms by which electron transport in the polymer layer may be controlled. Depending on the experimental conditions and the nature of the polymer matrix used, the rate-determining step may be dictated by: (1) polymer movement (in cases where the catalytic centers are strongly bound to the polymer chain) or diffusion of the catalysts within the polymer (when interactions are not strong); (2) diffusion of the substrate and/or counter ions, or; (3) electron hopping [49]. Diffusion of the electrocatalysts in these polymer matrices is proposed to be faster than electron hopping and, therefore, is the most likely mechanism for the electrocatalytic processes [47,50,51]. This is due to the weak interaction of the polymer matrix and the complex. This type of electron transport mechanism is observed for Co(III)TPP/Co(II)TPP (TPP = tetraphenylporphyrin) incorporated in P(VP-St) and Nafion® [51] and also for MV^{2+}/MV^{+} in Nafion® (MV^{2+} = methyl viologen) [52]. Electron hopping is expected to be dominant for $[Ru(bpy)_3]^{3+}/[Ru(bpy)_3]^{2+}$ in Nafion® [53].

When reduction occurs within a polymer film, the charge on the reduced complex will be compensated. This may happen by one of two pathways: (1) by cation migration from the electrolyte solution into the polymer film or (2) by anion migration from the polymer matrix to the solution. This charge compensation also influences electron transport rate. In Nafion® the sulphonate anions are immobilized in the polymer and so charge migration takes place from the bulk electrolyte into the Nafion® film. In aqueous media, charge migration in the form of protons from the bulk solution balances the negative charge associated with the reduced catalytic species at the electrode surface, as protons have a higher mobility than any other cations in the film. Charge compensation in P(VP-St) occurs via proton migration from the bulk solution into the layer, a process that is more likely than the migration of bulky anions such as $H_2PO_4^-$ from the polymer layer to the bulk solution. However, positively charged ions may be prevented from moving into the polymer matrix by the protonated pyridines of the P(VP-St) matrix, resulting in a lower electron transfer rate [47].

Charge-transfer through a polymer film can be described by the apparent diffusion coefficient, D_{app}, assuming semi-infinite diffusion behavior, as defined by Cottrell's equation [54],

$$j = \frac{nFC\left(D_{app}\right)^{1/2}}{(\pi t)^{1/2}}$$

where j is the current density ($A\,cm^{-2}$), n is the electron stoichiometry, F is Faraday's constant ($96{,}485\,C\,mol^{-1}$), C is the catalyst concentration ($mol\,cm^{-3}$), and t is time (s). D_{app} values were obtained following a potential step from 0 V to −0.6 V vs. Ag/AgCl for an electrode modified with [Zn-**1**] embedded in a P(VP-St) matrix, denoted [Zn-**1**]/P(VP-St) and [Zn-**1**] incorporated in a Nafion® matrix, denoted [Zn-**1**]/Nafion® adsorbed on a BPG (basal plane pyrolytic graphite electrode). The D_{app} values calculated were almost independent of the concentration of MPc complex in the matrix, at low catalyst concentrations (<20 mM) [47]. Reported D_{app} values for [Zn-**1**]/Nafion® ($\sim 1.9 \times 10^{-8}\,cm^2\,s^{-1}$) were almost four times higher than those observed for [Zn-**1**]/P(VP-St) ($\sim 5.5 \times 10^{-9}\,cm^2\,s^{-1}$) due to the interaction of the redox complex with the polymer matrix and counterion migration. This behavior was also observed for [Co-**1**], [Co-**2**] and [Co-**3**] complexes incorporated in P(VP-St) [50]. The D_{app} values (calculated in a potential step from 0 V to −0.6 V vs. Ag/AgCl) were almost independent of complex concentration in the polymer matrix for [Co-**1**] and [Co-**2**], where concentrations ranged from 2.5 mM to 10 mM produced D_{app} from $\sim 21 \times 10^{-9}\,cm^2\,s^{-1}$ to $\sim 6.6 \times 10^{-9}\,cm^2\,s^{-1}$ respectively. However, for [Co-**3**], D_{app} values decreased with an increase of the complex concentration in the polymer matrix. The electron transfer rate is highly dependent upon the interaction between complex and matrix, with physical diffusion of the complexes ascribed as the mechanism of electron transfer for each of the three complexes. These D_{app} values which illustrate the rates of charge transport in through the catalytic layer highlight the importance of the choice of appropriate matrix for the electrochemical processes [50].

The electronic properties of ring substituents play a key role in the catalytic activity of the MPc towards hydrogen evolution. Many researchers have explored this idea, varying both the nature of the metal and the structure of the phthalocyanine ring. Kaneko et al. have reported the electrocatalytic properties of a series of

Co(II) phthalocyanines. [Co-**1**], [Co-**2**] and [Co-**3**] were incorporated in P(VP-St) polymer and adsorbed onto a BPG electrode. All three displayed electrocatalytic activity for hydrogen formation [50]. A commonly reported performance indicator that is used to describe catalyst activity is turnover number (TON), which, in these studies, reports the number of moles of product generated per mole of immobilized, electrochemically active catalyst over the duration of the experiment. TON figures suffer from several drawbacks. First, the amount of product is dependent on the electrolysis time. This may be offset by reporting the turnover frequency (TOF, or TON per unit time). However, non-linear product formation has been observed over time. For [Co-**1**] embedded in a P(VP-St) polymer matrix, a TON as high as 2×10^5 in 1 h for H_2 generation was observed under constant potential electrolyses at −0.9 V vs. Ag/AgCl in acidic phosphate buffer. This TON value is one of the highest values reported when compared with other molecular based catalysts. Upon substitution of [Co-**1**] with cyano- or sulphato- groups, the catalytic efficiency and D_{app} decreased in the order [Co-**1**] > [Co-**2**] > [Co-**3**]. This decrease in efficiency is also observed by the TON calculated for [Co-**2**] and [Co-**3**] as $5 \times 10^4\ h^{-1}$ and $\sim 1.2 \times 10^3\ h^{-1}$ under the same conditions as used for [Co-**1**]. This trend suggests that catalytic efficiency is dependent upon the rate of electron transfer within the matrix as discussed above. Another important factor to consider is the redox state that is responsible for proton reduction. For [Co-**1**] and [Co-**3**], it has been proposed that the second reduction wave catalyzes hydrogen formation, while for [Co-**2**] the third reduction is most likely involved, even though this complex displays the most positive Co(II)/(I) reduction of the three complexes. Clearly the nature of the functional groups on the Pc ring strongly affects catalytic efficiency which is reflected in the mechanism as discussed above and also in redox potentials observed for the compounds [50]. It is also worthwhile pointing out that for the [Zn-**1**] CMEs discussed above the redox process that catalyzes hydrogen formation is based on the ring and is not metal centered, as further discussed below.

It was initially assumed that redox-active metals are required to catalyze hydrogen evolution, however, ring-based mediation has been observed [43,47,55–59]. This shift in the nature of the redox state is related to the *d*-orbitals of the central metal ion. If the central metal has no available *d* orbital levels that lie between the HOMO and LUMO energy gap of Pc, the metal center is not involved when the complex is either oxidized or reduced implying that electrocatalytic steps are mediated by the phthalocyanine ring. Ni(II), Zn(II), Pb(II), Pd(II), and Cu(II) are metals which display this type of electrochemical behavior [41,43–45,47,55] while Mn(II), Fe(II) and Co(II) can experience metal-based reductions as well as ligand-based reductions [39,41,43–45,50,57,58,60]. In general, the more polarizing the central metal ion, the easier the reduction (i.e., less negative reduction potentials, thus less energy required) [43]. Koca investigated a range of copper complexes adsorbed on a GC working electrode. [Cu-**1**] exhibited ligand-based redox processes that efficiently catalyzed proton reduction to H_2 [55]. Koca reported that in acidic phosphate buffer for [Cu-**1**], a decrease in overpotential for H^+/H_2 was observed when compared against experiments using a bare GC electrode. (Catalyst concentration on the GC electrode was calculated as 2.5×10^{-9} mol per electrode surface.) This indicates that [Cu-**1**] physically adsorbed on an electrode surface can work as a catalyst for proton reduction. For a [Cu-**1**]/Nafion® modified GC electrode, a decrease in overpotential for H^+/H_2 was observed compared to the adsorbed catalyst (i.e. without a polymer) by almost 600 mV in phosphate buffer solution at pH 10.4. No TON was reported for this catalyst. When [Cu-**1**] was substituted with fluorophenoxy functional groups ([Cu-**4**]) and adsorbed onto a GC electrode (catalyst concentration 2.5×10^{-9} mol), higher electrocatalytic activity for proton reduction was observed than for the cobalt analogue, [Co-**4**]. While electrocatalytic activity begins at −1.27 V vs. Ag/AgCl for a bare GC electrode in aqueous phosphate buffer at pH 9.2, the onset potentials for the catalytic reduction of H^+ to H_2 (as indicated by the appearance of a sharp cathodic process) were −0.84 V and −1.04 V for [Cu-**4**] and [Co-**4**], respectively; however, no TON data were reported for these compounds [59].

Zhao et al. examined [Zn-**1**] embedded in Nafion® and [P(VP-St)] matrices adsorbed on BPG electrodes, which displayed ring-based redox processes that catalyzed hydrogen formation [47]. TON values reached 4.3×10^4 and 2.9×10^4 for [Zn-**1**]/Nafion® and [Zn-**1**]/P(VP-St), respectively, after a 1 h electrolysis at −0.9 V vs. Ag/AgCl with a catalyst/polymer concentration on the electrode surface calculated as 5×10^{-8} mol per electrode surface.

The Nernst equation for these processes reveals that the pH of the electrolyte solution plays an important role in the potential required for hydrogen evolution. For [Co-**1**], the electrocatalytic activity of the complex varies with increasing pH due to the different mechanistic pathways for interaction between protons and [Co-**1**] coated onto the surface of a GC electrode [50]. Formation of a proposed metal–hydride intermediate occurs after the first reduction of the complex which is dependent upon electron transfer rate and pH of the electrolyte. The effect of pH on the catalytic proton reduction for MPc's was investigated. Osmanbaş et al. have reported that in acidic media for [Co-**5**] adsorbed on a GC electrode, the electrocatalytic activity increases while in neutral conditions, the least electrocatalytic activity is observed [57]. The mechanism proposed suggests that in acidic media, the first step is the reduction of [Co(II)Pc(−2)] to $[Co(I)Pc(-2)]^-$, which is protonated to form a stable hydride complex [Co(I)Pc(−2)H]. Proton reduction occurs following a second protonation of the protonated, reduced species, [Co(I)Pc(−2)H], to yield molecular H_2 [57]. Thus in acidic conditions, [Co-**5**] can bind a proton firmly so electrocatalytic activity increases.

The pathway for [Co-**5**], described above, agrees with work carried out using titanyl phthalocyanines, as reported by Koca et al. for films on GC electrodes. At low pH, [Ti-**6a-c**] complexes are reduced to anionic forms, followed by protonation to form stable hydrides, which yield H_2 through a 1 proton, 1 e− sequence (ECCE mechanism overall) [61]. By increasing the pH to neutral conditions, the electrocatalytic activity of the complexes decreases. When the pH is made more basic for [Ti-**6b-c**], the potential difference between the reduced species $[M(II)Pc(-2)]/[M(I)Pc(-2)]^-$ and the proton reduction process increases. It is suggested that this difference may cause deprotonation of the hydride before its reduction can occur to evolve hydrogen. As a result, there is a decrease in electrocatalytic activity. For [Ti-**6a**] however, electrocatalytic activity increases in basic media. This increase may arise from the axially bound ligand. Upon reduction of [Ti-**6a**] to form $[Ti\text{-}\mathbf{6a}]^-$, protonation occurs to yield the hydride. This is followed by a second reduction and then successive protonation and reduction steps (ECECE overall), leading to the increase in catalytic activity. Hence at different pH's, the difference in electrocatalytic activity is due to the ability to (1) bind a proton and (2) form a stable metal–hydride intermediate.

Incorporation of [Ti-**6a-c**] in a Nafion® matrix adsorbed on a glassy carbon electrode surface yields an enhancement in electrocatalytic activity for [Ti-**6a**] and [Ti-**6b**] in neutral and acidic media. This observation suggests that the nature of the ring substituents along with the axial ligands for [Ti-**6a-c**] can affect the ability of the polymer/catalyst to bind a proton, and that the polymer matrix plays an important role in the electrocatalytic activity over a range of pHs.

For certain MPc complexes, different mechanisms to that described above have been reported. Koca et al. noted the effect of changing pH of the electrolyte buffer, for cobalt(II) tetratricarboxyethyl phthalocyanine, [Co-**7**], incorporated in a Nafion® film absorbed on the surface of an ITO working electrode. In acidic

conditions, the reduction potential of the Co(II)/Co(I) process is pH dependent until the electrolyte solution reaches a neutral pH. TONs reported for [Co-**7**] embedded in a Nafion® matrix were 20.1, 39.9 and 31.5 at pH 1.4, 2.2 and 4.0, respectively. (As these electrocatalytic experiments were carried out on an ITO electrode, the concentration of catalyst immobilized on the surface was not given.) At neutral pH (7.2), [Co-**7**] displayed poor activity for binding protons, reflected by the TON of 6.18. The reduction potential for [Co-**7**] is shifted negatively in basic media, yielding an increase in the electrocatalytic activity for proton reduction. At pH 10.3, a TON of 34.2 was reported for H_2 formation. The central metal ion influences electrocatalytic activity over a range of pH's with the formation of metal–hydride intermediates; however, it appears that proton reduction is also reliant upon the nature of the substituents in both acidic and basic conditions [39].

2.2. Metalloporphyrin-modified electrodes

Macrocyclic metalloporphyrin complexes are used for various applications such as phototherapeutic agents for treatment of cancer (PDT) [62] and as catalysts for the reduction of H^+ to H_2 in solution [63–65]. Research carried out by Kaneko et al. reported the electrocatalytic properties of various metal porphyrins [66–68]. Substitution of the porphyrin ring with a range of functional groups and using different central metal ions have revealed diverse electrocatalytic activities for the hydrogen evolution reaction. The natures of the substituent and central metal ion are crucial for this reaction to proceed.

[Co-**8**] incorporated in a Nafion® membrane and absorbed on a Pt working electrode was examined for hydrogen evolution [67]. This assembly acts as a catalyst in acidic conditions at potentials close to the theoretical redox potential of H^+/H_2 (−0.25 V vs. Ag/AgCl). [Co-**8**] immobilized in a Nafion® membrane displayed higher catalytic activity compared to [Co-**8**] immobilized directly on the bare Pt electrode (i.e. without the aid of polymer matrix). Hydrogen evolution occurred at potentials more positive than the bare Pt electrode in these studies. After a 1 h potentiostatic electrolysis at −0.3 V at pH 1, the TON reached 2.3×10^2. (The catalyst concentration on electrode surface was estimated to be 2×10^{-9} mol.) However, the values obtained were lower than those for [Co-**1**] (TON: 2×10^5; catalyst concentration: 1.25×10^{-8} mol per electrode surface) incorporated in P(VP-St) after 1 h [50]. The relatively high electrocatalytic activity of [Co-**8**]/Nafion® was assigned to the strongly acidic properties of Nafion®, where a high concentration of protons in the Nafion® membrane at pH 1 favors H_2 production [69]. As previously discussed for metal phthalocyanines, diffusion based electron transfer occurs for this system due to a weak interaction between the redox couple and the polymer matrix and as a result, electron transfer occurs faster than the electron-hopping mechanism [50]. For this complex, it is suggested that a bimolecular catalysis mechanism is responsible for the reduction of Co(II)-TPP to catalyze H_2. The formation of two intermediates was proposed; (1) metal–hydride formation (M–H) and (2) a phenyl group of the TPP substituents acts as an active site to form a protonated intermediate-complex due to cation (H^+)–π interaction.

[Mn-**8**] and [Fe-**8**] [66] complexes embedded in a Nafion® polymer and adsorbed onto a Pt working electrode are also active as catalysts, although they are less effective than [Co-**1**] [50]. Similar to the findings for [Co-**8**], proton reduction was observed for these complexes at more positive potentials (approx. 50 mV) than for the bare Pt electrode. A comparison of the amounts of H_2 produced after the potentiostatic electrolysis step for each of [M-**8**] incorporated into Nafion® and [M-**8**] films adsorbed directly onto the Pt electrode surface showed that the molecular based system embedded in Nafion® exhibited the highest electrocatalytic activity, 23.6 μL and 34.7 μL for [Mn-**8**] and [Fe-**8**] respectively. Thus the [M-**8**]/Nafion® system works as an efficient electrocatalyst for proton reduction. The TON reported for [M-**8**] was $5.0 \times 10^2\ h^{-1}$ at −0.8 V in pH 1 buffer solution with a catalyst concentration on the electrode surface of 1×10^{-8} mol cm^{-2}. For this complex, a bimolecular catalysis mechanism for electron transfer was considered, which involves a one-electron reduced catalyst species with the possible formation of two intermediates; (1) metal–hydride formation (M–H) and (2) formation of π–H^+ complex of a phenyl group of the TPP substituent. Importantly, Buttry and Anson reported the presence of Co-TPP in the hydrophobic region of the Nafion® [48] and this may suggest formation of the second intermediate. Choi et al. reported similar behavior for the [Fe-**8**] and [Mn-**8**] complexes [70].

Abe et al. investigated the effect of using light to enhance the electrocatalytic activity of [Zn-**8**] immobilized in a matrix and adsorbed on a Pt electrode. This modified electrode showed a photocurrent at a potential window below −0.4 V vs. Ag/AgCl when PVP as a polymer was employed at pH 4.4 [68a]. The coated amount of catalyst embedded in the PVP matrix on the Pt electrode was determined to be 1×10^{-7} mol cm^{-2}. [Zn-**8**] works as a photosensitizer in the visible region for photoinduced electron transfer [71–74]. These findings suggest that quenching of the singlet [Zn-**8**]* species to [Zn-**8**]$^-$ occurred by reduction of the Pt electrode. This reduced [Zn-**8**]$^-$ species was expected to mediate proton reduction to H_2. Nafion® was also used as a polymer for these electrocatalytic experiments using light [68b]. Potentiostatic electrolyses were carried out at −0.25 V vs. Ag/AgCl for 1 h in pH 1.01 aqueous solution. It was observed that photoinduced H_2 formation takes place efficiently for this system. The concentration of [Zn-**8**] incorporated in a Nafion® polymer was determined to be 1×10^{-8} mol cm^{-2}. Although no TON was reported, 19.6 μL of H_2 was obtained on electrolysis. Thus, these systems [Zn-**8**], when either PVP or Nafion® were employed as polymers, displayed photoelectrochemical H_2 production without employing an electron relay, while [Zn-**8**] acts as the sensitizer in the polymer membrane.

Electrocatalytic hydrogen generation in non-aqueous solvents displayed by metalloporphyrins will be briefly discussed. Collman et al. report the potential application of Ru and Os metalloporphyrins for electrocatalytic hydrogen evolution in solution [75]. Following the reduction of the metal center to form a metal hydride complex, these species formed octahedral complexes where an axially bound ligand resulted in a *trans*-binding to the hydride. Taguchi et al. propose a similar bimolecular catalysis mechanism for these Ru and Os-metalloporphyrins, compared to the [M-**8**] compound discussed above [66,67]. Cobalt hydrides have been suggested as intermediates in the catalysis of proton reduction to H_2, with hydrogen production proposed to occur via two parallel pathways. One route is the bimolecular reductive elimination of dihydrogen from two metal–hydrides. The second route involves protonation of a metal hydride resulting in elimination of molecular H_2 [75]. These pathways are in agreement with Kaneko's proposed routes for a bimolecular catalysis mechanism. Savéant reported metalloporphyrins in solution capable of reducing protons to H_2 following the reduction of the metal center. The reduction of Fe(II) porphyrin to Fe(0) [63a] in acidic solution is the species responsible for the catalytic H^+ reduction for [Fe-**8**], while Rh(III) hydrides in solution [63b] [Rh-**8**] at negative potentials allow for the electrocatalytic activity for hydrogen evolution in acidic conditions. It is proposed that hydride transfer from Rh(II)H^- to acid produces H_2. Similar to metal phthalocyanines, the nature of the substituents varies the properties of the porphyrins. Savéant reported that the absence/presence of axial ligands played a key role in the stability of the catalyst and the hydrogen evolution process. The reactivity of the Rh(II) hydride is dependent on the nature of the axial ligand and can be explained in terms of the electron density distribution of the rhodium metal and the hydrogen atoms bound to it. The nature of the axial ligand also affects the

stability of the Rh(II) porphyrin, which is attributed to the changes of electron density distribution within the porphyrin ring [63b].

2.3. Modified electrodes incorporating complexes having polypyridine-ligands

The incorporation of a bis(2,2′:6′2″-terpyridine) cobalt(II) complex [Co-**9**] in a Nafion® membrane adsorbed on a BPG yielded a modified electrode which showed catalytic activity towards the hydrogen evolution reaction [76]. In solution, cyclic voltammetry revealed a sharp growth of a catalytic current below −1.5 V vs. Ag/AgCl in 4:1 DMA:H_2O, indicative of proton reduction. In the absence of H_2O, the reversible redox couple Co(I)/Co(0) occurs at −1.51 V, thus it was postulated that electrocatalytic H^+ reduction can occur upon formation of the zero-valent Co(0) species. When [Co-**9**]/Nafion® is adsorbed to the surface of a BPG electrode, the behavior of these films displayed a dependence on the pH of the electrolyte solution employed. TON obtained after 1 h potentiostatic electrolysis at −1.0 V vs. Ag/AgCl in acidic conditions was 13.9. However, in more basic conditions, TON reached 20.7 after 1 h at −1.45 V vs. Ag/AgCl indicating a slight improvement in catalytic activity at higher pH. The average concentration of catalyst in the membrane was calculated as 1.3×10^{-8} mol per electrode surface. As the formal potential for H^+/H_2 at pH 3 is −0.37 V vs. Ag/AgCl, acidic conditions will in general produce reduced overpotentials for the formation of H_2. Under these conditions, catalytic H^+ reduction occurs after the reduction of Co(II)/Co(I)-hydride, as this metal–hydride acts as a reducing agent. When Co(II) was reduced to the Co(I) species at higher pH, Co(I) did not catalyze the reduction of H^+, as it was further reduced to Co(0). This intermediate forms a metal–hydride Co(0)–H, followed by the reduction of H^+ to molecular H_2 [76].

Platinum complexes have been investigated for their catalytic behavior. Polypyridyl Pt complexes have been used in photochemical proton reduction experiments with organic/inorganic semiconductors or sensitizers [77–79]. A range of polypyridyl Pt complexes has been studied for electrocatalytic proton reduction. Bis(2,2′-bipyridine) platinum (II) nitrate [Pt-**10**] incorporated in a Nafion® membrane adsorbed on a BPG electrode exhibited activity at potentials below −0.4 V vs. Ag/AgCl compared to that of a bare BPG under the same conditions [80]. Proton reduction occurred after the formation of a zero-valent Pt species, as indicated by XPS (X-ray photoelectron spectroscopy). Potentiostatic electrolysis was performed at −0.6 V vs. Ag/AgCl using this Pt-complex/polymer absorbed on an ITO electrode. The TON reported for $[Pt(bpy)_2]^{2+}$/Nafion® after 1 h was 6×10^3 in pH = 1.0 aqueous solution. The catalyst amount on the electrode surface was determined to be 4.6×10^{-9} mol per electrode surface.

Chloro(2,2′:6′,2″terpyridine)platinum(II) chloride [Pt-**11**] embedded in a Nafion® membrane has been examined as an electrocatalyst [81] and showed a TON of 55.2 h^{-1} when potentiostatic electrolysis was applied at −0.95 V vs. Ag/AgCl in pH 5.9 phosphate solution. However, these results are lower than observed for $[Pt(bpy)_2]^{2+}$ under the same conditions, which exhibited a TOF for H_2 evolution of 238.3 h^{-1}. The amount of catalyst employed for the electrolysis experiments were given as 0.31 M and 0.52 M for [Pt-**11**] and $[Pt(bpy)_2]^{2+}$ ([Pt-**10**]) respectively. The mechanism for catalytic H^+ reduction by this complex was proposed to be the reduced state of Pt-complex (zero-valent) which generates a catalytically active form.

2.4. Modified electrodes incorporating glyoxime-type complexes

Pantini et al. describe a study involving the glyoximes [Co-**12,13**] and [Ni-**12,13**] dispersed onto carbon black, which are plated to the surface of GC electrodes incorporated in a Nafion® film [82]. These were used as electrodes for the electrocatalytic proton reduction in aqueous acidic solution but no TONs are reported to indicate H_2 evolution performance. For these metal glyoximes proton reduction takes place as indicated by cyclic voltammetry, on the second reduction process assigned to Co(II)/Co(I) for Co-glyoxime [Co-**12**] at −0.61 V vs. Ag/AgCl in acetonitrile. The addition of increasing amounts of $HClO_4$ resulted in the appearance of larger currents at the redox potential of Co(II)/Co(I). For the Ni(II) complexes catalytic activity begins with the addition of increasing amounts of $HClO_4$, at the first Ni(II)/Ni(I) based reduction at −0.76 V and −0.46 V for [Ni-**12**] and [Ni-**13**], respectively in DMF. Concentrations of these metal glyoximes used for these experiments were given as 2 mM. To improve the catalytic activity of this system, Pantini suggests that modification of the ligands can result in a shift of the redox potential of the compound to more positive values.

Hu et al. report Co-macrocyclic diglyoximes [Co-**14–16**] which are electrocatalytically active in solution ($TsOH{\cdot}H_2O$/acetonitrile/DMF) at −0.51 V vs. Ag/AgCl requiring a low overpotential for H^+ to H_2 [83]. The concentrations of catalyst used in solution were 0.3 mM and 0.6 mM for [Co-**14**] and [Co-**15**] respectively. The catalytic activity was observed upon the addition of $TsOH{\cdot}H_2O$, close to the reduction of the redox couple Co(II)/Co(I), indicating that the metal center is involved in the reaction. Formation of a Co-hydride intermediate is thought to assist the catalytic activity for hydrogen evolution reaction. The potential for electrocatalytic formation of H_2 from the reduction of protons is close to the formal potential of the reduction of $TsOH{\cdot}H_2O$ in acetonitrile solution, $E^{\circ\prime}$ −0.19 V vs. Ag/AgCl.

Peters et al. also report a series of Co-tetraamines ([Co-**17,18**], Co-[**19–22**], and [Co-**23-26**]) as catalysts which show electrocatalytic activity for hydrogen evolution while adsorbed on ITO (chemisorbed for [Co-**25**]) and GC electrodes as modified surface electrodes [84]. These tetramine complexes (typical concentration of catalyst adsorbed on the electrode surface 1×10^{-9} mol cm^{-2} as calculated from the area under the cathodic peak by cyclic voltammetry), modified with carboxylic acid functionalities and BF_2 substituents, are active for hydrogen evolution reaction in aqueous solution at pH <4.5 with low overpotentials required. When the pH was lowered to 2 for [Co-**17**], the onset of the catalytic current occurred at −0.56 V vs. Ag/AgCl with an overpotential of 240 mV. Jacques et al. describe a series of cobalt dioxime complexes [Co-**27–30**] and nickel diimine complexes [Ni-**31–33**] which are electrocatalytically active in acidic non-aqueous solutions for H_2 production requiring low overpotentials [85]. Potentiostatic electrolysis was carried out using a graphite rod as a working electrode in a 0.1 M $TBABF_4$ acetonitrile solution containing 50 mM of [M-**27–33**] and 50 mM acid (see Table 1). Although TON reported after 3 h electrolysis was low (maximum TON for H_2 reached 50 for [Co-**30**]), Faradaic yields calculated were very efficient; 100% efficiency for H_2 evolution for [Co-**29**] and [Co-**30**]. Lower efficiencies were noted for Ni-based electrocatalysts (70–30%). Bernhardt and Jones have also employed metal–macrocyclic complexes for electrocatalytic proton reduction, using macrocyclic Co(III)-hexaamines [86]. These complexes, [Co-**34**] (*trans*) and [Co-**35**] (*cis*) electrocatalytically reduce H^+ to H_2 while reducing the overpotential for hydrogen evolution in aqueous phosphate solution. During the reaction, the reduced protons involve the re-oxidation of Co(II) to Co(III) at neutral pH, however the stability of such complexes is dependent upon pH and the coordination properties of the supporting electrolyte. No TON was reported for these complexes.

2.5. Modified electrodes incorporating miscellaneous transition metal complexes

Abe et al. report Prussian White [87] $K_4Fe^{II}{}_4[Fe^{II}(CN)_6]_3$ [Fe-**36**], a polynuclear iron–cyanide complex immobilized on a Pt working

electrode as an active catalyst for H^+ reduction. Prussian white produced a larger current compared to a bare Pt electrode at the theoretical potential of H^+/H_2 at −0.274 V vs. Ag/AgCl in pH 1.35 aqueous solution. The amount of H_2 produced for [Fe-**36**] was also greater than that produced by a bare Pt electrode; 6.35 μL and 0.23 μL, respectively. Thus, a TOF reaching 67 h^{-1} at −0.8 V vs. Ag/AgCl in acidic solution (pH 1.35) was achieved with a catalyst amount of 1.8×10^{-8} mol per electrode surface, as determined from cyclic voltammetry. It has been suggested that cyanide ions work as the active sites for proton reduction by coordinating protons, which are reduced to H_2. Abe et al. have investigated ruthenium purple denoted RP [Ru-**37**] (ferric ruthenocyanide) for use as an electrocatalyst adsorbed on a basal pyrolytic graphite (BPG) electrode [88]. Under acidic conditions (pH 1.5) using NaH_2PO_4 as an electrolyte, electrocatalytic H^+ reduction to H_2 was found to occur for a potentiostatic electrolysis carried out at −0.8 V vs. Ag/AgCl. A very low TON value was reported after 1 h (For this study, the amount of catalyst on the electrode surface was reported to be about the magnitude of a monolayer; 3.6×10^{-10} mol per electrode surface). As the redox potential of Fe(III)/Fe(II) occurs at +0.2 V vs. Ag/AgCl, this potential is more positive than that for redox potential of H^+/H_2 couple, thus RP must be reduced to allow for proton reduction to take place. It was observed that the electrocatalytic activity depended upon the nature of the electrolyte. This dependency is reflected by the TON, reaching only 2.1×10^{-3} after 1 h electrolysis at −0.8 V vs. Ag/AgCl when a solution of 0.1 M NaCl in HCl is employed as the electrolyte. A monolayer of 7.3×10^{-10} mol of catalyst was present on the electrode. It was concluded from these results that the sodium counter ion plays a key role in the electrocatalytic reduction of H^+ to H_2 as higher TON are achieved using sodium dihydrogen phosphate as an electrolyte solution.

Ruthenium Red ($[(NH_3)_5Ru^{III}\text{-}O\text{-}Ru^{IV}(NH_3)_4\text{-}O\text{-}Ru^{III}(NH_3)_5]Cl_6$) [Ru-**38**] incorporated in a Nafion® matrix adsorbed on a BPG electrode displayed catalytic activity for hydrogen evolution in pH 1 conditions with TON reaching 1.8×10^2 h^{-1} at −0.6 V potentiostatic electrolysis [89]. The amount of catalyst on the electrode surface was determined to be 6.3×10^{-9} mol per electrode surface. Catalysis of H^+ to H_2 was observed following the formation of a catalytically active species from [Ru-**38**] within a polymer matrix. Abe et al. postulate that this active species is formed after an irreversible second electrochemical reduction of the reduced complex (either $[Ru^{III}(NH_3)_5(H_2O)]^{3+}$ or $[Ru^{III}(NH_3)_4(H_2O)_2]^{3+}$) resulting in a zerovalent Ru(0) complex which facilitates the catalytic reduction.

Paunović et al. reported a series of nanostructured Co-based catalytic phases such as non-stoichiometric TiO_2 (Magneli or Ebonex®), Vulcan XC72, TiO_2 (anatase) and MWCNT (multi-walled carbon nanotubes) designed as new electrode material for hydrogen evolution [90–92]. The main criteria for these nanostructured catalytic phases are; (1) a surface area with excellent dispersion of these nanoscaled particles, (2) allow efficient electron transfer to ions involved in an electrochemical reaction by having a high electric conductivity, (3) desirable mechanical properties, (4) chemical stability and (5) improved intrinsic catalytic activity.

Magneli phases meet the criteria outlined above as they offer chemical stability and high electric conductivity, and thus are considered as attractive support material. The interaction of the Co-based catalyst within the support phases allows for an enhancement in the intrinsic catalytic activity. However, the low surface area of the Magneli phases is a disadvantage. It was shown that mechanical treating of these phases can lead to an improved catalytic surface area. Studies revealed that the optimum duration for this treatment was between 16 h and 20 h [92]. Shorter treatment resulted in larger phase sizes, leading to a decrease in catalytic activity. Although these nanostructured catalytic phases display catalytic activity, the activity is smaller compared to Co-based catalysts deposited on other support materials such as Vulcan XC72 [90], TiO_2 (anatase) and MWCNT (multi-walled carbon nanotubes) [91]. This activity can be related in terms of the overpotential required for H_2 evolution to occur. The Co-Magneli phase exhibits an overpotential of 365 mV at a current density of 60 mA/cm^2. This is the largest overpotential reported for these Co-based electrocatalysts incorporated in this range of support materials.

Co-based catalysts embedded within support materials as mentioned above were also investigated in conjunction with a second metal, Pt in a 4:1 weight ratio (Co:Pt) which was deposited on MWCNT with TiO_2 (anatase) as a substrate [91]. Paunović found that the addition of the Pt to the Co-based electrocatalysts affects the particle size of Pt, reducing it by almost three times from 11 nm to 4 nm. Efficiency of the system is enhanced with the addition of Pt. The overpotential required for a Co:Pt (4:1 ratio) based catalyst deposited on MWCNT with TiO_2 (anatase) with a current density of 60 mA/cm^2 is 135 mV. This potential is only 20 mV more negative than that for the Pt only based phase of 125 mV. Remarkably a reduction in the ratio to equal amounts (1:1) Co:Pt ratio displayed the lowest overpotential required of 115 mV. The aim of employing Co-based metal electrocatalysts is to replace Pt as an electrode material and this work shows that Pt use can at least be minimized. Thus, Co-based nanostructured catalysts embedded within the support materials can work as catalysts for hydrogen formation as indicated above. TONs were not reported here as a performance indicator for any of these nanostructured Co-based catalytic phases for hydrogen evolution.

Another metal-based nanostructure electrocatalyst was reported by Raoof et al. entailing a bimetallic Cu–Pt nanoparticle incorporated into a poly(8-hydroxyquinoline) matrix [93]. The preparation of the chemically modified electrode (CME) was carried out by electropolymerization of 8-hydroxyquinoline on a glassy carbon electrode (GC). The incorporation of the copper nanoparticles was carried out by immersion of the poly(8-hydroxyquinoline) modified electrode into a concentrated solution of copper (II) ions, followed by electrochemical reduction step at −0.9 V vs. SCE in order to obtain the desired electrocatalyst, denoted Cu/P(8-HQ)/M. The Cu/P(8-HQ)/M modified electrode showed a catalytic current in 0.1 M H_2SO_4 at approximately −0.7 V vs. SCE. Replacement of Cu nanoparticles occurs by an irreversible and spontaneous redox process in which Cu is oxidatively dissolved by a noble metal ion, Pt(IV) which is simultaneously reduced and deposited on the P(8-HQ)/M modified electrode, denoted Cu/Pt-P(8-HQ)/M. The catalytic active Cu/Pt-P(8-HQ)/M produced a large cathodic current at −0.23 V vs. SCE indicating the reduction of H^+ to H_2. (The Pt catalyst amount on the modified electrode surface was calculated as 1.5×10^{-9} mol per electrode surface). The potential at which this catalytic current occurred was at a more positive potential compared to both the bare GC electrode and the Cu/P(8-HQ)/M in 0.1 M H_2SO_4. These results indicate that this bimetallic Cu/Pt nanoparticle can be used as a convenient conducting substrate for the electrocatalysis of H^+ to H_2. This method for preparation may be applicable to other bimetallic nanoparticles based on Cu as catalyst.

3. Electrocatalytic reduction of CO_2

Carbon dioxide is a major contributor to climate change, and quantities of CO_2 in the earth's atmosphere have increased steadily since the industrial revolution by over 40% [94]. Despite a general awareness of this issue, and international political initiatives aimed at curbing the production of greenhouse gases, the major source of energy for industry continues to be fossil fuels. Furthermore, because emerging economic "superpowers" in Asia and India – two of the world's most populated regions – expect to rely heavily on petroleum and coal to meet their energy demands, it is conceivable that the problem will worsen significantly within the timeframe of the next generation.

The possibility of utilizing CO_2 as a feedstock for carbon-based fuels is very appealing [95,96]. Since CO_2 is one of the products of hydrocarbon combustion, ostensibly, there is an inexhaustible supply of this substance that would be available for reactions which could generate other, more useful carbon-containing compounds. Photosynthesis permits conversion of CO_2 and water to carbohydrates and O_2, with energy from sunlight. In combustion reactions, energy is obtained by virtue of the high bond enthalpies of the products. Because CO_2 is a very stable molecule, approaches aimed at the conversion of CO_2 to other chemical forms are faced with significant challenges.

The one-electron reduction potential for CO_2 reflects the high stability of this oxide:

$$CO_2 + e^- \rightarrow CO_2^- E^\circ = -1.9\,\text{V vs. NHE}$$

Depending on the solvent/electrolyte system, this value can be as low as −2.5 V. Proton-coupled electrochemical reactions, however, are possible at much less negative potentials (E° vs. SHE, pH 7):

$$CO_2 + 2H^+ + 2e^- \rightarrow CO + H_2O \quad E^\circ = -0.52\,\text{V}$$

$$CO_2 + 2H^+ + 2e^- \rightarrow HCO_2H \quad E^\circ = -0.61\,\text{V}$$

$$CO_2 + 4H^+ + 4e^- \rightarrow HCHO + H_2O \quad E^\circ = -0.48\,\text{V}$$

$$CO_2 + 6H^+ + 6e^- \rightarrow CH_3OH + H_2O \quad E^\circ = -0.38\,\text{V}$$

$$CO_2 + 8H^+ + 8e^- \rightarrow CH_4 + 2H_2O \quad E^\circ = -0.24\,\text{V}$$

Thus reduction of CO_2 to either CH_3OH or CH_4 is significantly more feasible, thermodynamically, than reduction of CO_2 to CO_2^- [97,98]. Methanol and methane are desirable targets in these reactions, since they can be directly utilized in existing technologies as high energy density fuels. However, the lower oxidation states of carbon in these substances are achieved through kinetically unfavorable pathways, as they require the transfer of six and eight electrons to each carbon center, respectively, along with chemical steps involving proton transfers. A further complication concerns competitive reduction of H^+ to H_2, which often occurs near the potentials required for CO_2 reduction. However, the use of non-aqueous, aprotic solvents for CO_2 reduction can suppress competitive H_2 formation (particularly in solvents like DMF or CH_3CN) and CO_2-solublity in these solvents is significantly higher than in water. The development of electrocatalysts which facilitate the transfer of multiple electrons (and protons) to CO_2 with minimum energy investments during selective transformations is thus a major goal in this area. A great variety of molecular electrocatalysts for CO_2 reduction have been reported, incorporating various metal centers and coordination spheres. For an extensive account of these homogeneous solution-based systems the reader is directed to Kubiak's recent review article [99].

3.1. Metal phthalocyanine-modified electrodes

Modified electrodes incorporating metal phthalocyanines have been studied by a number of research groups. Phthalocyanines may be deposited from solutions onto electrodes, forming aggregated systems which exhibit very low solubility in water. The most reactive metal phthalocyanines for CO_2 reduction are [Co-**1**] and its derivatives [20,100–102]. These systems have produced high turnover numbers for CO in electrocatalytic experiments under constant applied potentials. Because H^+ reduction is competitive with CO_2 reduction at the potentials studied, the pH was varied to influence the selectivity of CO/H_2, with better selectivities for CO being obtained (See Table 2) at higher solution pH (ca. 2:1 at pH 6.8 at an electrolysis potential of −1.16 V vs. Ag/AgCl), as expected, considering the Nernst equations that describe these reactions [20]. The mechanism proposed by Kaneko for CO_2 reduction for [Co-**1**], elucidated through the use of in situ potential step chronoamperospectroscopy (PSCAS) experiments, is believed to involve an intermediate, protonated form, $[Co(I)Pc(-3)H]^-$ (see Fig. 2). This complex is formed after one-electron reduction of Co(II)Pc(−2) to yield $[Co(I)Pc(-2)]^-$, followed by ring protonation and a second, one-electron reduction to yield $[Co(I)Pc(-3)H]^-$. The last species is nucleophilic enough to bind CO_2 in a catalytic cycle. After binding of CO_2 to the catalyst, another reduction (3rd reduction step) of this intermediate produces CO, regenerating the $1e^-$ reduced $[Co(I)Pc(-2)]^-$ species through an overall $2e^-$ reduction of CO_2 by the reduced intermediate. Although CO_2-reduction should be mediated by the metal center according to this scheme, proton reduction was suggested to occur at the protonated ring structure instead. A report by Lewis and Lieber concerning [Co-**1**] cited turnover numbers as high as 3.7×10^5 for CO in pH 5 solution at −1.11 V (vs. Ag/AgCl) for films of [Co-**1**] adsorbed on carbon cloth [103]. Additionally, trace quantities of $HCOO^-$ and $C_2O_4^{2-}$ were detected. Results obtained in the course of this work also implied that electrode-supported catalysts possessed greater stability during catalytic cycles than the homogeneous form.

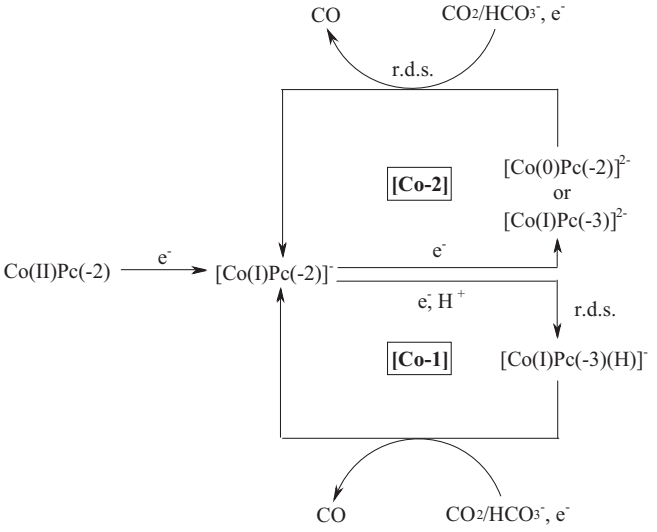

Fig. 2. Mechanisms for CO_2 reduction for [Co-**1**] (bottom) and [Co-**2**] (top). The label, "r.d.s." means rate-determining step for the catalytic cycle.
Adapted from ref. [102].

The cobalt octacyanophthalocyanine compound [Co-**2**], was also investigated and showed less negative electrolysis potentials, higher selectivity and improved Faradaic efficiency for CO formation compared to [Co-**1**] [102]. The positive shift in potentials required for CO_2 reduction for this complex can be attributed to the inductive effects of the electron-withdrawing CN groups. The CO/H_2 selectivity for adsorbed films of [Co-**2**] was around 9.5 at −1.20 V vs. Ag/AgCl in solutions with a pH of 9.3. At more negative potentials, H_2 evolution was favored and CO formation was suppressed, presumably because electrons are used for H^+ reduction at bare BPG surface positions, rather than for regenerating the catalytically active form of the complex. PSCAS experiments revealed that the rate-determining step for CO_2 reduction for this complex was different than that for unsubstituted [Co-**1**] and its octasubstituted derivative, [Co-**39**]. For [Co-**2**], the formation of the intermediate (CO_2-bound) complex was rate-determining, not the reduction of the $[Co(I)Pc(-2)]^-$ species, as was found for [Co-**1**] and [Co-**39**]. The expected mechanism of CO_2 reduction for [Co-**2**] is shown in Fig. 2.

Further work in this area was carried out on cobalt(II) octabutoxyphthalocyanine, [Co-**39**], a complex which possesses electron-donating n-butoxy substituents on the phthalocyanine ring structure [101]. For this complex, as expected, a more negative potential was required for the electrocatalytic reduction of CO_2 compared to the unsubstituted form, [Co-**1**]. However, turnover numbers of 10^6 were obtained at pH 4.4, with a CO/H_2 selectivity of ca. 4.2. The butoxy-substituents push the potential for the electrocatalytic reduction reaction to lower values and enhance the electron density at the cobalt center, thus improving the ability of [Co-**39**] to coordinate CO_2 relative to [Co-**1**] and [Co-**2**]. As above, it was found that more negative potentials favored H_2 evolution; however, [Co-**39**] remained more active for CO_2 reduction than [Co-**1**] at lower potentials. The authors proposed that the more basic [Co-**39**] was better at reducing CO_2 at these potentials due to the better donor properties of this complex.

Studies of [Co-**1**] supported in PVP matrices describe the effect of the polymer environment on CO_2 coordination and CO/H_2 selectivity [20,100–102]. PVP should serve as an electron-donor through its pyridine groups, acting as an axial ligand which enhances the electron density at the catalyst centers to facilitate CO_2 coordination. Also, because of the polymer's weakly basic properties, it should act as an H^+ supply line, provided the solution pH is comparable to/below the pK_a of PVP. Furthermore, CO_2 should exhibit a greater solubility in this material than in water through Lewis acid–base interactions. Thus, it should be possible to achieve better performance figures for CO_2 reduction with PVP-encapsulated catalysts. [Co-**1**] exhibited superior CO/H_2 selectivity and significantly higher turnover numbers in PVP films compared to adsorb films at similar pH values. At low pH, the selectivity was not as good, presumably because H_2 evolution occurred at faster rates than CO_2 reduction. For example, the maximum CO/H_2 selectivity for [Co-**1**] in PVP at pH 2.3 in CO_2-saturated phosphate buffer was ca. 1 (at −1.06 V vs. Ag/AgCl), while at pH 6.8 the maximum selectivity was almost 4.7 (at −1.26 V vs. Ag/AgCl). At pH 4.4, the maximum selectivity for the immobilized catalyst was ca. 3.4 at −1.16 V vs. Ag/AgCl. These results are impressive, considering the lower effective concentration of [Co-**1**] near the electrode surface (due to its dispersion in the polymer film) relative to neat films.

Hackerman et al. immobilized [Co-**1**] and [Ni-**1**] on carbon rod electrodes and used the resulting CMEs in CO_2 reduction experiments in aqueous solutions. $HCOO^-$ was found to be the major product for [Co-**1**] in solutions having a pH between 3 and 7 [104]. Methanol was produced with low efficiencies at films of [Co-**1**] in solutions having pH <4 (CH_3OH was produced with a 5% current efficiency at pH 3) which suggests that HCOOH is produced first under these conditions. When electrolyses were conducted for an extended period (72 h) at a current density of 1 mA/cm^2 in 0.1 M $NaHCO_3$, $HCOO^-$ was produced with 60% current efficiency. There is a lack of information concerning the electrolysis experiments and product analyses of this report which makes it difficult to gauge exactly how the % efficiency figures cited were determined.

A variety of metal phthalocyanines ([M-**1**], M = Co, Ni, Mn, Pd, Cu, and Fe) were studied in aqueous solutions of 0.1 M tetraalkylammonium salts as adsorbed films on graphite rods by Meshituka et al. [105]. For [Co-**1**] and [Ni-**1**], oxalic acid and glycolic acid were detected, but not HCOOH. [Mn-**1**] and [Pd-**1**] complexes were inactive, while [Cu-**1**] and [Fe-**1**] complexes displayed weak activity. In this work, the authors call attention to the fact that the doubly reduced forms of [Co-**1**] and [Ni-**1**] possess occupied d_z^2 orbitals and an excess of ligand π-electrons, while [Mn-**1**] and [Fe-**1**] (which displayed poor activity) do not, perhaps shedding light on the CO_2 coordination mode during catalytic reactions.

Magdesieva et al. utilized metal phthalocyanine-coated graphite rods to study the electrocatalytic reduction of CO_2, employing [Cu-**40**], [Cu-**41**] (monomeric and polymeric), [Lu-(**1**)-OAc], and the dimers, [Lu-(**1**)$_2$], [Dy-(**1**)$_2$], and [Lu-(**42**)$_2$] (Fig. 1) in order to study the effects of dimeric and polymer structures on CO_2 reduction [106]. The main product of the electrolyses, carried out in 0.1 M $LiClO_4/CH_3OH$, was $HCOOCH_3$; however, [Cu-**40**] produced CH_4 in significant quantities (32%). In stark contrast to [Cu-**40**], monomeric [Cu-**41**] and poly[Cu-**41**] did not produce significant quantities of CH_4. Instead, they produced $HCOOCH_3$ as a major product. Poly[Cu-**41**] produced CO in high yields at low potentials (−1.5 V and lower), and produced $HCOOCH_3$ at up to 60% efficiency at −1.1 V. Based on a comparison of the Cu complexes, it is clear that the phthalocyanine ring plays a major role in the reduction reaction. The t-butyl substituents of [Cu-**40**] make the reduced form of this complex a strong reducing agent. The complex can reduce CO_2 to its radical form, which can either be transformed to $HCOOCH_3$ or undergo further reaction to form CO. CO is strongly bound by the Cu center in this complex, making CO yields low, but enabling further reduction to CH_4. In the tetra-amino complex, [Cu-**41**], the strong donor substituents enhance both ring and metal-center electron density, thereby increasing the d_z^2 orbital energy high enough that its interaction with CO is no longer efficient. Because CO is not as strongly bound as for [Cu-**41**], it does not participate in further reductions and is released as CO. For the case of [Lu-(**42**)$_2$], the d-orbitals of the rare earth metal are low in energy and do not participate in bonding interactions. The catalytic process involves the phthalocyanine ring in this case, and produces $HCOOCH_3$ as a main product. The dimeric complexes impede interactions between CO_2 and the metal center. For these complexes, $HCOOCH_3$ was again the major electrolysis product.

Gas-diffusion electrodes were modified by metal phthalocyanines in order to exploit the microporous structure of these materials, generating substantial current densities in CO_2 reduction reactions. Mahmwood et al. modified PTFE-bonded gas-diffusion electrodes by coating them with carbon which had been impregnated with metal phthalocyanines, and used them for the reduction of CO_2 [107]. The products of these reactions were CO and H_2 or HCOOH and H_2, depending on the metal center. For the [Co-**1**] system, CO was obtained with good selectivity at a potential of −1.46 V vs. Ag/AgCl and a partial current density of 22 mA/cm^2 (H_2 at 3 mA/cm^2) in aqueous Na_2SO_4 at pH 2. At more negative potentials, higher current densities were achieved at the cost of lower CO selectivity. The high current densities reported in this work are a reflection of the high active surface areas of the electrodes. In some experiments, total current densities of ca. 140 mA/cm^2 were noted. For [Mn-**1**] phthalocyanine, HCOOH was produced at 26% efficiency at a potential of −1.96 V vs. Ag/AgCl (H_2: ca. 74%; no CO was produced). For [Cu-**1**] and [Zn-**1**], HCOOH was produced, along with the major product, H_2. The results indicate that the products of the electrolyses are highly dependent on the nature of the metal center in these complexes, and are not as dependent on the electronic properties of the ligand. For Mn, Cu, and Zn complexes, CO_2 is expected to be reduced through a reduced phthalocyanine radical anion. It is worth noting that the authors estimated partial current densities to calculate % efficiency figures for each experiment, and cite inaccuracies in the determination of these current densities to explain variations in the data. For example, a total current efficiency of 114% was reported in one case (see Table 2). Unfortunately, no experimental data were presented that show how these partial current densities were determined.

Magdesieva et al. modified gas-diffusion electrodes using [Co-**1**], [Cu-**1**], [Co-**40**], [Cu-**40**], and the cobalt porphyrin, [Co-**43**] [108]. The ligands were selected to study interactions with activated carbon fiber (ACF) gas-diffusion electrodes. This support is advantageous for CO_2 reduction studies because CO_2 exhibits strong adsorption tendencies in the nanospaces of ACF fibers, producing effective CO_2 pressures of over 20 mPa [109]. All catalysts were effective for CO_2 to CO reduction, with current efficiencies of higher

than 70% being observed. Curiously, it was found that the optimal range for CO production was similar for all complexes, regardless of ligand structure or metal center. The authors suggested that the benefits of the nanospace environment might be ineffective for these complexes because they are too bulky to adsorb within the pores of the ACF material. Generally, performance data for the bulky (t-Bu substituted) complexes was inferior to that found for the smaller complexes in the ACF supports. However, on activated carbon (AC), the performance of the bulkier, t-Bu-substituted complexes was good (ca. 80% efficiency for CO formation for [Cu-**40**]). For the smaller [M-**1**] complexes, the CO selectivity appeared to be relatively unaffected by the nature of the ligands and metal centers in the ACF environment.

Furuya and Matsui prepared [M-**1**]-impregnated gas-diffusion electrodes using 17 different transition metallophthalocyanine complexes [110]. The results showed that [Co-**1**] and [Ni-**1**] complexes displayed the highest activity for CO_2, generating CO as a product with near 100% current efficiency in each case. Other metal phthalocyanines were not as active. Sn, Pb, or In phthalocyanines (group IIIB or IVB metals) mainly yielded HCOOH and H_2, with the best current efficiency being ca. 70% for [Sn-**1**]. For Cu, Ga, and Ti phthalocyanines, CH_4 was a significant product, with current efficiencies of ca. 30–40% being observed; the main products were CO and H_2. For [Ga-**1**] and [Ti-**1**], significantly low potentials were required to reduce CO_2 (ca. −2 V or lower). Zn, Fe and Pd phthalocyanines yielded CO as a main product, but with low yields relative to Co and Ni forms. Mg, V, Pt, and Mn phthalocyanines yielded only H_2 in significant quantities.

Zhang et al. prepared rotating ring-disk modified electrodes involving the cationic phthalocyanine structure, [Co-**44**], coated by Nafion® films [111]. In this research, a Pt ring-edged pyrolytic graphite disk assembly provided a means of assessing the performance of the CO_2-to-CO reduction pathway. CO was detected as an adsorbed species on the Pt ring which could be stripped during scans to higher potentials (ca. +0.45 V vs. Ag/AgCl). The amount of adsorbed CO depended on the CO_2 concentration in the electrolysis solution, indicating that this approach can be used for the quantification of CO formation. CO_2 was studied in this manner over a concentration range of 1×10^{-4} M to 3.2×10^{-2} M.

Isaacs et al. polymerized [M-**45**] (M = Co, Ni, Fe) to obtain modified electrode surfaces that incorporated reactive phthalocyanine units [112]. The electrolysis products in these experiments were dependent on the identity of the metal center. For the polymeric Co system studied, HCOOH was produced exclusively at an applied potential of −0.96 V vs. Ag/AgCl (with no H_2), with a TON of 7.9×10^4 during the 1.5 h^{-1} electrolysis. No change in the electrochemical behavior was seen over a 10-day period for this system. The Ni polymer produced both HCOOH and HCHO in an approximate ratio of 2:1, while films incorporating Fe centers produced HCHO and H_2. Metal-free polymer films produced only H_2. Spectroelectrochemical experiments showed that for poly-[Co-**45**], reduction of CO_2 required both reduced metal centers and reduced ligands, while for poly-[Ni-**45**], CO_2 was reduced at potentials that corresponded to ligand reduction, offering an explanation for the different products obtained in electrolyses for these two metallopolymers.

3.2. Metalloporphyrin-modified electrodes

Glassy carbon electrode surfaces were modified with various cobalt macrocycles, including the phthalocyanines [Co-**1**] and [Co-**46**], the porphyrins [Co-**8**] and [Co-**43**], the oxamide [Co-**47**], and two varieties of vitamin B_{12}, [Co-**48**] and [Co-**49**], using —CONH-C_5H_4N tethers (C_5H_4N = 4-pyridyl) [113]. The pyridyl tethers were coordinated to the cobalt centers so as to anchor the complexes at the electrode surface. The modified electrodes were then used for electrocatalytic reduction of CO_2 in 0.1 M phosphate buffer (pH 6.3). In all cases except [Co-**47**] (which yielded only H_2), the reduction product was CO. [Co-**1**] and [Co-**46**] yielded the highest current densities, while the porphyrin systems exhibited the highest current efficiencies. The porphyrin complexes were predicted to undergo slow H_2 evolution reactions from a hydride intermediate, relative to competing steps that produced CO.

Ramirez et al. tethered the cobalt(II) tetrabenzoporphyrin, [Co-**50**], to electrode surfaces through coordination of the macrocycle to electrodes derivatized by 4-aminopyridine [114]. This produced an electrocatalyst for which the fifth cobalt coordination site was occupied by a pyridine ligand. This arrangement is quite interesting: acting as an electron-donor, the tether facilitates CO_2 coordination to cobalt through the *trans*-effect. The modified electrodes generated in this way were then boiled in DMF to encourage the formation of axially bonded macrocycles. Although no performance data were given, the electrochemical response of the catalyst in the presence of CO_2 indicated high catalytic activity with long-term stability.

[Co-**8**] was chemically bound to glassy carbon electrodes by 4-(pyridyl)-NH-CO-, 4-(pyridyl)-CH_2-NH-CO-, and 4-(piperidyl)-CH_2-NH-CO- groups and to SnO_2 electrodes with 4-(pyridyl)ethylsiloxane groups to catalyze the electroreduction of CO_2 in aqueous solutions [115–117]. Fixation of the complexes to the electrode surface was accomplished by coordination of the cobalt centers through chemically tethered pyridines (Fig. 3). The first of these modified electrodes produced CO with 92% current efficiency at −1.11 V vs. Ag/AgCl, and a TON = 10^7 (CO_2 reduction to CO); at lower potentials, H_2 evolution was the dominant process (assuming only $2e^-$ reduction processes) [115]. These electrodes were very stable, exhibiting negligible loss of electroactivity after 3 days when stored in CO_2-saturated phosphate buffer solutions. The binding group exerted an influence on the CO_2 reduction behavior, attributable to the basic properties of the links, with the more basic 4-(pyridyl)-CH_2-NH-CO- and 4-(piperidyl)-CH_2-NH-CO- groups pushing the CO-producing potentials to lower values where H_2 evolution is more competitive (and thus % efficiency for CO is less) [116]. For a siloxane-tethered Co(II)TPP complex, no CO_2 reduction was noted at potentials as low as −1.06 V, although significant changes in the cyclic voltammograms collected for this CME seemed to indicate axial bonding of CO_2 to the cobalt center, suggesting that CO_2 is too stable to undergo reduction once coordinated [117]. A mechanism for CO_2 reduction was proposed (Fig. 4).

In two other reports, Aramata et al. described electrode surfaces that were modified in a manner similar to that described above. In the first case, [Co-**8**] CMEs were made by immobilization of the metalloporphyrin onto chemically bound pyridine substituents [118]. Electrochemical reduction of CO_2 was believed to occur through a reduced form of [Co-**8**], since the CO_2 reduction wave coincided with the Co(II/I) process. Constant potential electrolyses at −1.16 V vs. Ag/AgCl yielded CO with 50% current efficiency (the balance of the current corresponding to H_2 evolution). Turnover numbers of 10^5 were obtained in 4 h, with no detectable decrease in the reduction current over that timeframe. Subsequent work concerned aminopyridyl radical cation bridged-[Co-**8**] catalysts, which were generated by the oxidation of aminopyridines (4-aminopyridine, 4-aminoethylpyridine, or imidazole) [119]. These electrodes catalyzed the reduction of CO_2 in an aqueous buffer (pH 6.3). Coordination of [Co-**8**] to the pyridine-modified surfaces resulted in a 120 mV negative shift of the Co(II/I) potential, in accordance with the higher electron density for this Co(II) center, following axial coordination of the pyridine substituent. Cyclic voltammograms collected for these films in the absence of CO_2 suggested the presence of a stacked [Co-**8**] motif, in which layers of the metalloporphyrin were piled upon the pyridine-bonded [Co-**8**]. Only the surface-bound complexes were capable of reducing

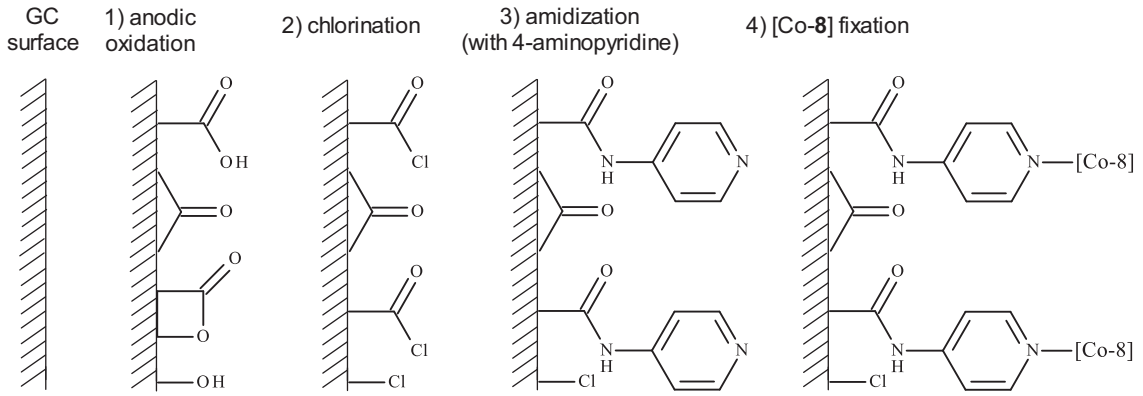

Fig. 3. Scheme for the derivatization of electrode surfaces through covalent tethers. Step 1, involves the oxidation of GC surface by holding the electrode at 2.5 V for 10 min; step 2, oxidized electrode surfaces were refluxed in $SOCl_2$ for 1 h; step 3, surface amidization was carried out by immersing the electrodes in an aminopyridine-saturated benzene solution at room temperature for 2 h (the electrodes were subsequently washed with benzene); step 4, derivatized electrodes were refluxed with 0.3 mM [Co-**8**] in 4:1 benzene/CH_2Cl_2 for 1 h and subsequently washed with water before use.
Adapted from ref. [115].

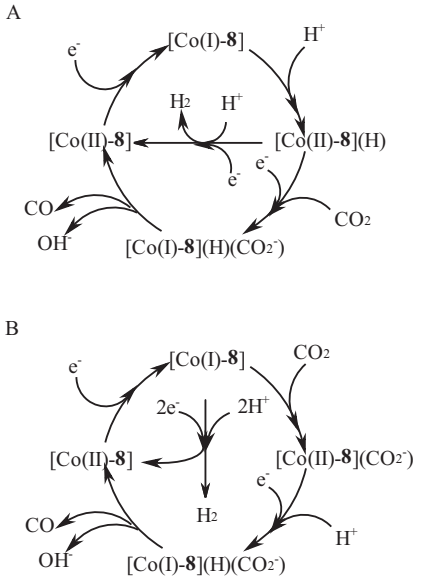

Fig. 4. Mechanism for CO_2 reduction using [Co-**8**] immobilized on glassy carbon electrode with a 4-pyridyl-NHCO-tether (A); for [Co-**8**] immobilized with either 4-pyridyl-CH_2-NHCO- or 4-piperidyl-CH_2-NHCO-tethers, or from evaporation of [Co-**8**] solution on the GC surface (B).
Adapted from ref. [116].

CO_2, which occurred through a hydride species [Co(II)-**8**](H). Only CO and H_2 were produced by the [Co-**8**] films.

Gas-diffusion electrodes impregnated with [M-**8**] (M = Co, Fe, Zn, Cu, Ni, and Mg) and H_2-tetraphenylporphyrin (H_2P) were compared in galvanostatic CO_2 reduction experiments under CO_2 at atmospheric pressure and 20 atm. At 1 atm, [Co-**8**] exhibited good CO selectivity in electrocatalytic reduction reactions, while [Fe-**8**] and [Zn-**8**] displayed moderate performance numbers [120]. The remaining metal porphyrins and H_2P (the metal-free macrocycle) displayed poor performance for CO production. At 20 atm, however, both [Co-**8**] and [Fe-**8**] displayed good selectivity (97% and 81%, respectively, for CO) while [Zn-**8**] also showed reasonably good performance (62% for CO). [Cu-**8**] showed modest CO selectivity, but also produced HCOOH (27% and 22%, respectively). CO_2 reduction potentials were observed to shift to less negative values under high CO_2 pressure. For [Co-**8**] and [Fe-**8**] complexes, the CO_2 wave in cyclic voltammetry experiments shifted to a potential that coincided with the M(I/0) process. For [Cu-**8**] and [Zn-**8**], this shift coincided with ligand-based reductions. It was thus inferred that [Co-**8**] and [Fe-**8**] reduced CO_2 at a [M(I)-**8**] center, while for [Cu-**8**] and [Zn-**8**], CO_2 reduction was expected to be mediated by reduced tetraphenylpyrrole ligands.

Riquelme et al. polymerized [Co-**51**] on glassy carbon electrodes and used the resulting modified surfaces as CO_2 reduction electrocatalysts in aqueous 0.1 M $LiClO_4$ [121]. The polymer-modified films produced CO and H_2 as major products, with small quantities of HCOOH also detected. The authors postulated that the rate-limiting step in the electrolysis was the Co(II/I) electron transfer process.

3.3. Modified electrodes incorporating complexes having polypyridine-ligands

[Co-**9**] immobilized in Nafion® exhibited good selectivity for HCOOH over H_2 in aqueous solutions at a potential of −1.06 V vs. Ag/AgCl (ca. 51% Faradaic efficiency, selectivity for CO_2/H^+ reduction = 4.0), as reported by Yoshida et al. [122]. HCOOH/H_2 selectivity was highly dependent on the applied potential, with H^+ reduction dominating at lower potentials. At a potential of −1.51 V vs. Ag/AgCl, H_2 was produced with 87% efficiency, while HCOOH was formed with only 4% efficiency at the same potential.

Abruña et al. electropolymerized [M-**9**, M-**52** and M-**53**] complexes of a range of transition metal centers (M = Cr, Fe, Co, Ni, Ru, and Os) yielding metallopolymer-coated glassy carbon electrodes that were used to reduce CO_2 in aqueous $NaClO_4$ [123–126]. The octahedral polymeric complexes present in these films contained two terdentate ligands, and partial de-coordination may have occurred during the reduction process to create a vacant site at the metal center. The metallopolymers produced HCHO, while no $HCOO^-$ or CO was detected [124]. Turnover numbers for the modified electrodes were high (up to 15,000, for poly-[Fe-**52**]). Poly-[Cr-**52**] exhibited the highest selectivity for HCHO, at 87%. Film thickness influenced reaction rates, with thinner films generally exhibiting faster reduction rates. It is likely that charge propagation through thicker films limits the rate of CO_2 reduction. Correlations were also drawn between catalyst activity and reduction potentials observed for the complexes under inert nitrogen atmospheres. Where there was good agreement between metal-based reduction waves and the potentials required for the complexes to reduce CO_2, high catalytic activity was observed, since reduced metal centers interact more favorably with Lewis acidic CO_2 (Fig. 5). Although the potential for the CO_2 reduction process mediated by poly-[Fe-**52**] does not coincide with the Fe-based

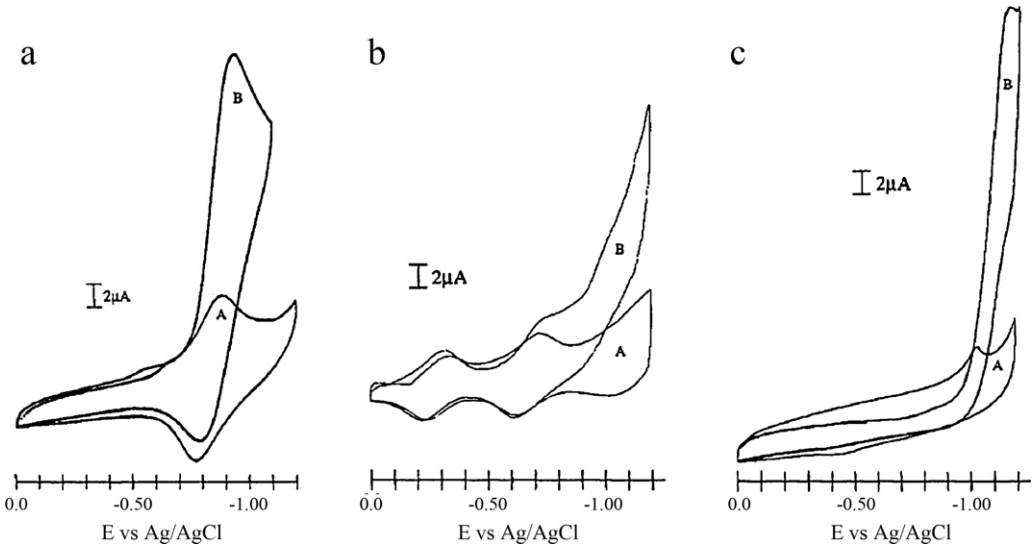

Fig. 5. Electrochemical reduction of CO_2 on electrodes modified with films of poly-[M-**52**], M = Co (**a**), Cr (**b**), Fe (**c**) under N_2 (curve "A") and CO_2 (curve "B") atmospheres in 0.10 M $NaClO_4$.
Adapted from ref. [124].

redox process, the activity for this CME is still high. However, for poly-[Fe-**52**], a ligand-based reduction coincides with the potential of the CO_2 process. It was postulated that interaction between the π^* ligand orbitals and e_g metal orbitals might also yield favorable interactions with CO_2. Complexes within the Fe, Ru, and Os grouping demonstrated the effect of row number on catalyst performance. The onset of CO_2 reduction occurred at more negative potentials along this series, reflecting of the relative stabilities of the complexes. Comparisons of [M-**52**] and [M-**53**] polymers suggested that the latter system exhibits better CO_2 reduction activity. The steric constraints introduced in polymers incorporating the 6-vinylpyridine substituent appeared to facilitate the creation of open coordination sites for CO_2 in poly-[Ru-**53**] compared to poly-[Ru-**52**], as evidenced by less negative reduction potentials under CO_2 atmosphere. Comparisons between thin-film behavior and solution-phase behavior were not direct, since the reduction product in DMF was mainly $HCOO^-$ ($2e^-$ product) rather than HCHO ($4e^-$ product).

In a separate study, Arana et al. polymerized complexes of the [M-**52**]-type (M = Fe, Ni, Co) and compared their performance in CO_2 reduction experiments in DMF/Bu_4NClO_4 with non-polymerized analogues [M-**9**] complexes in solution [123]. In general, it was observed that electrodes modified with the polymerized complexes demonstrated much higher activity in CO_2 reduction than the same catalysts in solution-phase experiments, as determined by the relative enhancements in the magnitudes of the reduction currents in the presence of CO_2 vs. those observed under a N_2 atmosphere. For poly-[Fe-**52**] and poly-[Co-**52**], a significant shift of the CO_2 reduction potential to less negative values was observed (700 mV shift for the Fe complex and ca. 1 V shift for the Co and Cr complexes relative to CO_2 reduction on a GC electrode). The superior performance exhibited by the modified electrodes was expected to be a result of the high concentration of catalyst centers in the film (e.g. cooperativity effects), and the data showed that the electrocatalytic behavior of the immobilized complexes (potentials for CO_2 reduction and the number of electrons transferred, gauged from complimentary work on O_2 reduction) was largely metal-center dependent.

Caix et al. also utilized this approach to form Ir(III) and Rh(III) polymer-supported catalysts for CO_2 reduction, using functionalized polypyrrole films on vitreous carbon electrodes [127]. For [Rh-**54**] (solution and polymer) the active species is a hydridocomplex, and studies of the effect of water concentration in this work showed that at about 20% H_2O/CH_3CN and at −1.36 V vs. Ag/AgCl, $HCOO^-$ was produced at close to 50% current efficiency in solution-phase experiments for [Rh-**54**]. (CO was formed at ca. 1% and H_2 at ca. 15% under these conditions.) The proposed mechanism for this catalyst is shown in Fig. 6. A $2e^-$ reduction of the chloro complex yields a hydrido form, which then undergoes $1e^-$ reduction and CO_2-insertion steps. This process competes with H_2 evolution (see Fig. 4). For these polymer films, both CO and H_2 were produced at higher efficiencies than in solution, under comparable conditions. The highest reported $HCOO^-$ efficiency was for a 5% H_2O/CH_3CN solution: $HCOO^-$ (22%); H_2 (60%); and CO (5%) at an applied potential of −1.26 V. The data obtained in constant potential electrolyses suggested that CO_2-insertion into Rh–hydride bonds in the polymer was hindered relative to solution-phase reactions. For the films of [Ir-**55**], $HCOO^-$ formation occurred to a lesser extent, at a maximum current efficiency of 5%.

Work by Yoshida et al. in this area involved Nafion®-supported [Re-**56**] and [Re-**57**] electrocatalysts for reduction of CO_2 in aqueous solutions [128]. Films of [Re-**56**]/Nafion® that were cast on basal plane pyrolytic graphite produced CO and HCOOH, with H_2 produced as a by-product. At −1.26 V vs. Ag/AgCl CO_2 reduction was

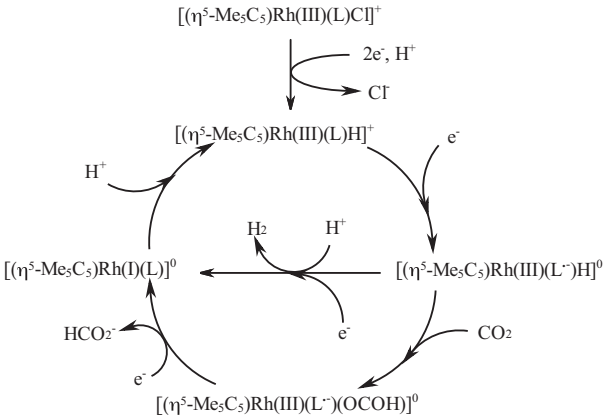

Fig. 6. Mechanism for CO_2 reduction by $[(\eta^5\text{-}Me_5C_5)Rh(III)(L)Cl](BF_4)$, [Rh-**54**], in poly-[Rh-**54**] film.
Adapted from ref. [127].

favored to H_2 evolution, but at lower potentials, H^+ reduction was more prominent. HCOOH was produced with 48% current efficiency at −1.26 V, while an efficiency of 28.5% for CO was found at −1.36 V. [Re-**56**] was more selective for HCOOH than CO at −1.26 V, but at lower potentials CO was favored. At a potential of −1.56 V, turnover numbers for HCOOH and CO were 401 and 0, respectively, in ca. 3.2 h for [Re-**57**].

O'Toole et al. were among the first to report on films of electropolymerized complexes of the [Re(bpy)$(CO)_3$Cl]-type compounds [129]. Films of poly-[Re-**58**] catalyzed CO_2 reduction to CO with ca. 92% efficiency; in an 80 min interval, a turnover number of 516 was recorded for this polymer, compared to 20–30 for a solution-phase experiment involving the non-polymerized analogue, over the same timeframe. However, the stability of the films in these experiments was not good. In subsequent work, modified electrodes involving complexes of this type were generated by co-polymerization with [Ru-**59**] [130]. Kinetic studies revealed that the rate-determining step depended strongly on film thickness. Kinetic data for thinner films exhibited a reliance on the rate of the reaction between reduced poly-[Re-**58**] and CO_2, while electrolysis rates for thicker films appeared to depend more on the rate of electron transport from the electrode, through the films, to the reaction sites. Thus catalyst performance was superior for thinner films. It was also observed that co-polymers exhibited better catalyst performance data, possibly due to a more open environment in the films created by the presence of dicationic ruthenium complexes and their counter ions.

Later, Cecchet et al. produced polymers of [Re-**58**] in mesoporous TiO_2 on a SnO_2 substrate, so as to enhance the accessible reaction surface sites and improve CO yields from electrochemical reduction of CO_2 [131]. Qu et al. accomplished a similar goal, using TiO_2 nanotubes and nanoparticles to load RuO_2 for support on Pt electrodes [132,133]. The performance of RuO_2 loaded on nanotubes/nanoparticles was superior to RuO_x on Pt, a consequence of the higher number of accessible reaction sites in the nanostructured materials. On TiO_2 nanotube structures, the Faradaic efficiency for CH_3OH production was 60.5%, roughly double what was reported for RuO_x on Pt [132].

Cosnier et al. used an alternative approach to polymerization of [Re(bpy)$(CO)_3$Cl]-type complexes, in which pyrrole-containing bipyridine ligands (rather than vinyl-substituted ones) were used [134]. With this polymerizable group, a series of complexes, [Re-**60**–**64**], were obtained via anodic deposition, producing conjugated polypyrrole linkages that joined the catalysts sites together. In this study, all complexes underwent electropolymerization; however, only poly-[Re-**60**–**62**] catalyzed the electrochemical reduction of CO_2. [Re-**63**] and [Re-**64**] both possess ester linkers rather than aliphatic ones present in [Re-**60**] and [Re-**61**], which connect the bipyridine chelating unit to the polymerizable pyrrole ring. The stability of the polymers was investigated with cyclic voltammetry experiments and the results indicate that poly-[Re-**63**] and poly-[Re-**64**] were most stable. This is most likely due to the presence of these ester groups, since the first reduction waves for these complexes appeared at potentials that were ca. 400 mV less negative than those of poly-[Re-**60**–**62**]. This potential shift might lower the orbital energies of the reduced forms of these complexes to the extent that they become poor matches for binding CO_2, as was outlined for Abruña's bis-terpyridine complexes (vide supra). Film thickness studies for poly-[Re-**60**–**62**] revealed an optimum thickness, beyond which no gains in CO_2 reduction performance were realized, and the reduction products for each of these films was a 1:1 mixture of CO and CO_3^{2-}.

Another interesting group of complexes containing polypyridine-ligands that are active for CO_2 reduction are polymeric $[M(bpy)(CO)_2]_n$ systems. These polymers can be produced by reduction of the parent complex to yield axially linked,

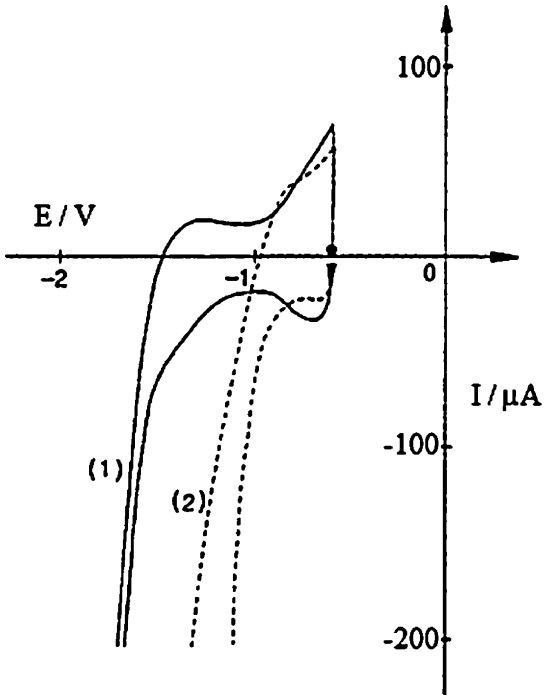

Fig. 7. Cyclic voltammograms in 0.1 M $LiClO_4$ for [Ru-**65**] under N_2 (curve "1") and CO_2 atmospheres (curve "2").
Adapted from ref. [136].

metal–metal bonded chains which consist of metal complex units that possess bipyridine and CO ligands (see Fig. 1). For *trans*-(Cl)-[Ru(bpy)$(CO)_2Cl_2$], polymerization is brought about through constant potential electrolysis in CH_3CN solution at −1.32 V vs. Ag/AgCl [135]. For the resulting polymer, [Ru-**65**], desorption and subsequent dissolution are accomplished during successive processes at potentials of ca. +0.34 V and +1.44 V vs. Ag/AgCl. Reductions of the polymer are bpy-localized, and two reversible reduction waves for this system were reported at −0.56 V and −1.21 V. In CH_3CN, films of this polymer proceeded to reduce CO_2 via a hydride intermediate, yielding CO and $HCOO^-$ in 58% and 2% yields, respectively. In 5% H_2O/CH_3CN under a CO_2 atmosphere the behavior was quite different: a very large cathodic wave (Fig. 7) corresponding to catalytic CO_2 reduction was observed, beginning at −0.76 V [136]. Constant potential electrolyses at −1.21 V in this solvent system yielded CO with 100% current efficiency, while in aqueous $LiClO_4$, the reduction was observed to begin at ca. −0.8 V; electrolyses at −1.16 V vs. Ag/AgCl produced CO with 97% efficiency. For a [Ru-**69**] system, anodic polymerization first yielded a polypyrrole metallopolymer, which was subsequently reduced to form Ru–Ru bonds within the existing polymer (Fig. 8). Electrocatalytic reduction of CO_2 with this polymer in either CH_3CN/5% H_2O or aqueous solution yielded CO with high efficiency (90% and 80%, respectively).

Deronzier reported the electrocatalytic activity of polymers synthesized by the electropolymerization of *trans*-Cl-[Ru(L)$(CO)_2Cl_2$] complexes, where L consisted of a range of bipyridine-type ligands. In this work, the complexes were electropolymerized reductively, producing the polymers [Ru-**65–71**] on electrode surfaces [137]. The electrolysis products in this work were highly dependent on the electron-donating or withdrawing nature of the bipyridine-type ligand. The electrolyses yielded CO with very high efficiencies when the bidentate ligand was either 2,2′-bipyridine (**65**) or other electron-donating ligands (**66**, **67**, **70**). The maximum efficiency for [Ru-**65**] at −0.86 V vs. Ag/AgCl was found in pH 9 buffer: 94% for CO formation; however, selectivity for this polymer depended

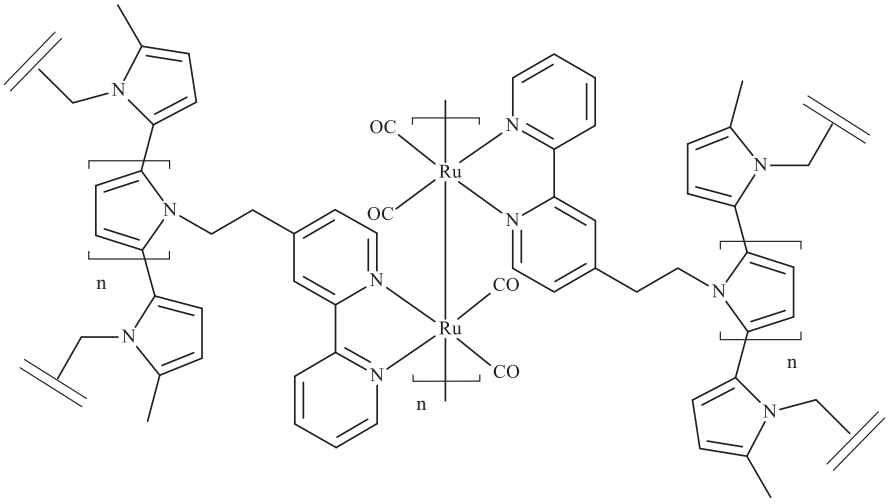

Fig. 8. Polymer structure proposed to exist in films of poly-[Ru-**69**] created by anodic electropolymerization and subsequently subjected to potentials that effect the formation of Ru–Ru bonds.

strongly on the pH of the medium. At pH 7, CO was produced with only ca. 54% efficiency, while $HCOO^-$ was produced at 33% efficiency. Selectivity in CO_2 reduction reactions exhibited a dependence on the electronics of the bipyridine ligand. For [Ru-**68**], a case where electron-withdrawing substituents are present, $HCOO^-$ was obtained as the major product in solutions having pH >5. At −0.86 V in pH 12 solution, $HCOO^-$ was obtained with ca. 90% current efficiency. The mechanism of CO_2 reduction for [Ru-**65–67,69,70**] is shown in Fig. 9. An initial $1e^-$ reduction of the complex produces a reduced form where the reduction is localized at the bipyridine ligand. This structure is proposed to lose a CO ligand to create a pentacoordinate complex that can bind CO_2. Following protonation of bound CO_2 to —COOH, a second protonation liberates H_2O and leaves a bound CO ligand in its wake. Films of these complexes were also generated by anodic polymerization of complexes that possessed pyrrole-substituted ligands (Fig. 8), since films grown by reductive polymerization are unstable at potentials that oxidize the films. In the case of polypyrrole-[Ru-**71**], polymer films produced $HCOO^-$ in 99% Faradaic yields in the presence of 0.5 M Na_2SO_4 + 0.1 M $NaHCO_3$, at only −0.75 V vs. Ag/AgCl. The osmium polymer, [Os-**65**] was synthesized by electropolymerization of *trans*-(Cl)-[Os(bpy)$(CO)_2Cl_2$] and investigated for its potential to

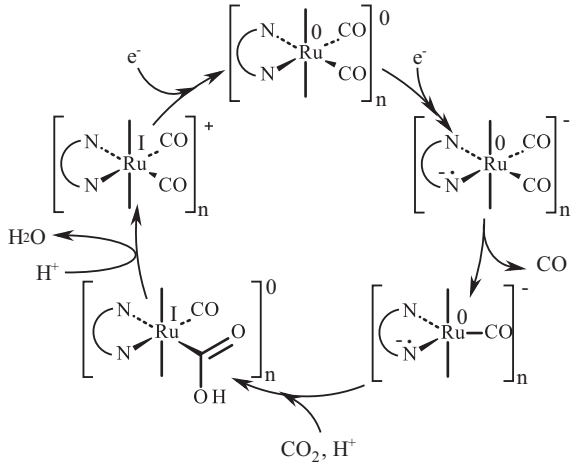

Fig. 9. Mechanism for CO_2 reduction in films of poly-[Ru-**65–67**] and poly-[Ru-**69,70**].
Adapted from ref. [137].

reduce CO_2 electrochemically [138]. Under a CO_2 atmosphere, films of this polymer on carbon felt electrodes were active at a potential of −0.96 V vs. Ag/AgCl in 10% H_2O/acetonitrile. In aqueous $LiClO_4$, $HCOO^-$ and CO were produced with 10% and 60% current efficiencies, respectively.

3.4. Modified electrodes incorporating cyclam-type complexes

Nickel complexes of tetraazacyclodecane and related ligands display structural features similar to porphyrin systems, and nickel and cobalt complexes incorporating these ligands exhibit catalytic activity toward CO_2 reduction in solution [139]. Langmuir–Blodgett films of nickel tetraazacyclodecanes were used to modify glassy carbon surfaces by Fujihira et al. [140,141]. The *N*-substituted complexes [Ni-**72**,**73**] were synthesized and used in CO_2 reduction experiments in work directed towards the construction of interfaces for artificial photosynthesis. Films of [Ni-**72**] underwent reduction at less negative potentials than the same complex did in solution, and were active for CO_2 reduction at a potential of −1.38 V vs. SCE [140]. Comparable studies of the adsorption of *N*-methyl-substituted tetraazacyclodecanes were carried out by Bilewicz et al. on mercury electrodes [142,143]. Although these kinds of complexes are photochemically active towards CO_2 reduction, this pathway demonstrates poor efficiencies [144]. On the other hand, the electrocatalytic reduction of CO_2 by Ni tetraazacyclodecanes proceeds with high efficiency and selectivity [145]. Bilewicz et al. attempted to effect changes in the catalytic activity of Ni(II) macrocycles toward CO_2 reduction through systematic structural changes in the tetraazacyclodecane skeleton. Increasing the degree of *N*-methyl substitution in these complexes was expected to decrease the ligands' σ-donor abilities and yield complexes with less negative reduction potentials; however, it also affects their stability in the reduced, $Ni(I)_{(ads)}$ state. Ni(II) complexes of this type become weakly adsorbed at mercury surfaces (see Fig. 10) and the degree of this adsorption increases with *N*-substitution. Before undergoing electrochemical reduction to the catalytically active $Ni(I)_{(ads)}$ state, a reorganization from the *trans*-III (or *RRSS*) form to the *trans*-I (or *RSRS*) form occurs [142]. The results obtained in this study showed that increasing the degree of *N*-substitution in the ligands yielded the more strongly adsorbed *trans*-I complex species on mercury. Presumably, the σ-donor properties of highly *N*-substituted macrocycles are reduced relative to the cyclams present in [Ni-**74**], enabling Hg to act as a strong donor at a fifth coordination site for those cases. For the most

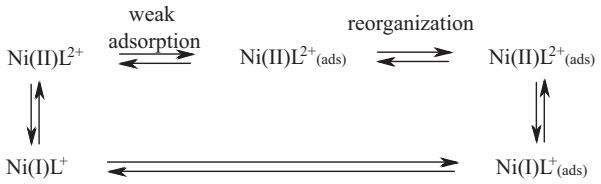

Fig. 10. Mechanism for adsorption of Ni–cyclam complexes. The reorganization step involves the transformation of *trans*-III (or *RRSS*) form to the *trans*-I (or *RSRS*) form which, following reduction, yields an adsorbed, catalytically active complex. Adapted from ref. [142].

highly substituted systems, [Ni-**77**,**78**], the interactions between the Ni(II) *RSRS*-form and mercury were so strong that very negative potentials were required to reduce the complex, and instead of the catalytically active, Ni(I) species, Ni(0) was produced. Since binding of CO_2 requires the catalyst to be in the adsorbed Ni(I) RSRS-form, CO_2 reduction for films incorporating [Ni-**77**,**78**] was not observed.

A comparison of the catalytic properties of this family of complexes in three different surface-confined forms was carried out in a study involving films that were deposited using either a Nafion® support phase, by anchoring monolayers to the electrode surface with pyridyl and anthracyl side-chains, or by the Langmuir–Blodgett (monolayer) technique [143]. Complexes supported in Nafion® films exhibited stable electrochemical behavior but showed low catalytic activity compared to monolayer CMEs, probably because the polymer matrix hindered adsorption of the complex to the electrode surface. Modified electrodes prepared by the Langmuir–Blodgett technique for [Ni-**73**] and [Ni-**79**] exhibited substantially higher currents in the presence of CO_2 compared to Ar-purged solutions at hydrophobic substrates (e.g. thin-film mercury electrodes and glassy carbon surfaces), but not hydrophilic substrates (e.g. indium–tin oxide). Complexes incorporating pyridyl and anthracyl side-chains, [Ni-**80**] and [Ni-**81**] were also active for CO_2 reduction but were not stable for long periods of time, probably because of poisoning of catalyst sites by carbonyl compounds formed during catalytic cycles.

3.5. Modified electrodes incorporating miscellaneous transition metal complexes

Losada et al. polymerized [Co-**82**] to create modified electrode surfaces that were active for both O_2 and CO_2 reductions [146]. CO_2 was reduced by this system at potentials beginning at −0.96 V vs. Ag/AgCl. The study also shows the importance of film preparation on catalyst performance. Films grown by potential cycling to a less positive potential limit (+0.90 V) had less compact morphologies, as determined by SEM. These films exhibited catalytic currents at potentials ca. 150 mV less negative than for films prepared by potential cycling between 0.04 V and +1.04 V.

A study employing a dual-film assembly was reported by Ogura et al. in which [Fe-**83**] was immobilized in a polyaniline|Prussian Blue modified electrode. This arrangement produced lactic acid with a selectivity of 88% at −0.8 V vs. SCE in 0.5 M KCl, along with small amounts of CH_3OH, C_2H_5OH, CH_3COH, $(CH_3)_2CO$, and CH_4 [147]. The modified electrodes consisted of a Pt |film 1|film two-setup, where film 1 (Prussian Blue) served to generate hydride species at the film 1–film 2 interface, and film 2 consisted of the electrocatalyst supported in polyaniline. Significantly, the onset of CO_2 reduction was observed at potentials as high as −0.3 V, close to the thermodynamic potentials for formation of some of the products found. In a similar study, 2-hydroxy-1-nitrosonaphthalene-3,6-disulfonatocobalt(II) [Co-**84**] was employed in a dual-film assembly (Prussian Blue|polyaniline), producing lactic acid, CH_3OH, C_2H_5OH, and $(CH_3)_2CO$ at −0.6 V vs. SCE, all with low current efficiencies [148].

4. Concluding remarks and future challenges

The present review reports on recent developments of the potential application of electrode surfaces modified with molecular electrocatalysts for the generation of hydrogen from water and the transformation of CO_2 into fuels and/or chemical feed stocks. In the 1980s and 1990s this area of research attracted considerable interest and as a result of reducing oil prices, interest declined rapidly. However, since the realization that fossil fuels are running out and because of the ever-worsening problem of climate change, its relevance to energy and environmental issues has placed this issue center stage.

The results presented in this review cover the electrocatalytic behavior of a wide variety of coordination complex types, most of them based on abundant (and cheap) first row transition metals. The approach used in these studies involves the immobilization of molecular electrocatalysts on a conducting electrode surface such as carbon. The electrocatalysts used are often identified from earlier, homogenous, solution-based studies. As is often the case with catalytic systems, the immobilization of a catalyst on an active surface can yield considerable dividends. Only small amounts of catalysts are needed, they can easily be separated from the reaction mixture and fast, heterogeneous electron transfer rates can often be obtained. The most direct means of such immobilization is the physical or chemical adsorption of electrocatalytic species as monolayers on electrode surfaces. This method, although widely used, has some problems such as the observation that only very small amounts of active materials are effectively bound to the surface, mostly in the order of a monolayer or less. A small amount of immobilized of electrocatalytic centers will hinder the development electrocatalytic electrodes with high current densities.

Therefore, alternative methods need to be developed, for example, ones that incorporate electrodes with high surfaces areas, such as nanocrystalline surfaces [149] or more traditional, porous electrodes. An alternative is the development of 3-D catalytic layers within an immobilizing polymer matrix. Such a layering might lead to higher concentrations of electrocatalytic species at the electrode surface and give better control of the electrochemical processes and/or higher product yields. For example, polymerized [M-**52**] complexes exhibited much higher activity toward CO_2 reduction than the same complexes in homogeneous, solution-phase experiments [124]. A dramatic ~1 V shift of the reduction potential for CO_2 observed at poly-[Co-**52**] and poly-[Cr-**52**]-coated surfaces compared to what was found for CO_2 reduction at a bare GC surface might be attributed in those cases to a combination of cooperativity effects (created by the close proximity of many active catalyst centers) as well as enhanced availability of open coordination sites for fixation of CO_2 in the reduced, Co(I) form of the polymeric complexes. It has also been shown that certain polymers such as polyvinyl pyridines and Nafion® can be used to concentrate electrocatalysts on electrode surfaces in high (up to molar concentrations) and can also used to control the proton concentration in the modifying layer. This again may provide higher reaction rates. Furthermore, immobilization within a polymer layer also offers the opportunity to tailor the orbital energies of metallic catalyst centers through binding to the polymer backbone. In certain metal complexes such as metallophthalocyanines and polypyridine compounds, ligands can, in addition to metal centers, also be reduced in a catalytically active form and store more redox equivalents that might be transferred to the substrate during catalytic cycles. This is an important point where CO_2 reduction is concerned, since higher

target products like CH_3OH or CH_4 are obtained electrochemically through multi-electron and multi-proton transfers.

A problem that may arise with polymer matrices, however, is that the electron and ion percolations to the underlying electrode surface have to be efficient and fast. It has been shown, for example, that the charge transport properties of electrode-immobilized osmium containing poly(4-vinylpyridine) electrocatalysts depend strongly on the layer thickness, the nature and concentration of the contacting electrolyte, the pH and the temperature [49,150]. Careful control of the reaction conditions is therefore needed to obtain optimum efficiency. Importantly, studies with polymer-modified electrodes have shown excellent film stability over many days.

Another point that needs to be considered is that film morphology will exert a major influence on the diffusion of substrates and ions through the film. During scale-up, reproducibility of film conditions might not be trivial. The development of new materials (e.g. polymers with better electrical conductivity, enhanced robustness, etc.) can be expected to give way to better catalytic electrodes. The issues outlined above are important for hydrogen generating systems as well as electrocatalytic assemblies for the transformation of CO_2. There are, however, a number of differences in approach needed to achieve successful devices in both cases. The electrolysis of water for the production of hydrogen is well understood. Most of the hydrogen produced on an industrial scale is at present obtained from fossil fuels but electrolysis is also utilized. However, in these processes expensive electrode materials, high pressures and temperatures are needed. There is therefore considerable interest in producing novel cells that are cost effective, showing high efficiencies and stability at room temperature using abundant, stable and cheap electrocatalysts. In the development of such systems the overpotential that has to be applied to achieve high turnover numbers is a very important factor. This is evident from the many different compounds discussed in this review where the introduction of substituents in, for example, metal-based porphyrins and metallophthalocyanines is aimed at lowering this overpotential. Therefore the energy cost for any catalyst to be utilized on a large-scale process is one of the most important factors that determine the feasibility of its use. This is reflected in the compounds discussed in this review. Although a small part of the studies presented in this review pertain to precious metal centers, the majority involve non-precious metals like cobalt, iron, nickel, copper, and zinc.

For CO_2-transforming devices, such efficiency and commercial criteria are critically important. For future development of electrocatalytic devices in this area, rhenium-based electrocatalysts are much less sustainable than devices based on cobalt or nickel and research should clearly develop in this direction. There are however a number of other problems to be considered. Firstly, there is currently much less information available about the mechanisms involved in these transformations than there needs to be, particularly where non-precious metal complexes are concerned. A deeper understanding of such catalytic cycles is required before embarking on device development steps. Then, there is the limited solubility of CO_2 in water and the range of products obtained in these studies, such as CO, H_2, CH_3OH, CH_4 and HCOOH. A related problem is the difficulty in the isolation of the products formed in the electrolysis solution. As mentioned, organic solvents can be used to increase the solubility of CO_2. More research into this aspect of CO_2 electrolysis (solvents/conditions that improve CO_2 solubility) may yield higher current densities and inherently better device efficiencies. Gas-diffusion electrodes may offer improvements over polymer films deposited on solid electrodes. The very high surface areas of these electrodes and the improved accessibility to CO_2 that they offer are both critical for obtaining high current densities in CO_2 reductions. If electrochemical techniques assume a larger role for energy storage in the future, these materials will probably find frequent use.

So while H^+ reduction in aqueous solutions yields H_2 only, product selectivity in CO_2 reductions is of ultimate importance and to obtain such selectivity is, at the moment, highly problematic. Many of the electrocatalysts discussed in this review reduce CO_2 to either CO or HCOOH. In some cases, the Faradaic efficiencies reported for these reductions are quite high, and the range of products in these cases can be narrow. High Faradaic efficiency also implies high catalyst stability, since the current in the electrolysis is used for substrate reduction and not some other process that involves the complex (e.g. decomposition). In certain cases cited here, catalyst stability has been evaluated on the basis of changes in electrochemical behavior over time. This is an important aspect of electrocatalyst performance that really needs to be explored for any catalyst that appears to be a promising candidate for larger-scale use.

In conclusion, even though electrocatalytic H_2 evolution and CO_2 reduction using cheap materials at ambient temperatures display considerable promise, there is an urgent need to conduct more structured investigations of these materials (for example, the systematic investigations of catalyst structures and polymer films carried out by Kaneko). As already noted by Savéant in a recent review [151], a considerable amount of work has been conducted in this area, but an understanding beyond an empirical level needs to be achieved in order to provide better knowledge of the fundamental, underlying processes. It can be expected that as further investigations are made into understanding reaction pathways, by concentrating where the effects of electrode materials, solvents, electrolytes, immobilization techniques and suitable substrates on device output used are considered in detail, a viable, cost effective electrochemical alternative to the use of fossil fuels for sustainable energy production will be developed.

Acknowledgments

The authors thank the EPA (Grant 2008-ET-MS-3-S2) and the SFI under (Grants Nos. 07/SRC/B1160 and 08/RFP/CHE13490) for supporting this work.

References

[1] M. Momirlan, T.N. Veziroglu, Int. J. Hydrogen Energy 30 (2005) 795.
[2] T. Abe, M. Kaneko, Prog. Polym. Sci. 28 (2003) 1441.
[3] S.C. Roy, O.K. Varghese, M. Paulose, C.A. Grimes, ACS Nano 4 (2010) 1259.
[4] (a) B. O'Regan, M. Grätzel, Nature 353 (1991) 737;
(b) A. Hagfeldt, M. Grätzel, Acc. Chem. Res. 33 (2000) 269.
[5] D. Gust, T.A. Moore, A.L. Moore, Acc. Chem. Res. 42 (2009) 1890.
[6] G. Centi, S. Perathoner, Greenhouse Gas Sci. Technol. 1 (2011) 21.
[7] BP Statistical Review of World Energy 2010, Christof Rühl, June, 2010 http://www.bp.com/genericarticle.do?categoryId=98&contentId=7062807.
[8] S. Dahl, I. Chorkendorff, Nat. Mater. 11 (2012) 100.
[9] (a) S. Rau, D. Walther, J.G. Vos, Dalton Trans. 9 (2007) 915;
(b) A.J. Morris, G. Meyer, E. Fujita, Acc. Chem. Res. 42 (2009) 1983;
(c) A. Inagaki, M. Akita, Coord. Chem. Rev. 254 (2010) 1220;
(d) S. Losse, J.G. Vos, S. Rau, Coord. Chem. Rev. 254 (2010) 2492;
(e) M. Schulz, M. Karnahl, M. Schwalbe, J.G. Vos, Coord. Chem. Rev. (2012) http://dx.doi.org/10.1016/j.ccr.2012.02.016, in press.
[10] (a) S. Rau, B. Schäfer, D. Gleich, E. Anders, M. Rudolph, M. Friedrich, H. Görls, W. Henry, J.G. Vos, Angew. Chem. Int. Ed. 45 (2006) 6215;
(b) M. Elvington, J. Brown, S.M. Arachchige, K.J. Brewer, J. Am. Chem. Soc. 129 (2007) 10644;
(c) V. Artero, M. Chavarot-Kerlidou, M. Fontecave, Angew. Chem. Int. Ed. 50 (2011) 7238;
(d) H. Ozawa, K. Sakai, Chem. Commun. 47 (2011) 2227;
(e) G.S. Bindra, M. Schulz, A. Paul, S. Soman, R. Groarke, J. Inglis, M.T. Pryce, W.R. Browne, S. Rau, B.J. MacLean, J.G. Vos, Dalton Trans. 40 (2011) 10812.
[11] (a) B. Gholamkhass, H. Mametsuka, K. Koike, T. Tanabe, M. Furue, O. Ishitani, Inorg. Chem. 44 (2005) 2326;
(b) H. Takeda, K. Koike, H. Inoue, O. Ishitani, J. Am. Chem. Soc. 130 (2008) 2023;
(c) T. Dhanasekaran, J. Grodkowski, P. Neta, P. Hambright, E. Fujita, J. Phys. Chem. A 103 (1999) 7742.
[12] A. Paul, D. Connolly, M. Schulz, M.T. Pryce, J.G. Vos, Inorg. Chem. 51 (2012) 1977.
[13] NREL Technical Report, NREL/TP-581-40605.
[14] European Fuel Cells and Hydrogen Joint Undertaking, EU Call FCH-JU-2011-1.

[15] W. Haije, H. Geerlings, Environ. Sci. Technol. 45 (2011) 8609.
[16] http://www.rsc.org/chemistryworld/Issues/2003/August/electrolysis.asp.
[17] A. Deronzier, J.C. Moutet, in: M.D. Ward (Ed.), Comprehensive Coordination Chemistry, II, Elsevier, Amsterdam, 2003.
[18] R.W. Murray, Acc. Chem. Res. 13 (1980) 135.
[19] A. Yesildag, D. Ekinci, Electrochim. Acta 55 (2010) 7000.
[20] T. Yoshida, K. Kamato, M. Tsukamoto, T. Iida, D. Schlettwein, D. Wohrle, M. Kaneko, J. Electroanal. Chem. 385 (1995) 209.
[21] A. Deronzier, J.C. Moutet, Acc. Chem. Res. 22 (1989) 249.
[22] Y. Shi, R.Z. Yang, P.K. Yuet, Carbon 47 (2009) 1146.
[23] (a) M. Kaneko, Prog. Poly. Sci. 26 (2001) 1101;
(b) H. Shiroishi, K. Ishikawa, K. Hirano, M. Kaneko, Polym. Advan. Technol. 12 (2001) 237.
[24] (a) O. Haas, M. Kriens, J.G. Vos, J. Am. Chem. Soc. 103 (1981) 1318;
(b) R.J. Forster, J.G. Vos, Macromolecules 23 (1990) 4372;
(c) R.J. Forster, J.G. Vos, Langmuir 10 (1994) 4330.
[25] (a) A.P. Doherty, M.A. Stanley, J.G. Vos, Analyst 120 (1995) 2371;
(b) A.P. Doherty, M.A. Stanley, D. Leech, J.G. Vos, Anal. Chim. Acta 319 (1996) 111;
(c) A. Heller, Acc. Chem. Res. 23 (1990) 128.
[26] J. Roncali, J. Mater. Chem. 9 (1999) 1875.
[27] J. Ochmanska, P.G. Pickup, Can. J. Chem. 69 (1991) 653.
[28] A. Deronzier, J.C. Moutet, Coord. Chem. Rev. 147 (1996) 339.
[29] B.J. MacLean, P.G. Pickup, J. Mater. Chem. 11 (2001) 1357.
[30] B.J. MacLean, P.G. Pickup, J. Phys. Chem. B 106 (2002) 4658.
[31] C.G. Cameron, B.J. MacLean, P.G. Pickup, Macromol. Symp. 196 (2003) 165.
[32] (a) B.J. MacLean, P.G. Pickup, Chem. Commun. (1999) 2471;
(b) D.T. Walker, C.G. Douglas, B.J. MacLean, Can. J. Chem. 87 (2009) 729;
(c) A.H. Murray, Z. Yue, A.L. Wallbank, T.S. Cameron, R. Vadavi, B.J. MacLean, M.A.S. Aquino, Polyhedron 27 (2008) 1270.
[33] P. Gregory, J. Porphyr. Phthalocyan. 4 (2000) 432.
[34] S. O'Malley, B. Schazmann, D. Diamond, K. Nolan, Tetrahedron Lett. 48 (2007) 9003.
[35] G. Guillaud, J. Simon, J.P. Germain, Coord. Chem. Rev. 180 (1998) 1433.
[36] N.B. McKeown, Structure and Function, Cambridge University Press, Cambridge, 1998.
[37] C.C. Leznoff, A.B.P. Lever, Phthalocyanines: Properties and Applications, Vol. 1, VCH, New York, 1989.
[38] J.R. Darwent, P. Douglas, A. Harriman, G. Porter, M.-C. Richoux, Coord. Chem. Rev. 44 (1982) 83.
[39] A. Koca, M.K. Şener, M.B. Koçak, A. Gül, Int. J. Hydrogen Energy 31 (2006) 2211.
[40] K. Hesse, D. Schlettwein, J. Electroanal. Chem. 476 (1999) 148.
[41] M.K. Şener, A. Koca, A. Gül, M.B. Koçak, Polyhedron 26 (2007) 1070.
[42] M.N. Yarasir, M. Kandaz, A. Koca, B. Salih, Polyhedron 26 (2007) 1139.
[43] A. Koca, M.K. Şener, M.B. Koçak, A. Gül, Transit. Metal Chem. 30 (2005) 399.
[44] A. Koca, Ş. Bayar, H.A. Dinçer, E. Gonca, Electrochim. Acta 54 (2009) 2684.
[45] M. Ozer, A. Altindal, A.R. Özkaya, M. Bulut, Ö. Bekaroglu, Polyhedron 25 (2006) 3593.
[46] N. Chebotareva, T. Nyokong, Electrochim. Acta 42 (23) (1997) 3519.
[47] F. Zhao, J. Zhang, D. Wöhrle, M. Kaneko, J. Porphyr. Phthalocya 4 (2000) 31.
[48] D.A. Buttry, F.C. Anson, J. Am. Chem. Soc. 106 (1984) 59.
[49] (a) W.J. Albery, A.R. Hillman, Annu. Rep. Prog. Chem. C78 (1981) 317;
(b) C.P. Andrieux, J.M. Dumas-Bouchiat, J.M. Saveant, J. Electroanal. Chem. 131 (1982) 131.
[50] F. Zhao, J. Zhang, T. Abe, D. Wöhrle, M. Kaneko, J. Mol. Catal. A: Chem. 145 (1999) 245.
[51] F. Zhao, J. Zhang, T. Abe, M. Kaneko, J. Porphyr. Phthalocya 3 (1999) 238.
[52] J. Zhang, T. Abe, M. Kaneko, J. Electroanal. Chem. 438 (1997) 133.
[53] J. Zhang, M. Yagi, X. Hou, M. Kaneko, J. Electroanal. Chem. 412 (1996) 159.
[54] J.A. Bard, Electroanalytical Chemistry, Vol. 18, Marcel Dekker, New York, 1986.
[55] A. Koca, Electrochem. Commun. 11 (2009) 838.
[56] A. Koca, A. Kalkan, Z. Altuntaş Bayir, Electroanalysis 22 (2010) 310.
[57] Ö.A. Osmanbaş, A. Koca, M. Kandaz, F. Karaca, Int. J. Hydrogen Energy 33 (2008) 3281.
[58] A. Alemdar, A.R. Özkaya, M. Bulut, Polyhedron 28 (2009) 3788.
[59] A. Koca, A. Kalkan, Z. Altuntaş Bayir, Electrochim. Acta 56 (2011) 5513.
[60] A. Koca, M. Özçeşmeci, E. Hamuryudan, Electroanalysis 14 (2010) 1623.
[61] A. Koca, Int. J. Hydrogen Energy 34 (2009) 2107.
[62] D. Wohrle, A. Wendt, A. Weitemeyer, J. Stark, W. Spiller, G. Schneider, S. Muller, U. Michelsen, H. Kliesch, A. Heuermann, A. Ardeschirpur, Russ. Chem. B+ 43 (1994) 1953.
[63] (a) I. Bhugan, D. Lexa, J.M. Savéant, J. Am. Chem. Soc. 118 (1996) 3982;
(b) V. Grass, D. Lexa, J.M. Savéant, J. Am. Chem. Soc. 119 (1997) 7526.
[64] R.M. Kellett, T.G. Spiro, Inorg. Chem. 24 (1985) 2373.
[65] R.M. Kellett, T.G. Spiro, Inorg. Chem. 24 (1985) 2378.
[66] F. Taguchi, T. Abe, M. Kaneko, J. Mol. Catal. A: Chem. 140 (1999) 41.
[67] T. Abe, F. Taguchi, H. Imaya, F. Zhao, J. Zhang, M. Kaneko, Polym. Adv. Tech. 9 (1998) 559.
[68] (a) T. Abe, H. Imaya, S. Tokita, D. Wöhrle, M. Kaneko, J. Porphyr. Phthalocya 1 (1997) 215.
[69] M. Yagi, K. Kinoshita, M. Kaneko, J. Phys. Chem. B 101 (1997) 3957.
[70] I.K. Choi, Y. Liu, Z. Wei, M.D. Ryan, Inorg. Chem. 36 (1997) 3113.
[71] K. Kalyanasundaram, N. Vlachopoulos, V. Krishnan, A. Monnier, M. Grätzel, J. Phys. Chem. 91 (1987) 2342.
[72] E. Tsuchida, M. Kaneko, H. Nishide, M. Hoshino, J. Phys. Chem. 90 (1986) 2283.
[73] M. Kaneko, E. Tsuchida, Y. Imai, J. Chem. Soc. Faraday Trans. 87 (1) (1991) 83.
[74] M. Kaneko, I. Okura (Eds.), Photocatalysis – Science and Technology, Kodansha-Springer, Japan, 2002, p. 294.
[75] J.P. Collman, P.S. Wangenknett, N.S. Lewis, J. Am. Chem. Soc. 114 (1992) 5665.
[76] T. Abe, M. Kaneko, J. Mol. Catal. A-Chem. 169 (2001) 177.
[77] T. Maruyama, T. Yamamoto, J. Phys. Chem. B 101 (1997) 3806.
[78] M. Suzuki, S. Kobayashi, S. Kimura, K. Hanabusa, H. Shirai, Chem. Commun. (1997) 227.
[79] R. Palmans, A.J. Frank, J. Phys. Chem. 95 (1991) 9438.
[80] T. Abe, K. Takahashi, Y. Shiraishi, N. Toshima, M. Kaneko, Macromol. Chem. Phys. 201 (2000) 102.
[81] T. Abe, K. Hirano, Y. Shiraishi, N. Toshima, M. Kaneko, Eur. Polym. J. 37 (2001) 753.
[82] O. Pantini, E. Anxolabéhère-Mallart, A. Aukauloo, P. Millet, Electrochem. Commun. 9 (2007) 54.
[83] X. Hu, B.S. Brunschwig, J.C. Peters, J. Am. Chem. Soc. 129 (2007) 8988.
[84] L.A. Berben, J.C. Peters, Chem. Commun. 46 (2010) 398.
[85] P.A. Jacques, V. Artero, J. Pécaut, M. Fontecave, PNAS 106 (49) (2009) 20627.
[86] P.V. Bernhardt, L.A. Jones, Inorg. Chem. 38 (1999) 5086.
[87] T. Abe, F. Taguchi, S. Tokita, M. Kaneko, J. Mol. Catal. A-Chem. 126 (1997) L89.
[88] T. Abe, G. Toda, A. Tajiri, M. Kaneko, Electroanal. Chem. 510 (2001) 35.
[89] T. Abe, T. Goto, K. Ohzeki, M. Kaneko, Electrochim. Acta 45 (2000) 4009.
[90] P. Paunović, O. Popovski, A. Dimitrov, D. Slakvok, E. Lefterova, S. Hadži-Jordanov, Electrochim. Acta 52 (2007) 4640.
[91] P. Paunović, I. Radev, A.T. Dimitrov, O. Popovski, E. Lefterova, E. Slavcheva, S. Hadži-Jordanov, Int. J. Hydrogen Energy 34 (2009) 2866.
[92] P. Paunović, O. Popovski, E. Fidančevska, B. Ranguelov, D.S. Gogovska, A.T. Dimitrov, S.H. Jordanov, Int. J. Hydrogen Energy 35 (2010) 10073.
[93] J.B. Raoof, R. Ojani, S.A. Esfeden, S.R. Nadimi, Int. J. Hydrogen Energy 35 (2010) 3937.
[94] http://www.ipcc.ch/publications_and_data/publications_ipcc_fourth_assessment_ report_synthesis _report.htm.
[95] G.A. Olah, A. Goeppert, G.K.S. Prakash, J. Org. Chem. 74 (2009) 487.
[96] G. Centi, S. Perathoner, Catal. Today 148 (2009) 191.
[97] J.P. Collin, J.P. Sauvage, Coord. Chem. Rev. 93 (1989) 245.
[98] M. Jitaru, J. Univ. Chem. Technol. Metallurgy 42 (2007) 333.
[99] E.E. Benson, C.P. Kubiak, A.J. Sathrum, J.M. Smieja, Chem. Soc. Rev. 38 (2009) 89.
[100] T. Abe, T. Yoshida, S. Tokita, F. Taguchi, H. Imaya, M. Kaneko, J. Electroanal. Chem. 412 (1996) 125.
[101] T. Abe, F. Taguchi, T. Yoshida, S. Tokita, G. Schnurpfeil, D. Wohrle, M. Kaneko, J. Mol. Catal. A-Chem. 112 (1996) 55.
[102] T. Abe, H. Imaya, T. Yoshida, S. Tokita, D. Schlettwein, D. Wohrle, M. Kaneko, J. Porphyr. Phthalocya 1 (1997) 315.
[103] N.S. Lewis, C.M. Lieber, J. Am. Chem. Soc. 106 (1984) 5033.
[104] S. Kapusta, N. Hackerman, J. Electrochem. Soc. 131 (1984) 1511.
[105] S. Meshituka, M. Ichikawa, K. Tamaru, J. Chem. Soc., Chem. Commun. (1974) 158.
[106] T.V. Magdesieva, I.V. Zhukov, D.N. Kravchuk, O.A. Semenikhin, L.G. Tomilova, K.P. Butin, Russ. Chem. B+ 51 (2002) 805.
[107] M.N. Mahmwood, D. Masheder, C.J. Harty, J. Appl. Electrochem. 17 (1987) 1223.
[108] T.V. Magdesieva, T. Yamamoto, D.A. Tryk, A. Fujishima, J. Electrochem. Soc. 149 (2002) D89.
[109] J. Imai, M. Souma, S. Ozeki, T. Suzuki, M. Kaneko, J. Phys. Chem. A 95 (1991) 9955.
[110] N. Furuya, K. Matsui, J. Electroanal. Chem. 271 (1989) 181.
[111] J.J. Zhang, W.J. Pietro, A.B.P. Lever, J. Electroanal. Chem. 403 (1996) 93.
[112] M. Isaacs, F. Armijo, G. Ramirez, E. Trollund, S.R. Biaggio, J. Costamagna, M.J. Aguirre, J. Mol. Catal. A-Chem. 229 (2005) 249.
[113] H. Aga, A. Aramata, Y. Hisaeda, J. Electroanal. Chem. 437 (1997) 111.
[114] G. Ramirez, M. Lucero, A. Riquelme, M. Villagran, J. Costamagna, E. Trollund, M.J. Aguirre, J. Coord. Chem. 57 (2004) 249.
[115] T. Atoguchi, A. Aramata, A. Kazusaka, M. Enyo, J. Electroanal. Chem. 318 (1991) 309.
[116] A. Aramata, A. Kazusaka, T. Atoguchi, M. Enyo, Denki Kagaku 60 (1992) 1063.
[117] A. Aramata, T. Atoguchi, A. Kazusaka, M. Enyo, Denki Kagaku 60 (1992) 565.
[118] T. Atoguchi, A. Aramata, A. Kazusaka, M. Enyo, J. Chem. Soc., Chem. Commun. (1991) 156.
[119] A. Aramata, H. Tanaka, J. Electroanal. Chem. 437 (1997) 29.
[120] N. Sonoyama, M. Kirii, T. Sakata, Electrochem. Commun. 1 (1999) 213.
[121] M.A. Riquelme, M. Isaacs, M. Lucero, E. Trollund, M.J. Aguirre, J. Chil. Chem. Soc. 48 (2003) 89.
[122] T. Yoshida, T. Iida, T. Shirasagi, R.J. Lin, M. Kaneko, J. Electroanal. Chem. 344 (1993) 355.
[123] C. Arana, M. Keshavarz, K.T. Potts, H.D. Abruña, Inorg. Chim. Acta 225 (1994) 285.
[124] J.A.R. Sende, C.R. Arana, L. Hernandez, K.T. Potts, M. Keshevarzk, H.D. Abruña, Inorg. Chem. 34 (1995) 3339.
[125] H.C. Hurrell, A.L. Mogstad, D.A. Usifer, K.T. Potts, H.D. Abruña, Inorg. Chem. 28 (1989) 1080.
[126] A.R. Guadalupe, D.A. Usifer, K.T. Potts, H.C. Hurrell, A.-E. Mogstad, H.D. Abruña, J. Am. Chem. Soc. 110 (1988) 3462.

[127] C. Caix, S. ChardonNoblat, A. Deronzier, J. Electroanal. Chem. 434 (1997) 163.
[128] T. Yoshida, K. Tsutsumida, S. Teratani, K. Yasufuku, M. Kaneko, J. Chem. Soc., Chem. Commun. (1993) 631.
[129] T.R. O'Toole, L.D. Magrgerum, T.D. Westmoreland, W.J. Vining, R.W. Murray, T.J. Meyer, J. Chem. Soc., Chem. Commun. (1985) 1416.
[130] T.R. O'Toole, B.P. Sullivan, M.R.M. Bruce, L.D. Margerum, R.W. Murray, T.J. Meyer, J. Electroanal. Chem. 259 (1989) 217.
[131] F. Cecchet, M. Alebbi, C.A. Bignozzi, F. Paolucci, Inorg. Chim. Acta 359 (2006) 3871.
[132] J.P. Qu, X.G. Zhang, Y.G. Wang, C.X. Xie, Electrochim. Acta 50 (2005) 3576.
[133] K. Ogura, N. Endo, M. Nakayama, H. Ootsuka, J. Electrochem. Soc. 142 (1995) 4026.
[134] S. Cosnier, A. Deronzier, J.-C. Moutet, J. Mol. Catal. 45 (1988) 381.
[135] S. Chardon-Noblat, M.N. Collomb-Dunand-Sauthier, A. Deronzier, R. Ziessel, D. Zsoldos, Inorg. Chem. 33 (1994) 4410.
[136] M.N. Collomb-Dunand-Sauthier, A. Deronzier, R. Ziessel, J. Chem. Soc., Chem. Commun. (1994) 189.
[137] S. Chardon-Noblat, A. Deronzier, R. Ziessel, D. Zsoldos, J. Electroanal. Chem. 444 (1998) 253.
[138] S. Chardon-Noblat, A. Deronzier, F. Hartl, J. van Slageren, T. Mahabiersing, Eur. J. Inorg. Chem. (2001) 613.
[139] M. Beley, J.P. Collin, R. Ruppert, J.P. Sauvage, J. Am. Chem. Soc. 108 (1986) 7461.
[140] Y. Hirata, K. Suga, M. Fujihira, Thin Solid Films 179 (1989) 95.
[141] U. Akiba, Y. Nakamura, K. Suga, M. Fujihira, Thin Solid Films 210 (1992) 381.
[142] K. Bujno, R. Bilewicz, L. Siegfried, T.A. Kaden, J. Electroanal. Chem. 445 (1998) 47.
[143] A. Jarzebinska, P. Rowinski, I. Zawisza, R. Bilewicz, L. Siegfried, T. Kaden, Anal. Chim. Acta 396 (1999) 1.
[144] J.L. Grant, K. Goswami, L.O. Spreer, J.W. Otvos, M. Calvin, J. Chem. Soc. Dalton Trans. (1987) 2105.
[145] M. Beley, J.-P. Collin, R. Ruppert, J.-P. Sauvage, J. Chem. Soc., Chem. Commun. (1984) 1315.
[146] J. Losada, I. Delpeso, L. Beyer, J. Hartung, V. Fernandez, M. Mobius, J. Electroanal. Chem. 398 (1995) 89.
[147] K. Ogura, M. Higasa, J. Yano, N. Endo, J. Electroanal. Chem. 379 (1994) 373.
[148] K. Ogura, K. Mine, J. Yano, H. Sugihara, J. Chem. Soc., Chem. Commun. (1993) 20.
[149] G. Centi, S. Perathoner, ChemsusChem 4 (2011) 913.
[150] (a) R.J. Forster, M.E.G. Lyons, J.G. Vos, J. Chem. Soc. Faraday Trans. (1991) 3761; (b) R.J. Forster, J.G. Vos, J. Electroanal. Chem. 314 (1991) 135; (c) R.J. Forster, J.G. Vos, Electrochim. Acta 37 (1992) 159; (d) R.J. Forster, J.G. Vos, J. Electrochem. Soc. 139 (1992) 1503.
[151] J.M. Savéant, Chem. Rev. 108 (2008) 2348.

Dalton Transactions

Cite this: *Dalton Trans.*, 2012, **41**, 13050

www.rsc.org/dalton

PAPER

The role of bridging ligand in hydrogen generation by photocatalytic Ru/Pd assemblies†‡

Gurmeet Singh Bindra,[a] Martin Schulz,[a,b] Avishek Paul,[a] Robert Groarke,[a] Suraj Soman,[a] Jane L. Inglis,[a] Wesley R. Browne,[c] Michael G. Pfeffer,[d] Sven Rau,[d] Brian J. MacLean,[e] Mary T. Pryce[a] and Johannes G. Vos*[a]

Received 1st May 2012, Accepted 15th June 2012
DOI: 10.1039/c2dt30948c

The synthesis and characterisation of two terpyridine based ruthenium/palladium heteronuclear compounds are presented. The photocatalytic behaviour of the Ru/Pd complex containing the linear 2,2′:5′,2″-terpyridine bridge (**1a**) and its analogue the non-linear 2,2′:6′,2″-terpyridine bridge (**2a**) are compared together with the respective mononuclear complexes **1** and **2**. Irradiation of **1a** with visible light (*e.g.*, 470 nm) results in the photocatalytic generation of dihydrogen gas. Photocatalysis was not observed with complex **2a** by contrast. A comparison with the photocatalytic behaviour of the precursors **1** and **2** indicates, that while for **1a** the photocatalysis is an intramolecular process, for the mononuclear precursors it is intermolecular. The photophysical and electrochemical properties of the mono- and heterobinuclear compounds are compared. Raman spectroscopy and DFT calculations indicate that there are substantial differences in the nature of the lowest energy ^{3}MLCT states of **1a** and **2a**, from which the contrasting photocatalytic activities of the complexes can be understood.

Introduction

Hydrogen is widely perceived to be one of the primary fuels of the future, in particular for the transport sector because of its exceptionally high energy-density/mass ratio. One of the most promising approaches towards the generation of hydrogen in an environmentally friendly and sustainable manner is the use of molecular photocatalysts that utilise visible light to drive proton reduction. Such systems are comprised of a light-harvesting antenna that can donate electrons to a catalytically active centre *via* a bridging ligand. Due to their exceptional photophysical and redox properties Ru(II) polypyridyl complexes are an excellent choice as the light harvesting centre[1] while Pd(II) or Pt(II) are often the metal of choice for the catalytically active centres.[2] Alternative combinations already reported are the combinations of Re/Co, Ru/Pd, Ru/Pt, Os/Rh, Ru/Rh, Pt/Co and Ir/Rh.[3] The perception that intramolecular electron transfer from the light harvesting centre to the catalytic centre *via* the bridging ligand has stimulated the search for suitable bridging ligands. However, changes to the peripheral ligand can influence the catalytic properties of the assemblies also.[2b,4]

In this contribution two new Ru(II)/Pd(II) heterobinuclear metal complexes **1a** and **2a** (Fig. 1) and their photocatalytic properties with regard to hydrogen production are reported. The complexes are based on terpyridine bridging ligands with the linear 2,2′:5′,2″-terpyridine bridge (2,5-bpp) used in **1a** and the angular 2,2′:6′,2″-terpyridine bridging moiety (2,6-bpp) in **2a**. We show here that **1a** (with the linear 2,5-bpp ligand) can catalyse the production of hydrogen while **2a** does not. In addition preliminary wavelength dependent studies on the catalytic

[a]*SRC for Solar Energy Conversion, School of Chemical Sciences, Dublin City University, Glasnevin, Dublin 9, Dublin, Ireland. E-mail: han.vos@dcu.ie*
[b]*Lehrstuhl für Pharmazeutische Radiochemie, Technische Universität München, Walther-Meißner-Str. 3, 85748 Garching, Germany*
[c]*Stratingh Institute for Chemistry, Faculty of Mathematics and Natural Sciences, University of Groningen, Nijenborgh 4, 9747 AG Groningen, The Netherlands*
[d]*Anorganische Chemie I, Universität Ulm, Albert-Einstein-Allee 11, 89081 Ulm, Germany*
[e]*Department of Chemistry, St. Francis Xavier University, Physical Sciences Building, P.O. Box 5000, Antigonish, Nova Scotia, B2G-2W5, Canada*

†Based on the presentation at Dalton Discussion No. 13, 10–12 September 2012, University of Sheffield, UK.
‡Electronic supplementary information (ESI) available: ^{1}H NMR spectra, cyclic voltammetry and orbital contributions tables. See DOI: 10.1039/c2dt30948c

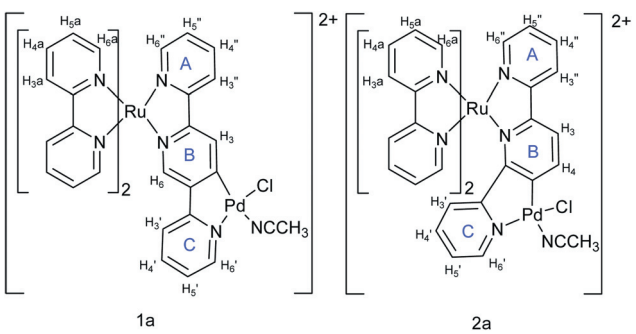

Fig. 1 Structure of complexes $[Ru(bipy)_2(2,5\text{-bpp})Pd(CH_3CN)Cl](PF_6)_2$ (**1a**) and $[Ru(bipy)_2(2,6\text{-bpp})Pd(CH_3CN)Cl](PF_6)_2$ (**2a**). The mononuclear precursor Ru(II)-complexes are denoted **1** and **2**.

efficiency suggest that the highest efficiency may be obtained when the lowest energy ^{3}MLCT states are localised on the bridging ligand.

Results and discussion

Synthesis

The linear 2,2′:5′,2″-terpyridine ligand was prepared through a Negishi coupling of 2,5-dibromopyridine with 2-pyridylzinc bromide using modified published procedures[5] and obtained with moderate yields. Complexes **1** and **2** were obtained in excellent yields from $[Ru(bipy)_2Cl_2]\cdot 2H_2O$. Heating **1** and **2** in alcoholic solution at reflux with $(NH_4)_2[PdCl_4]$ for several days afforded the heterodinuclear complexes **1a** and **2a** in good yield.

A key issue is the actual molecular structure of the active compounds. In Fig. 1 the Pd centre is coordinated to the bridging bpp ligand, as well as to a chlorido and an acetonitrile ligand, and elemental analysis supports this structure. However, a tetranuclear structure such as in Fig. 2 is also possible, whereby the acetonitrile is not bound to the Pd(II) centre but is solvent of crystallisation.

The ^{1}H NMR spectrum of **1a** is shown in Fig. S2a, ESI.‡ The resonance at 2.06 ppm, when compared with related Pd(II) complexes, can be assigned to coordinated acetonitrile.[6] A similar assignment can be made for **2a** (Fig. S2b, ESI‡). Hence, in solution the structure is most likely to be that shown in Fig. 1. It is worth noting that the products obtained from the reaction between **1** (or **2**) and the Pd(II) precursor are insoluble in a range of solvents except upon addition of acetonitrile (*e.g.*, to acetone) when dissolution occurs. This suggests that the product obtained from this reaction may have the structure as shown in Fig. 2, but that upon addition of acetonitrile the solvent adduct is formed. For the photocatalytic and electrochemical experiments it is assumed that the molecular structure of the compounds is that shown in Fig. 1.

Steric interactions between the 2,6-bpp ligand and the bipy ligands results in the pyridine ring not coordinated to the Ru(II) centre sitting out of the plane of the other two pyridine rings (*vide infra*). ^{1}H NMR spectroscopy shows that for **1**, which contains the sterically constrained 2,5-bpp ligand (Fig. S1, ESI‡), and for **1a** four sets of bipyridine multiplets (8.64–8.54, 8.15–8.07, 7.95–7.78, 7.48–7.38 ppm) were observed due to the similar chemical environment of all bipyridine ligands. In contrast, up to twelve resolved sets of signals were observed for the bipyridine ligands of **2** and **2a**, indicating the different chemical environments that these ligands are in (Fig. S2, ESI‡). The chemical shifts of the bridging ligands are similar for all complexes. Assignment of the signals observed was facilitated by deuteriation[7] of the bipy ligands (see Fig. S1 and S2, ESI‡) and by the use of ^{1}H COSY NMR spectroscopy.

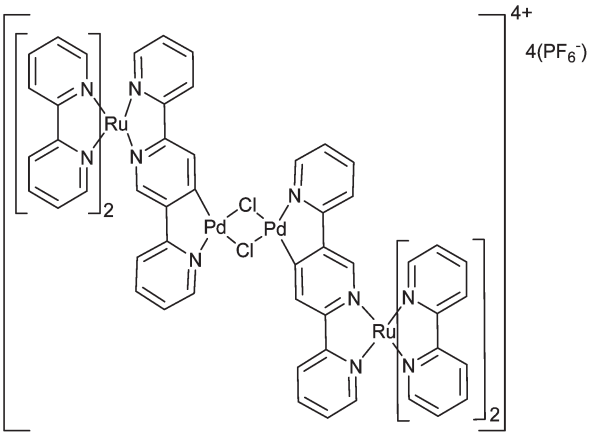

Fig. 2 Possible structure for RuPd photocatalyst **1a** in the solid state.

UV/Vis spectroscopic and redox properties

The spectroscopic and electrochemical properties of the compounds are shown in Table 1 and Fig. 3. The absorption and emission maxima show only minor changes upon addition of the Pd(II) centre; however, a considerable decrease in emission lifetime is observed *e.g.*, from 442 ns for **1** to 105 ns for **1a**. The decrease in emission lifetime, however, is not accompanied by a corresponding decrease in emission quantum yield, which suggests that the coordination of the palladium centre increases the rate of radiative relaxation possible through increased spin orbit coupling effects. A similar observation was made by Sakai and co-workers.[8] This also suggests that the lowest excited states are bipy based for both mono- and heterodinuclear complexes in agreement with transient Raman studies. The DFT calculations suggest however that other excited states with similar energy which are bridge based are also present (*vide infra*).

The electrochemical properties of the complexes were investigated using both CV (cyclic voltammetry) and DPV (differential pulse voltammetry) in DMF (Fig. S3, ESI‡). In acetonitrile very similar results were obtained. **1** and **2** show well-defined oxidation waves {Ru(II)/Ru(III)} and reductions assigned to ligand based reductions.

Interpretation of the cyclic voltammetry of the heterodinuclear complexes is, in contrast, not straightforward due to the observation of a number of irreversible processes (Fig. S3, ESI‡). The data obtained for **1a** and **2a** were compared with those obtained for **1**, **2** and $[(2\text{-phenylpyridine})Pd(\mu\text{-}Cl)]_2$ (**3**). Compounds **1a** and **2a** show three oxidative processes, the second wave at *ca.* 0.84 V for **1a** and at 0.78 V for **2a** is quasi reversible, while the first and third are irreversible. The irreversible processes are assigned to Pd based oxidations by comparison with **3** (Table 1). It is worth noting that the Ru(II)/(III) redox potential does not change significantly upon the coordination of Pd(II). This suggests that the energy of the ground state is largely unaffected. A number of ill-defined processes are observed at negative potentials for both **1a** and **2a**, and assignment of individual redox couples is therefore not possible. Previous studies of related ruthenium complexes have shown that a 2,5-bpp based reduction generally occurs at more positive potentials than for bipy based reductions.[9]

Of particular interest at negative potentials are the Pd(II) based reduction waves. Again a definitive assignment cannot be made, however the least negative processes at −1.67 V (**1a**) and −1.92 V (**2a**) are most likely ligand centred reductions. In compounds **1** and **2** a wave is observed at similar potentials, however assuming that this reduction is bpp based, it can be expected that this

Table 1 UV/Vis spectroscopic and electrochemical properties of **1**, **1a**, **2** and **2a**

	Abs./nm {ε 10^4 M^{-1} cm^{-1}}	Em./nm {τ^a/ns}	Φ_{Em}	$E_{ox}{}^b$ (V)	$E_{red}{}^b$ (V)
1	455 {1.18}	630 {442}	0.047	0.83	−1.64, −1.95, −2.16, −2.53
1a	463 {1.33}	635 {105}	0.032	0.73[c], 0.84, 1.02[c]	−1.43[c], −1.67, −1.88, −2.10, −2.37[d,c], −2.55[d]
2	449 {1.88}	627 {33}	0.003	0.77	−1.77, −1.97, −2.27
2a	449 {1.72}	635 {[e]}	0.001	0.66[c], 0.78, 0.93[c]	−1.76[c], −1.92, −2.10, −2.31, −2.27, −2.37[d]
3				0.70[c], 1.03[c]	−2.31[c], −2.45[c], −2.49

[a] By TCSPC at 293 K in de-aerated acetonitrile solution. [b] Cyclic voltammetry in DMF with 0.1 M $TBAPF_6$ *vs.* Fc/Fc^+ couple. Data were obtained at 263.15 K for **1a** and **2a**. [c] Peak potentials for irreversible processes. [d] Determined using differential pulse voltammetry. [e] lifetime less than instrument response (<1 ns).

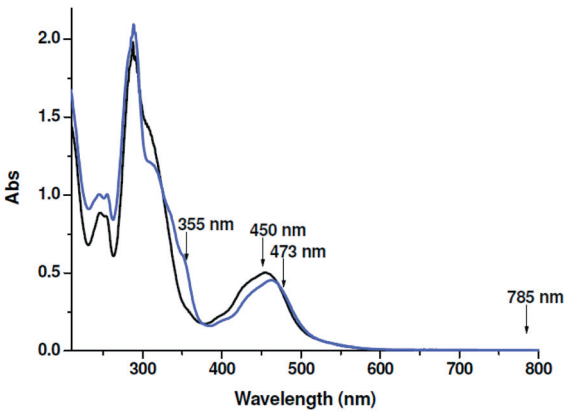

Fig. 3 UV-Vis absorption spectra of **1** (black) and **1a** (blue). Wavelengths used to record Raman spectra are indicated.

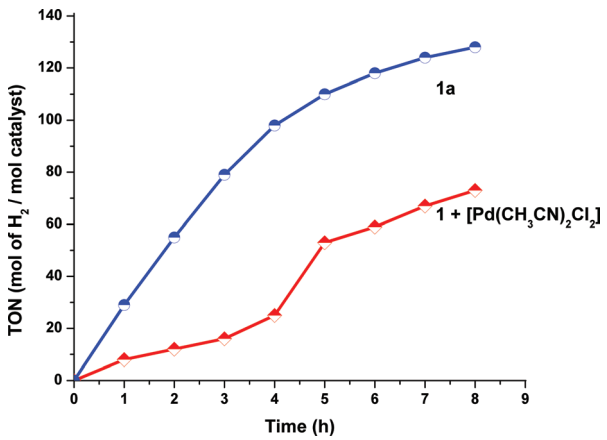

Fig. 4 Time-dependence of the TON achieved for H_2 evolution in the presence of 10% water for **1a** (blue) and **1** with $[Pd(CH_3CN)_2Cl_2]$ (red).

wave will be at more negative potentials when the ligand is cyclo-metallated.

These UV/Vis spectroscopic and electrochemical data overall indicate that coordination of Pd(II) to **1** (and **2**) has only a modest effect and the photophysical properties of the ruthenium centre remain largely unchanged, albeit with a red-shift in the ππ* absorption bands of the bpp ligands to *ca.* 350 nm. The absence of a substantial change in the absorption and emission maxima and the indication from electrochemical data that the Ru(II) centred HOMO orbitals are unchanged in terms of energy suggest that the primary effect of complexation of the Pd(II) centre is to reduce the radiative lifetimes and to introduce an additional excited state deactivation channel (*e.g.*, energy or electron transfer to the palladium centre).

Table 2 Turnover numbers (TON) for hydrogen generation

Compounds / Water content	TON as function of water content[a] (v/v) 0%	5%	10%
1a	0	108	130
2a	0	0	0
1 + $(NH_4)_2[PdCl_4]$[b]	—	50	48
1 + $[Pd(CH_3CN)_2Cl_2]$[b]	—	79	70
2 + $(NH_4)_2[PdCl_4]$[b]	—	0	0
2 + $[Pd(CH_3CN)_2Cl_2]$[b]	—	0	0

[a] Determined by GC after irradiation for 18 h. [b] The reaction mixture contains an equimolar mix of the mononuclear complex and Pd species 3.0×10^{-5} M, [TEA] = 2.30 M.

Photocatalysis

The photocatalytic properties of **1a** and **2a** were investigated in acetonitrile with the sacrificial reductant triethylamine (TEA) and compared with solutions containing the mononuclear complexes **1** or **2** and $[Pd(CH_3CN)_2Cl_2]$. As anticipated no photocatalytic water-splitting, was observed in the absence of water, however when solutions contained 5 or 10 vol% water H_2 was generated with turnover numbers shown in Table 2. The turnover numbers (TONs) for H_2 production obtained after irradiation at 470 nm for 18 h are given in Table 2. TONs of up to 130 (16 μmol after 18 h) were obtained for **1a**. The time dependence of H_2 evolution by **1a**, and **1** with $[Pd(CH_3CN)_2Cl_2]$, expressed as TON over an 8 h period is shown in Fig. 4. Remarkably, H_2 production was not observed with **2a**.

Photocatalytic hydrogen production was also observed when the catalyst was prepared by mixing **1** with $[Pd(CH_3CN)_2Cl_2]$ or $(NH_4)_2[PdCl_4]$ *in situ*; however lower TONs were obtained than for **1a** under the same conditions. Furthermore the lack of activity of the *in situ* prepared catalyst over the first 4 h of the reaction and the absence of conversion when $[Pd(CH_3CN)_2Cl_2]$ was used alone support the conclusion that the H_2 evolution originates from an intramolecular process in the heterodinuclear complex. Furthermore, it is clear from Fig. 4 that the activity is highest in the early stages of the reaction (t < 4 h). Control

experiments with the mononuclear precursors **1** and **2** without Pd species present or by mixing **2a** with $[Pd(CH_3CN)_2Cl_2]$ did not show evidence of H_2 production.

The formation of colloids for H_2 generation has been discussed by several authors.[10] Since both complexes have comparable binding properties for Pd it seems unlikely that one should act as a precursor for catalytically active colloids while the other does not. Indeed given the greater steric demands that the coordination of palladium places on complex **2a**, it would be expected to be this complex that releases palladium more rapidly. This is not the case, however. The formation of a black precipitate is observed for **1**/$[Pd(CH_3CN)_2Cl_2]$ and for **1a** under catalytic conditions and suggests dissociation of the palladium. By contrast precipitates were not observed for **2a** under the same conditions. It should be noted that the standard mercury test,[11] used to identify the presence of Pd nanoparticles, has previously been found to be inappropriate for these types of complexes.[4]

The wavelength dependence of H_2 production by **1a** was examined (Fig. 5). A maximum TON of 130 with 10% water was obtained close to the maximum absorption (463 nm, ε = 1.33 × 10^4 M^{-1} cm^{-1}) when irradiated at 470 nm (ε = 1.28 × 10^4 M^{-1} cm^{-1}) for 18 h (Table 2). For other excitation wavelengths the TON decreased according to the absorption spectrum; at 520 nm (ε = 0.21 × 10^4 M^{-1} cm^{-1}), TON = 51; at 590 nm (ε = 0.03 × 10^4 M^{-1} cm^{-1}), TON = 5; and at 630 nm (ε = 0 M^{-1} cm^{-1}), TON = 0. When differences in molar absorptivity are taken into account, the efficiency is higher when excitation is at longer wavelengths, *i.e.* efficiency is not constant over the visible spectrum.

For heterogeneous photocatalytic hydrogen production with graphitic C_3N_4 (g-C_3N_4) the catalytic activity follows the absorption spectrum strictly.[12,13] However, Rau and co-workers, have observed wavelength dependence for the efficiency of the complex $[Ru(tbbpy)_2(tpphz)PdCl_2](PF_6)_2$ where the catalytic activity did not follow the absorption spectrum strictly.[14] The origin of this effect could lie in the involvement of a one electron reduced intermediate state; *i.e.* excitation of **1a** is followed either by relaxation to **1a** or reduction of the excited complex by TEA to yield **1a**$^-$. The absorption spectrum of this species would be expected to be substantially different and hence the second excitation, if rate limiting, will depend not on the spectrum of **1a** but on the one electron reduced **1a**$^-$. Alternatively, recent studies on related iridium compounds[3j] indicate that the efficiency of hydrogen formation may depend on the nature of the excited state populated as also suggested in ref. 14. These latter investigations on a tpphz based photocatalyst utilised laser excitation sources with a constant photon flux. This is technically not easily accomplished with LED excitations. More detailed studies into these observations are necessary especially with more accurate excitation sources in order to obtain more detailed information.

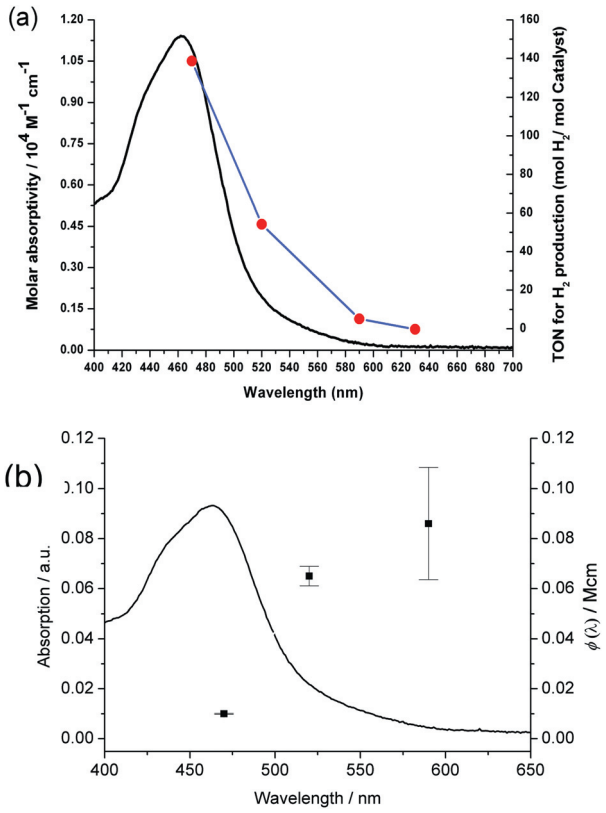

Fig. 5 (a) Wavelength dependence of photocatalytic hydrogen generation and (b) the efficiency spectrum $\Phi(\lambda)$ for complex **1a**. For conditions see the Experimental section.

Raman spectroscopy

Resonance Raman spectroscopy has proven to be a powerful tool in the association of electronic absorption bands with individual ligands, in particular metal to ligand change transfer bands in Ru(II) polypyridyl complexes.[15] In addition the use of nanosecond pulsed lasers can provide information regarding the nature of the lowest electronically excited states.[16] This technique was therefore used to further investigate the electronic properties of the hydrogen producing compound **1a** and its precursor **1**. The excitation wavelengths used to record these spectra are shown in Fig. 3. The (non-resonant) Raman spectra of **1** and **1a** are shown in Fig. 6. For both compounds Raman bands typical of 2,2-bipyridyl ligands are present at 1604, 1556, 1487, 1317, 1274, 1173, 1108, 1039, 1028, 766, 662 and 646 cm^{-1},[17] however, in each case additional bands were observed that can be ascribed to the 2,5-bpp and orthometallated 2,5-bpp$^-$ ligands, respectively. For **1**, bands assignable to the 2,5-bpp ligand are evident at 1604, 1590, 1505, 1474, 1435, 1377, 1324(sh), 1302, 1234, 1030, 991, 805, 678 and 649 cm^{-1}. For **1a** the bands are shifted

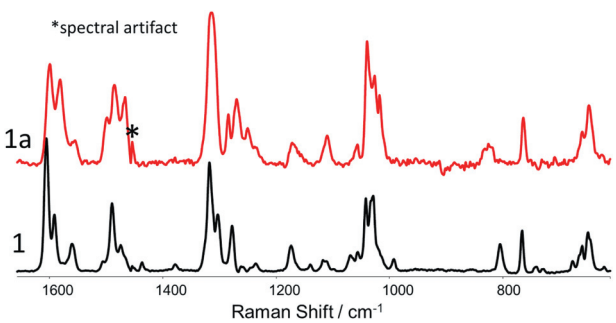

Fig. 6 (Non-resonant) Raman spectra of **1** and **1a** (photocatalyst) in the solid state (λ_{exc} 785 nm).

compared with **1** as expected due to the deprotonation of the 2,5-bpp ligand and are at 1599, 1581, 1499, 1466, 1312, 1283, 1250, 1109, 1027 and 1016 and 647 cm^{-1}. Of particular interest, with regard to the discussion of the resonance Raman data below, are the bands at around 1490 cm^{-1}, as the bands of the 2,5-bpp and (−H)2,5-bpp^- ligands are of comparable intensity to that of the bipy ligands. Importantly, however, it is clear from the non-resonant Raman spectra that vibrational modes of the 2,5-bpp ligand can easily be distinguished from those of the bipy ligands and that the vibrational modes of the bpp ligand change considerably upon orthometallation by the palladium.

The electronic absorption bands observed in **1** and **1a** at 355 nm are absent in $[Ru(bipy)_3]^{2+}$ and are therefore tentatively assigned as 2,5-bpp and 2.5-bpp^- π–π* transitions, respectively. This assignment is confirmed by the resonance Raman spectra recorded at 355 nm (Fig. 7 and 8) in which bands assignable to the 2,5-bpp and 2,5-bpp^- ligands are observed and the well-known bipy modes are completely absent.

Of particular interest in the present study is the nature and localisation of the ^{1}MLCT transitions present in the visible region since they are expected to be heavily involved in the photocatalytic process. Although the relatively strong emission observed for both **1** and **1a** precludes acquisition of spectra at the longest wavelength absorption available (*e.g.*, 532 nm), good quality resonance enhanced Raman spectra could be obtained at 450 and 473 nm, which represent the maximum and red shoulder of the ^{1}MLCT absorption manifolds. For **1**, bands assignable to a bipy based ($^1MLCT_{bipy}$ ← GS) (where GS is ground state) absorption could be observed at 1605, 1560, 1490 cm^{-1} with no significant resonant enhancement of the 2,5-bpp modes. This suggests that for this compound the red side of the MLCT manifold is dominated by bipy based transitions. In stark contrast, for **1a** excitation at both 450 and 473 nm showed strong contributions from modes originating from both the bipy ligands and the 2,5-bpp^- ligand, with the 2,5-bpp^- modes dominating the Raman spectrum when excitation was at the red edge of the absorption manifold (*i.e.* 473 nm), Fig. 8. This indicates that for

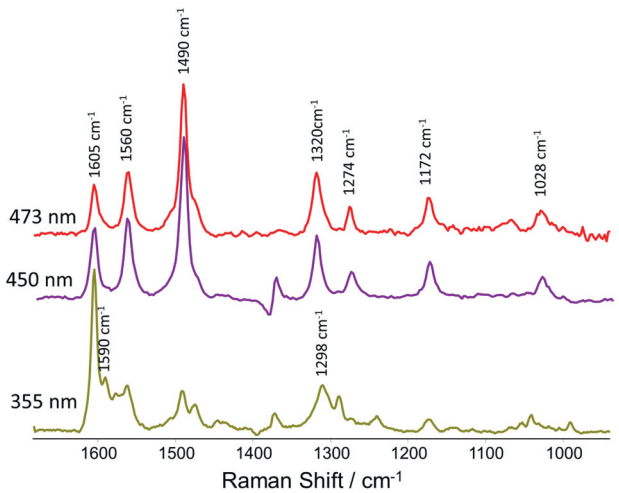

Fig. 7 Resonance Raman spectra of **1** in CH_3CN (solvent subtracted) at 355, 450 and 473 nm.

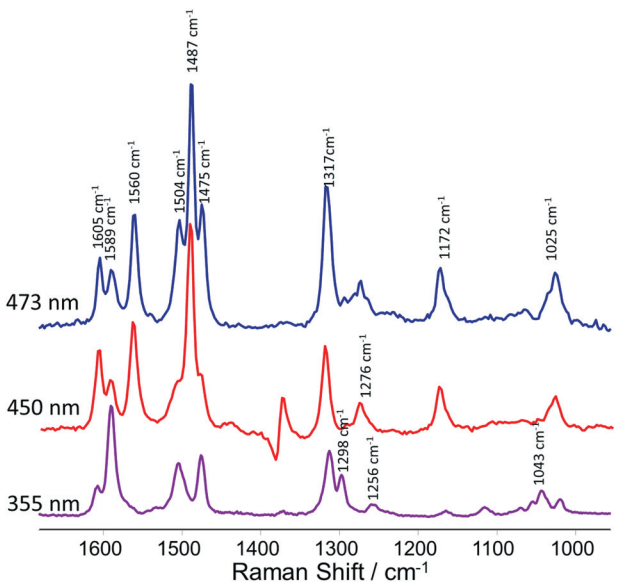

Fig. 8 Resonance Raman spectra of **1a** in CH_3CN (solvent subtracted) at 355, 450 and 473 nm.

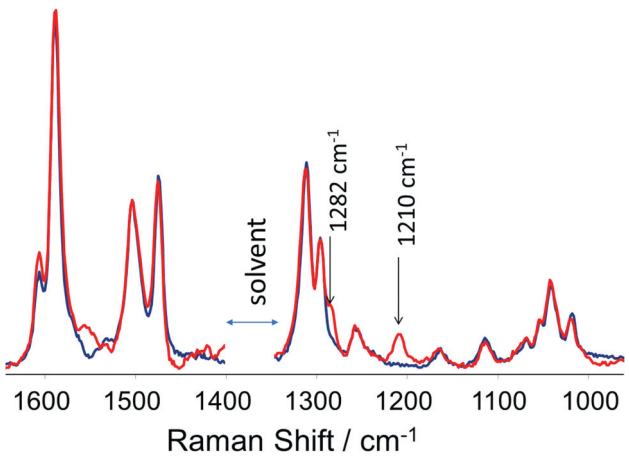

Fig. 9 Resonance Raman spectra of **1a** in CH_3CN (solvent subtracted) at 355 nm with (blue) continuous wave (CW) and (red) pulsed excitation. The characteristic modes of the bipy anion radical are observed at 1282 and 1210 cm^{-1}.

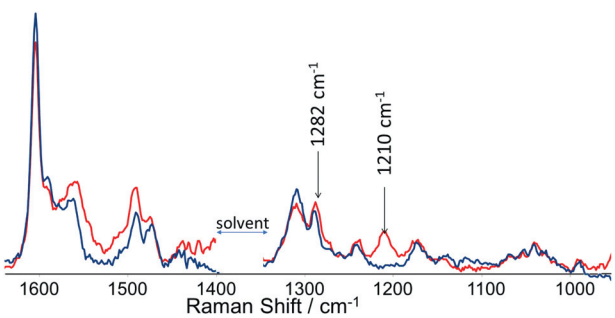

Fig. 10 Resonance Raman spectra of **1** in CH_3CN (solvent subtracted) at 355 nm with (blue) CW and (red) pulsed excitation. The characteristic modes of the bipy anion radical are observed at 1282 and 1210 cm^{-1}.

1a, ^{1}MLCT$_{bpp^-}$ ← GS transitions are generally lower or equal in energy to the ^{1}MLCT$_{bipy}$ ← GS transitions.

Resonance Raman spectra obtained with pulsed rather than continuous wave excitation at 355 nm can potentially provide further information as to the nature of the lowest ^{3}MLCT excited state as shown in Fig. 9 and 10. For **1** and **1a** the strong resonance enhancement of Raman scattering from the 2,5-bpp ligand (*vide supra*) means that the spectra obtained with pulsed excitation are dominated by ground state modes. Nevertheless, comparison of spectra obtained at 355 nm using CW and pulsed excitation shows the appearance of bands characteristic of the bipy anion radical[17] and hence although significant population of a 2,5-bpp based ^{3}MLCT excited cannot be excluded, it is clear that the lowest ^{3}MLCT manifold also involves bipy based ^{3}MLCT states.

Computational studies

The data described above confirm that the Ru/Pd complexes **1a** and **2a** have different catalytic behaviours. High level DFT calculations were carried out to further investigate the electronic properties of the complexes. The geometries of complexes **1**, **1a**, **2** and **2a** were calculated as minimum structures and the IEF-PCM formalism was used to model the influence of the solvent acetonitrile (for details see Experimental part). Although the singlet states of Ru(II) polypyridyl complexes can be reasonably well described by the popular B3LYP functional (20% Hartree–Fock exchange) it failed for the calculation of the lowest energy triplet states. We thus tested three τ-dependent functionals with varying Hartree–Fock contributions, namely, M06-L (0%), M06 (27%) and M06-HF (100%).[18] M06-L and M06 were successfully applied for the modelling of the lowest energy triplet state of **1a** and **2a** but M06-HF failed. M06 was then chosen for the re-calculation of the singlet states and also for the modelling of the singly reduced doublet states, since the M06 results give a more delocalised picture. It is worth noting that the calculations are sensitive to the chosen functional and hence great care must be taken. A comparison of selected calculated and experimental bond lengths is given in Table 3 and the structures of the calculated complexes are given in Fig. 11. The differences due to the metallation and the different structures of the bridging ligands were studied by comparing the calculated geometric parameters of the dinuclear complexes **1a** and **2a** with each other as well as with their mononuclear counterparts. In agreement with the UV/Vis absorption data, the 2,5-bpp ligand of **1a** can be considered as a pyridyl substituted bipyridine with electronic communication between the two parts. In contrast the 2,6-bpp ligand can be viewed as a bipyridine in which there is little communication with its pyridyl substituent. This is due to the geometric distortions discussed above and is apparent in the results of the calculations (Fig. 11). Delocalisation of bridge based molecular orbitals is not hindered by the metallation of the central pyridine ring. Comparison of the M06 geometries of **1** and **1a** as well as **2** and **2a** revealed no induced alteration of the bridging ligand bond lengths on addition of palladium. Analysis of the charges on each atom also shows that the presence of palladium does not result in changes except for the metallated carbon atom having a more negative value. In summary, the charge of the cyclo-metallated carbon is localised and the electronic properties of the bridge remain mainly unchanged. The only exception is the metallation induced planarity of the 2,5-bpp-bridge of **1a** that allows for greater delocalisation of bridge-based orbitals and hence a red shift of transitions that have significant contributions from the bpp ligand. The geometric distortion of the 2,6-bpp-bridge remains in the metallated complex **2a** and hence prevents substantial delocalisation of bridge based orbitals. The out of plane nature of the 2,6-bpp bridge leads to larger Ru–N bond lengths varying between 220 pm for the Ru–N(ring-A) and 206 pm Ru–N(bipy).

Table 3 Comparison of experimental values with the M06 geometries of singlet-**1a** and singlet-**2a**

Bond lengths [pm]	**1a** (M06)	**2a** (M06)	Exp	Ref.
Ru–N	208[a]	211[a]	205[a]	19
Pd–Cl	235	235	236	20
Pd–N	208	207	202	20
Pd–ACN	214	214	214	20
Pd–C	198	198	199	20

The angular nature of the 2,6-bpp bridge leads to larger Ru–N(py) bond lengths.[a] Average values.

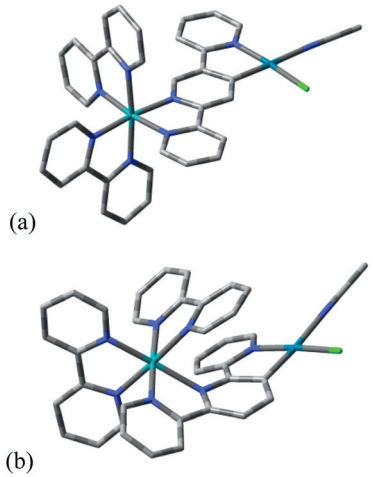

Fig. 11 Presentation of the optimised structures of (a) singlet-**1a** and (b) singlet-**2a**.

The spatial localisation of the molecular orbitals was calculated through a population analysis. Their localisation on a certain part of the molecule is expressed as per cent contribution and given in Tables S1–S6, ESI.‡ The calculations indicate that the localisation of the SOMOs in the triplet states of **1a** and **2a** differ from the localisation of the LUMO of their singlet states. However, the LUMO of the singlet state and the SOMO of the mono-reduced doublet state have a similar spatial localisation.

Analysis of the frontier orbitals of the singlet ground state of ^{1}**1a** and ^{1}**2a** shows the expected electronic configuration. The three highest energy occupied orbitals (HOMO-2–HOMO) are localised on the Ru(II) centre (Fig. 12 and Tables S1–S6, ESI‡). The LUMO is a bridge based orbital while L+1 and L+2 are localised on the bipy ligands. This is in agreement with resonance Raman results that show electronic transitions to the bpp ligand at lower energy than the electronic transitions to the bipy

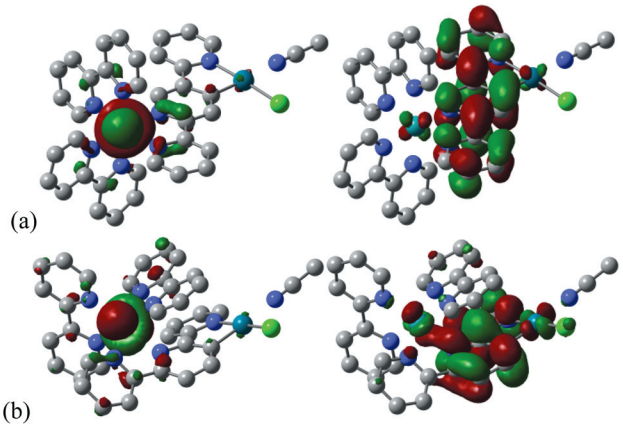

Fig. 12 Presentation of selected frontier orbitals. (a) ^{1}**1a** HOMO and LUMO and (b) ^{1}**2a** HOMO and LUMO.

ligands. The lowest energy triplet states are assumed to be the emissive state and were calculated as fully relaxed minimum structures, thus the energy difference between the triplet and the singlet state should match the E^{0-0} emission energy. Indeed, the M06 SCF energy difference (ΔSCF = SCF (Triplet) − SCF (Singlet)) for **1a** is 15 481 cm^{-1} (646 nm), which is only a slightly longer wavelength than the actual emission maximum, λ_{em} = 15 748 cm^{-1} (635 nm). The M06 ΔSCF energy of **2a** is 10 633 cm^{-1}, which is much lower than the experimentally determined emission (Table 1), which precludes a detailed comparison between theory and experiment in this case.

Analysis of the localisation of the two unpaired electrons of ^{3}**1a** and ^{3}**2a** reveals several interesting differences. The highest energy singly occupied molecular orbital (SOMO) of ^{3}**1a** is located on the bridge while for ^{3}**2a** it is localised on the ruthenium centre (Fig. 12 and ESI‡). The SOMO-1 of ^{3}**1a** and ^{3}**2a** are both delocalised on the Pd centre and the bridging ligand. These results are surprising as it would be expected that the triplet state SOMO (of highest energy) would resemble the singlet state LUMO. It is furthermore surprising that the ruthenium centre of **1a** makes only negligible contributions to the SOMOs. The one electron reduced complexes are possible candidates for the resting state during the catalysis and may be formed *via* excitation followed by reduction from the sacrificial donor or direct one electron reduction in an electrochemical experiment. We modelled the minimum structure of the species ^{2}**1a** and ^{2}**2a** having a net charge of +1 and a multiplicity of 2. Both, ^{2}**1a** and ^{2}**2a** were calculated with the M06 functional showing a delocalisation of the unpaired electron over the whole bridge for ^{2}**1a** and a delocalisation over the central pyridine ring and the Pd-bound pyridine ring for ^{2}**2a** (Tables S5 and S6, ESI‡). This suggests that the first reduction is indeed a bridge based process as discussed above.

Conclusions

In the present contribution, the importance of the structure of the bridging ligand to the effectiveness of heterodinuclear Ru/Pd complexes is demonstrated as is the potential of a system in which an intramolecular approach is taken with regard to combining a light harvesting component and a catalyst within the same molecule. This approach contrasts with the more widely used approach where these functions are carried out by distinct components.

In the present study the photocatalytic ability of two structurally and electronically similar complexes are shown to be very different and that the activity of **1a** is not due to the formation of nanoparticles or other palladium species. However, the nature of the actual catalytically active species remains elusive. The origin of the differences in catalytic ability of **1a** and **2a** may be related to the localisation of the LUMO since the first step in the catalytic cycle involves the formation of a one electron reduced complex. In **1a** the LUMO is mainly based on the bridge according to DFT calculations and furthermore the triplet excited state is based on the bridging ligand with only a minor contribution on the Ru centre. By contrast for ^{3}**2a** this orbital is mostly based on the bipy ligands and the Ru centre. This latter arrangement is not as favourable for electron transfer as that observed for **1a**. Although excited state lifetimes do not correlate with hydrogen production the short excited state lifetime of **2a** may also be a possible reason for the absence of catalytic activity.[3g]

Future studies will focus on the preparation of less labile complexes, the use of less corrosive sacrificial agents or ultimately their elimination by the developing surface bound assemblies.

Experimental

Reagents for synthesis were purchased as reagent grade and were used without further purification. 2,2′:6′,2″-terpyridine (2,6-bpp) was obtained commercially and used as received.

Synthesis and characterisation

2,2′:5′,2″-terpyridine (2,5-bpp) was synthesised using the procedure of Kozhevnikov *et al.* with modifications.[5] $Pd(PPh_3)_4$ (0.3 g, 0.26 mmol) and 2,5-dibromopyridine (1 g, 4.22 mmol) were added under a nitrogen atmosphere to a dried two neck round bottom flask. The mixture was cooled to 0 °C in an ice bath and a 0.5 M solution of 2-pyridylzinc bromide in tetrahydrofuran (19.5 cm^3, 9.75 mmol) was added *via* syringe. The temperature was kept constant at 0 °C during addition. Subsequently the reaction mixture was stirred for 12 h at room temperature under a nitrogen atmosphere and a white precipitate formed. The reaction mixture was poured onto 200 cm^3 of a saturated aqueous solution of EDTA and Na_2CO_3 and stirred until the precipitate dissolved and a yellow precipitate formed. The aqueous solution and the precipitate were extracted with dichloromethane and the combined organic phase was dried over $MgSO_4$. Removal of the solvent *in vacuo* yielded the crude product which was purified by column chromatography (neutral alumina, hexane–ethyl acetate (9.5 : 0.5 v/v), TLC: R_f = 0.15). Yield: 0.5 g (51%). ^{1}H-NMR (DMSO-d_6, 400 MHz): δ = 9.40 (d, J = 2.4 Hz, 1H, H_6), 8.74 (m, 2H, $H_{6'}$, $H_{6''}$), 8.62 (dd, J = 8.4 Hz, J = 2.0 Hz, 1H, H_4), 8.52 (d, J = 8.4 Hz, 1H, H_3), 8.47 (d, J = 7.8 Hz, 1H, $H_{3''}$), 8.15 (d, J = 8.1 Hz, 1H, $H_{3'}$), 7.98 (m, 2H, $H_{4'}$, $H_{4''}$), 7.48 (m, 2H, $H_{5'}$, $H_{5''}$).

$[Ru(bipy)_2(2,5\text{-bpp})](PF_6)_2 \cdot 0.5(CH_3)_2CO$ (**1**): $[Ru(bipy)_2Cl_2] \cdot 2H_2O$ (0.339 g, 0.65 mmol) dissolved in 5 cm^3 of ethanol was

added drop-wise to a solution of 2,2′:5′,2″-terpyridine (0.152 g, 0.65 mmol) in 10 cm^3 of ethanol–water (3 : 1 v/v). The reaction mixture was heated at reflux for 8 h. Subsequently, the mixture was allowed to cool to room temperature and the solvent was removed *in vacuo*. The residue was precipitated in saturated aqueous solution of NH_4PF_6 followed by filtration of the product, which was then washed with 10 cm^3 of diethyl ether. Recrystallisation from acetone–water (3 : 1 v/v) afforded a red solid. Yield: 0.576 g, 92%. Anal. Calcd for $C_{35}H_{27}F_{12}N_7P_2Ru{\cdot}0.5\ (CH_3)_2CO$ (965.67): C, 45.39; H, 3.13; N, 10.15%. Found: C, 45.06; H, 2.95; N, 9.88%. ^{1}H-NMR (acetonitrile-d_3, 400 MHz): δ = 8.64–8.54 (m, 4H, bipy H_{3a}), 8.60–8.58 (m, 2H, H_3, H_4), 8.54–8.52 (m, 2H, $H_{3''}$, $H_{6'}$), 8.30 (s, 1H, H_6), 8.15–8.07 (m, 4H, bipy H_{4a}), 8.07 (t, 1H, J = 8.0 Hz, $H_{4''}$), 7.95–7.78 (m, 4H, bipy H_{6a}), 7.83 (t, 1H, J = 7.8 Hz, $H_{4'}$), 7.75 (d, 1H, J = 5.6 Hz, $H_{6''}$), 7.67 (d, 1H, J = 7.6 Hz, $H_{3'}$), 7.48–7.38 (m, 4H, bipy H_{5a}), 7.41 (m, 1H, $H_{5''}$), 7.36 (m, 1H, $H_{5'}$).

$[Ru(bipy)_2(2,5\text{-bpp})Pd(CH_3CN)Cl](PF_6)_2$ (**1a**): $[Ru(bipy)_2(2,5\text{-bpp})](PF_6)_2$ (0.100 mg, 0.11 mmol) was dissolved in 5 cm^3 of methanol and added drop wise to a solution of $(NH_4)_2PdCl_4$ (0.027 g, 0.10 mmol) in 10 cm^3 of methanol. The reaction mixture was heated at reflux for 48 h. Subsequently the mixture was allowed to cool to room temperature. The product was precipitated by addition of 20 cm^3 of *n*-hexane. After filtration and washing with 10 ml of diethyl ether the red solid was recrystallised from acetone–acetonitrile (1 : 1 v/v). Yield: 0.100 g, 84%. Anal. Calcd for $C_{37}H_{29}ClF_{12}N_8P_2PdRu{\cdot}$(1118.55): C, 39.73; H, 2.61; N, 10.02%. Found: C, 39.49; H, 2.82; N, 10.04%. ^{1}H-NMR (acetonitrile-d_3, 400 MHz): δ = 9.51 (d, J = 6.0 Hz, 1H, $H_{6'}$), 9.13 (s, 1H, H_3), 8.64–8.54 (m, 4H, bipy H_{3a}), 8.45 (d, J = 8.4 Hz, 1H, $H_{3''}$), 8.15–8.07 (m, 4H, bipy H_{4a}), 8.01 (m, 1H, $H_{4''}$), 7.95–7.78 (m, 4H, bipy H_{6a}), 7.86 (m, 1H, $H_{4'}$), 7.67 (d, J = 5.6 Hz, 1H, $H_{6''}$), 7.46 (s, 1H, H_6), 7.48–7.38 (m, 4H, bipy H_{5a}), 7.39 (m, 1H, $H_{5'}$), 7.34 (m, 1H, $H_{5''}$), 7.18 (d, J = 7.6 Hz, $H_{3'}$), 2.06 (s, 3H, CH_3CN).

$[Ru(bipy)_2(2,6\text{-bpp})](PF_6)_2{\cdot}2H_2O$ (**2**): $[Ru(bipy)_2Cl_2]{\cdot}2H_2O$ (0.500 g, 0.96 mmol) dissolved in 6 cm^3 ethanol was added drop-wise to a solution of 2,2′;6′,2″-terpyridine (0.224 g, 0.96 mmol) in 40 cm^3 ethanol–water (3 : 1). The reaction mixture was heated at reflux for 6 h. Subsequently, the mixture was allowed to cool to room temperature and the solvent was removed *in vacuo*. The residue was precipitated in saturated aqueous solution of NH_4PF_6 followed by filtration of the product, which was then washed with 10 cm^3 of diethyl ether. Recrystallisation from acetone–water (3 : 1 v/v) afforded a red solid. Yield: 0.510 g, 54%. Anal. Calcd for $C_{35}H_{27}F_{12}N_7P_2Ru{\cdot}2H_2O$: C, 43.22; H, 3.21; N, 10.08%. Found: C, 43.15; H, 2.82; N, 9.99% ^{1}H-NMR (acetonitrile-d_3, 400 MHz): δ = 8.75 (br s, 1H, bipy H_{3a}), 8.63 (m, 2H, H_5, $H_{3''}$), 8.48 (d, 1H, J = 7.5 Hz, bipy H_{3a}), 8.42–8.39 (m, 2H, bipy H_{3a}), 8.17–8.07 (m, 6H, H_4, $H_{4''}$, $H_{3'}$, bipy H_{4a} (3H)), 7.96 (t, 1H, J = 7.8 Hz, bipy H_{4a}), 7.67 (d, 1H, J = 6.0 Hz, bipy H_{6a}), 7.62 (t, 1H, J = 7.5 Hz, bipy H_{5a}), 7.58–7.53 (m, 2H, $H_{6''}$, bpy H_{6a} (1H)), 7.41–7.28 (m, 5H, H_3, $H_{5''}$, $H_{5'}$, bipy H_{6a} (1H), bipy H_{5a} (1H)), 7.21 (t, 1H, J = 7.6 Hz, bipy H_{5a}), 6.99 (t, 1H, J = 7.5 Hz, $H_{4'}$), 6.88 (d, 1H, J = 7.6 Hz, bipy H_{6a}), 6.85–6.76 (m, 2H, $H_{6'}$, bipy H_{5a} (1H)).

$[Ru(bipy)_2(2,6\text{-bpp})Pd(CH_3CN)Cl](PF_6)_2H_2O$ (**2a**): $[Ru(bipy)_2(2,6\text{-bpp})](PF_6)_2$ (0.102 g, 0.11 mmol) dissolved in 5 cm^3 of methanol was added drop-wise to a solution of $(NH_4)_2[PdCl_4]$ (0.029 g, 0.11 mmol) in 10 cm^3 of methanol. The reaction mixture was heated at reflux for 72 h. Subsequently the mixture was allowed to cool to room temperature. The product was precipitated by addition of 20 cm^3 of *n*-hexane. After filtration and washing with 10 cm^3 of diethyl ether a red solid was recrystallised from acetone–acetonitrile (1 : 1 v/v). Yield: 0.058 g, 50%. Anal. Calcd for $C_{37}H_{29}ClF_{12}N_8P_2PdRu{\cdot}H_2O$: (1136.55): C, 39.10; H, 2.75; N, 9.86%. Found: C, 38.96; H, 2.49; N, 9.84%. ^{1}H-NMR (acetonitrile-d_3, 400 MHz): δ = 9.12 (br s, 1H, $H_{6'}$), 9.01 (br s, 1H, bipy H_{3a}), 8.75 (d, 1H, J = 7.5 Hz, bipy H_{3a}), 8.66 (d, 1H, J = 7.5 Hz, bipy H_{3a}), 8.42 (d, 1H, J = 7.8 Hz, $H_{3''}$), 8.40 (d, 1H, J = 7.5 Hz, bipy H_{3a}), 8.24 (ddd, 1H, J = 7.5 Hz, J = 1.5 Hz, bipy H_{4a}), 8.12–8.00 (m, 4H, $H_{4''}$, bipy H_{4a}), 7.93 (d, 1H, J = 7.5 Hz, H_4), 7.88 (d, 1H, J = 7.6 Hz, bipy H_{6a}), 7.80 (d, 1H, J = 7.7 Hz, $H_{3'}$), 7.70 (d, 1H, J = 7.5 Hz, H_3), 7.69–7.59 (m, 3H, bipy H_{6a}), 7.55 (d, 1H, J = 7.5 Hz, bipy H_{5a}), 7.50 (t, 1H, J = 7.8 Hz, $H_{4'}$), 7.46 (d, 1H, J = 7.8 Hz, $H_{6''}$), 7.29 (t, 1H, J = 7.5 Hz, bipy H_{5a}), 7.27 (t, 1H, J = 7.8 Hz, $H_{5''}$), 7.18 (t, 1H, J = 7.5 Hz, bipy H_{5a}), 7.09 (t, 1H, J = 7.4 Hz, bipy H_{5a}), 7.02 (t, 1H, J = 7.8 Hz, $H_{5'}$), 2.07 (s, 3H, CH_3CN).

NMR spectra were recorded on a Bruker Advance 400 spectrometer and referenced to the solvent signal. Elemental analysis was carried out on an Exador Analytical CE440 by the Microanalytical Department of the University College Dublin. UV/Vis absorption spectra were recorded on Varian Cary 50 spectrophotometer at 20 ± 1 °C in a 1 cm pathlength quartz cuvette. Acetonitrile for spectrophotometric measurements was purchased from Aldrich in spectrophotometric grade and used as received. Electrochemical data were obtained by cyclic voltammetry and differential pulse voltammetry using a either a two-neck, V-shaped cell or a three-neck cell equipped with a Luggin capillary. Data were collected using a Ag wire quasi-reference electrode with ferrocene added as an internal reference at the end of each experiment ($E^{o'}_{Fc/Fc+}$ = 0.652 V); a Pt wire served as counter electrode. Potentials were corrected with iR compensation during data collection. Complexes were dissolved and de-aerated with UHP-grade argon in anhydrous DMF/0.1 M Bu_4NPF_6.

Emission and excitation spectra were obtained on a Perkin Elmer LS 50B at 20 ± 1 °C. Quantum yields were obtained from de-aerated acetonitrile solutions with [ruthenium(II)-tris(2,2′-bipyridine)] dichloride in water as a standard. Excited-state lifetimes were measured by time-correlated single photon counting on an Edinburgh Analytical Instruments TCSPC instrument (at 293 K) in de-aerated acetonitrile solution (freeze–pump–thaw triple sequence). Samples were excited with a LED at 360 nm. Raman spectra at 785 nm excitation were recorded using a Perkin Elmer Raman station. Continuous wave Raman Spectra at 355 nm (10 mW, Cobolt lasers), 450 nm (50 mW, Power technology) and 473 nm (75 mW, Cobolt lasers) were recorded using a 180° backscattering arrangement as described previously.[21] Raman scattering was focused into a Shamrock 303i spectrograph and dispersed with either a 500 nm blaze 1800 l mm^{-1} or 400 blaze 2400 l mm^{-1} grating onto an iDus-BU2 CCD camera (Andor technology) cooled at −60 °C. Transient Raman spectra were recorded using the same system as for CW Raman studies except that a frequency tripled Nd-YAG laser (355 nm, 6 ns FWHM, between 0.5 and 4 mJ per pulse, operating at 10 Hz, Innolas Spitlight 200). UV/Vis absorption spectra of samples

before and after measurements were recorded to verify that photo-decomposition did not occur during the recording of Raman spectra.

Calculations

All calculations were carried out with the Gaussian 09 program suite.[22] The compounds **1**, **1a**, **2** and **2a** were optimized using the M06 functional. The MWB28[23] basis with an effective core potential was used for the heavy Ru and Pd atoms while 6-31G (d) was used for the remainder. Tight convergence criteria were applied for the geometry optimization process and local minima were confirmed by a frequency calculation. All calculations were carried out in the presence of a solvent sphere, which was modelled by the IEF-PCM[24] method in acetonitrile (ε = 35.688000). Orbital contributions were calculated by a Mulliken population analysis and evaluated using GaussSum.[25]

Photocatalysis

All manipulations were carried out under strictly anaerobic inert conditions. Acetonitrile was dried over calcium hydride and triethylamine over sodium according to common procedures and freshly distilled under nitrogen prior to use. Photocatalytic hydrogen production experiments were carried out using a home-built air-cooled apparatus (at 22 °C) under constant irradiation (LED 470 nm) of the sample. For the photocatalysis experiments 2 cm^3 of the sample solution were added to GC vials (total volume 5 cm^3, diameter 13 mm, 3 cm^3 headspace) in the dark and under a stream of nitrogen. The vials were closed with gas-tight septum caps. A typical sample solution was prepared by mixing 0.65 cm^3 of a 1.8×10^{-4} M Ru/Pd complex in acetonitrile, 0.6 ml of triethylamine, 0.0–0.2 ml (0–10 vol%) of thoroughly degassed water and 0.55–0.75 ml of anhydrous acetonitrile. Subsequently, the GC vials were irradiated at 470 nm using an LED for 18 h. After irradiation, 20 µl samples were drawn from the headspace with a gas tight syringe (50 µl, SGE Analytical Science) and determined by GC, a Varian CP3800 chromatograph, with a thermal conductivity detector and a CP7536 Plot Fused Silica 25 MX 0.32 MMID column (length 25 m, layer thickness 30 µm) with nitrogen carrier gas (purity 99.999%). The GC was calibrated using 100% hydrogen gas. The obtained signal (retention time for H_2 = 1.58 min) was plotted against the calibration curve and multiplied accordingly to determine the total amount of hydrogen in the headspace. The LED-torch consists of a stick-shaped printed board (19 × 1 cm) with 30 blue LEDs (Kingbright, type L-7113PBC-G, 470 ± 20 nm) with a luminous efficiency of 2000 mcd per LED. LEDs are soldered closely on front and backside in a range of 9 cm. The torch was then placed within the home built reactor. The utilised LED excitation sources have comparable but different light intensities measured in candela, however the candela unit is not linear but has to be referenced to the CIE eye sensitivity function, $V(\lambda)$. This sensitivity function has a nearly Gaussian distribution with maximum sensitivity at 555 nm and steep tails to approximately 370 nm and 760 nm. As a consequence the photon flux of a 470 nm LED and a 520 nm LED with similar candela strength is different [International Commission on Illumination (usually abbreviated CIE for its French name, Commission Internationale de l'éclairage), 1978]. For wavelength dependent catalysis the GC vials containing the catalytic solution were irradiated with High Power LEDs with a diameter of 10 mm and constantly cooled to room temperature as described above. The manufacturer's data of the LEDs used are as follows: 470 nm LED: I = 5 lumen, 20 000 mcd; 520 nm LED: I = 15 lumen, 50 000 mcd; 590 nm LED: I = 8 lumen, 32 000 mcd; 630 nm LED: I = 9 lumen, 20 000 mcd. Analysis of the catalytic activity by GC was performed as described above.

Acknowledgements

This research is supported by the EPA grant 2008-ET-MS-3-S2 and the SFI under Grants No. 07/SRC/B1160 and 08/RFP/CHE1349, the Netherlands Organisation for Scientific Research through a VIDI grant (WRB) and the German Research Association (DFG SFB 583, SR and GRK 1626; MPG).

References

1 (*a*) P. Chen and T. J. Meyer, *Chem. Rev.*, 1998, **98**, 1439; (*b*) B. S. Brunschwig, C. Creutz and N. Sutin, *Chem. Soc. Rev.*, 2002, **31**, 168; (*c*) K. D. Demadis, C. M. Hartshorn and T. J. Meyer, *Chem. Rev.*, 2001, **101**, 2655; (*d*) W. R. Browne, R. Hage and J. G. Vos, *Coord. Chem. Rev.*, 2006, **250**, 1653; (*e*) J. G. Vos and J. M. Kelly, *Dalton Trans.*, 2006, 4869; (*f*) W. R. Browne, N. M. O'Boyle, J. J. McGarvey and J. G. Vos, *Chem. Soc. Rev.*, 2005, **34**, 641.

2 (*a*) S. Rau, B. Schäfer, D. Gleich, E. Anders, M. Rudolph, M. Friedrich, H. Görls, W. Henry and J. G. Vos, *Angew. Chem., Int. Ed.*, 2006, **45**, 6215; (*b*) S. Rau, D. Walther and J. G. Vos, *Dalton Trans.*, 2007, 915; (*c*) H. Ozawa and K. Sakai, *Chem. Commun.*, 2011, **47**, 2227.

3 (*a*) H. Ozawa, Y. Yokoyama, M. Haga and K. Sakai, *Dalton Trans.*, 2007, 1197; (*b*) S. A. Arachchige, J. Brown and K. J. Brewer, *J. Photochem. Photobiol., A*, 2008, **197**, 13; (*c*) E. D. Cline, S. E. Adamson and S. Bernhard, *Inorg. Chem.*, 2008, **47**, 10378; (*d*) P. W. Du, K. Knowles and R. Eisenberg, *J. Am. Chem. Soc.*, 2008, **130**, 12576; (*e*) A. Fihri, V. Artero, M. Razavet, C. Baffert, W. Leibl and M. Fontecave, *Angew. Chem., Int. Ed.*, 2008, **47**, 564; (*f*) C. Li, M. Wang, J. X. Pan, P. Zhang, R. Zhang and L. C. Sun, *J. Organomet. Chem.*, 2009, **694**, 2814; (*g*) Y. Miyake, K. Nakajima, K. Sasaki, R. Saito, H. Nakanishi and Y. Nishibayashi, *Organometallics*, 2009, **28**, 5240; (*h*) B. Probst, C. Kolano, P. Hamm and R. Alberto, *Inorg. Chem.*, 2009, **48**, 1836; (*i*) M. Schulz, M. Karnahl, M. Schwalbe and J. G. Vos, *Coord. Chem. Rev.*, 2012, **256**, 1682; (*j*) S. Soman, G. Singh Bindra, A. Paul, R. Groarke, J. C. Manton, F. M. Connaughton, M. Schultz, D. Dini, C. Long, M. T. Pryce and J. G. Vos, *Dalton Trans.*, 2012, DOI: 10.1039/c2dt32028b.

4 G. Singh Bindra, M. Schulz, A. Paul, S. Soman, R. Groarke, J. Inglis, M. T. Pryce, W. R. Browne, S. Rau, B. J. Maclean and J. G. Vos, *Dalton Trans.*, 2011, **40**, 10812.

5 (*a*) V. N. Kozhevnikov, D. N. Kozhevnikov, O. V. Shabunina, V. L. Rusinov and O. N. Chupakhin, *Tetrahedron Lett.*, 2005, **46**, 1791; (*b*) V. N. Kozhevnikov, O. V. Shabunina, D. S. Kopchuk, M. M. Ustinova, B. König and D. N. Kozhevnikov, *Tetrahedron*, 2008, **64**, 8963.

6 C. J. Mathews, P. J. Smith and T. Welton, *J. Mol. Catal. A: Chem.*, 2004, **214**, 27.

7 W. R. Browne, C. M. O'Connor, J. S. Killeen, A. L. Guckian, M. Burke, P. James, M. Burke and J. G. Vos, *Inorg. Chem.*, 2002, **41**, 4245.

8 K. Sakai, H. Ozawa, H. Yamada, T. Tsubomura, M. Hara, A. Higuchi and M. Haga, *Dalton Trans.*, 2006, 3300–3305.

9 (*a*) L. Cassidy, S. Horn, L. Cleary, Y. Halpin, W. R. Browne and J. G. Vos, *Dalton Trans.*, 2009, 3923; (*b*) Y. Halpin, L. Cleary, L. Cassidy, S. Horne, D. Dini, W. R. Browne and J. G. Vos, *Dalton Trans.*, 2009, 4146.

10 (*a*) P. Du, J. Schneider, L. Fan, W. Zhao, U. Patel, F. N. Castellano and R. Eisenberg, *J. Am. Chem. Soc.*, 2008, **130**, 5056; (*b*) P. Lei,

M. Hedlund, R. Lomoth, H. Rensmo, O. Johansson and L. Hammarström, *J. Am. Chem. Soc.*, 2008, **130**, 26.
11 (*a*) R. Baba, S. Nakabayashi, A. Fujishima and K. Honda, *J. Phys. Chem.*, 1985, **89**, 1902; (*b*) D. R. Anton and R. H. Crabtree, *Organometallics*, 1983, **2**, 855.
12 H. Ozawa, M. Haga and K. Sakai, *J. Am. Chem. Soc.*, 2006, **128**, 4926.
13 X. Wang, K. Maeda, A. Thomas, K. Takanabe, G. Xin, J. M. Carlsson, K. Domen and M. Antonietti, *Nat. Mater.*, 2009, **8**, 76.
14 S. Tschierlei, M. Karnahl, M. Presselt, B. Dietzek, J. Guthmüller, L. Gonzalez, M. Schmitt, S. Rau and J. Popp, *Angew. Chem., Int. Ed.*, 2010, **49**, 3981.
15 (*a*) J. R. Ferraro and K. Nakamoto, *Introductory Raman Spectroscopy*, Academic Press Limited, London, 1994; (*b*) D. F. Morris and W. H. Woodruff, in *Spectroscopy of Inorganic Based Materials*, ed. R. J. H. Clark and R. E. Hester, John Wiley & Sons, New York, 1987; (*c*) D. P. Strommen and K. Nakamoto, *J. Chem. Educ.*, 1977, **54**, 474; (*d*) W. R. Browne, N. M. O'Boyle, J. J. McGarvey and J. G. Vos, *Chem. Soc. Rev.*, 2005, **34**, 641.
16 (*a*) P. J. Carroll and L. E. Brus, *J. Am. Chem. Soc.*, 1987, **109**, 7613; (*b*) C. Kumar, J. Barton, I. Gould, N. Turro and J. van Houten, *Inorg. Chem.*, 1988, **27**, 648; (*c*) C. Kumar, J. Barton, I. Gould and N. Turro, *Inorg. Chem.*, 1987, **26**, 1455; (*d*) S. E. J. Bell, *Analyst*, 1996, **121**, 107R; (*e*) J. J. McGarvey, P. Callaghan, C. G. Coates, J. R. Schoonover, J. M. Kelly, L. Jacquet and K. C. Gordon, *J. Phys. Chem. B*, 1998, **102**, 5941; (*f*) C. G. Coates, T. E. Keyes, H. P. Hughes, P. M. Jayaweera, J. J. McGarvey and J. G. Vos, *J. Phys. Chem. A*, 1998, **102**, 5013.
17 (*a*) D. P. Strommen, P. K. Mallick, G. D. Danzer, R. S. Lumpkin and J. R. Kincaid, *J. Phys. Chem.*, 1990, **94**, 1357; (*b*) R. F. Dallinger and W. H. Woodruff, *J. Am. Chem. Soc.*, 1979, **101**, 4391.
18 Y. Zhao and D. G. Truhlar, *Theor. Chem. Acc.*, 2008, **120**, 215.
19 M. Biner, H. B. Buergi, A. Ludi and C. Roehr, *J. Am. Chem. Soc.*, 1992, **114**, 5197.
20 J. E. Bercaw, A. C. Durrell, H. B. Gray, J. C. Green, N. Hazari, J. A. Labinger and J. R. Winkler, *Inorg. Chem.*, 2010, **49**, 1801.
21 A. Draksharapu, Q. Li, H. Logtenberg, T. A. van den Berg, A. Meetsma, J. S. Killeen, B. L. Feringa, R. Hage, G. Roelfes and W. R. Browne, *Inorg. Chem.*, 2012, **51**, 900.
22 M. J. Frisch, G. W. Trucks, H. B. Schlegel, G. E. Scuseria, M. A. Robb, J. R. Cheeseman, G. Scalmani, V. Barone, B. Mennucci, G. A. Petersson, H. Nakatsuji, M. Caricato, X. Li, H. P. Hratchian, A. F. Izmaylov, J. Bloino, G. Zheng, J. L. Sonnenberg, M. Hada, M. Ehara, K. Toyota, R. Fukuda, J. Hasegawa, M. Ishida, T. Nakajima, Y. Honda, O. Kitao, H. Nakai, T. Vreven, J. A. Montgomery, Jr., J. E. Peralta, F. Ogliaro, M. Bearpark, J. J. Heyd, E. Brothers, K. N. Kudin, V. N. Staroverov, R. Kobayashi, J. Normand, K. Raghavachari, A. Rendell, J. C. Burant, S. S. Iyengar, J. Tomasi, M. Cossi, N. Rega, J. M. Millam, M. Klene, J. E. Knox, J. B. Cross, V. Bakken, C. Adamo, J. Jaramillo, R. Gomperts, R. E. Stratmann, O. Yazyev, A. J. Austin, R. Cammi, C. Pomelli, J. Ochterski, R. L. Martin, K. Morokuma, V. G. Zakrzewski, G. A. Voth, P. Salvador, J. J. Dannenberg, S. Dapprich, A. D. Daniels, O. Farkas, J. B. Foresman, J. V. Ortiz, J. Cioslowski and D. J. Fox, *GAUSSIAN 09 (Revision A.2)*, Gaussian, Inc., Wallingford, CT, 2009.
23 (*a*) X. Cao, *THEOCHEM*, 2002, **581**, 139; (*b*) T. H. Dunning Jr. and P. J. Hay, in *Modern Theoretical Chemistry*, ed. H. F. Schaefer III, Plenum, New York, 1976, vol. 3, pp. 1–28; (*c*) D. Andrae, U. Haussermann, M. Dolg, H. Stoll and H. Preuss, *Theor. Chim. Acta*, 1990, **77**, 123.
24 J. Tomasi, B. Mennucci and R. Cammi, *Chem. Rev.*, 2005, **105**, 2999.
25 N. M. O'Boyle, A. L. Tenderholt and K. M. Langner, *J. Comput. Chem.*, 2008, **29**, 839.

PCCP

View Online / Journal Homepage
Dynamic Article Links

Cite this: DOI: 10.1039/c2cp42938a

www.rsc.org/pccp

PAPER

Resonance-Raman microspectroscopy for quality assurance of dye-sensitized NiO_x films with respect to dye desorption kinetics in water†

Maximilian Bräutigam,*[ab] Martin Schulz,‡[c] Jane Inglis,[c] Jürgen Popp,[ab] Johannes G. Vos[c] and Benjamin Dietzek[ab]

Received 21st August 2012, Accepted 12th September 2012
DOI: 10.1039/c2cp42938a

Resonance Raman microspectroscopy is used to investigate dye-sensitized NiO_x nanoparticle films to be used as photocathodes in tandem dye-sensitized solar cells. It is shown that rR microspectroscopy has potential for applications in quality assurance in such systems and also in integrated dye-sensitized solar cell modules. Here, ruthenium dye-sensitized NiO_x nanoparticle layers were produced both as single and double NiO_x films using a one or two-step deposition process, respectively. The distribution of the sensitizer on the surfaces was investigated by rR microspectroscopy. The chemical images obtained from rR microspectroscopy yield complementary information to bright field microscope pictures and provide detailed insight into the sensitization pattern *e.g.* in the vicinity of surface vacancies and other inhomogeneities. Furthermore, based on the mapping results the dye desorption kinetics upon addition of water has been analysed. Desorption on the single NiO_x film is faster and more efficient than on the double film. These changes are attributed to binding sites on the NiO_x surface that are passivated with regard to water penetration. This passivation is introduced by the second synthesis step in building the second film of NiO_x on the glass substrate. Both findings highlight the potential of rR microspectroscopy for quality assurance of dye-sensitized solar cell electrodes.

Introduction

Recent forecasts reveal a growth of the world energy consumption by up to 53% from 2008 to 2035.[1] In order to reduce the carbon emission while generating this vast amount of energy, renewable energy sources are the only alternative to fossil fuels. Especially, solar energy has a large potential and paramount importance since the amount of solar energy striking the earth per year is much larger than the world's annual energy consumption.[2–4] Therefore, a variety of solar cell concepts are developed in particular with respect to an increased efficiency and lifetime and production lines are optimized to enable mass production and to reduce the production costs. The huge number of solar cell concepts investigated[5] includes dye-sensitized solar cells (DSC). This promising concept was introduced in 1991 and was awarded the Millennium Technology Prize in 2010.[6–8]

Various DSCs have been built using a variety of dyes and different semiconductor substrates.[9] A state-of-the-art DSC consists of a Ru–polypyridine dye-sensitized TiO_2 photoanode and a passive Pt cathode.[10] In order to activate the photocathode and to thereby increase the light-conversion efficiency, so-called tandem solar cells are currently investigated, which raise the theoretical efficiency limit from 30% for single junction DSCs to 43% in tandem DSCs. These tandem cells consist of the well established dye-sensitized TiO_2 photoanode and a dye-sensitized p-type semiconductor photocathode; mainly NiO_x is used for this purpose.[9] Both TiO_2 photoanodes and NiO_x photocathodes were realized with different dyes, *e.g.* purely organic dyes such as coumarin 343[11] and P1[12,13] or Ru dyes.[14,15] One central challenge in the development of tandem DSCs is to increase their long-term stability, which – amongst other factors – is determined by their limited stability against humidity. Degradation of the photocathode performance is caused by water-induced desorption of the dyes from the semiconductor surface.[9] Several approaches had been pursued to increase the long-term stability of cells by decreasing the sensitivity of the cells to water by *e.g.* modifying the dyes utilizing hydrophobic groups[16] or their anchor groups.[17]

[a] *Institute of Photonic Technology (IPHT) Jena e. V., Albert-Einstein-Straße 9, D-07745 Jena, Germany. E-mail: benjamin.dietzek@ipht-jena.de; Tel: +49 3641206-332*
[b] *Institute for Physical Chemistry and Abbe Center of Photonics, Friedrich-Schiller University Jena, Helmholtzweg 4, D-07743 Jena, Germany*
[c] *SRC for Solar Energy Conversion, School of Chemical Sciences, Dublin City University, Dublin 9, Ireland*
† Electronic supplementary information (ESI) available. See DOI: 10.1039/c2cp42938a
‡ Current address: Pharmaceutical Radiochemistry, Technical University Munich, Walther-Meissner-Str. 3, D-85748 Garching, Germany.

Alternative approaches focus on the modification of the semiconductor with NAFION polymeric films (TiO_2) to protect an adsorbed layer of Ru dye on TiO_2 against desorption.[18] Further attempts focused on the development of water-based DSCs. However, their light-conversion efficiency is low under these conditions.[19] In the context of these recent developments a systematic microspectroscopic study of the desorption process is needed to understand this process on the surface in more detail in order to support further development of novel semiconductor based assemblies and to increase the photocathode stability.

This paper aims at a detailed analysis of the desorption of the ruthenium dye $[Ru(4,4'\text{-}(COOCH_2CH_3)_2\text{-}2,2'\text{-bipyridine})_3]^{2+}$, **Ru1**, from a NiO_x surface utilizing resonance-Raman (rR) microspectroscopy. Ruthenium–polypyridine dyes are commonly used for the fabrication of dye-sensitized solar cells due to their stability, their broad absorption spectra in the visible part of the spectrum, and their favourable photovoltaic properties.[13] **Ru1** in particular has been chosen for this study as its parent complex $[Ru(bpy)_3]^{2+}$ is one of the best studied complexes. In order to ensure binding to the surface **Ru1** carries esterificated carboxyl anchor groups.[14,20,21] The obvious advantage of rR microspectroscopy is the combination of surface mapping capability with high spatial resolution and chemical fingerprint information of the dyes adsorbed to the surface. As will be shown below that rR imaging can be utilized to investigate the quality of photocathode assemblies regarding the integrity of the dye, its concentration on the NiO_x surface and to map the distribution of the dye on the surface. In addition when used in combination with bright field spectroscopy, detailed information concerning the presence of defects on the metal oxide NiO_x surface can also be obtained. The integrity of the dye-semiconductor junction is of great importance for the performance of solar cells that are based on these electrodes since the initial electron dynamics after excitation (excited state decay, electron injection, electron transport through the mesoporous oxide film) take place here.[9]

Resonance-Raman spectroscopy was already used to investigate several aspects relevant for the design and function of DSCs.[5] For example, the mechanisms of ligand-exchange reactions between the redox couple $3I^-/I_3^-$ and of the thiocyanato ligands of ruthenium complex N3 were studied.[22] Furthermore – as solvents largely impact the efficiency and function of the solar cells – rR spectroscopy has been used to screen widely used solvents propylene carbonate, methoxypropionitrile, γ-butyrolactone for effects on the photoelectrode/electrolyte interface.[23] The surface interactions of substituted bipyridyl complexes of ruthenium(II) on TiO_2 were studied using time-resolved rR spectroscopy.[24]

In this paper in contrast to the aforementioned studies, rR spectroscopy and imaging techniques[25] are combined to create a powerful new approach to determine the quality of the NiO_x-based photocathodes and to thoroughly investigate dye-desorption kinetics.

Experimental

Sample preparation

The synthesis of the NiO_x surfaces was performed with minor alterations of the protocol described in the literature.[13,26] The polymer–$NiCl_2$ solution was spin coated onto the glass substrate. As the polymer–$NiCl_2$ solution is highly viscose the surface of the glass substrate was completely covered with the mixture and the subsequent spinning of the glass slide led to very homogeneous polymer–$NiCl_2$ films. The burning temperature of these films was set to 420 °C. Double NiO_x films were produced by a subsequent analogue second spin-coating/burning step.[13] After cleaning the NiO_x surface with deionized water (MilliQ) the films were soaked in ACN–dye solution (10^{-3} M) for 24 h to sensitize the NiO_x nanoparticles.

The ruthenium dye **Ru1** = $[Ru(4,4'\text{-}(COOCH_2CH_3)_2\text{-}2,2'\text{-bipyridine})_3]^{2+}$ has been immobilized on the NiO_x nanoparticle films. The dye **Ru2** = $[Ru(4,4'\text{-}(COOH)_2\text{-}2,2'\text{-bipyridine})(2,2'\text{-bipyridine})_2]^{2+}$ was included in the spectroscopic studies. The relevant data are listed in the ESI.†

Experimental setup and data processing

For the rR microspectroscopy measurements, a conventional micro-Raman setup (Labram HR, Horiba Jobin Yvon) was used. The spectrometer was equipped with 600 lines per millimeter grating and combined with an Olympus microscope (BX 41). The excitation wavelengths were delivered by a krypton-ion laser (Model Coherent Innova 301C, λ = 413 and 476 nm) and a frequency-doubled Nd:YAG laser (λ = 532 nm). For the measurements, the laser was focused onto the dye-sensitized NiO_x surface using an Olympus 40 × UPlan FLN microscope objective. Incident laser powers of about 2.5 mW were applied to the sample during the measurements with a spot size of about 1 μm. The spectra were recorded with an integration time of 2 s per spectrum. Repeated measurements at the same position were performed in order to test the decomposition of the dye. No decrease in signal intensity is observed during the first two minutes. Thus, the method is non-destructive within the range of parameters, *i.e.* focussing conditions, laser power, pixel dwell time *etc.*, used. All spectra presented in this paper are mean spectra of a quadratic map (66 μm edge length, 10 × 10 spectra) which builds a profound and statistically reliable basis for the comparison of rR intensities. For iterated measurements that were performed to detail the effect of individual washing steps with water, the exact position on the surface was marked with a crosshair carved into the NiO_x surface. All measurements were taken in the first quadrant of the crosshair. The mean spectra were processed by the statistics-sensitive non-linear iterative peak-clipping (SNIP) algorithm[27] for background correction using Gnu R[28] and the library "Peaks" with 30 iterations.

UV-vis measurements were carried out on a Jasco V-530 spectrometer. Absorption spectra of NiO_x films were taken in transmission mode.

Results and discussion

The most widely used method to investigate the composition and integrity of DSC modules and the respective photoelectrodes is UV-vis spectroscopy. It will be shown that UV-vis absorption spectroscopy reveals the amount of dye bound to the surface, which depends on the solvent used for cleaning the surface after sensitization. In addition, the choice of solvent – especially

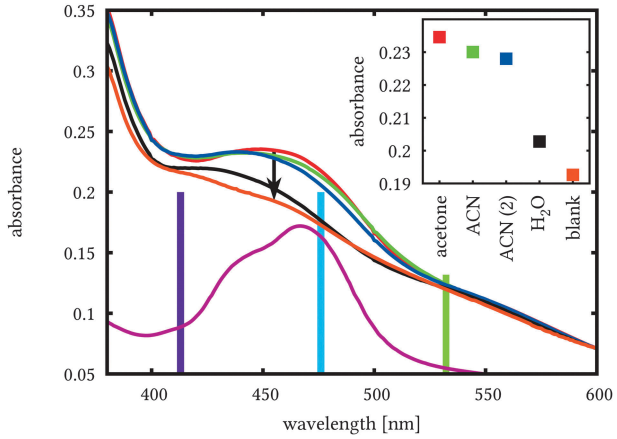

Fig. 1 UV-vis spectra of a **Ru1** dye-sensitized NiO_x surface after the 4 washing steps: first step – (i) acetone (red), second step – (ii) ACN (green), third step – (iii) ACN (blue), fourth step – (iv) water (black). In addition, the spectra of the bare NiO_x surface (brown) and **Ru1** in ACN (violet) are given. Coloured bars indicate wavelengths used for rR measurements (413, 476 and 532 nm). The inset shows the UV-vis absorbance at 455 nm after the series of washing procedures.

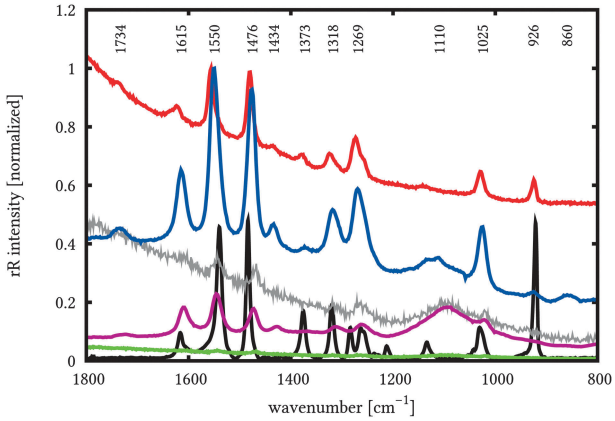

Fig. 2 rR spectra of **Ru1** on NiO_x excited at 413 nm (violet), 476 nm (blue) and 532 nm (green) without background correction. Due to the low quality of the spectrum at 532 nm (green), this spectrum has been multiplied by factor 10 to detail the vibrational modes (grey). The ACN solution spectra of **Ru1** at 476 nm excitation (red) and $[Ru(bis\text{-}tert\text{-}butyl\text{-}bpy)_3]^{2+}$ at 458 nm excitation (black) are added for comparison (solvent bands at 1374 and 919 cm^{-1}).

when water is used – might influence the long-term stability of the solar cell due to desorption of the Ru dye.

Fig. 1 shows the impact of several cleaning solvents on the UV-vis absorption of **Ru1**-sensitized NiO_x films. The ^{3}MLCT band[29] at about 460 nm is the dominant feature and is characteristic of the presence of dye on the NiO_x film. As can be deduced from Fig. 1 the largest amount of dye remains on the surface when washing with acetone. Upon further cleaning with ACN a small fraction of the dye is removed as can be seen by the slightly reduced contribution of the ^{3}MLCT absorption to the UV-vis spectra. This amount is attributed to physisorbed dye on the surface, while acetone just removes excess unbound dye. The differences observed between the two solvents are most likely due to the solubility of the dye in these solvents. For example, acetone is used for recrystallization of Ru dyes due to the limited solubility.[30] Similar results are obtained when investigating **Ru2** as shown in the ESI.† A subsequent second cleaning step with ACN basically leaves the composition of the surface unaffected. Finally, washing of the module with water almost completely removes the ^{3}MLCT band in the UV-vis spectrum indicating an almost complete loss of the dye. The 4 step cleaning protocol, *i.e.* (i) acetone, (ii) ACN, (iii) ACN, and (iv) water, reduces the dye absorbance compared to cleaning with acetone alone by about (0.24–0.20)/(0.24–0.19) = 80%. In order to detail this effect rR microspectroscopic investigations have been carried out. With rR microspectroscopy the effect of wide-area inhomogeneities of the surface can be ruled out as all measurements are carried out at the same position on the surface. These inhomogeneities that will be detailed later might influence the UV-vis measurements when placing the surface at a slightly different position in the beam-line of the UV-vis spectrometer after the respective washing steps. Furthermore, rR microspectroscopy has the advantage of solely detecting the dye that is bound to the NiO_x surface since the UV-vis measurements only provide information on the transmission of the functionalized surface, *i.e.* contributions from both the dye and the NiO_x are overlapping. Furthermore, not only absorption but also scattering contributes to the recorded spectra in Fig. 1, which are recorded in transmission mode.

To overcome these limitations, rR investigations were performed using excitation at 413, 476, and 532 nm (see Fig. 1). A comparison of the rR spectra at these wavelengths is depicted in Fig. 2: Strong rR enhancement is observed at 476 nm excitation but is poor at 532 nm. Consequently, a low signal-to-noise ratio is recorded. This finding correlates with the absorption spectra as shown in Fig. 1: while 476 nm excitation matches the resonance condition (maximum MLCT absorption of **Ru1**), 532 nm falls outside the range of the MLCT band and is therefore off resonance. When comparing 476 and 413 nm excitation, the strong background of NiO_x in the UV-vis spectrum at 413 nm has to be taken into account. Despite a comparable absorbance at 413 and 476 nm, the dye's contribution to the UV-vis spectrum at 413 nm is smaller because of reduced extinction coefficients, leading to a less intense rR signal. The rR spectra of **Ru1** attached to the NiO_x surfaces exhibit the typical Ru–bipyridine band pattern as can be seen from the comparison with the rR spectrum of $[Ru(bis\text{-}tert\text{-}butyl\text{-}bpy)_3]^{2+}$, which is shown for reference. The **Ru1** rR band pattern is dominated by the triplet of (ring) stretching vibrations of the bipyridine ligand at 1476 (ν-CC), 1550 (ν_{sym}-ring), and 1615 cm^{-1} (ν_{sym}-ring).[31] Further prominent bands can be found in the spectra of **Ru1** on the NiO_x surface and the spectra of the reference dye at 1318 (ν-C_2–C_2'), 1269 (ν-ring, δ-CH), and 1025 cm^{-1} (ring breathing).[32] The spectra of **Ru1** on NiO_x exhibit all features of the solution spectra of $[Ru(4,4'\text{–}(COOCH_3)_2\text{–}2,2'\text{-bipyridine})_3]^{2+}$.[33]

As excitation at 476 nm leads to the best rR enhancement, all further measurements were carried out with this excitation wavelength. The potential of rR microspectroscopy for detailing inhomogeneous regions on the NiO_x surface was tested by measuring at different positions on the sensitized semiconductor film. Furthermore, comparison of dye-sensitized NiO_x film and the glass substrate was performed as shown in Fig. 3.

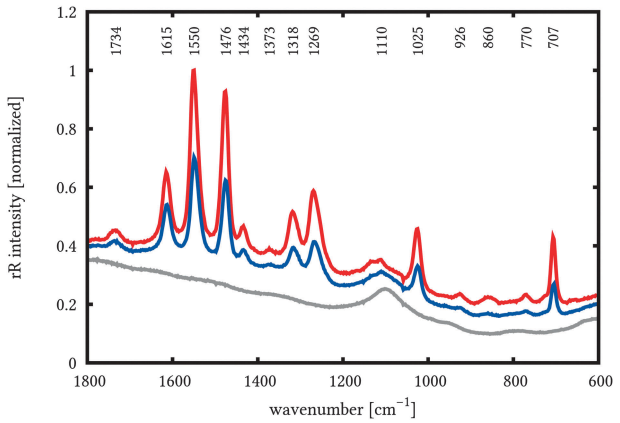

Fig. 3 rR spectra at 476 nm excitation of **Ru1** on NiO_x: at the centre of the surface (red) and at the edge of the NiO_x surface in close vicinity to the blank glass slide (blue). The rR spectrum of the clean glass substrate (grey) is added for comparison.

The background in the rR spectra of the dye-sensitized NiO_x films originates from the glass substrate, is relatively low compared to the fluorescence background of the dye in ACN (see Fig. 2) and does not hamper quality assurance of the sensitized film by rR microspectroscopy. During measurements different areas on the surface were investigated. As evidenced in Fig. 3 rR bands of **Ru1** appear to be twice as strong in the centre of the NiO_x surface as compared to the edges. This effect can be attributed to the fact that the quality of the surface decreases from the centre to the edges due to the fabrication process of the surface, *i.e.* the spin coating during synthesis. This leads to a decreased Ru-dye loading at the edges of the surface.

The quality of the rR spectra is very high and spatial variations of the rR intensity on the dye-sensitizes NiO_x films are visible as shown above. Hence, in combination with a scanning microscope it is possible to detail the distribution of the ruthenium dye on the surface, which presents an indispensable step towards an exhaustive quality assurance of the tandem-DSC modules. In order to map the distribution of the sensitizer on the surface, the prominent rR region from 1400 to 1700 cm^{-1} with its bipyridine (ring) stretching vibrations was spectrally integrated after SNIP background correction (see Experimental section) and used for mapping various areas of interest. Regions of interest were chosen based on bright field images of the sensitized NiO_x films that contain either inhomogeneities or vacancies at the surface.

Fig. 4A shows a bright field white light microscopic image of a **Ru1**-functionalized NiO_x film. In the centre of the bright field image is a rectangular inhomogeneity in the film. Notably, the rR map (B) does not reveal the same pattern as the white light image (A) but the shapes of the inhomogeneity as seen in the different spectroscopic modalities differ strongly. While the white light image shows a close-to-square defect in the centre of the image, the rR map reveals an elongated structure in the upper part of the map with reduced rR intensities. This difference can be rationalized when considering that the bright field picture originates from absorption and scattering of both dye and NiO_x surface while the rR mapping only depends on the rR signal intensity of the dye. Therefore, both imaging modalities yield complementary results. But rR mapping is not only able to map those wide-area

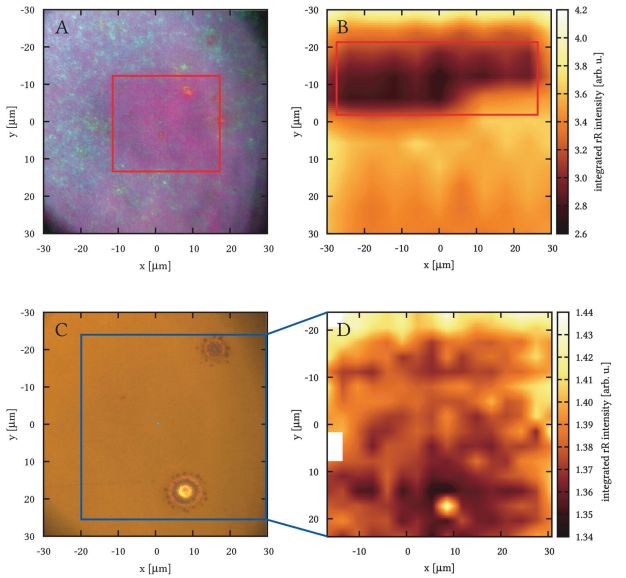

Fig. 4 **Ru1**-sensitized NiO_x surface: comparison of bright field microscope picture (A and C) *versus* mapping of an integrated rR signal in the region of 1400 to 1700 cm^{-1} (B and D). A and B: area with an inhomogeneity. Red rectangles indicate the approximate shape of the inhomogeneity. C and D: vacancy on the surface. The blue rectangle indicates the zoom from C to D.

defects but also smaller vacancies. Such vacancies are exemplarily depicted in Fig. 4C and D. Here, a circular vacancy on the NiO_x surface can be seen on the bottom of the bright field picture (C). This appears to be an artefact of the synthesis probably caused by an impurity or an inhomogeneous temperature distribution in the furnace. Using rR micro-spectroscopy it is relatively easy to visualize the decreased dye loading (a reduced rR signal of **Ru1**) in the corona of this vacancy (D). This might be attributed to a lower quality of the NiO_x surface in the vicinity of the vacancy. The second vacancy at the top of image C cannot be unequivocally detected by rR microspectroscopy since the changes in **Ru1** dye concentration appear to be small. As the comparison of bright field and rR mapping evidence, rR microspectroscopy is capable of investigating local inhomogeneities in the dye loading on the surface. Thus, rR microspectroscopy – due to its high chemical specificity – is a powerful tool for the quality assurance of photoelectrodes and in perspective DSC modules.

Furthermore, this high chemical specificity allows for tracking of changes of the dye's concentration on the surface, which *e.g.* occurs as a result of desorption upon addition of water. As mentioned before, water causes rapid desorption of sensitizers from the NiO_x surface. Therefore, water and humidity influence the performance of DSC, and hence, a robust technique for the analysis is desirable. Dye-desorption kinetics were followed by rR microspectroscopy and the results are shown in Fig. 5. In particular its capability to monitor the dye concentration with high spatial resolution over large areas, allows the technique to achieve statistically reliable results for the desorption kinetics. The spatial resolution in combination with the spectral component yields multidimensional data that contain much more information than most other techniques such as UV-vis spectroscopy or bright field microscopy.

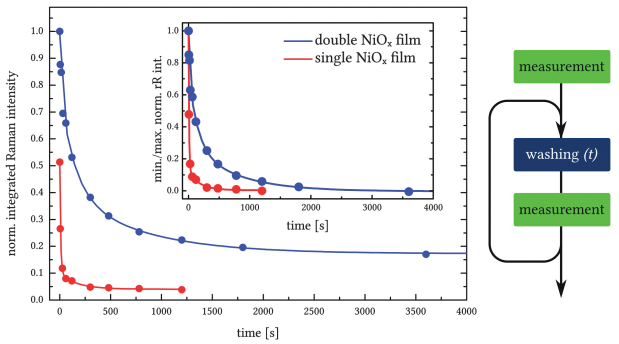

Fig. 5 Resonance Raman intensity of **Ru1** on single and double NiO_x films as a function of the exposure time in water. The data are fitted using a multi-exponential model. The two processes of measuring the surface for gaining the intensity and the washing step that determines the time axis are carried out in a serialized mode. The inset shows the minimum–maximum normalized kinetics.

As can be seen in the scheme in Fig. 5, the surface was initially measured without any washing step. Then the dye-sensitized NiO_x surface was dipped in water for certain time periods as shown in the figure. Subsequently rR measurements were performed. These two steps were repeated several times to yield the desorption kinetics of the dye in water as can be seen in the graph in Fig. 5. Three statements can be deduced from the kinetics shown there. First, the double film can bind more sensitizer, *i.e.* without washing the rR signal and thus the amount of dye on the surface of the double NiO_x film is twice as high as on the single film. The initial value of the dye's rR signal on the single film is 0.51 as compared to 1 on the double film. This behaviour is the expected as a second NiO_x deposition step should provide more binding sites for the sensitizer.[8] Second, the double film binds the sensitizers more strongly, *i.e.* the ratio of the dye remaining on the surfaces after the cleaning procedure, which is determined from the long-time offset in the integrated rR signal (at 1200 s), increases from 0.04 (single film) to 0.22 (double film). Thus, the quotient of the rR signal of the double film to the single film in dependence on the water exposure shifts from 1.9 (1 : 0.51 – initial value) to 5.5 (0.22 : 0.04 – long term offset). This can be interpreted in terms of vaults in the double NiO_x film that are small and passivated upon chemisorption of the dye. **Ru1** might increase the number of carboxylic groups bound to NiO_x when the dye penetrates these vaults. As a consequence, water cannot penetrate these binding sites and the dye does not desorb effectively. Apparently such "vault" structures are – to a significant extent – introduced upon fabrication of the second NiO_x layer. Finally, desorption of the sensitizers slowed in the double NiO_x film structure as can be deduced from the minimum–maximum normalized washing kinetics as plotted in the inset of Fig. 5. Again, this might be due to the passivated surface when depositing a second NiO_x layer. Thus, statements (3) and (2) are strongly related to each other. This work shows that the sensitized double film structure is significantly more stable against water exposure. This finding might influence further synthesis of NiO_x nanoparticle layers for the use in tandem-DSCs.

Conclusion

The potential of resonance Raman (rR) microspectroscopy for assuring the quality of NiO_x based photocathodes has been demonstrated. The combination of rR spectroscopy and the microscopic spatial resolution allows us to map both wide areas and small vacancies with chemical sensitivity. Thereby, the spatial distribution of *e.g.* Ru-bipyridine dyes, which are sorbed to the surface, can be unambiguously identified with chemical specificity. The quality of the rR spectra is very high and spatial variations of the rR intensity on the dye-sensitizes NiO_x layers are visible. Hence, in combination with a scanning microscope it is possible to detail the distribution of the ruthenium dye on the surface. It is shown that bright field microscope pictures and rR images are complimentary in nature, *i.e.* shapes of inhomogeneous regions on the surface appear to be different when evaluating on a molecular level with rR imaging. Thus, the distribution of dye on the NiO_x surface might not correlate with the bright field microscope picture. Furthermore, rR microspectroscopy has been used to detailed analysis of the dye-desorption kinetics upon addition of water on single film and double NiO_x film substrates. As a result, the intensity of Ru dye concentration without any washing step on the double film is twice as high as on the single film. Furthermore, after several washing steps relatively more Ru dye remains bound to the double NiO_x film as compared to the single layer. This observation is additionally accompanied by a slower desorption of the sensitizers from the NiO_x surfaces in the case of the double film structure. This can be interpreted in terms of a passivated surface that is introduced upon sintering and the second synthetic step during the double film production. This paper has successfully investigated Ru-dye-sensitized NiO_x nanoparticle surfaces with rR microspectroscopy and particularly detailed the dye-desorption kinetics upon addition of water, which will – partially – influences the long-term stability of DSC modules constructed from such materials. Here, it is shown that deposition of a second NiO_x layer increases the stability of the surface against desorption of the dye. The ability to exclusively detect the dye's distribution on the surface is the key feature of the rR microspectroscopy and makes it applicable to most systems that consist of (some) Raman-active components. Thus, rR microspectroscopy – due to its high chemical specificity – is a powerful tool for the quality assurance of photoelectrodes and in perspective DSC modules.

Acknowledgements

Financial support is gratefully acknowledged from the *Studienstiftung des deutschen Volkes* (M.B.), and the *Fonds der Chemischen Industrie* (B.D. and J.P.). J.I., M.S., and J.G.V. thank Science Foundation Ireland for supporting this work (Grants No. 07/SRC/B1160 and 08/RFP/CHE13490).

Notes and references

1 J. Conti and P. Holtberg, *International Energy Outlook 2011*, U.S. Energy Information Administration, Washington, DC, 2011.
2 R. F. Service, *Science*, 2005, **309**, 548–551.
3 J. Potočnik, *Science*, 2007, **315**, 810–811.
4 Q. Schiermeier, *Nat. News*, 2008, **454**, 816–823.
5 M. Wächtler, J. Guthmuller, L. González and B. Dietzek, *Coord. Chem. Rev.*, 2012, **256**, 1479–1508.
6 B. O'Regan and M. Grätzel, *Nature*, 1991, **353**, 737–740.
7 M. D. McGehee, *Science*, 2011, **334**, 607–608.
8 G. J. Meyer, *ACS Nano*, 2010, **4**, 4337–4343.

9 A. Hagfeldt, G. Boschloo, L. Sun, L. Kloo and H. Pettersson, *Chem. Rev.*, 2010, **110**, 6595–6663.
10 J. He, H. Lindström, A. Hagfeldt and S.-E. Lindquist, *Sol. Energy Mater. Sol. Cells*, 2000, **62**, 265–273.
11 A. Morandeira, G. Boschloo, A. Hagfeldt and L. Hammarström, *J. Phys. Chem. B*, 2005, **109**, 19403–19410.
12 P. Qin, H. Zhu, T. Edvinsson, G. Boschloo, A. Hagfeldt and L. Sun, *J. Am. Chem. Soc.*, 2008, **130**, 8570–8571.
13 L. Li, E. A. Gibson, P. Qin, G. Boschloo, M. Gorlov, A. Hagfeldt and L. Sun, *Adv. Mater.*, 2010, **22**, 1759–1762.
14 Y. Pellegrin, L. Le Pleux, E. Blart, A. Renaud, B. Chavillon, N. Szuwarski, M. Boujtita, L. Cario, S. Jobic, D. Jacquemin and F. Odobel, *J. Photochem. Photobiol., A*, 2011, **219**, 235–242.
15 B. Schulze, D. Escudero, C. Friebe, R. Siebert, H. Görls, S. Sinn, M. Thomas, S. Mai, J. Popp, B. Dietzek, L. González and U. S. Schubert, *Chem.–Eur. J.*, 2012, **18**, 4010–4025.
16 H. Choi, C. Baik, S. O. Kang, J. Ko, M. Kang, M. K. Nazeeruddin and M. Grätzel, *Angew. Chem., Int. Ed.*, 2008, **47**, 327–330.
17 P. Péchy, F. P. Rotzinger, M. K. Nazeeruddin, O. Kohle, S. M. Zakeeruddin, R. Humphry-Baker and M. Grätzel, *J. Chem. Soc., Chem. Commun.*, 1995, 65–66.
18 L. Kavan and M. Grätzel, *Electrochim. Acta*, 1989, **34**, 1327–1334.
19 W. H. Lai, Y. H. Su, L. G. Teoh and M. H. Hon, *J. Photochem. Photobiol., A*, 2008, **195**, 307–313.
20 S. Ardo and G. J. Meyer, *Chem. Soc. Rev.*, 2009, **38**, 115.
21 M. Awais, M. Rahman, J. M. Don MacElroy, N. Coburn, D. Dini, J. G. Vos and D. P. Dowling, *Surf. Coat. Technol.*, 2010, **204**, 2729–2736.
22 H. Greijer, J. Lindgren and A. Hagfeldt, *J. Phys. Chem. B*, 2001, **105**, 6314–6320.
23 T. Stergiopoulos, A. G. Kontos, V. Likodimos, D. Perganti and P. Falaras, *J. Phys. Chem. C*, 2011, **115**, 10236–10244.
24 S. Umapathy, A. M. Cartner, A. W. Parker and R. E. Hester, *J. Phys. Chem.*, 1990, **94**, 8880–8885.
25 K. Grosser, L. Zedler, M. Schmitt, B. Dietzek, J. Popp and G. Pohnert, *Biofouling*, 2012, **28**, 687–696.
26 S. Sumikura, S. Mori, S. Shimizu, H. Usami and E. Suzuki, *J. Photochem. Photobiol., A*, 2008, **199**, 1–7.
27 C. G. Ryan, E. Clayton, W. L. Griffin, S. H. Sie and D. R. Cousens, *Nucl. Instrum. Methods Phys. Res., Sect. B*, 1988, **34**, 396–402.
28 R Development Core Team, A Language and Environment for Statistical Computing, Vienna, Austria, 2012.
29 C. Daul, E. J. Baerends and P. Vernooijs, *Inorg. Chem.*, 1994, **33**, 3538–3543.
30 K.-S. Chen, W.-H. Liu, Y.-H. Wang, C.-H. Lai, P.-T. Chou, G.-H. Lee, K. Chen, H.-Y. Chen, Y. Chi and F.-C. Tung, *Adv. Funct. Mater.*, 2007, **17**, 2964–2974.
31 C. Kuhnt, S. Tschierlei, M. Karnahl, S. Rau, B. Dietzek, M. Schmitt and J. Popp, *J. Raman Spectrosc.*, 2010, **41**, 922–932.
32 T. J. Dines and R. D. Peacock, *J. Chem. Soc., Faraday Trans. 1*, 1988, **84**, 3445.
33 M. Schwalbe, B. Schäfer, H. Görls, S. Rau, S. Tschierlei, M. Schmitt, J. Popp, G. Vaughan, W. Henry and J. G. Vos, *Eur. J. Inorg. Chem.*, 2008, 3310–3319.

Dalton Transactions

Cite this: *Dalton Trans.*, 2011, **40**, 10812

www.rsc.org/dalton

COMMUNICATION

The effect of peripheral bipyridine ligands on the photocatalytic hydrogen production activity of Ru/Pd catalysts†

Gurmeet Singh Bindra,[a] Martin Schulz,[a] Avishek Paul,[a] Suraj Soman,[a] Robert Groarke,[a] Jane Inglis,[a] Mary T. Pryce,[a] Wesley R. Browne,[b] Sven Rau,[c] Brian J. Maclean[d] and Johannes G. Vos*[a]

Received 29th June 2011, Accepted 23rd August 2011
DOI: 10.1039/c1dt11241d

A pyrazine bridged ruthenium/palladium bimetallic photocatalyst with peripheral 4,4′-dicarboxyethyl-2,2′-bipyridine ligands, EtOOC-RuPd, is reported, together with its 2,2′-bipyridine analogue. Upon irradiation with visible light, EtOOC-RuPd catalyses the production of hydrogen gas whereas the complex RuPd does not.

Hydrogen is widely perceived to be one of the primary replacement fuels, in particular for transport, due to its exceptionally high energy density/mass ratio. The photocatalytic production of hydrogen is therefore a major challenge in converting solar energy directly to chemical energy. One of the most promising approaches towards this goal is the use of molecular photocatalysts that utilise visible light to drive proton reduction and it can be envisaged that such systems comprise of a light-harvesting antenna (photosensitiser) that can donate electrons to a catalytically active centre to which it is connected *via* a bridging ligand.

Due to their exceptional photophysical and redox properties Ru(II) polypyridyl complexes are an excellent choice as the light harvesting centre while Pd(II) or Pt(II) are the metal of choice for the catalytically active centres.[1] Alternative combinations already reported are Re/Co, Ru/Pd, Ru/Pt, Os/Rh, Ru/Rh, Pt/Co, Ir/Rh.[2–10] The intramolecular approach in which a bridging ligand facilitates photoinduced electron transfer from the light harvesting centre to the hydrogen forming centre requires vectorial electron transfer to be mediated by the bridging ligand. This realisation has led to the application of bridging ligands that are more electron deficient than the peripheral ligands. However, recently Rau *et al.* have proposed that in addition to the final (lowest lying) excited state, higher lying excited (Franck–Condon) states can also play an important role, as seen from the excitation wavelength dependency of turnover numbers (TONs).[11] However, other factors such as lifetime of the charge separated states and secondary processes during the multiple electron transfer steps may influence catalytic activity.

Here we report direct evidence of the importance of the peripheral 2,2′-bipyridyl (bpy) ligands in the photocatalytic process. The photocatalytic activity of the Ru(II)/Pd(II) complex based on the non-substituted 2,2′-bipyridyl (bpy) ligand (**RuPd**) is contrasted with that of the analogous heterobimetallic complex in which the more electron deficient 4,4′-di(carboxyethyl)bipyridine ligand replaces bipy (*i.e.* **EtOOC-RuPd**). The structures of both complexes are shown in Fig. 1. The bridging ligand is 2,5-di(pyridin-2-yl)pyrazine (2,5-dpp).

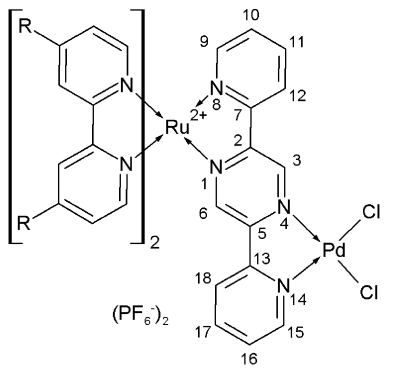

R = H (**RuPd**), COOEt (**EtOOC-RuPd**)

Fig. 1 Structure of complexes described in the text.

In agreement with the earlier report by Sakai and Ozawa,[12] the complex **RuPd** was found to show no photocatalytic activity towards hydrogen production. In stark contrast we found that the dinuclear catalyst **EtOOC-RuPd** could achieve TONs for H_2 production of up to 400 (32 μmol after 18 h).

Photocatalytic reactions were performed by irradiation of the reaction mixtures at 470 nm using triethylamine (TEA) as the terminal reductant to regenerate the Ru(II) complex. The presence of water was found to be a key factor for photocatalytic hydrogen production,‡ with hydrogen formation not observed in its absence. The role played by water in the catalysis is however manifold: (1) as a source of protons, and hence an increase in water content accelerates to a certain point the reaction, (2) to facilitate

[a]*SRC for Solar Energy Conversion, School of Chemical Sciences, Dublin City University, Glasnevin, Dublin 9, Dublin, Ireland. E-mail: han.vos@dcu.ie*
[b]*Stratingh Institute for Chemistry, Faculty of Mathematics and Natural Sciences, University of Groningen, Nijenborgh 4, 9747 AG, Groningen, The Netherlands*
[c]*Anorganische Chemie I, Universität Ulm, Albert-Einstein-Allee 11, 89081, Ulm, Germany*
[d]*Department of Chemistry, St. Francis Xavier University, Physical Sciences Building, P.O. Box 5000, Antigonish, Nova Scotia, B2G 2W5, Canada*

† Electronic supplementary information (ESI) available: Synthesis of **Ru**, **RuPd**, **EtOOC-Ru** and **EtOOC-RuPd** and experimental details on the catalysis. See DOI: 10.1039/c1dt11241d

proton-transfer and (3) to increase solvent polarity thereby stabilizing polar intermediates. Control experiments with the mononuclear precursor compounds **Ru** and **EtOOC-Ru** confirmed the necessity of the presence of the Pd(II) centre. The time-dependence of dihydrogen formation is shown in Fig. S2 (ESI†). Different behaviour is observed for the preformed complex **EtOOC-RuPd** and the *in situ* formed complex (*i.e.* **EtOOC-Ru** + $Pd(CH_3CN)_2Cl_2$, 1 : 1 molar ratio). Both graphs show a sigmoidal time profile eventually reaching a plateau that indicates deactivation of the catalyst. An induction period was observed with dihydrogen production reaching a maximum after *ca.* 3.5 h for **EtOOC-RuPd** and *ca.* 5.5 h for **EtOOC-Ru** + $Pd(CH_3CN)_2Cl_2$. The longer induction period for the *in situ* formed binuclear complex supports the conclusion that the active catalyst is a binuclear **EtOOC-Ru/Pd** complex. For further details on the photocatalytic reactions see the ESI.†

Colloid formation has been discussed as a possible process in catalysis with Ru/Pd complexes[13,14] and although this behaviour cannot be excluded in the present system it is important to note that the formation of a precipitate was not observed during the photocatalysis with either **RuPd** or **EtOOC-RuPd**.§

Previous investigations have shown that the 2,5-dpp bridge enables relatively strong coupling between the metal centres and that the emissive state for the $[(bpy)_2Ru\text{-}(2,5\text{-}dpp)]^{2+}$ and $[(bpy)_2Ru\text{-}(2,5\text{-}dpp)\text{-}Ru(bpy)_2]^{4+}$ compounds is dpp-based.[15–23] Absorption spectroscopy shows that **RuPd** and **EtOOC-RuPd** have similar features with the intraligand and metal-to-bpy charge transfer bands being shifted towards lower energy by *ca.* 15–40 nm. However, the lowest energy MLCT of **EtOOC-RuPd** is shifted by 10 nm to higher energy compared with the **RuPd** complex (Table 1). Similarly the emission spectrum of **EtOOC-RuPd** is shifted by 30 nm to the blue compared to **RuPd**. Due to the lower π* energy of the EtOOC-bpy ligands they are better π-acceptors which leads to a stabilisation of the ground state and is manifested in a red shift of 40 nm in the ^{1}MLCT ← GS transition involving the peripheral bpy/$(EtOOC)_2$bpy ligands. This is in agreement with the higher oxidation potential of **EtOOC-RuPd** with respect to **RuPd**. These data suggest as expected that the π*-energy levels for the carboxyethyl ligands are lower in energy than those of the bpy ligands. The UV/Vis absorption spectrum of the complex undergoes several changes already when TEA is added, as indicated by absorption and emission spectroscopy. Similar changes are observed when following the photocatalysis by absorption spectroscopy, assigned tentatively to exchange of the chloride ligands.

Table 1 Photophysical and electrochemical properties of the dinuclear complexes **RuPd**, **EtOOC-RuPd** and their mononuclear precursors **Ru**, **EtOOC-Ru**

Compounds	Abs. (log ε)/nm	Em./nm	τ^a/ns	Oxidation^b/mV
RuPd	539 (4.00)	807	< 0.5	+1.56
EtOOC-RuPd	526 (4.20)	778	< 0.5	+1.75
Ru	483 (3.98)	685	266	+1.33
EtOOC-Ru	467 (4.25)	630	564	+1.68

[a] Determined by time correlated single photon counting at 293 K in aerated acetonitrile solution. [b] From cyclic voltammetry in acetonitrile (0.1 M $TBAPF_6$) *vs.* Ag/AgCl. All data were acquired at 293 K.

The dramatic differences in the photocatalytic activities towards H_2 production between the polypyridyl-Ru/Pd complexes **RuPd** and **EtOOC-RuPd**, *i.e.* with the former inactive and the latter highly active (TONs of 400), is surprising. Both heterobimetallic complexes exhibit very short excited state lifetimes, indicating efficient interaction between the two metal centres (electron transfer quenching). The observations indicate the importance of the peripheral ligand for photoinduced electron transfer as proposed earlier by Rau *et al.*[11] It is also important to note that hydrogen formation is not directly linked to the formation of precipitates as is observed for other systems.[14]

Further investigations concerning the nature of the electron transfer and additional factors governing the overall catalytic activity of intramolecular photocatalysts such as the nature and location of the involved electronic states are in progress.

This research is supported by the EPA grant 2008-ET-MS-3-S2, the SFI under Grants No. 07/SRC/B1160, 08/RFP/CHE1349, the Netherlands Organisation for Scientific Research through a VIDI grant (WRB) and the German Research Association (DFG SFB 583, GRK 1626; SR).

Notes and references

‡ TONs were determined by gas chromatography after irradiation of the reaction mixture for 18 h. Reaction mixture: *c*(cat.) = 4.08×10^{-5} M, *c*(TEA) = 2.15 M, 5 vol% of water in acetonitrile. The mixture was irradiated with an LED torch at 470 nm. The TON is the average of three independent measurements.

§ The addition of mercury has been proposed as a method to identify the involvement of colloids (by quenching their activity). In the present system however addition of mercury leads to decomposition of the complexes even in the absence of light and hence this standard test is not applicable here. It should be noted that the coordination of $PdCl_2$ to both **Ru** and **EtCOO-Ru** would be essentially the same and hence dissociation to form Pd-colloids would be expected from both complexes if it occurred. The absence of H_2 evolution in the case of **RuPd** suggests that Pd dissociation to yield an active colloid does not occur in the present system.

1 P. Chen and T. J. Meyer, *Chem. Rev.*, 1998, **98**, 1439–1477; B. S. Brunschwig, C. Creutz and N. Sutin, *Chem. Soc. Rev.*, 2002, **31**, 168–184; K. D. Demadis, C. M. Hartshorn and T. J. Meyer, *Chem. Rev.*, 2001, **101**, 2655–2685; W. R. Browne, R. Hage and J. G. Vos, *Coord. Chem. Rev.*, 2006, **250**, 1653–1668.
2 S. Rau, B. Schäfer, D. Gleich, E. Anders, M. Rudolph, M. Friedrich, H. Görls, W. Henry and J. G. Vos, *Angew. Chem., Int. Ed.*, 2006, **45**, 6215–6218.
3 H. Ozawa, Y. Yokoyama, M. Haga and K. Sakai, *Dalton Trans.*, 2007, 1197–1206.
4 S. A. Arachchige, J. Brown and K. J. Brewer, *J. Photochem. Photobiol., A*, 2008, **197**, 13–17.
5 E. D. Cline, S. E. Adamson and S. Bernhard, *Inorg. Chem.*, 2008, **47**, 10378–10388.
6 P. W. Du, K. Knowles and R. Eisenberg, *J. Am. Chem. Soc.*, 2008, **130**, 12576–12577.
7 A. Fihri, V. Artero, M. Razavet, C. Baffert, W. Leibl and M. Fontecave, *Angew. Chem., Int. Ed.*, 2008, **47**, 564–567.
8 C. Li, M. Wang, J. X. Pan, P. Zhang, R. Zhang and L. C. Sun, *J. Organomet. Chem.*, 2009, **694**, 2814–2819.
9 Y. Miyake, K. Nakajima, K. Sasaki, R. Saito, H. Nakanishi and Y. Nishibayashi, *Organometallics*, 2009, **28**, 5240–5243.
10 B. Probst, C. Kolano, P. Hamm and R. Alberto, *Inorg. Chem.*, 2009, **48**, 1836–1843.
11 S. Tschierlei, M. Karnahl, M. Presselt, B. Dietzek, J. Guthmüller, L. Gonzalez, M. Schmitt, S. Rau and J. Popp, *Angew. Chem., Int. Ed.*, 2010, **49**, 3981–3984.
12 H. Ozawa and K. Sakai, *Chem. Commun.*, 2011, **47**, 2227–2242.
13 P. Du, J. Schneider, L. Fan, W. Zhao, U. Patel, F. N. Castellano and R. Eisenberg, *J. Am. Chem. Soc.*, 2008, **130**, 5056–5058.

14 P. Lei, M. Hedlund, R. Lomoth, H. Rensmo, O. Johansson and L. Hammarström, *J. Am. Chem. Soc.*, 2008, **130**, 26–27.
15 S. Ernst, V. Kasack and W. Kaim, *Inorg. Chem.*, 1988, **27**, 1146–1148; S. D. Ernst and W. Kaim, *Inorg. Chem.*, 1989, **28**, 1520–1528.
16 D. M. D'Alessandro and F. R. Keene, *New J. Chem.*, 2006, **30**, 228–237.
17 S. Campagna, G. Denti, S. Serroni, M. Ciano and V. Balzani, *Inorg. Chem.*, 1991, **30**, 3728–3732; P. Ceroni, F. Paolucci, S. Roffia, S. Serroni, S. Campagna and A. J. Bard, *Inorg. Chem.*, 1998, **37**, 2829–2832.
18 G. Denti, S. Serroni, S. Campagna, V. Ricevuto and V. Balzani, *Inorg. Chim. Acta*, 1991, **182**, 127–129.
19 G. Denti, S. Campagna, L. Sabatino, S. Serroni, M. Ciano and V. Balzani, *Inorg. Chem.*, 1990, **29**, 4750–4758.
20 M. Marcaccio, F. Paolucci, C. Paradisi, S. Roffia, C. Fontanesi, L. J. Yellowlees, S. Serroni, S. Campagna, G. Denti and V. Balzani, *J. Am. Chem. Soc.*, 1999, **121**, 10081–10091.
21 M. Marcaccio, F. Paolucci, C. Paradisi, M. Carano, S. Roffia, C. Fontanesi, L. J. Yellowlees, S. Serroni, S. Campagna and V. Balzani, *J. Electroanal. Chem.*, 2002, **532**, 99–112.
22 M. Sommovigo, G. Denti, S. Serroni, S. Campagna, C. Mingazzini, C. Mariotti and A. Juris, *Inorg. Chem.*, 2001, **40**, 3318–3323.
23 M. Schulz, J. Hirschmann, A. Draksharapu, G. Singh Bindra, S. Soman, A. Paul, R. Groarke, M. T. Pryce, S. Rau, W. R. Browne and J. G. Vos, *Dalton Trans.*, 2011, DOI: 10.1039/c1dt10960j.

Appendix B

Chapter 3

3.2.1 UV Absorbance Spectra

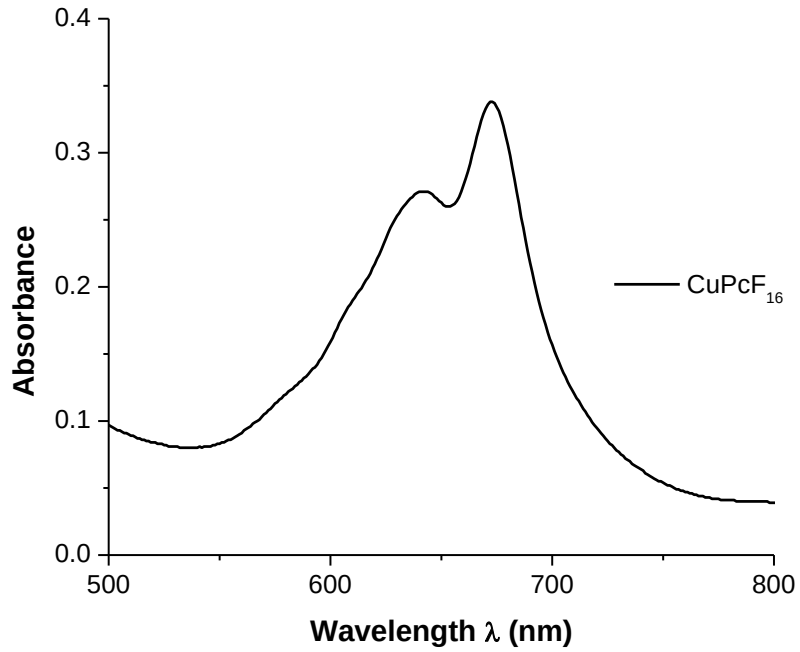

Figure B.1: *Absorbance spectrum of $CuPcF_{16}$ in DMF solution.*

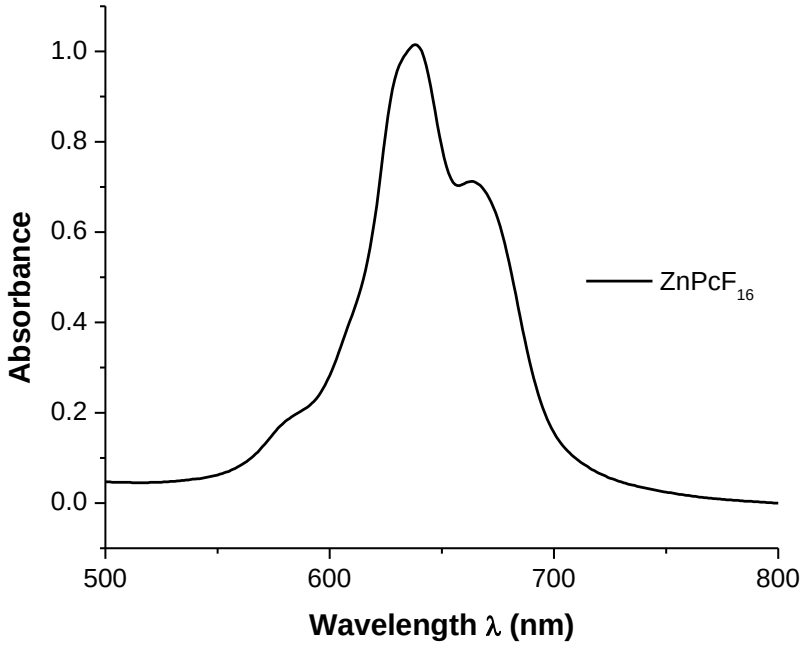

Figure B.2: *Absorbance spectrum of $ZnPcF_{16}$ in DMF solution.*

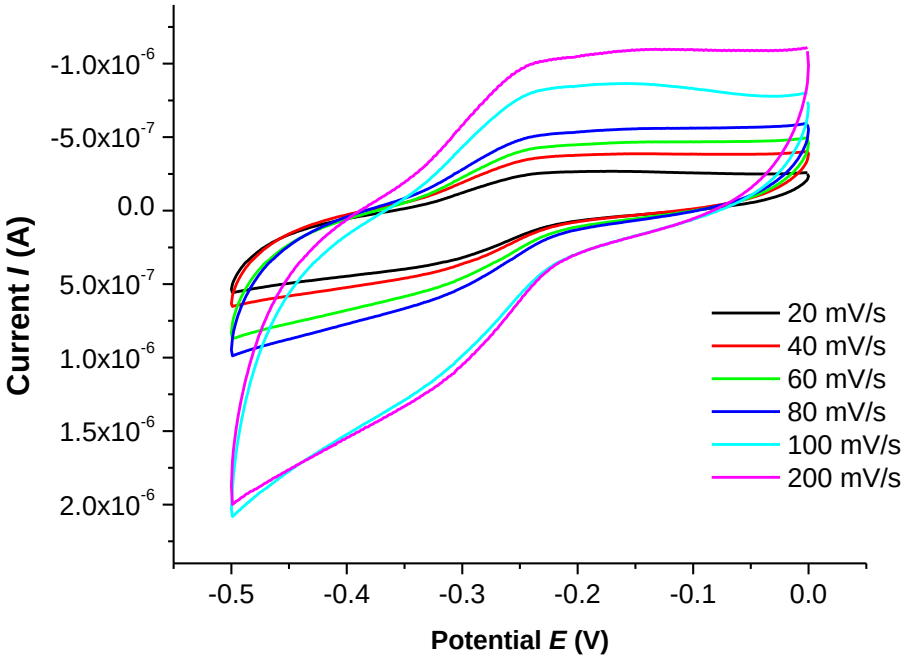

Figure B.3: *Scan rate dependence of the first reduction process of $ZnPcF_{16}$ modified electrode in 0.1 M NaH_2PO_4/H_3PO_4 (pH 2) vs. Ag/AgCl.*

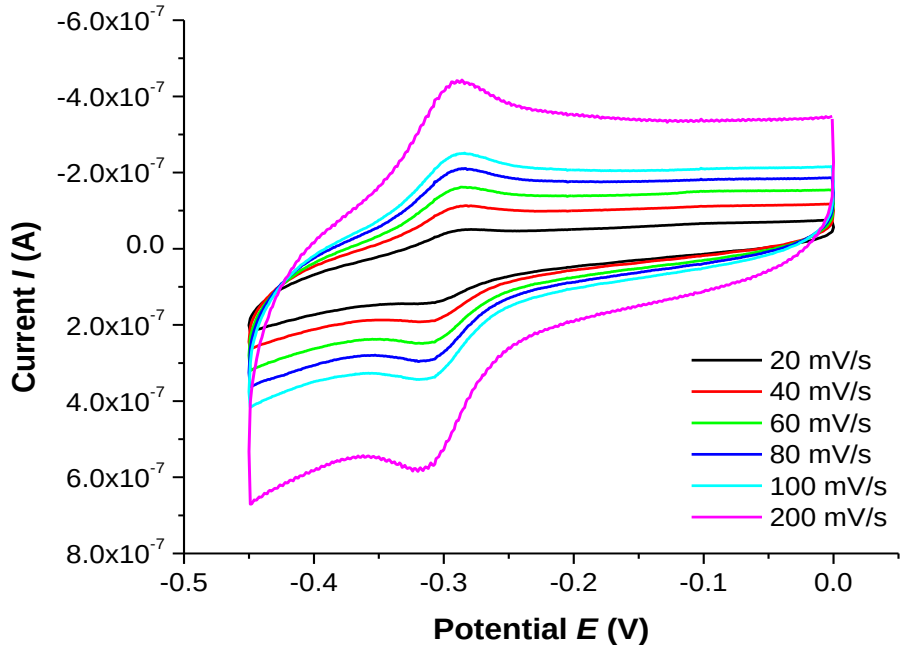

Figure B.4: *Scan rate dependence of the first reduction process of $CuPcF_{16}$ modified electrode in 0.1 M NaH_2PO_4/H_3PO_4 (pH 2) vs. Ag/AgCl.*

Appendix C

Chapter 4

4.2.2.1 Applied Potential

Applied Potential (V)	***-0.8***	***-0.9***	***-1.0***	***-1.1***	***-1.2***
TOF (hr^{-1}) (Electrochemical)	*9.2 x10^3*	*3.1 x10^4*	*7.7 x10^5*	*1.4 x10^6*	*1.9 x10^6*
TOF (hr^{-1}) (GC)	*2.5 x 10^3*	*1.2 x 10^4*	*1.1 x 10^5*	*2.2 x 10^5*	*1.4 x 10^6*
Faradaic Efficiency (%)	*27*	*39*	*15*	*16*	*74*

Table C.1: *$CoPcF_{16}$ with varying electrolysis potentials in 0.1 M NaH_2PO_4/H_3PO_4 (pH 2).*

Applied Potential (V)	***-0.8***	***-0.9***	***-1.0***	***-1.1***	***-1.2***
TOF (hr^{-1}) (Electrochemical)	*1.9 x 10^5*	*1.1 x 10^6*	*2.3 x 10^6*	*3.2 x 10^6*	*4.7 x 10^6*
TOF (hr^{-1}) (GC)	-	*3 x10^5*	*7.3 x10^5*	*1.8 x10^6*	*3.5 x10^6*
Faradaic Efficiency (%)	-	*25*	*32*	*56*	*74*

Table C.2: *$CuPcF_{16}$ with varying electrolysis potentials in 0.1 M NaH_2PO_4/H_3PO_4 (pH 2).*

Applied Potential (V)	***-0.8***	***-0.9***	***-1.0***	***-1.1***	***-1.2***
TOF (hr^{-1}) (Electrochemical)	*5 x 10^3*	*1.4 x 10^5*	*1.9 x 10^6*	*3.2 x 10^6*	*2.0 x 10^6*
TOF (hr^{-1}) (GC)	-	-	*1.4 x10^6*	*1.7 x10^6*	*8.0 x10^5*
Faradaic Efficiency (%)	-	-	*68*	*54*	*40*

Table C.3: *$ZnPcF_{16}$ with varying electrolysis potentials in 0.1 M NaH_2PO_4/H_3PO_4 (pH 2).*

4.2.2.2 Effect of temperature

Temperature T (°C)	***3°C***	***20°C***	***40°C***
TOF (hr^{-1}) (Electrochemical)	*7.4 x 10^5*	*1.9 x 10^6*	*3.8 x 10^6*
TOF (hr^{-1}) (GC)	*3.3 x10^5*	*1.4 x10^6*	*1.9 x10^6*
Faradaic Efficiency (%)	*46*	*74*	*50*

Table C.4: *$CoPcF_{16}$ with temperature in 0.1 M NaH_2PO_4/H_3PO_4 (pH 2).*

Temperature T (°C)	***3°C***	***20°C***	***40°C***
TOF (hr^{-1}) (Electrochemical)	*1.1 x 10^6*	*4.7 x 10^6*	*8.5 x 10^6*
TOF (hr^{-1}) (GC)	*1.5 x 10^5*	*3.5 x 10^6*	*3.9 x 10^6*
Faradaic Efficiency (%)	*15*	*74*	*46*

Table C.5: *$CuPcF_{16}$ with varying electrolysis potentials in 0.1 M NaH_2PO_4/H_3PO_4 (pH 2).*

Temperature T (°C)	***3°C***	***20°C***	***40°C***
TOF (hr^{-1}) (Electrochemical)	*7.6 x 10^5*	*3.2 x 10^6*	*3.8 x 10^6*
TOF (hr^{-1}) (GC)	*2.7 x 10^5*	*1.7 x 10^6*	*3.4 x 10^6*
Faradaic Efficiency (%)	*36*	*54*	*89*

Table C.6: *$ZnPcF_{16}$ with varying electrolysis potentials in 0.1 M NaH_2PO_4/H_3PO_4 (pH 2).*

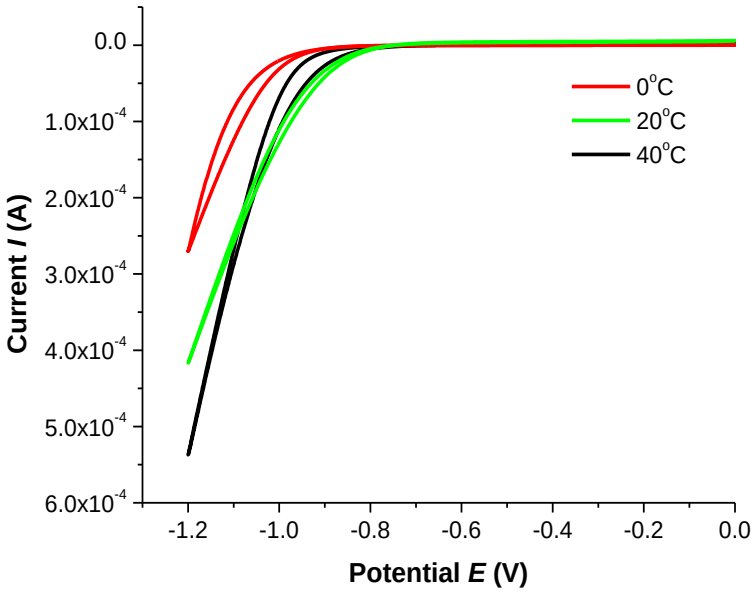

Figure C.1: *Cyclic voltammogram of $CuPcF_{16}$ vs. Ag/AgCl in 0.1 M NaH_2PO_4/H_3PO_4 (pH 2) at 100 mV/s where the red, green and black lines represent the catalytic currents at 0°C, 20°C and 40°C respectively.*

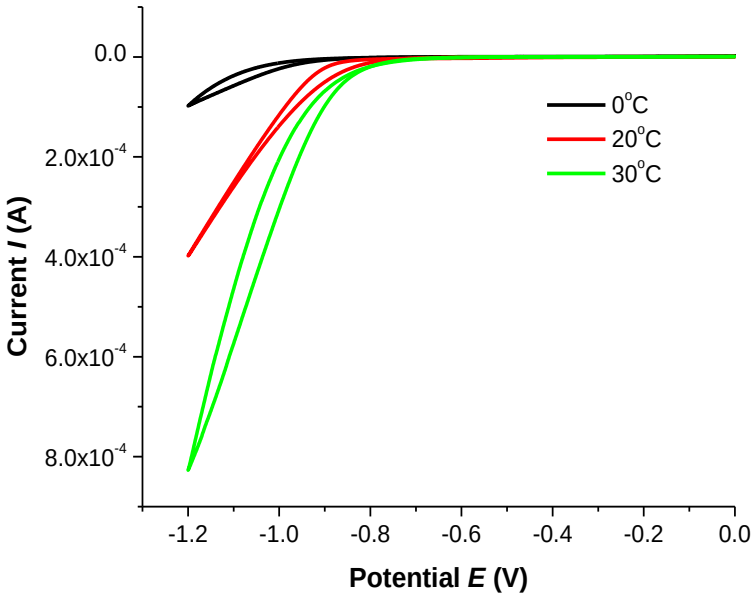

Figure C.2: *Cyclic voltammogram of $ZnPcF_{16}$ vs. Ag/AgCl in 0.1 M NaH_2PO_4/H_3PO_4 (pH 2) at 100 mV/s where the black, red and green lines represent the catalytic currents at 0°C, 20°C and 30°C respectively.*

4.2.2.3 Effect of using ethyl acetate for preparation of catalyst solutions

No. of layers drop cast	***1***	***2***	***5***
TOF (hr^{-1}) (Electrochemical)	*7.9 x 10^5*	*4.6 x 10^5*	*2.4 x 10^6*
TOF (hr^{-1}) (GC)	*4.8 x 10^5*	*2.6 x 10^5*	*1.3 x 10^6*
Faradaic Efficiency (%)	*60*	*56*	*56*

Table C.7: *$CoPcF_{16}$ (prepared in ethyl acetate), effect of additional layers in 0.1 M NaH_2PO_4/H_3PO_4 (pH 2).*

4.2.2.4 Casting additional layers using DMF catalyst solution

Catalyst	***$CoPcF_{16}$***	
No. of layers cast	***1***	***2***
TOF (hr^{-1}) (Electrochemical)	*1.9 x 10^6*	*9.6 x 10^5*
TOF (hr^{-1}) (GC)	*1.4 x 10^6*	*4.1 x 10^5*
Faradaic Efficiency %	*74*	*43*

Table C.8: *Varying the number of layers of catalyst deposited (from a catalyst solution prepared in DMF) for $CoPcF_{16}$ in 0.1 M NaH_2PO_4/H_3PO_4 (pH 2).*

Catalyst	***$CuPcF_{16}$***		***$ZnPcF_{16}$***	
No. of layers cast	***1***	***2***	***1***	***2***
Average Charge ($C\ hr^{-1}$)	*0.23*	*0.12*	*0.44*	*0.24*
TOF ($GC\ hr^{-1}$)	*2.1×10^6*	*1.9×10^6*	*1.9×10^6*	*1.1×10^6*
[1]Current Density J (mA/cm^2)	*0.9*	*0.7*	*1.8*	*1.0*
Electroactive $MPcF_{16}$ %	*1.0*	*0.4*	*0.1*	*0.1*

Table C.9: *Performance data obtained for $CuPcF_{16}$ and $ZnPcF_{16}$ by CV and BE vs. Ag/AgCl in 0.1 M NaH_2PO_4/H_3PO_4 (pH 2) with varying the number of layers of catalyst deposited on the electrode.*

4.2.2.5 Effect of varying the pH and ionic strength of electrolyte

Applied Potential (V)	***-1.2*** *(pH 2)*	***-1.4*** *(pH 4)*	***-1.8*** *(pH 7)*	***-1.8*** *(pH 9)*
TOF Electrochemistry (hr^{-1})	*1.9×10^6*	*9.1×10^5*	*2.7×10^6*	*2.6×10^6*
TOF GC (hr^{-1})	*1.4×10^6*	*5.5×10^5*	*2.2×10^6*	*2.0×10^6*
Faradaic Efficiency %	*74*	*60*	*82*	*77*

Table C.10: *Effect of pH of electrolyte on the performance indicators for $CoPcF_{16}$ obtained by CV and BE (using varying applied potentials).*

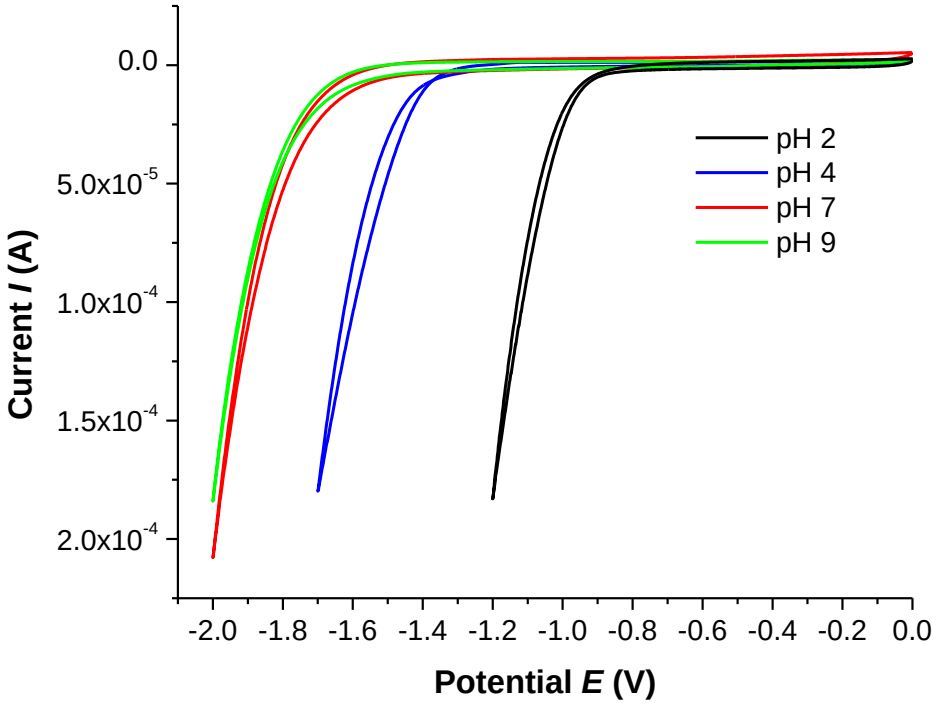

Figure C.3: *Typical currents observed for $CuPcF_{16}$ in 0.1 M NaH_2PO_4 at various pH. Scan rate = 100 mV/s.*

pH	***2***	***4***	***7***	***9***
Applied Potential (V)	*-1.2*	*-1.7*	*-2.0*	*-2.0*
Average Charge (C hr^{-1})	*0.23*	*0.35*	*0.70*	*0.51*
Electroactive $CuPcF_{16}$ (%)	*1.0*	*0.4*	*0.3*	*1.8*
TOF Electrochemistry (hr^{-1})	*4.7×10^6*	*6.6×10^6*	*3.9×10^7*	*9.2×10^6*
TOF GC (hr^{-1})	*3.5×10^6*	*3.0×10^6*	*1.4×10^7*	*7.5×10^6*
Faradaic Efficiency %	*74*	*45*	*36*	*82*

Table C.11: *Effect of pH of electrolyte on the performance indicators for $CuPcF_{16}$ obtained by CV and BE (using varying applied potentials).*

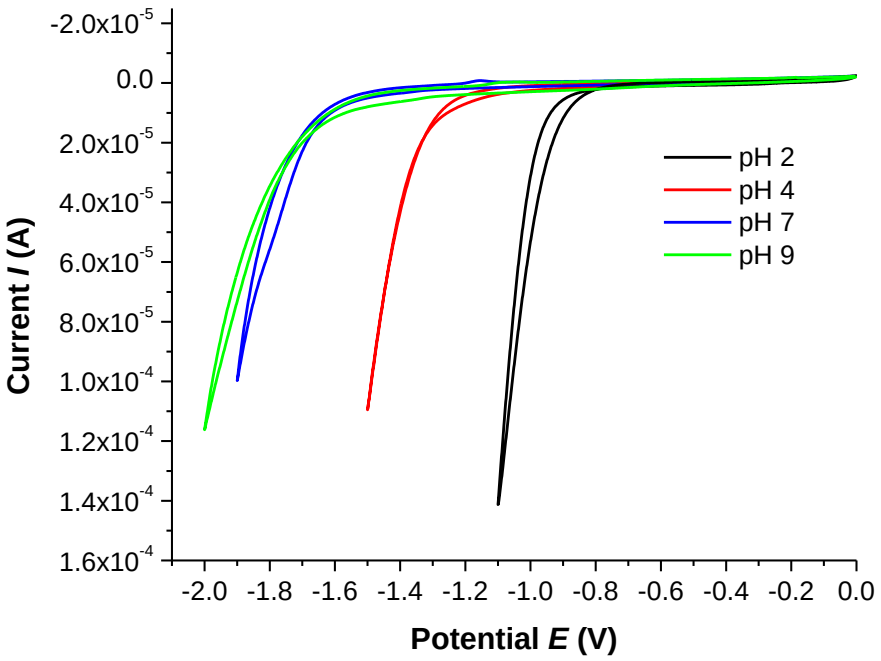

Figure C.4: *Typical currents observed for $ZnPcF_{16}$ in 0.1 M NaH_2PO_4 at various pH. Scan rate = 100 mV/s.*

pH	***2***	***4***	***7***	***9***
Applied Potential (V)	*-1.1*	*-1.5*	*-1.9*	*-2.0*
Average Charge (C hr^{-1})	*0.4*	*0.3*	*0.6*	*0.7*
Electroactive $ZnPcF_{16}$ (%)	*0.1*	*0.03*	*0.5*	*0.3*
TOF Electrochemistry (hr^{-1})	*3.2×10^6*	*6.6×10^6*	*1.4×10^6*	*2.1×10^6*
TOF GC (hr^{-1})	*1.7×10^6*	*3.5×10^6*	*1.2×10^6*	*1.9×10^6*
Faradaic Efficiency %	*54*	*53*	*86*	*91*

Table C.12: *Effect of pH of electrolyte on the performance indicators for $ZnPcF_{16}$ obtained by CV and BE (using varying applied potentials).*

4.2.2.6 Varying the catalyst concentration in coating solutions

Catalyst Concentration (x 10^{-5} M)	***0.7***	***1.4***	***2.1***
Moles of electroactive catalyst (mol)	*6.6 x10^{-13}*	*1.4 x10^{-12}*	*1.4 x10^{-12}*
TOF (hr^{-1}) (Electrochemical)	*1.3 x 10^{6}*	*1.1 x 10^{6}*	*9.0 x 10^{5}*
TOF (hr^{-1}) (GC)	*5.9 x 10^{5}*	*4.3 x 10^{5}*	*4.1 x 10^{5}*
Faradaic Efficiency (%)	*46*	*39*	*45*

Table C.13: *Performance data obtained for $CoPcF_{16}$ by CV and BE (at -1.2 V for 1 hour) vs. Ag/AgCl in 0.1 M NaH_2PO_4/H_3PO_4 (pH 2) with varying catalyst concentration.*

4.2.2.8 Using Chloride as an electrolyte

Temperature (°C)	***0***	***20***	***40***
TOF (hr^{-1}) (Electrochemical)	*5.3 x 10^{5}*	*6.8 x 10^{5}*	*8.2 x 10^{5}*
TOF (hr^{-1}) (GC)	*3.4 x 10^{5}*	*6.1 x 10^{5}*	*7.3 x 10^{5}*
Faradaic Efficiency (%)	*64*	*89*	*89*

Table C.14: *Performance data obtained for $CoPcF_{16}$ by CV and BE (at -1.2 V for 1 hour) vs. Ag/AgCl in 0.1 M HCl/KCl (pH 1.8) with varying temperature.*

4.2.2.9 Stability

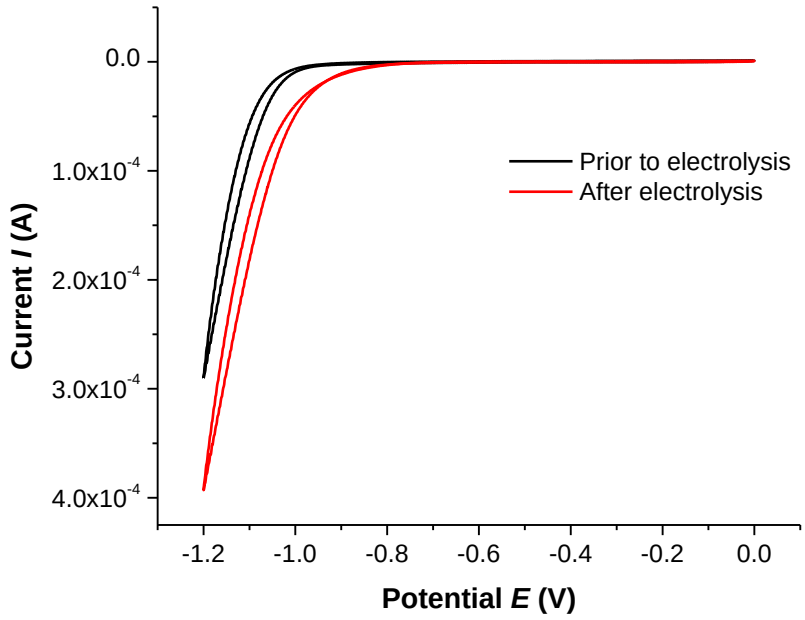

Figure C.5: *Cyclic voltammograms of $CoPcF_{16}$ vs. Ag/AgCl in 0.1 M NaH_2PO_4/H_3PO_4 (pH 2). Scan rate = 100 mV/s.*

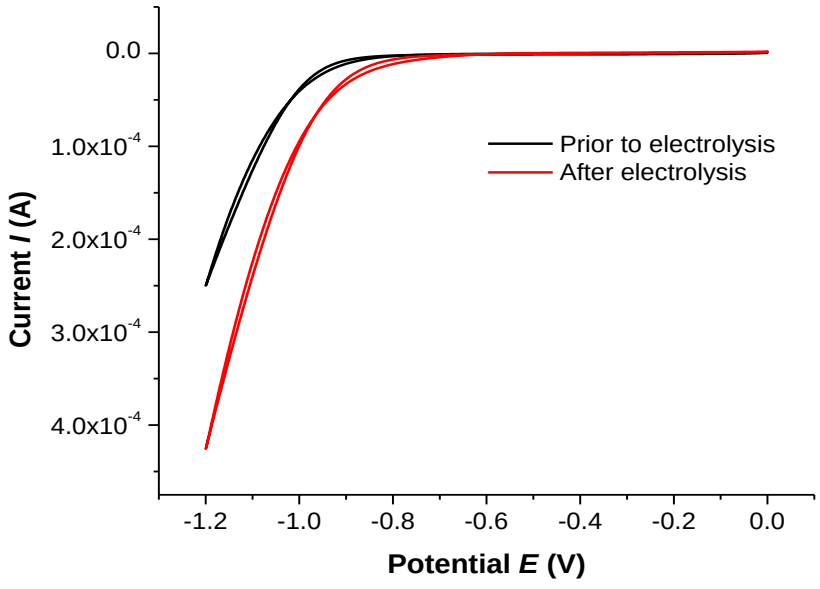

Figure C.6: *Cyclic voltammograms of $CuPcF_{16}$ vs. Ag/AgCl in 0.1 M NaH_2PO_4/H_3PO_4 (pH 2). Scan rate = 100 mV/s.*

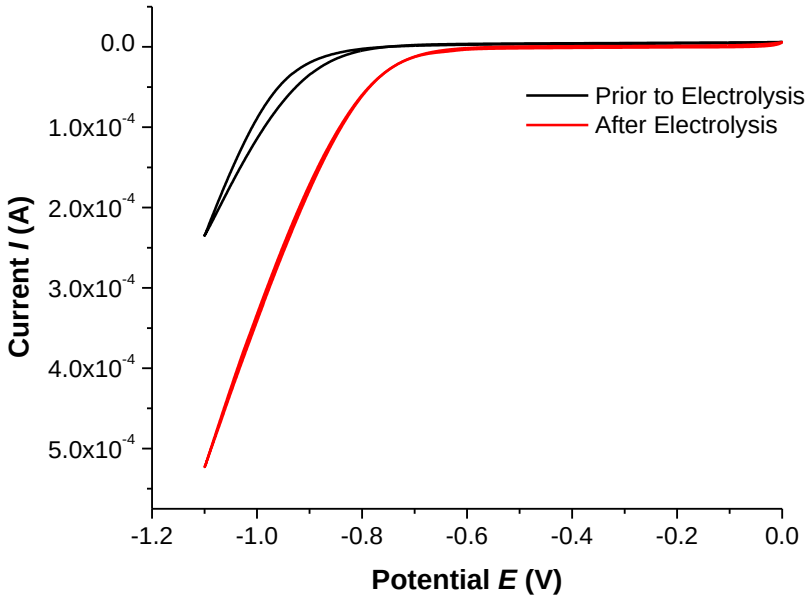

Figure C.7: *Cyclic voltammograms of $ZnPcF_{16}$ vs. Ag/AgCl in 0.1 M NaH_2PO_4 (pH 2). Scan rate = 100 mV/s.*

4.2.2.10 Duration of Electrolysis

Time (hr)	***1***	***5***	***11***	***24***
TON (hr^{-1}) (Electrochemical)	*1.9×10^6*	*2.7×10^6*	*6.6×10^6*	*4×10^7*
TON (hr^{-1}) (GC)	*1.4×10^6*	*1.9×10^6*	*3.8×10^6*	*7.9×10^6*
Faradaic Efficiency (%)	*74*	*70*	*58*	*20*

Table C.15: *Turnover numbers (TON) obtained for $CoPcF_{16}$ over 1 to 24 hours.*

4.2.2.11 Repeated Use of ME

	First Use	***Second Use***
TOF (hr^{-1}) (Electrochemical)	*1.2×10^6*	*1.3×10^6*
TOF (hr^{-1}) (GC)	*5.8×10^5*	*2.4×10^5*
Faradaic Efficiency (%)	*49*	*19*

Table C.16: *Turnover frequencies obtained for $CoPcF_{16}$ for the first and second use of the modified electrode.*

4.2.2.12 Photo- electrocatalytic generation of hydrogen

	Co	***Cu***	***Zn***
TOF (hr^{-1}) (Electrochemical)	*1.1×10^6*	*8.8×10^5*	*1.5×10^5*
TOF (hr^{-1}) (GC)	*6.7×10^5*	*6.6×10^4*	*3.5×10^4*
Faradaic Efficiency (%)	*63*	*8*	*31*

Table C.17: *Performance data obtained in the dark for $CoPcF_{16}$/ $CuPcF_{16}$/ $ZnPcF_{16}$ by CV and BE (at -1.2 V for 1 hour) vs. Ag/AgCl in 0.1 M NaH_2PO_4/H_3PO_4 (pH 2)*

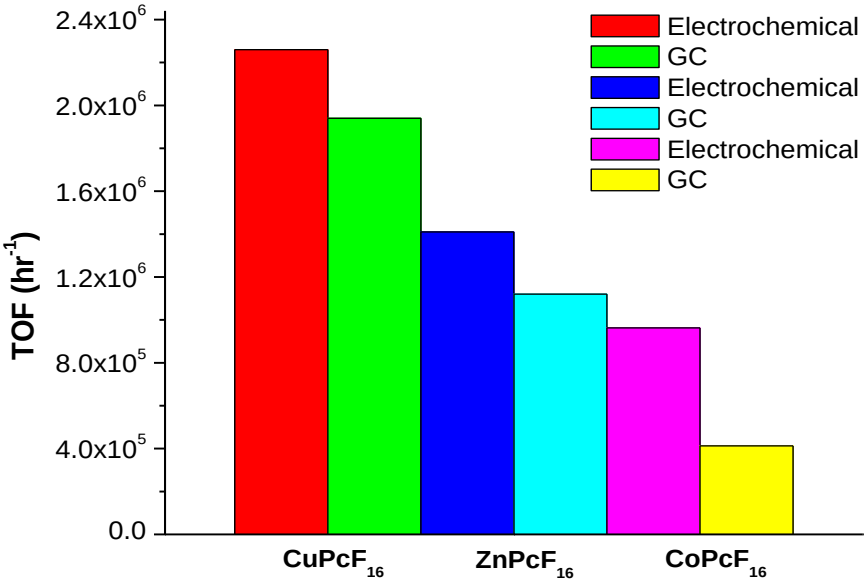

Figure C.8: *Electrochemical and gas chromatography TOF values obtained for each of the three catalysts where 2 layers were deposited on the working electrode.*

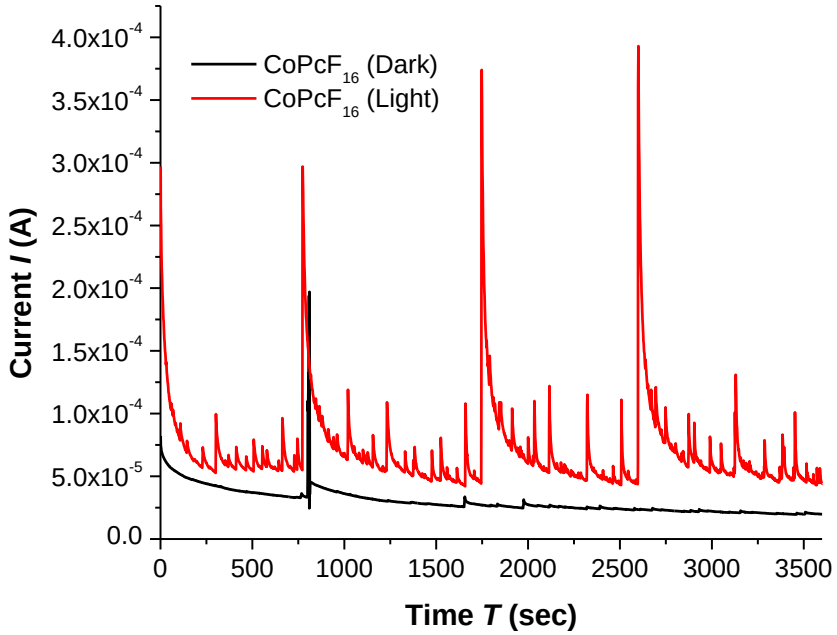

Figure C.9: *Electrochemical and gas chromatography TOF values obtained for each of the three catalysts where 2 layers were deposited on the working electrode.*

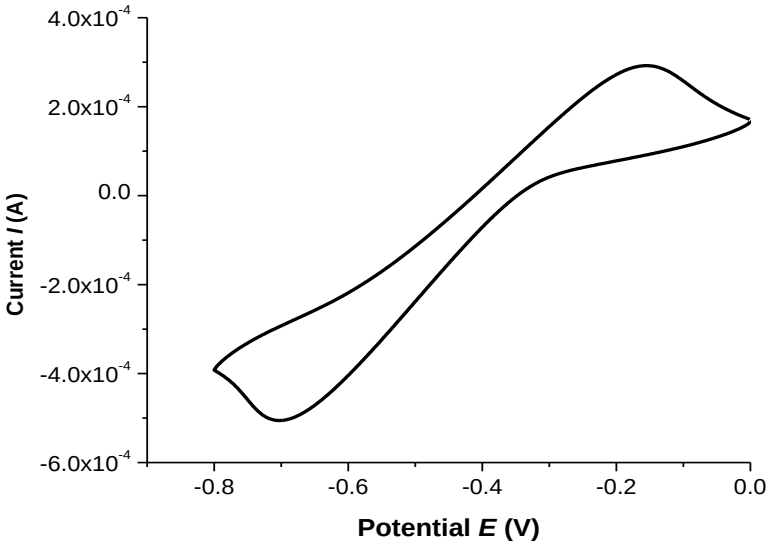

Figure C.10: *Cyclic voltammetry of a bare Pt electrode (geometrical area = 0.03cm^2) vs. Ag/AgCl in 0.1 M NaH_2PO_4/H_3PO_4 (pH 2). Scan rate = 100 mV/s.*

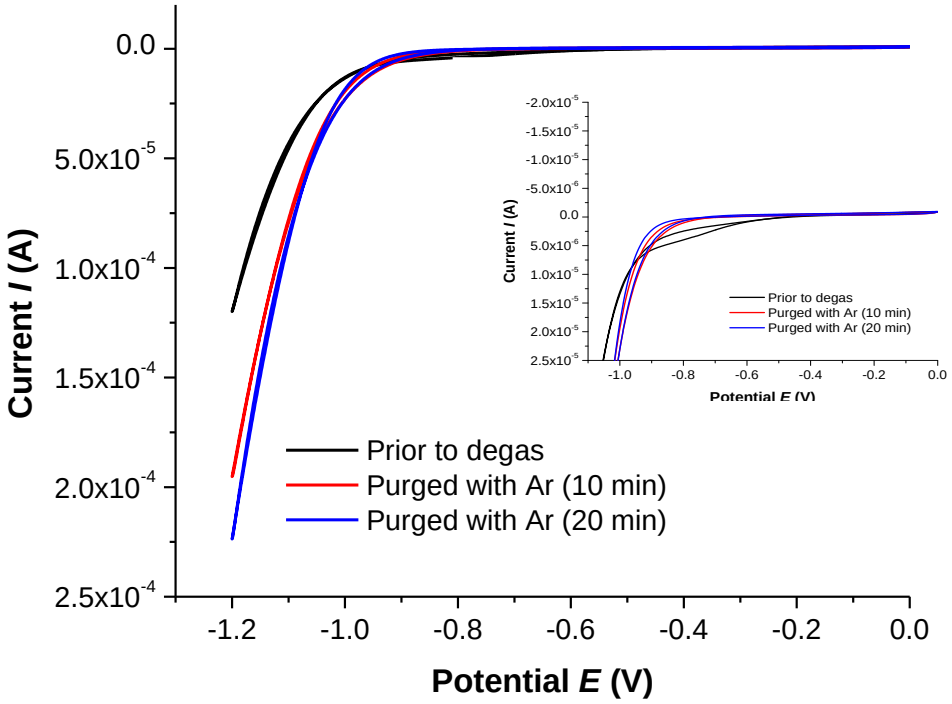

Figure C.11: *Cyclic voltammetry of a modified electrode coated with $CoPcF_{16}$ vs. Ag/AgCl in 0.1 M NaH_2PO_4/H_3PO_4 (pH 2). Scan rate = 100 mV/s. Catalytic currents produced with increasing degassing times.*

Appendix D

Chapter 5

5.2.1.2 Electrochemical reactivity of M(II)PcF$_{16}$ embedded in Nafion®

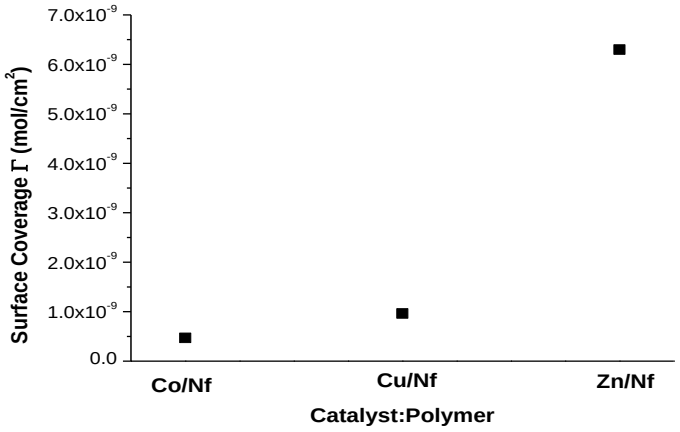

Figure D.0: *Additional data* concerning *surface coverage*.

5.2.2.1 Applied Electrolysis

Applied Potential (V)	***-0.8***	***-0.9***	***-1.0***	***-1.1***	***-1.2***
TOF (hr^{-1}) (Electrochemical)	*2.2 x10^4*	*8.4 x10^4*	*1.9 x10^5*	*2.2 x10^5*	*6.2 x10^5*
TOF (hr^{-1}) (GC)	*1.5 x10^4*	*2.0 x10^4*	*7.8 x10^4*	*9.2 x10^4*	*4.4 x10^5*
Faradaic Efficiency (%)	*68*	*25*	*41*	*42*	*71*

Table D.1: *CoPcF$_{16}$/Nf with varying electrolysis potentials in 0.1 M NaH_2PO_4/H_3PO_4 (pH 2).*

Applied Potential (V)	***-0.8***	***-0.9***	***-1.0***	***-1.1***	***-1.2***
TOF (hr^{-1}) (Electrochemical)	*9.1 x 10^4*	*1.5 x 10^5*	*5.4 x 10^5*	*5.2 x 10^5*	*6.0 x 10^5*
TOF (hr^{-1}) (GC)	*1.8 x 10^4*	*2.6 x 10^4*	*1.3 x 10^5*	*1.5 x 10^5*	*2.3 x 10^5*
Faradaic Efficiency (%)	*19*	*18*	*25*	*29*	*39*

Table D.2: *$CuPcF_{16}$/Nf with varying electrolysis potentials in 0.1 M NaH_2PO_4/H_3PO_4 (pH 2).*

Applied Potential (V)	***-0.8***	***-0.9***	***-1.0***	***-1.1***	***-1.2***
TOF (hr^{-1}) (Electrochemical)	*8.5×10^3*	*6.3×10^3*	*7.7×10^3*	*7.9×10^4*	*2.7×10^5*
TOF (hr^{-1}) (GC)	-	-	-	*1.9×10^4*	*5.8×10^4*
Faradaic Efficiency (%)	-	-	-	*25*	*22*

Table D.3: *$ZnPcF_{16}$/Nf with varying electrolysis potentials in 0.1 M NaH_2PO_4/H_3PO_4 (pH 2).*

5.2.2.2 Effect of Temperature

Temperature (°C)	***0***	***20***	***40***
TOF (hr^{-1}) (Electrochemical)	*2.0×10^5*	*6.2×10^5*	*1.1×10^6*
TOF (hr^{-1}) (GC)	*1.3×10^5*	*4.4×10^5*	*8.1×10^5*
Faradaic Efficiency (%)	*66*	*71*	*77*

Table D.4: *$CoPcF_{16}$/Nf with varying temperature in 0.1 M NaH_2PO_4/H_3PO_4 (pH 2).*

Temperature (°C)	***0***	***20***	***40***
TOF (hr^{-1}) (Electrochemical)	*1.3×10^5*	*6×10^5*	*1.1×10^6*
TOF (hr^{-1}) (GC)	*5×10^4*	*2.3×10^5*	*8.1×10^5*
Faradaic Efficiency (%)	*39*	*39*	*74*

Table D.5: *$CuPcF_{16}$/Nf with varying temperature in 0.1 M NaH_2PO_4/H_3PO_4 (pH 2).*

Temperature (°C)	***0***	***20***	***40***
TOF (hr^{-1}) (Electrochemical)	*5.4×10^4*	*2.4×10^5*	*4.3×10^5*
TOF (hr^{-1}) (GC)	*1.4×10^4*	*5.8×10^4*	*3.0×10^5*
Faradaic Efficiency (%)	*25*	*24*	*70*

Table D.6: *$ZnPcF_{16}$/Nf with varying temperature in 0.1 M NaH_2PO_4/H_3PO_4 (pH 2).*

5.2.2.3 Effect of pH and Ionic Strength

pH	***2***	***4***	***7***	***9***
TOF (hr^{-1}) (Electrochemical)	*6.2×10^5*	*2.0×10^5*	*4.3×10^6*	-
TOF (hr^{-1}) (GC)	*4.4×10^5*	*1.1×10^5*	*1.5×10^6*	-
Faradaic Efficiency (%)	*71*	*55*	*35*	-

Table D.7: *$CoPcF_{16}$/Nf with varying pH in 0.1 M NaH_2PO_4.*

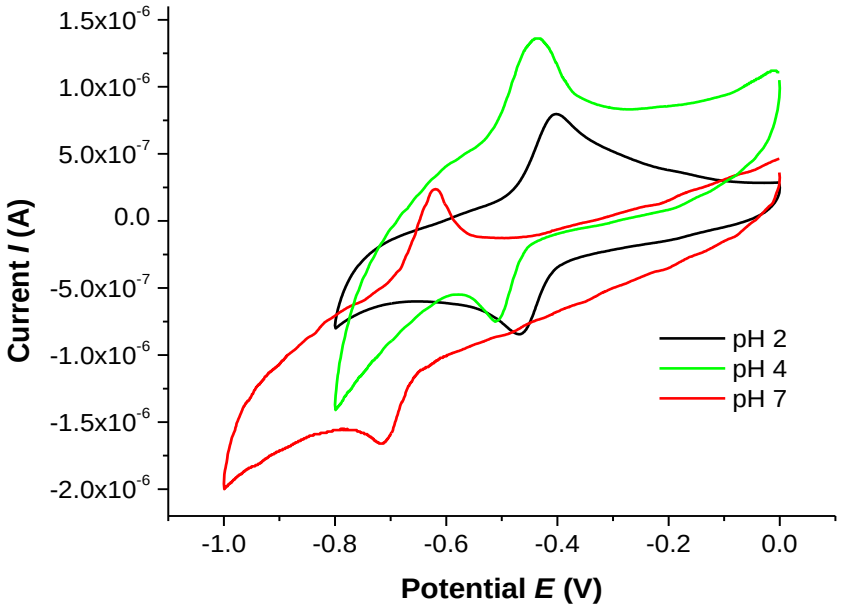

Figure D.1: *Comparison of redox potentials of $CoPcF_{16}$/Nf in 0.1 M NaH_2PO_4 vs. Ag/AgCl, ranging in pH 2-7. Scan rate = 20 mV/s*

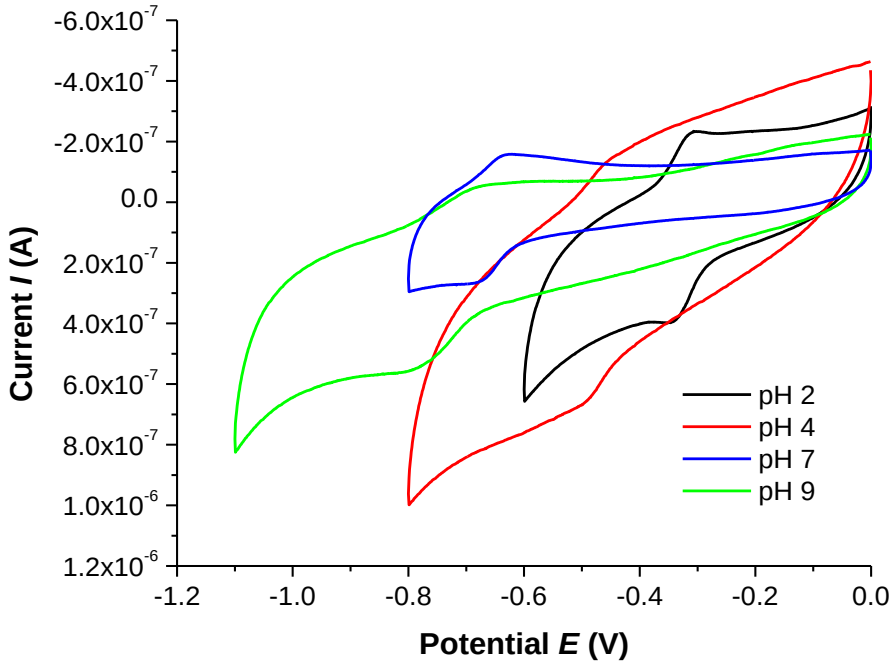

Figure D.2: *Comparison of redox potentials of $CuPcF_{16}$/Nf in 0.1 M NaH_2PO_4 vs. Ag/AgCl, ranging in pH 2-9. Scan rate = 20 mV/s*

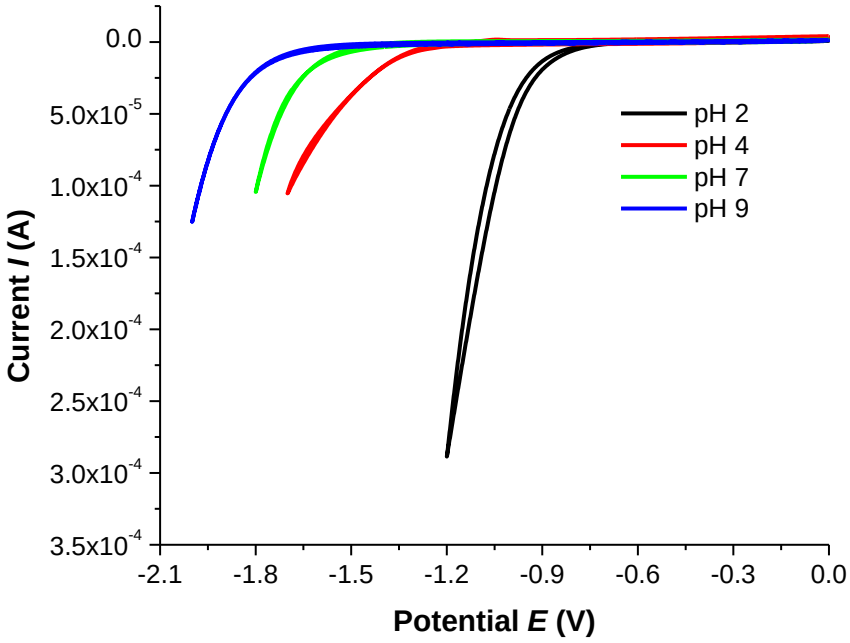

Figure D.3: *Typical currents observed for $CuPcF_{16}$/ in 0.1 M NaH_2PO_4 vs. Ag/AgCl, ranging in pH 2-9. Scan rate = 20 mV/s*

pH	E ½ Potential (V)	$E_{pc} - E_{pa}$ (V)	Onset Potential (V)
2	-0.32	0.04	-0.87
4	-0.46	0.06	-1.33
7	-0.65	0.50	-1.55
9	-0.73	0.11	-1.70

Table D.8: *Reduction potentials of $CuPcF_{16}$/Nf in 0.1 M NaH_2PO_4 electrolyte over a range of pH.*

Applied Potential (V)	***-1.2*** *(pH 2)*	***-1.7*** *(pH 4)*	***-1.8*** *(pH 7)*	***-2.0*** *(pH 9)*
Average Charge (C hr^{-1})	*0.17*	*0.28*	*1.78*	*1.02*
Electroactive $CuPcF_{16}$/Nf (%)	*3.4*	*3.2*	*1.0*	*3.2*
TOF (hr^{-1}) (Electrochemical)	*6.0 x 10^5*	*7.6 x 10^5*	*3.8 x 10^6*	*2.2 x 10^6*
TOF (hr^{-1}) (GC)	*2.3 x 10^5*	*2.9 x 10^5*	*3.5 x 10^6*	*1.6 x 10^6*
Faradaic Efficiency (%)	*39*	*38*	*92*	*73*

Table D.9: *Effect of pH of electrolyte on the performance indicators for $CuPcF_{16}$/Nf (using varying applied potentials).*

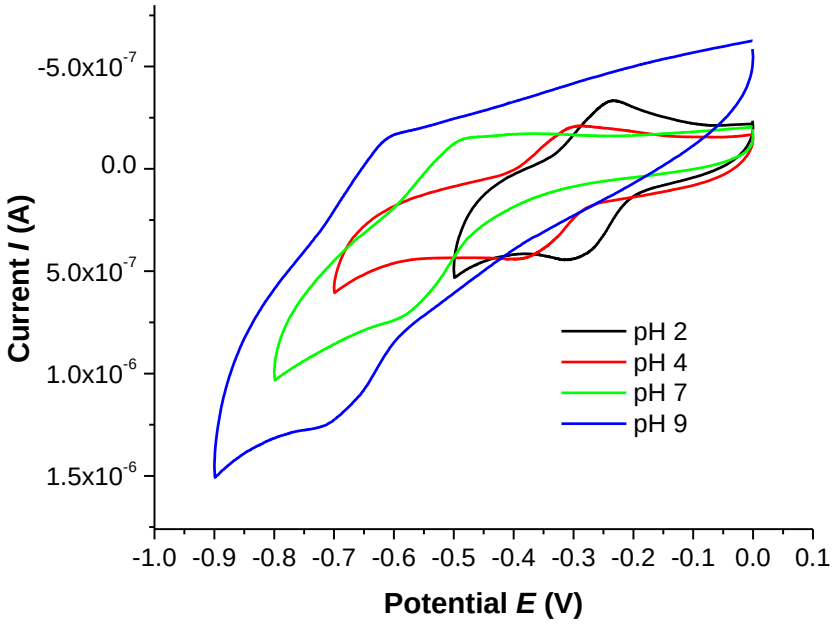

Figure D.4: *Comparison of redox potentials of $ZnPcF_{16}$/Nf in 0.1 M NaH_2PO_4 vs. Ag/AgCl, ranging in pH 2-9. Scan rate = 20 mV/s*

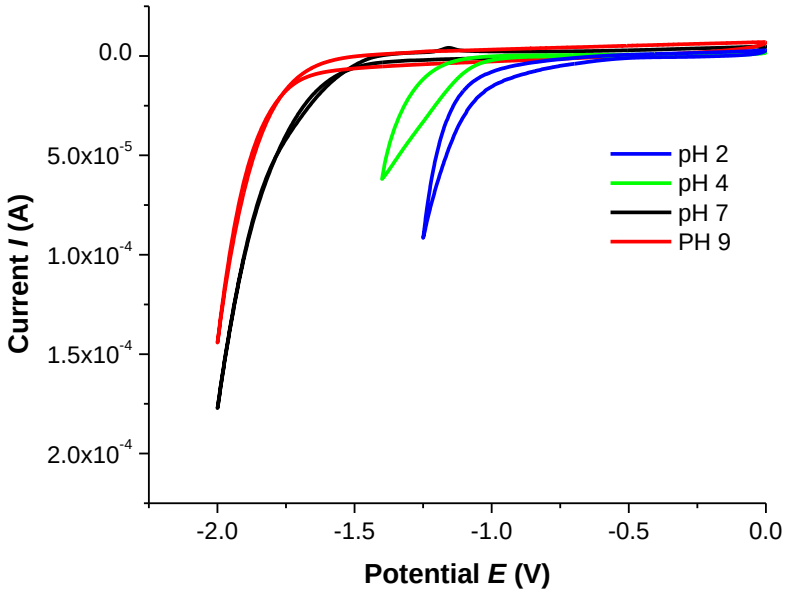

Figure D.5: *Typical currents observed for $ZnPcF_{16}$/Nf in 0.1 M NaH_2PO_4 vs. Ag/AgCl, ranging in pH 2-9. Scan rate = 20 mV/s*

pH	E ½ Potential (V)	$E_{pc} - E_{pa}$ (V)	Onset Potential (V)
2	-0.25	0.08	-1.00
4	-0.35	0.09	-1.04
7	-0.53	0.10	-1.53
9	-0.66	0.10	-1.74

Table D.10: *Reduction potentials of $ZnPcF_{16}$/Nf in 0.1 M NaH_2PO_4 electrolyte over a range of pH.*

Applied Potential (V)	***-1.2*** *(pH 2)*	***-1.4*** *(pH 4)*	***-2.0*** *(pH 7)*	***-2.0*** *(pH 9)*
Average Charge (C hr^{-1})	*0.24*	*0.05*	*0.72*	*0.25*
Electroactive $ZnPcF_{16}$/Nf (%)	*0.7*	*1.1*	*1.1*	*0.8*

TOF (hr^{-1}) (Electrochemical)	*2.4×10^5*	*5.4×10^4*	*7.6×10^5*	*3.7×10^5*
TOF (hr^{-1}) (GC)	*5.8×10^4*	-	*2.0×10^5*	*7.1×10^4*
Faradaic Efficiency (%)	*24*	-	*26*	*21*

Table D.11: *Effect of pH of electrolyte on the performance indicators for $ZnPcF_{16}$/Nf obtained using varying applied potentials.*

5.2.2.3 Ionic Strength

Electrolyte at pH 2	**0.01 M NaH_2PO_4/H_3PO_4**	**0.1 M NaH_2PO_4/H_3PO_4**
TOF (hr^{-1}) (Electrochemical)	*2.7×10^4*	*1.9×10^5*
TOF (hr^{-1}) (GC)	-	*7.8×10^4*
Faradaic Efficiency %	-	*41*

Table D.12: *Performance data obtained for $CoPcF_{16}$ vs. Ag/AgCl using both 0.01 M and 0.1 M NaH_2PO_4/H_3PO_4 (pH 2).*

5.2.2.4 Using Chloride as an electrolyte

Temperature (°C)	**0**	**20**	**40**
TOF (hr^{-1}) (Electrochemical)	*1.5×10^5*	*5.1×10^5*	*1.1×10^6*
TOF (hr^{-1}) (GC)	*9.2×10^4*	*3.5×10^5*	*8.1×10^5*
Faradaic Efficieny %	*63*	*69*	*77*

Table D.13: *Performance data obtained for $CoPcF_{16}/Nf$ (at -1.2 V for 1 hour) vs. Ag/AgCl in 0.1 M HCl/KCl (pH 1.8) with varying temperature.*

5.2.2.5 Varying the catalyst concentration in coating solution

Catalyst Concentration (x 10^{-5} M)	**0.6**	**1.1**	**1.7**
TOF (hr^{-1}) (Electrochemical)	*3.3×10^5*	*2.2×10^5*	*1.5×10^5*
TOF (hr^{-1}) (GC)	*2.9×10^5*	*2.0×10^5*	*1.2×10^5*
Faradaic Efficiency (%)	*90*	*89*	*74*

Table D.14: *$CoPcF_{16}/Nf$ vs. Ag/AgCl in 0.1 M NaH_2PO_4/H_3PO_4 (pH 2) with varying catalyst concentration.*

5.2.2.7 Casting additional layers using DMF catalyst solution

Layers	**Co/Nf 2 layers**	**Zn/Nf 2 layer**	**Cu/Nf 2 layers**
TOF (hr^{-1}) (Electrochemical)	*1.2×10^5*	*4.7×10^4*	*1.7×10^5*
TOF (hr^{-1}) (GC)	*7.8×10^4*	*2.1×10^4*	*6.6×10^4*
Faradaic Efficiency (%)	*65*	*45*	*39*

Table D.15: *$CoPcF_{16}/Nf$, $ZnPcF_{16}/Nf$ and $CuPcF_{16}/Nf$ vs. Ag/AgCl in 0.1 M NaH_2PO_4/H_3PO_4 (pH 2) with additional layers cast.*

5.2.2.8 Stability

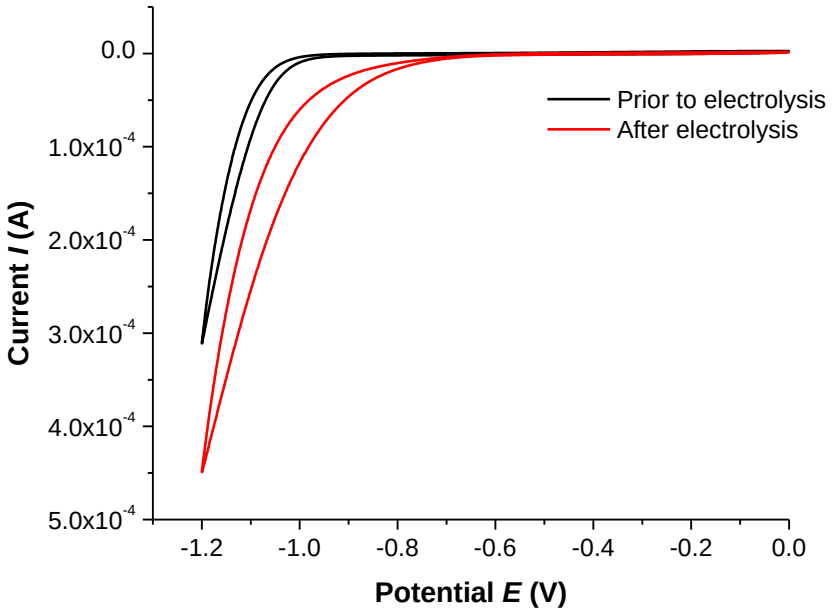

Figure D.6: *Cyclic voltammograms of $CoPcF_{16}$/Nf vs. Ag/AgCl in NaH_2PO_4/H_3PO_4 (pH 2). Scan rate = 100 mV/s.*

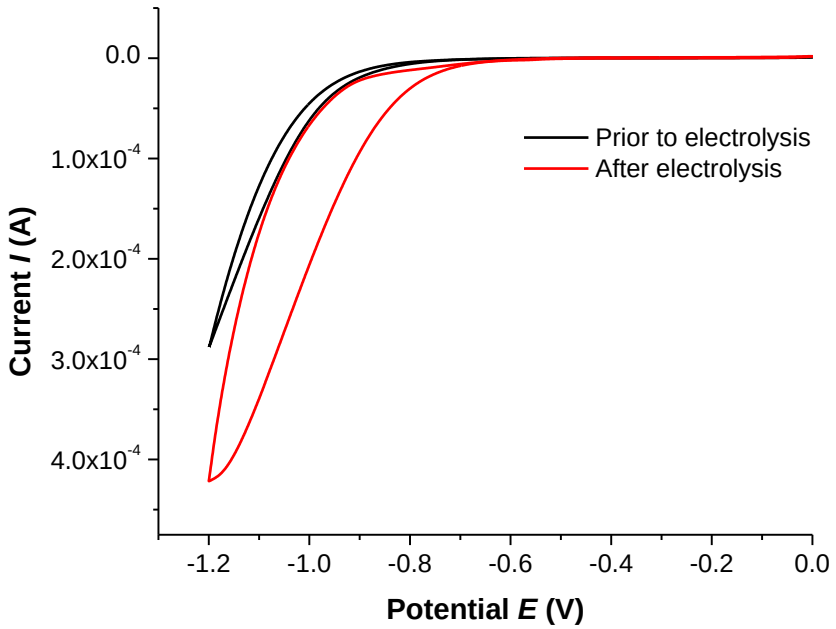

Figure D.7: *Cyclic voltammograms of $CuPcF_{16}$/Nf vs. Ag/AgCl in NaH_2PO_4/H_3PO_4 (pH 2). Scan rate = 100 mV/s.*

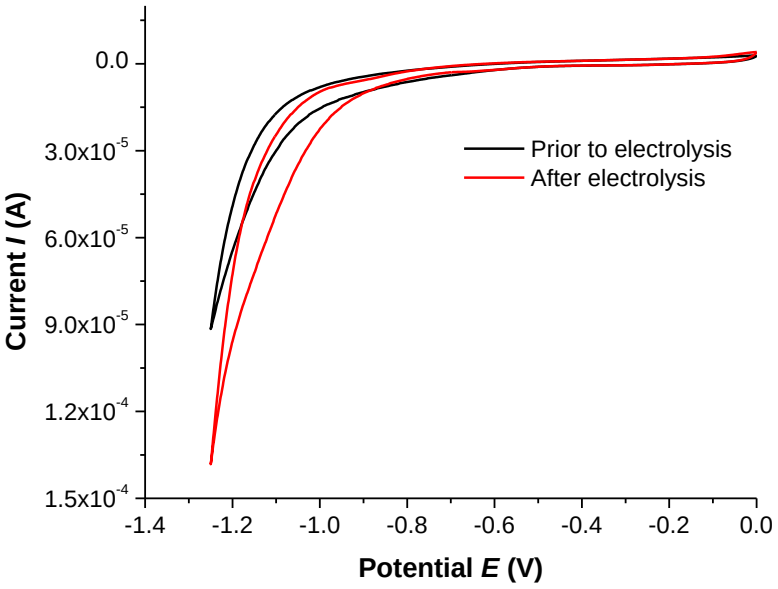

Figure D.8: *Cyclic voltammograms of $ZnPcF_{16}$/Nf vs. Ag/AgCl in NaH_2PO_4/H_3PO_4 (pH 2). Scan rate = 100 mV/s.*

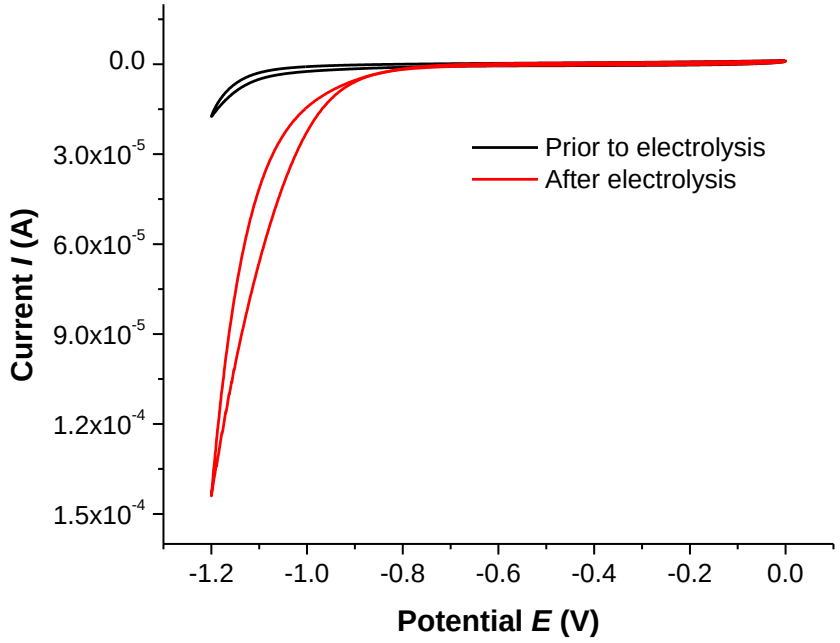

Figure D.9: *Cyclic voltammograms of Nafion vs. Ag/AgCl in 0.1 M NaH_2PO_4/H_3PO_4 (pH 2). Scan rate = 100 mV/s.*

5.2.2.9 Duration of Electrolysis

Time (hr)	**1**	**6**	**24**
TOF (hr^{-1}) (Electrochemical)	*6.2×10^6*	*2.1×10^6*	*1.7×10^7*
TOF (hr^{-1}) (GC)	*4.4×10^5*	*1.1×10^6*	*2.9×10^6*
Faradaic Efficiency (%)	*71*	*52*	*17*

Table D.16: *$CoPcF_{16}$/Nf (at -1.2 V) vs. Ag/AgCl in 0.1 M NaH_2PO_4/H_3PO_4 (pH 2) as a function of time.*

5.2.2.10 Photo- electrocatalytic generation of hydrogen

Variable	**Co/Nf Dark**	**Cu/Nf Dark**	**Zn/Nf Dark**
TOF (hr^{-1}) (Electrochemical)	*5.9×10^5*	*3.9×10^5*	*2.7×10^5*
TOF (hr^{-1}) (GC)	*3.8×10^5*	*2.1×10^5*	*4.3×10^4*
Faradaic Efficiency (%)	*64*	*54*	*16*

Table D.17: *$CoPcF_{16}$/Nf, $CuPcF_{16}$/Nf, and $ZnPcF_{16}$/Nf (at -1.2 V for 1 hour) vs. Ag/AgCl in 0.1 M NaH_2PO_4/H_3PO_4 (pH 2) in darkness.*

5.2.3 Effect of varying ratio of MPc to Nafion®- Additional calculations

Calculations in w/v % for catalyst systems *1*-$CuPcF_{16}$/Nf, *2*-$CuPcF_{16}$/Nf and 3-$CuPcF_{16}$/Nf

1-$CuPcF_{16}$/Nf (1 ml of 5 % w/w Nafion + 4 ml of $CuPcF_{16}$/DMF):

1 ml of 5 % w/w Nafion = 50 mg/ml

Cu = 0.039 mg/ml

1300 times less Cu in *1*-$CuPcF_{16}$/Nf

2-$CuPcF_{16}$/Nf (1 ml of 5 % w/w Nafion + 1 ml of $CuPcF_{16}$/DMF):

1 ml of 5 % w/w Nafion = 50 mg/ml

Cu = 0.025 mg/ml

2000 times less Cu in *2*-$CuPcF_{16}$/Nf

3-$CuPcF_{16}$/Nf (4 ml of 5 % w/w Nafion + 1 ml of $CuPcF_{16}$/DMF):

4 ml of 5 % w/w Nafion = 200 mg/ml

Cu = 0.01 mg/ml

20000 times less Cu in 3-$CuPcF_{16}$/Nf

Calculation of the diffusion coefficient.

$$i_p = (2.69 \times 10^5) n^{3/2} A D_O^{1/2} C_O^* \upsilon^{1/2}$$

$$\frac{i_p}{A\upsilon^{1/2}} = 1.84x10^{-5} = (2.69 \times 10^5) n^{3/2} D_O^{1/2} C_O^*$$

$$\frac{1.84 * 10^{-5}}{(2.69 \times 10^5) n^{3/2} \left(1.0x10^{-6} \frac{mol}{cm^3}\right)} = D_O^{1/2}$$

$$D_o = 4.67x10^{-9} \frac{cm^2}{s}$$

5.2.3.1 Varying the ratio of $CuPcF_{16}$: Nafion®

Ratio of $CuPcF_{16}$:Nafion®	***4:1***	***1:1***	***1:4***
TOF (hr^{-1}) (Electrochemical)	*6×10^5*	*2.3×10^6*	*1.7×10^6*
TOF (hr^{-1}) (GC)	*2.3×10^5*	*1.1×10^6*	*2.1×10^5*
Faradaic Efficiency (%)	*39*	*48*	*13*

Table D.18: *$CuPcF_{16}$/Nf vs. Ag/AgCl in 0.1 M NaH_2PO_4/H_3PO_4 (pH 2) with varying ratios of catalyst: Nafion® deposited on the electrodes.*

Varying the ratio of $CoPcF_{16}$: Nafion®

Ratio of $CoPcF_{16}$:Nafion®	***4:1***	***1:1***	***1:4***
Average Charge (C hr^{-1})	*0.19*	*0.18*	*0.24*
[1]Current Density *J* (mA/cm^2)	*1.1*	*0.9*	*1.4*
[2]Current Density *J* (mA/cm^2)	*4.5*	*4.6*	*5.6*
(%) Electroactive $CoPcF_{16}$/Nf	*10.5*	*5.9*	*9.0*
TOF (hr^{-1}) (Electrochemical)	*6.2×10^5*	*8.3×10^5*	*6.3×10^5*
TOF (hr^{-1}) (GC)	*4.4×10^5*	*7.7×10^5*	*5.5×10^6*
Faradaic Efficiency (%)	*71*	*93*	*88*

Table D.19: *Performance data obtained for $CoPcF_{16}$/Nf by CV and BE (at -1.2 V for 1 hour) vs. Ag/AgCl in 0.1 M NaH_2PO_4/H_3PO_4 (pH 2) with varying ratios of*

catalyst: Nafion® deposited on the electrodes. Current densities obtained by [1]BE and [2]CV.

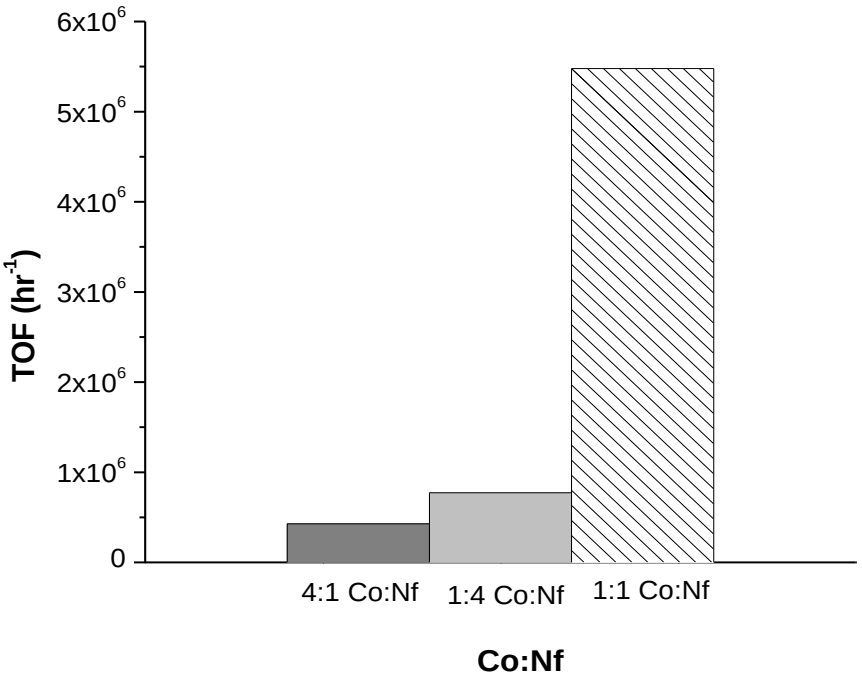

Figure D.10: *Effect of varying the ratios of $CoPcF_{16}$ and Nafion® on turnover frequencies TOF (hr^{-1}) for ratios of 4:1, 1:4 and 1:1 $CoPcF_{16}$/Nf respectively.*

Varying the ratio of $ZnPcF_{16}$: Nafion®

Ratio of $ZnPcF_{16}$:Nafion®	***4:1***	***1:1***	***1:4***
Average Charge (C hr^{-1})	*0.24*	*0.12*	*0.40*
[1]Current Density *J* (mA/cm^2)	*0.7*	*0.5*	*1.6*
[2]Current Density *J* (mA/cm^2)	*1.4*	*1.3*	*2.1*
Electroactive $ZnPcF_{16}$/Nf (%)	*1.2*	*0.5*	*0.5*
TOF (hr^{-1}) (Electrochemical)	*2.4×10^5*	*1.4×10^5*	*5.5×10^5*
TOF (hr^{-1}) (GC)	*5.8×10^4*	*2.7×10^4*	*1.3×10^5*
Faradaic Efficiency (%)	*24*	*20*	*24*

Table D.20: *Performance data obtained for $ZnPcF_{16}$/Nf by CV and BE (at -1.2 V for 1 hour) vs. Ag/AgCl in 0.1 M NaH_2PO_4/H_3PO_4 (pH 2) with varying ratios of catalyst: Nafion® deposited on the electrodes. Current densities obtained by [1]BE and [2]CV.*

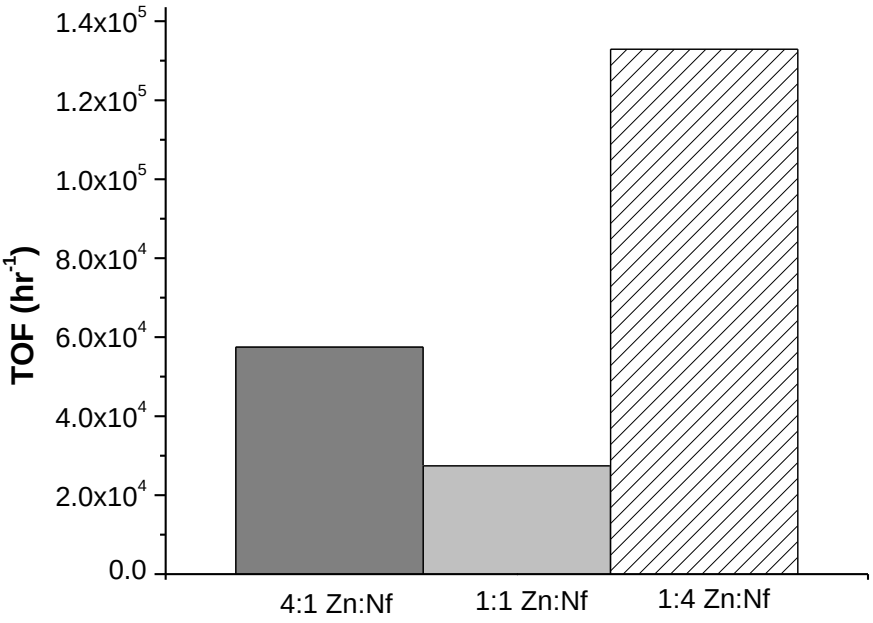

Figure D.11: *Effect of varying the ratios of $ZnPcF_{16}$ and Nafion® on turnover frequencies for ratios of 4:1, 1:1 and 1: 4 $ZnPcF_{16}$/Nf respectively.*

5.2.3.2 Varying the ratio of Catalyst:Nafion® using KCl as the electrolyte

MPc: Nafion®	**4:1**	**1:1**	**1:4**
TOF (hr^{-1}) (Electrochemical)	*7.3×10^5*	*9.4×10^5*	*6.3×10^6*
TOF (hr^{-1}) (GC)	*6.9×10^5*	*8.7×10^5*	*5.5×10^6*
Faradaic Efficiency %	*94*	*93*	*88*

Table D.21: *$CoPcF_{16}$/Nf (at -1.2 V for 1 hour) vs. Ag/AgCl in 0.1 M HCl/KCl (pH 1.8) at 20°C with varying ratios of catalyst: Nafion®.*

Appendix E

Chapter 6

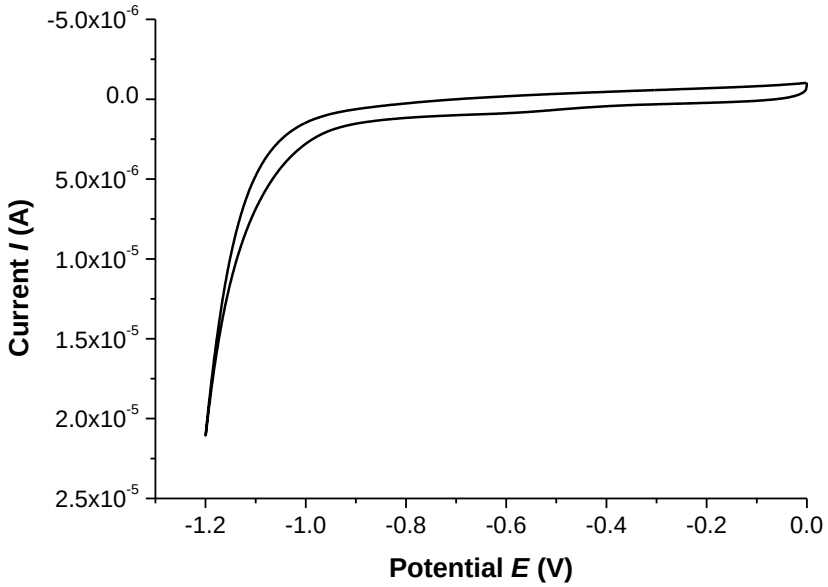

Figure E.1: *Cyclic voltammogram of bare CM/DDAB vs. Ag/AgCl in 0.1 M NaH_2PO_4/H_3PO_4 (pH 2). Scan rate = 100 mV/s.*

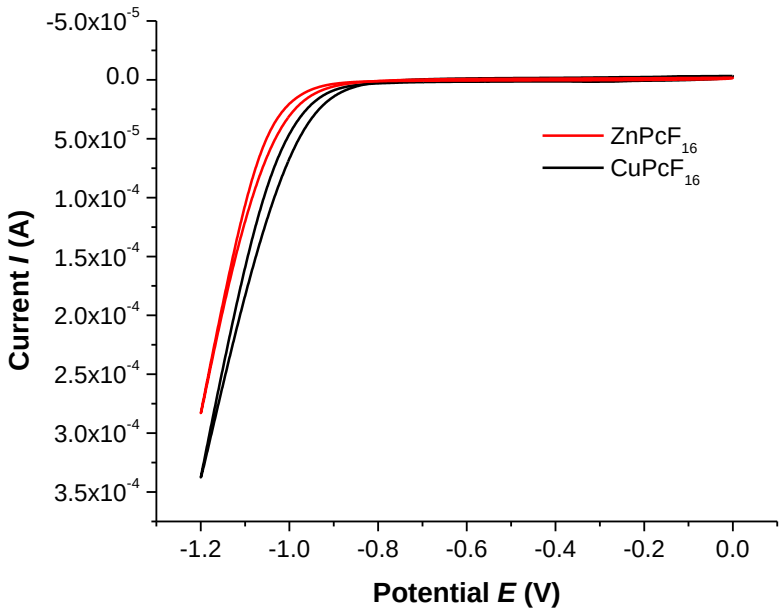

Figure E.2: *Cyclic voltammogram of 1:1 CM:$CuPcF_{16}$ (black line) and 1:1 CM:$ZnPcF_{16}$ (red line) vs. Ag/AgCl in 0.1 M NaH_2PO_4/H_3PO_4 (pH 2). Scan rate = 100 mV/s.*

Modified Electrode	***MCM***	***1:1***	***1:2***	***1:3***	***1:4***
TOF (hr^{-1}) Electrochemical	*2.4 x 10^6*	*2.3 x 10^5*	*8.2 x 10^4*	*9.3 x 10^4*	*6.2 x 10^4*
TOF (hr^{-1}) GC	*5.9 x 10^5*	*7.5 x 10^4*	*2.7 x 10^4*	*3.2 x 10^4*	*3.9 x 10^4*
Faradaic Efficiency %	*25*	*32*	*33*	*33*	*63*

Table E.1: *Performance data obtained by CV and BE vs. Ag/AgCl for 1 hour for $CoPcF_{16}$ adsorbed in carbon monolith fragments MCM, and from DDAB supported catalysts on carbon using ratios of CM:$CoPcF_{16}$ in 0.1 M NaH_2PO_4/H_3PO_4 (pH 2). Current densities obtained by [1]BE and [2]CV data.*

Modified Electrode	**$CuPcF_{16}$**	**$ZnPcF_{16}$**
TOF (hr^{-1}) Electrochemical	*1.4x 10^6*	*1.1x 10^5*
TOF (hr^{-1}) GC	*5.0 x 10^5*	*3.5 x 10^4*
Faradaic Efficiency %	*36*	*32*

Table E.2: *$CuPcF_{16}$ and $ZnPcF_{16}$ dispersed in carbon monolith fragments in a ratio of 1:1 in 0.1 M NaH_2PO_4/H_3PO_4 (pH 2).*

ME Ratio	***1:1***	***1:2***	***1:3***	***1:4***
TOF (hr^{-1}) Electrochemical	*7.4 x 10^5*	*1.0 x 10^5*	*8.8 x 10^4*	*6.4 x 10^4*
TOF (hr^{-1}) GC	*2.9 x 10^5*	*4.7 x 10^4*	*4.8 x 10^4*	*3.9 x 10^4*
Faradaic Efficiency %	*39*	*47*	*55*	*61*

Table E.3: *Performance data obtained for varying ratios of CM:$CoPcF_{16}$ in 0.1 M NaH_2PO_4/H_3PO_4 (pH 2) at 40°C.*

Modified Electrode	**$CuPcF_{16}$**	**$ZnPcF_{16}$**
TOF (hr^{-1}) Electrochemical	2.0 x 10^6	1.3 x 10^5
TOF (hr^{-1}) GC	8.6 x 10^5	6.0 x 10^4
Faradaic Efficiency %	43	46

Table E.4: *Performance data obtained for $CuPcF_{16}$ and $ZnPcF_{16}$ respectively in a 1:1 mix of carbon monolith at 40°C in 0.1 M NaH_2PO_4/H_3PO_4 (pH 2).*

	$CoPcF_{16}$	***$CuPcF_{16}$***	***$ZnPcF_{16}$***
TOF (hr^{-1}) Electrochemical	*1.5 x 10^6*	*1.4 x 10^6*	*4.7 x 10^5*
TOF (hr^{-1}) GC	*1.3 x 10^5*	*8.7 x 10^5*	*3.7 x 10^5*
Faradaic Efficiency (%)	*82*	*62*	*79*

Table E.5: *Performance indicators for $CoPcF_{16,}$ $CuPcF_{16}$ and $ZnPcF_{16}$ in carbon monolith in a ratio of 4:1 mix MPc:CM at 40°C using 0.1 M HCl/KCl (pH 1.8).*